Distribution Agreement

In presenting this thesis or dissertation as a partial fulfillment of the requirements for an advanced degree from Emory University, I hereby grant to Emory University and its agents the non-exclusive license to archive, make accessible, and display my thesis or dissertation in whole or in part in all forms of media, now or hereafter known, including display on the world wide web. I understand that I may select some access restrictions as part of the online submission of this thesis or dissertation. I retain all ownership rights to the copyright of the thesis or dissertation. I also retain the right to use in future works (such as articles or books) all or part of this thesis or dissertation.

Signature:

_____ _____

Esra Sefik Date

A genetics-first, rare variant approach to understanding the neurobiological substrates of schizophrenia and associated disorders

By

Esra Sefik
Doctor of Philosophy

Graduate Division of Biological and Biomedical Sciences
Neuroscience

_____
Jennifer G. Mulle, Ph.D.
Advisor

_____
Elaine F. Walker, Ph.D.
Advisor

_____
Joseph F. Cubells, MD, Ph.D.
Committee Member

_____
Sarah Shultz, Ph.D.
Committee Member

_____
David Weinshenker, Ph.D.
Committee Member

Accepted:

_____
Kimberly J. Arriola, Ph.D.
Dean of the James T. Laney School of Graduate Studies

_____
Date

A genetics-first, rare variant approach to understanding the neurobiological substrates of schizophrenia and associated disorders

By

Esra Sefik
B.A., Tufts University, 2015

Advisor: Jennifer G. Mulle, Ph.D.
Advisor: Elaine F. Walker, Ph.D.

An abstract of
A dissertation submitted to the Faculty of the
James T. Laney School of Graduate Studies of Emory University
in partial fulfillment of the requirements for the degree of
Doctor of Philosophy
in Graduate Division of Biological and Biomedical Sciences
Neuroscience
2022

Abstract

A genetics-first, rare variant approach to understanding the neurobiological substrates of schizophrenia and associated disorders
By Esra Sefik

It has long been known that schizophrenia has a substantial genetic component, but large-scale genomic investigations have only recently begun to illuminate the exact nature of this genetic architecture. There are now at least eight copy number variants (CNVs) with genome-wide significance for association with schizophrenia, which provide new substrates to investigate the etiology and pathogenesis of this complex and heterogeneous disorder. Among these, the 3q29 deletion (3q29Del) confers the highest known risk for schizophrenia (>40-fold increase); but the neurobiological mechanisms contributing to the abnormal neurodevelopmental phenotypes are not yet understood. The objective of this dissertation was to address this knowledge gap by employing a multidisciplinary approach that integrates tools from high-throughput RNA-sequencing, network analysis, neuroimaging, behavioral and clinical phenotyping, and statistical modeling. First, we used a systems-biology approach to interrogate the network-level behavior of 3q29 interval genes within the global protein-coding transcriptome of the healthy human prefrontal cortex. The modular properties and connectivity patterns yielded key predictions about novel biological roles, functional interactions and putative disease associations for individual 3q29 genes. Next, we performed the first known *in vivo* quantitative neuroimaging study in individuals with 3q29Del, and assessed the relationship between neuroanatomical findings and standardized measures of cognitive and sensorimotor abilities. Our findings showed that abnormal development of posterior fossa structures, particularly the cerebellum, may be a neuroimaging-based biomarker in 3q29Del. We additionally found that cerebellar volumetric changes are associated with cognitive disability, and diminished visual-motor integration skills, suggesting that the cerebellum is a possible mechanistic intermediary between this genetic lesion and motor and non-motor syndromic phenotypes. Furthermore, we conducted the first in-depth evaluation of psychotic symptoms in subjects with 3q29Del, compared this profile to 22q11.2Del, and investigated the relationship between psychotic symptoms and findings from structural brain imaging. Results from this work established the unique and shared profiles of psychotic symptoms across two high-impact CNVs and revealed cerebellar involvement in elevated psychosis-risk in 3q29Del. Altogether, the presented findings substantially advance our understanding of the role that 3q29Del plays in vulnerability for severe neurodevelopmental and psychiatric disorders and provide novel insights into neurogenetic mechanisms shaping human behavior and development.

A genetics-first, rare variant approach to understanding the neurobiological substrates of schizophrenia and associated disorders

By

Esra Sefik
B.A., Tufts University, 2015

Advisor: Jennifer G. Mulle, Ph.D.
Advisor: Elaine F. Walker, Ph.D.

A dissertation submitted to the Faculty of the
James T. Laney School of Graduate Studies of Emory University
in partial fulfillment of the requirements for the degree of
Doctor of Philosophy
in Graduate Division of Biological and Biomedical Sciences
Neuroscience
2022

Acknowledgements

This dissertation would not have been possible without the support of many people.

I would first and foremost like to thank my co-advisors, Jennifer Mulle and Elaine Walker, for their invaluable mentorship, continuous support and endless supply of fascinating research ideas during the course of my graduate work. I am extremely grateful that you took me on as a trainee and continued to have faith in me over the years.

Thank you to the members of my dissertation committee, Sarah Shultz, David Weinshenker, and Joseph Cubells. Your encouraging words and insightful feedback pushed me to sharpen my thinking and raised my work to a higher level. I would like to especially thank Sarah Shultz for everything she taught me in the world of neuroimaging.

I would like to acknowledge several other collaborators whom I was fortunate to work with and learn from, including Ryan Purcell, Steven Sloan, Longchuan Li, and Gary Bassell. I would like to especially thank Ryan Purcell for taking me under his wing, teaching me wet lab skills (starting with how to hold a pipette), and engaging in a great many discussions on complex disease mechanisms. I express my sincere gratitude to Steven Sloan for introducing me to the captivating subject of single cell transcriptomics, which formed an invaluable part of my doctoral training outside the scope of the work reported herein.

I would also like to thank all current and former lab members, with whom I was lucky to have shared my time at Emory. They have enriched my Ph.D. journey in myriad ways.

Thank you to my Neuroscience cohort, particularly Thomas Shiu, Nuri Jeong, and Mallika Halder for their comradery – you were instrumental in making Atlanta a home for me over these past five years.

My earnest thanks to my partner, Eric Feltham for giving me unconditional love, support, and understanding as I maneuvered my way through graduate school. I appreciate the encouragement that you gave me when the tasks seemed arduous and insurmountable – you are my rock.

An extra special thanks to my sister Esen Sefik and my niece Su Sefik Karatepe, who was born the same year I started my PhD. Thank you SuSu for all the drawings, rainbow GIFs and voice messages that you send me; they cheer me up every time. And thank you Esen Sefik for always being there for me through thick and thin – you are an incredibly strong role model and my closest confidant.

I owe much gratitude to my parents, Nurcihan Sefik and Bedri Sefik for their unwavering support, love and sacrifices that allowed me to achieve my dreams.

Finally, I would like to express the utmost gratitude to our study participants and their families. This work would not have been possible without their contributions.

Table of Contents

CHAPTER 1. Introduction 1

A clinical and epidemiological introduction to schizophrenia 1

Schizophrenia neuroanatomy 3

The neurodevelopmental hypothesis of schizophrenia 6

Genetic architecture of schizophrenia 7

Copy number variation 11

Research aims 14

Figures 16

Figure 1. The canonical 3q29 deletion locus, modified from the National Center for Biotechnology Information's Genome Data Viewer. 16

References 17

CHAPTER 2. Convergent and distributed effects of the 3q29 deletion on the human neural transcriptome 35

Abstract 36

Introduction 37

Methods and Materials 38

Results 43

Discussion 50

Data availability 55

Figures 56

Figure 1. Unbiased weighted gene co-expression network analysis (WGCNA) of the human transcriptome

in the healthy adult prefrontal cortex (PFC). 56

Figure 2. Network-based inference of the functional impact of 3q29Del on the adult human prefrontal cortex (PFC). 59

Figure 3. 3q29 interval genes form transcriptomic subnetworks enriched for known schizophrenia, autism and intellectual / developmental disability-risk genes. 61

Figure 4. Network of prioritized drivers predicted to contribute to the neuropsychiatric sequelae of 3q29Del. 63

Figure 5. Weighted gene co-expression network analysis (WGCNA) predicts differentially expressed genes in the mouse mode of 3q29Del. 65

References 67

Supplemental Materials 78

Extended Methods 78

Extended Results 97

Supplemental Figures 114

Figure S1. Tissue sample attributes and donor phenotypes of the GTEx dataset used for reference network construction. 114

Figure S2. Pre-processing of the reference dataset: outlier removal. 116

Figure S3. Determination of the soft-thresholding power (β) in weighted gene co-expression network analysis (WGCNA). 117

Figure S4. Determination of network reproducibility and module preservation in an independent test dataset. 119

Figure S5. Individual module preservation and quality statistics underlying composite Zsummary scores. 122

Figure S6. Publication numbers for 3q29 genes and historic schizophrenia spectrum disorder candidate genes. 123

Figure S7. Overlap between known protein-protein interactions (PPI) and gene co-expression patterns

of 3q29 interval genes. ... 124
Figure S8. STRING protein-protein interaction (PPI) networks of genes co-expressed in 3q29 modules. ... 126
Figure S9. Amalgamated illustration of top biological processes and pathways enriched in 3q29 modules. ... 133
Supplemental References ... 134
CHAPTER 3. Structural deviations of the posterior fossa and the cerebellum and their cognitive links in a neurodevelopmental deletion syndrome ... 142
Abstract ... 143
Introduction ... 144
Methods and Materials ... 145
Results ... 151
Discussion ... 154
Acknowledgements ... 162
Data availability ... 162
Tables ... 163
Table 1. Demographic characteristics of the study sample in volumetric analyses, stratified by diagnostic group. ... 163
Table 2. Summary of multiple linear regression results testing for differences in volumetric measures of interest between 3q29Del and control subjects. ... 164
Table 3. Post hoc analysis of the sex-specific effects of diagnostic group on eICV. ... 166
Table 4. Exploratory analysis of the relationship between volumetric measures of interest and posterior fossa arachnoid cyst and mega cisterna magna findings among 3q29Del subjects. ... 167
Table 5. Summary of multiple linear regression results showing the relationships between cerebellar white

matter volume and standardized test scores for sensorimotor and cognitive abilities among 3q29Del subjects. 169

Figures 171

Figure 1. Histogram showing the age distribution of study participants in volumetric analyses, stratified by sex and diagnostic group. 171

Figure 2. Scatter plots showing the distribution of A) total cerebellum volume, B) cerebellar cortex volume, C) cerebellar white matter volume, and D) eICV as a function of age among male and female subjects in each diagnostic group. 172

Figure 3. Predictor effect plots showing the effect of diagnostic group on volumetric measures of interest. 173

Figure 4. Predictor effect plot showing the moderating effect of sex on the relationship between diagnostic group and eICV. 175

Figure 5. Prevalence of posterior fossa arachnoid cyst and mega cisterna magna findings in structural MRI scans of 3q29Del and control subjects. 176

Figure 6. Predictor effect plots showing the relationships between cerebellar white matter volume and visual-motor integration skills, composite IQ, verbal IQ and non-verbal IQ among 3q29Del subjects. 178

References 180

Supplemental Materials 198

Extended Methods 198

Supplemental Tables 209

Table S1. Demographic characteristics of the study sample in volumetric analyses, stratified by diagnostic group and sex. 209

Table S2. Comparison of structural magnetic resonance imaging (MRI) protocols 210

Table S3. Extended linear regression results testing the effect of diagnostic group on volumetric measures of interest and polynomial modeling of age. 212

Table S4. Summary of supplemental results from penalized cubic spline models testing the effect of diagnostic group on volumetric measures of interest. 221
Table S5. Exploratory modeling of diagnostic group by sex interaction effects on volumetric measures. 223
Table S6. Post hoc analysis of the suggestive sex by diagnostic group interaction effect on eICV-adjusted cerebellar white matter volumes 226
Table S7. Summary of multiple linear regression findings and descriptive statistics for volumetric measures of interest in 3q29Del and control groups. 229
Table S8. Demographic and relevant clinical characteristics of 3q29Del subjects with versus without posterior fossa arachnoid cyst or mega cisterna magna findings. 230
Table S9. Descriptive statistics for standardized test scores for sensorimotor and cognitive abilities among 3q29Del subjects. 232
Table S10. Extended multiple linear regression results testing the relationships between tissue-specific cerebellar volumes and sensorimotor and cognitive abilities among 3q29Del subjects. 234
Table S11. Standardized test scores for sensorimotor and cognitive abilities in 3q29Del subjects with versus without posterior fossa arachnoid cyst or mega cisterna magna findings. 235
Supplemental Figures 236
Figure S1. Example cerebellar segmentation masks for representative age- and sex-matched 3q29Del and healthy control pairs. 237
Figure S2. Relationships between estimated total intracranial volume, total brain volume and head circumference among 3q29Del subjects. 239
Figure S3. Relationships between eICV and A) total cerebellum, B) cerebellar cortex, and C) cerebellar white matter volumes among 3q29Del subjects versus controls. 241
Figure S4. Correction of cerebellar volumes for head size variation in volumetric case-control analyses. 243
Figure S5. Scatter plots showing the distribution of eICV-adjusted A) total cerebellum volume, B)

cerebellar cortex volume, and C) cerebellar white matter volume as a function of age among male and female subjects in each diagnostic group. 245

Figure S6. Regression diagnostics: testing the assumptions of ordinary least squares regression for best-fitting models from Table S3. 247

Figure S7. Developmental trajectories for volumetric measures of interest estimated by the penalized cubic spline approach. 248

Figure S8. Predictor effect plot showing a suggestive interaction effect between diagnostic group and sex on eICV-adjusted cerebellar white matter volumes. 249

Figure S9. Estimated normative percentile curves for cerebellar volumes and eICV, stratified by sex. 252

Figure S10. Scatter plots showing the distribution of A) total cerebellum volume, B) cerebellar cortex volume, C) cerebellar white matter volume, and D) eICV as a function of age among 3q29Del subjects with versus without posterior fossa arachnoid cyst or mega cisterna magna findings. 253

Figure S11. Violin plots with box plots visualizing the distribution of standardized test scores for sensorimotor and cognitive abilities among 3q29Del subjects. 254

Figure S12. Heatmap visualization of pairwise Pearson's correlations between standardized test scores for sensorimotor and cognitive abilities among 3q29Del subjects. 255

Figure S13. Cerebellar protein expression profiles of 3q29 interval genes annotated by the Human Protein Atlas. 257

Supplemental References 259

CHAPTER 4. Psychosis spectrum symptoms among individuals with schizophrenia-associated copy number variants and evidence of cerebellar correlates of symptom severity 262

Abstract 263

Introduction 264

Methods and Materials 265

Results 269

Discussion 273

Acknowledgements 278

Data availability 278

Tables 278

Table 1. Demographic and relevant clinical information for individuals with 3q29Del. 279

Table 2. Rates of clinically significant psychotic symptoms (i.e., at least one SIPS item rated ≥ 3) among subjects with 3q29Del and 22q11.2Del. 280

Table 3. The overall results of the ANCOVA between the SIPS ratings of each diagnostic group and pairwise comparisons. 281

Figures 283

Figure 1. The unadjusted means of individual SIPS ratings for each diagnostic group 283

Figure 2. The relationships between cerebellar structure and psychosis-risk symptoms in 3q29Del 284

References 286

Supplemental Materials 300

Extended Methods 300

Extended Results 304

Supplemental Tables 306

Table S1. Demographic and relevant clinical information for the HC and 22q11.2Del samples and comparison with 3q29Del. 306

Table S2. Correlations between SIPS symptom ratings and age at visit, stratified by symptom domain and diagnostic group. 308

Table S3. Sex-adjusted means and standard errors of SIPS ratings after log-transformation. 309

Table S4. Demographic, clinical, and MRI-derived volumetric information for the 3q29Del subsample

with available neuroimaging and SIPS data. 310
Table S5. Extended linear regression results: The effect of cerebellar volumetric measures on domain-specific symptom ratings in 3q29Del and polynomial modeling of age. 311
Table S6. Extended logistic regression results: The effect of cerebellar volumetric measures on the probability of a psychotic disorder or APSS diagnosis in 3q29Del and polynomial modeling of age. 320
Table S7. Nested comparison of diagnostic and dimensional phenotypes in 3q29Del subjects with versus without posterior fossa arachnoid cyst and mega cisterna magna findings. 323
Supplemental Figures 325
Figure S1. Age-stratified prevalence rates of florid or attenuated psychotic symptoms in 3q29Del. 325
Figure S2. Scatter plots of the relationship between SIPS symptom ratings and age at visit, stratified by symptom domain and diagnostic group. 327
Figure S3. Sex-specific SIPS ratings among deletion groups and HCs. 328
Figure S4. Comparison of hemisphere-specific ROI volumes in the 3q29Del subsample with available neuroimaging and SIPS data. 329
Figure S5. Sensitivity analysis: The relationship between cerebellar cortex volume and positive symptom severity in 3q29Del after removal of an extreme data point. 330
Supplemental References 331
CHAPTER 5. Conclusions 332
References 340

CHAPTER 1. Introduction

A clinical and epidemiological introduction to schizophrenia

Schizophrenia is a highly debilitating, chronic and complex mental illness that has a lifetime prevalence of about 0.5-1% (1, 2), with comparable rates observed across diverse populations (3). Despite a century of research since Emil Kraepelin's original formulation of the nosology of schizophrenia under the name of "dementia praecox" (4, 5), our knowledge of the etiology and pathogenetic unfolding of this disorder remains scarce.

Schizophrenia is characterized by positive symptoms (i.e., delusions, hallucinations, and grossly disorganized speech and behavior), negative symptoms (i.e., amotivation, social withdrawal, and blunted affect), and cognitive impairment (i.e., executive function deficits) (6). Minor neurological abnormalities (also known as neurological "soft signs") including motor coordination and sequencing impairments, as well as sensory integration deficits are also commonly reported by patients (7-9). Although positive symptoms, such as hearing voices that are not there, are often the primary reason why patients are brought to medical attention, negative, cognitive and motor symptoms can also produce significant adverse effects on everyday functioning (10). Typically, the clinical onset of schizophrenia occurs in late adolescence or early adulthood (11), although earlier and later forms of onset can also be seen. The specific combinations of these symptoms, and the course of the disease itself reveal considerable heterogeneity across individuals.

Antipsychotic medications targeting dopamine neurotransmission have been the principal mean of therapeutic intervention for schizophrenia since the 1950s (12), but side effects, such as cardiometabolic abnormalities and extrapyramidal symptoms play a key role in discontinuation of treatment (13-16), and there is substantial variation in observed treatment responses (17). In approximately one-third of patients, available antipsychotics are partially or not effective in the management and treatment of schizophrenia (18, 19), suggesting that there may be differences in the etiology and consequent pathophysiology of this illness across patients and that schizophrenia may not be a single disease entity. Notably, the mean life expectancy among individuals with schizophrenia is approximately 15-20 years shorter than that of the general population, and there is a substantial risk of death by suicide early in the course of the illness: ~1 in 3 people with schizophrenia

attempt suicide during their lifetime. (20-23). In addition, it is estimated that 70-90% of individuals with schizophrenia experience challenges with living and working independently (24-28). These outcomes urgently implore us to develop more effective, and possibly individualized, interventions.

It is worth noting that the diagnostic definitions and clinical boundaries of schizophrenia have changed over time according to the scientific zeitgeist (6, 29, 30). In recent years, the limitations of using a categorical diagnosis system have garnered increasing attention, with many camps advocating for a more transdiagnostic approach to evaluating dimensions of psychopathology. Accordingly, the classical subtypes of schizophrenia were eliminated from the most recent edition of the *Diagnostic and Statistical Manual of the American Psychiatric Association, DSM-5* (31), and schizophrenia is now conceptualized on a psychosis continuum. The *DSM-5* currently defines schizophrenia using the following operational criteria under the section on "schizophrenia spectrum and other psychotic disorders" (31):

A. Two (or more) of the following, each present for a significant portion of time during a 1-month period (or less if successfully treated). At least one of these must be [1], [2], or [3]:
    1. Delusions.
    2. Hallucinations.
    3. Disorganized speech (e.g., frequent derailment or incoherence).
    4. Grossly disorganized or catatonic behavior.
    5. Negative symptoms (i.e., diminished emotional expression or avolition).
B. For a significant portion of the time since the onset of the disturbance, level of functioning in one or more major areas, such as work, interpersonal relations, or self-care, is markedly below the level achieved prior to the onset (or when the onset is in childhood or adolescence, there is failure to achieve expected level of interpersonal, academic, or occupational functioning).
C. Continuous signs of the disturbance persist for at least 6 months. This 6-month period must include at least 1 month of symptoms (or less if successfully treated) that meet Criterion A (i.e., active-phase symptoms) and may include periods of prodromal or residual symptoms. During these prodromal or residual periods, the signs of the disturbance may be manifested by only negative symptoms or by two

or more symptoms listed in Criterion A present in an attenuated form (e.g., odd beliefs, unusual perceptual experiences).

D. Schizoaffective disorder and depressive or bipolar disorder with psychotic features have been ruled out because either 1) no major depressive or manic episodes have occurred concurrently with the active-phase symptoms, or 2) if mood episodes have occurred during active-phase symptoms, they have been present for a minority of the total duration of the active and residual periods of the illness.

E. The disturbance is not attributable to the physiological effects of a substance (e.g., a drug of abuse, a medication) or another medical condition.

F. If there is a history of autism spectrum disorder or a communication disorder of childhood onset, the additional diagnosis of schizophrenia is made only if prominent delusions or hallucinations, in addition to the other required symptoms of schizophrenia, are also present for at least 1 month (or less if successfully treated).

These diagnostic criteria play a critical role in not only the psychiatric management and treatment of patients with schizophrenia, but also in the very conceptualization of research studies that aim to elucidate the risk factors and causal mechanisms underlying this complex and heterogeneous disorder. Since the neurobiology underlying this condition is insufficiently understood, most diagnostic attributes that define schizophrenia remain inferential and heavily rely on subjective experiences reported by patients and their caregivers. Currently, there is no externally validated biomarker or objective diagnostic test that can be used for the identification, prevention, or treatment of schizophrenia in clinical practice.

Schizophrenia neuroanatomy

A plethora of noninvasive *in vivo* neuroimaging studies using cross-sectional or longitudinal study designs and sampling techniques based on clinical presentation have shown structural brain alterations in both patients with chronic schizophrenia and patients with first episode psychosis. These studies have been instrumental for advancing our understanding of disorder-related pathophysiological mechanisms, but there is

extensive heterogeneity and inconsistencies across structural neuroimaging findings, possibly due in part to etiologic heterogeneity, but also as a consequence of methodological differences (e.g., differences in inclusion criteria, sample sizes, age range of study participants, duration of treatment etc.). This presents a major challenge for interpreting and integrating results from different studies. This section aims to present a selective review of structural neuroimaging findings in schizophrenia, primarily based on magnetic resonance imaging (MRI), to provide background knowledge for contextualizing later findings presented in this dissertation.

When all morphological changes demonstrated by structural neuroimaging studies of patients with schizophrenia are reviewed, enlarged lateral ventricles and reduced gray matter volumes in the prefrontal cortex and medial temporal lobe structures (including the hippocampus) emerge as some of the most consistent neuroanatomical abnormalities in this disorder (32-40). Multiple meta-analyses in patients with schizophrenia also identified gray matter deficits in the insula, anterior cingulate cortex, parietal cortex, thalamus, amygdala and basal ganglia structures, as well as diffuse abnormalities in white matter tracts, including the uncinate fasciculus, the cingulum bundle, corpus callosum, and internal capsule (32-35, 41-44), although there is substantial variability across these reports.

A meta-analysis of over 300 MRI studies investigating brain alterations in both medicated and antipsychotic-naive schizophrenia patients showed that intracranial and total brain volumes were significantly decreased among individuals with schizophrenia, with the largest effect sizes observed in gray matter structures (45). Among antipsychotic-naive patients, volume reductions in the caudate and thalamus were more pronounced than in medicated patients, suggesting that subcortical abnormalities are present before antipsychotics are introduced and may be attenuated by treatment. Similar reductions in white matter volume were observed in both groups, while reductions in gray matter were less extensive in antipsychotic-naive patients. Interestingly, total gray matter reduction was found to be associated with longer illness duration and higher doses of antipsychotic treatment at time of scanning. These findings altogether suggest that structural brain alternations among schizophrenia patients are related to a combination of both early neurodevelopmental processes that go awry (as reflected in intracranial volume reductions) as well as factors related to illness progression and differential exposure to psychotropic medications.

Notably, divergent brain abnormalities have been reported for earlier versus later-onset psychosis patients, which may be related to disparities in underlying vulnerabilities and different brain structures maturing at different ages and rates (46-51). For example, in very early-onset psychosis, such as childhood-onset schizophrenia (before the age of 13) (52), parietal abnormalities have been reported (53, 54), whereas among patients with psychosis onset during adolescence, the frontal and temporal regions were shown to be principally affected (55-58). During normative brain development, the parietal cortex reaches peak maturity in late childhood, while frontal and temporal cortices mature later during adolescence (49). It has been theorized that if onset of psychosis coincides with active maturational changes in a brain structure, then development of that particular brain structure will be most affected by the disease (49, 59-61). Hence, age at onset appears to modulate structural brain changes in schizophrenia and may explain an important component of the heterogeneity observed in studies aimed at understanding the neurobiological underpinnings of this illness.

To date, significant inroads have been made towards describing the regional brain abnormalities associated with schizophrenia, but it should be highlighted that not all parts of the brain have received equal attention or coverage. For many years, schizophrenia was considered a disease that primarily affects the cerebrum ("the seat of intelligence"), hence the cerebellum – a hindbrain structure that plays a well-established role in sensory-motor functions (62) – was traditionally overlooked due to its apparent involvement in "lower" functions unrelated to cognition (63). However, this trend is changing. Emerging evidence indicate that the cerebellum is wired not only to cerebral areas involved in motor control but also to areas involved in higher-order cognitive and affective functions (64-67). The reciprocal influence between the brain regions making up the cerebello-basal ganglia-thalamo-cortical system is gaining increasing attention in a variety of learning processes (68).

Newer findings indicate that cerebellar structural abnormalities are present in both patients with chronic schizophrenia and patients at the early stages of schizophrenia (independent of antipsychotic medication effects or illness duration), with some studies also reporting cerebellar associations with cognitive abilities and disease symptoms among patients (69-75). Hence, our conceptualization of the roles that regions outside the cerebrum play in schizophrenia pathophysiology is rapidly evolving. However, the etiological

underpinnings and precise neurobiological mechanisms driving these structural changes remain unknown.

The neurodevelopmental hypothesis of schizophrenia

The neurodevelopmental hypothesis of schizophrenia, originally formulated by Weinberger (76), Murray and Lewis (77), provides a valuable framework for understanding schizophrenia (an adult-onset disorder) as a condition that has its roots at least in part in events occurring early in development. The idea that schizophrenia is a disorder that may arise from aberrant brain development is not new, but new impetus in favor of this paradigm has been given by growing evidence implicating a combination of genetic and environmental factors that act on brain development as significant risk factors for schizophrenia (77-83).

In this context, it is now largely established that although schizophrenia is typically diagnosed in late adolescence or early adulthood, psychotic episodes and other disease characteristics rarely emerge with an acute onset. A prodromal period which is marked by a gradual decline in cognitive and social functioning, as well as the emergence of attenuated or sub-threshold positive symptoms, often precedes the first psychotic episode among patients with schizophrenia spectrum and other psychotic disorders (84-86). Previous work, including studies that have evaluated childhood home movies of schizophrenia patients and comparison subjects, has also shown that premorbid signs of social and neuromotor deficits are already present during childhood, long before clinical symptoms of the disease appear in the second or third decade of life (87-89). An array of neuroanatomical abnormalities, including gray matter reductions in the frontal and temporal cortices of the cerebrum, deviations in cerebellar structure and widespread alterations in white matter connectivity, has been identified among youth exhibiting prodromal signs and symptoms compared with healthy controls; these abnormalities appear to be similar to but more subtle than those seen in patients with frank psychosis (90-95), implying that deviations in brain structure predate illness onset and likely have a neurodevelopmental component.

The neurodevelopmental hypothesis of schizophrenia is further supported by multiple strands of evidence indicating that individuals who experience an excess of prenatal and/or perinatal complications, such as maternal infection *in utero*, prenatal malnutrition or obstetric complications (e.g., prematurity, low birth

weight, fetal hypoxia) have an increased risk of developing schizophrenia later in life (96-100). A significant relationship between early childhood trauma and risk of psychosis has also been reported (101, 102). Moreover, there is robust evidence showing that urban birth and upbringing are associated with psychotic illness (103, 104), although there is still no consensus on what aspects of the urban environment underly this increased risk (possibilities include stress, pollution, and infections adversely impacting brain development).

At the same time, results from numerous family, twin and adoption studies have revealed that schizophrenia has a considerable (although not deterministic) genetic component. Concordance rates of schizophrenia for monozygotic and dizygotic twins are around 50% and 20%, respectively, and the heritability estimate for this disorder (i.e., the proportion of phenotypic variance attributable to genetic variance in a population, h^2) is approximately 80% (105-110), which is roughly equal to that of type I diabetes (111). These findings indicate that, besides environmental sources of risk, genetic factors also play an important role in increasing susceptibility for schizophrenia, which implies that abnormal neurodevelopmental processes that arise as a consequence of aberrant gene expression events likely predate illness onset in certain subsets of schizophrenia patients.

However, knowing the heritability of a trait does not directly provide information about which genes or how many genes are involved in disease etiology (i.e., its molecular genetics). In recent decades, it has become clear from genetic epidemiological data that schizophrenia's mode of transmission is complex (112, 113), but the search for the exact genetic substrates of schizophrenia has been fraught with many dead ends. The next section will present a selective review of specific genetic loci that have been shown to be associated with increased risk for developing schizophrenia, with an emphasis on robust and replicable findings.

Genetic architecture of schizophrenia

Multiple approaches have been applied to understand the genetic basis of schizophrenia. Prior to the era of genome-wide association studies (GWAS), "candidate gene" studies were highly prominent in the literature. Given the high cost and difficulty of genotyping large areas of the human genome at the time, these earlier studies used a case-control study design and genotyped a limited number of genetic markers in a

candidate gene that was selected based on existing theories about the etiology of schizophrenia or on findings from linkage or cytogenetic studies. Over 1,000 candidate gene papers have been published using this approach (114). Some of the most cited candidate genes in schizophrenia research are *DISC1* (Disrupted in schizophrenia 1; rationale for study: translocation in a pedigree), *DRD2, DRD3* and *DRD4* (Dopamine receptors D2-4; rationale for study: antipsychotic pharmacology), *GRM3* (Glutamate receptor, metabotropic 3; rationale for study: glutamate hypothesis), *HTR2A* (Serotonin receptor 2A; rationale for study: antipsychotic pharmacology), *SLC6A3* (Dopamine transporter; rationale for study: dopamine hypothesis), *SLC6A4* (Serotonin transporter; rationale for study: implicated in mood disorders), *TNF* (Tumor necrosis factor; rationale for study: immune hypothesis), *BDNF* (Brain-derived neurotrophic factor; rationale for study: neurodevelopment hypothesis), *APOE* (Apolipoprotein E; rationale for study: implicated in Alzheimer's disease), *NRG1* (Neuregulin 1; rationale for study: linkage analysis), and *DTNBP1* (Dystrobrevin binding protein 1; rationale for study: linkage analysis) (115).

The candidate gene strategy paved the way for several notable successes in identifying specific risk variants for complex brain disorders like Alzheimer's disease (e.g., *APOE*) (116), but this approach failed to yield clear insights into the genetic basis of schizophrenia, since most findings suffered from low reproducibility (possibly in part due to inadequate statistical power) and much of the genome was ignored. Today, findings from candidate gene association studies of schizophrenia are considered controversial due to inconsistencies and their potential pathogenetic involvement in schizophrenia etiology remains debated (117-120).

Starting with the first schizophrenia GWAS that appeared in 2008 (121), cost-effective advancements in genotyping and sequencing technologies coupled with international consortia efforts (e. g., Psychiatric Genomics Consortium) that accrued large sample sizes have led to a considerable increase in our knowledge of schizophrenia's true genetic architecture. Similar to the candidate gene approach, GWAS uses a case-control study design, but as opposed to testing relatively few genetic markers on *a priori* selected candidate genes, GWAS undertakes an agnostic evaluation and casts a wide net of genetic markers across the entire genome (122). Its objective is to identify common genetic risk variants (almost exclusively single nucleotide polymorphisms, SNPs) associated with a disease of interest with greater power to detect small to modest effect sizes using a

stringent threshold of significance ($p < 5 \times 10^{-8}$). To date, more than 30 schizophrenia GWASs have been published (see https://www.ebi.ac.uk/gwas/) and collectively over 200 common risk loci have been shown to display robust associations with schizophrenia (121, 123-131). Each new increase in sample size has led to the identification of new associations. Some of these genomic loci, most notably the major histocompatibility complex (MHC; also known as human leukocyte antigen (HLA) complex), which is essential for adaptive immunity (123, 124, 132), have been repeatedly implicated in risk for schizophrenia in multiple independent GWASs, which is especially promising given previous difficulties in replicating genetic findings in schizophrenia research.

Pathway or gene-set enrichment analyses have been applied to GWAS results to provide a biological context for evaluating the molecular mechanisms through which these common variants may operate. Studies using such systems genomics approaches point to the involvement of multiple key biological processes and cellular compartments in the pathophysiology of schizophrenia, including neuron differentiation, intracellular signal transduction in synapses, trans-synaptic signaling and cell adhesion, synaptic plasticity, postsynaptic density, dopaminergic and cholinergic neurotransmission, long-term potentiation through the glutamatergic system, histone modifications, targets of the fragile X mental retardation protein (FMRP), immune signaling pathways, and glucose metabolism (125, 133-136). Involvement of calcium signaling and ion channels as well as glial biology have also been reported in gene-set analyses using schizophrenia GWAS data (137, 138).

It is worth noting that although compelling genetic signals have been found, the enthusiasm surrounding GWAS findings for schizophrenia has been tempered by the following observations: 1) Genetic variants detected by GWAS may not be causal for disease due to linkage disequilibrium (refer to (139) for a detailed discussion on linkage disequilibrium), 2) The identified loci individually confer relatively small risk for disease (typically odds ratios < 1.2), and 3) GWAS offers limited power to capture structural variants and rare variants of any type with low minor allele frequencies (e.g., ≤ 1-5%) (140).

As noted above, the heritability of schizophrenia is approximately 80%, but common SNPs alone explain only about 20% of the variance in schizophrenia liability (141-143), which means that most of the heritability of schizophrenia remains unexplained by GWAS findings. Thanks to advances in chromosomal

microarray and next generation sequencing technologies, there is now compelling evidence that rare variants, including single nucleotide variants (SNVs) and copy number variants (CNVs), which are not detectable by GWAS because of their low frequencies, also play an important role in the genetic architecture of schizophrenia (144-150). In fact, in schizophrenia's known genetic landscape, some of the most robust and replicable findings have come from studies of rare CNVs, which is the focus of the present dissertation.

While SNPs arise from variations in single nucleotide base pairs due to point mutations, CNVs arise from large-scale (>100Kb) structural variations (i.e., chromosomal rearrangements) in the human genome, involving both duplications and deletions of genetic material that often overlap multiple genes (151-156). According to a prior case-control study that has evaluated the frequency of 15 CNVs at schizophrenia-associated loci, approximately 2.5% of cases with schizophrenia were found to carry at least one of these known pathogenic variants, as opposed to 0.9% of the control group (155), confirming that CNVs are significantly enriched among patients, but tend to be uncommon. This is consistent with the theory that evolution places negative selection pressure on alleles with deleterious effects on fitness (157). Although common risk variants collectively account for a greater proportion of the genetic liability to schizophrenia, rare CNVs individually exhibit a much higher penetrance for the disorder (odds ratios between 2 and <40) (155, 158), which provides an important foothold for uncovering biological mechanisms that can serve as targets for novel pharmacotherapies.

A 2017 meta-analysis by the Psychiatric Genomics Consortium showed that particularly eight CNV loci have genome-wide significant associations with schizophrenia (153). These loci are 1q21.1, 2p16.3, 3q29, 7q11.2, 15q13.3, distal 16p11.2, proximal 16p11.2 and 22q11.2. Many additional, possibly rarer CNVs or CNVs with smaller odds ratios are likely to be identified as risk factors for schizophrenia in the near future. However, despite accumulating evidence that CNVs are some of the strongest risk factors for schizophrenia, many remain understudied.

Interestingly, recent studies have shown that there are overlaps between common and rare variants that are associated with risk for schizophrenia and genetic loci that are associated with a variety of other neurodevelopmental and psychiatric conditions, such as autism spectrum disorder (ASD), attention deficit

hyperactivity disorder (ADHD) and intellectual disability (159-162). These findings suggest that schizophrenia, ASD and several other neurodevelopmental disorders may share underlying pathogenic mechanisms, which challenges the traditional ways in which such disorders have been diagnosed and researched. Elucidating the neurobiological mechanisms affected by these genetic variants can help disentangle the extensive heterogeneity within schizophrenia and elucidate its relationship to other diagnostic entities.

To this end, the present dissertation investigates the neurobiology of the 3q29 deletion. To further orient the reader, we present a more detailed overview of the general topic of CNVs in the next section.

Copy number variation

Unlike SNPs, structural variants like CNVs cannot be easily identified by studying single sequence reads. As a result, the characterization of this class of genetic variants has lagged behind our understanding of other forms of genetic variation. The first discovery of CNVs in humans can be traced back to the 1900s, but two landmark studies that came out in 2004 have been especially instrumental in demonstrating that submicroscopic variations in DNA copy number, which are much smaller than those identified cytogenetically, are widespread in normal human genomes (163, 164). Since this initial discovery, many more CNVs that change the dosage of particular genomic regions have been identified and the quantity of structural variation data is expected to increase as our ability to identify novel variants at greater resolutions advances (165).

In 2006, Redon and colleagues constructed the first CNV map of the human genome in four populations with ancestry in Europe, Africa or Asia and identified nearly 1,500 CNV regions cumulatively covering approximately 12% (~360 million nucleotides) of the human genome (154). Subsequent studies reported that 4.8-9.7% of the human genome contributes to CNVs (166), and within a single human genome, CNVs can result in a 1.2% difference compared to the reference human genome (167). Altogether, these findings demonstrate the surprising ubiquity of CNVs and highlight this class of genetic variants as an important source of human genetic diversity.

CNVs can be inherited from a parental genome, arise *de novo* as a somatic mutation, or occur during meiosis (typically during prophase I). CNVs that are found in less than 1% of the general population are referred

to as rare CNVs and those that recur with approximately the same breakpoints in independent individuals are described as recurrent CNVs (168, 169). A hallmark feature of recurrent CNVs is the presence of segmental duplications (also known as "low copy repeats") flanking the affected intervals. CNVs can be generated by a variety of mutational mechanisms, including non-allelic homologous recombination (NAHR), which is a form of homologous recombination that occurs between two segments of DNA that share high sequence similarity, but are not alleles (170). Due to unequal crossing over between misaligned sequences that recombine, NAHR leads to copy gains or losses. Particularly sub-telomeric and pericentromeric regions of the genome that are rich in duplicated sequences tend to be more susceptible to this mutational mechanism and are thus more variable in structure (154, 171).

Although significant advances have been achieved in this relatively new area of genetic research, our understanding of the functional importance of many CNVs remains incomplete. To date, at least 100 genes that can be deleted without engendering apparent phenotypic consequences have been found (166). However, the spectrum of CNV effects can range from adaptive traits to embryonic lethality (172-176). As noted above, a meta-analysis by the Psychiatric Genomics Consortium showed that at least eight recurrent CNV loci have genome-wide significant associations with increased risk of developing schizophrenia (153), but the mechanisms by which most of these CNVs lead to disease onset are unclear.

The 22q11.2 deletion (22q11.2Del) was the first CNV to be implicated in schizophrenia (177-179) and this association has been extensively replicated over the years (152, 153). This deletion spans more than 50 genes including the highly cited *COMT (*catecholamine-degrading enzyme*)* gene, which plays a critical role in the metabolic degradation of synaptic dopamine and norepinephrine (180). Since there are multiple segmental duplications within the 22q11.2 region, the deletion can vary in size. The most common (90% of cases) version is a ~3Mb deletion, followed by a ~1.5Mb deletion (8% of cases) (181, 182). Notably, the reciprocal duplication of this locus has been reported to be protective against schizophrenia (183).

Another well-known schizophrenia CNV is the 16p11.2 duplication (16p11.2Dup) (184), which affects a ~600Kb region encompassing 29 annotated genes. It has been suggested that the major driver of neurodevelopmental abnormalities in this CNV may be the *KCTD13* (Potassium Channel Tetramerization

Domain Containing 13) gene, which contributes to the dendritic maturation of cerebral cortical neurons (185, 186). Notably, the deletion of a more distal and smaller region on 16p11.2 has also been shown to be associated with schizophrenia (187, 188).

The 15q13.3 deletion (15q13.3Del) also has genome-wide significant evidence of being associated with schizophrenia. This locus also has variable breakpoints but usually spans six protein-coding genes. Similar to other CNVs, the exact contribution of the genes in the 15q13.3 region to clinical phenotypes remains unclear, but the *CHRNA7* (Cholinergic Receptor Nicotinic Alpha 7 Subunit) gene, which encodes the A7 nicotinic acetylcholine receptor (189) and the *OTUD7A* (OTU Deubiquitinase 7A) gene, which has been implicated in the development of cortical dendritic spines and dendrite outgrowth (190) are considered strong candidates.

Another CNV with genome-wide significant association with schizophrenia is the deletion of the 2p16.3 region (2p16.3Del), which includes the *NRXN1* (Neurexin 1) gene. *NRXN1* (one of the largest known human genes) encodes a presynaptic cell adhesion molecule that plays a crucial role in synapse formation and maturation through its interactions with neuroligins (191, 192). The reciprocal 1q21.1 deletion and duplication (1q21.1Del & Dup), the 7q11.23 duplication (7q11.23Dup, reciprocal to the Williams-Beuren syndrome (193)) and the 15q11.2 deletion (15q11.2Del) are also linked with schizophrenia (153, 156, 194).

Finally, the 3q29 deletion (3q29Del), which is the focus of the present dissertation, is another rare and recurrent CNV that is a strong risk factor for schizophrenia (153, 195-197). This deletion encompasses 21 protein-coding genes. It was first described as a risk factor for intellectual disability (198) prior to its link with psychosis was identified. An extended description of our current knowledge of 3q29Del is presented in the following sections.

It is important to note that a common characteristic across these genomic rearrangements is "variable expressivity", which refers to the range of signs and symptoms that can occur in different people with the same genetic variant. CNVs like 22q11.2Del and 3q29Del are often associated with a broad spectrum of physical and neurodevelopmental manifestations besides schizophrenia, including global developmental delay, varying degrees of intellectual disability, ASD and various congenital malformations (151, 199, 200). What determines the neurodevelopmental trajectory towards schizophrenia versus other clinical phenotypes for carriers of the

same CNV is unclear. Possibilities include genetic modifiers on the same allele or on other chromosomes, environmental exposures, and their interactions. The exact drivers and modifiers and the neurobiological mechanisms through which most schizophrenia associated CNVs operate remain largely unknown.

Research aims

The present dissertation takes a genetics-first, rare variant approach to investigate the neurobiology of schizophrenia and associated disorders, with a focus on 3q29Del: a rare, recurrent 1.6Mb CNV on the long arm of the third chromosome (Fig. 1) that confers exceptionally high genetic risk for a range of neurodevelopmental and psychiatric disorders, including mild to moderate intellectual disability, ASD, ADHD and the largest known effect size for schizophrenia (>40-fold increase in risk) (153, 195-197). Although several genes within this interval have been proposed as putative drivers, it is not currently known which genes or neurobiological mechanisms contribute to the emergence of abnormal neurodevelopmental and psychiatric phenotypes in 3q29Del. The overarching objective of this dissertation was to address this knowledge gap by employing a multidisciplinary approach that integrates a breath of tools from neuroscience, genetics, clinical psychology, and bioinformatics.

The present thesis consists of five chapters and is structured based on the "three paper" model, consisting of three conceptually related, publication-quality manuscripts, where each presents a significant finding, but together yield a richer and deeper narrative.

In chapter 1, a general introduction of the background and overarching aims of the project are presented. The three papers are presented in chapters 2-4. Chapter 5 closes this dissertation with a summary of the foregoing chapters, the broader implications of our findings for the fields of neuroscience and psychiatric genetics and future directions.

In chapter 2, we perform an unbiased systems-biology analysis to interrogate the network-level behavior of 3q29 interval genes within the global protein-coding transcriptome of the healthy human cortex. We assess the validity of our graph-based predictions in an experimental system by conducting RNA-sequencing in mice harboring a homologous deletion to the human 3q29Del locus. The emerging modular

properties and connectivity patterns of 3q29 genes yield key predictions about novel biological roles, functional interactions, and putative disease associations for individual 3q29 genes. The data included in this report advance our understanding of 3q29Del-associated neuropsychiatric risk and present evidence-based mechanistic hypotheses untethered from annotation bias. The contents of this chapter have been peer-reviewed and are now published in *Translational Psychiatry*.

In chapter 3, we conduct the first ever quantitative neuroimaging study in subjects with 3q29Del using structural MRI and compare these morphometric data with a large sample of healthy controls. We also perform whole-brain radiological analyses and assess the relationship between neuroanatomical findings and standardized measures of cognitive and sensorimotor abilities in 3q29Del. Our findings from these analyses point to the abnormal development of specific brain structures as potential neuroimaging-based biomarkers of 3q29Del. These data also reveal novel brain-behavior relationships that bring us closer to delineating specific brain regions that may function as a mechanistic intermediary between this genetic lesion and syndromic phenotypes. The contents of this chapter are currently under peer review.

In chapter 4, we report the first in-depth evaluation of psychotic symptoms in study subjects with 3q29Del, using the gold-standard Structured Interview for Psychosis-Risk Syndromes (SIPS). We compare this profile to a large sample of healthy controls and participants with another well-known schizophrenia associated CNV, the 22q11.2Del. Additionally, we examine the effect of age and sex on symptom severity and investigate the relationship between psychotic symptoms and findings from structural brain imaging in 3q29Del to probe the neural substrates of elevated psychosis risk in this syndrome. The contents of this chapter are currently under peer review as well.

As outlined in this introduction, systematic research on high-impact CNVs offers a promising opportunity to link specific genetic mechanisms to brain and behavioral phenotypes underlying schizophrenia and associated disorders. The ultimate objective of this dissertation was to improve our current understanding of 3q29Del in pursuit of this goal.

Figures

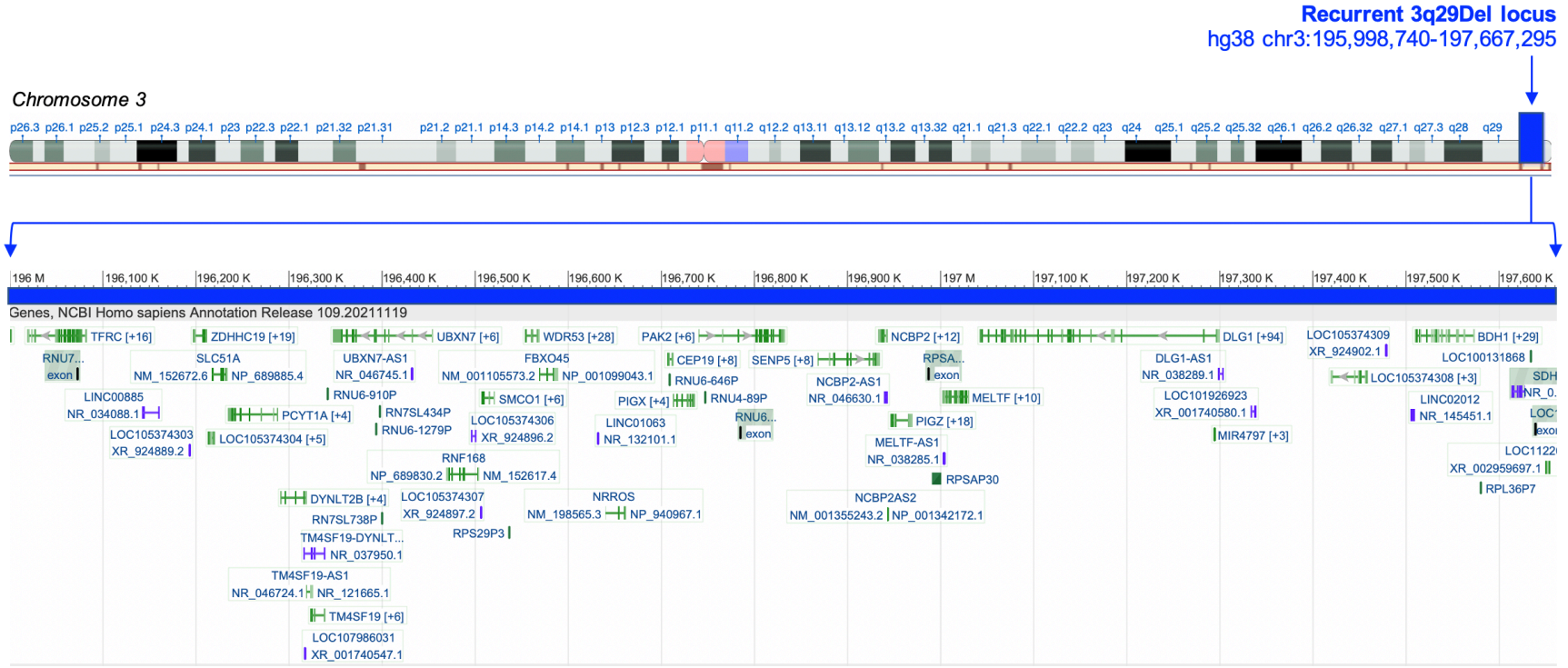

Figure 1. The canonical 3q29 deletion locus, modified from the National Center for Biotechnology Information's Genome Data Viewer. The ideogram represents human chromosome 3 and the boxed area in blue denotes the cytological region corresponding to the canonical 3q29 deletion (3q29Del) locus. The *Sequence Viewer* below provides an expanded view of this locus using a linear graphical representation of features annotated/aligned to the sequence coordinates noted in the top right corner of the figure. The sequence and track data that were used to generate this figure can be accessed via https://www.ncbi.nlm.nih.gov/genome/gdv.

References

1. Saha S, Chant D, Welham J, McGrath J (2005): A systematic review of the prevalence of schizophrenia. *PLoS Med.* 2:e141.

2. Perala J, Suvisaari J, Saarni SI, Kuoppasalmi K, Isometsa E, Pirkola S, et al. (2007): Lifetime prevalence of psychotic and bipolar I disorders in a general population. *Arch Gen Psychiatry.* 64:19-28.

3. Jablensky A, Sartorius N, Ernberg G, Anker M, Korten A, Cooper JE, et al. (1992): Schizophrenia: manifestations, incidence and course in different cultures. A World Health Organization ten-country study. *Psychol Med Monogr Suppl.* 20:1-97.

4. Kraepelin E (1990): Psychiatrie. 6 Auflage. Leipzig, Austria: Barth 1899. English translation by Metoui H, Ayed S: Psychiatry, A Textbook for Students and Physicians, Canton, MA. Science History Publications. Ein Lehrbuch für Studierende und Aerzte.

5. Kraepelin E (1919): *Dementia praecox and paraphrenia.* Livingstone.

6. Rahman T, Lauriello J (2016): Schizophrenia: An Overview. *Focus (Am Psychiatr Publ).* 14:300-307.

7. Bachmann S, Bottmer C, Schroder J (2005): Neurological soft signs in first-episode schizophrenia: a follow-up study. *Am J Psychiatry.* 162:2337-2343.

8. Bombin I, Arango C, Buchanan RW (2005): Significance and meaning of neurological signs in schizophrenia: two decades later. *Schizophr Bull.* 31:962-977.

9. Compton MT, Bollini AM, McKenzie Mack L, Kryda AD, Rutland J, Weiss PS, et al. (2007): Neurological soft signs and minor physical anomalies in patients with schizophrenia and related disorders, their first-degree biological relatives, and non-psychiatric controls. *Schizophr Res.* 94:64-73.

10. Harvey PD (2014): Assessing disability in schizophrenia: tools and contributors. *J Clin Psychiatry.* 75:e27.

11. Hafner H, Maurer K, Loffler W, Fatkenheuer B, an der Heiden W, Riecher-Rossler A, et al. (1994): The epidemiology of early schizophrenia. Influence of age and gender on onset and early course. *Br J Psychiatry Suppl.*29-38.

12. Lopez-Munoz F, Alamo C, Cuenca E, Shen WW, Clervoy P, Rubio G (2005): History of the discovery and clinical introduction of chlorpromazine. *Ann Clin Psychiatry.* 17:113-135.

13. Lambert M, Conus P, Eide P, Mass R, Karow A, Moritz S, et al. (2004): Impact of present and past antipsychotic side effects on attitude toward typical antipsychotic treatment and adherence. *Eur Psychiatry*. 19:415-422.

14. Kane JM, Kishimoto T, Correll CU (2013): Non-adherence to medication in patients with psychotic disorders: epidemiology, contributing factors and management strategies. *World Psychiatry*. 12:216-226.

15. Sendt KV, Tracy DK, Bhattacharyya S (2015): A systematic review of factors influencing adherence to antipsychotic medication in schizophrenia-spectrum disorders. *Psychiatry Res*. 225:14-30.

16. Neumeier MS, Homan S, Vetter S, Seifritz E, Kane JM, Huhn M, et al. (2021): Examining Side Effect Variability of Antipsychotic Treatment in Schizophrenia Spectrum Disorders: A Meta-analysis of Variance. *Schizophr Bull*. 47:1601-1610.

17. Garver DL, Holcomb JA, Christensen JD (2000): Heterogeneity of response to antipsychotics from multiple disorders in the schizophrenia spectrum. *J Clin Psychiatry*. 61:964-972; quiz 973.

18. Haddad PM, Correll CU (2018): The acute efficacy of antipsychotics in schizophrenia: a review of recent meta-analyses. *Ther Adv Psychopharmacol*. 8:303-318.

19. Leucht S, Leucht C, Huhn M, Chaimani A, Mavridis D, Helfer B, et al. (2017): Sixty Years of Placebo-Controlled Antipsychotic Drug Trials in Acute Schizophrenia: Systematic Review, Bayesian Meta-Analysis, and Meta-Regression of Efficacy Predictors. *Am J Psychiatry*. 174:927-942.

20. Hjorthoj C, Sturup AE, McGrath JJ, Nordentoft M (2017): Years of potential life lost and life expectancy in schizophrenia: a systematic review and meta-analysis. *Lancet Psychiatry*. 4:295-301.

21. Laursen TM, Nordentoft M, Mortensen PB (2014): Excess early mortality in schizophrenia. *Annu Rev Clin Psychol*. 10:425-448.

22. McGrath J, Saha S, Chant D, Welham J (2008): Schizophrenia: a concise overview of incidence, prevalence, and mortality. *Epidemiol Rev*. 30:67-76.

23. Pompili M, Amador XF, Girardi P, Harkavy-Friedman J, Harrow M, Kaplan K, et al. (2007): Suicide risk in schizophrenia: learning from the past to change the future. *Ann Gen Psychiatry*. 6:10.

24. Bowie CR, Reichenberg A, Patterson TL, Heaton RK, Harvey PD (2006): Determinants of real-world functional performance in schizophrenia subjects: correlations with cognition, functional capacity, and symptoms. *Am J Psychiatry*. 163:418-425.

25. Twamley EW, Doshi RR, Nayak GV, Palmer BW, Golshan S, Heaton RK, et al. (2002): Generalized cognitive impairments, ability to perform everyday tasks, and level of independence in community living situations of older patients with psychosis. *Am J Psychiatry*. 159:2013-2020.

26. Lee RS, Hermens DF, Naismith SL, Lagopoulos J, Jones A, Scott J, et al. (2015): Neuropsychological and functional outcomes in recent-onset major depression, bipolar disorder and schizophrenia-spectrum disorders: a longitudinal cohort study. *Transl Psychiatry*. 5:e555.

27. Harvey PD, Heaton RK, Carpenter WT, Jr., Green MF, Gold JM, Schoenbaum M (2012): Functional impairment in people with schizophrenia: focus on employability and eligibility for disability compensation. *Schizophr Res*. 140:1-8.

28. Strassnig M, Kotov R, Fochtmann L, Kalin M, Bromet EJ, Harvey PD (2018): Associations of independent living and labor force participation with impairment indicators in schizophrenia and bipolar disorder at 20-year follow-up. *Schizophr Res*. 197:150-155.

29. Tandon R, Gaebel W, Barch DM, Bustillo J, Gur RE, Heckers S, et al. (2013): Definition and description of schizophrenia in the DSM-5. *Schizophr Res*. 150:3-10.

30. Tandon R (2013): Schizophrenia and other psychotic disorders in DSM-5. *Clin Schizophr Relat Psychoses*. 7:16-19.

31. American Psychiatric Association D, Association AP (2013): *Diagnostic and statistical manual of mental disorders: DSM-5*. American psychiatric association Washington, DC.

32. Ellison-Wright I, Glahn DC, Laird AR, Thelen SM, Bullmore E (2008): The anatomy of first-episode and chronic schizophrenia: an anatomical likelihood estimation meta-analysis. *Am J Psychiatry*. 165:1015-1023.

33. Ellison-Wright I, Bullmore E (2010): Anatomy of bipolar disorder and schizophrenia: a meta-analysis. *Schizophr Res*. 117:1-12.

34. Glahn DC, Laird AR, Ellison-Wright I, Thelen SM, Robinson JL, Lancaster JL, et al. (2008): Meta-analysis of gray matter anomalies in schizophrenia: application of anatomic likelihood estimation and network analysis. *Biol Psychiatry*. 64:774-781.

35. Fornito A, Yucel M, Patti J, Wood SJ, Pantelis C (2009): Mapping grey matter reductions in schizophrenia: an anatomical likelihood estimation analysis of voxel-based morphometry studies. *Schizophr Res*. 108:104-113.

36. Ren W, Lui S, Deng W, Li F, Li M, Huang X, et al. (2013): Anatomical and functional brain abnormalities in drug-naive first-episode schizophrenia. *Am J Psychiatry*. 170:1308-1316.

37. Gong Q, Lui S, Sweeney JA (2016): A Selective Review of Cerebral Abnormalities in Patients With First-Episode Schizophrenia Before and After Treatment. *Am J Psychiatry*. 173:232-243.

38. Vita A, De Peri L, Silenzi C, Dieci M (2006): Brain morphology in first-episode schizophrenia: a meta-analysis of quantitative magnetic resonance imaging studies. *Schizophr Res*. 82:75-88.

39. Wright IC, Rabe-Hesketh S, Woodruff PW, David AS, Murray RM, Bullmore ET (2000): Meta-analysis of regional brain volumes in schizophrenia. *Am J Psychiatry*. 157:16-25.

40. Mathew I, Gardin TM, Tandon N, Eack S, Francis AN, Seidman LJ, et al. (2014): Medial temporal lobe structures and hippocampal subfields in psychotic disorders: findings from the Bipolar-Schizophrenia Network on Intermediate Phenotypes (B-SNIP) study. *JAMA Psychiatry*. 71:769-777.

41. Bora E, Fornito A, Radua J, Walterfang M, Seal M, Wood SJ, et al. (2011): Neuroanatomical abnormalities in schizophrenia: a multimodal voxelwise meta-analysis and meta-regression analysis. *Schizophr Res*. 127:46-57.

42. Cetin-Karayumak S, Di Biase MA, Chunga N, Reid B, Somes N, Lyall AE, et al. (2020): White matter abnormalities across the lifespan of schizophrenia: a harmonized multi-site diffusion MRI study. *Mol Psychiatry*. 25:3208-3219.

43. Birur B, Kraguljac NV, Shelton RC, Lahti AC (2017): Brain structure, function, and neurochemistry in schizophrenia and bipolar disorder-a systematic review of the magnetic resonance neuroimaging literature. *NPJ Schizophr*. 3:15.

44. Yao L, Lui S, Liao Y, Du MY, Hu N, Thomas JA, et al. (2013): White matter deficits in first episode schizophrenia: an activation likelihood estimation meta-analysis. *Prog Neuropsychopharmacol Biol Psychiatry*. 45:100-106.

45. Haijma SV, Van Haren N, Cahn W, Koolschijn PC, Hulshoff Pol HE, Kahn RS (2013): Brain volumes in schizophrenia: a meta-analysis in over 18 000 subjects. *Schizophr Bull.* 39:1129-1138.

46. Courchesne E, Chisum HJ, Townsend J, Cowles A, Covington J, Egaas B, et al. (2000): Normal brain development and aging: quantitative analysis at in vivo MR imaging in healthy volunteers. *Radiology*. 216:672-682.

47. Gogtay N, Giedd JN, Lusk L, Hayashi KM, Greenstein D, Vaituzis AC, et al. (2004): Dynamic mapping of human cortical development during childhood through early adulthood. *Proc Natl Acad Sci U S A*. 101:8174-8179.

48. Shaw P, Kabani NJ, Lerch JP, Eckstrand K, Lenroot R, Gogtay N, et al. (2008): Neurodevelopmental trajectories of the human cerebral cortex. *J Neurosci.* 28:3586-3594.

49. Giedd JN, Raznahan A, Alexander-Bloch A, Schmitt E, Gogtay N, Rapoport JL (2015): Child psychiatry branch of the National Institute of Mental Health longitudinal structural magnetic resonance imaging study of human brain development. *Neuropsychopharmacology*. 40:43-49.

50. Nie J, Li G, Shen D (2013): Development of cortical anatomical properties from early childhood to early adulthood. *Neuroimage*. 76:216-224.

51. Sowell ER, Thompson PM, Leonard CM, Welcome SE, Kan E, Toga AW (2004): Longitudinal mapping of cortical thickness and brain growth in normal children. *J Neurosci.* 24:8223-8231.

52. Nicolson R, Rapoport JL (1999): Childhood-onset schizophrenia: rare but worth studying. *Biol Psychiatry*. 46:1418-1428.

53. Greenstein D, Lerch J, Shaw P, Clasen L, Giedd J, Gochman P, et al. (2006): Childhood onset schizophrenia: cortical brain abnormalities as young adults. *J Child Psychol Psychiatry*. 47:1003-1012.

54. Thompson PM, Vidal C, Giedd JN, Gochman P, Blumenthal J, Nicolson R, et al. (2001): Mapping adolescent brain change reveals dynamic wave of accelerated gray matter loss in very early-onset schizophrenia. *Proc Natl Acad Sci U S A*. 98:11650-11655.

55. Janssen J, Aleman-Gomez Y, Schnack H, Balaban E, Pina-Camacho L, Alfaro-Almagro F, et al. (2014): Cortical morphology of adolescents with bipolar disorder and with schizophrenia. *Schizophr Res*. 158:91-99.

56. Rimol LM, Hartberg CB, Nesvag R, Fennema-Notestine C, Hagler DJ, Jr., Pung CJ, et al. (2010): Cortical thickness and subcortical volumes in schizophrenia and bipolar disorder. *Biol Psychiatry*. 68:41-50.

57. Rimol LM, Nesvag R, Hagler DJ, Jr., Bergmann O, Fennema-Notestine C, Hartberg CB, et al. (2012): Cortical volume, surface area, and thickness in schizophrenia and bipolar disorder. *Biol Psychiatry*. 71:552-560.

58. Voets NL, Hough MG, Douaud G, Matthews PM, James A, Winmill L, et al. (2008): Evidence for abnormalities of cortical development in adolescent-onset schizophrenia. *Neuroimage*. 43:665-675.

59. Pina-Camacho L, Del Rey-Mejias A, Janssen J, Bioque M, Gonzalez-Pinto A, Arango C, et al. (2016): Age at First Episode Modulates Diagnosis-Related Structural Brain Abnormalities in Psychosis. *Schizophr Bull*. 42:344-357.

60. Arango C, Fraguas D, Parellada M (2014): Differential neurodevelopmental trajectories in patients with early-onset bipolar and schizophrenia disorders. *Schizophr Bull*. 40 Suppl 2:S138-146.

61. Pina-Camacho L, Martinez K, Diaz-Caneja CM, Mezquida G, Cuesta MJ, Moreno C, et al. (2022): Cortical thinning over two years after first-episode psychosis depends on age of onset. *NPJ Schizophr*. 8:20.

62. Manto M, Bower JM, Conforto AB, Delgado-Garcia JM, da Guarda SN, Gerwig M, et al. (2012): Consensus paper: roles of the cerebellum in motor control--the diversity of ideas on cerebellar involvement in movement. *Cerebellum*. 11:457-487.

63. Andreasen NC, Pierson R (2008): The role of the cerebellum in schizophrenia. *Biol Psychiatry*. 64:81-88.

64. Van Overwalle F, Manto M, Cattaneo Z, Clausi S, Ferrari C, Gabrieli JDE, et al. (2020): Consensus Paper: Cerebellum and Social Cognition. *Cerebellum*. 19:833-868.

65. Bodranghien F, Bastian A, Casali C, Hallett M, Louis ED, Manto M, et al. (2016): Consensus Paper: Revisiting the Symptoms and Signs of Cerebellar Syndrome. *Cerebellum*. 15:369-391.

66. Koziol LF, Budding D, Andreasen N, D'Arrigo S, Bulgheroni S, Imamizu H, et al. (2014): Consensus paper: the cerebellum's role in movement and cognition. *Cerebellum*. 13:151-177.

67. Buckner RL (2013): The cerebellum and cognitive function: 25 years of insight from anatomy and neuroimaging. *Neuron*. 80:807-815.

68. Caligiore D, Pezzulo G, Baldassarre G, Bostan AC, Strick PL, Doya K, et al. (2017): Consensus Paper: Towards a Systems-Level View of Cerebellar Function: the Interplay Between Cerebellum, Basal Ganglia, and Cortex. *Cerebellum*. 16:203-229.

69. Kim T, Lee KH, Oh H, Lee TY, Cho KIK, Lee J, et al. (2018): Cerebellar Structural Abnormalities Associated With Cognitive Function in Patients With First-Episode Psychosis. *Front Psychiatry*. 9:286.

70. Moberget T, Doan NT, Alnaes D, Kaufmann T, Cordova-Palomera A, Lagerberg TV, et al. (2018): Cerebellar volume and cerebellocerebral structural covariance in schizophrenia: a multisite mega-analysis of 983 patients and 1349 healthy controls. *Mol Psychiatry*. 23:1512-1520.

71. Rasser PE, Schall U, Peck G, Cohen M, Johnston P, Khoo K, et al. (2010): Cerebellar grey matter deficits in first-episode schizophrenia mapped using cortical pattern matching. *Neuroimage*. 53:1175-1180.

72. Kuhn S, Romanowski A, Schubert F, Gallinat J (2012): Reduction of cerebellar grey matter in Crus I and II in schizophrenia. *Brain Struct Funct*. 217:523-529.

73. Gupta CN, Calhoun VD, Rachakonda S, Chen J, Patel V, Liu J, et al. (2015): Patterns of Gray Matter Abnormalities in Schizophrenia Based on an International Mega-analysis. *Schizophr Bull*. 41:1133-1142.

74. Yuksel C, McCarthy J, Shinn A, Pfaff DL, Baker JT, Heckers S, et al. (2012): Gray matter volume in schizophrenia and bipolar disorder with psychotic features. *Schizophr Res*. 138:177-182.

75. Lawyer G, Nesvag R, Varnas K, Okugawa G, Agartz I (2009): Grey and white matter proportional relationships in the cerebellar vermis altered in schizophrenia. *Cerebellum*. 8:52-60.

76. Weinberger DR (1986): The pathogenesis of schizophrenia; a neurodevelopmental theory. *The neurology of schizophrenia*.397-406.

77. Murray RM, Lewis SW (1987): Is schizophrenia a neurodevelopmental disorder? *Br Med J (Clin Res Ed)*. 295:681-682.

78. Owen MJ, O'Donovan MC, Thapar A, Craddock N (2011): Neurodevelopmental hypothesis of schizophrenia. *Br J Psychiatry*. 198:173-175.

79. Howes OD, Murray RM (2014): Schizophrenia: an integrated sociodevelopmental-cognitive model. *Lancet*. 383:1677-1687.

80. Sullivan PF (2012): Puzzling over schizophrenia: schizophrenia as a pathway disease. *Nat Med*. 18:210-211.

81. Kahn RS, Sommer IE, Murray RM, Meyer-Lindenberg A, Weinberger DR, Cannon TD, et al. (2015): Schizophrenia. *Nat Rev Dis Primers*. 1:15067.

82. Walker EF (1994): Developmentally moderated expressions of the neuropathology underlying schizophrenia. *Schizophr Bull*. 20:453-480.

83. Weinberger DR (1987): Implications of normal brain development for the pathogenesis of schizophrenia. *Arch Gen Psychiatry*. 44:660-669.

84. Cornblatt BA, Lencz T, Smith CW, Correll CU, Auther AM, Nakayama E (2003): The schizophrenia prodrome revisited: a neurodevelopmental perspective. *Schizophr Bull*. 29:633-651.

85. Yung AR, McGorry PD (1996): The prodromal phase of first-episode psychosis: past and current conceptualizations. *Schizophr Bull*. 22:353-370.

86. Niendam TA, Bearden CE, Johnson JK, McKinley M, Loewy R, O'Brien M, et al. (2006): Neurocognitive performance and functional disability in the psychosis prodrome. *Schizophr Res*. 84:100-111.

87. Walker EF, Savoie T, Davis D (1994): Neuromotor precursors of schizophrenia. *Schizophr Bull*. 20:441-451.

88. Walker EF, Grimes KE, Davis DM, Smith AJ (1993): Childhood precursors of schizophrenia: facial expressions of emotion. *Am J Psychiatry*. 150:1654-1660.

89. Schiffman J, Walker E, Ekstrom M, Schulsinger F, Sorensen H, Mednick S (2004): Childhood videotaped social and neuromotor precursors of schizophrenia: a prospective investigation. *Am J Psychiatry*. 161:2021-2027.

90. Fusar-Poli P, Radua J, McGuire P, Borgwardt S (2012): Neuroanatomical maps of psychosis onset: voxel-wise meta-analysis of antipsychotic-naive VBM studies. *Schizophr Bull*. 38:1297-1307.

91. Fusar-Poli P, Borgwardt S, Crescini A, Deste G, Kempton MJ, Lawrie S, et al. (2011): Neuroanatomy of vulnerability to psychosis: a voxel-based meta-analysis. *Neurosci Biobehav Rev*. 35:1175-1185.

92. Mechelli A, Riecher-Rossler A, Meisenzahl EM, Tognin S, Wood SJ, Borgwardt SJ, et al. (2011): Neuroanatomical abnormalities that predate the onset of psychosis: a multicenter study. *Arch Gen Psychiatry*. 68:489-495.

93. Ellis JK, Walker EF, Goldsmith DR (2020): Selective Review of Neuroimaging Findings in Youth at Clinical High Risk for Psychosis: On the Path to Biomarkers for Conversion. *Front Psychiatry*. 11:567534.

94. Chung Y, Allswede D, Addington J, Bearden CE, Cadenhead K, Cornblatt B, et al. (2019): Cortical abnormalities in youth at clinical high-risk for psychosis: Findings from the NAPLS2 cohort. *Neuroimage Clin*. 23:101862.

95. Witthaus H, Kaufmann C, Bohner G, Ozgurdal S, Gudlowski Y, Gallinat J, et al. (2009): Gray matter abnormalities in subjects at ultra-high risk for schizophrenia and first-episode schizophrenic patients compared to healthy controls. *Psychiatry Res*. 173:163-169.

96. Cannon M, Jones PB, Murray RM (2002): Obstetric complications and schizophrenia: historical and meta-analytic review. *Am J Psychiatry*. 159:1080-1092.

97. Brown AS, Derkits EJ (2010): Prenatal infection and schizophrenia: a review of epidemiologic and translational studies. *Am J Psychiatry*. 167:261-280.

98. Mortensen PB, Norgaard-Pedersen B, Waltoft BL, Sorensen TL, Hougaard D, Torrey EF, et al. (2007): Toxoplasma gondii as a risk factor for early-onset schizophrenia: analysis of filter paper blood samples obtained at birth. *Biol Psychiatry*. 61:688-693.

99. St Clair D, Xu M, Wang P, Yu Y, Fang Y, Zhang F, et al. (2005): Rates of adult schizophrenia following prenatal exposure to the Chinese famine of 1959-1961. *JAMA*. 294:557-562.

100. Xu MQ, Sun WS, Liu BX, Feng GY, Yu L, Yang L, et al. (2009): Prenatal malnutrition and adult schizophrenia: further evidence from the 1959-1961 Chinese famine. *Schizophr Bull*. 35:568-576.

101. Cutajar MC, Mullen PE, Ogloff JR, Thomas SD, Wells DL, Spataro J (2010): Schizophrenia and other psychotic disorders in a cohort of sexually abused children. *Arch Gen Psychiatry*. 67:1114-1119.

102. Morgan C, Fisher H (2007): Environment and schizophrenia: environmental factors in schizophrenia: childhood trauma--a critical review. *Schizophr Bull*. 33:3-10.

103. McGrath J, Scott J (2006): Urban birth and risk of schizophrenia: a worrying example of epidemiology where the data are stronger than the hypotheses. *Epidemiol Psichiatr Soc*. 15:243-246.

104. Vassos E, Pedersen CB, Murray RM, Collier DA, Lewis CM (2012): Meta-analysis of the association of urbanicity with schizophrenia. *Schizophr Bull*. 38:1118-1123.

105. Hilker R, Helenius D, Fagerlund B, Skytthe A, Christensen K, Werge TM, et al. (2018): Heritability of Schizophrenia and Schizophrenia Spectrum Based on the Nationwide Danish Twin Register. *Biol Psychiatry*. 83:492-498.

106. Cardno AG, Gottesman, II (2000): Twin studies of schizophrenia: from bow-and-arrow concordances to star wars Mx and functional genomics. *Am J Med Genet*. 97:12-17.

107. Sullivan PF, Kendler KS, Neale MC (2003): Schizophrenia as a complex trait: evidence from a meta-analysis of twin studies. *Arch Gen Psychiatry*. 60:1187-1192.

108. Gejman PV, Sanders AR, Duan J (2010): The role of genetics in the etiology of schizophrenia. *Psychiatr Clin North Am*. 33:35-66.

109. McGuffin P, Farmer AE, Gottesman, II, Murray RM, Reveley AM (1984): Twin concordance for operationally defined schizophrenia. Confirmation of familiality and heritability. *Arch Gen Psychiatry*. 41:541-545.

110. Cannon TD, Kaprio J, Lonnqvist J, Huttunen M, Koskenvuo M (1998): The genetic epidemiology of schizophrenia in a Finnish twin cohort. A population-based modeling study. *Arch Gen Psychiatry*. 55:67-74.

111. Hyttinen V, Kaprio J, Kinnunen L, Koskenvuo M, Tuomilehto J (2003): Genetic liability of type 1 diabetes and the onset age among 22,650 young Finnish twin pairs: a nationwide follow-up study. *Diabetes*. 52:1052-1055.

112. Gottesman, II, Shields J (1967): A polygenic theory of schizophrenia. *Proc Natl Acad Sci U S A*. 58:199-205.

113. McGue M, Gottesman, II (1989): A single dominant gene still cannot account for the transmission of schizophrenia. *Arch Gen Psychiatry*. 46:478-480.

114. Allen NC, Bagade S, McQueen MB, Ioannidis JP, Kavvoura FK, Khoury MJ, et al. (2008): Systematic meta-analyses and field synopsis of genetic association studies in schizophrenia: the SzGene database. *Nat Genet*. 40:827-834.

115. Farrell MS, Werge T, Sklar P, Owen MJ, Ophoff RA, O'Donovan MC, et al. (2015): Evaluating historical candidate genes for schizophrenia. *Mol Psychiatry*. 20:555-562.

116. Zou Z, Liu C, Che C, Huang H (2014): Clinical genetics of Alzheimer's disease. *Biomed Res Int*. 2014:291862.

117. Sullivan PF (2007): Spurious genetic associations. *Biol Psychiatry*. 61:1121-1126.

118. Ioannidis JP (2006): Commentary: grading the credibility of molecular evidence for complex diseases. *Int J Epidemiol*. 35:572-578; discussion 593-576.

119. Neale BM, Sham PC (2004): The future of association studies: gene-based analysis and replication. *Am J Hum Genet*. 75:353-362.

120. Gejman PV, Sanders AR, Kendler KS (2011): Genetics of schizophrenia: new findings and challenges. *Annu Rev Genomics Hum Genet*. 12:121-144.

121. Lencz T, Morgan TV, Athanasiou M, Dain B, Reed CR, Kane JM, et al. (2007): Converging evidence for a pseudoautosomal cytokine receptor gene locus in schizophrenia. *Mol Psychiatry*. 12:572-580.

122. Witte JS (2010): Genome-wide association studies and beyond. *Annu Rev Public Health*. 31:9-20 24 p following 20.

123. Stefansson H, Ophoff RA, Steinberg S, Andreassen OA, Cichon S, Rujescu D, et al. (2009): Common variants conferring risk of schizophrenia. *Nature*. 460:744-747.

124. International Schizophrenia C, Purcell SM, Wray NR, Stone JL, Visscher PM, O'Donovan MC, et al. (2009): Common polygenic variation contributes to risk of schizophrenia and bipolar disorder. *Nature*. 460:748-752.

125. Pardinas AF, Holmans P, Pocklington AJ, Escott-Price V, Ripke S, Carrera N, et al. (2018): Common schizophrenia alleles are enriched in mutation-intolerant genes and in regions under strong background selection. *Nat Genet*. 50:381-389.

126. O'Donovan MC, Craddock N, Norton N, Williams H, Peirce T, Moskvina V, et al. (2008): Identification of loci associated with schizophrenia by genome-wide association and follow-up. *Nat Genet*. 40:1053-1055.

127. Li Z, Chen J, Yu H, He L, Xu Y, Zhang D, et al. (2017): Genome-wide association analysis identifies 30 new susceptibility loci for schizophrenia. *Nat Genet*. 49:1576-1583.

128. Lam M, Chen CY, Li Z, Martin AR, Bryois J, Ma X, et al. (2019): Comparative genetic architectures of schizophrenia in East Asian and European populations. *Nat Genet*. 51:1670-1678.

129. Schizophrenia Working Group of the Psychiatric Genomics C (2014): Biological insights from 108 schizophrenia-associated genetic loci. *Nature*. 511:421-427.

130. Schizophrenia Psychiatric Genome-Wide Association Study C (2011): Genome-wide association study identifies five new schizophrenia loci. *Nat Genet*. 43:969-976.

131. Liu J, Li S, Li X, Li W, Yang Y, Guo S, et al. (2021): Genome-wide association study followed by trans-ancestry meta-analysis identify 17 new risk loci for schizophrenia. *BMC Med*. 19:177.

132. Corvin A, Morris DW (2014): Genome-wide association studies: findings at the major histocompatibility complex locus in psychosis. *Biol Psychiatry*. 75:276-283.

133. Lips ES, Cornelisse LN, Toonen RF, Min JL, Hultman CM, International Schizophrenia C, et al. (2012): Functional gene group analysis identifies synaptic gene groups as risk factor for schizophrenia. *Mol Psychiatry*. 17:996-1006.

134. Schijven D, Kofink D, Tragante V, Verkerke M, Pulit SL, Kahn RS, et al. (2018): Comprehensive pathway analyses of schizophrenia risk loci point to dysfunctional postsynaptic signaling. *Schizophr Res*. 199:195-202.

135. Network, Pathway Analysis Subgroup of Psychiatric Genomics C (2015): Psychiatric genome-wide association study analyses implicate neuronal, immune and histone pathways. *Nat Neurosci*. 18:199-209.

136. Chan MK, Cooper JD, Heilmann-Heimbach S, Frank J, Witt SH, Nothen MM, et al. (2017): Associations between SNPs and immune-related circulating proteins in schizophrenia. *Sci Rep*. 7:12586.

137. Hertzberg L, Katsel P, Roussos P, Haroutunian V, Domany E (2015): Integration of gene expression and GWAS results supports involvement of calcium signaling in Schizophrenia. *Schizophr Res*. 164:92-99.

138. Duncan LE, Holmans PA, Lee PH, O'Dushlaine CT, Kirby AW, Smoller JW, et al. (2014): Pathway analyses implicate glial cells in schizophrenia. *PLoS One*. 9:e89441.

139. Slatkin M (2008): Linkage disequilibrium--understanding the evolutionary past and mapping the medical future. *Nat Rev Genet*. 9:477-485.

140. McCarthy MI, Abecasis GR, Cardon LR, Goldstein DB, Little J, Ioannidis JP, et al. (2008): Genome-wide association studies for complex traits: consensus, uncertainty and challenges. *Nat Rev Genet*. 9:356-369.

141. Cross-Disorder Group of the Psychiatric Genomics C, Lee SH, Ripke S, Neale BM, Faraone SV, Purcell SM, et al. (2013): Genetic relationship between five psychiatric disorders estimated from genome-wide SNPs. *Nat Genet*. 45:984-994.

142. Shi H, Kichaev G, Pasaniuc B (2016): Contrasting the Genetic Architecture of 30 Complex Traits from Summary Association Data. *Am J Hum Genet*. 99:139-153.

143. Lee SH, DeCandia TR, Ripke S, Yang J, Schizophrenia Psychiatric Genome-Wide Association Study C, International Schizophrenia C, et al. (2012): Estimating the proportion of variation in susceptibility to schizophrenia captured by common SNPs. *Nat Genet*. 44:247-250.

144. Kirov G, O'Donovan MC, Owen MJ (2005): Finding schizophrenia genes. *J Clin Invest*. 115:1440-1448.

145. Escudero I, Johnstone M (2014): Genetics of schizophrenia. *Curr Psychiatry Rep*. 16:502.

146. Legge SE, Santoro ML, Periyasamy S, Okewole A, Arsalan A, Kowalec K (2021): Genetic architecture of schizophrenia: a review of major advancements. *Psychol Med*. 51:2168-2177.

147. Sullivan PF, Daly MJ, O'Donovan M (2012): Genetic architectures of psychiatric disorders: the emerging picture and its implications. *Nat Rev Genet*. 13:537-551.

148. Avramopoulos D (2018): Recent Advances in the Genetics of Schizophrenia. *Mol Neuropsychiatry*. 4:35-51.

149. Rhoades R, Jackson F, Teng S (2019): Discovery of rare variants implicated in schizophrenia using next-generation sequencing. *J Transl Genet Genom*. 3:1-20.

150. Purcell SM, Moran JL, Fromer M, Ruderfer D, Solovieff N, Roussos P, et al. (2014): A polygenic burden of rare disruptive mutations in schizophrenia. *Nature*. 506:185-190.

151. Malhotra D, Sebat J (2012): CNVs: harbingers of a rare variant revolution in psychiatric genetics. *Cell*. 148:1223-1241.

152. Levinson DF, Duan J, Oh S, Wang K, Sanders AR, Shi J, et al. (2011): Copy number variants in schizophrenia: confirmation of five previous findings and new evidence for 3q29 microdeletions and VIPR2 duplications. *Am J Psychiatry*. 168:302-316.

153. Marshall CR, Howrigan DP, Merico D, Thiruvahindrapuram B, Wu W, Greer DS, et al. (2017): Contribution of copy number variants to schizophrenia from a genome-wide study of 41,321 subjects. *Nat Genet*. 49:27-35.

154. Redon R, Ishikawa S, Fitch KR, Feuk L, Perry GH, Andrews TD, et al. (2006): Global variation in copy number in the human genome. *Nature*. 444:444-454.

155. Rees E, Walters JT, Georgieva L, Isles AR, Chambert KD, Richards AL, et al. (2014): Analysis of copy number variations at 15 schizophrenia-associated loci. *Br J Psychiatry*. 204:108-114.

156. Stefansson H, Rujescu D, Cichon S, Pietilainen OP, Ingason A, Steinberg S, et al. (2008): Large recurrent microdeletions associated with schizophrenia. *Nature*. 455:232-236.

157. Fay JC, Wyckoff GJ, Wu CI (2001): Positive and negative selection on the human genome. *Genetics*. 158:1227-1234.

158. Kirov G, Rees E, Walters JT, Escott-Price V, Georgieva L, Richards AL, et al. (2014): The penetrance of copy number variations for schizophrenia and developmental delay. *Biol Psychiatry*. 75:378-385.

159. Brainstorm C, Anttila V, Bulik-Sullivan B, Finucane HK, Walters RK, Bras J, et al. (2018): Analysis of shared heritability in common disorders of the brain. *Science*. 360.

160. Rees E, Creeth HDJ, Hwu HG, Chen WJ, Tsuang M, Glatt SJ, et al. (2021): Schizophrenia, autism spectrum disorders and developmental disorders share specific disruptive coding mutations. *Nat Commun*. 12:5353.

161. Rees E, Kendall K, Pardinas AF, Legge SE, Pocklington A, Escott-Price V, et al. (2016): Analysis of Intellectual Disability Copy Number Variants for Association With Schizophrenia. *JAMA Psychiatry*. 73:963-969.

162. O'Donovan MC, Owen MJ (2016): The implications of the shared genetics of psychiatric disorders. *Nat Med*. 22:1214-1219.

163. Iafrate AJ, Feuk L, Rivera MN, Listewnik ML, Donahoe PK, Qi Y, et al. (2004): Detection of large-scale variation in the human genome. *Nat Genet*. 36:949-951.

164. Sebat J, Lakshmi B, Troge J, Alexander J, Young J, Lundin P, et al. (2004): Large-scale copy number polymorphism in the human genome. *Science*. 305:525-528.

165. Scherer SW, Lee C, Birney E, Altshuler DM, Eichler EE, Carter NP, et al. (2007): Challenges and standards in integrating surveys of structural variation. *Nat Genet*. 39:S7-15.

166. Zarrei M, MacDonald JR, Merico D, Scherer SW (2015): A copy number variation map of the human genome. *Nat Rev Genet*. 16:172-183.

167. Pang AW, MacDonald JR, Pinto D, Wei J, Rafiq MA, Conrad DF, et al. (2010): Towards a comprehensive structural variation map of an individual human genome. *Genome Biol*. 11:R52.

168. Carvalho CM, Lupski JR (2016): Mechanisms underlying structural variant formation in genomic disorders. *Nat Rev Genet*. 17:224-238.

169. Liu P, Carvalho CM, Hastings PJ, Lupski JR (2012): Mechanisms for recurrent and complex human genomic rearrangements. *Curr Opin Genet Dev*. 22:211-220.

170. Stankiewicz P, Lupski JR (2002): Genome architecture, rearrangements and genomic disorders. *Trends Genet*. 18:74-82.

171. Sharp AJ, Locke DP, McGrath SD, Cheng Z, Bailey JA, Vallente RU, et al. (2005): Segmental duplications and copy-number variation in the human genome. *Am J Hum Genet*. 77:78-88.

172. Beckmann JS, Estivill X, Antonarakis SE (2007): Copy number variants and genetic traits: closer to the resolution of phenotypic to genotypic variability. *Nat Rev Genet*. 8:639-646.

173. Hurles ME, Dermitzakis ET, Tyler-Smith C (2008): The functional impact of structural variation in humans. *Trends Genet*. 24:238-245.

174. Feuk L, Carson AR, Scherer SW (2006): Structural variation in the human genome. *Nat Rev Genet*. 7:85-97.

175. Freeman JL, Perry GH, Feuk L, Redon R, McCarroll SA, Altshuler DM, et al. (2006): Copy number variation: new insights in genome diversity. *Genome Res*. 16:949-961.

176. Girirajan S, Campbell CD, Eichler EE (2011): Human copy number variation and complex genetic disease. *Annu Rev Genet*. 45:203-226.

177. McDonald-McGinn DM, Sullivan KE, Marino B, Philip N, Swillen A, Vorstman JA, et al. (2015): 22q11.2 deletion syndrome. *Nat Rev Dis Primers*. 1:15071.

178. Karayiorgou M, Morris MA, Morrow B, Shprintzen RJ, Goldberg R, Borrow J, et al. (1995): Schizophrenia susceptibility associated with interstitial deletions of chromosome 22q11. *Proc Natl Acad Sci U S A*. 92:7612-7616.

179. Shprintzen RJ, Goldberg R, Golding-Kushner KJ, Marion RW (1992): Late-onset psychosis in the velo-cardio-facial syndrome. *Am J Med Genet*. 42:141-142.

180. Lachman HM, Papolos DF, Saito T, Yu YM, Szumlanski CL, Weinshilboum RM (1996): Human catechol-O-methyltransferase pharmacogenetics: description of a functional polymorphism and its potential application to neuropsychiatric disorders. *Pharmacogenetics*. 6:243-250.

181. Carlson C, Sirotkin H, Pandita R, Goldberg R, McKie J, Wadey R, et al. (1997): Molecular definition of 22q11 deletions in 151 velo-cardio-facial syndrome patients. *Am J Hum Genet*. 61:620-629.

182. Ivanov D, Kirov G, Norton N, Williams HJ, Williams NM, Nikolov I, et al. (2003): Chromosome 22q11 deletions, velo-cardio-facial syndrome and early-onset psychosis. Molecular genetic study. *Br J Psychiatry*. 183:409-413.

183. Rees E, Kirov G, Sanders A, Walters JT, Chambert KD, Shi J, et al. (2014): Evidence that duplications of 22q11.2 protect against schizophrenia. *Mol Psychiatry*. 19:37-40.

184. McCarthy SE, Makarov V, Kirov G, Addington AM, McClellan J, Yoon S, et al. (2009): Microduplications of 16p11.2 are associated with schizophrenia. *Nat Genet*. 41:1223-1227.

185. Golzio C, Willer J, Talkowski ME, Oh EC, Taniguchi Y, Jacquemont S, et al. (2012): KCTD13 is a major driver of mirrored neuroanatomical phenotypes of the 16p11.2 copy number variant. *Nature*. 485:363-367.

186. Gladwyn-Ng I, Huang L, Ngo L, Li SS, Qu Z, Vanyai HK, et al. (2016): Bacurd1/Kctd13 and Bacurd2/Tnfaip1 are interacting partners to Rnd proteins which influence the long-term positioning and dendritic maturation of cerebral cortical neurons. *Neural Dev*. 11:7.

187. Guha S, Rees E, Darvasi A, Ivanov D, Ikeda M, Bergen SE, et al. (2013): Implication of a rare deletion at distal 16p11.2 in schizophrenia. *JAMA Psychiatry*. 70:253-260.

188. Barge-Schaapveld DQ, Maas SM, Polstra A, Knegt LC, Hennekam RC (2011): The atypical 16p11.2 deletion: a not so atypical microdeletion syndrome? *Am J Med Genet A*. 155A:1066-1072.

189. Hoppman-Chaney N, Wain K, Seger PR, Superneau DW, Hodge JC (2013): Identification of single gene deletions at 15q13.3: further evidence that CHRNA7 causes the 15q13.3 microdeletion syndrome phenotype. *Clin Genet*. 83:345-351.

190. Uddin M, Unda BK, Kwan V, Holzapfel NT, White SH, Chalil L, et al. (2018): OTUD7A Regulates Neurodevelopmental Phenotypes in the 15q13.3 Microdeletion Syndrome. *Am J Hum Genet*. 102:278-295.

191. Cao X, Tabuchi K (2017): Functions of synapse adhesion molecules neurexin/neuroligins and neurodevelopmental disorders. *Neurosci Res*. 116:3-9.

192. Kirov G, Gumus D, Chen W, Norton N, Georgieva L, Sari M, et al. (2008): Comparative genome hybridization suggests a role for NRXN1 and APBA2 in schizophrenia. *Hum Mol Genet*. 17:458-465.

193. Nickerson E, Greenberg F, Keating MT, McCaskill C, Shaffer LG (1995): Deletions of the elastin gene at 7q11.23 occur in approximately 90% of patients with Williams syndrome. *Am J Hum Genet*. 56:1156-1161.

194. International Schizophrenia C (2008): Rare chromosomal deletions and duplications increase risk of schizophrenia. *Nature*. 455:237-241.

195. Mulle JG (2015): The 3q29 deletion confers >40-fold increase in risk for schizophrenia. *Mol Psychiatry*. 20:1028-1029.

196. Mulle JG, Dodd AF, McGrath JA, Wolyniec PS, Mitchell AA, Shetty AC, et al. (2010): Microdeletions of 3q29 confer high risk for schizophrenia. *Am J Hum Genet*. 87:229-236.

197. Sanchez Russo R, Gambello MJ, Murphy MM, Aberizk K, Black E, Burrell TL, et al. (2021): Deep phenotyping in 3q29 deletion syndrome: recommendations for clinical care. *Genet Med*. 23:872-880.

198. Willatt L, Cox J, Barber J, Cabanas ED, Collins A, Donnai D, et al. (2005): 3q29 microdeletion syndrome: clinical and molecular characterization of a new syndrome. *Am J Hum Genet*. 77:154-160.

199. Vassos E, Collier DA, Holden S, Patch C, Rujescu D, St Clair D, et al. (2010): Penetrance for copy number variants associated with schizophrenia. *Hum Mol Genet*. 19:3477-3481.

200. Girirajan S, Rosenfeld JA, Coe BP, Parikh S, Friedman N, Goldstein A, et al. (2012): Phenotypic heterogeneity of genomic disorders and rare copy-number variants. *N Engl J Med*. 367:1321-1331.

CHAPTER 2. Convergent and distributed effects of the 3q29 deletion on the human neural transcriptome

Esra Sefik, Ryan H. Purcell, The Emory 3q29 Project, Elaine F. Walker, Gary J. Bassell, Jennifer G. Mulle

Adapted from an original publication, as cited below:

Sefik E, Purcell RH, Emory 3q P, Walker EF, Bassell GJ, Mulle JG (2021): Convergent and distributed effects of the 3q29 deletion on the human neural transcriptome. *Transl Psychiatry*. 11:357.

Abstract

The 3q29 deletion (3q29Del) confers high risk for schizophrenia and other neurodevelopmental and psychiatric disorders. However, no single gene in this interval is definitively associated with disease, prompting the hypothesis that neuropsychiatric sequelae emerge upon loss of multiple functionally connected genes. 3q29 genes are unevenly annotated and the impact of 3q29Del on the human neural transcriptome is unknown. To systematically formulate unbiased hypotheses about molecular mechanisms linking 3q29Del to neuropsychiatric illness, we conducted a systems-level network analysis of the non-pathological adult human cortical transcriptome and generated evidence-based predictions that relate 3q29 genes to novel functions and disease associations. The 21 protein-coding genes located in the interval segregated into seven clusters of highly co-expressed genes, demonstrating both convergent and distributed effects of 3q29Del across the interrogated transcriptomic landscape. Pathway analysis of these clusters indicated involvement in nervous-system functions, including synaptic signaling and organization, as well as core cellular functions, including transcriptional regulation, post-translational modifications, chromatin remodeling and mitochondrial metabolism. Top network-neighbors of 3q29 genes showed significant overlap with known schizophrenia, autism spectrum disorder and intellectual disability-risk genes, suggesting that 3q29Del biology is relevant to idiopathic disease. Leveraging "guilt by association", we propose nine 3q29 genes, including one hub gene, as prioritized drivers of neuropsychiatric risk. These results provide testable hypotheses for experimental analysis on causal drivers and mechanisms of the largest known genetic risk factor for schizophrenia and highlight the study of normal function in non-pathological post-mortem tissue to further our understanding of psychiatric genetics, especially for rare syndromes like 3q29Del, where access to neural tissue from carriers is unavailable or limited.

Introduction

Copy number variants (CNVs) offer tractable entry points to investigate the genetic contributions to complex neuropsychiatric diseases. The recurrent 1.6Mb deletion of the 3q29 interval (3q29Del) is robustly associated with schizophrenia spectrum and other non-affective psychotic disorders (SZ) (1-4) and is the strongest known risk allele for the disease with an estimated odds ratio >40 (5). The associated syndrome is a rare (~1 in 30,000) and typically *de novo* genomic disorder that is often accompanied by reduced birth weight, failure to thrive, dysmorphic craniofacial features and varied medical manifestations, including congenital heart defects (6-8). Autism spectrum disorders (ASD) and intellectual disability / developmental delay (IDD) are also enriched in 3q29Del carriers (7, 9, 10). However, it is not currently known which genes within the interval are responsible for the increased neuropsychiatric risk. No single 3q29 interval gene has been definitively associated with SZ, ASD, or ID, prompting the hypothesis that haploinsufficiency of more than one gene is required (11). The paucity of information regarding the functional roles of most 3q29 interval genes hampers the development of evidence-based hypotheses for deciphering this link. No transcriptomic investigation of 3q29Del in humans has been reported, and it is unclear what impact hemizygous loss of these genes might have in the nervous system.

Among the 21 protein-coding genes of the 3q29Del locus, several have been proposed as drivers of the behavioral phenotypes (12), yet the evidence for their individual association with neuropsychiatric disease remains suggestive. *DLG1* produces a synaptic scaffold protein that interacts with AMPA and NMDA-type glutamate receptors (13-16), the latter of which is hypothesized to be involved in SZ pathogenesis (17). A *DLG1* polymorphism has been genetically linked to SZ (18, 19). However, the mouse-specific phenotypes of 3q29Del are not recapitulated by haploinsufficiency of *Dlg1* alone (20). Another prominent candidate, *PAK2* encodes a brain-expressed protein kinase involved in cytoskeletal dynamics (21) and dendritic spine morphology (22). Both *DLG1* and *PAK2* are homologous to genes linked to ID (23, 24) and evidence from *Drosophila* indicates that joint haploinsufficiency of both genes simultaneously may be required for synaptic defects rather than either gene individually (25). A recent study generated select combinatorial knockdowns of 3q29 gene homologs in *Drosophila* and *Xenopus laevis* and proposed that a component of the nuclear cap-binding complex, *NCBP2*

(26), mediates neurodevelopmental defects in 3q29Del syndrome (11). However, in the 3q29Del mouse model, NCBP2 is not decreased at the protein level in brain tissue (20), dampening enthusiasm for this gene as a causal element. It remains unclear which genes and their potential interactions are responsible for 3q29-associated phenotypes.

To avoid annotation-bias (27) and address the knowledge gap for 3q29 genes, we employed a gene co-expression network analysis approach that is rooted in systems biology (28-31), and generated evidence-based predictions that relate individual 3q29 genes to novel functions and disease phenotypes. Accumulating evidence indicates that genes work in conjunction, rather than in isolation, to realize most cellular functions (11, 25, 32). Genes participating in the same molecular and biological pathways tend to show positively correlated expression with each other (co-expression), as they are often expressed under the control of a coordinated transcriptional regulatory system (33, 34). In this holistic context, well-characterized genes can be leveraged to infer the functions of understudied genes by studying network patterns that emerge by means of co-expression (35-37). This *in silico* approach to investigating unknown biology extends the "guilt by association" paradigm (38) that is extensively used for inductive reasoning in other domains to gene-gene interactions in complex biological systems (39-41). Weighted gene co-expression network analysis (WGCNA) (29, 42) has been successfully deployed to study how genes embedded in network structures jointly affect complex human diseases (43-53). We employed this paradigm to glean new biological insights into the 3q29Del syndrome.

Methods and Materials

The reference dataset

To uncover the network-level operations of genes located in the recurrent 3q29Del locus, we employed WGCNA (29, 42) and organized the non-pathological adult human cortical transcriptome into modules of highly co-expressed genes (Fig. 1A). Given the strong genetic link between 3q29Del and risk for SZ (5), we focused the present network analysis on revealing the clustering patterns of 3q29 interval genes as a function of their expression similarity during adulthood: a period when SZ typically manifests diagnostically, with peak onset in late adolescence and early adulthood (54), and a substantial proportion of patients becoming ill during

middle adulthood (55). A prior study has shown that only 0.7% of genes detected in the neocortex show a temporally regulated profile of differential expression during adulthood (between ages 20-60 years) (56); hence, gene expression data were pooled across adulthood to derive the present dataset. We further focused our analysis spatially on gene-gene relationships in the PFC: a brain region that subserves a diverse range of cognitive and emotional operations, is implicated in the etiology of SZ and may be particularly vulnerable to the effects of genetic disruption due to its protracted development (57). For these reasons, the network was constructed on publicly available transcriptomic data from the Genotype Tissue Expression Project (GTEx) (58), using prefrontal cortex (PFC; Brodmann Area 9) samples from male and female adults (age range = 20-79, 68.2% male) with no known history of psychiatric or neurological disorder (Fig. S1). Transcriptome profiling was performed by RNA-Seq as described in (58).

Protein-coding transcripts were extracted from the dataset, normalized expression values were $\log_2$ transformed and summarized at the gene-level, and outlier samples were removed (Fig. S2). The data were corrected for covariance mediated by age, sex, death classification, post-mortem interval (PMI) and batch effect (59, 60) (Fig. 1B, Fig. S1). Genes with zero variance and genes and samples with greater than 50% missing entries (default) were removed (29, 42). The normalized, outlier-removed, residualized expression values of 18,410 protein-coding genes from 107 samples constituted the final dataset.

Weighted and signed gene co-expression network construction

The single-block pipeline implemented in the WGCNA R package was employed for network construction (29, 42). Co-expression similarity was defined by biweight midcorrelation (61, 62). To capture the continuous nature of interactions and accentuate strong positive correlations, co-expression similarity was transformed into a signed and weighted adjacency matrix by a soft-thresholding procedure that yielded approximate scale-free topology (63-66) (Fig. 1C, Fig. S3). Topological overlap measures (TOM) were calculated from the resulting adjacency matrix to capture not only the univariate correlational relationship between gene-pairs but also the large-scale connections among "neighborhoods" of genes (67, 68) (Fig. 1A). Hence, we measure the interconnectedness of gene-pairs in relation to the commonality of the nodes they connect to.

The modular structure of the data was revealed by average linkage hierarchical clustering on TOM following its transformation into a dissimilarity metric (Fig. 1D). Module definitions used in this study do not use *a priori* knowledge of functionally defined gene-sets. Instead, modules were detected in a data-driven fashion through adaptively pruning the branches of the resulting dendrogram by the dynamic-hybrid-tree-cut method (69). The expression profile of each identified module was subsequently summarized by a module eigengene (ME) (70) , defined as its first principal component. Calculation of MEs amounted to a data reduction method used for effectively correlating entire modules to one another and for establishing the eigengene-based module connectivity measure (kME) of individual genes (42). To eliminate spurious assignment of genes into separate modules, modules with strongly correlated MEs were amalgamated (Pearson's $r > 0.8$, $P < 0.05$, cut height = 0.2) (Fig. 1D).

Module preservation and quality analyses

To validate the reproducibility of the network modules derived from the GTEx dataset (considered the reference dataset/network), we evaluated module preservation in an independently ascertained, demographically comparable transcriptomic dataset, referred to as the test dataset/network (Fig. S4A). For this purpose, publicly available transcriptomic data was obtained from the BrainSpan Developmental Transcriptome Project (56). 30 non-pathological post-mortem samples from the PFC of male and female adults (age range = 18-37, 50% male) with no known neurological or psychiatric disorder comprised the test dataset (Fig. S4B). Transcriptome profiling was performed by RNA-Seq as described in (71).

The pre-processed test dataset consisted of normalized and residualized expression values for 18,339 protein-coding genes from 30 samples that were pooled from four sub-regions of the PFC to test whether the co-expression patterns derived from Brodmann Area 9 of the PFC in the reference dataset could be commonly found and robustly defined in broader sampling of tissue across the PFC. Prior to preservation analysis, a sample-level hierarchical clustering of the test dataset was conducted, which revealed no distribution bias associated with PFC sub-region, ruling out tissue of origin as a potential confound in test network construction. (Fig. S4C).

To determine whether properties of within-module topology were preserved in the test network, we calculated a composite, network-based preservation statistic for each module ($Z_{summary.pres}$) by using the *modulePreservation* function of the WGCNA package in R (72). $Z_{summary.pres}$ is a summary statistic that encompasses multiple density-based and connectivity-based preservation statistics, which are equally important for establishing the overall preservation of a module. To determine whether the observed preservation statistics were higher than expected by chance, we randomly permuted the module assignments in the test dataset (200 times) and derived a standardized $Z_{summary.pres}$ score for each module. To account for this metric's dependence on module-size, we reduced large modules by randomly sampling 1000 intra-modular nodes. The resulting scores were evaluated according to established thresholds: $Z_{summary.pres} < 2$, no evidence for preservation; $2 < Z_{summary.pres} < 10$, moderate evidence for preservation; $Z_{summary.pres} > 10$, strong evidence for preservation.

In addition to testing preservation, we measured the quality of the modules defined in the reference network by employing a resampling technique that applied the preservation statistics outlined above to repeated random splits of the reference dataset. We assessed the robustness of the identified modules (i.e., how distinct a module is from the background) by calculating a standardized, composite quality statistic ($Z_{summary.qual}$), as described in (72). The same $Z_{summary.pres}$ thresholds outlined above were used to evaluate $Z_{summary.qual}$.

Functional characterization of network modules harboring 3q29 genes

Pathway analyses of individual modules found to harbor 3q29 genes were performed by g:Profiler (http://biit.cs.ut.ee/gprofiler), using annotations from the Gene Ontology (GO), Reactome and Kyoto Encyclopedia of Genes and Genomes (KEGG) databases. Enriched terms surpassing the adjusted g:SCS significance threshold of $P < 0.05$ were filtered for size and semantic similarity (73).

To further interrogate whether the gene co-expression modules identified in this study represent biologically meaningful units with shared membership of the same molecular complex or functional pathway, we also investigated whether the genes co-clustering in the same transcriptomic module tend to interact at the protein level. First, we queried the known protein interactors of 3q29 interval genes based on the Human Reference Protein Interactome Mapping Project (HuRI; http:/interactome-atlas.org/) (see (74)). We identified

qualitative overlaps between these known protein interactors and gene co-expression partners of 3q29 interval genes at module and meta-module levels of network organization. Second, we tested the co-expression modules harboring 3q29 interval genes for enrichment of known and predicted protein-protein interactions (PPIs) curated from the STRING database (v.11, https://string-db.org/). The STRING enrichment analysis tool was used to test whether the observed number of protein interactions (edges) in each interrogated module is significantly higher than the number of edges expected if the nodes were to be selected from the genome at random (see (75)). See Supplemental Methods for details.

Identification of prioritized driver genes and biological mechanisms

Disease-associated genes are often more closely connected to each other than random gene-pairs in a biological network; this non-random network characteristic has enabled the identification of novel genetic risk loci for many diseases (76-80). To generate data-driven hypotheses about which 3q29 genes are causally linked to the major neuropsychiatric phenotypes of 3q29Del, we tested the overlap between "top neighbors" of individual 3q29 genes and known risk genes for SZ and related disorders (Fig. 3A). A top neighbor was defined as any node whose gene expression profile has a moderate-to-high correlation (Spearman's rho (ϱ) ≥ 0.5), $P < 0.05$) with a given 3q29 gene (considered a "seed") within the same module. Hence, top neighbors were identified by a hard-thresholding method applied only to intramodular edges of a seed that were initially defined by the topological overlap principle. Hypergeometric tests were conducted to gauge the probability of the overlap between curated gene-sets and top neighbors, as implemented in the *GeneOverlap* package in R (81), followed by Benjamini-Hochberg multiple testing correction.

Lastly, to formulate testable hypotheses about key biological mechanisms that link the 3q29 locus to neuropsychiatric disease, we interrogated the functional enrichment of prioritized driver genes, using the same pathway analysis approach applied to modules. See Supplemental Methods for details.

Proof of concept for testing the validity of WGCNA-based predictions

A necessary step in determining the utility of network-based predictions is a proof of concept of their

validity in an experimental system. To this end, we assessed the validity of our WGCNA-derived predictions by testing the enrichment of co-expression network-partners of 3q29 interval genes for differential expression in a mouse model of 3q29Del (20).

Mice harboring a heterozygous deletion of 1.26Mb ($Del16^{+/Bdh1\text{-}Tfrc}$) that is homologous to the human 3q29Del locus were generated by CRISPR/Cas9 technology previously (20). At postnatal day seven, five mutant and five wild-type male pups were anesthetized under isoflurane and rapidly decapitated. The bilateral cortical sheet was dissected, chopped with a scalpel, and homogenized in QIAzol (Qiagen) in a Bullet Blender Tissue Homogenizer (Next Advance, Inc., Troy, NY). Total RNA was isolated using the miRNeasy Mini Kit (Qiagen) with on-column DNAse I treatment (Qiagen). RNA-sequencing libraries were generated using the SMART-Seq Stranded Kit (Takara Bio, Mountain View, CA). 50M paired-end 150bp read sequencing was performed on an Illumina platform. Sequences were quality-checked and aligned to the mm10 reference genome. Gene quantification was conducted using HTSeq-count (82). We used two analysis tools (DESeq2 (83) and edgeR (84)) to identify differentially expressed genes (DEGs). Only the protein-coding consensus DEGs with nominal significance ($P < 0.05$) were carried into downstream analysis.

The statistical significance of the overlap between identified DEGs and the network co-expression partners of 3q29 interval genes was tested via hypergeometric tests, using the *GeneOverlap* package in R (81). All compared gene-sets were filtered for mouse-human homology based on the HomoloGene database of the National Center for Biotechnology Information (NCBI) (85). See Supplemental Methods for details.

Results

Unbiased gene co-expression network analysis reveals convergent and distributed effects of 3q29 interval genes across the adult human cortical transcriptome.

Applying an unsupervised WGCNA approach (29, 42) to publicly-available data from the GTEx Project (58) revealed that the protein-coding transcriptome of the healthy adult human PFC can be organized into a gene co-expression network of 19 modules (labeled by color) (Fig. 1D, Fig. 2A). The identified modules group genes with highly similar expression profiles and likely represent shared function and/or co-regulation. The

resulting module sizes ranged from 43 (steel-blue module) to 4,746 (green module) genes, with an average module size of 1,014 genes. To obtain high-quality module definitions, one module (grey module) was reserved for genes that could not be unequivocally assigned to any module. Thus, the grey module was excluded from downstream analysis. The resulting set of modules was screened for membership of 3q29 genes; modules that were found to harbor at least one 3q29 gene are rereferred to as "3q29 modules".

To ensure the reproducibility and robustness of our network analysis results, we tested the preservation and quality of the identified modules in an independent dataset obtained from the BrainSpan Developmental Transcriptome Project (56) (Fig. S4) and in repeated random splits of the reference dataset. All identified modules, except for the grey module (unassigned genes), were found to be successfully preserved in the test network ($Z_{summary.pres} > 2$) (Fig. 1E, Fig. S5). Specifically, 3/18 modules exhibited moderate evidence of preservation ($2 < Z_{summary.pres} < 10$), and 15/18 modules, including all 3q29 modules, exhibited strong evidence of preservation ($Z_{summary.pres} > 10$). In addition to preservation statistics, we calculated multiple module quality statistics that measure how well-defined or robust the boundaries of individual modules are in the reference network. All 18 modules showed strong evidence for high cluster quality ($Z_{summary.qual} > 10$), revealing robust module definitions (Fig. 1E, Fig. S5). Specifically, all 3q29 modules had a $Z_{summary.qual}$ score ≥ 20. These analyses revealed the replicable, well defined, and non-random nature of the identified network modules. For extended results, see Supplemental Results.

The 21 protein-coding genes located in the 3q29 interval clustered into seven modules (Fig. 2A): black (one 3q29 gene), brown (four 3q29 genes), dark-turquoise (one 3q29 gene), green (six 3q29 genes), magenta (one 3q29 gene), midnight-blue (three 3q29 genes), and turquoise (five 3q29 genes). Within this network, 18 (86%) of the 3q29 interval genes concentrate into just four modules (Fig. 2A), suggesting that the haploinsufficiency of sets of genes within the locus may perturb the same biological processes via multiple hits, cumulatively disrupting redundancy and compensatory resiliency in the normative regulation of cellular functions.

To evaluate whether modules further clustered within larger meta-modules that represent the higher-order organization of the transcriptome, we identified meta-modules as tight clusters of positively correlated MEs, detectable as major branches of the eigengene dendrogram (86) (Fig. 2A-B). Meta-modules were screened to

identify the grouping patterns among 3q29 modules, allowing exploration of extra-modular interactions. This analysis revealed that the 3q29 modules further cluster into three higher level meta-modules (Fig. 2B), which likely reflect dependencies and interactions between pathways involving 3q29 genes. Simultaneously, leading presumptive candidates *DLG1* and *PAK2* were found in opposite branches of the network, demonstrating the distributed effects of this CNV across the transcriptomic landscape.

Pathway analysis points to functional involvement of the 3q29 locus in nervous-system functions and core aspects of cell biology.

Since highly co-expressed genes often share similar functions (33, 34), biological processes and pathways that are enriched in a co-expression module can be used to infer functional information for poorly annotated genes of that module. Functional enrichment analysis of 3q29 modules showed that their constituent genes converge onto canonical biological processes and known / predicted PPI networks at proportions greater than expected by chance, indicating that these modules are biologically relevant units (Fig. 2D, Fig. S8-9).

The turquoise and green modules showed overrepresentation of roles specific to the neuronal system and implicate involvement in multiple synaptic properties. Other 3q29 modules point to biological pathways that may also underlie neuropsychiatric pathology in 3q29Del. The magenta module was predominantly enriched for protein modification, turnover, and localization. Additionally, a link was identified between the magenta module and the initiation of major histocompatibility complex class-I (MHC-I)-dependent immune responses, driven by a genomic locus implicated in the etiology of SZ (87, 88). On the other hand, overrepresented pathways in the black module encompass regulation of gene expression and maintenance of the integrity of the cellular genome, including DNA repair, and the metabolism and processing of RNA. The midnight-blue module shared enriched roles with the black module, validating their shared meta-module structure, yet it was set apart by its involvement in cell cycle regulation. The brown module revealed primary enrichment for cellular metabolism and mitochondrial function, whereas the dark-turquoise module coalesced genes involved in epigenetic mechanisms and in signal transduction pathways mediated by Rho GTPases. This latter function may be attributable to *PAK2*, which encodes a known Rho GTPase effector. Intriguingly, this module was also

enriched for estrogen receptor-mediated signaling, suggesting a potential mechanism for sex-specific effects. Taken together, functional characterization of the 3q29 modules point to novel mechanisms of shared or synchronized action for co-clustering 3q29 interval genes (Fig. 2D, Fig. S9).

Simultaneously, PPI network enrichment analysis revealed that all 3q29 modules show significant enrichment for PPIs that were systematically curated from the STRING protein interactome database (Fig. S8), augmenting confidence in our RNA-Seq based network predictions with proteomic evidence (midnight blue, black, brown, and magenta modules: *P*-value < 1.00e-16; dark turquoise module: *P*-value = 1.11e-16; green module: *P*-value = 8.62e-08; turquoise module: *P*-value = 4.30e-09).

Additionally, we identified qualitative overlaps between the transcriptomic co-expression partners of 3q29 interval genes identified via WGCNA and known protein partners of 3q29 interval genes curated from the HuRI database (Fig. S7). Notably, of the 21 protein coding genes located in the 3q29 interval, only 14 were found to have an entry on HuRI, 50% of which had less than eight known proteome-wide interactors. For reference, in the yeast proteome, an average of five interactors are estimated per protein (89). Given that the average domain content of human proteins is higher than that of yeast (90), a much higher number of PPIs per protein is expected in humans. This finding is consistent with prior studies reporting that technological limitations in measuring the proteome with enough coverage results in a high rate of missing entries, which leads to significant bias and loss of information on human PPIs that may be disease relevant (91-93). The missing PPI data for over one fourth of the genes located in the 3q29 interval corroborate the paucity of information regarding the functional roles of most 3q29 interval genes, and further reveal the need for novel approaches that are free of annotation-bias (27). For extended results, see Supplemental Results.

UBXN7 is a highly connected cortical hub-gene predicted to play a crucial role in the neuropsychiatric sequela of 3q29Del.

Targeted disruption of a highly connected "hub" gene produces a more deleterious effect on network function and yields a larger number of phenotypic outcomes than randomly selected or less connected genes (94, 95). Hence, we sought to measure how strongly connected individual 3q29 genes are to their modules by

evaluating their intramodular kME (Fig. 2C), defined as the Pearson's correlation between the expression profile of a gene and the eigengene of its assigned module (29, 42, 70).

Genes with high intramodular kME are considered hub genes that are predicted to be critical components of the overall function of their module (29). Nodes with high intramodular kME often have high intramodular connectivity (kIM), which reflects sum of adjacencies to other nodes (42). However, an advantage of using kME over other connectivity metrics, is its defined *P*-value and values that lie between -1 and 1, allowing comparison across modules that differ in size. To generate rigorous predictions about which 3q29 genes, if any, are intramodular hub genes, we adopted a conservative criterion that defines hub genes as nodes with kME > 0.8 ($P < 0.05$). Only one 3q29 interval gene was identified as a hub gene: *UBXN7* (kME = 0.84, *P* = 8.33E-30), which encodes a ubiquitin ligase-substrate adaptor (96, 97).

SMCO1, SLC51A, and *MFI2* had non-significant kMEs ($P < 0.05$) for their module, suggesting low intramodular connectivity. These 3q29 genes are detected but display very low abundance in the human cerebral cortex (98), which may relate to their peripheral network assignments in our analysis. Consequently, *SMCO1, SLC51A* and *MFI2* were excluded from downstream analysis to derive the most parsimonious prioritization of driver genes based on tight network connections.

Nine 3q29 interval genes form transcriptomic subnetworks enriched for known SZ, ASD and IDD-risk genes.

We next identified a refined subset of target genes (top neighbors) that not only co-cluster based on TOM but also have a strong pairwise correlation with 3q29 genes (Fig. 3A). Several 3q29 genes were found to be top neighbors of one another. *FBXO45* ($\varrho = 0.5$, *P* = 5.43E-09) and *PIGX* ($\varrho = 0.6$, *P* = 1.24E-10) are top-neighbors of *CEP19*, while *SENP5* and *WDR53* are top-neighbors of each other ($\varrho = 0.5$, *P* = 1.05E-07). On the other hand, intramodular connections of *TM4SF19* and *ZDHHC19* did not meet top neighborhood criteria; hence they were not included in downstream analysis. Similar to *SMCO1, SLC51A* and *MFI2,* their mRNA expression profiles indicate low abundance in the cerebral cortex, which likely reflects their lack of strong network connections.

The human transcriptome is theorized to demonstrate non-random topological characteristics, where

disease genes interact with other disease genes that underlie a common pathophenotype (99). Concordant with this prediction, within the top neighbors of 3q29 genes, we found several genes that have been extensively implicated in neuropsychiatric disease. These include *MECP2*, *NRXN1*, *GRIN2A*, *GRIN2B*, *CHD8*, *SATB2*, *CNTNAP2*, *FOXP1*, *PTEN*, and *SCN2A*. Motivated by this observation, we asked whether top neighbors of individual 3q29 genes significantly overlap with known SZ, ASD or intellectual disability / developmental delay (IDD)-risk genes (Fig. 3A). We curated six evidence-based lists of SZ (100-104), ASD (105, 106) and IDD-risk genes (107), which span a wide range of the allele frequency spectrum and include post-mortem findings from case-control gene expression studies. 3q29 genes whose top neighbors showed an overrepresentation of SZ, ASD and/or IDD risk genes (adjusted $P < 0.05$) were subsequently prioritized as likely genetic drivers of neuropsychiatric risk in 3q29Del syndrome, along with their SZ, ASD, and/or IDD-related top neighbors from the enrichment findings (Fig. 3A). We found overrepresentation of one or more established risk gene-sets among the top neighbors of nine 3q29 genes (Benjamini-Hochberg adjusted-$P < 0.05$) (Fig. 3B).

To evaluate the specificity of the identified patterns of polygenic disease burden, we also tested these top neighbors for overlap with known Parkinson's disease (PD) (108), late-onset Alzheimer's disease (AD) (109), and inflammatory bowel disease (IBD) risk genes (110). These phenotypes have no known link to 3q29Del, thus, their risk loci were considered negative controls. Common variants associated with height (111) were included as a fourth negative control to rule out a potential bias associated with large differences in the sizes of curated gene-sets.

Concurrently, we found no statistically significant evidence for overrepresentation of AD or IBD-risk genes among the interrogated top neighbors (Fig. 3B). Only the top neighbors of *SENP5* showed a significant overlap with height-associated genes (adjusted-P = 2.36E-02), and the top neighbors of *NRROS*, which did not show an enrichment for known IDD, ASD, or SZ risk genes, exhibited a small but significant overlap with known PD-risk genes (adjusted-P = 2.00E-02) (Fig. 3B). Overall, 19 out of 96 hypergeometric tests (20%) revealed a significant overrepresentation of SZ, ASD, and/or IDD-risk gene-sets among the top neighbors of 3q29 genes. By contrast, only 2 out of 64 (3%) hypergeometric tests indicated a significant overlap with the negative control gene-sets. The substantial margin between these two enrichment ratios supports the high specificity of our

network-derived inferences for uncovering biology relevant to 3q29Del. By leveraging guilt by association, we prioritize *BDH1, CEP19, DLG1, FBXO45, PIGZ, RNF168, SENP5, UBXN7, and WDR53*, along with their 284 unique SZ, ASD, and/or IDD-related top neighbors from significant overlap tests as likely drivers of the neuropsychiatric consequences of 3q29Del (Fig. 4A).

Disease-relevant driver genes prioritized by network analysis load onto key biological pathways linked to neuropsychiatric disorders.

To formulate testable hypotheses about the biological mechanisms linking the 3q29 locus to neuropsychiatric phenotypes, we interrogated whether the prioritized driver genes identified in our network analysis assemble into known biological pathways. Functional enrichment analysis on the union of 293 prioritized driver genes (including nine 3q29 genes) revealed significant overrepresentation of eight biological pathways annotated by the Reactome and KEGG databases (Fig. 4B). These include axon guidance (adjusted-*P* = 3.64E-03), long-term potentiation (adjusted-*P* = 7.29E-03), and regulation of actin cytoskeleton (adjusted-*P* = 1.17E-02). Additionally, several GO biological processes (GO:BP), including chromosome organization (adjusted-*P* = 3.81E-09), histone modification (adjusted-*P* = 3.31E-08), neuron differentiation (adjusted-*P* = 1.88E-04), neurogenesis (adjusted-*P* = 1.89E-03), and excitatory postsynaptic potential (adjusted-*P* = 8.97E-03) were overrepresented among the predicted drivers (Fig. 4B-C). We hypothesize that the disruption of one or more of these biological pathways and processes, some of which have been demonstrated to be altered in idiopathic SZ and ASD (2, 112), lie on the casual pathway to neuropsychopathology in 3q29Del syndrome. For extended results, see Supplemental Results.

Network-derived targets predict differentially expressed genes in the mouse model of 3q29Del.

Perturbation of 3q29 gene dosage in neural tissue is expected to lead to the differential expression of the true transcriptomic network partners of 3q29 genes. Following this premise, we tested the enrichment of the network targets identified in this study for differential expression in Del16$^{+/Bdh1\text{-}Tfrc}$ mice compared with wild-type (WT) littermates. RNA-Seq analysis revealed 290 protein-coding DEGs with known human homologs (*P*

< 0.05), 17 of which were identified as 3q29 interval genes (*Bdh1, Cep19, Dlg1, Fbxo45, Mfi2, Ncbp2, Nrros, Pak2, Pcyt1a, Pigx, Pigz, Rnf168, Senp5, Tctex1d2, Tfrc, Ubxn7, Wdr53*) (Fig. 5). The scaled expression of these 3q29 genes showed a consistent reduction proportional to gene copy number (Fig. 5A).

All 290 DEGs were tested for enrichment of network-derived targets identified via WGCNA at three scales of network interconnectedness: i) broad 3q29 network (11,924 genes), ii) top-neighbor-based 3q29 subnetwork (5,087 genes), and iii) prioritized drivers (280 genes). Hypergeometric tests revealed significant enrichment of the interrogated DEGs for network-derived ties at all three levels of this analysis ($P < 0.05$; Fig. 5B). See Supplemental Results for extended results.

Discussion

The 3q29Del has been reliably associated with extraordinary risk for serious neuropsychiatric illness and therefore may offer key insights to advance our understanding of the biological basis of these complex disorders. Currently, the driver genes and affected biological pathways that link 3q29Del to neuropsychiatric pathology remain unknown. To avoid bias introduced by annotation-based criteria in the formulation of mechanistic hypotheses, we engaged a system-level vantage point and interrogated the collective behavior of 3q29 interval genes with the global protein-coding transcriptome of the healthy human brain. We leveraged publicly available transcriptomic data from the GTEx Project (58) to perform WGCNA (29, 42) on postmortem cortical samples from donors with no known history of psychiatric or neurological disease. We focused our analysis on the adult PFC and analyzed the resulting network to identify the modular properties and undirected connectivity patterns of the 3q29 interval, which yielded key predictions into inter-related functions and disease associations. Finally, we assessed the validity of our graph-based predictions in an experimental system by conducting RNA-sequencing in mice harboring a homologous deletion to the human 3q29Del locus (20). Our findings provide foundational information to formulate rigorous, targeted and testable hypotheses on the causal drivers and mechanisms underlying the largest known single genetic risk factor for SZ.

Genomic studies have identified several recurrent CNVs that confer high risk for neuropsychiatric disorders (2, 10). The current challenge is to understand which genes within these loci are the major drivers of

risk. In the 3q29 locus, *DLG1* and *PAK2* have been most often proposed as candidate drivers of neuropsychiatric phenotypes (12, 25, 113). Indeed, a recent literature search revealed more publications related to these genes than of all other 3q29Del genes combined (Fig. S6). Consistent with previous reports of an association between *DLG1* and SZ (18, 19), the current study presents network-level evidence for prioritizing *DLG1* as a neuropsychiatric disease-linked gene. Surprisingly, however, our analysis does not support inclusion of *PAK2* as a predicted driver of neuropsychiatric risk. Instead, our results lend support to *DLG1* and eight other 3q29 genes, most of which are largely understudied, as key players in 3q29Del syndrome. Our unbiased approach prioritizes *BDH1, CEP19*, *DLG1*, *FBXO45, PIGZ, RNF168, SENP5, UBXN7* and *WDR53* as primary drivers.

It is currently unknown whether the biological basis of neuropsychiatric risk associated with recurrent CNVs overlaps with that of individuals who share the same clinical diagnosis but do not share the same rare genetic variant. Our findings suggest that molecular perturbations caused by the hemizygous deletion of select 3q29 genes may overlap with the genetic etiologies contributing to idiopathic forms of SZ, ASD and ID. Disease-relevant driver genes prioritized by our network analysis are enriched for canonical biological pathways, such as neurogenesis, neuron differentiation, synapse organization, excitatory postsynaptic potential, long-term potentiation, axon guidance, regulation of actin cytoskeleton, signal transduction, post-translational protein modifications, chromatin organization and histone modification. We hypothesize that the disruption of one or more of these biological processes, some of which are altered in idiopathic SZ and ASD (2, 112), lie on the casual pathway to neuropsychopathology in 3q29Del syndrome.

No single gene within the interval has been definitively associated with neuropsychiatric disease, prompting the hypothesis that neuropathology in 3q29Del emerges upon loss of multiple genes that are functionally connected. While a single nucleotide polymorphism in *DLG1* has been associated with SZ in a case-control study (18, 19), the risk associated with this variant does not approach that of 3q29Del, suggesting that the neuropsychiatric risk associated with this CNV is distributed across more than one gene in the locus. To investigate functional connections across multiple 3q29 genes, we conducted an unsupervised analysis of the modular organization of the adult human PFC. We found the 21 3q29 genes distributed into three meta-

modules and seven modules, with 18 genes converging into just four modules. Hence, 3q29 genes display both distributed and convergent effects in the adult human cortical transcriptome. Rather than functioning as independent agents, sets of 3q29 genes may have shared and/or synchronized function and constitute interacting sources of pathology. It is conceivable that the consequences of the haploinsufficiency arise through the weakening of multiple distinct pathways that normally provide protective redundancies (distributed model), and/or through multiple insults to a functionally connected module that cumulatively disrupt resiliency (convergent biology model). These hypotheses warrant further testing.

A major goal was to infer unknown functions for understudied 3q29 genes by leveraging well-studied co-clustering genes. Pathway analysis of modules harboring 3q29 genes revealed likely functional involvement of the 3q29 locus in not only nervous-system specific functions, but also in core aspects of cell biology non-specific to an organ system. The closely related black and midnight-blue modules were significantly associated with regulation of gene expression, chromatin organization and DNA repair. The green and turquoise modules were associated with nervous system development and function, and in particular, regulation and organization of synaptic signaling and components. This finding is surprising because most of the 3q29 genes located in these latter two modules have not been identified as synaptic genes. Similarly, the 3q29 genes in the black and midnight-blue modules have not been implicated in gene regulatory pathways or DNA repair. We maintain that biological functions of poorly annotated genes can be inferred through the graph-based modeling of inter-gene relationships. Thereby, we predict novel roles for individual 3q29 genes in functions related to synaptic transmission, modulation of neurotransmission, synapse structure and function, mitochondrial metabolism, transcriptional and translational regulation, chromatin remodeling, cell cycle regulation, and protein modification, localization, and turnover. We propose that the subset of predicted functions that are non-specific to an organ system likely contribute to global developmental outcomes in 3q29Del.

Analysis of eigengene-based connectivity revealed that *UBXN7* is a hub gene, with top neighbors enriched for known association with all three major neuropsychiatric phenotypes of 3q29Del. Hub nodes of biological networks are often associated with human disease (114, 115). Disease-genes, identified from OMIM's Morbid Map of the Human Genome, disproportionately exhibit hub-gene characteristics, with protein products

participating in more known protein-protein interactions than that of non-disease genes (116). Supported by this literature, we predict that (1) *UBXN7* exerts critical influence on a large network of co-expressed genes, and (2) loss-of-function (LoF) mutations in *UBXN7* can cause major dysfunction in affiliated biological pathways (indeed, its pLI score = 0.99, i.e. extremely intolerant to LoF (117)). We prioritize *UBXN7* as a major driver in 3q29Del syndrome. *UBXN7* has not been previously linked to neuropsychiatric disorders or proposed as a candidate driver of 3q29Del syndrome. However, *UBXN7* has been reported to regulate the ASD-associated E3 ubiquitin ligase Cullin-3 (*CUL3*) (118), an interaction that deserves more attention in light of our findings (97). In fact, *UBXN7* is one of three genes involved in the ubiquitin-proteasome system (UPS) – along with *RNF168* and *FBXO45* – that were prioritized in our analysis. Accumulating evidence indicates multiple links between the UPS and SZ, though the causal relationship is still unclear (reviewed by (119)). Our analysis indicates that the UPS may be disrupted at multiple levels by haploinsufficiency of these three genes in 3q29Del.

The network described here was built from adult human PFC gene expression data, while the experimental system used to test the validity of the identified network targets was the mouse model of 3q29Del at postnatal day seven (20), which most closely matches the perinatal stage of brain development in humans (120). Notwithstanding this considerable difference in developmental phase, we found significant enrichment of network-derived targets among DEGs identified in this model, presenting proof of concept for the validity of our network analysis approach for uncovering biologically meaningful associations. These results also indicate that a significant fraction of transcriptomic network connections formed by the 3q29 locus may be relatively stable through development and are evolutionarily conserved in mice.

One limitation of the current study is its singular focus on protein-coding elements. How the non-coding elements of the interval, along with splice variants, integrate into the predictions formulated in this study is ripe for future investigation. Overall, the transcriptomic network identified in this study is predicted to connect 3q29 interval genes with gene-sets outside the interval that participate in the same or overlapping biological process and associate with similar disease phenotypes. Perturbation of 3q29 interval gene dosage is expected to also perturb the functioning of network-partners outside the recurrent 3q29Del locus. However, note that the underlying structure of weighted gene co-expression networks is agnostic to the mechanistic order of cellular

and molecular events. The information necessary to derive the order of biological interactions is not an explicit outcome of gene co-expression itself, since such inferences require time-dependent analysis of combinatorial interactions between nodes. As a result, some of the network partners identified in this study are expected to function upstream of their co-expressed 3q29 gene partner and would likely not be affected by 3q29Del. Simultaneously, this direction-agnostic property also suggests that network-based predictions formulated in this study are likely relevant to biological pathways and processes implicated in 3q29 duplication syndrome (121), which was recently shown to manifest phenotypic concordance with 3q29Del syndrome in multiple clinical areas, similar to relationships identified in other reciprocal CNV disorders (122).

Moreover, the complex interactions between molecules can be dynamic across time and space (56). Hence, a future direction will be to ask whether the network connections formed by 3q29 interval genes in the adult PFC show differential expression in the neural tissue of 3q29Del carriers and whether they show temporal and/or spatial variation. Finally, our analysis does not preclude the possibility that other 3q29 interval genes moderate phenotypic expressivity. For example, while the dark turquoise module (including *PAK2*) did not harbor prioritized driver genes, it was significantly associated with estrogen receptor-mediated signaling. An intriguing emerging feature of 3q29Del syndrome is the markedly reduced sex bias in risk for ASD (9). Additional studies will be required to assess the drivers of sex-specific phenotypes of 3q29Del syndrome.

Now that recurrent, highly penetrant CNV loci have been identified as important risk factors for neuropsychiatric disorders, determination of the component genes driving this risk is the next step toward deciphering mechanisms. We used an unbiased systems biology approach that leveraged the power of open data to infer unknown functions for understudied 3q29 interval genes, and to refine the 3q29 locus to nine prioritized driver genes, including one hub gene. Importantly, this approach can partially overcome barriers to formulation of relevant hypotheses that are introduced by poor annotation of interval genes, without requiring laborious, expensive, and time-consuming experiments to functionally characterize all genes within the interval. Our results reveal the power of this approach for prioritization of putative drivers. Ongoing and future studies will be directed at understanding how these genes work in concert and how multiple haploinsufficiencies confer risk for neuropsychiatric disease.

Data availability

The GTEx data (release version 6) used for the analyses described in this manuscript were downloaded from the GTEx portal on 01/08/2019 (http://www.gtexportal.org/home/datasets/, file name: "GTEx_Analysis_v6_RNA-seq_RNA-SeQCv1.1.8_gene_rpkm.gct.gz"); dbGaP accession number: phs000424.v6.p1. The Genotype-Tissue Expression (GTEx) Project was supported by the Common Fund of the Office of the Director of the National Institutes of Health, and by NCI, NHGRI, NHLBI, NIDA, NIMH, and NINDS.

The BrainSpan Developmental Transcriptome dataset used to construct the test network was downloaded from the Allen Brain Atlas portal on 01/12/2019 (https://www.brainspan.org/static/download/, file name: "RNA-Seq Gencode v10 summarized to genes"); dbGaP accession number: phs000755.v2.p1.

Figures

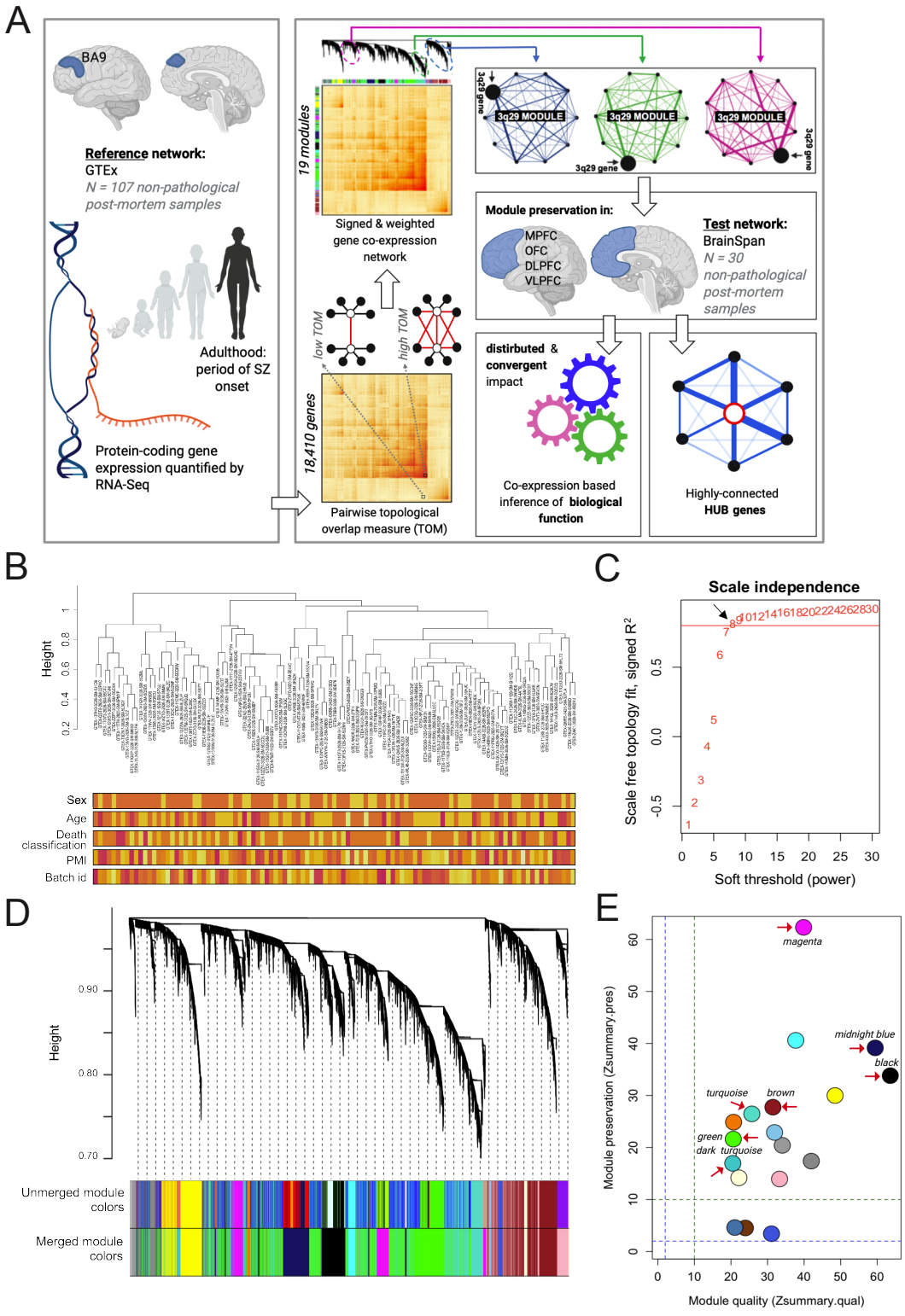

Figure 1. Unbiased weighted gene co-expression network analysis (WGCNA) of the human transcriptome in the healthy adult prefrontal cortex (PFC). (a) A schematic of the data analysis workflow

underlying WGCNA-derived predictions for functional interrogation of the 3q29Del interval. The reference dataset was obtained from the GTEx Project to construct a systems-level network representation of coordinated gene expression patterns across 107 non-pathological post-mortem samples collected from the Brodmann Area 9 (BA9) of male and female adults with no known history of psychiatric or neurological disorder. Modules of highly co-expressed genes were identified based on their topological overlap measure (TOM). The TOM between two genes is high if the genes have many overlapping network connections, yielding an interconnectedness measure that is proportional to the number of shared neighbors between pairs of genes. The resulting network was screened for modules harboring 3q29 interval genes (3q29 modules), which were then interrogated for biological function and hub genes. A test dataset obtained from the BrainSpan Project was used to validate the reproducibility of this network in an independent sample of 30 non-pathological post-mortem specimens collected from four sub-regions of the PFC from adult males and females with no known history of psychiatric or neurological disorder. These sub-regions are the OFC: orbital frontal cortex, DLPFC: dorsolateral PFC, VLPFC: ventrolateral PFC, and MPFC: medial PFC. **(b)** Sample-level dendrogram and trait heatmaps of the reference dataset. The dendrogram was yielded by hierarchical clustering of 107 GTEx samples using normalized, outlier-removed and residualized gene expression values for 18,410 protein-coding genes. Color bars represent trait heatmaps for sex, age-group (range = 20-79 years), death-classification based on the Hardy scale (range = 0-4), post-mortem interval (PMI) and batch id. The color intensity (from light yellow to red) is proportional to continuous or categorical values (in increasing order) of each variable. For sex, yellow and orange indicate female and male, respectively. Transcriptomic data were corrected for covariance mediated by these variables prior to network construction. Adjusted data reveal no distribution bias associated with the interrogated confounds in sample-level clustering patterns. **(c)** Determination of the soft-thresholding power (β) used for WGCNA. A β of 8 (black arrow) was identified as the lowest possible power yielding a degree distribution that results in approximate scale-free network topology (SFT R^2 fit index = 0.8; red line). **(d)** Clustering dendrogram and module assignments of genes, with dissimilarity based on TOM. 18,410 protein coding genes (leaves = genes) clustered into 19 final modules (bottom color bar), detected by the dynamic hybrid tree cut method. Modules with strongly correlated eigengenes (Pearson's $r > 0.8$, $P < 0.05$) were

amalgamated to eliminate spurious assignment of highly co-expressed genes into separate modules. Color bars reflect module assignments before and after the merging of close modules. **(e)** Composite *Zsummary* scores for module-preservation (how well-defined modules are in an independent test dataset) and module-quality (how well-defined modules are in repeated random splits of the reference dataset). Permutation tests were performed to adjust the observed preservation and quality statistics of each module for random chance by defining Z statistics. All modules (labeled by color) identified in the reference network were preserved (reproducible) in the test network (*Zsummary* > 2; blue line). 15/18 modules, including all 3q29 modules (red arrows), exhibited strong preservation (*Zsummary* > 10; green line). 3/18 modules exhibited moderate preservation (2 < *Zsummary* < 10). All modules demonstrated strong evidence for high quality (*Zsummary* > 10), confirming that the modules identified in the reference network were well-defined and non-random.

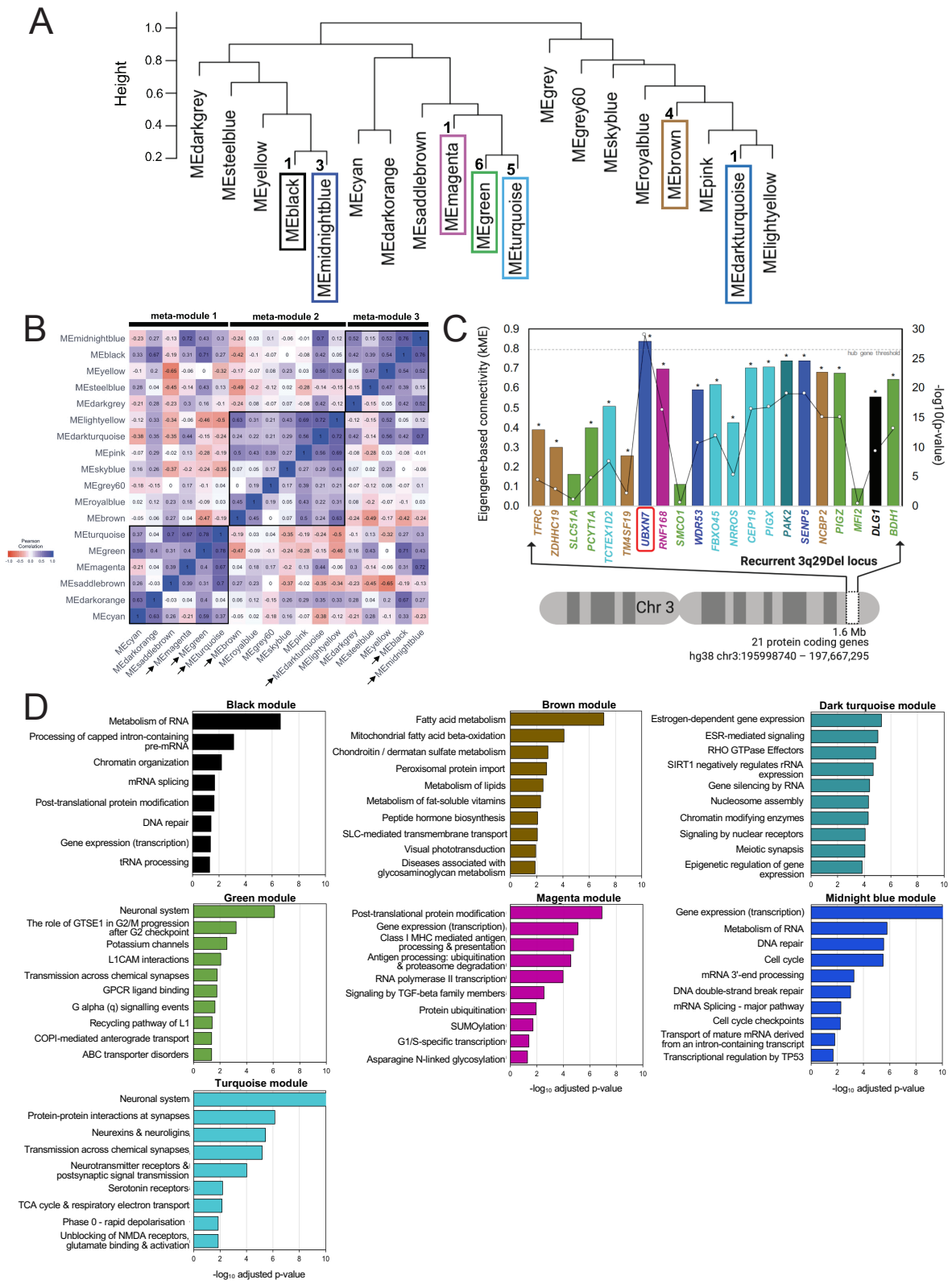

Figure 2. Network-based inference of the functional impact of 3q29Del on the adult human prefrontal cortex (PFC). (a) Hierarchical clustering of module eigengenes (ME) that summarize the 19 modules identified

by WGCNA. The 21 protein-coding genes located in the recurrent 3q29Del locus were found to be distributed into 7 co-expression modules (3q29 modules; framed), The numbers next to dendrogram branches indicate the total number of 3q29 interval genes found in each 3q29 module. **(b)** Heatmap representing the strength of Pearson's correlation (*r*) between ME-pairs. The seven 3q29 modules (arrows) further clustered into three higher-level meta-modules, corresponding to squares of blue color (high positive correlation) along the diagonal, also detected as major dendrogram branches in (a). **(c)** Eigengene-based connectivity strength (kME; y-axis) of 3q29 interval genes (x-axis; in chromosomal order) within their respective modules. kME is defined as the Pearson's correlation between a query gene and a given ME. The line graph indicates the $-\log_{10}$(*P-value*) of the plotted correlation coefficients (z-axis); the asterisks above the graph indicate $P < 0.05$. kME > 0.8 ($P < 0.05$; dotted line) indicates hub (highly connected) gene status. *UBXN7* (red frame) was found to be the only hub gene (kME > 0.8, P = 8.33E-30) within the 3q29Del locus. *SMCO1 (*kME = 0.11, P = 0.25*), SLC51A (*kME = 0.17, P = 0.09) and *MFI2* (kME = 0.09, P = 0.35) were found to have non-significant kMEs (P > 0.05) for their respective modules, suggesting peripheral membership. Color indicates module label. **(d)** Top 10 biological pathways (Reactome database) significantly enriched in 3q29 modules (adjusted-$P < 0.05$; capped at $-\log_{10}$ (adjusted-P = 10)). The g:SCS method was used for multiple testing correction. The observed enrichment profile of the queried modules for known biological processes and pathways indicates that genes co-clustering in 3q29 modules show coordinated expression and converge upon overlapping biological functions, more than expected by chance. The functional associations of gene-sets comprising individual 3q29 modules were leveraged to infer likely molecular consequences of 3q29Del in the adult human PFC.

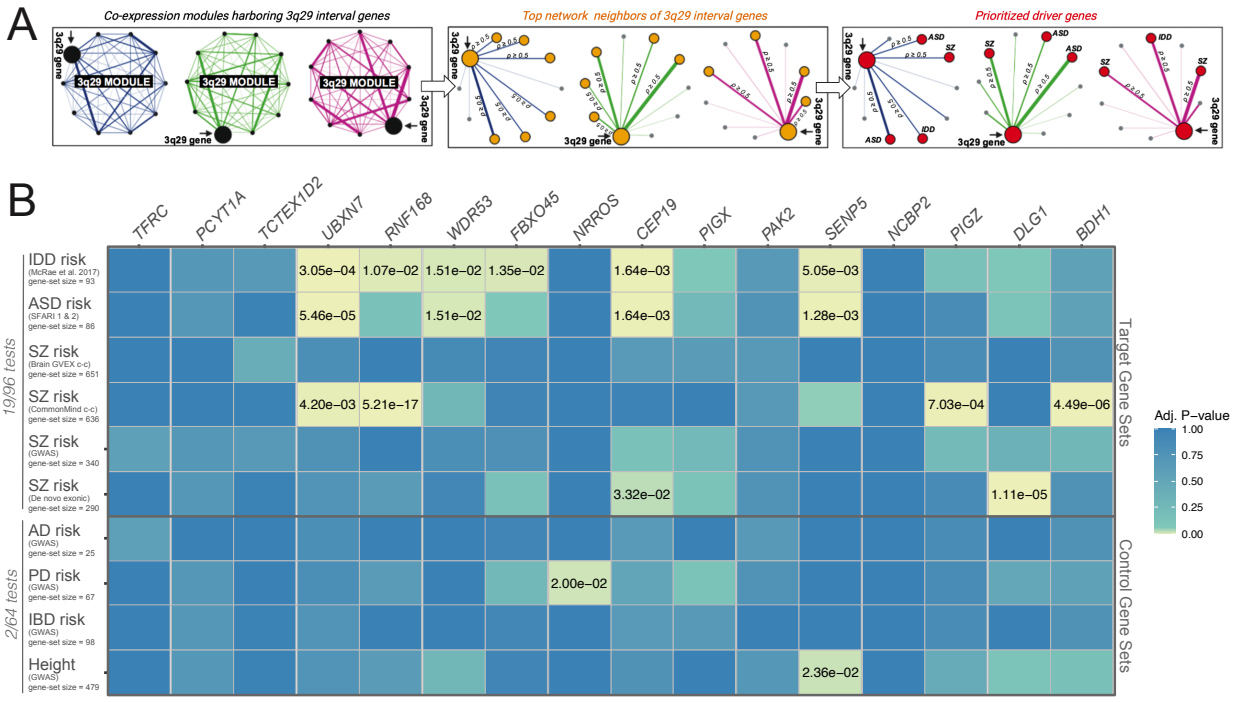

Figure 3. 3q29 interval genes form transcriptomic subnetworks enriched for known schizophrenia, autism and intellectual / developmental disability-risk genes. (**a**) Schematic of strategy to test the neuropsychiatric disease burden associated with top network neighbors of 3q29 interval genes and to refine a list of prioritized driver genes. To minimize false positives, 3q29 modules were reduced to strongly connected top neighbors (yellow nodes) of individual 3q29 genes, which were then screened for a significant overlap with known risk genes (red nodes) for schizophrenia (SZ), autism spectrum disorders (ASD), and intellectual / developmental disability (IDD), spanning known associations over a wide spectrum of allele frequencies. A top neighbor was defined as any node whose gene expression profile had a moderate-to-high pairwise correlation (Spearman's rho (ϱ) ≥ 0.5, $P < 0.05$) with a 3q29 interval gene within the same module. By leveraging the guilt by association principle, the 3q29 interval genes that showed a significant enrichment of known SZ, ASD, and/or IDD risk genes among their respective top neighbors were prioritized as likely drivers of the neurodevelopmental and psychiatric consequences of 3q29Del, along with their SZ, ASD, and/or IDD-related top neighbors from significant overlap tests. (**b**) Adjusted p-values from hypergeometric tests identifying the significance of the overlap between top neighbors of individual 3q29 genes and known risk genes for SZ, ASD,

and IDD. Risk gene-sets for three traits with no known association to the 3q29Del syndrome were also tested for over-representation as negative controls. Common variants associated with height were included as another negative control to rule out a potential bias introduced by gene-set size. Nine protein-coding genes from the 3q29 interval formed transcriptomic subnetworks that are significantly enriched for known SZ, ASD and/or IDD risk genes (orange highlight, adjusted-$P < 0.05$). The proportion of hypergeometric tests with significant overrepresentation of SZ, ASD, and IDD gene-sets (19/96) was found to be an order of magnitude larger than that of the negative control tests (2/64), demonstrating the high specificity of the identified enrichment patterns for reported 3q29Del-associated phenotypes.

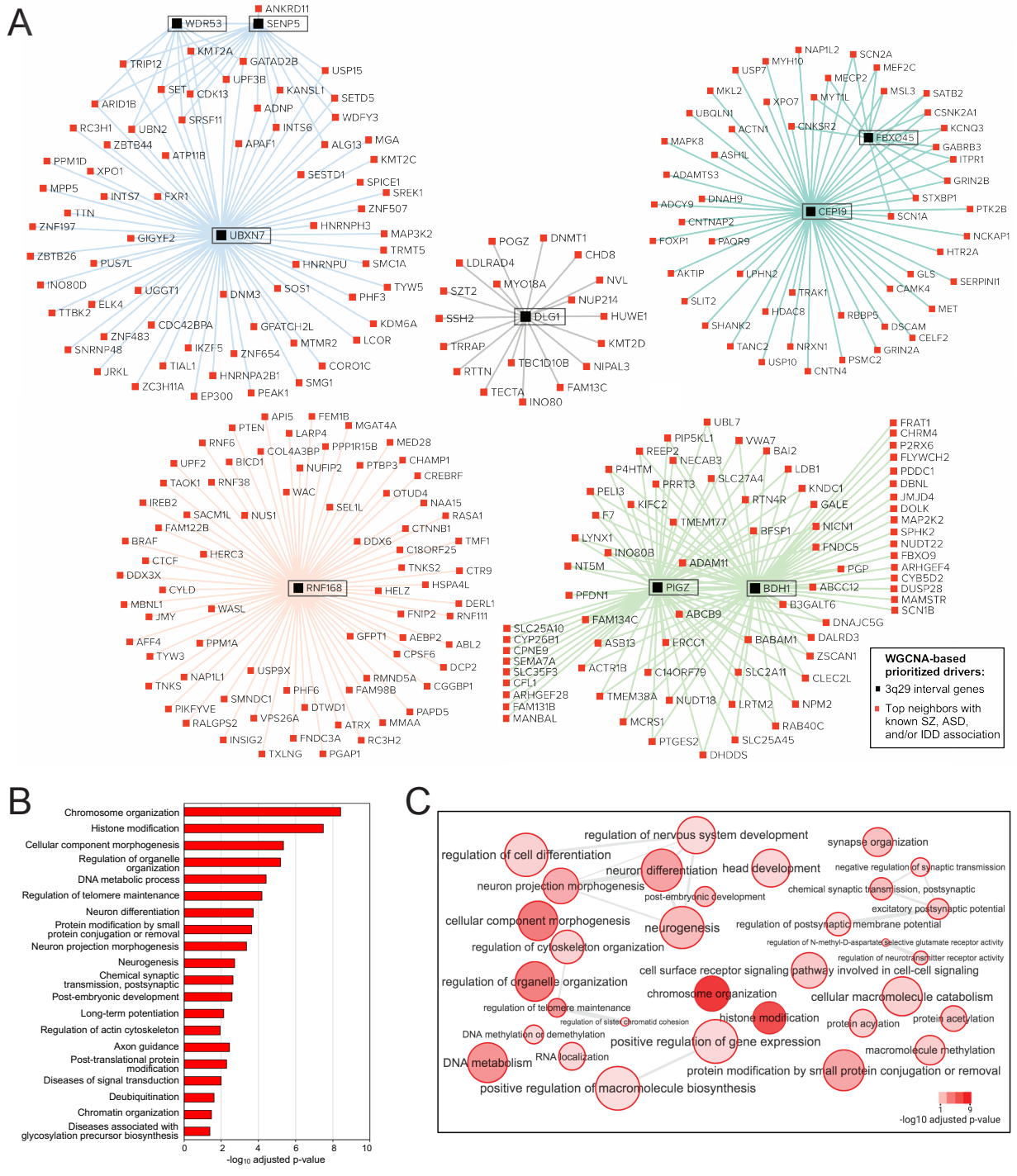

Figure 4. Network of prioritized drivers predicted to contribute to the neuropsychiatric sequelae of 3q29Del. (a) Nine protein-coding genes from the 3q29 interval formed top-neighbor-based transcriptomic subnetworks that were significantly enriched for known schizophrenia (SZ), autism spectrum disorder (ASD) and intellectual / developmental disability (IDD)-risk genes (adjusted-$P < 0.05$). Black and red nodes illustrated

in this network diagram represent these 9 3q29 genes and their 284 top neighbors with known SZ, ASD and/or IDD-association, respectively. The union of these prioritized genes constitute 293 genetic drivers predicted to contribute to the neurodevelopmental and psychiatric phenotypes of 3q29Del. The color of network edges that connect node-pairs represents module assignment. **(b)** Top 20 biological processes and pathways with significant enrichment among prioritized drivers (adjusted-$P < 0.05$). The identified Gene Ontology biological processes (GO: BP) and Reactome and KEGG biological pathways point to key mechanisms through which select genes within the 3q29Del locus and their likely partners outside the interval are predicted to influence susceptibility to SZ, ASD, and IDD. **(c)** Organization of all statistically significant biological processes enriched in prioritized drivers into a network of related functional annotation categories. GO:BP terms are connected if they have a high overlap (share many genes); edge width represents magnitude of the overlap**.**

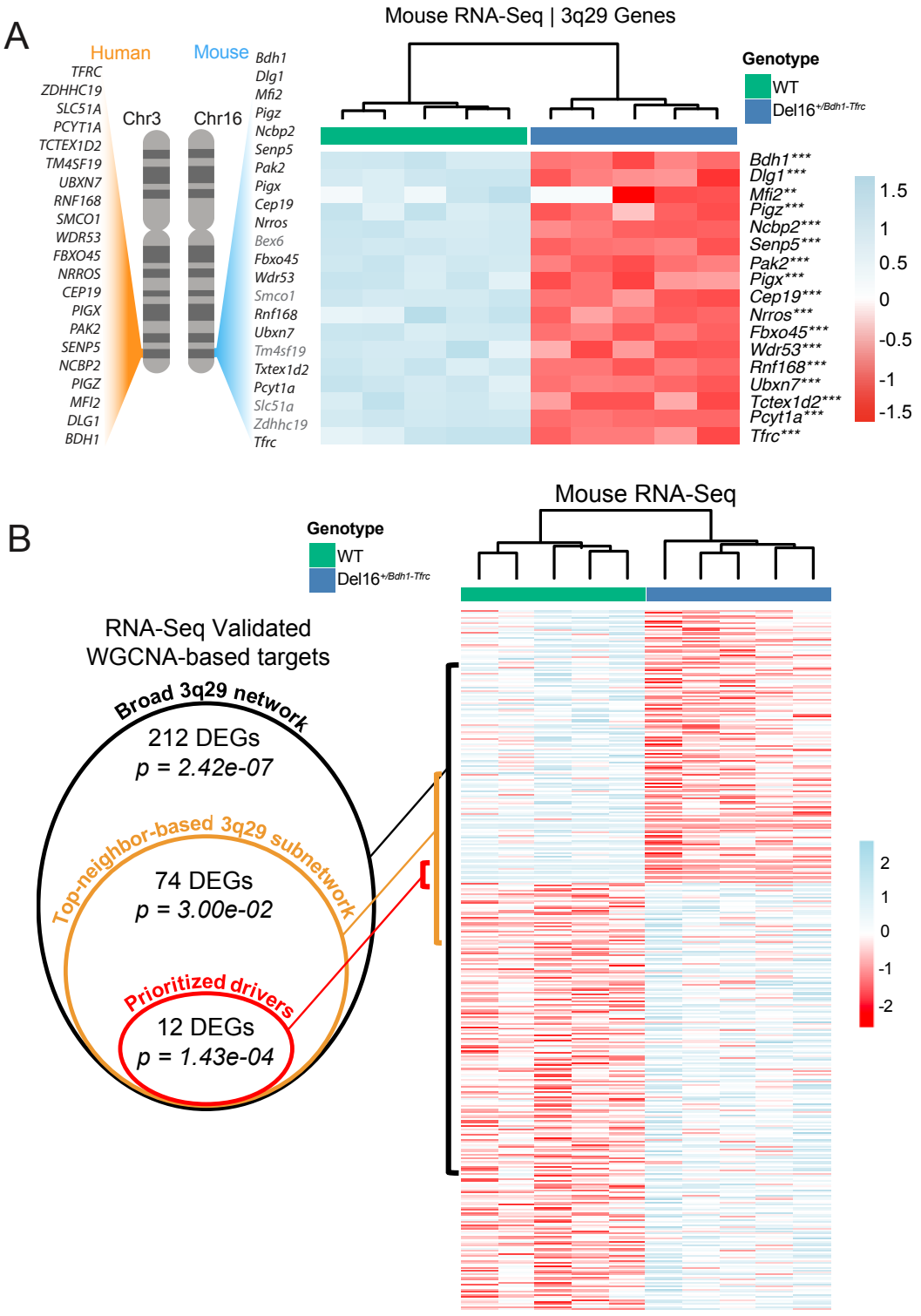

Figure 5. Weighted gene co-expression network analysis (WGCNA) predicts differentially expressed genes in the mouse mode of 3q29Del. (a) Gene-scaled expression of all detected protein-coding genes within the homologous 3q29 interval shows a consistent reduction in Del16$^{+/Bdh1\text{-}Tfrc}$ mice relative to wild-type (WT)

littermates, proportional to gene copy number. Genes in gray were not detected by RNA-Seq. Asterisks indicate level of significance (***$P < 0.0001$, **$P < 0.001$). (**b**) 290 protein-coding genes with known mouse-human homologs were found to be differentially expressed ($P < 0.05$) in Del16$^{+/Bdh1\text{-}Tfrc}$ mice relative to wild-type (WT) littermates. These DEGs were tested for enrichment of genes found in the broad 3q29 network (all genes in 3q29 modules), top-neighbor based 3q29 subnetwork, and disease-associated prioritized drivers. A significant enrichment was found at each level of network interconnectedness ($P < 0.05$). Up-regulated genes are in blue and down-regulated genes are in red.

References

1. Levinson DF, Duan J, Oh S, Wang K, Sanders AR, Shi J, et al. (2011): Copy number variants in schizophrenia: confirmation of five previous findings and new evidence for 3q29 microdeletions and VIPR2 duplications. *Am J Psychiatry*. 168:302-316.

2. Marshall CR, Howrigan DP, Merico D, Thiruvahindrapuram B, Wu W, Greer DS, et al. (2017): Contribution of copy number variants to schizophrenia from a genome-wide study of 41,321 subjects. *Nat Genet*. 49:27-35.

3. Mulle JG, Dodd AF, McGrath JA, Wolyniec PS, Mitchell AA, Shetty AC, et al. (2010): Microdeletions of 3q29 confer high risk for schizophrenia. *Am J Hum Genet*. 87:229-236.

4. Szatkiewicz JP, O'Dushlaine C, Chen G, Chambert K, Moran JL, Neale BM, et al. (2014): Copy number variation in schizophrenia in Sweden. *Mol Psychiatry*. 19:762-773.

5. Mulle JG (2015): The 3q29 deletion confers >40-fold increase in risk for schizophrenia. *Mol Psychiatry*. 20:1028-1029.

6. Sanchez Russo R, Gambello MJ, Murphy MM, Aberizk K, Black E, Burrell TL, et al. (2021): Deep phenotyping in 3q29 deletion syndrome: recommendations for clinical care. *Genet Med*.

7. Glassford MR, Rosenfeld JA, Freedman AA, Zwick ME, Mulle JG, Unique Rare Chromosome Disorder Support G (2016): Novel features of 3q29 deletion syndrome: Results from the 3q29 registry. *Am J Med Genet A*. 170A:999-1006.

8. Cox DM, Butler MG (2015): A clinical case report and literature review of the 3q29 microdeletion syndrome. *Clin Dysmorphol*. 24:89-94.

9. Pollak RM, Murphy MM, Epstein MP, Zwick ME, Klaiman C, Saulnier CA, et al. (2019): Neuropsychiatric phenotypes and a distinct constellation of ASD features in 3q29 deletion syndrome: results from the 3q29 registry. *Mol Autism*. 10:30.

10. Sanders SJ, He X, Willsey AJ, Ercan-Sencicek AG, Samocha KE, Cicek AE, et al. (2015): Insights into Autism Spectrum Disorder Genomic Architecture and Biology from 71 Risk Loci. *Neuron*. 87:1215-1233.

11. Singh MD, Jensen M, Lasser M, Huber E, Yusuff T, Pizzo L, et al. (2020): NCBP2 modulates neurodevelopmental defects of the 3q29 deletion in Drosophila and Xenopus laevis models. *PLoS Genet*. 16:e1008590.

12. Carroll LS, Williams HJ, Walters J, Kirov G, O'Donovan MC, Owen MJ (2011): Mutation screening of the 3q29 microdeletion syndrome candidate genes DLG1 and PAK2 in schizophrenia. *Am J Med Genet B Neuropsychiatr Genet*. 156B:844-849.

13. Gardoni F, Mauceri D, Fiorentini C, Bellone C, Missale C, Cattabeni F, et al. (2003): CaMKII-dependent phosphorylation regulates SAP97/NR2A interaction. *J Biol Chem*. 278:44745-44752.

14. Leonard AS, Davare MA, Horne MC, Garner CC, Hell JW (1998): SAP97 is associated with the alpha-amino-3-hydroxy-5-methylisoxazole-4-propionic acid receptor GluR1 subunit. *J Biol Chem*. 273:19518-19524.

15. Lin EI, Jeyifous O, Green WN (2013): CASK regulates SAP97 conformation and its interactions with AMPA and NMDA receptors. *J Neurosci*. 33:12067-12076.

16. Zhou W, Zhang L, Guoxiang X, Mojsilovic-Petrovic J, Takamaya K, Sattler R, et al. (2008): GluR1 controls dendrite growth through its binding partner, SAP97. *J Neurosci*. 28:10220-10233.

17. Moghaddam B, Javitt D (2012): From revolution to evolution: the glutamate hypothesis of schizophrenia and its implication for treatment. *Neuropsychopharmacology*. 37:4-15.

18. Uezato A, Kimura-Sato J, Yamamoto N, Iijima Y, Kunugi H, Nishikawa T (2012): Further evidence for a male-selective genetic association of synapse-associated protein 97 (SAP97) gene with schizophrenia. *Behav Brain Funct*. 8:2.

19. Uezato A, Yamamoto N, Jitoku D, Haramo E, Hiraaki E, Iwayama Y, et al. (2017): Genetic and molecular risk factors within the newly identified primate-specific exon of the SAP97/DLG1 gene in the 3q29 schizophrenia-associated locus. *Am J Med Genet B Neuropsychiatr Genet*. 174:798-807.

20. Rutkowski TP, Purcell RH, Pollak RM, Grewenow SM, Gafford GM, Malone T, et al. (2019): Behavioral changes and growth deficits in a CRISPR engineered mouse model of the schizophrenia-associated 3q29 deletion. *Mol Psychiatry*.

21. Bokoch GM (2003): Biology of the p21-activated kinases. *Annu Rev Biochem*. 72:743-781.

22. Wang Y, Zeng C, Li J, Zhou Z, Ju X, Xia S, et al. (2018): PAK2 Haploinsufficiency Results in Synaptic Cytoskeleton Impairment and Autism-Related Behavior. *Cell Rep*. 24:2029-2041.

23. Allen KM, Gleeson JG, Bagrodia S, Partington MW, MacMillan JC, Cerione RA, et al. (1998): PAK3 mutation in nonsyndromic X-linked mental retardation. *Nat Genet*. 20:25-30.

24. Tarpey P, Parnau J, Blow M, Woffendin H, Bignell G, Cox C, et al. (2004): Mutations in the DLG3 gene cause nonsyndromic X-linked mental retardation. *Am J Hum Genet*. 75:318-324.

25. Grice SJ, Liu JL, Webber C (2015): Synergistic interactions between Drosophila orthologues of genes spanned by de novo human CNVs support multiple-hit models of autism. *PLoS Genet*. 11:e1004998.

26. Pabis M, Neufeld N, Shav-Tal Y, Neugebauer KM (2010): Binding properties and dynamic localization of an alternative isoform of the cap-binding complex subunit CBP20. *Nucleus*. 1:412-421.

27. Johnson EC, Border R, Melroy-Greif WE, de Leeuw CA, Ehringer MA, Keller MC (2017): No Evidence That Schizophrenia Candidate Genes Are More Associated With Schizophrenia Than Noncandidate Genes. *Biol Psychiatry*. 82:702-708.

28. Eisenberg D, Marcotte EM, Xenarios I, Yeates TO (2000): Protein function in the post-genomic era. *Nature*. 405:823-826.

29. Zhang B, Horvath S (2005): A general framework for weighted gene co-expression network analysis. *Stat Appl Genet Mol Biol*. 4:Article17.

30. Ma'ayan A, Blitzer RD, Iyengar R (2005): Toward predictive models of mammalian cells. *Annu Rev Biophys Biomol Struct*. 34:319-349.

31. Barabasi AL, Gulbahce N, Loscalzo J (2011): Network medicine: a network-based approach to human disease. *Nat Rev Genet*. 12:56-68.

32. Qiu Y, Arbogast T, Lorenzo SM, Li H, Tang SC, Richardson E, et al. (2019): Oligogenic Effects of 16p11.2 Copy-Number Variation on Craniofacial Development. *Cell Rep*. 28:3320-3328 e3324.

33. Singer GA, Lloyd AT, Huminiecki LB, Wolfe KH (2005): Clusters of co-expressed genes in mammalian genomes are conserved by natural selection. *Mol Biol Evol*. 22:767-775.

34. de la Fuente A (2010): From 'differential expression' to 'differential networking' - identification of dysfunctional regulatory networks in diseases. *Trends Genet.* 26:326-333.

35. Wolfe CJ, Kohane IS, Butte AJ (2005): Systematic survey reveals general applicability of "guilt-by-association" within gene coexpression networks. *BMC Bioinformatics.* 6:227.

36. Horan K, Jang C, Bailey-Serres J, Mittler R, Shelton C, Harper JF, et al. (2008): Annotating genes of known and unknown function by large-scale coexpression analysis. *Plant Physiol.* 147:41-57.

37. Ahn AC, Tewari M, Poon CS, Phillips RS (2006): The limits of reductionism in medicine: could systems biology offer an alternative? *PLoS Med.* 3:e208.

38. Oliver S (2000): Guilt-by-association goes global. *Nature.* 403:601-603.

39. Lee HK, Hsu AK, Sajdak J, Qin J, Pavlidis P (2004): Coexpression analysis of human genes across many microarray data sets. *Genome Res.* 14:1085-1094.

40. Moreau Y, Tranchevent LC (2012): Computational tools for prioritizing candidate genes: boosting disease gene discovery. *Nat Rev Genet.* 13:523-536.

41. Oti M, Brunner HG (2007): The modular nature of genetic diseases. *Clin Genet.* 71:1-11.

42. Langfelder P, Horvath S (2008): WGCNA: an R package for weighted correlation network analysis. *BMC Bioinformatics.* 9:559.

43. Radulescu E, Jaffe AE, Straub RE, Chen Q, Shin JH, Hyde TM, et al. (2020): Identification and prioritization of gene sets associated with schizophrenia risk by co-expression network analysis in human brain. *Mol Psychiatry.* 25:791-804.

44. Etemadikhah M, Niazi A, Wetterberg L, Feuk L (2020): Transcriptome analysis of fibroblasts from schizophrenia patients reveals differential expression of schizophrenia-related genes. *Sci Rep.* 10:630.

45. Gordon A, Forsingdal A, Klewe IV, Nielsen J, Didriksen M, Werge T, et al. (2019): Transcriptomic networks implicate neuronal energetic abnormalities in three mouse models harboring autism and schizophrenia-associated mutations. *Mol Psychiatry.*

46. Chen C, Cheng L, Grennan K, Pibiri F, Zhang C, Badner JA, et al. (2013): Two gene co-expression modules differentiate psychotics and controls. *Mol Psychiatry.* 18:1308-1314.

47. Oron O, Getselter D, Shohat S, Reuveni E, Lukic I, Shifman S, et al. (2019): Gene network analysis reveals a role for striatal glutamatergic receptors in dysregulated risk-assessment behavior of autism mouse models. *Transl Psychiatry*. 9:257.

48. Lin M, Pedrosa E, Hrabovsky A, Chen J, Puliafito BR, Gilbert SR, et al. (2016): Integrative transcriptome network analysis of iPSC-derived neurons from schizophrenia and schizoaffective disorder patients with 22q11.2 deletion. *BMC Syst Biol*. 10:105.

49. Brennand K, Savas JN, Kim Y, Tran N, Simone A, Hashimoto-Torii K, et al. (2015): Phenotypic differences in hiPSC NPCs derived from patients with schizophrenia. *Mol Psychiatry*. 20:361-368.

50. Steinberg J, Webber C (2013): The roles of FMRP-regulated genes in autism spectrum disorder: single- and multiple-hit genetic etiologies. *Am J Hum Genet*. 93:825-839.

51. Jalbrzikowski M, Lazaro MT, Gao F, Huang A, Chow C, Geschwind DH, et al. (2015): Transcriptome Profiling of Peripheral Blood in 22q11.2 Deletion Syndrome Reveals Functional Pathways Related to Psychosis and Autism Spectrum Disorder. *PLoS One*. 10:e0132542.

52. Wang P, Zhao D, Lachman HM, Zheng D (2018): Enriched expression of genes associated with autism spectrum disorders in human inhibitory neurons. *Transl Psychiatry*. 8:13.

53. Maschietto M, Tahira AC, Puga R, Lima L, Mariani D, Paulsen Bda S, et al. (2015): Co-expression network of neural-differentiation genes shows specific pattern in schizophrenia. *BMC Med Genomics*. 8:23.

54. Hafner H, Maurer K, Loffler W, Fatkenheuer B, an der Heiden W, Riecher-Rossler A, et al. (1994): The epidemiology of early schizophrenia. Influence of age and gender on onset and early course. *Br J Psychiatry Suppl*.29-38.

55. Howard R, Rabins PV, Seeman MV, Jeste DV (2000): Late-onset schizophrenia and very-late-onset schizophrenia-like psychosis: an international consensus. The International Late-Onset Schizophrenia Group. *Am J Psychiatry*. 157:172-178.

56. Kang HJ, Kawasawa YI, Cheng F, Zhu Y, Xu X, Li M, et al. (2011): Spatio-temporal transcriptome of the human brain. *Nature*. 478:483-489.

57. Fuster JM (2002): Frontal lobe and cognitive development. *J Neurocytol*. 31:373-385.

58. Consortium GT (2015): Human genomics. The Genotype-Tissue Expression (GTEx) pilot analysis: multitissue gene regulation in humans. *Science*. 348:648-660.

59. Leek JT, Johnson WE, Parker HS, Jaffe AE, Storey JD (2012): The sva package for removing batch effects and other unwanted variation in high-throughput experiments. *Bioinformatics*. 28:882-883.

60. Johnson WE, Li C, Rabinovic A (2007): Adjusting batch effects in microarray expression data using empirical Bayes methods. *Biostatistics*. 8:118-127.

61. Wilcox R (1997): *Introduction to Robust Estimation and Hypothesis Testing*. San Diego: Academic Press.

62. Song L, Langfelder P, Horvath S (2012): Comparison of co-expression measures: mutual information, correlation, and model based indices. *BMC Bioinformatics*. 13:328.

63. Barabasi AL, Oltvai ZN (2004): Network biology: understanding the cell's functional organization. *Nat Rev Genet*. 5:101-113.

64. Fu J, Keurentjes JJ, Bouwmeester H, America T, Verstappen FW, Ward JL, et al. (2009): System-wide molecular evidence for phenotypic buffering in Arabidopsis. *Nat Genet*. 41:166-167.

65. Ouma WZ, Pogacar K, Grotewold E (2018): Topological and statistical analyses of gene regulatory networks reveal unifying yet quantitatively different emergent properties. *PLoS Comput Biol*. 14:e1006098.

66. Lachowiec J, Queitsch C, Kliebenstein DJ (2016): Molecular mechanisms governing differential robustness of development and environmental responses in plants. *Ann Bot*. 117:795-809.

67. Yip AM, Horvath S (2007): Gene network interconnectedness and the generalized topological overlap measure. *BMC Bioinformatics*. 8:22.

68. Ravasz E, Somera AL, Mongru DA, Oltvai ZN, Barabasi AL (2002): Hierarchical organization of modularity in metabolic networks. *Science*. 297:1551-1555.

69. Langfelder P, Zhang B, Horvath S (2008): Defining clusters from a hierarchical cluster tree: the Dynamic Tree Cut package for R. *Bioinformatics*. 24:719-720.

70. Horvath S, Dong J (2008): Geometric interpretation of gene coexpression network analysis. *PLoS Comput Biol*. 4:e1000117.

71. BrainSpan Atlas of the Developing Human Brain (2013): Technical white paper: transcriptome profiling by RNA sequencing and exon microarray (v.5).

72. Langfelder P, Luo R, Oldham MC, Horvath S (2011): Is My Network Module Preserved and Reproducible? *Plos Computational Biology*. 7.

73. Reimand J, Isserlin R, Voisin V, Kucera M, Tannus-Lopes C, Rostamianfar A, et al. (2019): Pathway enrichment analysis and visualization of omics data using g:Profiler, GSEA, Cytoscape and EnrichmentMap. *Nat Protoc*. 14:482-517.

74. Luck K, Kim DK, Lambourne L, Spirohn K, Begg BE, Bian W, et al. (2020): A reference map of the human binary protein interactome. *Nature*. 580:402-408.

75. Szklarczyk D, Gable AL, Lyon D, Junge A, Wyder S, Huerta-Cepas J, et al. (2019): STRING v11: protein-protein association networks with increased coverage, supporting functional discovery in genome-wide experimental datasets. *Nucleic Acids Res*. 47:D607-D613.

76. Ala U, Piro RM, Grassi E, Damasco C, Silengo L, Oti M, et al. (2008): Prediction of human disease genes by human-mouse conserved coexpression analysis. *PLoS Comput Biol*. 4:e1000043.

77. Segal E, Friedman N, Koller D, Regev A (2004): A module map showing conditional activity of expression modules in cancer. *Nat Genet*. 36:1090-1098.

78. Torkamani A, Dean B, Schork NJ, Thomas EA (2010): Coexpression network analysis of neural tissue reveals perturbations in developmental processes in schizophrenia. *Genome Res*. 20:403-412.

79. van Dam S, Cordeiro R, Craig T, van Dam J, Wood SH, de Magalhaes JP (2012): GeneFriends: an online co-expression analysis tool to identify novel gene targets for aging and complex diseases. *BMC Genomics*. 13:535.

80. McCarroll SA, Murphy CT, Zou S, Pletcher SD, Chin CS, Jan YN, et al. (2004): Comparing genomic expression patterns across species identifies shared transcriptional profile in aging. *Nat Genet*. 36:197-204.

81. Shen L (2019): GeneOverlap: Test and visualize gene overlaps. R package version 1.20.0 ed.

82. Anders S, Pyl PT, Huber W (2015): HTSeq--a Python framework to work with high-throughput sequencing data. *Bioinformatics*. 31:166-169.

83. Love MI, Huber W, Anders S (2014): Moderated estimation of fold change and dispersion for RNA-seq data with DESeq2. *Genome Biol.* 15:550.

84. Robinson MD, McCarthy DJ, Smyth GK (2010): edgeR: a Bioconductor package for differential expression analysis of digital gene expression data. *Bioinformatics.* 26:139-140.

85. Sayers EW, Beck J, Bolton EE, Bourexis D, Brister JR, Canese K, et al. (2021): Database resources of the National Center for Biotechnology Information. *Nucleic Acids Res.* 49:D10-D17.

86. Langfelder P, Horvath S (2007): Eigengene networks for studying the relationships between co-expression modules. *BMC Syst Biol.* 1:54.

87. Mokhtari R, Lachman HM (2016): The Major Histocompatibility Complex (MHC) in Schizophrenia: A Review. *J Clin Cell Immunol.* 7.

88. Sekar A, Bialas AR, de Rivera H, Davis A, Hammond TR, Kamitaki N, et al. (2016): Schizophrenia risk from complex variation of complement component 4. *Nature.* 530:177-183.

89. Grigoriev A (2003): On the number of protein-protein interactions in the yeast proteome. *Nucleic Acids Res.* 31:4157-4161.

90. Lander ES, Linton LM, Birren B, Nusbaum C, Zody MC, Baldwin J, et al. (2001): Initial sequencing and analysis of the human genome. *Nature.* 409:860-921.

91. Hart GT, Ramani AK, Marcotte EM (2006): How complete are current yeast and human protein-interaction networks? *Genome Biol.* 7:120.

92. Huang H, Jedynak BM, Bader JS (2007): Where have all the interactions gone? Estimating the coverage of two-hybrid protein interaction maps. *PLoS Comput Biol.* 3:e214.

93. Stumpf MP, Thorne T, de Silva E, Stewart R, An HJ, Lappe M, et al. (2008): Estimating the size of the human interactome. *Proc Natl Acad Sci U S A.* 105:6959-6964.

94. Cooper TF, Morby AP, Gunn A, Schneider D (2006): Effect of random and hub gene disruptions on environmental and mutational robustness in Escherichia coli. *BMC Genomics.* 7:237.

95. Yu H, Braun P, Yildirim MA, Lemmens I, Venkatesan K, Sahalie J, et al. (2008): High-quality binary protein interaction map of the yeast interactome network. *Science.* 322:104-110.

96. Alexandru G, Graumann J, Smith GT, Kolawa NJ, Fang R, Deshaies RJ (2008): UBXD7 binds multiple ubiquitin ligases and implicates p97 in HIF1alpha turnover. *Cell.* 134:804-816.

97. Tao S, Liu P, Luo G, Rojo de la Vega M, Chen H, Wu T, et al. (2017): p97 Negatively Regulates NRF2 by Extracting Ubiquitylated NRF2 from the KEAP1-CUL3 E3 Complex. *Mol Cell Biol.* 37.

98. Uhlen M, Fagerberg L, Hallstrom BM, Lindskog C, Oksvold P, Mardinoglu A, et al. (2015): Proteomics. Tissue-based map of the human proteome. *Science.* 347:1260419.

99. Chan SY, Loscalzo J (2012): The emerging paradigm of network medicine in the study of human disease. *Circ Res.* 111:359-374.

100. Fromer M, Roussos P, Sieberts SK, Johnson JS, Kavanagh DH, Perumal TM, et al. (2016): Gene expression elucidates functional impact of polygenic risk for schizophrenia. *Nat Neurosci.* 19:1442-1453.

101. Li J, Cai T, Jiang Y, Chen H, He X, Chen C, et al. (2016): Genes with de novo mutations are shared by four neuropsychiatric disorders discovered from NPdenovo database. *Mol Psychiatry.* 21:290-297.

102. Meng Q, Wang K, Brunetti T, Xia Y, Jiao C, Dai R, et al. (2018): The DGCR5 long noncoding RNA may regulate expression of several schizophrenia-related genes. *Sci Transl Med.* 10.

103. Psych EC, Akbarian S, Liu C, Knowles JA, Vaccarino FM, Farnham PJ, et al. (2015): The PsychENCODE project. *Nat Neurosci.* 18:1707-1712.

104. Schizophrenia Working Group of the Psychiatric Genomics C (2014): Biological insights from 108 schizophrenia-associated genetic loci. *Nature.* 511:421-427.

105. Banerjee-Basu S, Packer A (2010): SFARI Gene: an evolving database for the autism research community. *Dis Model Mech.* 3:133-135.

106. Abrahams BS, Arking DE, Campbell DB, Mefford HC, Morrow EM, Weiss LA, et al. (2013): SFARI Gene 2.0: a community-driven knowledgebase for the autism spectrum disorders (ASDs). *Mol Autism.* 4:36.

107. Deciphering Developmental Disorders S (2017): Prevalence and architecture of de novo mutations in developmental disorders. *Nature.* 542:433-438.

108. Chang D, Nalls MA, Hallgrimsdottir IB, Hunkapiller J, van der Brug M, Cai F, et al. (2017): A meta-analysis of genome-wide association studies identifies 17 new Parkinson's disease risk loci. *Nat Genet*. 49:1511-1516.

109. Kunkle BW, Grenier-Boley B, Sims R, Bis JC, Damotte V, Naj AC, et al. (2019): Genetic meta-analysis of diagnosed Alzheimer's disease identifies new risk loci and implicates Abeta, tau, immunity and lipid processing. *Nat Genet*. 51:414-430.

110. Momozawa Y, Dmitrieva J, Theatre E, Deffontaine V, Rahmouni S, Charloteaux B, et al. (2018): IBD risk loci are enriched in multigenic regulatory modules encompassing putative causative genes. *Nat Commun*. 9:2427.

111. Yengo L, Sidorenko J, Kemper KE, Zheng Z, Wood AR, Weedon MN, et al. (2018): Meta-analysis of genome-wide association studies for height and body mass index in approximately 700000 individuals of European ancestry. *Hum Mol Genet*. 27:3641-3649.

112. Guan J, Cai JJ, Ji G, Sham PC (2019): Commonality in dysregulated expression of gene sets in cortical brains of individuals with autism, schizophrenia, and bipolar disorder. *Transl Psychiatry*. 9:152.

113. Willatt L, Cox J, Barber J, Cabanas ED, Collins A, Donnai D, et al. (2005): 3q29 microdeletion syndrome: clinical and molecular characterization of a new syndrome. *Am J Hum Genet*. 77:154-160.

114. Wachi S, Yoneda K, Wu R (2005): Interactome-transcriptome analysis reveals the high centrality of genes differentially expressed in lung cancer tissues. *Bioinformatics*. 21:4205-4208.

115. Jonsson PF, Bates PA (2006): Global topological features of cancer proteins in the human interactome. *Bioinformatics*. 22:2291-2297.

116. Xu J, Li Y (2006): Discovering disease-genes by topological features in human protein-protein interaction network. *Bioinformatics*. 22:2800-2805.

117. Lek M, Karczewski KJ, Minikel EV, Samocha KE, Banks E, Fennell T, et al. (2016): Analysis of protein-coding genetic variation in 60,706 humans. *Nature*. 536:285-291.

118. O'Roak BJ, Vives L, Girirajan S, Karakoc E, Krumm N, Coe BP, et al. (2012): Sporadic autism exomes reveal a highly interconnected protein network of de novo mutations. *Nature*. 485:246-250.

119. Luza S, Opazo CM, Bousman CA, Pantelis C, Bush AI, Everall IP (2020): The ubiquitin proteasome system and schizophrenia. *Lancet Psychiatry*. 7:528-537.

120. Semple BD, Blomgren K, Gimlin K, Ferriero DM, Noble-Haeusslein LJ (2013): Brain development in rodents and humans: Identifying benchmarks of maturation and vulnerability to injury across species. *Prog Neurobiol*. 106-107:1-16.

121. Pollak RM, Zinsmeister MC, Murphy MM, Zwick ME, Emory 3q P, Mulle JG (2020): New phenotypes associated with 3q29 duplication syndrome: Results from the 3q29 registry. *Am J Med Genet A*. 182:1152-1166.

122. Golzio C, Katsanis N (2013): Genetic architecture of reciprocal CNVs. *Curr Opin Genet Dev*. 23:240-248.

Supplemental Materials

Extended Methods

Overview

For this analysis, we selected the most appropriate publicly available transcriptomic dataset and cleaned and processed the data before constructing an unsupervised gene co-expression network that can group functionally correlated genes into modules (1). Genes participating in the same molecular and biological pathways tend to show correlated expression (co-expression) with each other, as they are expressed under the control of a coordinated transcriptional regulatory system (2). Constructed on this principle, the transcriptomic network identified in this study amounts to a systems-level representation of gene-gene relationships in the healthy adult human prefrontal cortex (PFC), providing novel insights into network-level operations of understudied genes located in the recurrent 3q29 deletion (3q29Del) locus.

Given the strong genetic link between 3q29Del and risk for schizophrenia spectrum disorders (SZ; estimated odds ratio >40) (3), we placed our focus on revealing the co-regulation patterns of 3q29 interval genes as a function of their expression similarity during adulthood. This is a period when SZ typically manifests itself diagnostically, with peak onset in late adolescence (age 18-20 years) and early adulthood (age 20 to 40 years) (4), and a substantial proportion of patients becoming ill during middle adulthood (age 40 to 60 years) (5). We also focused our analysis on uncovering gene-gene relationships in the PFC: a brain region that subserves a diverse range of cognitive and emotional operations, is implicated in the etiology of SZ and may be particularly vulnerable to the effects of genetic disruption due to its protracted development (6). To validate the reproducibility of this transcriptomic network, we used an independent test dataset that was demographically comparable to our reference dataset and assessed the preservation (i.e., how well-defined modules are in an independent test dataset) of each identified network module by permutation tests. Using a similar approach, we also assessed the quality (i.e., how well-defined modules are relative to the background) of each network module in repeated random splits of our reference dataset.

We next identified and interrogated the modules that were found to harbor at least one 3q29 interval gene for (1) functional enrichment, (2) higher-level organization into meta-modules, (3) highly connected "hub"

genes and (4) "top" network neighbors of 3q29 interval genes. To generate testable hypotheses about which 3q29 interval genes may be causally linked to the major neuropsychiatric phenotypes of 3q29Del, we tested whether the top network neighbors of individual 3q29 interval genes show significant overrepresentation of known risk genes for SZ, or for two other clinical phenotypes associated with 3q29Del: autism spectrum disorders (ASD) and intellectual / developmental disability (IDD) ASD and IDD share genetic risk and pathogenic mechanisms with SZ, despite differences in the timing of clinical symptoms (7). Based on the identified enrichment patterns, we developed a list of "prioritized driver genes", consisting of select 3q29 interval genes and their tightly correlated SZ, ASD and IDD-associated top network neighbors, which were subsequently found to converge onto canonical biological pathways.

We predict that dysregulation of these prioritized molecular targets, including a hub gene within the 3q29 interval, and their associated biological pathways may be implicated in the neuropsychiatric phenotype in 3q29Del syndrome. Overall, our findings highlight the advantage to using unbiased systems approaches that integrate gene-level information into a higher-order, network-level framework to infer gene function, particularly for understudied genes with disease relevance. The molecular pathways and the prioritized gene-set identified in this study will inform new directions of neurobiological inquiry that can mechanistically connect 3q29Del with severe mental illness. Our approach also highlights the study of normal function in non-pathological post-mortem tissue to further our understanding of psychiatric genetics, especially for rare genetic syndromes like 3q29Del, where access to post-mortem neural tissue from carriers is unavailable or limited. The steps described in this overview are described in detail below.

Weighted gene co-expression network analysis (WGCNA)

Samples used for network construction: To interrogate the functional consequences of the 3q29Del at the individual gene level, we employed unbiased weighted gene co-expression network analysis (WGCNA package (1, 8) in R, version 1.68) and organized the adult human cortical transcriptome into clusters (modules) of highly correlated genes (nodes). The network was constructed on publicly available RNA-Seq data obtained from the Genotype Tissue Expression Project (GTEx) (9) (Fig. S1), the largest multi-tissue open-data initiative using

postmortem samples from human donors. 113 non-pathological post-mortem samples from the PFC (Brodmann Area 9) of male and female adults (age range = 20-79) with no known history of psychiatric or neurological disorder were included in this study. Transcriptome profiling was performed using Illumina TruSeq RNA sequencing as described in GTEx Consortium et al. (2013, 2015) (9). The GTEx data (release version 6) used for the analyses described in this manuscript were downloaded from the GTEx portal (http://www.gtexportal.org/home/datasets/) on 01/08/2019; the corresponding dbGaP study accession number is phs000424.v6.p1.

Data cleaning: Six outlier samples were removed from the original dataset prior to network construction to prevent an outlier-driven bias in network structure and module detection (Fig. S2). Inter-sample correlation (ISC) was used as an unbiased statistical diagnostic for identifying outliers with divergent gene expression profiles, defined as the Pearson's correlation between pairs of samples across the expression levels of all detected genes. Samples with a mean ISC greater than two standard deviations away from the mean of the sample-set were flagged as outliers and removed (as described in (10)), reducing the sample size to 107. Details on sample attributes and donor phenotypes are available in Fig. S1.

Protein-coding genes were extracted from the dataset based on GENCODE v19 annotations for gene-type (11), followed by $\log_2$ transformation of gene expression values. For genes indexed by multiple splice variants, the data were further pre-processed to limit the transcriptome to a single transcript per gene. This step was conducted by using the *collapseRows* function of the WGCNA package in R (method = MaxMean), that identifies the transcript with fewest number of missing values and highest mean expression value across samples (12). We limit the scope of this study to protein-coding genes with expression profiles summarized at the gene-level, in light of previously demonstrated drawbacks of isoform-level networks encompassing the non-coding transcriptome (13). Inclusion of splice variants and non-coding RNAs increases network size by 100-fold (13), which in turn dramatically increases the computational resources necessary for network analysis. Although this high computational demand can theoretically be overcome by using a block-wise design where automatically selected subsets of the original data are used to build a co-expression network in a block-by-block fashion (1), previous work has shown that networks generated by block-wise design reflect only an approximation of

networks generated by single-block design, which negatively influences the accuracy of subsequent module detection (13). To avoid the shortcomings of a block-wise approach and pursue the most parsimonious hypothesis, our dataset included only protein-coding genes, with expression values summarized at the gene-level. This approach yielded a trimmed protein-coding gene expression matrix of 18,410 unique HGNC gene symbols.

To remove non-biological experimental variation, the dataset was adjusted for known batch effect (nucleic acid isolation batch) using the empirical Bayes framework employed by the *ComBat* function of the Surrogate Variable Analysis (SVA) package in R (14) (as described in (15)). The gene expression data were further corrected for age, sex, death classification (assessed by the 4-point Hardy Scale) and post-mortem interval (PMI)-mediated covariance (16), added to the regression model as categorical or continuous variables as applicable (Fig. 1B, Fig. S1). The residuals calculated from this model were carried to downstream analysis. Finally, since low-expressed or non-varying genes usually represent noise in the data, we used the *goodSamplesGenes* function of the WGCNA package in R to iteratively identify and remove genes and samples with greater than 50% missing entries (default parameter) and genes with zero variance. The normalized, outlier-removed, residualized cortical expression values of 18,410 protein-coding genes from 107 samples constitute the final dataset for construction of the network.

Network construction and module detection: The single-block pipeline implemented in the WGCNA R package was employed to build a signed and weighted gene co-expression network using the final dataset. Co-expression similarity was defined as the biweight midcorrelation (bicor) coefficient between the expression profiles of gene-pairs calculated for all possible comparisons. Bicor is a median-based measure of co-expression that was chosen as a robust alternative to mean-based similarity metrics (i.e., Pearson correlation) in evaluating similarity in gene expression (17). To capture the continuous nature of pairwise interactions in biological systems and accentuate strong positive correlations, the resulting co-expression similarity matrix was transformed into a signed and weighted adjacency matrix. This step was conducted by using the soft-thresholding procedure implemented in the *pickSoftThreshold* and *scaleFreePlot* functions of the WGCNA package in R. A soft-thresholding power (β) of 8 was identified as the lowest possible β yielding a power-law degree

distribution that approximately fits one with a scale-free network topology, (signed R^2 fit index = 0.8), while maintaining a relatively high mean connectivity (mean k > 100) (Fig. 1C, Fig. S3). The rationale behind our choice to establish a scale-free topology is the demonstrated biological relevance of its degree distribution as a unifying property of many biological networks in nature, where a few hub nodes have many connections while most nodes have few connections (18-21). Additionally, note that a demonstrated advantage of weighted correlation networks is the high robustness of the network construction to the choice of β parameter (22).

A signed adjacency matrix (Equation 1) was chosen over an unsigned adjacency matrix (Equation 2) to re-scale the underlying pairwise correlations from the [−1, 1] interval to the [0, 1] interval, as opposed to treating negative correlations as positive. In other words, since the adjacency matrix that underlies network construction is always non-negative, a signed network was chosen to respect the direction (up vs. down) of the co-expression relationships to prevent a clustering structure that mixes negatively correlated nodes, which often belong to different biological categories, with positively correlated nodes. The biological relevance of signed adjacency was demonstrated by previous work indicating that genes showing positive transcriptional correlation are more likely to exhibit known protein-protein interactions than uncorrelated or negatively correlated genes (10, 23, 24). This approach is further supported by the recommendations of the creators of the WGCNA package in R (as described in https://peterlangfelder.com/ 2018/11/25/signed-or-unsigned-which-network-type-is-preferable/).

Signed adjacency A_{ij}^{signed} for genes i and j is defined as:

$$A_{ij}^{signed} = \left|\frac{1+bicor\,(x_i,x_j)}{2}\right|^{\beta} \qquad (1)$$

Unsigned adjacency $A_{ij}^{unsigned}$ for genes i and j is defined as:

$$A_{ij}^{unsigned} = \left|bicor\,(x_i,x_j)\right|^{\beta} \qquad (2)$$

The resulting signed and weighted adjacency matrix was transformed into a topological overlap (TO) matrix to capture not only the correlation between pairs of genes but also the connections among

"neighborhoods" of genes (25, 26). The TO measure (TOM) between two genes is high if the genes have many overlapping network connections, yielding a network interconnectedness measure that is proportional to the number of common neighbors shared between a pair of nodes. Several studies have shown that gene/protein-pairs with higher TO are more likely to play a role in the same functional class than gene/protein-pairs with lower TO (26-31), demonstrating that TOM yields biologically meaningful modules that can successfully capture the co-expression profile of genes encoding interacting proteins. Additionally, TOM was shown by previous work to be more robust to identifying spurious connections than pairwise correlation alone (32).

To explore the clustering structure of the nodes underlying our undirected network, we conducted average linkage hierarchical clustering on pairwise TOM, following its transformation into a dissimilarity measure (dissTOM = 1-TOM). To define network modules, we adaptively pruned the branches of the resulting dendrogram by using the dynamic-hybrid-tree-cut algorithm of the WGCNA package in R (Fig. 1D). This method employs a bottom-up approach that considers the shape of dendrogram branches in identifying clusters, yielding improved detection of outlying cluster members. This method was chosen, since it has been shown to outperform the traditional fixed-height branch cutting method for identifying biologically meaningful clusters, particularly in networks that exhibit a nested dendrogram structure (33). Standard parameters were used to conduct this analysis: cut height = 99% of the truncated height range in the dendrogram, module detection sensitivity (deep split) = 2, minimum module size = 30, signed network with partitioning about medoids (PAM) respecting the dendrogram. To avoid over-clustering, we set the smallest number of genes that can be considered a module (minimum module size) to 30; this is a standard parameter used in the literature to establish a compromise between large modules that are robust and biologically informative and small modules that are possibly informative but less robust (34-36). This approach yielded 31 modules, with module-sizes ranging from 43 to 3,319 genes; similar ranges have been reported in other applications.

We summarized the gene expression profiles of individual modules by eigengenes (1), identified as the first principal component of the expression data in a given module. Construction of eigengenes amounts to a network-based data reduction method that serves as a means to effectively correlate entire modules. Leveraging this approach, we amalgamated modules with very similar expression profiles to eliminate spurious assignment

of highly co-expressed genes into separate modules. To this end, we conducted average linkage hierarchical clustering of module eigengenes (ME) on a correlation-based dissimilarity metric (1-pairwise Pearson's correlation between MEs) and merged modules that are strongly correlated ($r > 0.8$ corresponding to cut height = 0.2) (Fig. 1D).

One of the resulting modules (grey module) was reserved for genes that could not be unequivocally assigned to any module (did not share similar co-expression patterns with the other genes of the network), as determined by the iterative refinement methodology used in our analysis pipeline to improve module detection. Therefore, the grey module was excluded from downstream analysis. Finally, we tested additional WGCNA parameters and determined that basic module structure in modules of interest (modules harboring 3q29 interval genes) was identifiable under variations of carefully selected algorithm parameters.

Module preservation and quality analysis

To validate the reproducibility of our identified modules, we evaluated network preservation in an independent transcriptomic dataset, hereafter referred to as the test dataset/network. Publicly available RNA-Seq data from the BrainSpan Developmental Transcriptome Project (37) was used to build the test network (Fig. S4). 30 non-pathological post-mortem samples from the PFC of male and female adults (age range = 18-37) with no known neurological or psychiatric disorder were used in this study. To exclude any confounding pathology, specimens had been confirmed by neuropathological evaluation to not contain obvious malformations, extensive neuronal loss, neuronal swelling, or dysmorphic neurons and neurites. Additionally, any donor with a reported prolonged agonal condition (i.e., coma, hypoxia, seizures etc.), ingestion of neurotoxic substances at the time of death, suicide, severe head injury, significant hemorrhages, prominent vascular abnormalities, tumors, prominent brain lesions, stroke, congenital neural abnormalities, and signs of neurodegeneration (i.e., amyloid plaques, Lewy bodies etc.) were also excluded (see technical white paper (38)). Transcriptome profiling was performed using Illumina TruSeq RNA sequencing. Details on sample attributes and donor phenotypes are available in Fig. S4. The BrainSpan data (Developmental Transcriptome Dataset; v10 summarized to genes) used for the analyses described in this manuscript were downloaded from the Allen

Brain Atlas portal (https://www.brainspan.org/ static/download/) on 01/12/2019; the corresponding dbGaP study accession number is phs000755.v2.p1.

The test dataset was pre-processed following the same pipeline used for the GTEx reference dataset. We were unable to correct the normalized gene expression values of the test dataset for batch effect and death classification-mediated covariance, due to absence of the pertinent information from publicly available data. However, we note that the highly selective inclusion/exclusion criteria used by the BrainSpan project for tissue qualification (37) mitigates a potential confounding effect of death classification on gene expression. The inclusion of age, sex and PMI in the regression model was consistent with the pre-processing pipeline applied to the reference dataset. No outlier sample was identified by the above described ISC method. Notably, the test dataset was assembled by the aggregation of transcriptomic data from four sub-regions of the PFC (orbital, dorsolateral, ventrolateral, and medial PFC). To rule out a potential bias in test network construction driven by tissue-type, we conducted average linkage hierarchical clustering on the BrainSpan samples used in this study. The similarity metric for clustering was defined as the Pearson's correlation between gene expression levels of pairs of samples. The resulting dendrogram revealed no clustering pattern driven by tissue-type, ruling out PFC sub-region as a factor that could bias network construction (Fig. S4). Upon completion of pre-processing, the test dataset consisted of normalized and residualized gene expression values for 18,339 unique HGNC symbols from 30 samples.

To determine whether properties of within-module topology that were identified in our reference network were preserved in the test network, we calculated a composite network-based preservation statistic ($Z_{summary.pres}$) (39) for each module by using the *modulePreservation* function of the WGCNA package in R. $Z_{summary.pres}$ is a summary statistic that encompasses multiple density-based and connectivity-based preservation statistics that test 1) whether nodes sharing the same module in the reference network remain highly connected in the test network (i.e., are groups of genes defined as modules in the reference network denser than random groups of genes in the test network?) and 2) whether connectivity patterns between nodes underlying the reference network remain similar in the test network (i.e., do hub nodes of the reference network preserve their high degree of connectivity in the test network?). To determine whether the observed preservation statistics

were higher than expected by chance and to derive a standardized Z score for each preservation statistic, we randomly permuted the module assignments in the test data (number of permutations = 200; twice as high as default) and derived a $Z_{summary.pres}$ score for each module. The resulting scores were evaluated according to established thresholds (39): $Z_{summary.pres} < 2$ indicates no evidence for preservation, $2 < Z_{summary.pres} < 10$ indicates moderate evidence for preservation, and $Z_{summary.pres} > 10$ indicates strong evidence for preservation. To account for the dependence of the $Z_{summary.pres}$ score and permutation test p-values on module-size, we set the maximum module-size parameter of the *modulePreservation* function to 1000 genes (default parameter), reducing large modules by randomly sampling 1000 intra-modular nodes. Note that the specific goal of this preservation analysis was to determine the preservation strength of individual modules in relation to established $Z_{summary.pres}$ score thresholds, as opposed to comparing the preservation statistics of modules with different sizes to one another (i.e., determine whether module A is more preserved than module B). Hence, aggregating multiple preservation statistics into an informative $Z_{summary.pres}$ score constitutes a valid and advantageous approach for our purposes, despite its sensitivity to module-size.

In addition to measuring the density and connectivity-based preservation of each module between the reference and test networks, we measured the quality of the identified modules in the reference network without a reference to the test network. The goal of this analysis was to assess the robustness of the identified modules (i.e., how distinct is a given module from other modules in the reference network?) by calculating a composite quality statistic ($Z_{summary.qual}$) (39) for each module, as implemented in the *modulePreservation* function of the WGCNA package in R. This approach is akin to a cluster stability analysis (40) and employs a resampling technique that applies the module preservation statistics outlined above to repeated random splits of the reference data. The resulting $Z_{summary.qual}$ score indicates the robustness of a given module definition (hence the parameters selected for network construction and module detection) across networks created from the original reference data. The same $Z_{summary.pres}$ thresholds outlined above were used to evaluate the $Z_{summary.qual}$ scores. Finally, in line with the recommendations (39) of the creators of the WGCNA package, we also evaluated the individual preservation and quality statistics underlying the composite scores for each module (Fig. S5). Results from the module preservation and quality analysis (Fig. 1E) revealed the replicable and robust nature of the

network, thus we commenced interrogation of the network for insights into 3q29 interval gene function.

Functional characterization of network modules harboring 3q29 genes

Understanding the functions of the 21 protein-coding genes hemizygously deleted in 3q29Del syndrome is an obligatory step towards gaining insights into the cellular mechanisms underlying disease etiology. Others have shown that each gene of the human genome is estimated on average to be involved in ten biological functions (41). Given that many of the genes in the 3q29Del interval are poorly annotated and some lack a functional annotation altogether (Fig. S6), we leveraged the transcriptomic co-expression approach to predict gene function. We screened each network module for membership of 3q29 interval genes and exploited major biological databases to derive a functional interpretation of the co-expression modules found to harbor at least one 3q29 interval gene (hereafter referred to as a 3q29 module).

Functional enrichment analyses of individual 3q29 modules (transformed into gene-sets) were run on the g:Profiler webserver (http://biit.cs.ut.ee/gprofiler; Ensembl version 96, Ensembl Genomes version 43) by using gene ontology biological processes (GO:BP), and Reactome (REACT) and Kyoto Encyclopedia of Genes and Genomes (KEGG) biological pathways. For high-confidence analysis, electronic GO annotations ("IEA"), which are assigned to gene products without curator verification (majority inferred *in silico*) and often cannot be traced to an experimental source, were discarded; filtering GO annotations based on evidence code has been recommended in previous literature to avoid erroneous results (42). The statistical domain scope for functional enrichment analysis was set to only genes with at least one known annotation (default parameter) to establish an effective genomic background for statistical testing using the hypergeometric probability function. Enriched terms surpassing the adjusted g:SCS significance threshold of $P < 0.05$ were filtered for gene-set size (allowed range: 10-2,000 genes) and semantic similarity to improve the specificity and interpretability of our results (43). The g:SCS (Set Counts and Sizes) method for multiple comparisons correction was our method of choice for pathway analysis, since it was shown to outperform standard approaches, such as Bonferroni correction, in estimating the true effect of multiple testing over the complex structure of functional profiling data (44). Functional classifications in databases such as gene ontology (GO) have a heavily overlapping hierarchical

structure, since any term is automatically related to all other terms included in its relational path. Hence, statistical assumptions underlying more traditional correction methods such as Bonferroni, which was designed for multiple independent tests, cannot be met in our application. Hence, we used the novel g:SCS method (refer to (43) for details) as an alternative solution to the multiple testing problem that is highly complex in functional data. Note that the g:Profiler software that was used to perform pathway analyses in this study also implements the g:SCS significance thresholds by default. The REVIGO webtool (http://revigo.irb.hr/) was used to reduce redundancy in the identified GO terms (default semantic similarity measure = SimRel, allowed similarity = 0.9 (large)) (45). Top 10 biological pathways (REACT) found to be enriched in individual 3q29 modules were ranked by statistical significance level (adjusted $P < 0.05$) and are shown in the main results.

Furthermore, findings of the functional enrichment analysis were also evaluated to determine whether identified co-expression modules reflect true biological signals as opposed to noise; this distinction was inferred by enrichment of the constituent genes for known biological processes and pathways. Our gene ontology-based approach complemented the module quality analysis described above.

To further interrogate whether the gene co-expression modules identified in this study represent biologically meaningful units of nodes with shared membership of the same molecular complex or functional pathway, we also investigated whether the genes co-clustering in the same transcriptomic module tend to interact at the protein level. First, we queried the known protein interactors of 3q29 interval genes identified by the Human Reference Protein Interactome Mapping Project (HuRI; http:/interactome-atlas.org/). The interaction data in HuRI were retrieved from two sources: 1) a systematic binary mapping pipeline using a high-throughput yeast two-hybrid assay, followed by retesting and validation, and 2) interactions curated from the literature and further filtered by HuRI to identify high-quality binary interactions (see details in (46)).

Second, we tested the co-expression modules harboring 3q29 interval genes for enrichment of known and predicted protein-protein interactions (PPIs) from the STRING database (v.11, https://string-db.org/). Using the STRING search tool, PPIs were retrieved from active interaction sources (species: "Homo sapiens"), including experiments (biochemical data), databases (previously curated pathway and protein-complex knowledge), genomic context prediction channels (neighborhood, fusion, gene co-occurrence), and text mining.

Interactions that rely on STRING's RNA-seq co-expression inference pipeline were excluded from this analysis. A minimum interaction confidence score of 0.4 (medium confidence, default setting) was applied to construct a PPI network for each module; this interaction score represents the approximate confidence of an association based on all available evidence from active sources. The STRING enrichment analysis tool was used to test whether the observed number of interactions (edges) in each interrogated module was significantly higher than the number of edges expected if the nodes were to be selected from the genome at random (see details in (47)). STRING enforces an upper limit on the number of query items and does not support the PPI network enrichment analysis of > 2,000 nodes. Hence, 2,000 genes from the green and turquoise modules, which harbor 4,746 and 3,319 genes respectively, were randomly subsampled without replacement, using the *sample* function in R (v. 4.0.3). The 3q29 interval genes clustering in each of these two modules were used as forced entries during this subsampling procedure to ensure that each resulting PPI subnetwork included our primary genes of interest.

Identification of meta-modules harboring 3q29 genes

Several studies have demonstrated that individual modules can be organized into biologically meaningful meta-modules that represent a higher-order organization of the transcriptome (48), likely reflecting pathway dependencies and synergistic function. To evaluate whether individual 3q29 modules clustered together within larger meta-modules of the co-expression network, we investigated the relationship among modules by leveraging their eigengenes (ME). We calculated the Pearson's correlations between all pairs of MEs and used this similarity metric to conduct average linkage hierarchical clustering of the MEs. Consistent with its use in other applications, we defined meta-modules as tight clusters of positively correlated MEs detectable as major branches of the resulting eigengene dendrogram (48). The identified meta-modules were screened to identify the grouping patterns among 3q29 modules across the co-expression network.

This eigengene-based network reduction framework was further utilized to determine whether individual 3q29 modules that were found to partake in larger meta-modules were truly distinct from each other. To this end, gene ontology information was leveraged to identify common versus distinct enrichment of

biological processes and pathways in individual 3q29 modules sharing a meta-module. This approach also complemented the module quality analysis described above.

Determination of module membership strength for 3q29 genes

To measure how strongly connected individual 3q29 genes are to their assigned modules, we used the *signedKME* function of the WGCNA package in R to calculate a module membership measure (kME) for each 3q29 gene. kME is an eigengene-based module connectivity measure, defined as the Pearson's correlation between the expression profile of a given gene and the eigengene (first principal component) of a given module(1). An advantage of using kME as a network connectivity metric is that it allows the direct comparison of module membership values across modules that differ in size. This property distinguishes kME from degree-based measures of module connectivity, which are derived by summing a node's *total* number and strength of *connections* within a module and result in a metric that can be biased by module size.

A kME of 0 indicates that a gene is uncorrelated with an ME of interest and is thus unlikely to be a member of that module. In contrast, kME > 0.8 describes a hub gene that is highly connected to other genes in its module, hence predicted to be a crucial component of the overall function of that module. Previous work has shown that targeted disruption of a hub gene has a more deleterious effect on the ability of the network to function and leads to a larger number of phenotypic outcomes than the disruption of randomly selected genes or targeted deletion of less connected genes (49, 50). These observations have led to the hypothesis that hub nodes of biological networks are typically associated with human disease genes. Indeed, several lines of evidence, particularly from cancer biology, have validated this hypothesis (51, 52). One study has shown that topological features of disease-genes identified from OMIM's Morbid Map of the Human Genome disproportionately exhibit hub-gene characteristics, with protein products participating in more known protein-protein interactions than that of non-disease genes(53)

Note that there is no established definition of a hub node in network analysis, since the selection criteria can vary depending on the sparsity of the network; examples of hub gene definitions based on kME ≥ 0.7 exist in the literature. To generate rigorous WGCNA-based predictions, we adopted a conservative criterion that

defines hub genes as nodes with kME > 0.8 ($P < 0.05$), a stringent threshold used by several other studies (54-56). We annotated 3q29 interval genes that surpassed this kME threshold as hub genes, whose loss of function is predicted to produce a highly deleterious impact on the system.

Additionally, we screened kME values to identify 3q29 genes with very weak module membership. Given that kME quantifies how close a gene is to its assigned cluster of co-expressed genes, we excluded 3q29 genes with non-significant kMEs ($P > 0.05$) from downstream analysis. Notably, we limited our evaluations to intra-modular kME values that describe a gene's correlation with the eigengene of its assigned module. In rare instances, the kME of a given gene was found to be slightly higher for a module other than its assigned module. This finding stems from the fact that TOM yields a measure of network interconnectedness that is similar but not identical to an only correlation-based approach (as described by the creators of the WGCNA package at https://support.bioconductor.org/p/101579/). As noted previously, TOM-based similarity was shown to outperform correlation-based similarity in identifying biologically meaningful modules (32).

Identification of prioritized driver genes

3q29Del confers >40-fold increased risk for SZ and constitutes a shared risk factor for IDD and ASD. However, no single gene in this interval has been definitively associated with SZ, IDD, or ASD. To generate testable hypotheses about which 3q29 interval genes are causally linked to the major neuropsychiatric phenotypes associated with 3q29Del, we further leveraged our gene co-expression network. We adopted the guilt-by-association approach and screened the intra-modular subnetworks of individual 3q29 interval genes for a significant overlap with known SZ, ASD and IDD-risk genes. Guilt-by-association is a widely used principle that operates on the assumption that disease-associated genes are more closely connected to each other than random pairs of nodes in a network. Ample evidence demonstrates the high utility of the guilt-by-association approach in identifying novel disease risk genes (57-61).

Previous work has shown that testing the overrepresentation of known disease-risk genes in entire network modules harboring a large number of genes produces an inflated false positive rate(13). To avoid this, we reduced 3q29 modules to top-neighbor-based subnetworks, maintaining only the close intra-modular

connections of individual 3q29 genes. A top neighbor was defined as any node whose gene expression profile has a moderate-to-high correlation (Spearman's rho (ϱ) $\geq$ 0.5) with a given 3q29 interval gene (considered a "seed" node) within the same module. Note that top neighbors were identified by a correlation-based hard-thresholding method applied only to intra-modular edges connecting seed-node pairs. Hence, the criterion for top neighbor identification combines the strength of scale free-topology and topological overlap principles of WGCNA for network construction and module detection, with subsequent application of a selective hard-thresholding method, resulting in a binary classification of top neighbors predicted to form direct functional links with 3q29 interval genes.

We conducted hypergeometric tests to determine whether top-neighbor-based intra-modular subnetworks of individual 3q29 genes are enriched for curated gene-sets with known SZ, ASD or IDD association. Six gene-sets were curated for this purpose from the following sources: 1) 93 IDD-risk genes enriched for damaging *de novo* mutations, identified by the Deciphering Developmental Disorders Study (62); 2) 86 ASD-risk genes categorized by the Simons Foundation Autism Research Initiative (SFARI) (63, 64) as "high-confidence candidate risk genes" with strong evidence for ASD association (categories = 1 & 2; downloaded on 2/15/2019 from https://gene.sfari.org/database/); 3) 651 SZ-related genes shown by Meng et al. (2018) (65) to demonstrate significant differential expression in the postmortem brain tissue of SZ cases/controls, identified from the PsychENCODE BrainGVEX dataset (66); 4) 636 SZ-related genes shown by Fromer et al. (2016) to demonstrate significant differential expression in the postmortem dorsolateral PFC tissue of SZ cases/controls, identified from the CommonMind Consortium dataset (67), 5) 340 SZ-risk genes adjacent to SZ-associated genetic loci, identified by the most recent genome-wide association study (GWAS) (68) conducted by the Psychiatric Genomics Consortium (PGC); 6) 290 SZ-risk genes with exonic *de novo* mutations, identified via the Neuropsychiatric Disorder *De Novo* Mutations Database (69) (downloaded on 2/17/2019 from http://www.wzgenomics.cn/NPdenovo/). Notably, these gene-sets were selectively curated from the literature to obtain a comprehensive yet reliable list of reported IDD, ASD and SZ-associated genetic variants spanning a wide range of the allele frequency spectrum. As noted previously, 3q29 genes with non-significant intra-modular kMEs ($P > 0.05$) (Fig. 2C) were excluded from this analysis.

To evaluate the specificity of the investigated disease enrichment patterns, we also tested the significance of the overlap between 3q29 subnetworks and negative control gene-sets associated with Parkinson's disease (PD), late-onset Alzheimer's disease (AD) and inflammatory bowel disease (IBD). The gene lists for these conditions were considered "negative controls," as they constitute disease phenotypes (two related and one unrelated to brain health) with no known association to 3q29Del. To rule out a potential bias that could be introduced to our enrichment analysis by differences in the sizes of curated gene-sets, common genetic variants associated with height (large gene-set size comparable to several SZ gene-set sizes) were included as another negative control. Four negative control gene-sets were curated for this purpose from the following sources: 1) 25 AD-risk genes identified by the largest published GWAS meta-analysis conducted by the Genetic and Environmental Risk in AD/Defining Genetic, Polygenic and Environmental Risk for AD Consortium (GERAD/PERADES) (70); 2) 67 PD-risk genes identified by the largest published GWAS meta-analysis conducted by the International PD Genomics Consortium (71); 3) 98 IBD-related genes identified by the International IBD Genetics Consortium as "strong positional candidate genes" in GWAS-identified risk loci (72); 4) 479 height-associated genes identified by the largest published GWAS meta-analysis conducted by the Genetic Investigation of Anthropometric Traits Consortium (GIANT) (73).

To accurately measure the union-size of the possible matches between the curated gene-sets and WGCNA-derived 3q29 subnetworks, genes that could only be present in one set (non-protein-coding genes; gene-type annotated by GENCODE v19) were excluded from the overlap analysis, yielding the final gene-set sizes listed above. Discrepancies in gene alias usage were accounted for to ensure consistency in nomenclature. The background list for the hypergeometric test was determined as the total number of unique genes used to conduct WGCNA. The *GeneOverlap* package(74) in R (version 1.20.0) was used for this analysis. The hypergeometric p-values obtained by overlap analysis were corrected for multiple testing using Benjamini-Hochberg (n = 10 gene-sets). 3q29 genes whose subnetworks were found to show a significant overlap with SZ, ASD and/or IDD risk genes (adjusted $P < 0.05$) were prioritized as driver genes, along with their SZ, ASD, and/or IDD-related top neighbors from the corresponding enriched disease gene-set. These prioritized drivers are predicted to contribute to the emergence of major neuropsychiatric phenotypes associated with 3q29Del.

Functional characterization of prioritized driver genes

According to the "local hypothesis" proposed by the emerging paradigm of network medicine, the human transcriptome and proteome demonstrate non-random topological characteristics, where disease genes tend to interact with other disease genes and play distinct roles in disrupting the same biochemical process underlying a common pathophenotype (75). Motivated by this theory, we sought to formulate testable hypotheses about the key biological mechanisms linking 3q29Del to SZ, ASD, and IDD by conducting a functional enrichment analysis on the union of our prioritized driver genes. We used the same analysis approach described above for testing the functional enrichment of 3q29 modules. The biological processes and pathways that were found to surpass the adjusted g:SCS significance threshold of $p<0.05$ were filtered for gene-set size and semantic similarity; the top 20 biological processes and pathways found to be enriched in our prioritized driver genes are shown in the main results. To provide a thorough illustration of all enriched GO:BP terms in the main results, GO:BP findings were further organized into a network visualization of related functional annotation categories.

Overall, the transcriptomic network identified in this study is predicted to connect 3q29 interval genes with gene-sets outside the interval that participate in the same or overlapping biological process and associate with similar disease phenotypes. Perturbation of 3q29 interval gene dosage is expected to also perturb the functioning of network-partners outside the recurrent 3q29Del locus. However, note that the underlying structure of weighted gene co-expression networks is agnostic to the mechanistic order of cellular and molecular events. The information necessary to derive the order of biological interactions is not an explicit outcome of gene co-expression itself, since such inferences require time-dependent analysis of combinatorial interactions between nodes. As a result, some of the network partners identified in this study are expected to function upstream of their 3q29 gene partner and would likely not be affected by 3q29Del.

Proof of concept study for testing the validity of WGCNA-based predictions

Overview: A necessary step in determining the utility of network-based predictions is a proof of concept

of their validity in an experimental system. To this end, we assessed the validity of our WGCNA-derived predictions by testing the enrichment of the identified network-partners of 3q29 interval genes for differential expression in the mouse model of 3q29Del (76).

RNA-sequencing in mouse cortex Mice harboring a heterozygous deletion of 1.26Mb ($Del16^{+/Bdh1\text{-}Tfrc}$) that is homologous to the human 3q29Del locus were generated by CRISPR/Cas9 technology previously (76). At postnatal day seven, five mutant and five wild-type male pups were anesthetized under isoflurane and rapidly decapitated. The bilateral cortical sheet was dissected, chopped with a scalpel, and homogenized in QIAzol (Qiagen) in a Bullet Blender Tissue Homogenizer (Next Advance, Inc., Troy, NY). Total RNA was isolated using the miRNeasy Mini Kit (Qiagen) with on-column DNAse I treatment (Qiagen). Sequencing libraries were generated using the SMART-Seq Stranded Kit (Takara Bio, Mountain View, CA). 50M paired-end 150bp read sequencing was performed on an Illumina platform. Sequences were quality-checked and aligned to the mm10 reference genome. Gene quantification was conducted using HTSeq-count (77).

Differential gene expression analysis: We used two analysis tools (DESeq2 (78) and edgeR (79)) using the negative binomial model to identify differentially expressed genes (DEGs). Since there is no established consensus on a gold-standard statistical pipeline for conducting differential expression analysis in transcriptomic research, we incorporated both programs into our analysis as two independent methodologies representing the state of the art in bioinformatics (80). Only the protein-coding consensus DEGs concurrently identified by DESeq2 (version 1.24.0) and edgeR (version 3.26.8) were carried into downstream analysis.

Read counts from technical replicates were summed up using the *collapseReplicates and sumTechReps* functions of the DESeq2 and edgeR packages, respectively. This approach effectively increases the sequencing depth of the individual biological replicates, thereby increasing the power to detect differential expression. Genes with low counts were filtered by mean normalized counts in DESeq2 and by expression in counts per million (CPM) in edgeR. To minimize false negatives, we cast a wide net and determined statistically significant differences in gene expression at the nominal significance level ($P < 0.05$); a similar approach has been taken in previous transcriptomic studies modelling neuropsychiatric disorders (81, 82).

Comparison of empirically identified DEGs and network-derived predictions: We tested the statistical significance

of the overlap identified between DEGs found in the mouse model of 3q29Del and the co-expression partners of 3q29 interval genes identified by WGCNA via hypergeometric tests. A similar proof of concept approach has been used in previous literature (65). The *GeneOverlap* package (74) in R was used for this analysis. We investigated intersections at three scales of network interconnectedness: i) the broad 3q29 network, ii) the top-neighbor-based 3q29 subnetwork, and iii) the prioritized driver genes. To accurately measure the union-size of the possible matches between mouse DEGs and WGCNA-based targets, all compared gene-sets were filtered for known human-mouse homologs as determined by the HomoloGene database of the National Center for Biotechnology Information (NCBI) (83), using the *homologene* package (version 1.4.68.19.3.27) in R.

i) The broad 3q29 network is comprised of the union of seven WGCNA-derived modules that were found to harbor at least one 3q29 interval gene. The constituent genes of 3q29 modules show high topological overlap with one or more 3q29 genes and with one another, forming tight clusters of nodes that not only show high pair-wise co-expression with one another but also share many network neighbors. The clustering structure derived from such coordinated expression patterns in local regions of the genome likely reflects co-regulation and/or shared function among constituting genes. Hence, the union of the 3q29 modules identified in this study represents a broad subset of the human protein-coding genome that shows coordinated expression at the mRNA level with the 21 protein-coding genes located in the interval. A total of 11,924 genes with known human-mouse homology, including 21 3q29 interval genes comprise this broad network.

ii) The top-neighbor-based 3q29 subnetwork represents a refined subgraph, where modules are restricted to only the "top neighbors" of 3q29 interval genes. These top neighbors are predicted to function as direct interacting partners of 3q29 genes, participating in the same or overlapping biological pathways within the modular organization of molecular systems. A top neighbor was defined as any node whose gene expression profile has a moderate-to-high pairwise correlation ($\varrho \geq 0.5$, $P < 0.05$) with a 3q29 interval gene (considered a "seed" node) within the same module. The network ties underlying this subnetwork were derived by a correlation-based hard-thresholding method applied only to intra-modular edges connecting seed-node pairs. Hence, the top neighbor criterion used to construct this sub-network combines the strengths of scale free-topology and topological overlap principles for network construction and module detection, with subsequent

application of a hard-thresholding method. The total number of genes in this subnetwork with known human-mouse homology is 5,087, including 21 3q29 interval genes.

iii) The prioritized driver genes constitute the most refined subset of the transcriptomic network connections identified in this study. These are comprised of select 3q29 genes and top neighbors that are predicted to function as the primary drivers of the neurodevelopmental and psychiatric consequences of 3q29Del. These drivers were identified by leveraging the widely used guilt-by-association principle predicated on the assumption that disease-associated genes are more closely connected to each other than random pairs of nodes in a network. As described in previous sections of our methods, we conducted hypergeometric tests to determine whether the top neighbors of individual 3q29 genes are enriched for curated gene-sets with known SZ, ASD or IDD association. 3q29 genes whose top neighbors were found to show a significant overlap with known risk genes (adjusted $P < 0.05$) were prioritized as driver genes, along with their disease-related top neighbors from the corresponding enrichment analyses. The total number of prioritized driver genes with known human-mouse homology is 280, including nine 3q29 interval genes.

Note that the underlying structure of weighted gene co-expression networks is agnostic to the mechanistic order of cellular and molecular events. As a result, some of the network targets identified in this study are expected to function upstream of their 3q29 gene partner and would likely not be affected in the mouse model of 3q29Del.

Extended Results

Unbiased gene co-expression network analysis reveals convergent and distributed effects of 3q29 interval genes across the adult human cortical transcriptome.

Our WGCNA-based unsupervised network analysis approach, applied to publicly available high-throughput GTEx data, revealed that the protein-coding transcriptome of the healthy adult human PFC can be organized into a co-expression network of 19 modules (labeled by color) (Fig. 1D, Fig. 2A). The identified modules group genes with highly similar expression profiles into densely interconnected clusters, which likely represent shared function and co-regulation. One of the identified modules (the grey module) contained genes

that could not be unequivocally assigned to any module; thus, it was excluded from downstream analysis. The resulting module sizes (number of genes assigned to a module) ranged from 43 (steel blue) to 4,746 (green) genes, with an average module size of 1,014 genes (excluding grey module). Similar ranges have been reported in other network analysis applications.

The 21 protein-coding genes located in the 3q29 interval were found to cluster into seven network modules, which represent local regions of the human protein-coding genome that demonstrate coordinated expression with the 3q29 locus (Fig. 2A). These modules are referred to as 3q29 modules, and were labeled as black (size = 1,170 genes), brown (size = 1,972 genes), dark turquoise (size = 496 genes), green (size = 4,746 genes), magenta (size = 1,437 genes), midnight blue (size = 1,414 genes), and turquoise (size = 3,319 genes) modules. Moreover, 18 / 21 3q29 interval genes were found to concentrate into just four modules (brown, green, midnight blue, turquoise) (Fig. 2A), suggesting that the haploinsufficiency of the 3q29 locus may perturb the same biological processes via multiple hits, cumulatively disrupting redundancy and compensatory resiliency in the normative regulation of cellular functions. Simultaneously, leading candidate genes *DLG1* (black) and *PAK2* (dark turquoise), which were previously hypothesized to contribute to neuropsychiatric pathology, were found in opposite branches of the network, demonstrating the potential distributed effects of this CNV across the transcriptomic landscape (Fig. 2A).

The average linkage hierarchical clustering of the module eigengenes revealed that the identified modules further clustered into three higher level meta-modules (clusters of highly correlated modules), detected as major branches of the resulting eigengene dendrogram (Fig. 2A-B). The magenta, green and turquoise 3q29 modules clustered together within the first meta-module, grouping 12 3q29 interval genes: *RNF168, BDH1, PIGZ, PCYT1A, SMCO1, SLC51A, MFI2, CEP19, FBXO45, PIGX, TCTEX1D2* and *NRROS*. The brown and dark turquoise 3q29 modules clustered together within a second meta-module, grouping five 3q29 interval genes: *NCBP2, TFRC, TM4SF19, ZDHHC19* and *PAK2*. Finally, the midnight blue and black 3q29 modules were found to cluster together within a third meta-module, grouping three 3q29 interval genes: *DLG1, UBXN7, SENP5* and *WDR53*. The observed grouping, as well as the segregation, of sets of 3q29 modules into distinct meta-modules represents a higher-order transcriptomic organization of the 3q29 locus, which likely reflects

pathway dependencies and interactions between biological processes involving 3q29 interval genes. These findings suggest that, rather than functioning as independent non-interacting units, sets of 3q29 interval genes and their co-expressed network partners may work in synergy at both the module and meta-module levels of transcriptomic organization (Fig. 2A-B), and likely constitute interacting sources of pathology in 3q29Del syndrome.

Pathway analysis points to functional involvement of the 3q29 locus in nervous-system functions and core aspects of cell biology.

The functional enrichment analysis of individual 3q29 modules showed that the constituent genes of each module load highly onto canonical biological processes and pathways (Fig. 2D). These functional enrichment findings validate that our co-expression-based 3q29 modules reflect clustering dynamics that are biologically meaningful.

Functional characterization of the black module: We observed that the biological processes and pathways that were significantly overrepresented in the black module mainly encompass terms related to regulation of gene expression and maintenance of the integrity of the cellular genome. Based on the ranking of p-values adjusted for multiple testing, the top biological pathways (annotated by the Reactome database) that were overrepresented in the black module include metabolism of RNA (REAC:R-HSA-8953854, adjusted P = 2.45E-07), processing of capped intron-containing pre-mRNA (REAC:R-HSA-72203, adjusted P = 7.74E-04), chromatin organization (REAC:R-HSA-4839726, adjusted P = 6.36E-03), mRNA splicing (REAC:R-HSA-72172, adjusted P = 2.11E-02), post-translational protein modification (REAC:R-HSA-597592, adjusted P = 2.33E-02), DNA Repair (REAC:R-HSA-73894, adjusted P = 4.02E-02) and tRNA processing (REAC:R-HSA-72306, adjusted P = 4.97E-02).

Functional characterization of the midnight-blue module: Similarly, the midnight-blue module, which is in the same meta-module as the black module, was found to be enriched for biological pathways and processes that are involved in DNA repair and regulation of gene expression at the levels of transcription and translation, as well as cellular response to stress. An important functional signature that set the midnight blue

module apart from the black module was its specific enrichment for terms related to cell cycle regulation. The top biological pathways that were overrepresented in the midnight blue module include gene expression (transcription) (REAC:R-HSA-74160, adjusted *P* = 2.10E-39), metabolism of RNA (REAC:R-HSA-8953854, adjusted *P* = 1.64E-06), DNA double-strand break repair (REAC:R-HSA-5693532, adjusted *P* = 9.79E-04), mRNA 3'-end processing (REAC:R-HSA-72187, adjusted *P* = 5.49E-04), cell cycle (REAC:R-HSA-1640170, adjusted *P* = 3.26E-06), mRNA splicing (major pathway) (REAC:R-HSA-72163, adjusted *P* = 5.33E-03), cell cycle checkpoints (REAC:R-HSA-69620, adjusted *P* = 5.73E-03), transport of mature mRNA derived from an intron-containing transcript (REAC:R-HSA-159236, adjusted *P* = 1.53E-02), and transcriptional regulation by the tumor suppressor TP53 (REAC:R-HSA-3700989, adjusted *P* = 2.10E-02).

Functional characterization of the brown module: Assessment of shared function among constituent genes of the brown module revealed primary enrichment for biological pathways and processes involved in cellular metabolism and mitochondrial function. The top biological pathways that were overrepresented in the brown module include fatty acid metabolism (REAC:R-HSA-8978868, adjusted *P* = 7.59E-08), mitochondrial fatty acid beta-oxidation (REAC:R-HSA-77289, adjusted *P* = 8.33E-05), chondroitin sulfate/dermatan sulfate metabolism (REAC:R-HSA-1793185, adjusted *P* = 1.42E-03), peroxisomal protein import (REAC:R-HSA-9033241, adjusted *P* = 1.79E-03), metabolism of fat-soluble vitamins (REAC:R-HSA-6806667, adjusted *P* = 4.99E-03), peptide hormone biosynthesis (REAC:R-HSA-209952, adjusted *P* = 8.72E-03), solute-carrier (SLC)-mediated transmembrane transport (REAC:R-HSA-425407, adjusted *P* = 8.94E-03), and diseases associated with glycosaminoglycan metabolism (REAC:R-HSA-3560782, adjusted *P* = 1.30E-02). Notably, the brown module was also found to be enriched for two canonical KEGG-annotated pathways: the Hippo signaling pathway (KEGG:04390, adjusted *P* = 4.82E-03) and the Wnt signaling pathway (KEGG:04310, adjusted *P* = 4.96E-02), which play crucial roles in growth and developmental pathways with substantial cross-talk (84).

Functional characterization of the dark turquoise module: The dark turquoise module was found to coalesce genes that are enriched for biological functions in epigenetic regulation of gene expression, as well as in signal transduction pathways that are mediated by Rho GTPases. This latter function is at least in part attributable to *PAK2*, the only 3q29 interval gene assigned to this module, which encodes a known Rho GTPase

effector. Intriguingly, this module was also found to be enriched for a functional role in estrogen receptor-mediated signaling. In particular, the top terms that were overrepresented in the dark turquoise module include estrogen-dependent gene expression (REAC:R-HSA-9018519, adjusted *P* = 5.08E-06), estrogen receptor (ESR)-mediated signaling (REAC:R-HSA-8939211, adjusted *P* = 9.52E-06), Rho GTPase effectors (REAC:R-HSA-195258, adjusted *P* = 1.35E-05), SIRT1 negatively regulates rRNA expression (REAC:R-HSA-427359, adjusted *P* = 2.09E-05), gene silencing by RNA (REAC:R-HSA-211000, adjusted *P* = 3.95E-05), nucleosome assembly (REAC:R-HSA-774815, adjusted *P* = 4.75E-05), chromatin modifying enzymes (REAC:R-HSA-3247509, adjusted *P* = 5.12E-05), signaling by nuclear receptors (REAC:R-HSA-9006931, adjusted *P* = 8.46E-05), meiotic synapsis (REAC:R-HSA-1221632, adjusted *P* = 8.73E-05), and epigenetic regulation of gene expression (REAC:R-HSA-212165, adjusted *P* = 1.44E-04). Notably, the dark turquoise module was found to share the same meta-module as the metabolism-related brown module, suggesting the involvement of several 3q29 interval genes in a hierarchical transcriptomic control structure that interconnects Rho GTPase-mediated signaling cascades and estrogen-regulated signal transduction pathways with metabolic regulation. Emerging empirical findings demonstrate the existence of a crosstalk between these fundamental pathways (85-87), supporting the biological relevance of the co-expression-based clustering patterns underlying the meta-module that harbors the brown and dark turquoise modules identified in this study.

Functional characterization of the turquoise module: The biological processes that were overrepresented in the turquoise module primarily encompass nervous-system specific terms comprising the regulation of nervous system development and function. Other enriched biological functions that are non-specific but cardinal to nervous-system operations involve ion transport, calcium signaling, cyclic adenosine monophosphate (cAMP)-dependent signal transduction and cell projection organization. Specifically, the top Reactome-based biological pathways that were enriched in the turquoise module include neuronal system (REAC:R-HSA-112316, adjusted *P* = 2.98E-12), protein-protein interactions at synapses (REAC:R-HSA-6794362, adjusted *P* = 7.12E-07), neurexins and neuroligins (REAC:R-HSA-6794361, adjusted *P* = 3.58E-06), transmission across chemical synapses (REAC:R-HSA-112315, adjusted *P* = 6.31E-06), neurotransmitter receptors and postsynaptic signal transmission (REAC:R-HSA-112314, adjusted *P* = 9.47E-05), serotonin

receptors (REAC:R-HSA-390666, adjusted *P* = 6.42E-03), the citric acid (TCA) cycle and respiratory electron transport (REAC:R-HSA-1428517, adjusted *P* = 7.00E-03), and unblocking of N-methyl-D-aspartate (NMDA) receptors, glutamate binding and activation (REAC:R-HAS 438066, adjusted *P* = 1.41E-02). Complementing these biological pathways, GO biological processes that were found to be enriched in the turquoise module include regulation of synaptic plasticity (GO:0048167, adjusted *P* = 6.68E-03), cognition (GO:0050890, adjusted *P* = 2.91E-02), neuron differentiation (GO:0030182, adjusted *P* = 3.19E-02), long-term potentiation (GO:0060291, adjusted *P* = 3.81E-02) and learning and memory (GO:0007611, adjusted *P* = 4.20E-02). Dysregulation of these biological processes and pathways has been implicated in the etiology of major neuropsychiatric and neurodevelopmental disorders, including SZ and ASD (88, 89). Hence, the observed functional enrichment profile highlights a likely pivotal role for the coordinated expression of the 3q29 interval genes and network partners that cluster in the turquoise module in establishing and maintaining the healthy functioning of the brain.

Functional characterization of the green module: Similar to the turquoise module, the pathway enrichment analysis of the genes constituting the green module revealed primary enrichment for shared function in several nervous-system specific biological processes. The overarching functional characteristics of this module are regulation of nervous system development, interactions between neuroactive ligands and receptors, synaptic vesicle cycle, intracellular trafficking systems (i.e., vesicle-mediated synaptic transport) and synapse assembly. The top Reactome-annotated biological pathways that were found to be enriched in the turquoise module include neuronal system (REAC:R-HSA-112316, adjusted *P* = 7.76E-07), the role of GTSE1 in G2/M progression after G2 checkpoint (REAC:R-HSA-8852276, adjusted *P* = 6.14E-04), potassium channels (REAC:R-HSA-1296071, adjusted *P* = 2.99E-03), L1 cell adhesion molecule (L1CAM) interactions (REAC:R-HSA-373760, adjusted *P* = 8.69E-03), transmission across chemical synapses (REAC:R-HSA-112315, adjusted *P* = 1.66E-02), G protein-coupled receptor (GPCR) ligand binding (REAC:R-HSA-500792, adjusted *P* = 1.74E-02), G alpha (q) signaling events (REAC:R-HSA-416476, adjusted *P* = 2.37E-02), recycling pathway of L1 (REAC:R-HSA-437239, adjusted *P* = 3.93E-02), coat protein complex I (COPI)-mediated anterograde transport (REAC:R-HSA-6807878, adjusted *P* = 4.27E-02), and adenosine triphosphate-binding

cassette (ABC) transporter disorders (REAC:R-HSA-5619084, adjusted *P* = 4.36E-02). The observed nervous system-specific functional enrichment findings suggest heightened disease-relevance for the 3q29 interval genes and intra-modular partners that coalesce in the green module. The neuropathology-associated functional characterization of the green module parallels that of the turquoise module, which shares the same meta-module as the green module. This functional overlap, which was identified agnostically to meta-module membership, presents further support for the utility of our approach in detecting biologically meaningful non-random network structures that organize gene expression in the healthy adult human cortex.

Functional characterization of the magenta module: The magenta module was found to be predominantly enriched for biological processes and pathways involved in post-translational protein modifications by small protein conjugation or removal, ubiquitin-dependent protein catabolism, intracellular protein transport and localization, and the ubiquitin-proteasome system. Hence, coordinated expression of the 3q29 interval genes and network partners that participate in the magenta module likely plays an important role in controlling the modification and spatiotemporal colocalization of substrates necessary for a variety of intracellular interactions. Moreover, pathway enrichment analysis revealed a link between magenta module genes and the initiation of MHC class I (MHC-I)-dependent immune responses, driven by a genomic locus that is increasingly implicated in the etiology of SZ (90). MHC-I antigen presentation has been shown to strictly depend on peptide supply by the ubiquitin-proteasome system to initiate an effective adaptive immune response(91); thus, the simultaneous enrichment of these interacting processes in a single module supports the biological relevance of the identified pattern of clustering. Specifically, the top Reactome-annotated biological pathways that were found to be significantly overrepresented in the magenta module include post-translational protein modification (REAC:R-HSA-597592, adjusted *P* = 1.22E-07), gene expression (transcription) (REAC:R-HSA-74160, adjusted *P* = 7.98E-06), MHC-I mediated antigen processing and presentation (REAC:R-HSA-983169, adjusted *P* = 1.69E-05), antigen processing: ubiquitination and proteasome degradation (REAC:R-HSA-983168, adjusted *P* = 2.78E-05), RNA polymerase II transcription (REAC:R-HSA-73857, adjusted *P* = 1.05E-04), signaling by TGF-beta family members (REAC:R-HSA-9006936, adjusted *P* = 2.87E-03), protein ubiquitination (REAC:R-HSA-8852135, adjusted *P* = 1.14E-02), and sumoylation (REAC:R-

HSA-2990846, adjusted *P* = 1.94E-02). Overall, the functional profile of the magenta module encompasses many known regulators of brain function, including synapse formation and trans-synaptic signaling. Hence, the functional characteristics of the magenta module complement that of its meta-module partners, the green and turquoise modules.

Taken together, functional characterization of the 3q29 modules (Fig. 2D) point to novel mechanisms of shared or overlapping action for sets of 3q29 interval genes that cluster in the same network module and further coalesce in the same meta-module. Simultaneously, the variety of biological pathways that were found to be enriched in 3q29 modules suggests distributed involvement of this locus in not only nervous-system specific functions, such as regulation and organization of synaptic signaling and components, but also in core aspects of cell biology, including cellular metabolism, transcriptional regulation, protein modifications, and cell cycle regulation.

Simultaneously, PPI network enrichment analysis revealed that all 3q29 modules show significant enrichment for PPIs that were systematically curated from the STRING protein interactome database (Fig. S8), augmenting confidence in our RNA-Seq based network predictions with proteomic evidence (midnight blue, black, brown, and magenta modules: *P*-value < 1.00e-16; dark turquoise module: *P*-value = 1.11e-16; green module: *P*-value = 8.62e-08; turquoise module: *P*-value = 4.30e-09). A small PPI enrichment p-value indicates that the protein products of genes that were found to be highly co-expressed with 3q29 interval genes in our transcriptomic network analysis are not organized into modules at random and that the observed number of edges calculated for each 3q29 module based on PPI pairs curated from STRING is significant ($P < 0.05$) (Fig. S8). The expected number of edges reflects how many edges are to be expected if the nodes were to be selected from the genome at random. More detail on active interaction sources and other parameters can be found in (47) and at https://string-db.org/.

Finally, we identified qualitative overlaps between the transcriptomic co-expression partners of 3q29 interval genes identified via WGCNA and known protein partners of 3q29 interval genes curated from the HuRI database (Fig. S7). Of the 21 protein coding genes located in the 3q29 interval, only 14 (*CEP19, DLG1, FBXO45, MFI2, NCBP2, PAK2, PCYT1A, RNF168, SLC51A, TCTEX1D2, TFRC, UBXN7*) were found to

have an entry on HuRI, 50% of which (*FBXO45, MFI2, NCBP2, RNF168, SLC51A, TCTEX1D2, TM4SF19*) had less than eight known proteome-wide interactors. A total of 193 distinct protein interactors were identified on HuRI for these 14 3q29 interval genes (after removing duplicates), 184 of which were identified as a node in our gene co-expression network. Of these 184, 137 (74%) were found to cluster in one of seven modules harboring 3q29 interval genes. 46% of the protein interactors identified in 3q29 modules share the same meta-module as their interacting 3q29 interval gene, 27% of which further show an overlap at the module level. Brief statistics and visual illustrations of the resulting PPI networks can be found in Fig. S7-8.

Network modules found to harbor 3q29 interval genes are robust and strongly reproducible in an independent test dataset.

To ensure the reproducibility of our network analysis results, we tested the preservation of various properties of graph structure that underly the modules identified in this study with respect to an independent dataset obtained from the BrainSpan Project (Fig. S4). We calculated multiple density-based and connectivity-based preservation statistics for each module using a permutation test procedure and summarized the observed statistics by a composite Z-statistic, $Z_{summary.pres}$. All identified modules, except for the grey module (unassigned genes), were found to be successfully preserved in the test network ($Z_{summary.pres} > 2$) (Fig. 1E). Specifically, 3/18 modules exhibited moderate evidence of preservation ($2 < Z_{summary.pres} < 10$), and 15/18 modules, including all 3q29 modules, exhibited strong evidence of preservation ($Z_{summary.pres} > 10$) (Fig. 1E). Moreover, the resulting composite preservation statistics of all 3q29 modules were substantially higher than that of a randomly drawn sample of 1,000 genes that represent the entire reference network as a single artificial module (labeled as the gold module, $Z_{summary.pres.gold} = 6.78$).

In addition to preservation statistics, we calculated multiple module quality statistics that measure how well-defined or robust the boundaries of individual modules are in the reference network. By employing a resampling technique that applies module preservation statistics to repeated random splits of our reference data, we obtained a composite Z-statistic for each module ($Z_{summary.qual}$) that standardizes and summarizes multiple cluster quality statistics. All 18 modules showed strong evidence for high cluster quality ($Z_{summary.qual} >$

10), revealing robust module definitions (Fig. S5). Specifically, all 3q29 modules had a $Z_{summary.qual}$ score ≥ 20 (Fig. 1E).

Finally, in line with the recommendations of the creators of the WGCNA package (39), we also evaluated the individual preservation and quality statistics underlying the composite $Z_{summary.pres}$ and $Z_{summary.qual}$ scores derived for each module. Individual module preservation statistics mostly converge on the finding that (1) nodes sharing the same module in the reference network remain highly connected in the test network and (2) connectivity patterns between nodes underlying the reference network remain similar in the test network (Fig. S5). Similarly, individual module quality statistics predominantly indicate strong evidence for high cluster quality in all identified modules across networks created from random splits of the original reference data (Fig. S5).

Overall, these findings support the strong reproducibility and robustness of our 3q29 modules, allowing high-confidence screening of the transcriptomic connectivity patterns formed by 3q29 interval genes in the healthy adult human PFC.

UBXN7 is a highly connected cortical hub-gene predicted to play a crucial role in the neuropsychiatric sequela of 3q29Del.

To measure how strongly connected individual 3q29 interval genes are to their assigned network modules, we calculated the eigengene-based module connectivity measure (kME) of each 3q29 interval gene for its respective module (Fig. 2C). To reiterate, this measure quantifies how close a node is to its assigned module and can be applied to identify hub genes (kME > 0.8, $P < 0.05$), which are highly correlated with their module eigengene and exhibit high connectivity in their module. Intriguingly, our results revealed that *UBXN7*, an understudied and poorly annotated 3q29 interval gene, is a hub gene of its module (kME = 0.84, P = 8.33E-30, midnight blue module size = 1,414 genes). Topological features of known disease-genes have been shown to disproportionately exhibit hub-gene characteristics compared to non-disease genes (53). Supported by this literature, we predict that (1) *UBXN7* exerts central influence on a large network of co-expressed genes, and (2) loss of function mutations in *UBXN7* can cause major dysfunction in the biological

pathways involving this gene. Consequently, we prioritize *UBXN7* as a major driver gene with likely disease relevance in 3q29Del.

Moreover, evaluation of the module membership strengths of 3q29 interval genes revealed that *SMCO1 (*kME = 0.11, *P* = 0.25*), SLC51A (*kME = 0.17, *P* = 0.09*) and MFI2 (*kME = 0.09, *P* = 0.35*)* have non-significant kMEs for their assigned module, suggesting poor module connectivity. The mRNA expression summaries obtained from the Human Protein Atlas (92) (HPA) for 3q29 interval genes indicate nearly negligible or very low mRNA expression levels for *SMCO1* (consensus normalized expression value = 0.1), *SLC51A,* (consensus normalized expression value = 0.4), *and MFI2* (consensus normalized expression value = 2.8) in the human cerebral cortex. These data indicate the low abundance of these 3q29 interval genes in our tissue of interest, which likely relates to their peripheral network assignments in our analysis. Consequently, *SMCO1, SLC51A* and *MFI2* were excluded from downstream analysis to ensure accurate refinement of tight network connections formed by 3q29 interval genes.

Nine 3q29 interval genes form transcriptomic subnetworks enriched for known SZ, ASD and IDD-risk genes.

To systematically generate testable hypotheses regarding which 3q29 interval genes are causally linked to the major neuropsychiatric phenotypes associated with 3q29Del, we reduced 3q29 modules to strongly connected top neighbors of individual 3q29 genes and screened the resulting top neighbors for a significant overlap with known SZ, ASD or IDD-risk genes. To reiterate, this approach leverages the extensively validated principle of guilt-by-association, which postulates that the disease-relevance of a particular gene is partially a property determined by its relationships in a biological network.

A top neighbor was defined as any node whose gene expression profile has a moderate-to-high pairwise correlation ($\varrho \geq 0.5$, $P < 0.05$) with a 3q29 interval gene within the same module. Intriguingly, our results revealed that several 3q29 interval genes are among the top neighbors of one another within the same module. *FBXO45* ($\varrho = 0.5$, *P* = 5.43E-09) and *PIGX* ($\varrho = 0.6$, *P* = 1.24E-10) were identified as top-neighbors of *CEP19* in the turquoise module. Similarly, *SENP5* and *WDR53* were top-neighbors of each other ($\varrho = 0.5$, *P* = 1.05E-07) in the midnight blue module. This finding further suggests that the correlated activity of subsets of 3q29

interval genes may converge upon the same or synchronized multicomponent biological processes in the adult PFC.

Moreover, *TM4SF19 (0 top neighbors)* and *ZDHHC19 (3 top neighbors)* were found to have no or < 5 intra-modular partners in the brown module that met the correlation threshold to qualify as top neighbors. Similar to *SMCO1, SLC51A* and *MFI2,* the mRNA expression summaries obtained from the HPA(92) for *TM4SF19* (consensus normalized expression value = 0.5) and *ZDHHC19* (consensus normalized expression value = 0) indicate negligible or very low mRNA expression levels in the human cerebral cortex. These data independently indicate the low abundance of these 3q29 interval genes in our tissue of interest, which likely reflects the reason behind their lack of strongly connected top neighbors in our network analysis. Hence, *TM4SF19* and *ZDHHC19* were excluded from our downstream disease-association analysis, along with *SMCO1, SLC51A* and *MFI2,* which were deprioritized earlier due to poor module connectivity.

The intra-modular top neighbors of the remaining 16 3q29 interval genes were interrogated for overlap with six curated lists of evidence-based IDD, ASD or SZ-risk genes, spanning a wide range of the allele frequency spectrum (Fig. 3A). Hypergeometric test results, corrected for multiple testing, revealed a significant overrepresentation of one or more of these established risk gene-sets among the top neighbors of nine 3q29 interval genes (adjusted $P < 0.05$): *BDH1, CEP19*, *DLG1*, *FBXO45, PIGZ, RNF168, SENP5, UBXN7* and *WDR53* (Fig. 3B). Details of the enrichment results with respect to module membership are provided below.

In the black module, top neighbors of *DLG1* (gene-set size = 294) were found to be enriched for known SZ-risk genes from the exonic *de novo* mutations gene-set (adjusted $P = 1.11E-05$). This identified intersection comprises 18 unique top neighbors of *DLG1* with known SZ association. Note that *DLG1* was the only 3q29 interval gene that clustered in the black module.

In the midnight blue module, all three constituent 3q29 interval genes had top neighbors that loaded highly onto known IDD, ASD and/or SZ-risk genes. Particularly, top neighbors of *UBXN7* (gene-set size = 811) were enriched for known IDD (overlap size = 14, adjusted $P = 3.05E-04$), ASD (overlap size = 15, adjusted $P = 5.46E-05$), and SZ-risk genes from the CommonMind case-control gene-set (overlap size = 45,

adjusted P = 4.20E-03). In addition, top neighbors of *SENP5* (gene-set size = 713) were enriched for known IDD (overlap size = 11, adjusted *P* = 5.05E-03) and ASD-risk genes (overlap size = 12, adjusted *P* = 1.28E-03). Similarly, top neighbors of *WDR53* (gene-set size = 278) had a significant overlap with known IDD (overlap size = 6, adjusted *P* = 1.51E-02) and ASD-risk genes (overlap size = 6, adjusted *P* = 1.51E-02). The union of these identified intersections adds up to a total of 67 unique top neighbors with known IDD, ASD and/or SZ association in this module.

In the green module, only two out of the six constituent 3q29 interval genes were found to have top neighbors that showed a significant overrepresentation of SZ-risk genes. Specifically, top neighbors of *BDH1* (gene-set size = 1008) were enriched for known SZ-risk genes from the CommonMind case-control gene-set (overlap size = 66, adjusted *P* = 4.49E-06). Similarly, top neighbors of *PIGZ* (gene-set size = 995) were also enriched for known SZ-risk genes from the CommonMind case-control gene-set (overlap size = 58, adjusted *P* = 7.03E-04). The union of these identified intersections adds up to a total of 75 unique top neighbors with known SZ association in this module.

In the magenta module, top neighbors of *RNF168* (gene-set size = 556) had a significant overlap with known IDD (overlap size = 9, adjusted *P* = 1.07E-02) and SZ-risk genes from the CommonMind case-control gene-set (overlap size = 65, adjusted *P* = 5.21E-17). The union of these identified intersections adds up to a total of 73 unique top neighbors with known SZ and/or IDD association in this module. Note that *RNF168* was the only 3q29 interval gene that clustered in the magenta module.

In the turquoise module, only two out of the five constituent 3q29 interval genes had top neighbors that loaded highly onto known IDD, ASD and/or SZ-risk genes. Specifically, top neighbors of *CEP19* (gene-set size = 1161) were enriched for known IDD (overlap size = 16 , adjusted *P* = 1.64E-03), ASD (overlap size = 15, adjusted *P* = 1.64E-03), and SZ-risk genes from the exonic *de novo* mutations gene-set (overlap size = 29, adjusted P = 3.32E-02). In addition, top neighbors of *FBXO45* (gene-set size = 1101) were also enriched for known IDD-risk genes (overlap size = 14, adjusted *P* = 1.35E-02). The union of these identified intersections adds up to a total of 51 unique top neighbors with known IDD and/or SZ association in this module.

Finally, there was no statistically significant evidence for overrepresentation of known disease genes of

interest among the top neighbors of 3q29 interval genes that clustered in the brown or dark turquoise modules.

To evaluate the specificity of the identified disease enrichment patterns, we also tested the top neighbors of 16 3q29 interval genes for overlap with known PD, late-onset AD and IBD risk genes. These disease phenotypes have no known link to 3q29Del syndrome, thus, genetic risk loci associated with these conditions were considered negative controls in this network analysis. In addition, a large list of common variants associated with height were included in our analysis as a fourth negative control to rule out a potential bias that could be introduced to our analysis by differences in the sizes of curated gene-sets. Our results indicate no statistically significant evidence for overrepresentation of AD or IBD-risk genes among the top neighbors of interrogated 3q29 interval genes. Only the top neighbors of *SENP5* (gene-set size = 713) showed a significant overlap with height-associated genes (overlap size = 30, adjusted P = 2.36E-02). Additionally, the top neighbors of *NRROS* (gene-set size = 68), which did not show an enrichment for known IDD, ASD, or SZ risk genes, exhibited a small but significant overlap with known PD-risk genes (overlap size = 3, adjusted P = 2.00E-02) (Fig. 3B).

Overall, 2 out of 64 hypergeometric tests indicated a significant overlap between the top neighbors of interrogated 3q29 interval genes and negative control gene-sets. In contrast, 19 out of 96 hypergeometric tests revealed a significant overrepresentation of SZ, ASD, and/or IDD-risk gene-sets among the same top neighbors, amounting to a proportion that is an order of magnitude larger than that of the negative controls (Fig. 3B). The substantial margin observed between these two enrichment ratios supports the high specificity and validity of our network-derived inferences for uncovering biology relevant to 3q29Del.

In summary, we identified 5,715 top neighbors of 3q29 interval genes, when combined across seven 3q29 modules. These top neighbors are predicted to function as direct interacting partners of 3q29 interval genes, participating in the same or overlapping biological pathways within the modular organization of molecular systems subserving the healthy functioning of the adult human PFC. Intriguingly, several 3q29 interval genes themselves were identified as top neighbors of other 3q29 interval genes, further suggesting functional convergence of subsets of genes within the 3q29 locus. Finally, our results revealed that *BDH1, CEP19*, *DLG1*, *FBXO45, PIGZ, RNF168, SENP5, UBXN7* and *WDR53* form strong co-expression-based ties

with network partners that show a significant overlap with known SZ, ASD and/or IDD-risk genes curated from evidence-based literature (Fig. 3B). By leveraging the guilt by association principle, we prioritize these nine 3q29 interval genes, along with their 284 SZ, ASD, and/or IDD-related top neighbors from significant overlap tests as primary drivers of the major neuropsychiatric consequences of 3q29Del (Fig. 3B, Fig. 4A).

Disease-relevant driver genes prioritized by network analysis load onto key biological pathways linked to neuropsychiatric disorders.

To formulate testable hypotheses about the key biological mechanisms linking the 3q29 locus to major neuropsychiatric phenotypes associated with 3q29Del syndrome, we interrogated whether the prioritized driver genes identified in our network analysis assemble into known biological pathways and processes that are annotated in major gene ontology databases. Functional enrichment analysis on the union of our 293 prioritized driver genes (Fig. 4A) revealed their significant overrepresentation in several key biological pathways and processes, some of which are specific to nervous system function, while others are core cellular processes that are non-specific to an organ system (Fig. 4B-C).

Specifically, our findings indicate enrichment of our prioritized driver genes in eight biological pathways annotated by the Reactome and KEGG databases. These are axon guidance (REAC:R-HSA-422475, adjusted P = 3.64E-03), post-translational protein modifications (REAC:R-HSA-597592, adjusted P = 5.24E-03), long-term potentiation (KEGG:04720, adjusted P = 7.29E-03), diseases of signal transduction (REAC:R-HSA-5663202, adjusted P = 1.00E-02), regulation of actin cytoskeleton (KEGG:04810, adjusted P = 1.17E-02), deubiquitination (REAC:R-HSA-5688426, adjusted P = 2.42E-02), chromatin organization (REAC:R-HSA-4839726, adjusted P = 3.32E-02), and diseases associated with glycosylation precursor biosynthesis (REAC:R-HSA-5609975, adjusted P = 4.06E-02). This analysis also revealed the enrichment of our prioritized driver genes for several fundamental biological processes annotated by the Gene Ontology Project (GO:BP), including chromosome organization (GO:0051276, adjusted P = 3.81E-09), histone modification (GO:0016570, adjusted P = 3.31E-08), cellular component morphogenesis (GO:0032989, adjusted P = 4.57E-06), regulation of organelle organization (GO:0033043, adjusted P = 6.40E-06), DNA metabolic process

(GO:0006259, adjusted *P* = 3.83E-05), regulation of telomere maintenance (GO:0032204, adjusted *P* = 6.62E-05), neuron differentiation (GO:0030182, adjusted *P* = 1.88E-04), protein modification by small protein conjugation or removal (GO:0070647, adjusted *P* = 2.34E-04), neuron projection morphogenesis (GO:0048812, adjusted *P* = 4.46E-04), neurogenesis (GO:0022008, adjusted *P* = 1.89E-03), chemical synaptic transmission, postsynaptic (GO:0099565, adjusted *P* = 2.37E-03), post-embryonic development (GO:0009791, adjusted *P* = 2.66E-03), synapse organization (GO:0050808, adjusted *P* = 3.20E-03), protein acetylation (GO:0006473, adjusted *P* = 5.48E-03), cell surface receptor signaling pathway involved in cell-cell signaling (GO:1905114, adjusted *P* = 6.41E-03), and excitatory postsynaptic potential (GO:0060079, adjusted *P* = 8.97E-03). We hypothesize that the disruption of one or more of these biological pathways and processes, some of which have been demonstrated to be altered in idiopathic SZ and ASD (88, 89), lie on the casual pathway to neuropsychopathology in 3q29Del syndrome.

The top 20 biological processes and pathways enriched among our prioritized driver genes is shown in Fig. 4B. For clear illustration of our findings, we organized all identified GO:BP terms into a network of related functional annotation categories in Fig. 4C.

Network-derived targets predict differentially expressed genes in the mouse model of 3q29Del.

We tested the enrichment of the network targets identified in this study for differential expression in Del16$^{+/Bdh1\text{-}Tfrc}$ mice compared with wild-type (WT) littermates (76). RNA-Seq analysis revealed 290 protein-coding DEGs with known human homologs (*P < 0.05*), 17 of which were identified as 3q29 interval genes (*Bdh1, Cep19, Dlg1, Fbxo45, Mfi2, Ncbp2, Nrros, Pak2, Pcyt1a, Pigx, Pigz, Rnf168, Senp5, Tctex1d2, Tfrc, Ubxn7, Wdr53*) (Fig. 5). All 290 DEGs were tested for enrichment of network-derived targets identified via WGCNA at three scales of network interconnectedness: i) broad 3q29 network (11,924 genes), ii) top-neighbor-based 3q29 subnetwork (5,087 genes), and iii) prioritized drivers (280 genes). All compared gene-sets were filtered for mouse-human homology. Hypergeometric tests revealed significant enrichment of the interrogated DEGs for network-derived ties at all three levels of this analysis ($P < 0.05$; Fig. 5B).

Specifically, 212 out of 290 DEGs were found to overlap with the broad 3q29 network (*P = 2.42e-07*),

with a 1.50-fold over-enrichment compared to what would be expected by random chance. 74 out of 290 DEGs were found to overlap with the top-neighbor-based 3q29 subnetwork (*P = 0.03*), with a 1.22-fold over-enrichment compared to what would be expected by random chance. Finally, 12 out of 290 DEGs were found to overlap with prioritized drivers predicted to be associated with the neurodevelopmental and psychiatric consequences of 3q29Del (*P = 1.43e-04*), with a 3.61-fold over-enrichment compared to what would be expected by random chance (Fig. 5B).

In conclusion, prediction of novel gene-function and gene-disease associations is an important goal in computational biology, particularly for un- or under-studied territories of the human genome, such as the recurrent 3q29Del locus. These genes have been neglected, in part, due to attention bias in biomedical research that disproportionately concentrates on isolated interrogation of well-studied genes (93). The network-based guilt-by-association approach used in this study is a promising strategy to rectify this skew and to advance our understanding of the full complement of the human genome and the full scope of genetic risk for severe mental illnesses in a systems biology framework.

Supplemental Figures

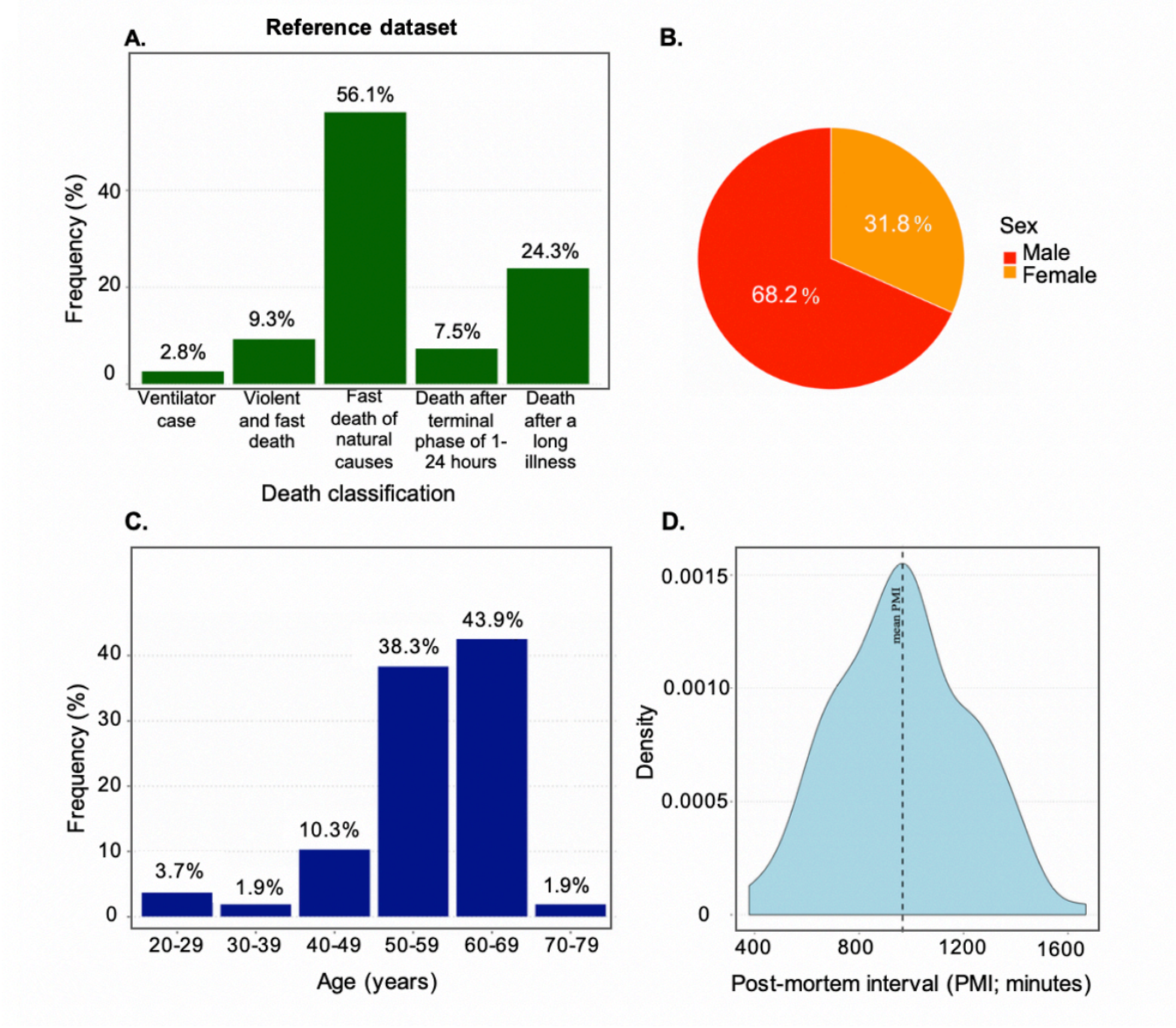

Figure S1. Tissue sample attributes and donor phenotypes of the GTEx dataset used for reference network construction. (A) Frequency distribution of donors' death-classification based on the 4-point Hardy scale. Majority of tissue samples (56.1%) were obtained from donors whose deaths were classified as "fast death of natural causes", which encompasses sudden (unexpected) deaths of people who had been reasonably healthy, following a terminal phase of <1 hour (e.g., sudden death from myocardial infarction). (B) Frequency distribution of donors' sex. Male:female ratio = 2.1:1.0. (C) Frequency distribution of donors' age-group based

on 4-year intervals determined by the GTEx project. Majority of donors (82.2%) were in the age-range of 50-69 years at the time of death. (D) Sample density plot of post-mortem interval (PMI), indicating time elapsed between donor's death and final tissue stabilization. Mean sample PMI (sd) = 966.2 (254.3) minutes. *N* = 107.

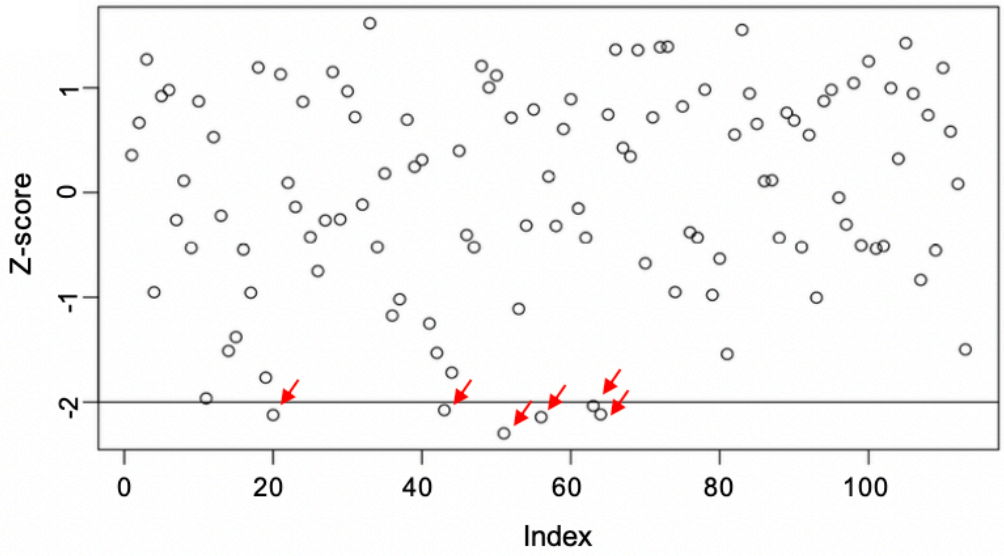

Figure S2. Pre-processing of the reference dataset: outlier removal. 6 outlier samples (red arrows) were removed from the reference dataset (GTEx Project) to prevent an outlier-driven bias in gene co-expression network construction. Inter-sample correlation (ISC) was used as the statistical diagnostic for identifying samples with divergent gene expression profiles. ISC was defined as the Pearson's correlation between pairs of samples across the expression levels of all detected genes. Samples with a mean ISC greater than 2 standard deviations away (black line) from the mean of the sample-set were removed, bringing the sample size used for weighted gene co-expression analysis to 107.

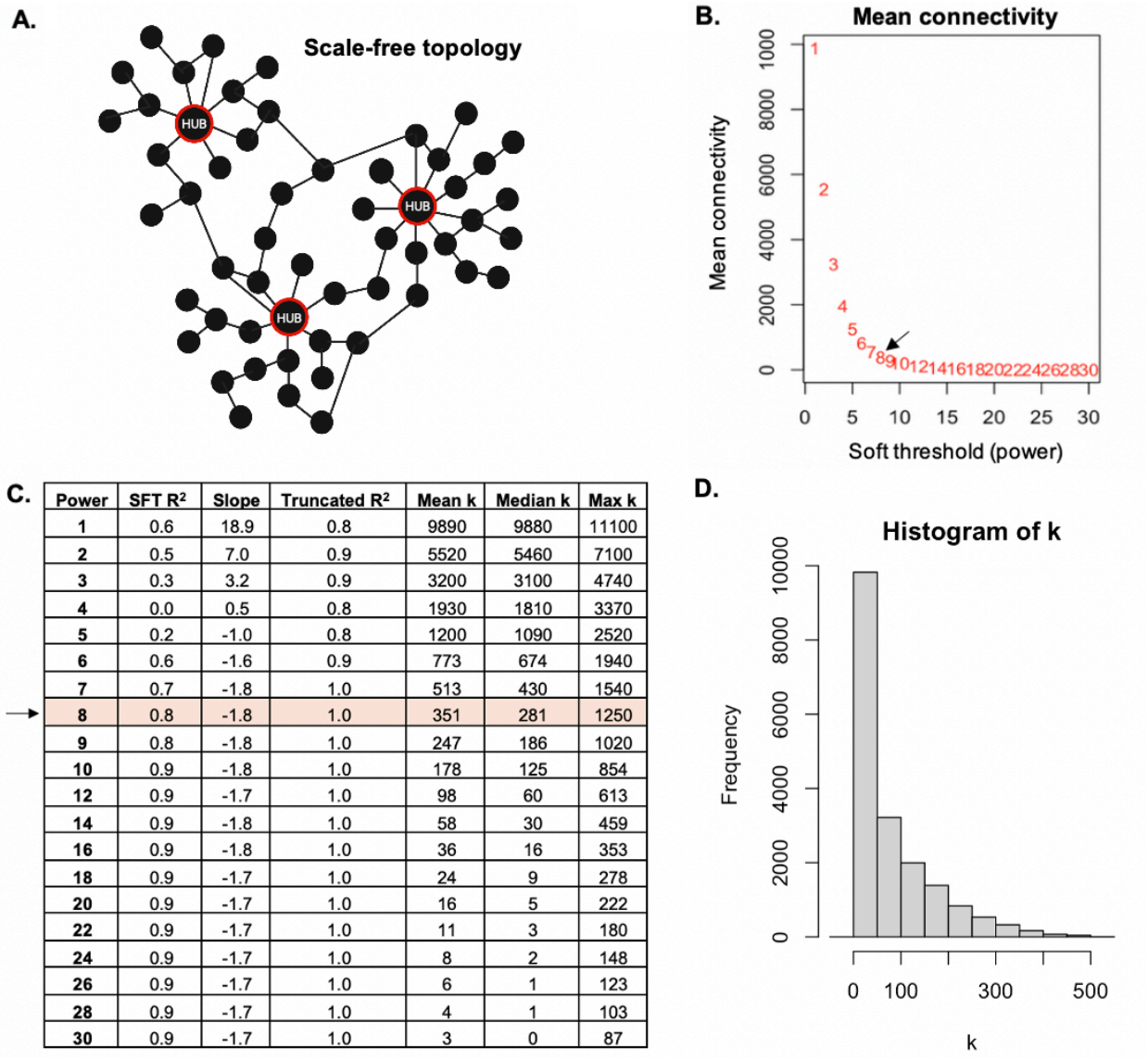

Power	SFT R^2	Slope	Truncated R^2	Mean k	Median k	Max k
1	0.6	18.9	0.8	9890	9880	11100
2	0.5	7.0	0.9	5520	5460	7100
3	0.3	3.2	0.9	3200	3100	4740
4	0.0	0.5	0.8	1930	1810	3370
5	0.2	-1.0	0.8	1200	1090	2520
6	0.6	-1.6	0.9	773	674	1940
7	0.7	-1.8	1.0	513	430	1540
→ 8	0.8	-1.8	1.0	351	281	1250
9	0.8	-1.8	1.0	247	186	1020
10	0.9	-1.8	1.0	178	125	854
12	0.9	-1.7	1.0	98	60	613
14	0.9	-1.8	1.0	58	30	459
16	0.9	-1.8	1.0	36	16	353
18	0.9	-1.7	1.0	24	9	278
20	0.9	-1.7	1.0	16	5	222
22	0.9	-1.7	1.0	11	3	180
24	0.9	-1.7	1.0	8	2	148
26	0.9	-1.7	1.0	6	1	123
28	0.9	-1.7	1.0	4	1	103
30	0.9	-1.7	1.0	3	0	87

Figure S3. Determination of the soft-thresholding power (β) in weighted gene co-expression network analysis (WGCNA). (A) Schematic of a representative scale-free network, whose degree distribution follows a power-law**:** most nodes have one or two connections but a few highly connected nodes (hub genes; marked by a red frame) have a large number of connections. Scale free topology (SFT) is a unifying property of biological networks in nature. **(B)** Mean connectivity (k) as a function of different β values. Mean k decreases as β increases. The arrow marks the β value used in this study. **(C)** List of SFT fitting indices for a wide range of β values. The highlighted row indicates the β used in this study. Given the necessary trade-off between SFT

index R^2 and mean connectivity (k), a β of 8 was identified as the lowest possible power yielding a degree distribution that results in approximate SFT (R^2 fit index = 0.8), while maintaining relatively high mean connectivity (mean k > 100), enabling the detection of modules and hub nodes. **(D)** Histogram of connectivity (k) distribution when a β of 8 was chosen for defining the adjacency matrix. The frequency distribution of k shows a large number of lowly connected genes and a small number of highly connected genes, indicating that the resulting network follows the SFT criterion.

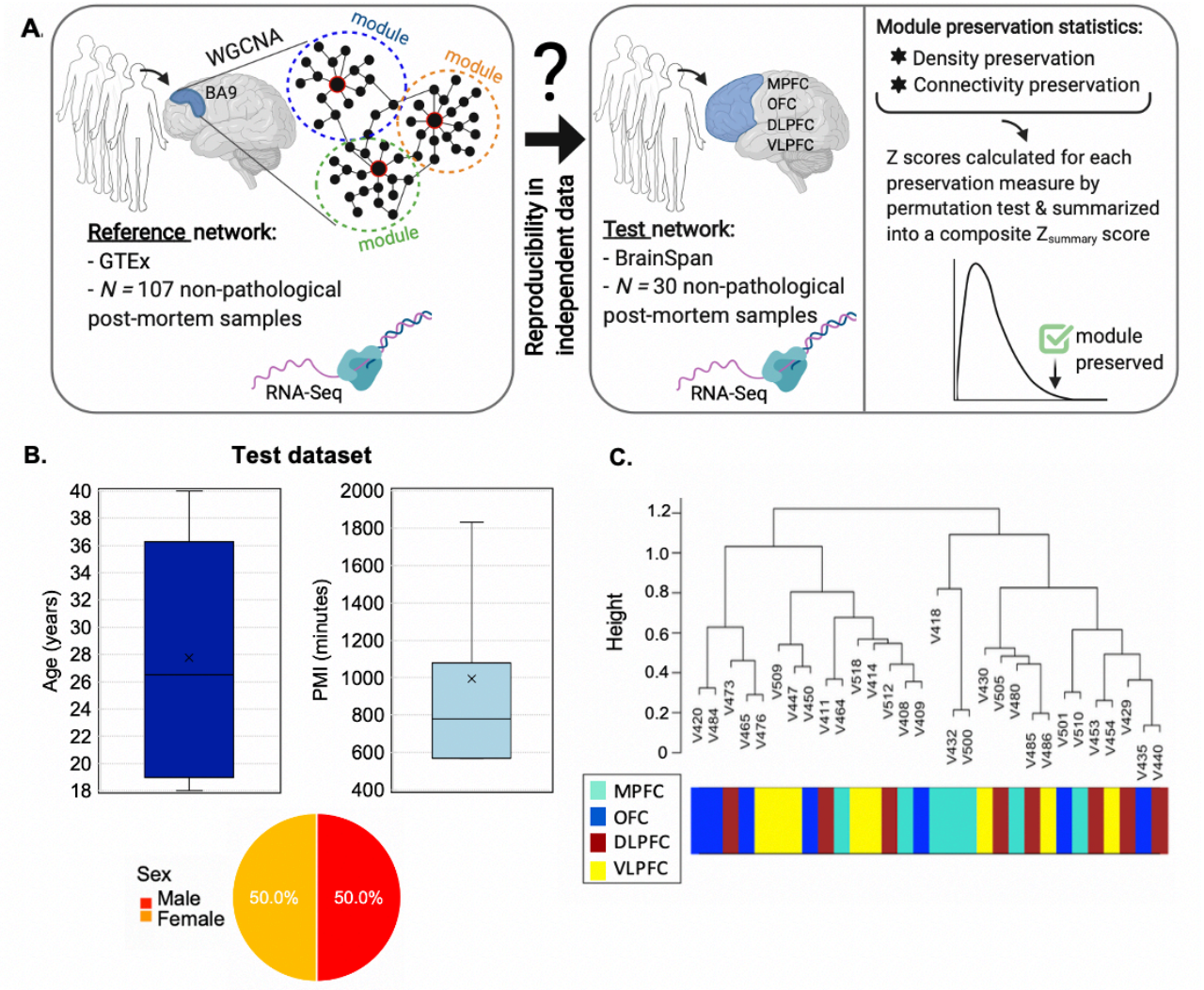

Figure S4. Determination of network reproducibility and module preservation in an independent test dataset. (A) Illustration of the network reproducibility approach used in this study. Preservation of all network modules that were identified in the reference dataset (GTEx Project, N=107) was established in an independent, demographically comparable test dataset obtained from the BrainSpan Project (N=30). Both transcriptomic datasets were corrected for covariance mediated by sex, age and post-mortem interval (PMI). **(B)** Tissue sample attributes and donor phenotypes of the BrainSpan test dataset. The dark blue box-plot indicates the distribution of donors' age at death (in years). Median age = 27 years (range: 18-40 years). Mean age (sd) = 28 (8.4) years and corresponds to the cross mark. The light blue box-plot indicates the distribution of PMI in the test dataset. Median PMI = 780 minutes. Mean PMI (sd) = 994 (446.2) minutes. Pie chart indicates

the percentage breakdown of donors' sex. Male:female ratio = 1:1. **(C)** Sample-level dendrogram of the test dataset plotted by hierarchical clustering of 30 non-pathological post-mortem samples obtained from four subregions of the prefrontal cortex (PFC) from male and female adults with no known history of neurological or psychiatric disorder. Clustering was conducted on normalized and residualized gene expression values for 18,339 protein-coding genes. Color bar below the dendrogram indicates tissue type corresponding to four subregions of the PFC that were pooled to derive the test dataset. The resulting dendrogram reveals no distribution bias associated with tissue-subtype in sample-level clustering patterns. OFC: orbital frontal cortex, DLPFC: dorsolateral PFC, VLPFC: ventrolateral PFC, MPFC: medial PFC.

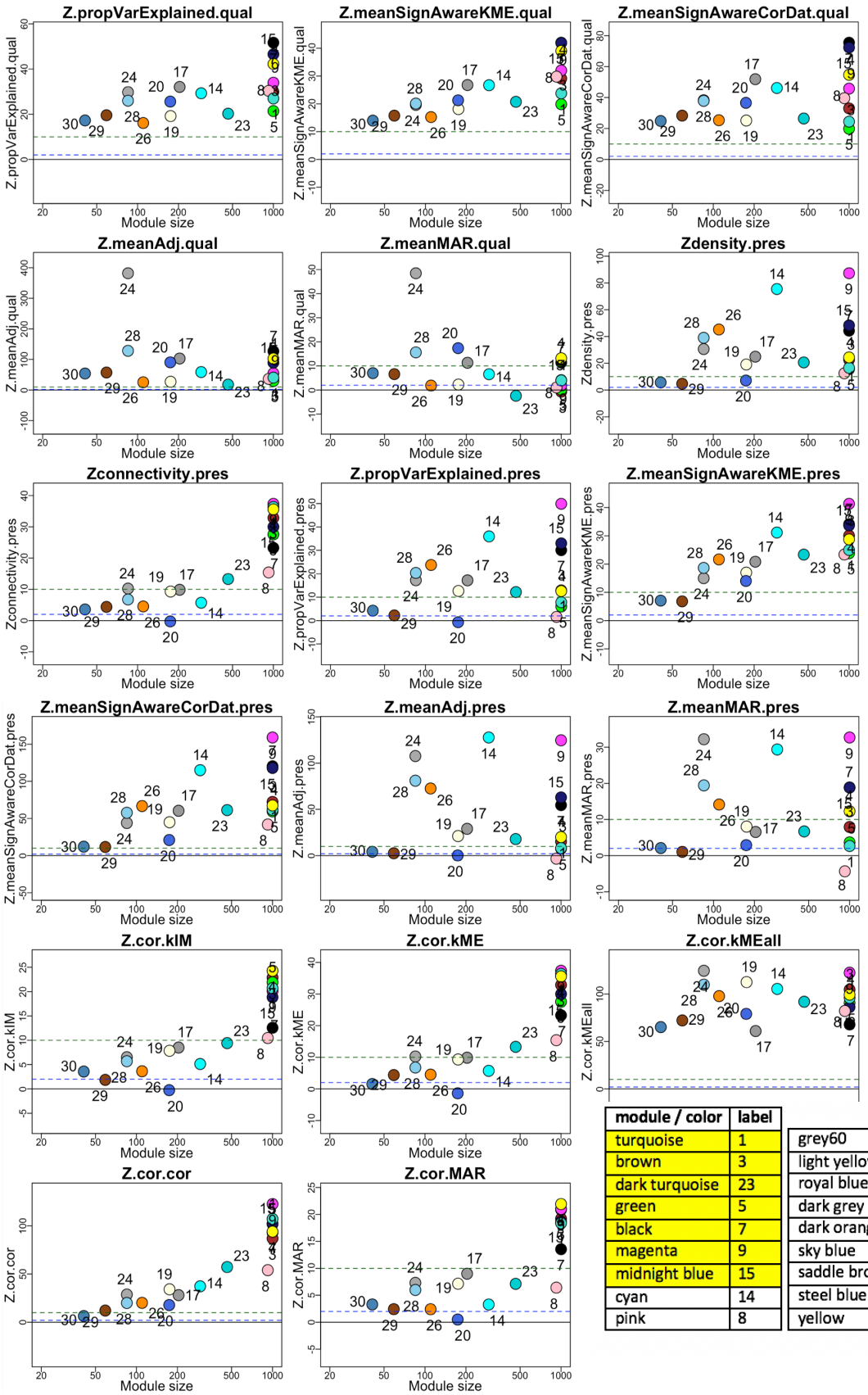

module / color	label
turquoise	1
brown	3
dark turquoise	23
green	5
black	7
magenta	9
midnight blue	15
cyan	14
pink	8

grey60	17
light yellow	19
royal blue	20
dark grey	24
dark orange	26
sky blue	28
saddle brown	29
steel blue	30
yellow	4

Figure S5. Individual module preservation and quality statistics underlying composite Zsummary scores. Multiple density-based and connectivity-based module-preservation statistics were assessed to determine the distinct properties of network structure preserved between the reference and test networks. In line with the composite $Z_{summary}$ statistic, individual module-preservation statistics mostly converged on the finding that 1) nodes sharing the same module in the reference network remain highly connected in the test network and 2) connectivity patterns between nodes underlying the reference network remain similar in the test network. Similarly, multiple module-quality based statistics were assessed to determine how distinct individual modules were from all other modules in the reference network. In line with the composite $Z_{summary}$ statistic, the majority of the evaluated module-quality statistics indicate robust module definitions across networks created from random splits of the original reference data. Permutation tests were performed to adjust the observed preservation and quality statistics of each module for random chance by defining Z statistics. Zstatistic < 2 (blue dotted line): no evidence for preservation/quality; 2 < Zstatistic < 10 (green dotted line): moderate evidence for preservation/quality; Zstatistic > 10: strong evidence for preservation/quality. Refer to Langfelder et al. (2017) for a detailed description of the individual module preservation and quality statistics plotted above. Both numeric and color-based labels were used to mark individual modules. The coding system corresponding to module labels is provided in the bottom right corner of the figure; labels highlighted in yellow indicate the 7 modules harboring 3q29 interval genes.

Langfelder P, Luo R, Oldham MC, Horvath S. Is My Network Module Preserved and Reproducible? *Plos Computational Biology* 2011; **7**(1).

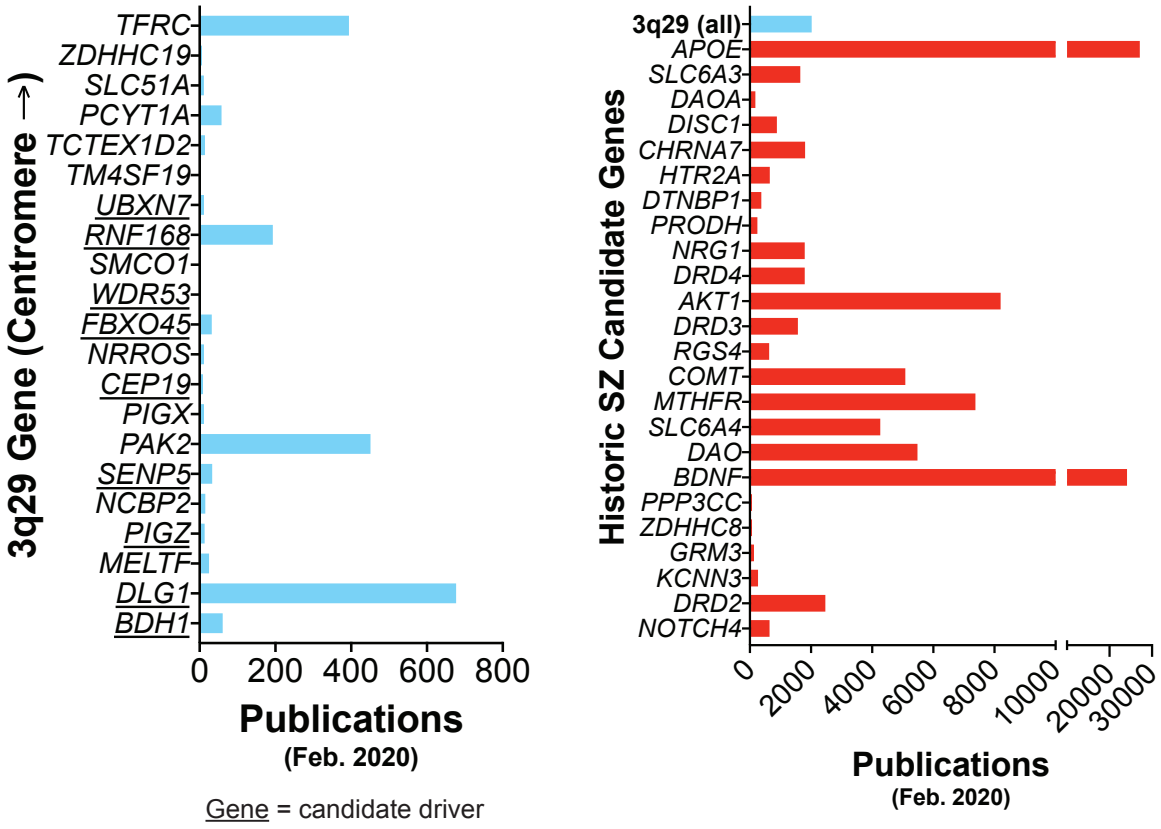

Figure S6. Publication numbers for 3q29 genes and historic schizophrenia spectrum disorder candidate genes. The total number of PubMed articles retrieved with a search for the symbol of each gene is shown above. Notably, of the prioritized driver genes (underlined) identified in this study (left), only *DLG1* has a publication history that compares favorably with historic schizophrenia spectrum disorder (SZ) candidate genes (right) that were typically identified by genetic linkage and association studies. The majority of 3q29 interval genes remain understudied.

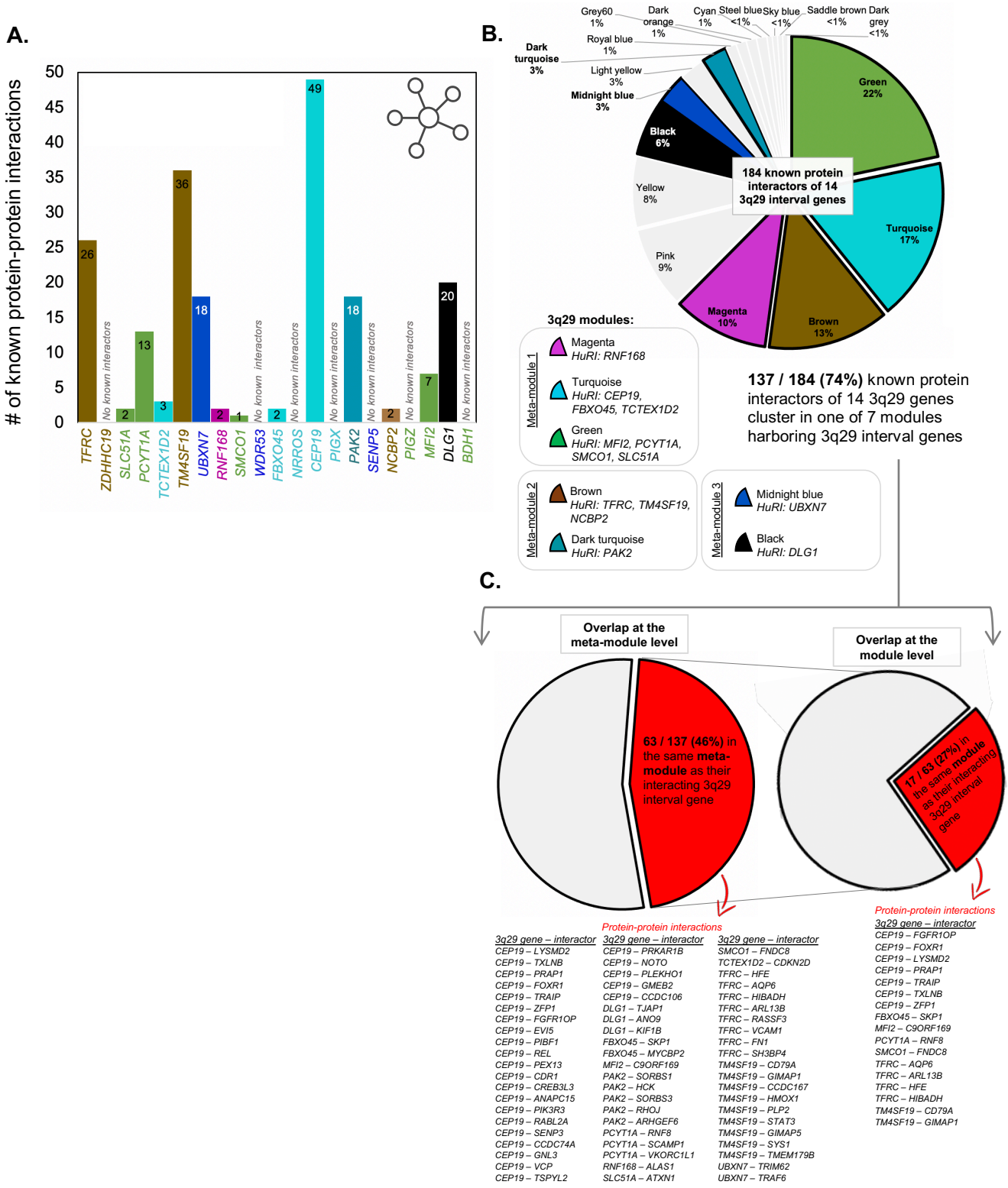

Figure S7. Overlap between known protein-protein interactions (PPI) and gene co-expression patterns of 3q29 interval genes. (A) Number of known binary protein interactors of 3q29 interval genes curated from

the Human Reference Protein Interactome (HuRI) database. Of the 21 protein coding genes located in the 3q29 interval, only 14 were found to have an entry on HuRI, 50% of which have less than 8 known proteome-wide interactors. X axis reflects the chromosomal order of the 3q29Del locus from centromere to telomere. Colors represent gene co-expression network modules. **(B)** Distribution of known protein interactors of 3q29 interval genes across our gene co-expression network. A total of 193 distinct protein interactors were identified on HuRI for 14 3q29 interval genes (after removing duplicates), 184 of which were identified as a node in our gene co-expression network. Of these 184, 137 (74%) were found to cluster in one of seven modules harboring 3q29 interval genes. **(C)** Overlap between 3q29 interval genes and their protein interactors at the module and meta-module levels of gene co-expression network organization. 46% of the protein interactors identified in 3q29 modules share the same meta-module as their interacting 3q29 interval gene, 27% of which further show an overlap at the module level.

Figure S8. STRING protein-protein interaction (PPI) networks of genes co-expressed in 3q29 modules. PPI network of genes co-clustering in the **(A)** black, **(B)** midnight blue, **(C)** brown, **(D)** magenta, **(E)** dark turquoise, **(F)** green, and **(G)** turquoise modules are visualized by node-link diagrams. Network nodes represent protein products of genes that were found to co-cluster in the same gene co-expression network modules as the 21 protein-coding 3q29 interval genes. Edges represent PPI curated from the STRING database (https://string-db.org/). Line thickness is proportional to the strength of available evidence for each PPI. For clear and effective visualization, only nodes from seven distinct 3q29 modules that are part of a known physical protein complex and are connected by at least a "high confidence" (0.7) strength of evidence for interaction are included in these illustrations. Based on these criteria, disconnected nodes were discarded from the graphs.

A. Black module

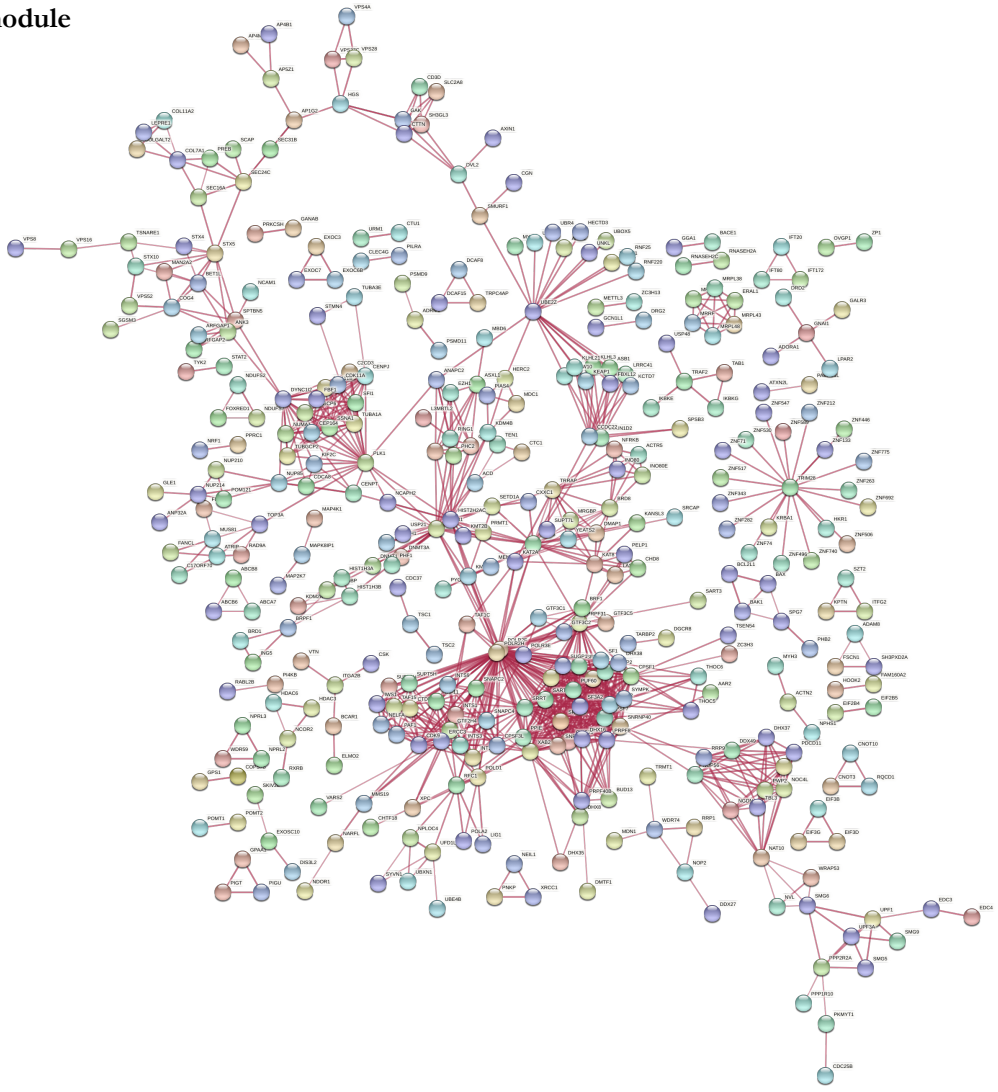

B. Midnight blue module

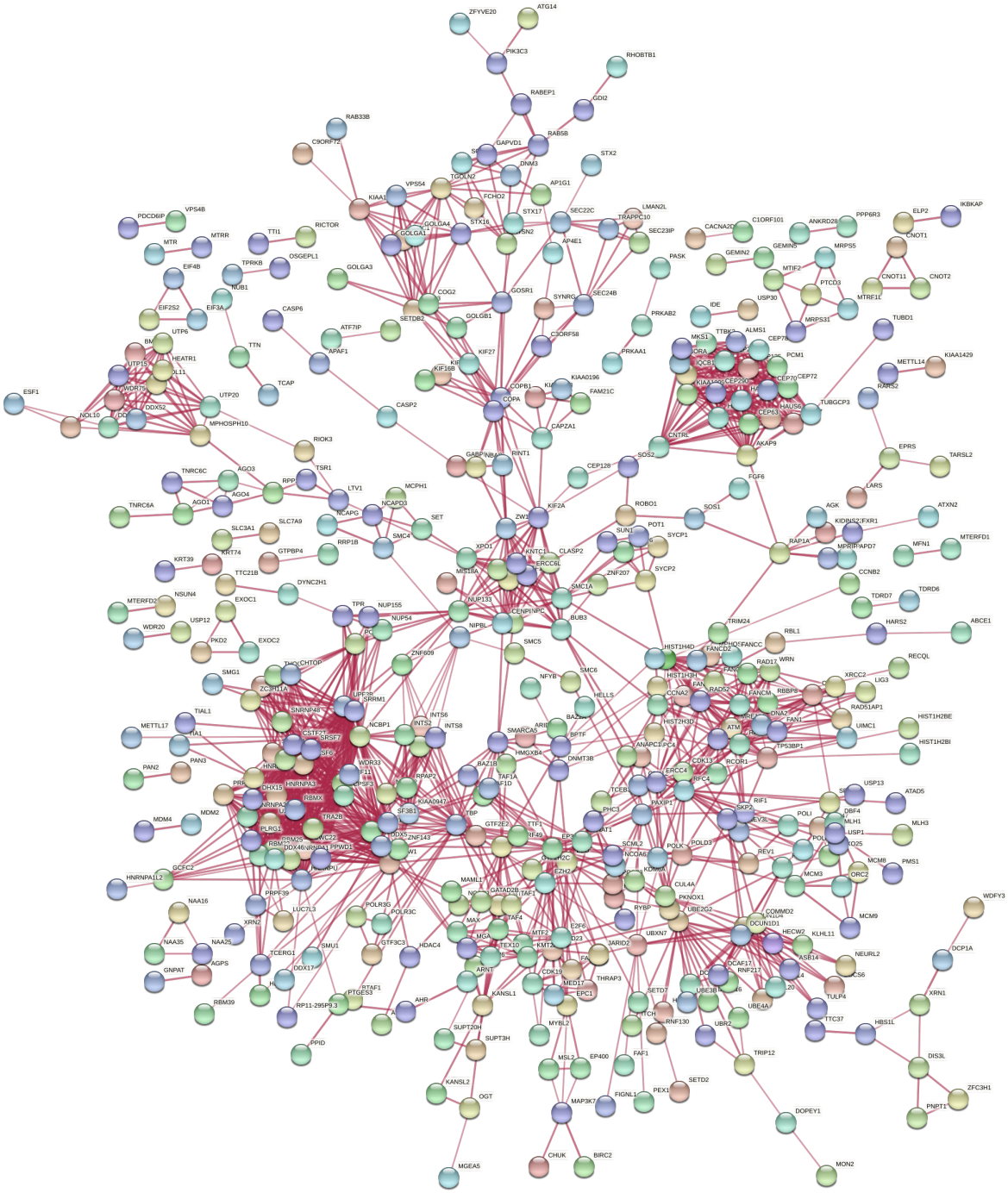
ATG14
ZFYVE20
PIK3C3
RHOBTB1
RABEP1
GDI2
RAB33B
C9ORF72
RAB5B
GAPVD1
STX2
DNM3
TGOLN2
AP1G1
VPS4A
KIAA1033
FCHO2
STX17
SEC22C
TRAPPC10
LMAN2L
SEC23IP
AP4E1
PASK
GOLGA4
GOLGA1
SNX2
VPS4B
PDCD6IP
MTRR
MTR
RICTOR
TTI1
OSGEPL1
TPRKB
NUB1
EIF4B
GOLGA3
COG2
GOSR1
SYNRG
SEC24B
EIF2S2
EIF3A
CASP6
SETD8
GOLGB1
ATF7IP
PRKAB2
IDE
USP30
MRPS31
TUBD1
UTP6
C3ORF58
APAF1
TTN
KIF27
KIF16B
PRKAA1
MKS1
TTBK2
ALMS1
CEP78
PCM1
CEP72
CEP70
KIAA1429
METTL14
RARS2
TUBGCP3
ESF1
UTP15
HEATR1
WDR75
UTP20
DDX52
TCAP
COPB1
COPA
KIAA0196
FAM21C
CASP2
CAPZA1
CNTRL
AKAP9
NOL10
MPHOSPH10
RIOK3
GABPB1
RINT1
CEP128
SOS2
EPRS
TARSL2
TNRC6C
AGO3
TSR1
RPP
AGO4
AGO1
TNRC6A
LTV1
MCPH1
NCAPD3
NCAPG
SET
SMC4
RRP1B
SLC3A1
SLC7A9
KRT74
GTPBP4
KRT39
TTC21B
DYNC2H1
NSUN4
MTERFD2
EXOC1
USP12
WDR20
PKD2
EXOC2
ZW10
KIF2A
ROBO1
SUN1
POT1
SYCP1
SYCP2
SOS1
FGF6
LARS
AGK
ATXN2
KIDINS220
EXR1
MPRIP
APD7
MFN1
MTERFD1
RAP1A
CCNB2
TDRD7
TDRD6
KNTC1
CLASP2
ERCC6L
MIS18A
SMC1A
ZNF207
XPO1
NUP133
CENPNPC
NUP155
NUP54
NIPBL
BUB3
TPR
SMC5
ZNF609
TRIM24
RBL1
HARS2
ABCE1
HIST1H4D
FANCD2
FANCC
RAD17
WRN
RECQL
HIST1H3H
FAN1
CCNA2
RAD52
FANCM
RBBP8
XRCC2
LIG3
RAD51AP1
HIST1H2BE
HIST1H2BI
UIMC1
HIST2H3D
ATM
DNA2
TP53BP1
RCOR1
CDK13
ERCC4
RFC4
ANAPC1
PCA
TCEB3
PAXIP1
PHC3
SKP2
RIF1
USP13
ATAD5
DBF4
MLH1
MLH3
USP1
POLI
REV1
POLD3
POLK
SCML2
NCOA6
KDM5A
EZH2
MCM8
PMS1
MCM3
ORC2
CUL4A
PKNOX1
UBE2D2
COMMD2
DCUN1D1
HECW2
KLHL11
ASB14
NEURL2
CS6
TULP4
TTC37
HBS1L
UBE4A
UBR2
RNF130
FITCH
SETD7
UBE3B
DCAF17
RNF217
L20
L4
MCM9
WDFY3
DCP1A
XRN1
DIS3L
ZFC3H1
PNPT1
DOPEY1
MON2
TRIP12
FAF1
EP400
MSL2
SETD2
PEX1
FIGNL1
MAP3K7
CHUK
BIRC2
MGEA5
KANSL2
OGT
SUPT20H
SUPT3H
MYBL2
EPC1
KANSL1
THRAP3
MED17
CDK19
ARNT
KMT2A
TEX10
MGA
MTF2
E2F6
DP3
UBXN7
JARID2
FAM
MAX
TAF4
TAF5
TAF1
GATAD2B
MAML1
NCOR2
PPID
RBM39
RP11-295P9.3
PTGES3
BTAF1
AHR
ARNT
GTF3C3
HDAC4
SMU1
TCERG1
DDX17
AGPS
GNPAT
NAA35
NAA25
XRN2
NAA16
LUC7L3
POLR3G
POLR3C
PRPF39
HNRNPA1L2
GCFC2
PPWD1
RBM25
WDR22
ZNF143
DDX5
SF3B1
TBP
GTF2E2
TTF1
RPAP2
CPSF3
WDR33
CPSF1
SF3
NCBP1
INTS2
INTS6
INTS8
SMARCA5
ARID1B
BPTF
HMGXB4
BAZ1B
TAF1A
TAF1D
DNMT3B
BAZ2A
SNRNP48
SRRM1
SRSF7
SF3
HNRNPA3
RBMX
TRA2B
KIAA0947
PRPF8
DHX15
PRP
HNR
PAN2
PAN3
MDM4
MDM2
METTL17
TIAL1
KIA1
ZC3H11A
THOC5
CHTOP
SMG1
NFYB
SMC6
HELLS
ZNF
SMG
UPF3B
ESF
SRRM
PC
NUP
NIPBL
BUB
SMC
ZNF
TPR
NUP
CENPNPC
MIS18A
SMC1A
ZNF207
XPO1
KNTC1
CLASP2
ERCC6L
ZW10
KIF2A
ROBO1
SUN1
POT1
SYCP1
SYCP2
SOS1
FGF6
LARS
AGK
ATXN2
KIDINS220
EXR1
MPRIP
APD7
MFN1
MTERFD1
RAP1A
CCNB2
TDRD7
TDRD6

C. Brown module

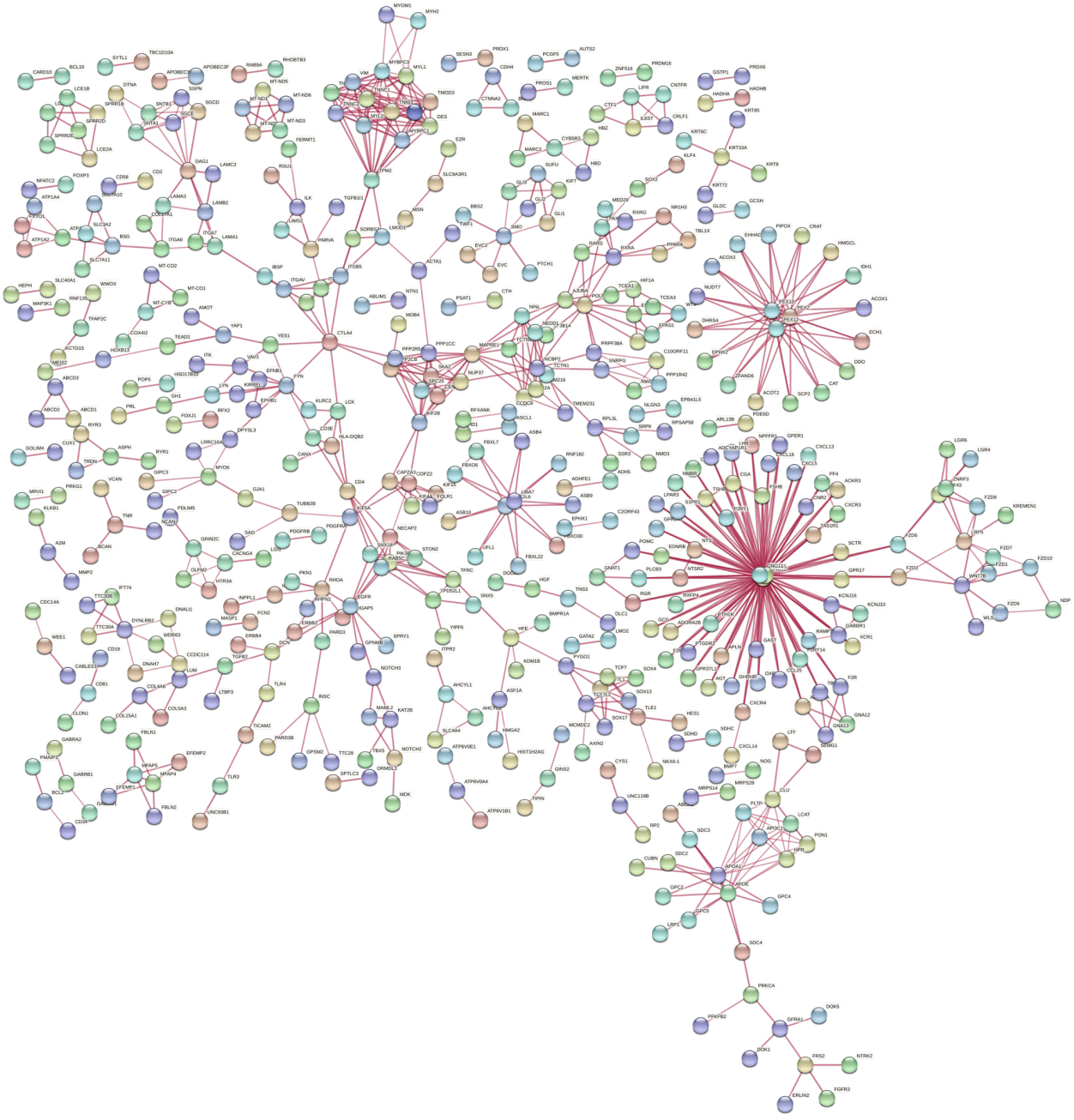

D. Magenta module

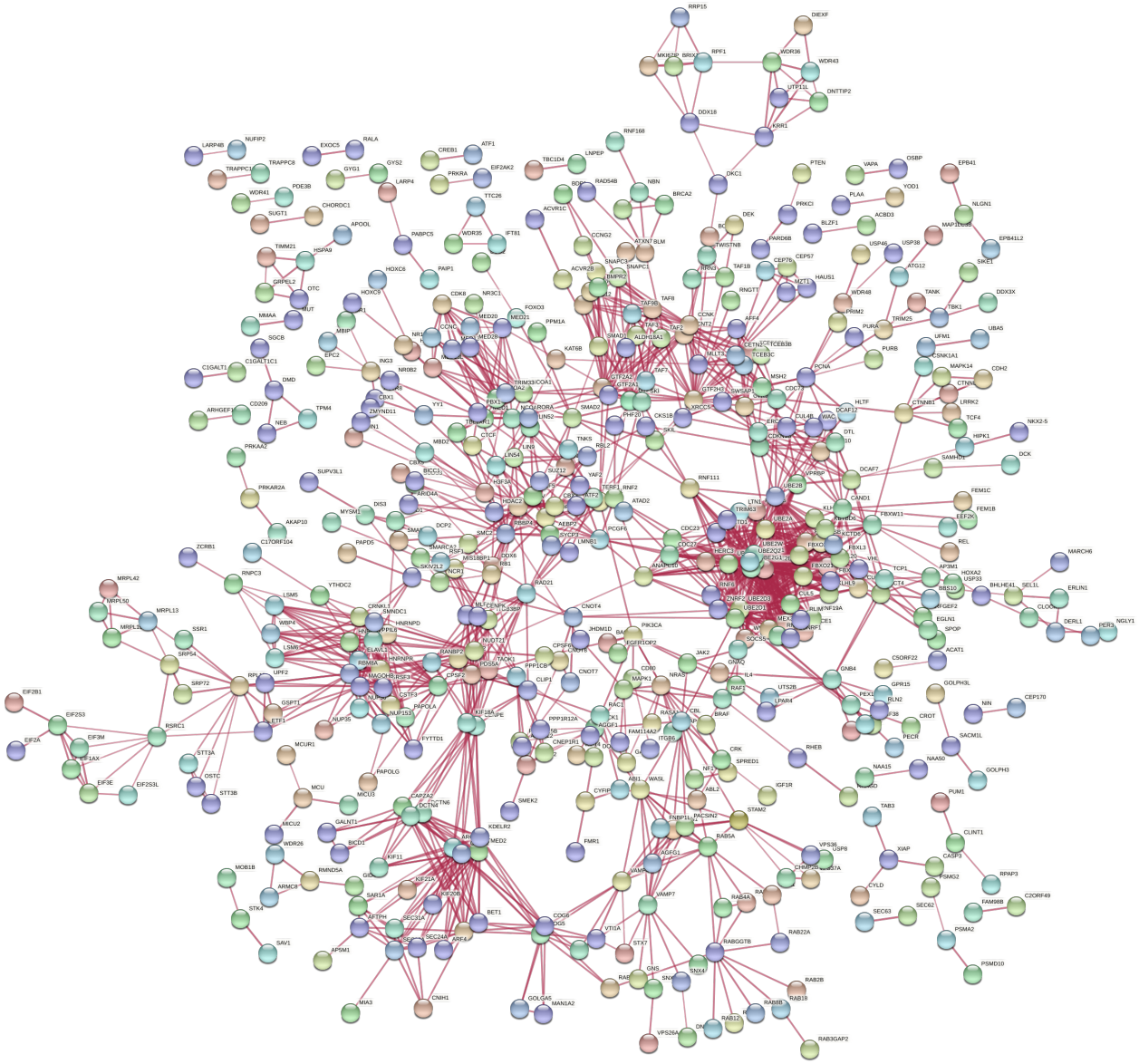

E. Dark turquoise module

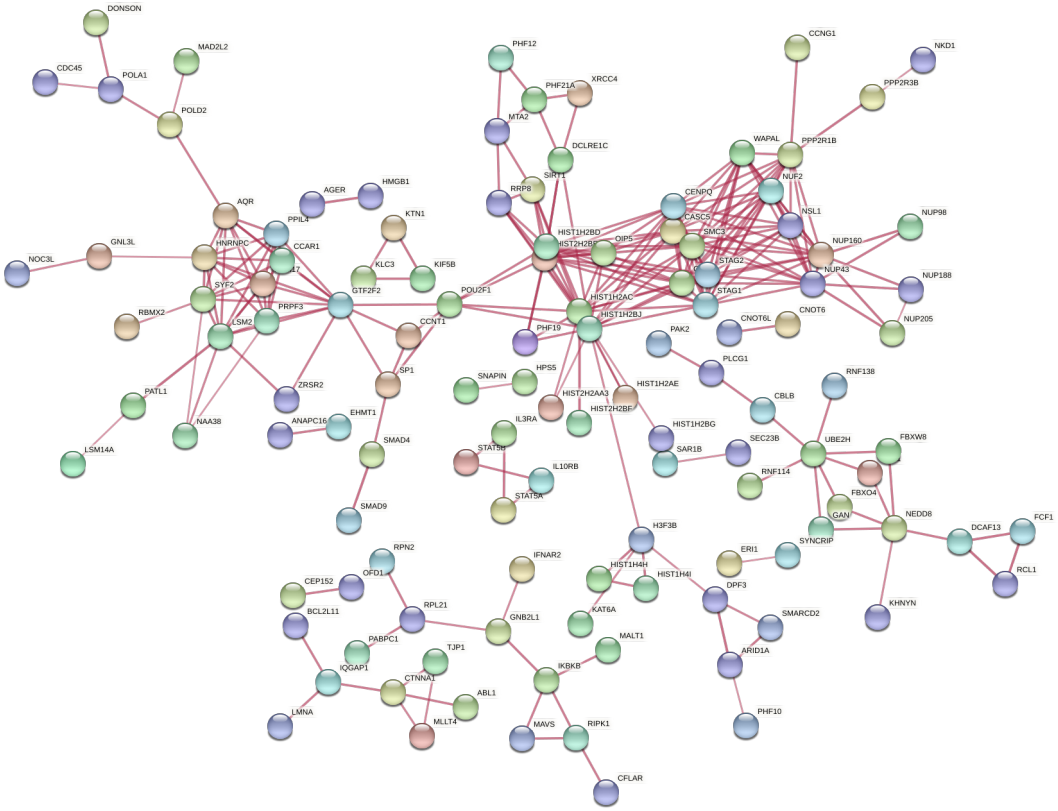

F. Green module

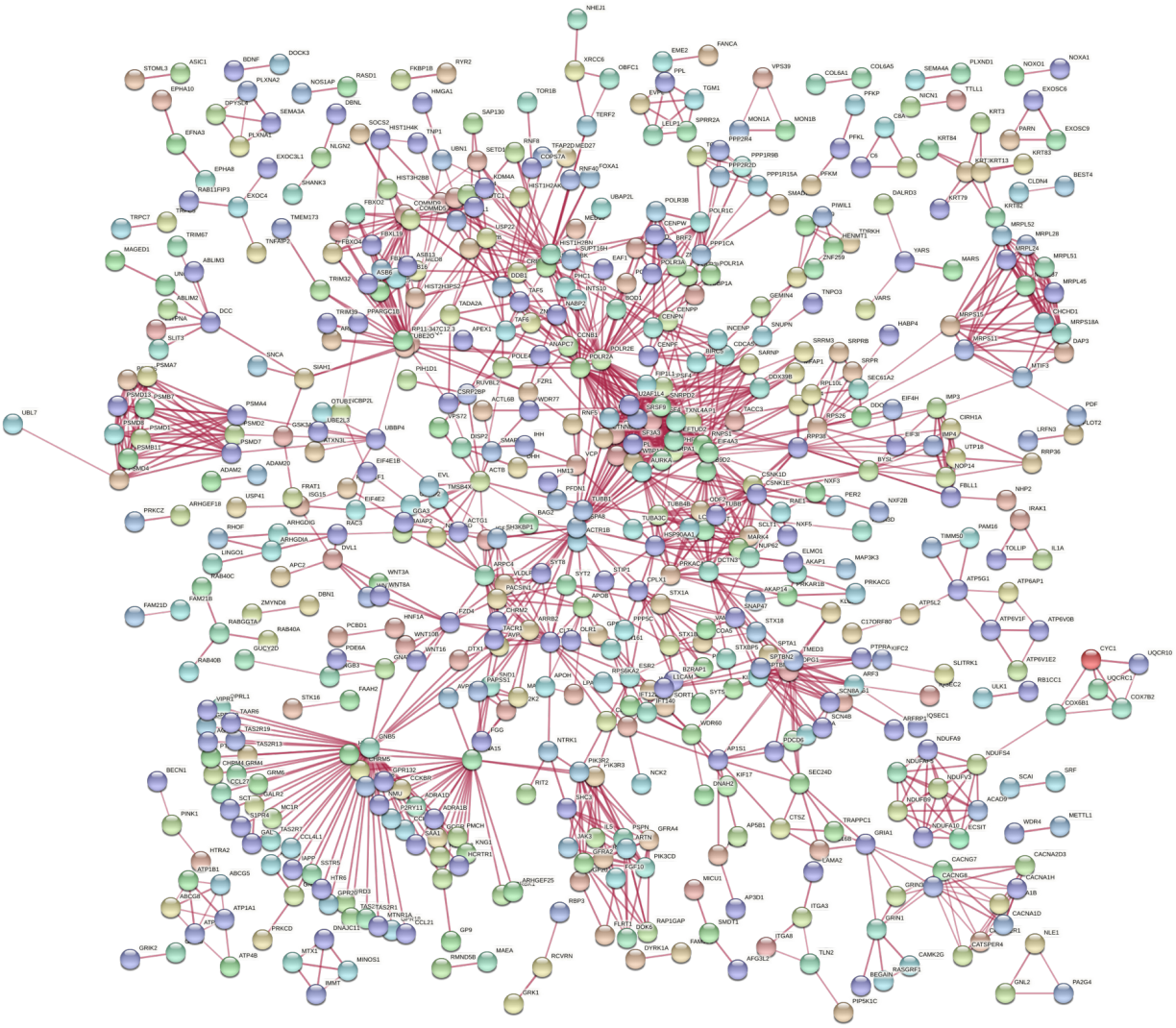

G. Turquoise module

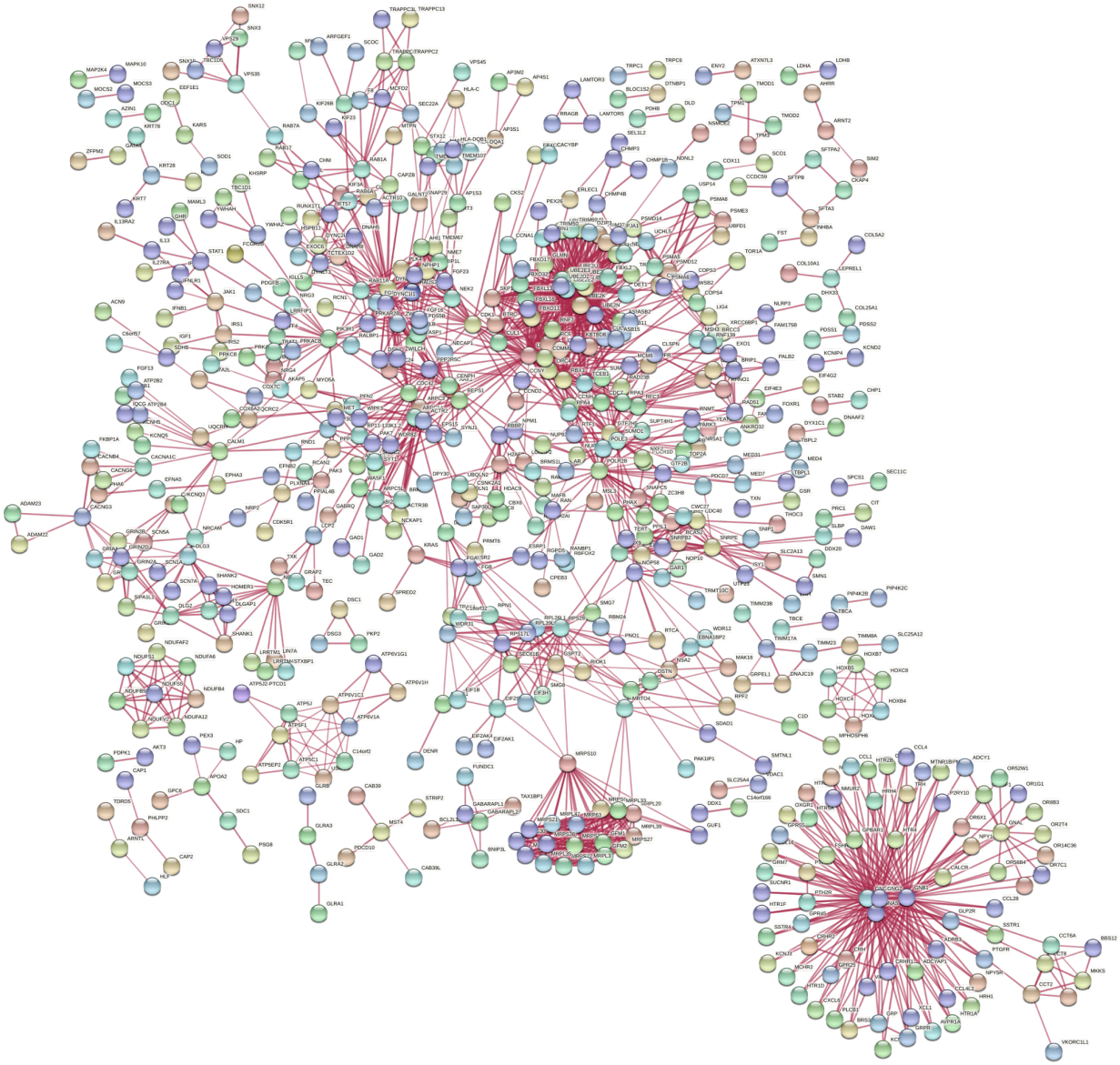

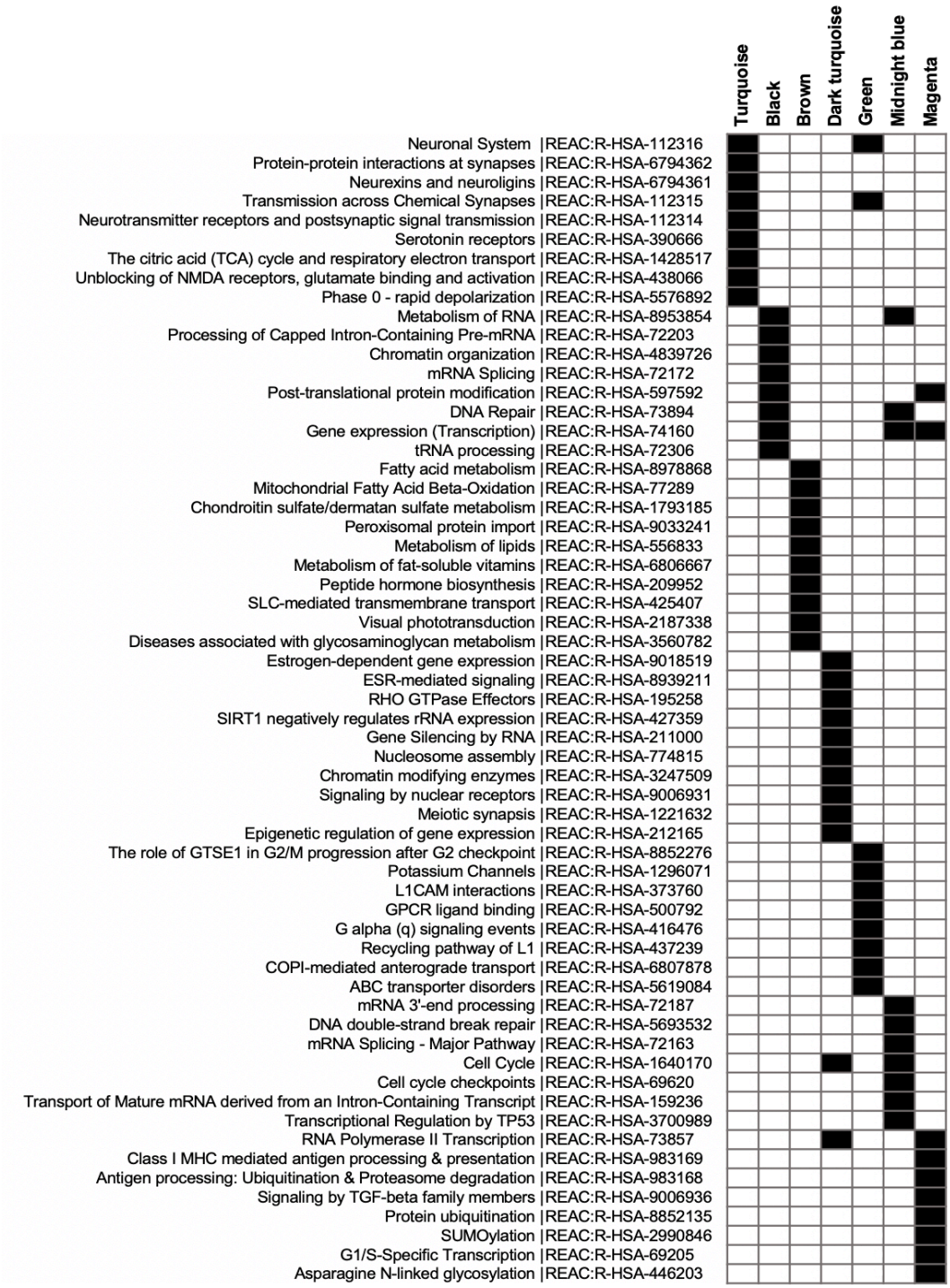

Figure S9. Amalgamated illustration of top biological processes and pathways enriched in 3q29 modules. Enrichment plots from Fig. 2D have been combined in this discrete heatmap to illustrate the distinct vs. shared enrichment profiles of the top Reactome terms overrepresented in different 3q29 modules. Black cells indicate significant enrichment at adjusted-$P < 0.05$.

Supplemental References

1. Langfelder P, Horvath S (2008): WGCNA: an R package for weighted correlation network analysis. *BMC Bioinformatics*. 9:559.

2. de la Fuente A (2010): From 'differential expression' to 'differential networking' - identification of dysfunctional regulatory networks in diseases. *Trends Genet*. 26:326-333.

3. Mulle JG (2015): The 3q29 deletion confers >40-fold increase in risk for schizophrenia. *Mol Psychiatry*. 20:1028-1029.

4. Hafner H, Maurer K, Loffler W, Fatkenheuer B, an der Heiden W, Riecher-Rossler A, et al. (1994): The epidemiology of early schizophrenia. Influence of age and gender on onset and early course. *Br J Psychiatry Suppl*.29-38.

5. Howard R, Rabins PV, Seeman MV, Jeste DV (2000): Late-onset schizophrenia and very-late-onset schizophrenia-like psychosis: an international consensus. The International Late-Onset Schizophrenia Group. *Am J Psychiatry*. 157:172-178.

6. Fuster JM (2002): Frontal lobe and cognitive development. *J Neurocytol*. 31:373-385.

7. Owen MJ, O'Donovan MC (2017): Schizophrenia and the neurodevelopmental continuum:evidence from genomics. *World Psychiatry*. 16:227-235.

8. Langfelder P, Horvath S (2012): Fast R Functions for Robust Correlations and Hierarchical Clustering. *J Stat Softw*. 46.

9. Consortium GT (2015): Human genomics. The Genotype-Tissue Expression (GTEx) pilot analysis: multitissue gene regulation in humans. *Science*. 348:648-660.

10. Oldham MC, Konopka G, Iwamoto K, Langfelder P, Kato T, Horvath S, et al. (2008): Functional organization of the transcriptome in human brain. *Nat Neurosci*. 11:1271-1282.

11. Harrow J, Frankish A, Gonzalez JM, Tapanari E, Diekhans M, Kokocinski F, et al. (2012): GENCODE: the reference human genome annotation for The ENCODE Project. *Genome Res*. 22:1760-1774.

12. Miller JA, Cai C, Langfelder P, Geschwind DH, Kurian SM, Salomon DR, et al. (2011): Strategies for aggregating gene expression data: the collapseRows R function. *BMC Bioinformatics*. 12:322.

13. van Dam S, Vosa U, van der Graaf A, Franke L, de Magalhaes JP (2018): Gene co-expression analysis for functional classification and gene-disease predictions. *Brief Bioinform*. 19:575-592.

14. Leek JT, Johnson WE, Parker HS, Jaffe AE, Storey JD (2012): The sva package for removing batch effects and other unwanted variation in high-throughput experiments. *Bioinformatics*. 28:882-883.

15. Johnson WE, Li C, Rabinovic A (2007): Adjusting batch effects in microarray expression data using empirical Bayes methods. *Biostatistics*. 8:118-127.

16. Ferreira PG, Munoz-Aguirre M, Reverter F, Sa Godinho CP, Sousa A, Amadoz A, et al. (2018): The effects of death and post-mortem cold ischemia on human tissue transcriptomes. *Nat Commun*. 9:490.

17. Wilcox R (1997): *Introduction to Robust Estimation and Hypothesis Testing*. San Diego: Academic Press.

18. Barabasi AL, Oltvai ZN (2004): Network biology: understanding the cell's functional organization. *Nat Rev Genet*. 5:101-113.

19. Fu J, Keurentjes JJ, Bouwmeester H, America T, Verstappen FW, Ward JL, et al. (2009): System-wide molecular evidence for phenotypic buffering in Arabidopsis. *Nat Genet*. 41:166-167.

20. Ouma WZ, Pogacar K, Grotewold E (2018): Topological and statistical analyses of gene regulatory networks reveal unifying yet quantitatively different emergent properties. *PLoS Comput Biol*. 14:e1006098.

21. Lachowiec J, Queitsch C, Kliebenstein DJ (2016): Molecular mechanisms governing differential robustness of development and environmental responses in plants. *Ann Bot*. 117:795-809.

22. Zhang B, Horvath S (2005): A general framework for weighted gene co-expression network analysis. *Stat Appl Genet Mol Biol*. 4:Article17.

23. Ge H, Liu Z, Church GM, Vidal M (2001): Correlation between transcriptome and interactome mapping data from Saccharomyces cerevisiae. *Nat Genet*. 29:482-486.

24. Miller JA, Horvath S, Geschwind DH (2010): Divergence of human and mouse brain transcriptome highlights Alzheimer disease pathways. *Proc Natl Acad Sci U S A*. 107:12698-12703.

25. Yip AM, Horvath S (2007): Gene network interconnectedness and the generalized topological overlap measure. *BMC Bioinformatics*. 8:22.

26. Ravasz E, Somera AL, Mongru DA, Oltvai ZN, Barabasi AL (2002): Hierarchical organization of modularity in metabolic networks. *Science*. 297:1551-1555.

27. Carlson MR, Zhang B, Fang Z, Mischel PS, Horvath S, Nelson SF (2006): Gene connectivity, function, and sequence conservation: predictions from modular yeast co-expression networks. *BMC Genomics*. 7:40.

28. Horvath S, Zhang B, Carlson M, Lu KV, Zhu S, Felciano RM, et al. (2006): Analysis of oncogenic signaling networks in glioblastoma identifies ASPM as a molecular target. *Proc Natl Acad Sci U S A*. 103:17402-17407.

29. Oldham MC, Horvath S, Geschwind DH (2006): Conservation and evolution of gene coexpression networks in human and chimpanzee brains. *Proc Natl Acad Sci U S A*. 103:17973-17978.

30. Ye Y, Godzik A (2004): Comparative analysis of protein domain organization. *Genome Res*. 14:343-353.

31. Li A, Horvath S (2007): Network neighborhood analysis with the multi-node topological overlap measure. *Bioinformatics*. 23:222-231.

32. Voigt A, Almaas E (2019): Assessment of weighted topological overlap (wTO) to improve fidelity of gene co-expression networks. *BMC Bioinformatics*. 20:58.

33. Langfelder P, Zhang B, Horvath S (2008): Defining clusters from a hierarchical cluster tree: the Dynamic Tree Cut package for R. *Bioinformatics*. 24:719-720.

34. Forsyth JK, Nachun D, Gandal MJ, Geschwind DH, Anderson AE, Coppola G, et al. (2020): Synaptic and Gene Regulatory Mechanisms in Schizophrenia, Autism, and 22q11.2 Copy Number Variant-Mediated Risk for Neuropsychiatric Disorders. *Biol Psychiatry*. 87:150-163.

35. Uddin M, Pellecchia G, Thiruvahindrapuram B, D'Abate L, Merico D, Chan A, et al. (2016): Indexing Effects of Copy Number Variation on Genes Involved in Developmental Delay. *Sci Rep*. 6:28663.

36. Gerring ZF, Gamazon ER, Derks EM, Major Depressive Disorder Working Group of the Psychiatric Genomics C (2019): A gene co-expression network-based analysis of multiple brain tissues reveals novel genes and molecular pathways underlying major depression. *PLoS Genet*. 15:e1008245.

37. Kang HJ, Kawasawa YI, Cheng F, Zhu Y, Xu X, Li M, et al. (2011): Spatio-temporal transcriptome of the human brain. *Nature*. 478:483-489.

38. BrainSpan Atlas of the Developing Human Brain (2013): Technical white paper: transcriptome profiling by RNA sequencing and exon microarray (v.5).

39. Langfelder P, Luo R, Oldham MC, Horvath S (2011): Is My Network Module Preserved and Reproducible? *Plos Computational Biology*. 7.

40. Luxburg Uv (2010): Clustering Stability: An Overview. *Foundations and Trends in Machine Learning*. 2:235-274.

41. Miklos GL, Rubin GM (1996): The role of the genome project in determining gene function: insights from model organisms. *Cell*. 86:521-529.

42. Rhee SY, Wood V, Dolinski K, Draghici S (2008): Use and misuse of the gene ontology annotations. *Nat Rev Genet*. 9:509-515.

43. Reimand J, Isserlin R, Voisin V, Kucera M, Tannus-Lopes C, Rostamianfar A, et al. (2019): Pathway enrichment analysis and visualization of omics data using g:Profiler, GSEA, Cytoscape and EnrichmentMap. *Nat Protoc*. 14:482-517.

44. Reimand J, Kull M, Peterson H, Hansen J, Vilo J (2007): g:Profiler--a web-based toolset for functional profiling of gene lists from large-scale experiments. *Nucleic Acids Res*. 35:W193-200.

45. Supek F, Bosnjak M, Skunca N, Smuc T (2011): REVIGO summarizes and visualizes long lists of gene ontology terms. *PLoS One*. 6:e21800.

46. Luck K, Kim DK, Lambourne L, Spirohn K, Begg BE, Bian W, et al. (2020): A reference map of the human binary protein interactome. *Nature*. 580:402-408.

47. Szklarczyk D, Gable AL, Lyon D, Junge A, Wyder S, Huerta-Cepas J, et al. (2019): STRING v11: protein-protein association networks with increased coverage, supporting functional discovery in genome-wide experimental datasets. *Nucleic Acids Res*. 47:D607-D613.

48. Langfelder P, Horvath S (2007): Eigengene networks for studying the relationships between co-expression modules. *BMC Syst Biol*. 1:54.

49. Cooper TF, Morby AP, Gunn A, Schneider D (2006): Effect of random and hub gene disruptions on environmental and mutational robustness in Escherichia coli. *BMC Genomics*. 7:237.

50. Yu H, Braun P, Yildirim MA, Lemmens I, Venkatesan K, Sahalie J, et al. (2008): High-quality binary protein interaction map of the yeast interactome network. *Science*. 322:104-110.

51. Wachi S, Yoneda K, Wu R (2005): Interactome-transcriptome analysis reveals the high centrality of genes differentially expressed in lung cancer tissues. *Bioinformatics*. 21:4205-4208.

52. Jonsson PF, Bates PA (2006): Global topological features of cancer proteins in the human interactome. *Bioinformatics*. 22:2291-2297.

53. Xu J, Li Y (2006): Discovering disease-genes by topological features in human protein-protein interaction network. *Bioinformatics*. 22:2800-2805.

54. Sanati N, Iancu OD, Wu G, Jacobs JE, McWeeney SK (2018): Network-Based Predictors of Progression in Head and Neck Squamous Cell Carcinoma. *Front Genet*. 9:183.

55. Laine VN, Verhagen I, Mateman AC, Pijl A, Williams TD, Gienapp P, et al. (2019): Exploration of tissue-specific gene expression patterns underlying timing of breeding in contrasting temperature environments in a song bird. *BMC Genomics*. 20:693.

56. Li W, Wang L, Wu Y, Yuan Z, Zhou J (2020): Weighted gene coexpression network analysis to identify key modules and hub genes associated with atrial fibrillation. *Int J Mol Med*. 45:401-416.

57. Ala U, Piro RM, Grassi E, Damasco C, Silengo L, Oti M, et al. (2008): Prediction of human disease genes by human-mouse conserved coexpression analysis. *PLoS Comput Biol*. 4:e1000043.

58. Segal E, Friedman N, Koller D, Regev A (2004): A module map showing conditional activity of expression modules in cancer. *Nat Genet*. 36:1090-1098.

59. Torkamani A, Dean B, Schork NJ, Thomas EA (2010): Coexpression network analysis of neural tissue reveals perturbations in developmental processes in schizophrenia. *Genome Res*. 20:403-412.

60. van Dam S, Cordeiro R, Craig T, van Dam J, Wood SH, de Magalhaes JP (2012): GeneFriends: an online co-expression analysis tool to identify novel gene targets for aging and complex diseases. *BMC Genomics*. 13:535.

61. McCarroll SA, Murphy CT, Zou S, Pletcher SD, Chin CS, Jan YN, et al. (2004): Comparing genomic expression patterns across species identifies shared transcriptional profile in aging. *Nat Genet*. 36:197-204.

62. Deciphering Developmental Disorders S (2017): Prevalence and architecture of de novo mutations in developmental disorders. *Nature*. 542:433-438.

63. Abrahams BS, Arking DE, Campbell DB, Mefford HC, Morrow EM, Weiss LA, et al. (2013): SFARI Gene 2.0: a community-driven knowledgebase for the autism spectrum disorders (ASDs). *Mol Autism*. 4:36.

64. Banerjee-Basu S, Packer A (2010): SFARI Gene: an evolving database for the autism research community. *Dis Model Mech*. 3:133-135.

65. Meng Q, Wang K, Brunetti T, Xia Y, Jiao C, Dai R, et al. (2018): The DGCR5 long noncoding RNA may regulate expression of several schizophrenia-related genes. *Sci Transl Med*. 10.

66. Psych EC, Akbarian S, Liu C, Knowles JA, Vaccarino FM, Farnham PJ, et al. (2015): The PsychENCODE project. *Nat Neurosci*. 18:1707-1712.

67. Fromer M, Roussos P, Sieberts SK, Johnson JS, Kavanagh DH, Perumal TM, et al. (2016): Gene expression elucidates functional impact of polygenic risk for schizophrenia. *Nat Neurosci*. 19:1442-1453.

68. Schizophrenia Working Group of the Psychiatric Genomics C (2014): Biological insights from 108 schizophrenia-associated genetic loci. *Nature*. 511:421-427.

69. Li J, Cai T, Jiang Y, Chen H, He X, Chen C, et al. (2016): Genes with de novo mutations are shared by four neuropsychiatric disorders discovered from NPdenovo database. *Mol Psychiatry*. 21:290-297.

70. Kunkle BW, Grenier-Boley B, Sims R, Bis JC, Damotte V, Naj AC, et al. (2019): Genetic meta-analysis of diagnosed Alzheimer's disease identifies new risk loci and implicates Abeta, tau, immunity and lipid processing. *Nat Genet*. 51:414-430.

71. Chang D, Nalls MA, Hallgrimsdottir IB, Hunkapiller J, van der Brug M, Cai F, et al. (2017): A meta-analysis of genome-wide association studies identifies 17 new Parkinson's disease risk loci. *Nat Genet*. 49:1511-1516.

72. Momozawa Y, Dmitrieva J, Theatre E, Deffontaine V, Rahmouni S, Charloteaux B, et al. (2018): IBD risk loci are enriched in multigenic regulatory modules encompassing putative causative genes. *Nat Commun*. 9:2427.

73. Yengo L, Sidorenko J, Kemper KE, Zheng Z, Wood AR, Weedon MN, et al. (2018): Meta-analysis of genome-wide association studies for height and body mass index in approximately 700000 individuals of European ancestry. *Hum Mol Genet.* 27:3641-3649.

74. Shen L (2019): GeneOverlap: Test and visualize gene overlaps. R package version 1.20.0 ed.

75. Chan SY, Loscalzo J (2012): The emerging paradigm of network medicine in the study of human disease. *Circ Res.* 111:359-374.

76. Rutkowski TP, Purcell RH, Pollak RM, Grewenow SM, Gafford GM, Malone T, et al. (2021): Behavioral changes and growth deficits in a CRISPR engineered mouse model of the schizophrenia-associated 3q29 deletion. *Mol Psychiatry.* 26:772-783.

77. Anders S, Pyl PT, Huber W (2015): HTSeq--a Python framework to work with high-throughput sequencing data. *Bioinformatics.* 31:166-169.

78. Love MI, Huber W, Anders S (2014): Moderated estimation of fold change and dispersion for RNA-seq data with DESeq2. *Genome Biol.* 15:550.

79. Robinson MD, McCarthy DJ, Smyth GK (2010): edgeR: a Bioconductor package for differential expression analysis of digital gene expression data. *Bioinformatics.* 26:139-140.

80. Costa-Silva J, Domingues D, Lopes FM (2017): RNA-Seq differential expression analysis: An extended review and a software tool. *PLoS One.* 12:e0190152.

81. Lin M, Pedrosa E, Hrabovsky A, Chen J, Puliafito BR, Gilbert SR, et al. (2016): Integrative transcriptome network analysis of iPSC-derived neurons from schizophrenia and schizoaffective disorder patients with 22q11.2 deletion. *BMC Syst Biol.* 10:105.

82. Brennand KJ, Simone A, Jou J, Gelboin-Burkhart C, Tran N, Sangar S, et al. (2011): Modelling schizophrenia using human induced pluripotent stem cells. *Nature.* 473:221-225.

83. Sayers EW, Beck J, Bolton EE, Bourexis D, Brister JR, Canese K, et al. (2021): Database resources of the National Center for Biotechnology Information. *Nucleic Acids Res.* 49:D10-D17.

84. Varelas X, Miller BW, Sopko R, Song S, Gregorieff A, Fellouse FA, et al. (2010): The Hippo pathway regulates Wnt/beta-catenin signaling. *Dev Cell.* 18:579-591.

85. Moller LLV, Klip A, Sylow L (2019): Rho GTPases-Emerging Regulators of Glucose Homeostasis and Metabolic Health. *Cells*. 8.

86. Madak-Erdogan Z, Charn TH, Jiang Y, Liu ET, Katzenellenbogen JA, Katzenellenbogen BS (2013): Integrative genomics of gene and metabolic regulation by estrogen receptors alpha and beta, and their coregulators. *Mol Syst Biol*. 9:676.

87. Su LF, Knoblauch R, Garabedian MJ (2001): Rho GTPases as modulators of the estrogen receptor transcriptional response. *J Biol Chem*. 276:3231-3237.

88. Marshall CR, Howrigan DP, Merico D, Thiruvahindrapuram B, Wu W, Greer DS, et al. (2017): Contribution of copy number variants to schizophrenia from a genome-wide study of 41,321 subjects. *Nat Genet*. 49:27-35.

89. Guan J, Cai JJ, Ji G, Sham PC (2019): Commonality in dysregulated expression of gene sets in cortical brains of individuals with autism, schizophrenia, and bipolar disorder. *Transl Psychiatry*. 9:152.

90. Mokhtari R, Lachman HM (2016): The Major Histocompatibility Complex (MHC) in Schizophrenia: A Review. *J Clin Cell Immunol*. 7.

91. Warnatsch A, Bergann T, Kruger E (2013): Oxidation matters: the ubiquitin proteasome system connects innate immune mechanisms with MHC class I antigen presentation. *Mol Immunol*. 55:106-109.

92. Uhlen M, Fagerberg L, Hallstrom BM, Lindskog C, Oksvold P, Mardinoglu A, et al. (2015): Proteomics. Tissue-based map of the human proteome. *Science*. 347:1260419.

93. Stoeger T, Gerlach M, Morimoto RI, Nunes Amaral LA (2018): Large-scale investigation of the reasons why potentially important genes are ignored. *PLoS Biol*. 16:e2006643.

CHAPTER 3. Structural deviations of the posterior fossa and the cerebellum and their cognitive links in a neurodevelopmental deletion syndrome

Esra Sefik, Yiheng Li, Brittney Sholar, Lindsey Evans, Jordan Pincus, Zeena Ammar, Melissa M. Murphy, Cheryl Klaiman, Celine A. Saulnier, Stormi P. White, Adam Ezra Goldman-Yassen, Ying Guo, Elaine F. Walker, Longchuan Li, Sarah Shultz, Jennifer G. Mulle

Adapted from manuscript currently under review. Preprint citation is provided below:

Sefik E, Li Y, Sholar B, Evans L, Pincus J, Ammar Z, et al. (2022): Structural deviations of the posterior fossa and the cerebellum and their cognitive links in a neurodevelopmental deletion syndrome. medRxiv.2022.2003.2001.22271659.

Abstract

High-impact genetic variants associated with neurodevelopmental disorders provide biologically defined entry points for etiological discovery. The 3q29 deletion (3q29Del) is one such variant that confers a ~40-fold increased risk for schizophrenia, and a ~30-fold increased risk for autism. However, the specific neural mechanisms underlying this link remain largely unknown. Here, we report the first *in vivo* quantitative neuroimaging study in 3q29Del subjects (N = 24) and healthy controls (N = 1,608) using structural MRI. Given prior reports of posterior fossa abnormalities in 3q29Del, we focus our investigation on the cerebellum and its primary tissue-types. Additionally, we compare the prevalence of cystic/cyst-like malformations of the posterior fossa between 3q29Del subjects and controls, and examine the association between neuroanatomical findings and standardized behavioral measures to probe gene-brain-behavior relationships. 3q29Del subjects had smaller cerebellar cortex volumes than controls, both before and after correction for intracranial volume (ICV). 3q29Del subjects also had larger cerebellar white matter volumes than controls following ICV-correction. The 3q29Del group displayed an elevated rate of posterior fossa arachnoid cysts and mega cisterna magna findings independent of cerebellar volume. Sex played a moderating role in a subset of findings. Cerebellar white matter volume was positively associated with visual-motor integration skills and cognitive ability, while cystic/cyst-like malformations yielded no behavioral link. Abnormal development of posterior fossa structures may represent neuroimaging-based biomarkers in 3q29Del. Results reveal cerebellar associations with sensorimotor and cognitive deficits in 3q29Del and present a novel point of genetic convergence with cerebellar pathology reported in idiopathic forms of neurodevelopmental disease.

Introduction

Copy number variation (CNV) of DNA sequences (gain/loss of >1-Kb genomic material) has been shown to represent a significant source of genetic diversity (1-5) and a far more important substrate for human evolution and adaptation than previously recognized (6-9). Accumulating findings indicate the existence of multiple rare CNVs that increase susceptibility to neurodevelopmental disorders (10-22). However, many CNVs remain understudied (23). Given their defined genomic boundaries, systematic investigation of recurring pathogenic CNVs can greatly further our understanding of the biology underlying complex neurodevelopmental disorders, such as schizophrenia (SZ), autism spectrum disorder (ASD), and intellectual disability.

Noninvasive neuroimaging technologies, such as high-resolution structural magnetic resonance imaging (MRI), offer an instrumental tool to elucidate the contribution of specific genetic variants to anatomical changes in the living human brain (24, 25). Such intermediate neuroanatomical phenotypes are crucial for bridging the gap between molecular/cellular mechanisms directly downstream of disease loci and behavioral endpoints (26, 27). The integration of genomics and imaging is especially promising for yielding biological insights into high-impact CNVs, as these variants are expected to produce highly disruptive and relatively consistent deviations in brain structure with greater etiological salience, which can help disentangle the extensive heterogeneity observed across studies of brain structure in idiopathic patient populations (28-32).

The 3q29 deletion (3q29Del) is one of eight recurrent CNVs shown to increase risk for SZ at genome-wide significance (10). 3q29Del confers an estimated >40-fold increased risk for SZ, which is one of the most robust and highest known effect sizes in the genetic landscape of this disorder (10, 33-37). It also confers a >30-fold increased risk for ASD, and exhibits pleiotropy for a range of phenotypes, including intellectual disability, developmental delay, attention deficit hyperactivity disorder (ADHD), and graphomotor deficits (38-41). 3q29Del has a prevalence of approximately 1 in 30,000 and usually arises *de novo* during parental meiosis due to the hemizygous deletion of a 1.6-Mb locus, spanning 21 protein-coding genes (39, 42). Although several genes within the interval have been proposed as putative drivers (43, 44), it is not currently known which genes or biological mechanisms contribute to the emergence of abnormal neurodevelopmental phenotypes in

3q29Del.

In a recent study, our group performed deep-phenotyping of the largest sample of 3q29Del participants with gold-standard instruments and structural MRI (39). Neuroradiological inspection revealed abnormal posterior fossa structures (between the tentorium cerebelli and foramen magnum) in over 70% of participants, including cerebellar hypoplasia and cystic/cyst-like malformations, suggesting that this brain region may be particularly relevant to 3q29Del biology. Other neuroimaging studies of 3q29Del have been based on descriptive single-case studies or small case-series with limited generalizability (41, 45-53). To our knowledge, no case-control analysis nor quantitative investigation of brain morphology has been reported in this syndrome.

Here, we report the first *in vivo* quantitative structural MRI study in individuals with 3q29Del and healthy controls. Motivated by previous findings on posterior fossa abnormalities (39), we focus our investigation on volumetric properties of the cerebellum and its primary tissue-types. Additionally, we expand our previous radiological investigation to the whole brain and test whether the prevalence of cystic/cyst-like malformations of the posterior fossa, which are typically considered incidental, asymptomatic findings in the general population (54-56), differ between 3q29Del and controls. Finally, given accumulating evidence implicating the cerebellum in high-order cognitive functions besides sensorimotor control (57-60), we examine the relationship between neuroanatomical findings and cognitive and sensorimotor deficits in 3q29Del to probe gene-brain-behavior relationships.

The findings reported in the present study have important implications for neuroimaging-based biomarker discovery in 3q29Del, and open novel directions for focusing cellular and molecular studies on target brain regions and circuits. These data also contribute to our knowledge of the genetic loci that subserve the normative development of the posterior fossa, particularly the cerebellum, which has been largely understudied in the context of neurodevelopmental and psychiatric disease.

Methods and Materials

Participants

The 3q29Del sample: 3q29Del participants were ascertained from the 3q29 Registry and traveled to

Atlanta, GA for evaluation with standardized tools and structural MRI. Data from 24 individuals with 3q29Del, ages 4-39 years (mean ± SD = 14.71 ± 9.21 years, 62.50% male) were included in this study. One participant was excluded from volumetric analyses due to inability to extract reliable volumetric measures but was retained for radiological examination. 3q29Del status was confirmed via the clinical genetics report and/or medical records. Participants provided informed consent/assent; if the participant was a minor, a parent/legal guardian additionally provided consent. All 3q29Del study procedures were approved by the Emory University Institutional Review Board. The project protocol and a summary of findings in the broader 3q29Del study sample, from which the current sample was drawn, have been detailed elsewhere (39, 61).

Healthy controls: To achieve reliable estimates for the structural variability observed in typically developing human brains, we used MRI data from the largest available, open-access sample of healthy controls (N = 1,765) from the Human Connectome Project (HCP), with cross-sectional continuity over a wide age range (5-37 years) overlapping with the 3q29Del sample (4-39 years). This dataset was selected to establish normative benchmarks around our study metrics with high statistical power, while accounting for linear and non-linear growth trajectories and sex differences. Data access was obtained in accordance with the terms outlined by the HCP. Upon inspection of the family relationships reported among controls, one sibling from each monozygotic twin-pair was randomly removed to minimize bias in standard error estimates (62, 63). Hence, 1,608 healthy controls (mean ± SD = 22.73 ± 8.21 years, 46.46% male) were included in the present study. See (64, 65) for an overview of HCP initiatives and eligibility criteria.

There were no significant differences in the sex, ethnicity, or race compositions of the two diagnostic groups (p's > 0.05). While there was a near complete overlap between their age ranges, the 3q29Del group was relatively younger than controls ($p \leq 0.001$). Hence, we considered age as a potential confound in downstream analyses. Demographic characteristics are presented in Table 1, Fig. 1, and Table S1.

Structural MRI acquisition and processing

High-resolution structural MRI data were collected from 3q29Del participants on a 3T Siemens Magnetom Prisma scanner, using a Siemens 32-channel head coil and an 80mT/m gradient. T1-weighted 3D

images were acquired in the sagittal plane using a single-echo MPRAGE sequence (66) with the following parameters: TE=2.24ms, TR=2400ms, TI=1000ms, bandwidth=210Hz/pixel, FOV=256x256mm, resolution=0.8mm isotropic. T2-weighted 3D images were acquired in the sagittal plane using a SPACE sequence (67) with the following parameters: TE=563ms, TR=3200ms, bandwidth=745Hz/pixel, FOV=256x256mm, resolution=0.8mm isotropic.

Control participants were imaged using a 3T Siemens Prisma or Skyra "Connectom" scanner by the HCP Development and Young Adult consortiums, using a Siemens 32-channel head coil with 80 or 100 mT/m gradients. T1- and T2-weighted 3D images were acquired in the sagittal plane using single- or multi-echo MPRAGE and SPACE sequences, respectively (65, 68, 69). Comparison of the 3q29Del and control protocols indicate that fundamental aspects of the hardware and acquisition parameters are either identical or highly comparable between study samples for combined hypothesis testing (see Table S2 for technical details).

For volumetrics, all 3q29Del scans were processed with the HCP "minimal pre-processing" pipeline to remove spatial artifacts/distortions, align images to MNI space and obtain brain masks/parcellations (70). Image processing for controls was performed by the HCP using this common framework. FreeSurfer software (https://surfer.nmr.mgh.harvard.edu) was used for automated segmentations, based on probabilistic information estimated from a manually labeled training set (71). Using this approach, we extracted volumetric measures for cerebellar cortex and white matter to distinguish the two primary tissue-types of the cerebellum; total cerebellar volume was defined as the sum of these metrics. See Supplemental Materials, Fig. S1 and Fig. S2 for extended methods.

Normalization of cerebellar volumes

Since skull dimensions and vertebrate brain size are correlated (72-74), correction for inter-subject variation in head size is recommended in analyses of brain volume (75, 76). We used the estimated total intracranial volume (eICV) generated by FreeSurfer as a proxy for head size (77). This method uses an automated atlas-based scaling factor estimated during affine transformation of images from native to standard space, and concords well with manually delineated ICV (78).

An important consideration in deciding whether and how regional brain volumes should be adjusted for head size, is the potential relevance of this variable to intrinsic disease processes (79, 80). Given prior reports of microcephaly in 3q29Del (41), this question is particularly germane to the present study. Hence, we evaluated the relationship between eICV and cerebellar volumes and tested for potential interaction effects between eICV and diagnostic group. Most cerebellar volumes did not scale directly proportionally with eICV, and the relationship between cerebellar white matter volume and eICV changed as a function of diagnostic group (p = 0.03) (Fig. S3). Consequently, all volumes were adjusted for eICV using the "residual" method (Fig. S4), based on normative regression slopes derived from the control group, as described in (75, 79, 81). The distributions of absolute and eICV-adjusted volumetric measures of interest (VOI) are visualized in Fig. 2 and Fig. S5.

Radiological evaluation of MRI scans

Prior work by our group using the same 3q29Del scans as in the present study has shown that posterior fossa arachnoid cysts (PFAC) are common among 3q29Del carriers (39). However, our original report did not explicitly evaluate regions outside the posterior fossa. To probe for patterns of relative regional specificity, all 3q29Del scans (N = 24) were reviewed qualitatively by a board-certified neuroradiologist (AEGY) at the whole-brain level. T1- and T2-weighted images were reviewed in axial, sagittal, and coronal reformats using Horos (https://horosproject.org). Given well-established challenges in differentiating PFAC from mega cisterna magna (MCM) (shared characteristics in appearance) (82, 83), their prevalence rates were considered jointly.

We also pulled radiographic data on incidental findings in healthy controls (N = 1,608) to define normative estimates for the prevalence of cystic/cyst-like malformations of the posterior fossa. Anatomical anomalies were identified by HCP raters and radiologists during standard quality control. Prior to case-control comparisons, the neuroradiologist who evaluated the 3q29Del scans independently confirmed the control findings for consistency. See Supplemental Materials for details.

Standardized behavioral measures

3q29Del participants also participated in a standardized, norm-referenced battery of cognitive and

sensorimotor tests, in the context of a broader deep-phenotyping study described elsewhere by our group (39, 61). Participants were administered the *Beery-Buktenica Developmental Test of Visual-Motor Integration* (VMI, 6th edition) to assess the extent to which they can integrate their visual and fine motor abilities in geometric design-copying tasks (84). Supplemental *Beery-VMI* tests were administered to measure visual perception and fine motor coordination, separately. Cognitive ability (composite, verbal, non-verbal IQ) was assessed using the *Differential Ability Scales* (DAS, 2nd edition) among participants aged 4-17 years (85), and the *Wechsler Abbreviated Scale of Intelligence* (WASI, 2nd edition) among participants aged 18-39 years (86).

Statistical analyses

Case-control comparison of volumetric measures

All statistical analyses were performed using *R* version 4.0.3 (87). Demographic characteristics of the diagnostic groups were compared using Wilcoxon rank sum test and Pearson's chi-squared test. We used multiple linear regression to model the main effect of diagnostic group on each VOI separately, while correcting for sex and age. Both absolute and eICV-adjusted cerebellar volumes, as well as eICV itself, were tested for group differences, as eICV variation may reflect a biological signal relevant to 3q29Del beyond nuisance variation. Analyses of variance (ANOVA) were performed to identify the best-fitting polynomial function of age for each VOI (see Table S3 for details). Multiple comparisons correction was applied at the VOI level (7 tests) to control the false discovery rate (FDR) using the Benjamini-Hochberg procedure. Since reliance on asymptotic theory can be problematic in small-moderate sample sizes, we additionally calculated exact p-values for model coefficients using marginal permutation tests (10,000 random permutations).

To evaluate whether the effects of diagnostic group on individual VOIs change as a function of sex, we also performed an exploratory analysis of diagnostic group and sex interactions, while correcting for age. In cases where a significant product term was identified ($p \leq 0.05$), males and females were subsequently tested separately. Given the exploratory nature of these analyses, FDR correction was not applied. Finally, in supplemental analyses, we adopted non-parametric spline modeling to build developmental trajectories for each VOI with increased flexibility and to estimate normative percentile curves for our VOIs akin to growth curves.

Since splines can capture a wide range of nonlinear trends, penalized cubic spline and quantile spline methods were incorporated to improve the statistical rigor of our central analyses. See Supplemental Materials for details.

Case-control comparison of radiological findings

The prevalence of PFAC/MCM findings was compared between 3q29Del and control groups using Fisher's exact test. Sex-specific differences in these rates were evaluated within each group using the same procedure. The demographic characteristics of 3q29Del participants with versus without cystic/cyst-like malformations were compared using Student's two sample t-test and Fisher's exact test. To rule out conceivable secondary (acquired) etiologies (88-90), differences in the distribution of past head injuries, maternal complications during pregnancy and neonatal complications during delivery were tested between these 3q29Del groups using Fisher's exact test. Finally, to determine whether the likelihood of these cystic/cyst-like malformations covary with volumetric measures among 3q29Del participants, we modeled the relationship between PFAC/MCM findings and our VOIs using linear regression, with sex, age, and eICV considered as covariates.

Tests of brain-behavior relationships in 3q29Del

To probe the functional relevance of our tissue-specific MRI findings, we investigated the association of cerebellar cortex and white matter volumes with composite IQ and VMI scores among 3q29Del participants in separate linear regression models, with adjustment for age and sex. Multiple comparisons correction was applied at the VOI level (4 tests) using Benjamini-Hochberg. Secondary analyses were conducted to investigate which cognitive (verbal / non-verbal IQ) and sensorimotor (visual perception / fine motor coordination) subprocesses may be associated with cerebellar volumes, using the same procedure. Given the exploratory nature of these analyses, FDR correction was not applied. In models where a significant relationship was identified ($p \leq 0.05$), we subsequently added eICV as an additional covariate to test whether results reflect a link with the cerebellum beyond global variability in head size. To examine the functional relevance of our radiological findings, we compared the standardized test scores of 3q29Del participants with versus without

cystic/cyst-like malformations of the posterior fossa using Student's two sample t-test and Wilcoxon rank sum test.

Standard diagnostics were performed to check all required assumptions. If parametric assumptions were not met, non-parametric alternatives were used. In cases where violations were observed for ordinary least squares regression (see Fig. S6), heteroscedasticity-robust estimates were calculated using the HC1 robust standard error estimator (91). All analyses were two-tailed. See Supplemental Materials for extended methods.

Results

Case-control differences in volumetric measures.

Using multiple linear regression, we first tested for diagnostic group differences in our VOIs, while correcting for age and sex (Table 2, Table S3A-H, Fig. 3A-G). Participants with 3q29Del had significantly smaller eICVs than controls (b = -197.99, $p \leq 0.001$, *FDR adjusted-p* ≤ 0.001); hence, we report case-control comparisons for both absolute and eICV-adjusted volumes while examining regional changes.

The 3q29Del group had significantly smaller total cerebellum volumes than controls (b = -15.26, $p \leq 0.001$, *FDR adjusted-p* ≤ 0.001), and this finding persisted after eICV-adjustment (b = -5.02, $p = 0.02$, *FDR adjusted-p* = 0.03). When the cerebellum was broken down to its two primary tissue-types, cerebellar cortex volumes were significantly smaller in the 3q29Del group (b = -15.38, $p \leq 0.001$, *FDR adjusted-p* ≤ 0.001), while cerebellar white matter volumes did not differ between the groups ($p = 0.93$). Case-control differences in cerebellar cortex remained significant after eICV-adjustment (b = -7.38, $p \leq 0.001$, *FDR adjusted-p* ≤ 0.001). Unexpectedly, 3q29Del participants also had significantly larger cerebellar white matter volumes than controls after eICV-adjustment (b = 2.69, $p = 0.04$, *FDR adjusted-p* = 0.05).

Considering these findings, we tested participants' cerebellar cortex to white matter volume ratios for group differences (Table S3D); this revealed significantly smaller ratios in 3q29Del (b = -0.49, $p \leq 0.01$). As an ancillary method, we fit generalized additive models (GAM) with a cubic spline basis to our data to identify group differences in VOIs with greater flexibly for modeling age. GAM results support the case-control differences identified using linear regression (Table S4, Fig. S7).

In exploratory analyses, we evaluated whether the effects of diagnostic group change as a function of sex, while correcting for age (Table S5A-H). There was a significant interaction between diagnostic group and sex on eICV (b = -149.64, $p \leq 0.01$). Both male and female 3q29Del participants had smaller eICVs than controls, however this reduction was greater among male (b = -237.09, $p \leq 0.001$) than female 3q29Del participants (b = -119.89, $p \leq 0.01$) (Fig. 4, Table 3). Both OLS-based asymptotic p-values and exact-p-values by permutation testing were concordant with heteroscedasticity-robust estimates across these analyses.

Additionally, OLS regression and permutation testing indicated a significant interaction between diagnostic group and sex on eICV-adjusted cerebellar white matter volumes (b = 2.73, p = 0.03); however, this effect failed to reach significance when heteroscedasticity-robust estimates were calculated (p = 0.29) (see Fig. S8 and Table S6 for sex-stratified results). Finally, using quantile splines as a supplemental method, we estimated sex-specific normative percentile curves for our VOIs. Fig. S9 visualizes the cerebellar volumes and eICV of each 3q29Del participant relative to developmental trajectories in controls, showing that many 3q29Del participants fall into extreme percentiles of growth, although within-group variability was observed in percentile ranks. A summary of case-control differences and descriptive statistics for each VOI are presented in Table S7.

Case-control differences in radiological findings.

Upon radiological evaluation, 11 controls (0.68%, out of 1,608) and 13 3q29Del participants (54.17%, out of 24) were found to have a PFAC/MCM finding. Comparison of these rates indicated a significantly higher prevalence in 3q29Del than controls (OR = 165.87, $p \leq 0.001$) (Fig. 5A-C). In sex-stratified analyses, among controls, 1 female (0.12%, out of 861) and 10 males (1.34%, out of 747) had a PFAC/MCM, while 5 females (55.56%, out of 9) and 8 males (53.33%, out of 15) had a PFAC/MCM in 3q29Del (Fig. 5D). Comparison of these sex-specific rates indicated an increase among male compared with female controls (OR = 11.66, $p \leq 0.01$), but no significant difference between male and female 3q29Del participants (OR = 0.92, $p > 0.05$).

Furthermore, there were no significant differences between 3q29Del participants with versus without PFAC/MCM findings in age, ethnicity, or race, nor in the distribution of past head injuries, maternal complications during pregnancy and/or neonatal complications during delivery (p's > 0.05) (Table S8),

suggesting that these findings are most likely of primary (congenital) origin and cannot be readily explained by conceivable secondary causes. Notably, in our whole-brain examination, only one 3q29Del participant (4.17%, out of 24) had an arachnoid cyst outside the posterior fossa (parietal lobe), highlighting increased vulnerability of the posterior fossa in this syndrome.

Lastly, regression results indicated no significant association between the likelihood of PFAC/MCM and volumetric variations in the cerebellum or eICV among 3q29Del participants, while controlling for age, sex, and/or eICV (p's > 0.05) (Table 4, Fig. S10), implying that VOI changes identified in the present study are not simply a byproduct of the cystic/cyst-like malformations enriched in this region.

Brain-behavior relationships in 3q29Del.

We next investigated the functional relevance of these neuroimaging findings to sensorimotor and cognitive deficits in 3q29Del. The mean standardized scores for both VMI and composite IQ were approximately two standard deviations below normative means, indicating clinical impairment (Fig. S11, Table S9). Both VMI (b = 1.38, $p \leq 0.01$, *FDR adjusted-p* = 0.02) and composite IQ (b = 1.33, $p \leq 0.01$, *FDR adjusted-p* = 0.02) were positively associated with cerebellar white matter volume, while controlling for sex and age, but not with cerebellar cortex volume (p's > 0.05) (Table S10).

In exploratory analyses, we aimed to differentiate the sensorimotor and cognitive subprocesses that may contribute to these findings. Cerebellar white matter volume was positively associated with both verbal (b = 1.51, p = 0.03) and non-verbal IQ (b = 1.28, p = 0.03) cognitive subtest scores, but not with visual perception or fine motor coordination skills (p's > 0.05) (Table S10). In models where a significant brain-behavior relationship was identified (p's ≤ 0.05), eICV was subsequently added as an additional covariate to consider the effect of head size. Cerebellar white matter volume remained significantly associated with VMI (b = 1.51, $p \leq$ 0.01), composite (b = 1.43, $p \leq 0.01$), verbal (b = 1.59, p = 0.03), and non-verbal IQ (b = 1.36, $p \leq 0.01$) after eICV-adjustment (Table 5, Fig. 6).

We also assessed whether these behavioral relationships may have been partially confounded by shared variance (Fig. S12). VMI had a significant positive correlation with composite IQ (r = 0.62, $p \leq 0.01$), and this

relationship was explained by a significant correlation between VMI and non-verbal IQ (overlapping constructs) ($r = 0.75$, $p \leq 0.001$). VMI did not correlate significantly with verbal IQ ($p > 0.05$), implying that VMI deficits do not explain the relationship between cerebellar white matter volume and verbal IQ in a significant way, and vice versa. Lastly, we found no significant differences between the standardized test scores of 3q29Del participants with versus without cystic/cyst-like malformations of the posterior fossa ($p's > 0.05$) (Table S11), which supports the specificity of our behavioral findings to cerebellar changes.

Discussion

It is now clear that the genetic component of many neurodevelopmental and psychiatric disorders includes CNVs arising from large structural rearrangements of the genome (10-18). However, there is a big gap in our understanding of the neurobiology underpinning many of these associations. To gain insights into pathogenesis, it is crucial to determine how these CNVs impact the structure and function of the human brain.

To this end, here we report the first *in vivo* quantitative neuroimaging study in individuals with 3q29Del: a recurrent CNV that confers exceptionally high genetic risk for neurodevelopmental and psychiatric disorders, including intellectual disability, ASD and the largest known effect size for SZ (10, 33-41). Using high-resolution MRI, standardized behavioral assessment tools, and a hypothesis-driven approach, our study revealed key findings on local alterations of brain structure and brain-behavior relationships in participants with 3q29Del.

First, by volumetric analysis, we showed that the average size of the cerebellum is significantly smaller among 3q29Del participants compared with healthy controls. This difference remained significant after adjustment for eICV, which was itself smaller among 3q29Del participants, indicating that the magnitude of reduction observed in the cerebellar volumes of individuals with this CNV shows regional specificity. This result corroborates radiological findings from several case reports (39, 50, 92). In our previous work on the same 3q29Del sample, we identified cerebellar hypoplasia in 14 males and females with 3q29Del aged six to 34 years (39). Citta et al. (2013) identified cerebellar "atrophy" in a 14-year-old female with 3q29Del, who had a history of intellectual disability and psychosis (50). Sargent et al. (1985) identified "absence" of the cerebellar vermis in a 16-month-old male with a 3q terminal deletion (proximal to 3q29), whose postmortem examination

at 26 months also revealed "small" cerebellar hemispheres (92). Hence, our volumetric findings converge with qualitative findings from case reports and for the first time quantitatively highlight the cerebellum as a region of marked pathology in 3q92Del.

For a more nuanced characterization, we next separated the cerebellum into its two primary tissue-types and found that the 3q29Del group had smaller cerebellar cortex volumes than controls, both with and without adjustment for eICV. In contrast, absolute volumes of cerebellar white matter did not differ between the groups, indicating that volumetric reduction is localized to the cerebellar cortex, which contains almost all neuronal cell bodies in the cerebellum and more than half of the neurons in the entire adult brain (93, 94). Surprisingly, 3q29Del participants also had larger cerebellar white matter volumes than controls after eICV-adjustment, implying that cerebellar white matter, which mostly contains myelinated axons, exhibits volumetric expansion in 3q29Del relative to what would be expected from controls with the same head size. Furthermore, the volumetric ratio of cerebellar cortex to white matter was smaller among 3q29Del participants, confirming that changes in these two cerebellar structures are nonuniform.

Unlike cerebral structures, the normative development of the cerebellum has been investigated in only a small number of studies. Based on this evidence, the human cerebellum starts differentiation during the first trimester (95) and displays a prolonged developmental course, with cerebellar cortex and white matter following distinct trajectories (96-101). In our large sample of healthy controls, cross-sectional modeling of cerebellar volumes revealed patterns consistent with earlier findings. From childhood to adulthood, the typical volume of cerebellar cortex roughly made an inverted U-shape, which is thought to reflect a period of transient exuberance followed by synaptic pruning (102). In contrast, the typical volume of cerebellar white matter showed a concomitant expansion continuing into adulthood, which is thought to reflect an increase in myelination and axonal diameter (102). It is conceivable that idiosyncrasies in the rate and type of these neuromaturational processes confer different susceptibilities to cerebellar cortex versus white matter development, which may partially explain the opposite direction of volumetric changes observed in these tissue-types in our 3q29Del sample.

It is also plausible that the expression of 3q29 genes themselves differ between cerebellar cortex and

white matter, which if true, would lead to tissue-specific consequences upon their hemizygosity. Accordingly, we queried the Human Protein Atlas (https://www.proteinatlas.org) (103, 104) for the 21 genes located in the 3q29 interval and found that 11 were detected in the cerebellar cortex at the protein level (Fig. S13). Notably, *BDH1*, *DLG1* and *PCYT1A* showed high protein expression profiles in the granular or Purkinje layers of the cerebellar cortex. *DLG1* encodes a synaptic scaffolding protein that interacts with AMPA and NMDA receptors (105), which are key components of glutamatergic synapses and mediators of synaptic plasticity. *BDH1 and PCYT1A* are involved in ketone body metabolism (106) and phosphatidylcholine biosynthesis (107), which are important regulators of bioenergetic homeostasis. Coincidently, both *DLG1* and *BDH1* were previously proposed as drivers of psychiatric and neurodevelopmental phenotypes in this CNV (43, 44). We conjecture that dosage alterations in these genes may be especially detrimental for cerebellar cortex development and function.

At the same time, *DLG1* was also detected in cerebellar white matter at the protein level (Fig. S13). Interestingly, *DLG1* was shown to regulate myelin thickness in the peripheral nervous system (108). Assuming a similar mechanism of action, larger cerebellar white matter volumes in our 3q29Del sample may reflect a failure in *DLG1*'s ability to put a break on myelination, although we highlight that haploinsufficiency of *Dlg1* alone was not sufficient to recapitulate the mouse-specific phenotypes of 3q29Del in an earlier study (109). Overall, these data lend molecular support to our volumetric findings implicating the 3q29 locus in cerebellar development.

It is also worth noting that larger cerebellar white matter volumes in 3q29Del may reflect a compensatory mechanism (as opposed to a primary disturbance) originating either internally within the white matter network of the cerebellum or externally through afferent pathways. Oligodendrocyte precursor cells continuously survey their environment and have the capacity to differentiate into oligodendrocytes well into adulthood, which can regenerate myelin following injury or disease (110-114). Hence, structural white matter alterations can serve compensatory functions by modifying conduction velocity. Altogether, mechanisms that may underly our structural findings include changes in number of neurons, neuronal size or dendritic arborization for cerebellar cortex, and changes in axon growth, guidance, or myelination for white

matter. Future work will aim to elucidate the relative contribution of these potential mechanisms to altered cerebellar development in 3q29Del.

Another key finding was the relationships identified between tissue-specific cerebellar volumes and sensorimotor and cognitive abilities among 3q29Del participants. Smaller cerebellar white matter volumes were associated with worse VMI, and composite, verbal, and non-verbal IQ scores. Interestingly, neither visual perception nor fine motor coordination skills separately had a significant relationship with cerebellar white matter, suggesting that the identified sensorimotor link is specific to the ability to integrate information from multiple modalities, as opposed to performing either one alone. Importantly, VMI and verbal IQ were not significantly correlated with each other in this sample, indicating that cerebellar associations identified with these motor and non-motor abilities are not secondary consequences of one another. Cumulatively, these findings suggest that structural cerebellar changes have functional significance for specific behavioral phenotypes in 3q29Del.

The role of the cerebellum in sensorimotor integration is long established (115). However, cerebellar contributions to cognitive processing have traditionally received less attention, in part due to a cortico-centric view of "higher" functions (116). A major shift has begun towards re-conceptualizing the cerebellum as a calibrator (i.e., "feed-forward controller") of the output and possibly the development of not only motor but also non-motor systems (57-59, 117-125), although skepticism about cerebellar roles beyond motor control remains. Recent anatomical studies have identified strong connections between the cerebellum and non-motor brain regions (117, 123, 126-128). Consistent with this, cerebellar activation has been reported in various cognitive tasks in functional neuroimaging (129-135), and cerebellar damage has been shown to produce impairments in linguistic processing, spatial cognition and executive functions (136-139).

In recent years, the cerebellum has also emerged as a site of renewed interest for a broad range of neurodevelopmental and psychiatric illnesses (58, 140, 141). Two independent studies have shown that structural alterations within the cerebellum are associated with general liability for common psychopathology (142, 143). Supporting these findings, perinatal injury to the cerebellum is now considered the largest known nongenetic risk factor for ASD (58, 144-147). Cerebellar abnormalities have also been reported in idiopathic

SZ, ASD and ADHD (148-160), although findings in this area show strong heterogeneity likely due to technical and physiological causes. Despite these advances, the precise molecular and neurobiological basis of cerebellar contributions to non-motor behaviors and mental illnesses remains largely unknown.

Our findings indicate that 3q29Del sits at the intersection of abnormal cerebellar development and increased risk for neurodevelopmental and psychiatric disease, which converges with growing evidence implicating the cerebellum in the pathophysiology of several other genomic variants, including well-known ASD or SZ-related genes such as *TSC1*, *FMR1*, *SHANK3*, *MECP2*, and *PTEN*, and CNVs like 22q11.2 deletion (161-167). The explanatory gap between these loci and disease mechanism has not yet been fully bridged, however altered cerebellar development may be a shared neuroanatomical endophenotype that contributes to heightened risk for a variety of neurodevelopmental and psychiatric disorders across these variants. Future work should investigate whether the biological mechanisms disrupted in 3q29Del converge onto pathways that are vulnerable to other genetic variants associated with cerebellar abnormalities.

Here, we would like to further elaborate on the significant positive relationship identified between cerebellar white matter volume, IQ and VMI scores in the 3q29Del sample, especially in light of the larger eICV-adjusted (but not unadjusted) cerebellar white matter volumes observed in this group compared with healthy controls. The direction of these relationships hints at neural compensation, which can be defined as changes in neural circuits that offset the loss of or aberrant functioning of neural cells in an attempt to preserve the cognitive and behavioral functions of an individual (168-170). Despite the seeming simplicity of this description, we highlight that neural compensation is an exceedingly complicated and poorly understood phenomenon. Improved white matter microstructure is one mechanism that has been distinguished as a key component of neural compensation that can build the groundwork for functional compensation (171). Building on this literature, we speculate that the expansion of cerebellar white matter volumes among 3q29Del carriers may be a compensatory mechanism initiated in response to the reduction in cerebellar cortex volumes, which is supported by significant changes in their relative ratios.

Previous literature, which primarily comes from studies of aging and neurodegenerative disorders, suggests that compensatory mechanisms can prevent or ease the manifestation of clinical symptoms up until

the burden of disease reaches a certain level of pathology, which cannot be counteracted anymore (171-173). This may explain why 3q29Del participants on average have IQ and VMI scores that are below the normative mean of 100, but that the individual scores of the participants range from 45–101 on the Beery and 31–106 on the WASI and DAS (Fig. S11, Table S9). The interplay between 3q29Del and other genetic and environmental risk factors and protectants may contribute to within-group variability in individual participants' ability/need to compensate for 3q29Del-related pathology, which could partially explain the variable clinical expression of this syndrome, similar to other CNVs (174). It has been proposed that the effects of neural compensation are likely time dependent (171), hence, longitudinal neuroimaging studies in this population may provide more robust evidence for compensatory changes and their association with motor and non-motor functions in 3q2Del beyond *post hoc* interpretations of cross-sectional results.

Finally, our findings also indicate that cystic/cyst-like malformations of the posterior fossa show an elevated prevalence among 3q29Del participants compared with controls. The prevalence of PFAC/MCM findings was approximately 1% among controls, and more common among males than females, consistent with prior estimates in the general population (55, 56). In contrast, their prevalence was approximately 54% among 3q29Del participants, with no sex differences. Consequently, besides cerebellar abnormalities, 3q29Del also confers a greater risk for cystic/cyst-like malformations in this region, suggesting a general vulnerability of the posterior fossa to this CNV. However, the likelihood of PFAC/MCM was not associated with cognitive or sensorimotor phenotypes in 3q29Del, supporting the specificity of behavioral associations to the cerebellum.

Furthermore, we found no significant association between the likelihood of PFAC/MCM findings and volumetric variations in the cerebellum among 3q29Del participants, indicating that VOI changes identified in the present study are not simply a byproduct (i.e., mass effect) of the cystic/cyst-like malformations enriched in this region. Several possible explanations for this result can be speculated. First, the absence of a statistically significant relationship between radiological PFAC/MCM findings and volumetric cerebellar changes may be due to lack of sufficient power to detect a genuine effect that may in fact exist in the general 3q29Del population from which the current sample was drawn. We highlight that absence of evidence does not necessarily reflect evidence of absence (175). In a similar vein, prior case studies have demonstrated that, although infrequently,

arachnoid cysts can resolve spontaneously without surgical intervention (176-182). Possible reasons for such disappearances include sudden ruptures when the intracystic tension is high, which can be accelerated by factors such as extreme breath holding, crying, Valsalva maneuver or head injury. We did not find any significant differences between the rates of reported past head injuries between 3q29Del participants with and without PFAC/MCM findings in the posterior fossa, but the possibility of spontaneous disappearance remains an unknown variable that may have biased our results towards the null.

A third possible explanation for the absence of a statistically significant relationship between PFAC/MCM findings and volumetric cerebellar changes in this sample may be related to potential differences in the precise neurobiological mechanisms that mediate and moderate their individual relationships with 3q29Del. The etiology and natural history of arachnoid cysts remain poorly understood and there is very limited knowledge about human meningeal development in general. The predominant theory argues that congenital arachnoid cysts arise from erroneous splitting or duplication of the arachnoid membrane *in utero* (183, 184), with familial and syndromic cases supporting a genetic contribution (185-189). It is also known that the meninges covering the cerebral and cerebellar hemispheres derive from the neural crest, which arises from the ectoderm, but there is regionalization of gene expression during the development of the anterior versus posterior meninges (190, 191). It is conceivable that the posterior fossa spatially emerges as a site of marked pathology in 3q29Del due to disruptions in the genetic programming of early patterning and specification of the ectoderm along the anteroposterior axis (also known as the rostral-caudal axis) (192). Following this initial insult, the ultimate emergence of cystic/cyst-like malformations and cerebellar defects in this region may unfold orthogonally through mechanisms that may be specific to cell-type and developmental time.

Notably, we found that 3q29Del confers greater influence on risk for cystic/cyst-like malformations of the posterior fossa among females than males. In prior work, we also identified a reduction in the male:female bias among participants with 3q29Del in ASD rates (38). In the general population the ratio of males:females with ASD is approximately 4:1 (193-195); in 3q29Del this ratio is 2:1 (38). According to the liability threshold model, females require a larger genetic burden than males before reaching affection status (196, 197), and the sex ratio in disease prevalence tends to approach 1:1 as the severity of a mutation increases (198). 3q29Del is

on the more severe end of this genetic spectrum, which may explain why the rate of PFAC/MCM is similar among males and females with this CNV. That said, we found a greater reduction in eICV among male than female 3q29Del participants, but no robust sex by diagnostic group interaction effect on cerebellar volumes. These results suggest regional variability in patterns of sexual dimorphism in 3q29Del and highlight that sex must be considered an important variable in studies of this CNV.

Several limitations should be addressed in future research. First, due to its rare prevalence, the 3q29Del sample size was limited, which prevented an in-depth analysis of complex interactions involving age and sex. Replication is needed in a larger sample of cases imaged on the same scanner as controls. Demands of study participation may have barred individuals with more severe disease manifestations from participating; this may have led to underestimation of effect sizes. For MRI, the complex architecture of the cerebellum introduced methodological challenges; future work with improved segmentation techniques will explore finer parcellations. Analyses will also be expanded to clinical phenotypes, and other measures of cognition for a more comprehensive investigation. Importantly, cerebellar connections with cerebral regions warrant investigation to expand questions to the circuitry-level. Finally, given our cross-sectional approach, reported findings do not necessarily reflect causation. Leveraging the mouse model of 3q29Del (109) may help elucidate mechanistic impacts on cerebellar development.

Acknowledgements

We acknowledge the 3q29Del study population, their families and the 3q29 Project members. We thank the Marcus Autism Center for providing clinical assessment resources. Funding for 3q29Del work was provided by National Institutes of Health (NIH) grants R01 MH110701, R01 MH118534, and National Institutes of Mental Health (NIMH) grant U01MH081988. REDCap is supported by grant UL1 TR000424. Healthy control data for the young-adult age range of the present study were provided in part by the Human Connectome Project, WU-Minn Consortium (Principal Investigators: David Van Essen and Kamil Ugurbil; 1U54MH091657) funded by the 16 NIH Institutes and Centers that support the NIH Blueprint for Neuroscience Research; and by the McDonnell Center for Systems Neuroscience at Washington University. Healthy control data for the developmental age range of the present study were provided by the Lifespan Human Connectome Project, supported by the NIMH under Award Number U01MH109589. The content is solely the responsibility of the authors and does not necessarily represent the official views of the NIH.

Data availability

The 3q29Del data collected in this study are deposited in the NIMH Data Archive (nda.nih.gov) (behavioral data: collection 2614, embargoed until September 2022; neuroimaging data: collection 3126, embargoed until November 2023). Prior to these dates, the 3q29Del data are available from Jennifer Mulle on reasonable request. Access to the Human Connectome Project data used in the present study is subject to the WU-Minn HCP Consortium's "Open Access and Restricted Data Use Terms" for the HCP-Young Adult dataset (1200 subjects data release; minimally preprocessed structural data available from the Connectome Coordination Facility via: https://humanconnectome.org/study/hcp-young-adult/document/1200-subjects-data-release) and the NIMH Data Archive's "Data Use Certification Agreement" for the HCP-Development dataset (HCP-Development Lifespan 2.0 release; data available from the NIMH Data Archive via: https://nda.nih.gov/general-query.html?q=query=featured-datasets:HCP%20Aging%20and%20Development)

Tables

Demographic variables	**Control** *N* = 1,608	**3q29Del** *N* = 23	**Test statistics**
Age (in years)			
Mean ± SD	22.73 ± 8.21	15.09 ± 9.22	*r* = 0.10 (small effect size), *W* = 9429.5, p-value [a] = 5.26E-05***
Median	25.00	14.00	
[Range]	[5 – 37]	[4 – 39]	
Sex, *N* (%)			
Male	747 (46.46%)	14 (60.87%)	X^2 = 1.36, DF = 1, p-value [b] = 0.24
Female	861 (53.54%)	9 (39.13%)	
Ethnicity, *N (%)*			
Non-Hispanic / Latino	1,397 (88.03%)	22 (95.65%)	X^2 = 0.64, DF = 1, p-value [b] = 0.42
Hispanic / Latino	190 (11.97%)	1 (4.35%)	
Race, *N (%)*			
White	1,112 (70.66%)	21 (91.30%)	X^2 = 6.25, DF = 4, p-value [b] = 0.18
Black / African American	222 (14.10%)	0 (0%)	
Asian / Native Hawaiian / Other Pacific Islander	108 (6.86%)	0 (0%)	
American Indian / Alaskan Native	4 (0.25%)	0 (0%)	
More than one race	128 (8.13%)	2 (8.70%)	

Table 1. Demographic characteristics of the study sample in volumetric analyses, stratified by diagnostic group. There were no significant differences in the sex, ethnicity, or race compositions of the two diagnostic groups (*p's* > 0.05). While there was a near complete overlap between the age ranges of the two groups, there was a significant age difference between 3q29Del subjects and controls on average ($p \leq 0.001$). Effect sizes are reported for significant test results only. Non-parametric statistics are reported in cases where the data do not meet parametric assumptions. [#]Control *N* = 1,587 for the ethnicity variable due to missing data. [##]Control *N* = 1,574 for the race variable due to missing data. Corresponding percentages reflect the fraction of controls with complete data. [a] Wilcoxon rank sum test with continuity correction, [b] Pearson's chi-squared test with Yates' continuity correction. p-value ≤ 0.001 '***', p-value ≤ 0.01 '**', p-value ≤ 0.05 '*', p-value ≤ 0.1 '•' *Abbreviations*: 3q29 deletion syndrome, 3q29Del; standard deviation, SD; degrees of freedom, DF.

Outcome variables	Explanatory variables	*b*	CI (95%)	p-value
Absolute Total Cerebellum Volume (cm^3)	Intercept	133.50	128.97 – 138.03	**< 2.00E-16*** **
	Age (years)	0.68	0.22 – 1.14	**3.72E-03** **
	Age^2	-0.02	-0.03 – -0.01	**6.22E-04*** **
	Sex [Male]	16.22	14.97 – 17.48	**< 2.00E-16*** **
	Diagnostic Group [3q29Del]	**-15.26**	**-20.01 – -10.51**	**3.76E-10*** **
	R^2 / R^2 adjusted	0.31 / 0.31		
	Robust Wald test	184.0 on 4 and 1626 DF, p-value < 2.20E-16***		
Absolute Cerebellar Cortex Volume (cm^3)	Intercept	113.52	109.73 – 117.31	**< 2.00E-16*** **
	Age (years)	0.13	-0.26 – 0.51	0.52
	Age^2	-0.01	-0.02 – -0.0001	**0.04***
	Sex [Male]	13.13	12.10 – 14.17	**< 2.00E-16*** **
	Diagnostic Group [3q29Del]	**-15.38**	**-19.53 – -11.22**	**5.86E-13*** **
	R^2 / R^2 adjusted	0.32 / 0.32		
	Robust Wald test	193.2 on 4 and 1626 DF, p-value < 2.20E-16***		
Absolute Cerebellar White Matter Volume (cm^3)	Intercept	19.98	18.82 – 21.15	**< 2.00E-16*** **
	Age (years)	0.55	0.43 – 0.67	**< 2.00E-16*** **
	Age^2	-0.01	-0.01 – -0.01	**8.88E-11*** **
	Sex [Male]	3.09	2.76 – 3.43	**< 2.00E-16*** **
	Diagnostic Group [3q29Del]	**0.11**	**-2.42 – 2.65**	**0.93**
	R^2 / R^2 adjusted	0.28 / 0.27		
	Robust Wald test	155.1 on 4 and 1626 DF, p-value < 2.20E-16***		
Estimated Total Intracranial Volume (eICV) (cm^3)	Intercept	1415.02	1367.87 – 1462.17	**< 2.00E-16*** **
	Age (years)	9.89	4.84 – 14.94	**1.26E-04*** **
	Age^2	-0.25	-0.37 – -0.13	**3.66E-05*** **
	Sex [Male]	206.00	192.06 – 219.93	**< 2.00E-16*** **
	Diagnostic Group [3q29Del]	**-197.99**	**-253.23 – -142.74**	**3.05E-12*** **
	R^2 / R^2 adjusted	0.37 / 0.37		
	Robust Wald test	232.5 on 4 and 1626 DF, p-value < 2.20E-16***		
eICV-Adjusted Total Cerebellum Volume (cm^3)	Intercept	144.44	142.97 – 145.92	**< 2.00E-16*** **
	Age (years)	-0.05	-0.11 – 0.01	0.12
	Sex [Male]	5.38	4.38 – 6.38	**< 2.00E-16*** **
	Diagnostic Group [3q29Del]	**-5.02**	**-9.25 – -0.80**	**0.02***
	R^2 / R^2 adjusted	0.07 / 0.07		
	Robust Wald test	39.0 on 3 and 1627 DF, p-value < 2.20E-16***		
eICV-Adjusted Cerebellar Cortex Volume (cm^3)	Intercept	119.88	118.60 – 121.17	**< 2.00E-16*** **
	Age (years)	-0.21	-0.26 – -0.16	**1.37E-15*** **
	Sex [Male]	4.87	4.03 – 5.72	**< 2.00E-16*** **
	Diagnostic Group [3q29Del]	**-7.38**	**-10.98 – -3.78**	**6.03E-05*** **
	R^2 / R^2 adjusted	0.11 / 0.11		
	Robust Wald test	67.5 on 3 and 1627 DF, p-value < 2.20E-16***		
eICV-Adjusted Cerebellar White Matter Volume (cm^3)	Intercept	22.22	21.22 – 23.23	**< 2.00E-16*** **
	Age (years)	0.42	0.31 – 0.53	**6.39E-14*** **
	Age^2	-0.01	-0.01 – -0.004	**3.94E-06*** **
	Sex [Male]	0.41	0.13 – 0.70	**4.51E-03** **
	Diagnostic Group [3q29Del]	**2.69**	**0.10 – 5.28**	**0.04***
	R^2 / R^2 adjusted	0.19 / 0.19		
	Robust Wald test	106.7 on 4 and 1626 DF, p-value < 2.20E-16***		

Table 2. Summary of multiple linear regression results testing for differences in volumetric measures of interest between 3q29Del and control subjects. Sex, age, and age^2 (when applicable) were included as

covariates in each regression equation based on the best-fitting polynomial function of age identified for each VOI (see Table S3 for details). The main effect of diagnostic group is reported in bold for clarity. Regression parameters reflect heteroskedasticity-robust estimates, which were computed as an alternative to ordinary least squares regression to address observed violations of statistical assumptions. Robust Wald test statistics are reported to assess the overall significance of each model. Control $N = 1{,}608$**,** 3q29Del $N = 23$. Contrast coding: reference levels for the categorical diagnostic group and sex variables are healthy control and female, respectively. p-value ≤ 0.001 '***', p-value ≤ 0.01 '**', p-value ≤ 0.05 '*', p-value ≤ 0.1 '†'. *Abbreviations*: 3q29 deletion syndrome, 3q29Del; VOI, volumetric measure of interest; eICV, estimated total intracranial volume; unstandardized coefficient estimate, *b*; confidence interval, CI; degrees of freedom, DF.

Outcome variable	Explanatory variables	*b*	CI (95%)	p-value
Estimated Total Intracranial Volume (eICV) (cm^3)	Intercept	1573.56	1502.04 – 1645.07	**< 2.00E-16*** **
	Age (years)	11.48	3.99 – 18.98	**2.72E-03** **
	Age^2	-0.23	-0.41 – -0.05	**0.01** **
	Diagnostic group [3q29Del]	**-237.09**	**-293.81 – -180.36**	**9.87E-16*** **
Sex: Male	R^2 / R^2 adjusted	0.08 / 0.07		
	Robust Wald test	32.3 on 3 and 757 DF, p-value **< 2.00E-16*** **		
Estimated Total Intracranial Volume (eICV) (cm^3)	Intercept	1463.47	1403.35 – 1523.58	**< 2.00E-16*** **
	Age (years)	7.28	0.73 – 13.83	**0.03***
	Age^2	-0.24	-0.39 – -0.08	**3.14E-03** **
	Diagnostic group [3q29Del]	**-119.89**	**-198.88 – -40.89**	**2.98E-03** **
Sex: Female	R^2 / R^2 adjusted	0.05 / 0.04		
	Robust Wald test	13.00 on 3 and 866 DF, p-value = 2.61E-08***		

Table 3. Post hoc analysis of the sex-specific effects of diagnostic group on eICV. Sex-stratified linear regression models include age and age^2 as covariates based on the best-fitting model reported for this VOI in Table 2. The main effect of diagnostic group is reported in bold for clarity. Heteroskedasticity-robust regression results indicated that both male and female 3q29Del subjects had smaller eICVs than controls (*p's* ≤ 0.01), however this reduction was greater among male 3q29Del subjects than female 3q29Del subjects. Robust Wald test statistics are reported to assess the overall significance of each model. Contrast coding: reference level for the diagnostic group variable is healthy control. Male *N* = 761 (Control *N* = 747, 3q29Del *N* = 14), Female *N* = 870 (Control *N* = 861, 3q29Del *N* = 9). p-value ≤ 0.001 '***', p-value ≤ 0.01 '**', p-value ≤ 0.05 '*', p-value ≤ 0.1 '†'. *Abbreviations*: 3q29 deletion syndrome, 3q29Del; estimated total intracranial volume, eICV; unstandardized coefficient estimate, *b*; confidence interval, CI; degrees of freedom, DF.

		Model 1			**Model 2** (with eICV-adjustment)		
Outcome variables	**Explanatory variables**	***b***	**CI (95%)**	**p-value**	***b***	**CI (95%)**	**p-value**
Total Cerebellum Volume (cm^3)	Intercept	138.53	123.93 – 153.12	3.59E-14***	79.17	20.03 – 138.32	**0.01****
	Age (years)	-0.57	-1.13 – -0.004	**0.04***	-0.46	-0.99 – 0.06	0.08†
	Sex [Male]	11.11	1.41 – 20.81	**0.03***	8.99	-0.15 – 18.13	0.05*
	eICV (cm^3)				0.04	0.001 – 0.08	**0.04***
	PFAC / MCM [Positive]	**-7.07**	**-17.22 – 3.09**	**0.16**	**-9.09**	**-18.62 – 0.44**	**0.06†**
	R^2 / R^2 adjusted	0.39 / 0.30			0.52 / 0.41		
	F-statistic	4.1 on 3 and 19 DF, p-value = 0.02*			4.8 on 4 and 18 DF, p-value = 0.01**		
Cerebellar Cortex Volume (cm^3)	Intercept	108.93	94.64 – 123.22	1.85E-12***	47.17	-9.75 – 104.10	0.10†
	Age (years)	-0.49	-1.04 – 0.07	0.08†	-0.38	-0.89 – 0.13	0.13
	Sex [Male]	7.89	-1.61 – 17.39	0.10†	5.69	-3.11 – 14.49	0.19
	eICV (cm^3)				0.04	0.005 – 0.08	**0.03***
	PFAC / MCM [Positive]	**-1.90**	**-11.84 – 8.04**	**0.69**	**-4.01**	**-13.18 – 5.17**	**0.37**
	R^2 / R^2 adjusted	0.28 / 0.17			0.45 / 0.33		
	F-statistic	2.5 on 3 and 19 DF, p-value = 0.09†			3.7 on 4 and 18 DF, p-value = 0.02*		
Cerebellar White Matter Volume (cm^3)	Intercept	37.25	28.70 – 45.80	3.40E-08***	41.34	11.67 – 71.02	9.15E-03**
	Age (years)	-1.22	-2.11 – -0.33	9.82E-03**	-1.23	-2.15 – -0.31	**0.01****
	Age^2	0.03	0.01 – 0.05	**0.01****	0.03	0.01 – 0.05	**0.01****
	Sex [Male]	2.93	-1.28 – 7.14	0.16	3.07	-1.38 – 7.53	0.16
	eICV (cm^3)				-0.003	-0.02 – 0.02	0.76
	PFAC / MCM [Positive]	**-3.97**	**-8.47 – 0.52**	**0.08†**	**-3.83**	**-8.57 – 0.91**	**0.11**
	R^2 / R^2 adjusted	0.48 / 0.37			0.48 / 0.33		
	F-statistic	4.2 on 4 and 18 DF, p-value = 0.01**			3.2 on 5 and 17 DF, p-value = 0.03*		
Estimated Total Intracranial Volume (eICV) (cm^3)	Intercept	1392.33	1236.74 – 1547.91	1.05E-13***			
	Age (years)	-2.39	-8.39 – 3.61	0.41			
	Sex [Male]	49.68	-53.72 – 153.08	0.33			
	PFAC / MCM [Positive]	**47.55**	**-60.68 – 155.79**	**0.37**			
	R^2 / R^2 adjusted	0.16 / 0.03					
	F-statistic	1.2 on 3 and 19 DF, p-value = 0.32					

Table 4. Exploratory analysis of the relationship between volumetric measures of interest and posterior fossa arachnoid cyst and mega cisterna magna findings among 3q29Del subjects. Multiple linear regression results for total cerebellum volume, cerebellar cortex volume**,** cerebellar white

matter volume and eICV indicate no significant relationship between the likelihood of PFAC/MCM findings and interrogated VOIs among 3q29Del subjects (*p's* > 0.05), while correcting for sex, age, age^2 (if appropriate) and eICV (in model 2 only). The main effect of the binary PFAC/MCM variable is reported in bold for clarity. The age term/s included in each model reflect the best-fitting polynomial expansion of age for a given VOI selected by ANOVA. Major assumptions for ordinary least squares regression were met in the current analysis, hence additional heteroskedasticity-robust estimates were not calculated. F-statistics are reported to assess the overall significance of each model. 3q29Del $N = 23$. Contrast coding: reference levels for the PFAC/MCM and sex variables are negative and female, respectively. p-value ≤ 0.001 '***', p-value ≤ 0.01 '**', p-value ≤ 0.05 '*', p-value ≤ 0.1 '·'. *Abbreviations*: 3q29 deletion syndrome, 3q29Del; volumetric measure of interest, VOI; posterior fossa arachnoid cyst, PFAC; mega cisterna magna, MCM; estimated total intracranial volume, eICV; analysis of variance, ANOVA; unstandardized coefficient estimate, *b*; confidence interval, CI; degrees of freedom, DF.

Outcome variables	Explanatory variables	*b*	CI (95%)	p-value
Visual-motor Integration *(standardized score, Beery VMI-6)*	Intercept	-38.13	-122.35 – 46.08	0.35
	Age (years)	-0.39	-0.97 – 0.19	0.18
	Sex [Male]	-13.59	-25.64 – -1.54	0.03*
	eICV (cm^3)	0.06	0.002 – 0.11	0.04*
	Cerebellar WM Volume (cm^3)	**1.51**	**0.64 – 2.39**	**1.87E-03****
	R^2 / R^2 adjusted	0.50 / 0.38		
	Robust Wald Test	5.1 on 4 and 18 DF, p-value = 6.08E-03**		
Composite IQ *(standardized score, WASI-II/ DAS-II)*	Intercept	-15.38	-76.16 – 45.39	0.60
	Age (years)	0.10	-0.42 – 0.61	0.70
	Sex [Male]	-10.85	-21.04 – -0.65	0.04*
	eICV (cm^3)	0.04	0.00 – 0.08	0.06†
	Cerebellar WM Volume (cm^3)	**1.43**	**0.50 – 2.35**	**4.66E-03****
	R^2 / R^2 adjusted	0.44 / 0.31		
	Robust Wald Test	6.2 on 4 and 18 DF, p-value = 2.57E-03**		
Verbal IQ *(standardized score, WASI-II/ DAS-II)*	Intercept	-2.26	-103.80 – 99.28	0.96
	Age (years)	0.20	-0.59 – 1.00	0.60
	Sex [Male]	-13.32	-29.75 – 3.10	0.11
	eICV (cm^3)	0.03	-0.03 – 0.09	0.31
	Cerebellar WM Volume (cm^3)	**1.59**	**0.17 – 3.01**	**0.03***
	R^2 / R^2 adjusted	0.26 / 0.10		
	Robust Wald Test	2.5 on 4 and 18 DF, p-value = 0.08†		
Non-verbal IQ *(standardized score, WASI-II/ DAS-II)*	Intercept	6.21	-54.98 – 67.40	0.83
	Age (years)	-0.41	-0.96 – 0.13	0.13
	Sex [Male]	-12.15	-22.77 – -1.53	0.03*
	eICV (cm^3)	0.03	-0.004 – 0.07	0.08†
	Cerebellar WM Volume (cm^3)	**1.36**	**0.31 – 2.40**	**0.01****
	R^2 / R^2 adjusted	0.47 / 0.35		
	Robust Wald Test	5.6 on 4 and 18 DF, p-value = 4.03E-03**		

Table 5. Summary of multiple linear regression results showing the relationships between cerebellar white matter volume and standardized test scores for sensorimotor and cognitive abilities among 3q29Del subjects. Only the significant test results from our investigation of brain-behavior relationships are reported in this table for brevity (p's ≤ 0.05) (see Table S10 for a complete summary of behavioral findings). Sex, age and eICV were included as covariates in each regression model. The main effect of cerebellar white matter volume is reported in bold for clarity. Regression parameters reflect heteroskedasticity-robust estimates. Robust Wald test statistics are reported to assess the overall significance of each model. Results indicate a significant relationship between cerebellar white matter volume and standardized test scores for visual-motor

integration skills ($p \leq 0.01$), composite IQ ($p \leq 0.01$), verbal IQ ($p \leq 0.05$), and non-verbal IQ ($p \leq 0.01$) among 3q29Del subjects. 3q29Del $N = 23$. Contrast coding: reference level for the categorical sex variable is female. p-value ≤ 0.001 '***', p-value ≤ 0.01 '**', p-value ≤ 0.05 '*', p-value ≤ 0.1 '†'. *Abbreviations*: 3q29 deletion syndrome, 3q29Del; estimated total intracranial volume, eICV; intelligence quotient, IQ; WASI, Wechsler Abbreviated Scale of Intelligence; DAS, Differential Ability Scales; VMI, visual-motor integration; unstandardized coefficient estimate, *b*; confidence interval, CI; degrees of freedom, DF.

Figures

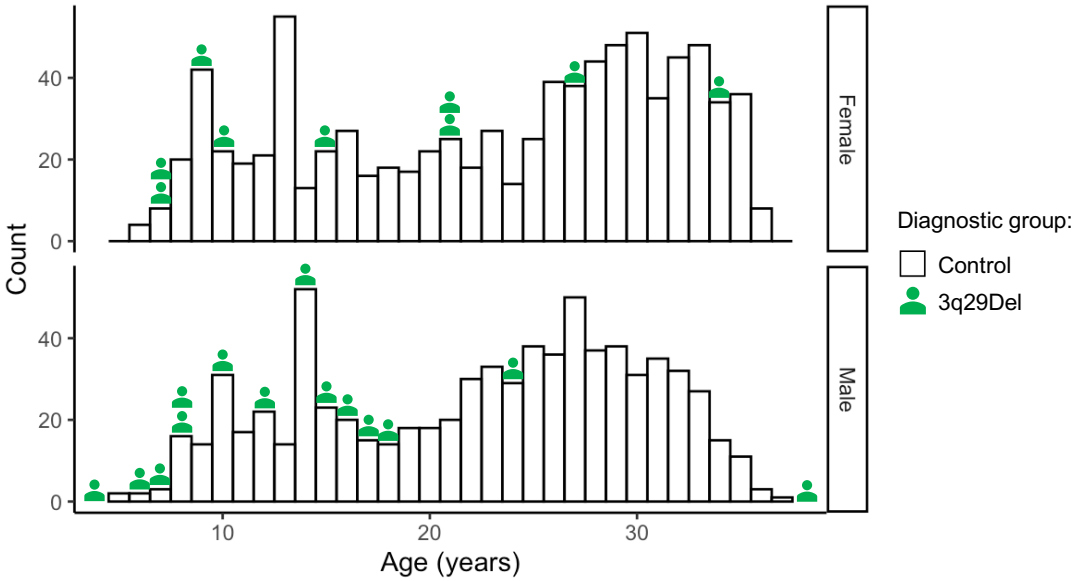

Figure 1. Histogram showing the age distribution of study participants in volumetric analyses, stratified by sex and diagnostic group. To define reliable estimates for the normative trajectory of cerebellar volumetric change across age, we used the largest available open-access sample of healthy controls from the Human Connectome Project, which cross-sectionally covers a wide age range [5 – 37 years] with near complete overlap with the 3q29Del sample [4 – 39 years]. Each histogram bin represents one year. Green icons above each bar symbolize the number of 3q29Del subjects included in volumetric analyses for a given age and sex. Control N = 1,608 (Female N = 861, Male N = 747)**,** 3q29Del N = 23 (Female N = 9, Male N = 14). *Abbreviations*: 3q29 deletion syndrome, 3q29Del.

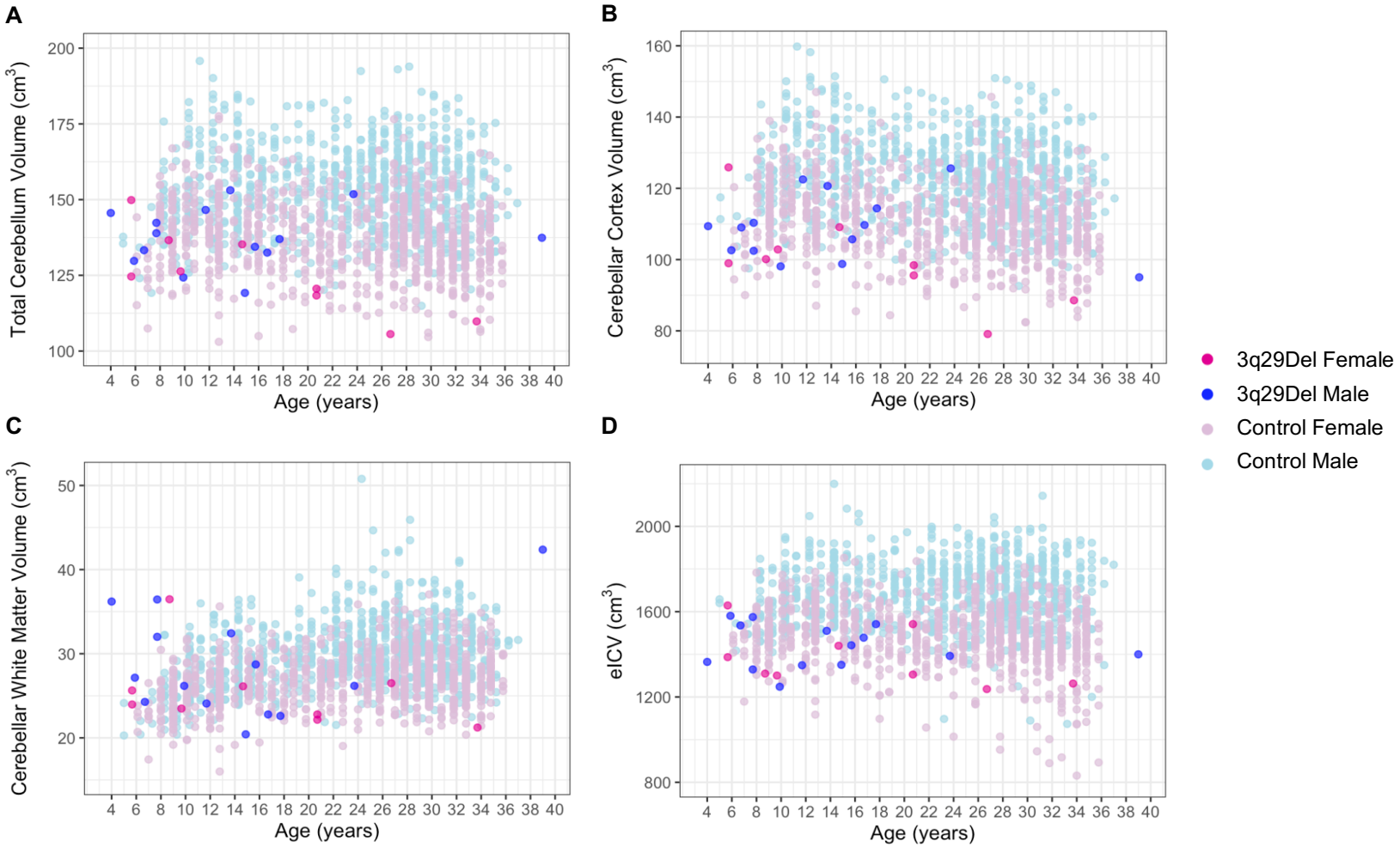

Figure 2. Scatter plots showing the distribution of A) total cerebellum volume, B) cerebellar cortex volume, C) cerebellar white matter volume, and D) eICV as a function of age among male and female subjects in each diagnostic group. A slight jitter was added systematically to all panels to minimize overplotting. Data reflect absolute volumes. Control *N* = 1,608 (Female *N* = 861, Male *N* = 747)**,** 3q29Del *N* = 23 (Female *N* = 9, Male *N* = 14). *Abbreviations*: 3q29 deletion syndrome, 3q29Del; estimated total intracranial volume, eICV.

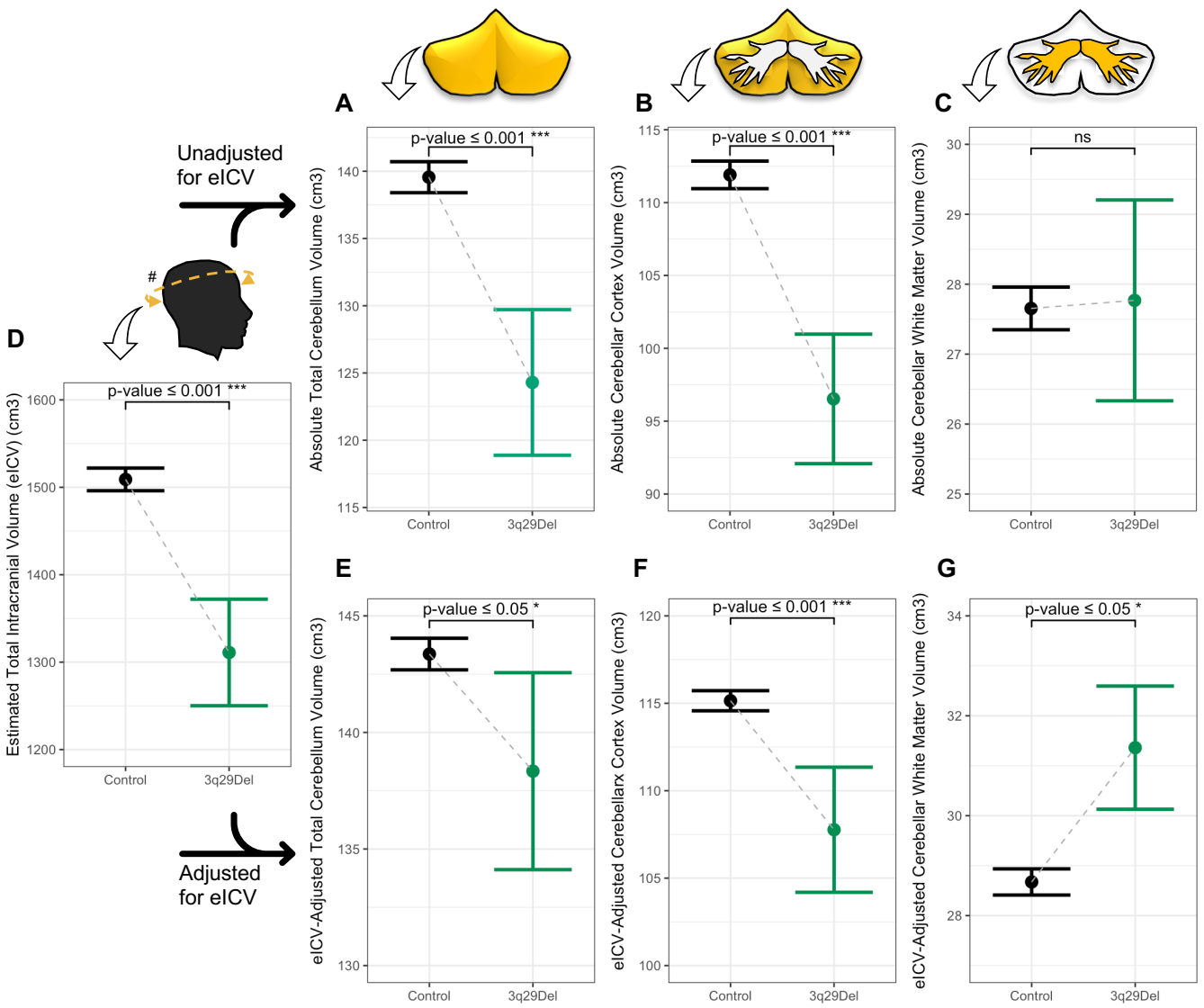

Figure 3. Predictor effect plots showing the effect of diagnostic group on volumetric measures of interest. A-G) Predicted values of VOIs across the 3q29Del and control groups were computed from the multiple linear regression models reported in Table 2, while covariates (sex, age, age² (when

applicable)) were held fixed. Error bars indicate the 95% confidence interval. P-values for the main effect of diagnostic group are indicated on each plot and reflect heteroskedasticity-robust estimates. A schematic of each VOI (yellow) is presented above the corresponding plot for clarity. Regression results indicate a significant difference between 3q29Del subjects and healthy controls in **A)** total cerebellum volume ($p \leq 0.001$), **B)** cerebellar cortex volume ($p \leq 0.001$), and **D)** eICV ($p \leq 0.001$), with smaller volumes observed in 3q29Del subjects compared with controls. This effect remained significant after **E)** total cerebellum volume ($p \leq 0.05$) and **F)** cerebellar cortex volume ($p \leq 0.001$) were adjusted for eICV. There was no significant effect of diagnostic group on **C)** absolute cerebellar white matter volume ($p > 0.05$), however **G)** after eICV-adjustment, 3q29Del subjects had significantly larger cerebellar white matter volumes than controls ($p \leq 0.05$). Control $N = 1{,}608$, 3q29Del $N = 23$. #eICV was calculated by FreeSurfer's atlas-based spatial normalization procedure. p-value ≤ 0.001 '***', p-value ≤ 0.01 '**', p-value ≤ 0.05 '*', p-value ≤ 0.1 '†' *Abbreviations*: 3q29 deletion syndrome, 3q29Del; volumetric measure of interest, VOI; estimated total intracranial volume, eICV; not significant, ns.

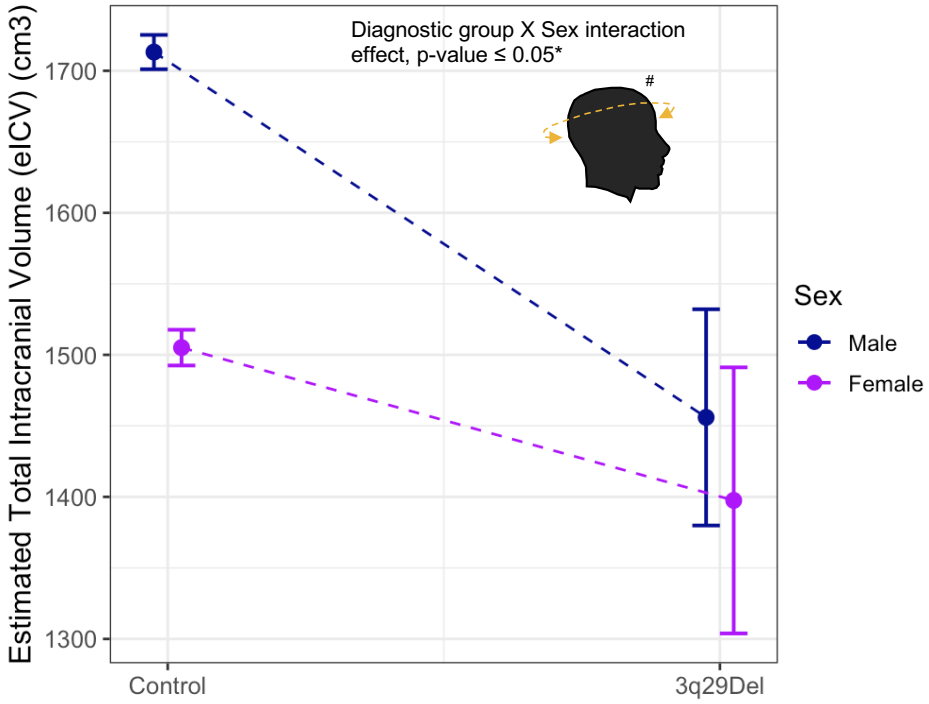

Figure 4. Predictor effect plot showing the moderating effect of sex on the relationship between diagnostic group and eICV. Predicted values of eICV across male versus female 3q29Del and control groups were computed from the exploratory interaction model reported in Table S4E, while covariates (age, age^2) were held fixed. Error bars indicate the 95% confidence interval. Heteroskedasticity-robust regression results indicate a significant diagnostic group by sex interaction effect on eICV ($p \leq 0.05$). Control N = 1,608 (Female N = 861, Male N = 747)**,** 3q29Del N = 23 (Female N = 9, Male N = 14). # eICV was calculated by FreeSurfer's atlas-based spatial normalization procedure. p-value ≤ 0.001 '***', p-value ≤ 0.01 '**', p-value ≤ 0.05 '*', p-value ≤ 0.1 '†' *Abbreviations*: 3q29 deletion syndrome, 3q29Del; estimated total intracranial volume, eICV.

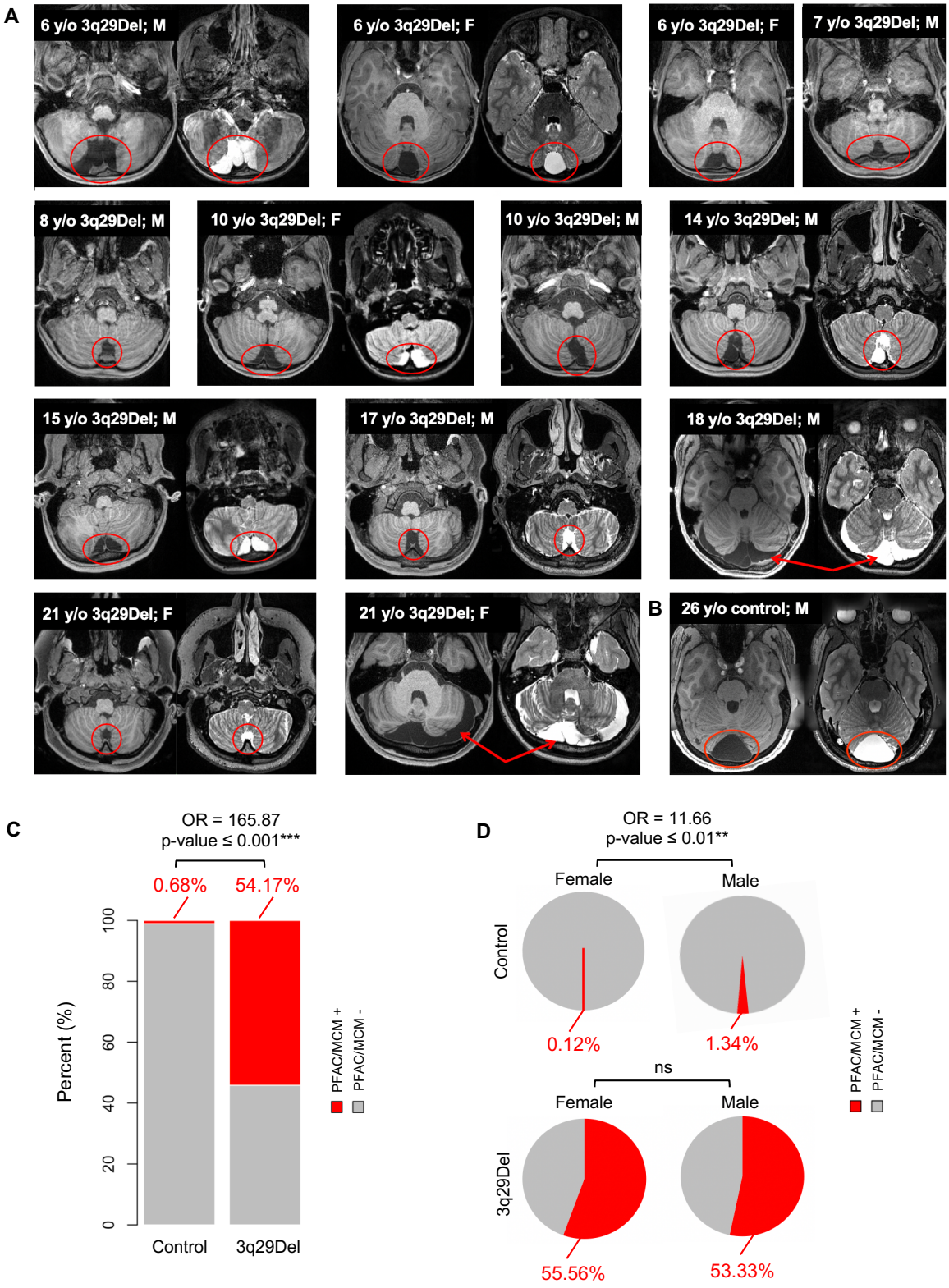

Figure 5. Prevalence of posterior fossa arachnoid cyst and mega cisterna magna findings in structural MRI scans of 3q29Del and control subjects. A) 13 3q29Del subjects had a PFAC/MCM finding (marked

in red) upon radiological evaluation of structural MRI scans. Representative T1- and/or T2-weighted MR images showing these radiological findings are provided in horizontal view for each 3q29Del subject, in chronological order of age. **B)** T1- and T2-weighted MR images of a representative control subject with a PFAC/MCM finding (marked in red). Age and sex information for each subject is indicated on individual images. **C)** Bar graphs represent the frequency of PFAC/MCM findings in the 3q29Del and control groups, separately. 3q29Del subjects had a significantly elevated rate of PFAC/MCM findings compared with controls ($p \leq 0.001$) **D)** Pie charts represent the sex-stratified frequency of PFAC/MCM findings in the 3q29Del and control groups, separately. Male controls had a significantly elevated rate of PFAC/MCM findings compared with female controls ($p \leq 0.01$), while there were no sex differences in these rates within the 3q29Del group ($p > 0.05$). Control $N = 1{,}608$ (Female $N = 861$, Male $N = 747$), 3q29Del $N = 24$ (Female $N = 9$, Male $N = 15$). p-value ≤ 0.001 '***', p-value ≤ 0.01 '**', p-value ≤ 0.05 '*', p-value ≤ 0.1 '†'. *Abbreviations*: 3q29 deletion syndrome, 3q29Del; posterior fossa arachnoid cyst, PFAC; mega cisterna magna, MCM; magnetic resonance imaging, MRI; years-old, y/o; male, M; female, F; odds ratio, OR; not significant, ns.

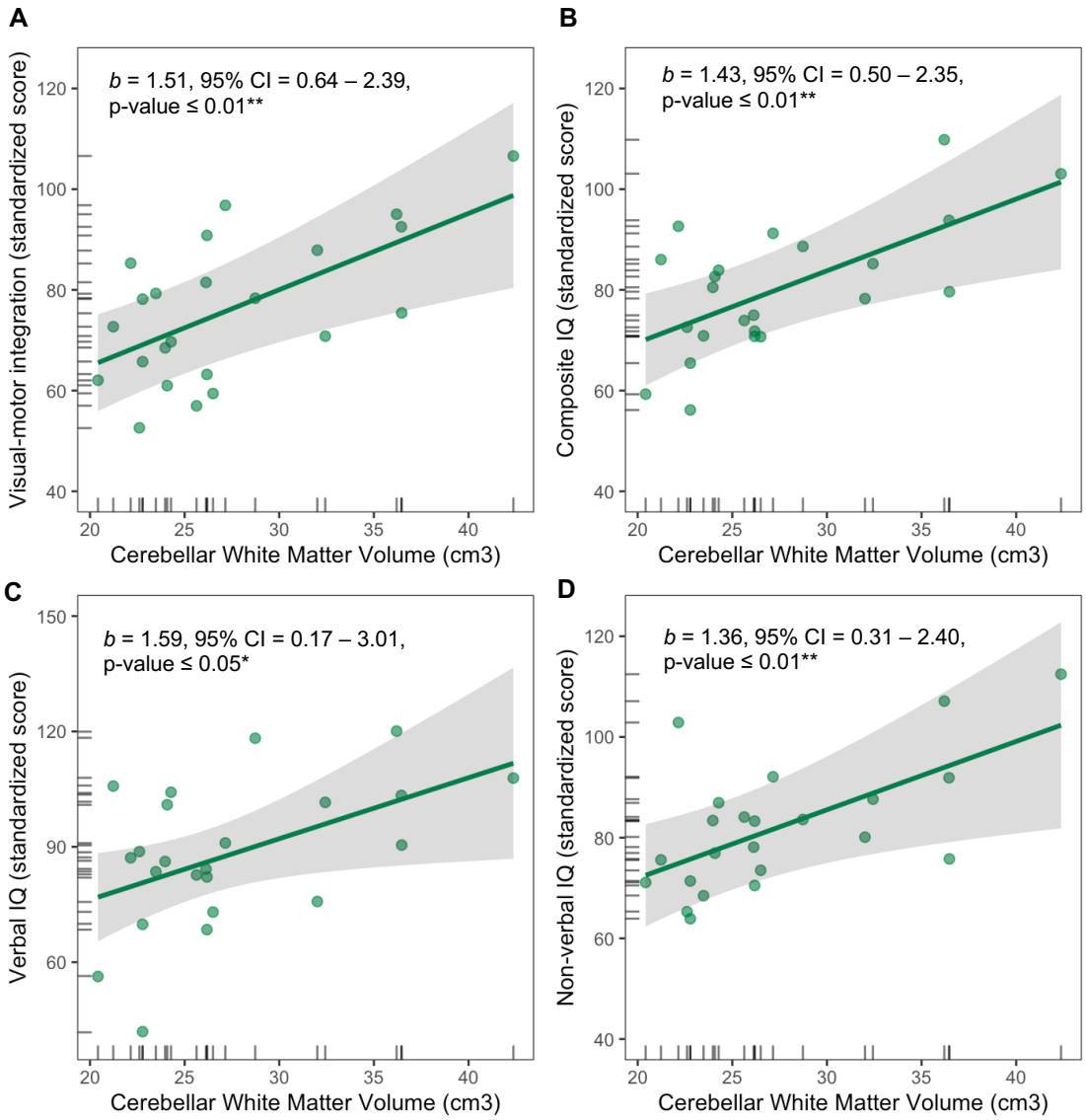

Figure 6. Predictor effect plots showing the relationships between cerebellar white matter volume and visual-motor integration skills, composite IQ, verbal IQ and non-verbal IQ among 3q29Del subjects. A-D) Predicted values for visual-motor integration, composite IQ, verbal IQ, and non-verbal IQ scores were computed from the multiple linear regression models reported in Table 5, while covariates (sex, age, eICV) were held fixed. Error bands indicate the 95% confidence interval, data points represent partial residuals, and rug plots show the distribution of the variables. Parameter estimates for the main effect of cerebellar white

matter volume are indicated on each plot and reflect heteroskedasticity-robust estimates. Regression results indicate significant relationships between cerebellar white matter volume and standardized test scores for **A)** visual-motor integration skills ($p \leq 0.01$), **B)** composite IQ ($p \leq 0.01$), **C)** verbal IQ ($p \leq 0.05$), and **D)** non-verbal IQ ($p \leq 0.01$), with larger volumes predicting higher scores among 3q29Del subjects. 3q29Del $N = 23$. p-value ≤ 0.001 '***', p-value ≤ 0.01 '**', p-value ≤ 0.05 '*', p-value ≤ 0.1 '†' *Abbreviations*: 3q29 deletion syndrome, 3q29Del; intelligence quotient, IQ; estimated total intracranial volume, eICV; unstandardized coefficient estimate, *b*; confidence interval, CI.

References

1. Iafrate AJ, Feuk L, Rivera MN, Listewnik ML, Donahoe PK, Qi Y, et al. (2004): Detection of large-scale variation in the human genome. *Nat Genet*. 36:949-951.

2. Sebat J, Lakshmi B, Troge J, Alexander J, Young J, Lundin P, et al. (2004): Large-scale copy number polymorphism in the human genome. *Science*. 305:525-528.

3. Redon R, Ishikawa S, Fitch KR, Feuk L, Perry GH, Andrews TD, et al. (2006): Global variation in copy number in the human genome. *Nature*. 444:444-454.

4. Korbel JO, Urban AE, Affourtit JP, Godwin B, Grubert F, Simons JF, et al. (2007): Paired-end mapping reveals extensive structural variation in the human genome. *Science*. 318:420-426.

5. Carvalho CM, Zhang F, Lupski JR (2011): Structural variation of the human genome: mechanisms, assays, and role in male infertility. *Syst Biol Reprod Med*. 57:3-16.

6. Cheng Z, Ventura M, She X, Khaitovich P, Graves T, Osoegawa K, et al. (2005): A genome-wide comparison of recent chimpanzee and human segmental duplications. *Nature*. 437:88-93.

7. Dumas L, Kim YH, Karimpour-Fard A, Cox M, Hopkins J, Pollack JR, et al. (2007): Gene copy number variation spanning 60 million years of human and primate evolution. *Genome Res*. 17:1266-1277.

8. Lupski JR (2007): An evolution revolution provides further revelation. *Bioessays*. 29:1182-1184.

9. Zhang F, Gu W, Hurles ME, Lupski JR (2009): Copy number variation in human health, disease, and evolution. *Annu Rev Genomics Hum Genet*. 10:451-481.

10. Marshall CR, Howrigan DP, Merico D, Thiruvahindrapuram B, Wu W, Greer DS, et al. (2017): Contribution of copy number variants to schizophrenia from a genome-wide study of 41,321 subjects. *Nat Genet*. 49:27-35.

11. Sanders SJ, He X, Willsey AJ, Ercan-Sencicek AG, Samocha KE, Cicek AE, et al. (2015): Insights into Autism Spectrum Disorder Genomic Architecture and Biology from 71 Risk Loci. *Neuron*. 87:1215-1233.

12. Leppa VM, Kravitz SN, Martin CL, Andrieux J, Le Caignec C, Martin-Coignard D, et al. (2016): Rare Inherited and De Novo CNVs Reveal Complex Contributions to ASD Risk in Multiplex Families. *Am J Hum Genet*. 99:540-554.

13. Takumi T, Tamada K (2018): CNV biology in neurodevelopmental disorders. *Curr Opin Neurobiol.* 48:183-192.

14. Malhotra D, Sebat J (2012): CNVs: harbingers of a rare variant revolution in psychiatric genetics. *Cell.* 148:1223-1241.

15. Kaminsky EB, Kaul V, Paschall J, Church DM, Bunke B, Kunig D, et al. (2011): An evidence-based approach to establish the functional and clinical significance of copy number variants in intellectual and developmental disabilities. *Genet Med.* 13:777-784.

16. Girirajan S, Campbell CD, Eichler EE (2011): Human copy number variation and complex genetic disease. *Annu Rev Genet.* 45:203-226.

17. Sebat J, Lakshmi B, Malhotra D, Troge J, Lese-Martin C, Walsh T, et al. (2007): Strong association of de novo copy number mutations with autism. *Science.* 316:445-449.

18. Girirajan S, Brkanac Z, Coe BP, Baker C, Vives L, Vu TH, et al. (2011): Relative burden of large CNVs on a range of neurodevelopmental phenotypes. *PLoS Genet.* 7:e1002334.

19. Cooper GM, Coe BP, Girirajan S, Rosenfeld JA, Vu TH, Baker C, et al. (2011): A copy number variation morbidity map of developmental delay. *Nat Genet.* 43:838-846.

20. Chawner SJ, Watson CJ, Owen MJ (2021): Clinical evaluation of patients with a neuropsychiatric risk copy number variant. *Curr Opin Genet Dev.* 68:26-34.

21. Moreno-De-Luca A, Myers SM, Challman TD, Moreno-De-Luca D, Evans DW, Ledbetter DH (2013): Developmental brain dysfunction: revival and expansion of old concepts based on new genetic evidence. *Lancet Neurol.* 12:406-414.

22. Moreno-De-Luca D, Cubells JF (2011): Copy number variants: a new molecular frontier in clinical psychiatry. *Curr Psychiatry Rep.* 13:129-137.

23. Lauer S, Gresham D (2019): An evolving view of copy number variants. *Curr Genet.* 65:1287-1295.

24. Mufford MS, Stein DJ, Dalvie S, Groenewold NA, Thompson PM, Jahanshad N (2017): Neuroimaging genomics in psychiatry-a translational approach. *Genome Med.* 9:102.

25. Bigos KL, Weinberger DR (2010): Imaging genetics--days of future past. *Neuroimage.* 53:804-809.

26. Meyer-Lindenberg A, Weinberger DR (2006): Intermediate phenotypes and genetic mechanisms of psychiatric disorders. *Nat Rev Neurosci*. 7:818-827.

27. Gottesman, II, Gould TD (2003): The endophenotype concept in psychiatry: etymology and strategic intentions. *Am J Psychiatry*. 160:636-645.

28. Amaral DG, Schumann CM, Nordahl CW (2008): Neuroanatomy of autism. *Trends Neurosci*. 31:137-145.

29. Wheeler AL, Voineskos AN (2014): A review of structural neuroimaging in schizophrenia: from connectivity to connectomics. *Front Hum Neurosci*. 8:653.

30. Zhang T, Koutsouleris N, Meisenzahl E, Davatzikos C (2015): Heterogeneity of structural brain changes in subtypes of schizophrenia revealed using magnetic resonance imaging pattern analysis. *Schizophr Bull*. 41:74-84.

31. Lenroot RK, Yeung PK (2013): Heterogeneity within Autism Spectrum Disorders: What have We Learned from Neuroimaging Studies? *Front Hum Neurosci*. 7:733.

32. Feczko E, Miranda-Dominguez O, Marr M, Graham AM, Nigg JT, Fair DA (2019): The Heterogeneity Problem: Approaches to Identify Psychiatric Subtypes. *Trends Cogn Sci*. 23:584-601.

33. Mulle JG (2015): The 3q29 deletion confers >40-fold increase in risk for schizophrenia. *Mol Psychiatry*. 20:1028-1029.

34. Singh T, Poterba T, Curtis D, Akil H, Aleissa M, Barchas J, et al. (2020): *Exome sequencing identifies rare coding variants in 10 genes which confer substantial risk for schizophrenia.*

35. Levinson DF, Duan J, Oh S, Wang K, Sanders AR, Shi J, et al. (2011): Copy number variants in schizophrenia: confirmation of five previous findings and new evidence for 3q29 microdeletions and VIPR2 duplications. *Am J Psychiatry*. 168:302-316.

36. Mulle JG, Dodd AF, McGrath JA, Wolyniec PS, Mitchell AA, Shetty AC, et al. (2010): Microdeletions of 3q29 confer high risk for schizophrenia. *Am J Hum Genet*. 87:229-236.

37. Kirov G, Pocklington AJ, Holmans P, Ivanov D, Ikeda M, Ruderfer D, et al. (2012): De novo CNV analysis implicates specific abnormalities of postsynaptic signalling complexes in the pathogenesis of schizophrenia. *Mol Psychiatry*. 17:142-153.

38. Pollak RM, Murphy MM, Epstein MP, Zwick ME, Klaiman C, Saulnier CA, et al. (2019): Neuropsychiatric phenotypes and a distinct constellation of ASD features in 3q29 deletion syndrome: results from the 3q29 registry. *Mol Autism*. 10:30.

39. Sanchez Russo R, Gambello MJ, Murphy MM, Aberizk K, Black E, Burrell TL, et al. (2021): Deep phenotyping in 3q29 deletion syndrome: recommendations for clinical care. *Genet Med*. 23:872-880.

40. Glassford MR, Rosenfeld JA, Freedman AA, Zwick ME, Mulle JG, Unique Rare Chromosome Disorder Support G (2016): Novel features of 3q29 deletion syndrome: Results from the 3q29 registry. *Am J Med Genet A*. 170A:999-1006.

41. Cox DM, Butler MG (2015): A clinical case report and literature review of the 3q29 microdeletion syndrome. *Clin Dysmorphol*. 24:89-94.

42. Mosley TJ, Johnston HR, Cutler DJ, Zwick ME, Mulle JG (2021): Sex-specific recombination patterns predict parent of origin for recurrent genomic disorders. *BMC Med Genomics*. 14:154.

43. Sefik E, Purcell RH, Emory 3q P, Walker EF, Bassell GJ, Mulle JG (2021): Convergent and distributed effects of the 3q29 deletion on the human neural transcriptome. *Transl Psychiatry*. 11:357.

44. Carroll LS, Williams HJ, Walters J, Kirov G, O'Donovan MC, Owen MJ (2011): Mutation screening of the 3q29 microdeletion syndrome candidate genes DLG1 and PAK2 in schizophrenia. *Am J Med Genet B Neuropsychiatr Genet*. 156B:844-849.

45. Baynam G, Goldblatt J, Townshend S (2006): A case of 3q29 microdeletion with novel features and a review of cytogenetically visible terminal 3q deletions. *Clin Dysmorphol*. 15:145-148.

46. Digilio MC, Bernardini L, Mingarelli R, Capolino R, Capalbo A, Giuffrida MG, et al. (2009): 3q29 Microdeletion: a mental retardation disorder unassociated with a recognizable phenotype in two mother-daughter pairs. *Am J Med Genet A*. 149A:1777-1781.

47. Tyshchenko N, Hackmann K, Gerlach EM, Neuhann T, Schrock E, Tinschert S (2009): 1.6Mb deletion in chromosome band 3q29 associated with eye abnormalities. *Eur J Med Genet*. 52:128-130.

48. Quintero-Rivera F, Sharifi-Hannauer P, Martinez-Agosto JA (2010): Autistic and psychiatric findings associated with the 3q29 microdeletion syndrome: case report and review. *Am J Med Genet A*. 152A:2459-2467.

49. Sagar A, Bishop JR, Tessman DC, Guter S, Martin CL, Cook EH (2013): Co-occurrence of autism, childhood psychosis, and intellectual disability associated with a de novo 3q29 microdeletion. *Am J Med Genet A*. 161A:845-849.

50. Citta S, Buono S, Greco D, Barone C, Alfei E, Bulgheroni S, et al. (2013): 3q29 microdeletion syndrome: Cognitive and behavioral phenotype in four patients. *Am J Med Genet A*. 161A:3018-3022.

51. Masarweh M (2011): Chromosome 3q29 deletion with gastrointestinal malformation: a case report. *J Med Case Rep*. 5:285.

52. Chirita Emandi A, Dobrescu AI, Doros G, Hyon C, Miclea D, Popoiu C, et al. (2019): A Novel 3q29 Deletion in Association With Developmental Delay and Heart Malformation-Case Report With Literature Review. *Front Pediatr*. 7:270.

53. Malt EA, Juhasz K, Frengen A, Wangensteen T, Emilsen NM, Hansen B, et al. (2019): Neuropsychiatric phenotype in relation to gene variants in the hemizygous allele in 3q29 deletion carriers: A case series. *Mol Genet Genomic Med*. 7:e889.

54. Bosemani T, Orman G, Boltshauser E, Tekes A, Huisman TA, Poretti A (2015): Congenital abnormalities of the posterior fossa. *Radiographics*. 35:200-220.

55. Al-Holou WN, Terman S, Kilburg C, Garton HJ, Muraszko KM, Maher CO (2013): Prevalence and natural history of arachnoid cysts in adults. *J Neurosurg*. 118:222-231.

56. Al-Holou WN, Yew AY, Boomsaad ZE, Garton HJ, Muraszko KM, Maher CO (2010): Prevalence and natural history of arachnoid cysts in children. *J Neurosurg Pediatr*. 5:578-585.

57. Rapoport M, van Reekum R, Mayberg H (2000): The role of the cerebellum in cognition and behavior: a selective review. *J Neuropsychiatry Clin Neurosci*. 12:193-198.

58. Wang SS, Kloth AD, Badura A (2014): The cerebellum, sensitive periods, and autism. *Neuron*. 83:518-532.

59. Koziol LF, Budding D, Andreasen N, D'Arrigo S, Bulgheroni S, Imamizu H, et al. (2014): Consensus paper: the cerebellum's role in movement and cognition. *Cerebellum*. 13:151-177.

60. Schmahmann JD (2019): The cerebellum and cognition. *Neurosci Lett*. 688:62-75.

61. Murphy MM, Lindsey Burrell T, Cubells JF, Espana RA, Gambello MJ, Goines KCB, et al. (2018): Study protocol for The Emory 3q29 Project: evaluation of neurodevelopmental, psychiatric, and medical symptoms in 3q29 deletion syndrome. *BMC Psychiatry*. 18:183.

62. White T, Andreasen NC, Nopoulos P (2002): Brain volumes and surface morphology in monozygotic twins. *Cereb Cortex*. 12:486-493.

63. Blokland GA, de Zubicaray GI, McMahon KL, Wright MJ (2012): Genetic and environmental influences on neuroimaging phenotypes: a meta-analytical perspective on twin imaging studies. *Twin Res Hum Genet*. 15:351-371.

64. Somerville LH, Bookheimer SY, Buckner RL, Burgess GC, Curtiss SW, Dapretto M, et al. (2018): The Lifespan Human Connectome Project in Development: A large-scale study of brain connectivity development in 5-21 year olds. *Neuroimage*. 183:456-468.

65. Van Essen DC, Smith SM, Barch DM, Behrens TE, Yacoub E, Ugurbil K, et al. (2013): The WU-Minn Human Connectome Project: an overview. *Neuroimage*. 80:62-79.

66. Mugler JP, 3rd, Brookeman JR (1990): Three-dimensional magnetization-prepared rapid gradient-echo imaging (3D MP RAGE). *Magn Reson Med*. 15:152-157.

67. Mugler JP, 3rd, Bao S, Mulkern RV, Guttmann CR, Robertson RL, Jolesz FA, et al. (2000): Optimized single-slab three-dimensional spin-echo MR imaging of the brain. *Radiology*. 216:891-899.

68. Harms MP, Somerville LH, Ances BM, Andersson J, Barch DM, Bastiani M, et al. (2018): Extending the Human Connectome Project across ages: Imaging protocols for the Lifespan Development and Aging projects. *Neuroimage*. 183:972-984.

69. Van Essen DC, Ugurbil K, Auerbach E, Barch D, Behrens TE, Bucholz R, et al. (2012): The Human Connectome Project: a data acquisition perspective. *Neuroimage*. 62:2222-2231.

70. Glasser MF, Sotiropoulos SN, Wilson JA, Coalson TS, Fischl B, Andersson JL, et al. (2013): The minimal preprocessing pipelines for the Human Connectome Project. *Neuroimage*. 80:105-124.

71. Fischl B, Salat DH, Busa E, Albert M, Dieterich M, Haselgrove C, et al. (2002): Whole brain segmentation: automated labeling of neuroanatomical structures in the human brain. *Neuron*. 33:341-355.

72. Fabbri M, Mongiardino Koch N, Pritchard AC, Hanson M, Hoffman E, Bever GS, et al. (2017): The skull roof tracks the brain during the evolution and development of reptiles including birds. *Nat Ecol Evol*. 1:1543-1550.

73. Koyabu D, Werneburg I, Morimoto N, Zollikofer CP, Forasiepi AM, Endo H, et al. (2014): Mammalian skull heterochrony reveals modular evolution and a link between cranial development and brain size. *Nature communications*. 5:1-9.

74. Bartholomeusz HH, Courchesne E, Karns CM (2002): Relationship between head circumference and brain volume in healthy normal toddlers, children, and adults. *Neuropediatrics*. 33:239-241.

75. Mathalon DH, Sullivan EV, Rawles JM, Pfefferbaum A (1993): Correction for head size in brain-imaging measurements. *Psychiatry Res*. 50:121-139.

76. Barnes J, Ridgway GR, Bartlett J, Henley SM, Lehmann M, Hobbs N, et al. (2010): Head size, age and gender adjustment in MRI studies: a necessary nuisance? *Neuroimage*. 53:1244-1255.

77. Davis P, Wright E (1977): A new method for measuring cranial cavity volume and its application to the assessment of cerebral atrophy at autopsy. *Neuropathology and applied neurobiology*. 3:341-358.

78. Buckner RL, Head D, Parker J, Fotenos AF, Marcus D, Morris JC, et al. (2004): A unified approach for morphometric and functional data analysis in young, old, and demented adults using automated atlas-based head size normalization: reliability and validation against manual measurement of total intracranial volume. *Neuroimage*. 23:724-738.

79. O'Brien LM, Ziegler DA, Deutsch CK, Frazier JA, Herbert MR, Locascio JJ (2011): Statistical adjustments for brain size in volumetric neuroimaging studies: some practical implications in methods. *Psychiatry Res*. 193:113-122.

80. Ueda K, Fujiwara H, Miyata J, Hirao K, Saze T, Kawada R, et al. (2010): Investigating association of brain volumes with intracranial capacity in schizophrenia. *Neuroimage*. 49:2503-2508.

81. Voevodskaya O, Simmons A, Nordenskjold R, Kullberg J, Ahlstrom H, Lind L, et al. (2014): The effects of intracranial volume adjustment approaches on multiple regional MRI volumes in healthy aging and Alzheimer's disease. *Front Aging Neurosci*. 6:264.

82. Kollias SS, Ball WS, Jr., Prenger EC (1993): Cystic malformations of the posterior fossa: differential diagnosis clarified through embryologic analysis. *Radiographics*. 13:1211-1231.

83. McKinney AM (2017): Mega Cisterna Magna and Retrocerebellar Arachnoid Cysts. *Atlas of Normal Imaging Variations of the Brain, Skull, and Craniocervical Vasculature*: Springer, pp 19-41.

84. Beery KE, Buktenica NA, Beery NA (2010): *The Beery–Buktenica Developmental Test of Visual–Motor Integration: Administration, scoring, and teaching manual*. 6 ed. Minneapolis, MN: Pearson.

85. Elliott CD (2007): *Differential abilities scales*. 2 ed. San Antonio, TX: Harcourt Assessment.

86. Wechsler D (2011): *Wechsler abbreviated scale of intelligence*. 2 ed. Bloomington, MN: Pearson.

87. R Development Core Team (2021): R: A Language and Environment for Statistical Computing. Vienna, Austria: R Foundation for Statistical Computing.

88. Kim TG, Kim DS, Choi JU (2010): Are arachnoid cysts localized hydrocephali? *Pediatr Neurosurg*. 46:362-367.

89. Choi JU, Kim DS (1998): Pathogenesis of arachnoid cyst: congenital or traumatic? *Pediatr Neurosurg*. 29:260-266.

90. Greene S, Ellenbogen RG (2005): Congenital Malformations of the Brain and Spinal Cord. *Pediatric Critical Care Mosby-Year Book (St Louis)*.

91. MacKinnon JG, White H (1985): Some heteroskedasticity-consistent covariance matrix estimators with improved finite sample properties. *Journal of econometrics*. 29:305-325.

92. Sargent C, Burn J, Baraitser M, Pembrey ME (1985): Trigonocephaly and the Opitz C syndrome. *J Med Genet*. 22:39-45.

93. Herculano-Houzel S (2010): Coordinated scaling of cortical and cerebellar numbers of neurons. *Frontiers in neuroanatomy*. 4:12.

94. Zagon IS, McLaughlin PJ, Smith S (1977): Neural populations in the human cerebellum: estimations from isolated cell nuclei. *Brain Res*. 127:279-282.

95. van Essen MJ, Nayler S, Becker EBE, Jacob J (2020): Deconstructing cerebellar development cell by cell. *PLoS Genet*. 16:e1008630.

96. Tiemeier H, Lenroot RK, Greenstein DK, Tran L, Pierson R, Giedd JN (2010): Cerebellum development during childhood and adolescence: a longitudinal morphometric MRI study. *Neuroimage*. 49:63-70.

97. Wierenga LM, Bos MGN, Schreuders E, Vd Kamp F, Peper JS, Tamnes CK, et al. (2018): Unraveling age, puberty and testosterone effects on subcortical brain development across adolescence. *Psychoneuroendocrinology*. 91:105-114.

98. Wierenga L, Langen M, Ambrosino S, van Dijk S, Oranje B, Durston S (2014): Typical development of basal ganglia, hippocampus, amygdala and cerebellum from age 7 to 24. *Neuroimage*. 96:67-72.

99. Ostby Y, Tamnes CK, Fjell AM, Westlye LT, Due-Tonnessen P, Walhovd KB (2009): Heterogeneity in subcortical brain development: A structural magnetic resonance imaging study of brain maturation from 8 to 30 years. *J Neurosci*. 29:11772-11782.

100. Wu KH, Chen CY, Shen EY (2011): The cerebellar development in chinese children-a study by voxel-based volume measurement of reconstructed 3D MRI scan. *Pediatr Res*. 69:80-83.

101. Sussman D, Leung RC, Chakravarty MM, Lerch JP, Taylor MJ (2016): The developing human brain: age-related changes in cortical, subcortical, and cerebellar anatomy. *Brain Behav*. 6:e00457.

102. Bray S, Krongold M, Cooper C, Lebel C (2015): Synergistic Effects of Age on Patterns of White and Gray Matter Volume across Childhood and Adolescence. *eNeuro*. 2.

103. Uhlen M, Oksvold P, Fagerberg L, Lundberg E, Jonasson K, Forsberg M, et al. (2010): Towards a knowledge-based Human Protein Atlas. *Nat Biotechnol*. 28:1248-1250.

104. Uhlen M, Fagerberg L, Hallstrom BM, Lindskog C, Oksvold P, Mardinoglu A, et al. (2015): Proteomics. Tissue-based map of the human proteome. *Science*. 347:1260419.

105. Howard MA, Elias GM, Elias LA, Swat W, Nicoll RA (2010): The role of SAP97 in synaptic glutamate receptor dynamics. *Proc Natl Acad Sci U S A*. 107:3805-3810.

106. Otsuka H, Kimura T, Ago Y, Nakama M, Aoyama Y, Abdelkreem E, et al. (2020): Deficiency of 3-hydroxybutyrate dehydrogenase (BDH1) in mice causes low ketone body levels and fatty liver during fasting. *J Inherit Metab Dis*. 43:960-968.

107. Haider A, Wei YC, Lim K, Barbosa AD, Liu CH, Weber U, et al. (2018): PCYT1A Regulates Phosphatidylcholine Homeostasis from the Inner Nuclear Membrane in Response to Membrane Stored Curvature Elastic Stress. *Dev Cell*. 45:481-495 e488.

108. Cotter L, Ozcelik M, Jacob C, Pereira JA, Locher V, Baumann R, et al. (2010): Dlg1-PTEN interaction regulates myelin thickness to prevent damaging peripheral nerve overmyelination. *Science*. 328:1415-1418.

109. Rutkowski TP, Purcell RH, Pollak RM, Grewenow SM, Gafford GM, Malone T, et al. (2021): Behavioral changes and growth deficits in a CRISPR engineered mouse model of the schizophrenia-associated 3q29 deletion. *Mol Psychiatry*. 26:772-783.

110. Purger D, Gibson EM, Monje M (2016): Myelin plasticity in the central nervous system. *Neuropharmacology*. 110:563-573.

111. Snaidero N, Mobius W, Czopka T, Hekking LH, Mathisen C, Verkleij D, et al. (2014): Myelin membrane wrapping of CNS axons by PI(3,4,5)P3-dependent polarized growth at the inner tongue. *Cell*. 156:277-290.

112. Sorond FA, Gorelick PB (2019): Brain White Matter: A Substrate for Resilience and a Substance for Subcortical Small Vessel Disease. *Brain Sci*. 9.

113. Bergles DE, Richardson WD (2015): Oligodendrocyte Development and Plasticity. *Cold Spring Harb Perspect Biol*. 8:a020453.

114. Bechler ME, Swire M, Ffrench-Constant C (2018): Intrinsic and adaptive myelination-A sequential mechanism for smart wiring in the brain. *Dev Neurobiol.* 78:68-79.

115. Evarts EV, Thach WT (1969): Motor mechanisms of the CNS: cerebrocerebellar interrelations. *Annu Rev Physiol.* 31:451-498.

116. Parvizi J (2009): Corticocentric myopia: old bias in new cognitive sciences. *Trends Cogn Sci.* 13:354-359.

117. Strick PL, Dum RP, Fiez JA (2009): Cerebellum and nonmotor function. *Annu Rev Neurosci.* 32:413-434.

118. Schmahmann JD (2010): The role of the cerebellum in cognition and emotion: personal reflections since 1982 on the dysmetria of thought hypothesis, and its historical evolution from theory to therapy. *Neuropsychol Rev.* 20:236-260.

119. Van Overwalle F, Manto M, Cattaneo Z, Clausi S, Ferrari C, Gabrieli JDE, et al. (2020): Consensus Paper: Cerebellum and Social Cognition. *Cerebellum.* 19:833-868.

120. Ito M (1993): Movement and thought: identical control mechanisms by the cerebellum. *Trends Neurosci.* 16:448-450; discussion 453-444.

121. Ito M (2008): Control of mental activities by internal models in the cerebellum. *Nat Rev Neurosci.* 9:304-313.

122. Leiner HC, Leiner AL, Dow RS (1991): The human cerebro-cerebellar system: its computing, cognitive, and language skills. *Behav Brain Res.* 44:113-128.

123. Badura A, Verpeut JL, Metzger JW, Pereira TD, Pisano TJ, Deverett B, et al. (2018): Normal cognitive and social development require posterior cerebellar activity. *Elife.* 7.

124. Popa LS, Hewitt AL, Ebner TJ (2014): The cerebellum for jocks and nerds alike. *Front Syst Neurosci.* 8:113.

125. Argyropoulos GPD, van Dun K, Adamaszek M, Leggio M, Manto M, Masciullo M, et al. (2020): The Cerebellar Cognitive Affective/Schmahmann Syndrome: a Task Force Paper. *Cerebellum.* 19:102-125.

126. Pisano TJ, Dhanerawala ZM, Kislin M, Bakshinskaya D, Engel EA, Hansen EJ, et al. (2021): Homologous organization of cerebellar pathways to sensory, motor, and associative forebrain. *Cell Rep.* 36:109721.

127. Kelly RM, Strick PL (2003): Cerebellar loops with motor cortex and prefrontal cortex of a nonhuman primate. *J Neurosci.* 23:8432-8444.

128. Keser Z, Hasan KM, Mwangi BI, Kamali A, Ucisik-Keser FE, Riascos RF, et al. (2015): Diffusion tensor imaging of the human cerebellar pathways and their interplay with cerebral macrostructure. *Front Neuroanat.* 9:41.

129. Stoodley CJ, Schmahmann JD (2009): Functional topography in the human cerebellum: a meta-analysis of neuroimaging studies. *Neuroimage.* 44:489-501.

130. E KH, Chen SH, Ho MH, Desmond JE (2014): A meta-analysis of cerebellar contributions to higher cognition from PET and fMRI studies. *Hum Brain Mapp.* 35:593-615.

131. Guell X, Gabrieli JDE, Schmahmann JD (2018): Triple representation of language, working memory, social and emotion processing in the cerebellum: convergent evidence from task and seed-based resting-state fMRI analyses in a single large cohort. *Neuroimage.* 172:437-449.

132. King M, Hernandez-Castillo CR, Poldrack RA, Ivry RB, Diedrichsen J (2019): Functional boundaries in the human cerebellum revealed by a multi-domain task battery. *Nat Neurosci.* 22:1371-1378.

133. Desmond JE, Fiez JA (1998): Neuroimaging studies of the cerebellum: language, learning and memory. *Trends Cogn Sci.* 2:355-362.

134. Stoodley CJ, Valera EM, Schmahmann JD (2010): An fMRI study of intra-individual functional topography in the human cerebellum. *Behav Neurol.* 23:65-79.

135. Stoodley CJ, Valera EM, Schmahmann JD (2012): Functional topography of the cerebellum for motor and cognitive tasks: an fMRI study. *Neuroimage.* 59:1560-1570.

136. Schmahmann JD, Sherman JC (1997): Cerebellar cognitive affective syndrome. *Int Rev Neurobiol.* 41:433-440.

137. Schmahmann JD (2004): Disorders of the cerebellum: ataxia, dysmetria of thought, and the cerebellar cognitive affective syndrome. *J Neuropsychiatry Clin Neurosci*. 16:367-378.

138. Levisohn L, Cronin-Golomb A, Schmahmann JD (2000): Neuropsychological consequences of cerebellar tumour resection in children: cerebellar cognitive affective syndrome in a paediatric population. *Brain*. 123 (Pt 5):1041-1050.

139. Schmahmann JD, Macmore J, Vangel M (2009): Cerebellar stroke without motor deficit: clinical evidence for motor and non-motor domains within the human cerebellum. *Neuroscience*. 162:852-861.

140. Phillips JR, Hewedi DH, Eissa AM, Moustafa AA (2015): The cerebellum and psychiatric disorders. *Front Public Health*. 3:66.

141. Hariri AR (2019): The Emerging Importance of the Cerebellum in Broad Risk for Psychopathology. *Neuron*. 102:17-20.

142. Moberget T, Alnaes D, Kaufmann T, Doan NT, Cordova-Palomera A, Norbom LB, et al. (2019): Cerebellar Gray Matter Volume Is Associated With Cognitive Function and Psychopathology in Adolescence. *Biol Psychiatry*. 86:65-75.

143. Romer AL, Knodt AR, Houts R, Brigidi BD, Moffitt TE, Caspi A, et al. (2018): Structural alterations within cerebellar circuitry are associated with general liability for common mental disorders. *Mol Psychiatry*. 23:1084-1090.

144. Limperopoulos C, Bassan H, Gauvreau K, Robertson RL, Jr., Sullivan NR, Benson CB, et al. (2007): Does cerebellar injury in premature infants contribute to the high prevalence of long-term cognitive, learning, and behavioral disability in survivors? *Pediatrics*. 120:584-593.

145. Bolduc ME, Du Plessis AJ, Sullivan N, Khwaja OS, Zhang X, Barnes K, et al. (2011): Spectrum of neurodevelopmental disabilities in children with cerebellar malformations. *Dev Med Child Neurol*. 53:409-416.

146. Limperopoulos C, Robertson RL, Sullivan NR, Bassan H, du Plessis AJ (2009): Cerebellar injury in term infants: clinical characteristics, magnetic resonance imaging findings, and outcome. *Pediatr Neurol*. 41:1-8.

147. Stoodley CJ, D'Mello AM, Ellegood J, Jakkamsetti V, Liu P, Nebel MB, et al. (2017): Altered cerebellar connectivity in autism and cerebellar-mediated rescue of autism-related behaviors in mice. *Nat Neurosci*. 20:1744-1751.

148. Bailey A, Luthert P, Dean A, Harding B, Janota I, Montgomery M, et al. (1998): A clinicopathological study of autism. *Brain*. 121 (Pt 5):889-905.

149. Kemper TL, Bauman ML (2002): Neuropathology of infantile autism. *Mol Psychiatry*. 7 Suppl 2:S12-13.

150. Wassink TH, Andreasen NC, Nopoulos P, Flaum M (1999): Cerebellar morphology as a predictor of symptom and psychosocial outcome in schizophrenia. *Biol Psychiatry*. 45:41-48.

151. Bottmer C, Bachmann S, Pantel J, Essig M, Amann M, Schad LR, et al. (2005): Reduced cerebellar volume and neurological soft signs in first-episode schizophrenia. *Psychiatry Res*. 140:239-250.

152. Gaser C, Volz HP, Kiebel S, Riehemann S, Sauer H (1999): Detecting structural changes in whole brain based on nonlinear deformations-application to schizophrenia research. *Neuroimage*. 10:107-113.

153. Kim T, Lee KH, Oh H, Lee TY, Cho KIK, Lee J, et al. (2018): Cerebellar Structural Abnormalities Associated With Cognitive Function in Patients With First-Episode Psychosis. *Front Psychiatry*. 9:286.

154. Stoodley CJ (2016): The Cerebellum and Neurodevelopmental Disorders. *Cerebellum*. 15:34-37.

155. Gupta CN, Calhoun VD, Rachakonda S, Chen J, Patel V, Liu J, et al. (2015): Patterns of Gray Matter Abnormalities in Schizophrenia Based on an International Mega-analysis. *Schizophr Bull*. 41:1133-1142.

156. Toal F, Bloemen OJ, Deeley Q, Tunstall N, Daly EM, Page L, et al. (2009): Psychosis and autism: magnetic resonance imaging study of brain anatomy. *Br J Psychiatry*. 194:418-425.

157. Skefos J, Cummings C, Enzer K, Holiday J, Weed K, Levy E, et al. (2014): Regional alterations in purkinje cell density in patients with autism. *PLoS One*. 9:e81255.

158. Whitney ER, Kemper TL, Bauman ML, Rosene DL, Blatt GJ (2008): Cerebellar Purkinje cells are reduced in a subpopulation of autistic brains: a stereological experiment using calbindin-D28k. *Cerebellum*. 7:406-416.

159. D'Mello AM, Crocetti D, Mostofsky SH, Stoodley CJ (2015): Cerebellar gray matter and lobular volumes correlate with core autism symptoms. *Neuroimage Clin*. 7:631-639.

160. Stanfield AC, McIntosh AM, Spencer MD, Philip R, Gaur S, Lawrie SM (2008): Towards a neuroanatomy of autism: a systematic review and meta-analysis of structural magnetic resonance imaging studies. *Eur Psychiatry*. 23:289-299.

161. Chambers T, Escott-Price V, Legge S, Baker E, Singh KD, Walters JTR, et al. (2022): Genetic common variants associated with cerebellar volume and their overlap with mental disorders: a study on 33,265 individuals from the UK-Biobank. *Mol Psychiatry*.

162. Tsai PT, Hull C, Chu Y, Greene-Colozzi E, Sadowski AR, Leech JM, et al. (2012): Autistic-like behaviour and cerebellar dysfunction in Purkinje cell Tsc1 mutant mice. *Nature*. 488:647-651.

163. Ellegood J, Anagnostou E, Babineau BA, Crawley JN, Lin L, Genestine M, et al. (2015): Clustering autism: using neuroanatomical differences in 26 mouse models to gain insight into the heterogeneity. *Mol Psychiatry*. 20:118-125.

164. Schmitt JE, DeBevits JJ, Roalf DR, Ruparel K, Gallagher RS, Gur RC, et al. (2021): A Comprehensive Analysis of Cerebellar Volumes in the 22q11.2 Deletion Syndrome. *Biol Psychiatry Cogn Neurosci Neuroimaging*.

165. Cupolillo D, Hoxha E, Faralli A, De Luca A, Rossi F, Tempia F, et al. (2016): Autistic-Like Traits and Cerebellar Dysfunction in Purkinje Cell PTEN Knock-Out Mice. *Neuropsychopharmacology*. 41:1457-1466.

166. Modenato C, Kumar K, Moreau C, Martin-Brevet S, Huguet G, Schramm C, et al. (2021): Effects of eight neuropsychiatric copy number variants on human brain structure. *Transl Psychiatry*. 11:399.

167. Kloth AD, Badura A, Li A, Cherskov A, Connolly SG, Giovannucci A, et al. (2015): Cerebellar associative sensory learning defects in five mouse autism models. *Elife*. 4:e06085.

168. Barulli D, Stern Y (2013): Efficiency, capacity, compensation, maintenance, plasticity: emerging concepts in cognitive reserve. *Trends Cogn Sci*. 17:502-509.

169. Papoutsi M, Labuschagne I, Tabrizi SJ, Stout JC (2014): The cognitive burden in Huntington's disease: pathology, phenotype, and mechanisms of compensation. *Mov Disord*. 29:673-683.

170. Scheller E, Minkova L, Leitner M, Kloppel S (2014): Attempted and successful compensation in preclinical and early manifest neurodegeneration - a review of task FMRI studies. *Front Psychiatry*. 5:132.

171. Sanjari Moghaddam H, Dolatshahi M, Mohebi F, Aarabi MH (2020): Structural white matter alterations as compensatory mechanisms in Parkinson's disease: A systematic review of diffusion tensor imaging studies. *J Neurosci Res.* 98:1398-1416.

172. Gregory S, Long JD, Tabrizi SJ, Rees G (2017): Measuring compensation in neurodegeneration using MRI. *Curr Opin Neurol.* 30:380-387.

173. Makovac E, Cercignani M, Serra L, Torso M, Spano B, Petrucci S, et al. (2016): Brain Connectivity Changes in Autosomal Recessive Parkinson Disease: A Model for the Sporadic Form. *PLoS One.* 11:e0163980.

174. Bassett AS, Scherer SW, Brzustowicz LM (2010): Copy number variations in schizophrenia: critical review and new perspectives on concepts of genetics and disease. *Am J Psychiatry.* 167:899-914.

175. Whitley E, Ball J (2002): Statistics review 4: sample size calculations. *Crit Care.* 6:335-341.

176. Yamauchi T, Saeki N, Yamaura A (1999): Spontaneous disappearance of temporo-frontal arachnoid cyst in a child. *Acta Neurochir (Wien).* 141:537-540.

177. Rakier A, Feinsod M (1995): Gradual resolution of an arachnoid cyst after spontaneous rupture into the subdural space. Case report. *J Neurosurg.* 83:1085-1086.

178. Beltramello A, Mazza C (1985): Spontaneous disappearance of a large middle fossa arachnoid cyst. *Surg Neurol.* 24:181-183.

179. Inoue T, Matsushima T, Tashima S, Fukui M, Hasuo K (1987): Spontaneous disappearance of a middle fossa arachnoid cyst associated with subdural hematoma. *Surg Neurol.* 28:447-450.

180. Mokri B, Houser OW, Dinapoli RP (1994): Spontaneous Resolution of arachnoid cysts. *J Neuroimaging.* 4:165-168.

181. Mori T, Fujimoto M, Sakae K, Sakakibara T, Shin H, Yamaki T, et al. (1995): Disappearance of arachnoid cysts after head injury. *Neurosurgery.* 36:938-941; discussion 941-932.

182. Yamanouchi Y, Someda K, Oka N (1986): Spontaneous disappearance of middle fossa arachnoid cyst after head injury. *Childs Nerv Syst.* 2:40-43.

183. Rengachary SS, Watanabe I, Brackett CE (1978): Pathogenesis of intracranial arachnoid cysts. *Surg Neurol.* 9:139-144.

184. Mustansir F, Bashir S, Darbar A (2018): Management of Arachnoid Cysts: A Comprehensive Review. *Cureus*. 10:e2458.

185. Boronat S, Caruso P, Auladell M, Van Eeghen A, Thiele EA (2014): Arachnoid cysts in tuberous sclerosis complex. *Brain Dev*. 36:801-806.

186. Pomeranz S, Constantini S, Lubetzki-Korn I, Amir N (1991): Familial intracranial arachnoid cysts. *Childs Nerv Syst*. 7:100-102.

187. Furey CG, Timberlake AT, Nelson-Williams C, Duran D, Li P, Jackson EM, et al. (2017): Xp22.2 Chromosomal Duplication in Familial Intracranial Arachnoid Cyst. *JAMA Neurol*. 74:1503-1504.

188. Orlacchio A, Gaudiello F, Totaro A, Floris R, St George-Hyslop PH, Bernardi G, et al. (2004): A new SPG4 mutation in a variant form of spastic paraplegia with congenital arachnoid cysts. *Neurology*. 62:1875-1878.

189. Qin X, Wang Y, Xu S, Hong X (2019): Familial arachnoid cysts: a review of 35 families. *Childs Nerv Syst*. 35:607-612.

190. Fountain DM, Smith MJ, O'Leary C, Pathmanaban ON, Roncaroli F, Bobola N, et al. (2021): The spatial phenotype of genotypically distinct meningiomas demonstrate potential implications of the embryology of the meninges. *Oncogene*. 40:875-884.

191. DeSisto J, O'Rourke R, Jones HE, Pawlikowski B, Malek AD, Bonney S, et al. (2020): Single-Cell Transcriptomic Analyses of the Developing Meninges Reveal Meningeal Fibroblast Diversity and Function. *Dev Cell*. 54:43-59 e44.

192. Barkovich AJ, Millen KJ, Dobyns WB (2009): A developmental and genetic classification for midbrain-hindbrain malformations. *Brain*. 132:3199-3230.

193. Fombonne E (2009): Epidemiology of pervasive developmental disorders. *Pediatr Res*. 65:591-598.

194. Werling DM, Geschwind DH (2013): Understanding sex bias in autism spectrum disorder. *Proc Natl Acad Sci U S A*. 110:4868-4869.

195. Idring S, Lundberg M, Sturm H, Dalman C, Gumpert C, Rai D, et al. (2015): Changes in prevalence of autism spectrum disorders in 2001-2011: findings from the Stockholm youth cohort. *J Autism Dev Disord*. 45:1766-1773.

196. Robinson EB, Lichtenstein P, Anckarsater H, Happe F, Ronald A (2013): Examining and interpreting the female protective effect against autistic behavior. *Proc Natl Acad Sci U S A*. 110:5258-5262.

197. Jacquemont S, Coe BP, Hersch M, Duyzend MH, Krumm N, Bergmann S, et al. (2014): A higher mutational burden in females supports a "female protective model" in neurodevelopmental disorders. *Am J Hum Genet*. 94:415-425.

198. De Rubeis S, He X, Goldberg AP, Poultney CS, Samocha K, Cicek AE, et al. (2014): Synaptic, transcriptional and chromatin genes disrupted in autism. *Nature*. 515:209-215.

Supplemental Materials

Extended Methods

Processing and quality control of structural magnetic resonance imaging (MRI) data

FreeSurfer software (http://surfer.nmr.mgh.harvard.edu/) was used for automated segmentation of all structural MR images, based on probabilistic information estimated from a manually labeled training set (Fischl et al., 2002). This approach has been shown to yield well-defined cerebellar boundaries comparable in accuracy to manual labeling (Fischl et al., 2002; Lee et al., 2015). Prior findings also indicate that the FreeSurfer algorithm is especially suitable for multi-center data acquired on different scanners, as it demonstrates relatively low sensitivity to noise and variable image quality (Mayer et al., 2016; Dewey et al., 2010). Note that a mock scanner training protocol was used in the 3q29Del project to minimize motion artifacts and attrition; participants with a contraindication for MRI were excluded.

Since it is currently unfeasible to accurately reconstruct and segment the cortical surface of the cerebellum using this harmonized framework, we treated the cerebellum as a volumetric structure. For quality control (QC), two trained evaluators (ES, LL) inspected all cerebellar segmentations obtained from 3q29Del subjects in axial, sagittal, and coronal reformats to determine whether technical problems (e.g., motion artifacts) or notable pathology (e.g., arachnoid cysts) interfered with registration or segmentation quality. One 3q29Del subject failed to pass QC due to a motion artifact and skull deformity interfering with the extraction of reliable volumetric measures (Fig. S1O). Similarly, the outputs of the structural pipeline for control subjects were inspected by the HCP, as described by Marcus et al. (2013) and Elam et al. (2021); no major errors were identified. Detailed QC information for the HCP dataset is available at https://wiki.humanconnectome.org/. To facilitate joint analysis, the two trained evaluators additionally cross-compared the image quality, tissue contrast and cerebellar segmentation masks of 23 age- and sex-matched case-control pairs randomly selected from the entire dataset (see Fig. S1A-N for representative images). No systematic irregularities were identified between the two diagnostic groups and no manual intervention was performed in either group to avoid adding subjectivity to volumetric measures.

Since visual QC of eICV segmentation masks is not attainable in the atlas-based head size

normalization approach used in the present study, we assessed the quality of our eICV measures by testing the correlations between eICV, total brain volume and head circumference among 3q29Del subjects using Pearson product moment analysis. As expected from previous literature (McKinney et al., 2017; Koyabu et al., 2014; Buckner et al., 2004; Sanfilipo et al., 2004; Kollias et al., 1993), these correlations were positive and significant with moderate to strong effect sizes (p's ≤ 0.05) (Fig. S2), providing an indirect means of quality assurance for the eICV data.

Extended methods for radiological evaluation of structural MRI data

T1- and T2-weighted images were reviewed qualitatively by a board-certified neuroradiologist (AEGY) in axial, sagittal, and coronal reformats using Horos (https://horosproject.org). The conditions that were evaluated for differential diagnosis of enlarged retrocerebellar cerebrospinal fluid (CSF) space includes Dandy-Walker malformation (DWM), Blake's pouch cyst, mega cisterna magna (MCM), posterior fossa arachnoid cyst (PFAC), and isolated inferior cerebellar vermian hypoplasia. DWM, the most common posterior fossa malformation in the general population, can occur in isolation or as part of chromosomal anomalies or Mendelian disorders (Doherty et al., 2013). Diagnostic features of DWM on neuroimaging include hypoplasia of the cerebellar vermis, which is elevated and upwardly rotated, and dilation of the fourth ventricle, which fills and enlarges the posterior fossa (Bosemani et al., 2015). DWM is often associated with additional malformations, including callosal dysgenesis, occipital encephaloceles, polymicrogyria, and grey matter heterotropia (Parisi et al., 2003). Hydrocephalus may be present. Blake's pouch cyst occurs sporadically due to a lack of fenestration of the Blake pouch, a normal developmental structure, resulting in absence of communication between the fourth ventricle and the subarachnoid space, and leading to hydrocephalus (Tortori-Donati et al., 1996; Cornips et al., 2010). The cerebellum has a normal size and shape. Imaging demonstrates an enlarged fourth ventricle that communicates with an infravermian cyst, often resulting in hydrocephalus. MCM is an enlarged cisterna magna (≥10 mm on midsagittal images) with an intact vermis and a normal fourth ventricle. The posterior fossa may be enlarged, with scalloping of the occipital bone, without hydrocephalus. MCM may be caused by delayed fenestration of the Blake's pouch, whereas the absence of

fenestration leads to a Blake's pouch cyst (Nelson et al., 2004). Arachnoid cysts result from duplication of the arachnoid membrane, with approximately 10% of arachnoid cysts in children occurring in the posterior fossa (Ali et al., 2014). Although PFACs may be asymptomatic and identified incidentally, they may present with macrocephaly, increased intracranial pressure, and developmental delay, particularly if CSF flow is obstructed (Marin-Sanabria et al., 2007). PFACs are isointense relative to CSF, well defined, can also result in scalloping of the occipital bone, and can exert mass effect on the cerebellum, with a normal appearance of the fourth ventricle and vermis. Isolated inferior vermian hypoplasia is characterized by partial absence of the inferior portion of the cerebellar vermis. More than 75% of patients with isolated inferior vermian hypoplasia have a favorable outcome, although in some patients, mild functional deficits in fine motor activity and receptive language may be present (Limperopoulos et al., 2006; Tarui et al., 2014).

Details on standardized behavioral measures

Subjects were administered the *Beery-Buktenica Developmental Test of Visual-Motor Integration* (VMI, 6th edition) to assess the extent to which they can integrate their visual and fine motor abilities in a geometric design-copying task. To measure VMI, subjects were asked to copy a set of geometric forms that increase in difficulty; the drawings were scored based on standard criteria outlined in the test manual according to how accurately each design was copied compared with the original.

The two supplemental tests included in the Beery VMI were additionally administered to assess visual and motor skills, separately. The visual perception supplemental test was used to assess visual analysis skills in a format requiring minimal motor input. In this task, subjects were shown a series of reference geometric designs with multiple similar shapes provided below them; the task required subjects to choose/match the shape that was identical to the reference design. The motor coordination supplemental test was used to assess fine motor coordination skills in a format requiring minimal visual analysis skills. In this task, subjects were asked to trace a set of geometric forms with a pencil without going outside a double-lined path. Raw scores were converted to age-appropriate standard scores based on the standardization sample reported for the corresponding tests (normative mean = 100, SD = 15). Higher scores indicate better performance.

Two measures of intellectual functioning were utilized in the present study given the age range of the participants. The general conceptual ability (GCA) and full-scale intelligence quotient (FSIQ) scores from the *Differential Ability Scales* (DAS, 2nd edition) and the *Wechsler Abbreviated Scale of Intelligence* (WASI, 2nd edition) were used as composite IQ scores. The verbal reasoning and verbal comprehension domains of the two scales were used to index verbal IQ, while the non-verbal reasoning and perceptual reasoning domains indexed non-verbal IQ. The contents of these tests are sufficiently similar for combination across scales in cross-sectional analyses. Raw scores were transformed into age-appropriate standard scores based on the standardization sample reported for the corresponding tests (normative mean = 100, SD = 15). Higher scores indicate better performance.

Extended statistical methods for penalized cubic spline and quantile spline models

The following analyses were performed to 1) build developmental trajectories for our volumetric measures of interest (VOI) and 2) to estimate normative percentile curves for our VOIs as an alternative to the polynomial linear regression models presented in the main manuscript for case-control comparisons. In these supplemental analyses, penalized cubic splines were fitted to volumetric data using the *mgcv* package in *R* (version 1.8-33) (Wood, 2011; Wood, 2017) and quantile splines were fitted to data using the *fields* package in *R* (version 12.5) (Nychka et al., 2021). Given the local nature of splines, these methods are capable of capturing a wide range of nonlinear neurodevelopmental trends in our data and were incorporated into the present study to improve the statistical rigor of our central analyses. We provide a detailed summary of each approach below.

1) Building developmental trajectories for VOIs: As a supplemental method, the penalized spline approach (Wahba, 1980; Eilers et al., 1996) was adopted to model volumetric changes in our brain regions of interest across age, since this method offers increased mathematical flexibility compared with parametric models that rely on delicate assumptions. As in regression splines (Eilers et al., 1996), penalized splines make use of piecewise polynomial approximation with a flexible selection of knots to effectively capture the underlying changes in a dataset, when given a fixed basis-dimension and appropriate positioning of the knots that provides fair coverage

of the covariate values (Wood, 2017). This creates computational efficiency compared with smoothing splines, which place a knot at every unique sample point. Moreover, penalized splines add a roughness (or "wiggliness") penalty to the model, as in smoothing splines (Reinsch, 1967), to control the smoothness of the fit while avoiding the problem of overfitting. In summary, penalized splines offer an effective compromise between regression splines and smoothing splines (two popular tools) for more closely approximating age-associated changes in our outcome variables of interest. Below, we will gradually build our way towards defining the penalized cubic spline approach that was used to characterize the developmental trajectories of our VOIs.

The definition of a natural spline is as follows (given a set of knots at $k_1, k_2, \ldots, k_K$):

1. $f(x)$ is a polynomial of degree p on each of the intervals $[k_1, k_2]$, $[k_2, k_3]$, ..., $[k_{K-1}, k_K]$.
2. $f(x)$ has continuous $(p-1)_{th}$ derivatives at knots $k_1, k_2, \ldots, k_K$.
3. $f(x)$is a polynomial of degree $\frac{(p-1)}{2}$ on $(-\infty, k_1]$ and $[k_K, \infty)$.

The last requirement forces a lower degree to the left (or right) of the leftmost (or rightmost) knot, to reduce the variance at the boundaries of the observations. In the present study, we used natural cubic splines $(p = 3)$, which are linear beyond the boundary knots.

The unique solution to the optimization problem described in *equation (1)* is a natural cubic spline with knots at every unique observation $x_1, x_2, \ldots, x_n$. The solution $f(x)$ is called a smoothing spline (Reinsch, 1967).

$$\min_f \{\frac{1}{n}\sum_{i=1}^{n}(y_i - f(x_i))^2 + \lambda \int (f''(x))^2 dx\} \qquad \textit{Equation (1)}$$

where $(x_i, y_i), i = 1, \ldots, n$ are a set of observations, $f(x)$ includes all that have continuous second derivatives and $\lambda > 0$ is a smoothing parameter that controls the trade-off between fidelity to the data and roughness of the function estimate.

Although smoothing splines enjoy the theoretical property of an optimizing solution (as described above), the degrees of freedom (i.e., number of knots) are comparable to the data to be smoothed and can be redundant, as the knots are placed at every unique observation. If the penalty term in *equation (1)* is removed and $f(x)$ is restricted to a natural spline with user-defined knots (as in the definition of a natural spline where the knot positions at $k_1, k_2, \ldots, k_K$ can be completely decided by users), the solution is reduced to a regression spline. Although regression splines ease the computational redundancy of smoothing splines by removing any restrictions in knot selection, they have the potential to be over-fitted. This can be handled by a regularization term, such as the integrated square second derivative in smoothing splines. Therefore, it is natural to combine the freely chosen degrees of freedom of a regression spline and the roughness penalty of a smoothing spline, which in turn gives penalized splines (Wahba, 1980). Specifically, we use penalized cubic splines in the present study, which is the solution to the optimization problem in *equation (2)*, where the number and positions of the knots are freely chosen in advance and the number of knots is usually much smaller than the sample size:

$$\begin{cases} \min_f \{\frac{1}{n}\sum_{i=1}^{n}(y_i - f(x_i))^2 + \lambda \int (f''(x))^2 dx\} \\ f \text{ is a natural cubic spline with predefined knots at } k_1, \ldots, k_K \end{cases} \qquad \textit{Equation (2)}$$

To obtain a satisfying fit, the knots should be arranged nicely to cover the distribution of the covariate in the original data set (Wood, 2017).

For each VOI (i.e., total cerebellum volume, cerebellar cortex volume, cerebellar white matter volume, estimated total intracranial volume (eICV), and the eICV-adjusted versions of cerebellar volumes), we denote y_i as the corresponding volume of the i_{th} subject in the pooled dataset (i.e., data aggregated across the two diagnostic groups). It is assumed that y_i is represented by a function of the subject's age, with sex and diagnostic group added as covariates, as expressed in *equation (3)*.

$$y_i = f(Age_i) + \alpha \cdot Sex_i + \beta \cdot Group_i + \epsilon_i,\ \epsilon_i \overset{\text{iid}}{\sim} N(0, \sigma^2) \qquad \textit{Equation (3)}$$

Sex_i is a sex indicator taking 1 for males and 0 for females. $Group_i$ is a diagnostic group indicator taking 1 for 3q29Del subjects and 0 for healthy control subjects. The residual random error ϵ_i is assumed to follow a Gaussian distribution with mean 0 and a common variance σ^2 across subjects (homoscedasticity). $f(Age_i)$ is a natural cubic spline term of age. The number of knots is chosen to be 10 and they evenly cover the quantiles of the age distribution (i.e., the knots are placed at the 0%, 11.11%, 22.22%, 33.33%, 44.44%, 55.56%, 66.67%, 77.78%, 88.89%, and 100% quantiles of age in the pooled data).

Following the optimization framework of a penalized cubic spline described in *equation (2)*, the parameter estimates are obtained via the objective function:

$$\begin{cases} \min_f \{\frac{1}{n}\sum_{i=1}^{n}(y_i - f(Age_i) - \alpha \cdot Sex_i - \beta \cdot Group_i)^2 + \lambda \int (f''(x))^2 dx\} \\ f \text{ is a natural cubic spline with with 10 knots spread evenly across the age quantiles} \end{cases} \quad \textit{Equation (4)}$$

where the smoothing parameter λ is selected by the restricted maximum likelihood (REML) method (Wood, 2011).

From the fitted penalized cubic splines, mean developmental trajectories for each VOI were estimated and laid onto the scatter plots of the original volumetric data points in Fig. S7. The effective degrees of freedom (EDF) reported in Table S4 represent how complex the neurodevelopmental pattern of the estimated volumetric trajectory of each VOI is across age. EDF = 1 is equivalent to a straight line, EDF = 2 is equivalent to a quadratic curve, etc., with higher EDFs describing increased wiggliness (Wood, 2017). The EDF of the smooth term is defined as the trace of the influence matrix. The significance of the smooth term $f(Age)$, the sex indicator and the diagnostic group indicator are also reported in Table S4 in the form of p-values. Note that the significance of the smooth term is derived from an approximate F-test of whether the smooth term of age is significant in the penalized cubic spline models for each VOI ($f(Age) = 0$). The p-values are approximate

in the sense that the components of the test statistic are weighted by the iterative fitting weights (Wood, 2017). A comprehensive description of how to obtain theoretical p-values is detailed by Wood (2013). The p-values for sex and diagnostic group are derived from standard t-tests of whether the indicator of sex/diagnostic group is significant in determining each VOI.

All of the aforementioned parameter estimates and p-values were obtained using the *gam()* function from the *mgcv* package in R (Wood, 2011; Wood, 2017). Using the function *gam.check()* from the same package, model diagnostics were performed, which confirmed that the required assumptions of the penalized cubic spline model in *equation (3)* were met and our basis dimension (10 knots of 9 basis dimension) was adequate to cover the age distribution of the present study sample. More specifically, QQ-plots were explored to justify the Gaussian assumption of the residuals; residuals versus linear predictors/fitted values were plotted to justify the homoscedasticity assumption; the histogram of residuals was plotted to check the normality of the residuals; and the p-value for the residual randomization test was explored to check the adequacy of the basis dimension.

2) Estimating normative percentile curves for VOIs: Besides estimating mean volumetric changes across age in the entire study sample (i.e., data pooled across the two diagnostic groups), another interest was in estimating sex-specific normative percentiles for volumetric changes observed across age in our healthy control subjects only. Here, our goal was to establish well-founded references (or "nomograms") for comparison against the VOIs of individual 3q29Del subjects to further characterize the degrees of neuroanatomical deviance observed within the 3q29Del sample. A secondary goal was to explore the relative distribution of 3q29Del data points in these normative charts to gain insights into potential age-windows of heightened structural vulnerability. However, the limited sample size of the 3q29Del group (especially when stratified by sex), and the paucity of data on control subjects younger than age 5 precluded our ability to reach any meaningful inferences in this regard. We foresee that these estimates may become particularly useful for future studies investigating longitudinal neuroimaging outcomes in 3q29Del subjects.

In the supplemental analyses described below, we characterized the 10th, 25th, 50th, 75th, and 90th percentiles of normative volumetric growth curves for each VOI, stratified by sex. Similar to modelling mean volume changes, our goal here was to model normative percentiles under a penalized spline framework, hence we used the quantile smoothing splines approach for this objective.

In quantile regression, the check loss shown in *equation (5)* is used as the objective of model fitting, where α represents the α quantile of the dependent variable y, x is the independent variable influencing y, and $1_{\{u<0\}}$ is an indicator taking 1 when $u < 0$ and 0 otherwise.

$$\rho_\alpha\big(y - g(x)\big) = (y - g(x))(\alpha - 1_{\{(y-g(x))<0\}}) \qquad \textit{Equation (5)}$$

To improve computation, Nychka et al. (1995) proposed a modified check loss which rounds out the corner of the check loss in a small interval around zero by piecing in a quadratic function, in order to make the loss function differentiable at zero. The modified check loss is shown in the following equation:

$$\rho_{\alpha,C}\big(y - g(x)\big) = \begin{cases} \rho_\alpha\big(y - g(x)\big), & if\ |y - g(x)| > C \\ \dfrac{1-\alpha}{C}(y - g(x))^2, & if\ 0 \le y - g(x) \le C \\ \dfrac{\alpha}{C}\big(y - g(x)\big)^2, & if\ -C \le y - g(x) < 0 \end{cases} \qquad \textit{Equation (6)}$$

where C is a scale factor for rounding out the absolute value function at zero to a quadratic (Nychka et al., 2021). According to Nychka et al. (1995), C should be chosen to be effectively zero relative to the magnitude of the data values.

After presenting the form of the modified check loss, we can adopt the optimization framework of smoothing splines shown in *equation (1)* by simply replacing the squared error loss to the modified check loss in *equation (6)*:

$$\min_g\{\frac{1}{n}\sum_{i=1}^{n}\rho_{\alpha,C}(y_i - g(x_i)) + \lambda\int(g''(x))^2dx\} \qquad \textit{Equation (7)}$$

Similar to least square smoothing splines, the quantile smoothing splines that we adopt use the L2 roughness penalty on the integral of the squared second derivative.

For each VOI (i.e., total cerebellum volume, cerebellar cortex volume, cerebellar white matter volume, estimated total intracranial volume (eICV), we denote y_i as the corresponding volume of the i_{th} healthy control subject, stratified by sex. It is assumed that the α quantile of y_i is represented by a function of the subject's age $g(Age_i)$ (i.e., $P(y_i \leq g(Age_i) = \alpha)$. Following the optimization framework of a quantile spline described in *equation (7)*, the parameter estimates are obtained via the following objective over all g, such that the roughness penalty is finite:

$$\min_g \{\frac{1}{n}\sum_{i=1}^{n} \rho_{\alpha, C}(y_i - g(Age_i)) + \lambda \int (g''(x))^2 dx\} \qquad \textit{Equation (8)}$$

where the smoothing parameter λ is selected by the generalized cross-validation (GCV) method (Graven, 1989), and C is set to 10^{-5} of the variance of the y's.

From the fitted quantile splines for α = 0.10, 0.25, 0.50, 0.75, 0.90, normative developmental trajectories for the 10th, 25th, 50th, 75th, and 90th percentiles of the VOIs were estimated, respectively. The computation was performed using the *qsreg()* function from the *fields* package in R (Douglas Nychka et al., 2021). In Fig. S9, the original VOIs of individual 3q29Del subjects are plotted against the normative percentile curves derived from male and female controls, separately. This case-by-case comparison provides a general idea of which age- and sex-specific normative percentile each 3q29Del subject's cerebellar and eICV volumes correspond to.

List of R packages used for statistical analyses and diagnostics

Multiple linear regression analyses were performed via the standard R *lm()* function. For model comparisons, analyses of variance (ANOVA) were performed by the standard R *anova()* function. Wald statistics were

calculated by the *waldtest()* function from the *lmtest* package (https://CRAN.R-project.org/package=lmtest). Heteroscedasticity-robust estimates were calculated using the *vcovHC()* function from the *sandwich* package (https://CRAN.R-project.org/package=sandwich). Permutation tests were performed using the *lmperm()* function of the *permuco* package https://CRAN.R-project.org/packages=permuco). Diagnostics plots for linear regression were created using the R base function *plot()*. Shapiro-Wilk tests were performed using the standard R *shapiro.test()* function to check for assumptions of normality. Breusch-Pagan and Levene's test were performed using the *bptest()* function from the *lmtest* package (https://CRAN.R-project.org/package=lmtest) and the *levene_test()* function from the *rstatix* package (https://CRAN.R-project.org/package=rstatix) to check for homogeneity of variances, respectively. Fisher's exact tests, Pearson's chi-squared tests, Student's two sample t-tests and Wilcoxon signed-rank tests were performed using the standard R *fisher.test(), chisq.test(), t.test()* and *wilcox.test()* functions. Effect sizes for Wilcoxon signed-rank tests were calculated using the *wilcox_effsize()* function from the *rstatix* package (https://CRAN.R-project.org/package=rstatix). The standard R *cor.test()* function was used to perform Pearson's correlations. The *pcor.test()* function from the *ppcor* package (https://CRAN.R-project.org/package=ppcor) was used to calculate partial correlations. For spline modeling, the *gam()* and *gam.check()* functions from the *mgcv* package (https://cran.r-project.org/package=mgcv) and the *qsreg()* function from the *fields* package (https://cran.r-project.org/package=fields) were used. Graphics were generated by the *ggplot2* (https://CRAN.R-project.org/package=ggplot2), *ggpubr (https://cran.r-project.org/package=ggpubr)* and *jtools* (https://cran.r-project.org/package=jtools) packages.

Supplemental Tables

Demographic variables	Males			Females		
	Control *N* = 747	**3q29Del** *N* = 14	**Test statistics**	**Control** *N* = 861	**3q29Del** *N* = 9	**Test statistics**
Age (in years)						
Mean ± SD	22.38 ± 7.74	14.14 ± 9.03	*r* = 0.13 (small effect size), *W* = 8146.5, p-value [a] = 3.40E-04***	23.03 ± 8.60	16.56 ± 9.86	*r* = 0.07 (small effect size), *W* = 5422, p-value [a] = 0.04*
Median	24.00	13.00		25.00	15.00	
[Range]	[5 – 37]	[4 – 39]		[6 – 36]	[6 – 34]	
Ethnicity[#], *N (%)*						
Non-Hispanic / Latino	64 (86.60%)	13 (92.86%)	X^2 = 0.08, DF = 1, p-value [b] = 0.78	757 (98.31%)	9 (100%)	X^2 = 0.25, DF = 1, p-value [b] = 0.62
Hispanic / Latino	99 (13.40%)	1 (7.14%)		91 (11.82%)	0 (0%)	
Race[##], *N (%)*						
White	52 (71.53%)	13 (92.86%)	X^2 = 3.83, DF = 4, p-value [b] = 0.43	587 (69.88%)	8 (88.89%)	X^2 = 2.43, DF = 4, p-value [b] = 0.66
Black / African American	97 (13.21%)	0 (0%)		125 (14.88%)	0 (0%)	
Asian / Native Hawaiian / Other Pacific Islander	55 (7.49%)	0 (0%)		53 (6.31%)	0 (0%)	
American Indian / Alaskan Native	3 (0.41%)	0 (0%)		1 (0.12%)	0 (0%)	
More than one race	54 (7.36%)	1 (7.14%)		74 (8.81%)	1 (11.11%)	

Table S1. Demographic characteristics of the study sample in volumetric analyses, stratified by diagnostic group and sex. While there was a near complete overlap between the age ranges of the two diagnostic groups in each sex, there was a significant age difference between male 3q29Del subjects and controls ($p \leq 0.001$), and female 3q29Del subjects and controls on average ($p \leq 0.05$). There were no significant differences in the ethnicity or race compositions of the two diagnostic groups in either sex (p's > 0.05). Effect sizes are reported for significant test results only. [#]Male control $N = 739$, Female control $N = 848$ for the ethnicity variable due to missing data. [##]Male control $N = 734$, Female control $N = 840$ for the race variable due to missing data. Corresponding percentages reflect the fraction of controls with complete data. [a]Wilcoxon rank sum test with continuity correction, [b]Pearson's chi-squared test with Yates' continuity correction. p-value ≤ 0.001 '***', p-value ≤ 0.01 '**', p-value ≤ 0.05 '*', p-value ≤ 0.1 '•' *Abbreviations*: 3q29 deletion syndrome, 3q29Del; volumetric measure of interest, VOI; standard deviation, SD; degrees of freedom, DF.

	3q29Del *N* = 24	HCP Young Adult *N* = 1,113	HCP Development *N* = 652
MRI Hardware			
Scanner	Siemens Magnetom Prisma 3T	Siemens Magnetom Skyra 3T (Customized 3T "Conectom")	Siemens Prisma 3T
Max gradient strength	80 mT/m gradient coil	100 mT/m gradient coil	80 mT/m gradient coil
Head coil	Siemens 32-channel Prisma head coil	Siemens 32-channel standard head coil	Siemens 32-channel Prisma head coil
Acquisition parameters | T1- & T2-weighted structurals			
Slice thickness (mm)	0.8	0.7	0.8
vNavs for prospective motion correction	NO	NO	YES
FOV read (mm)	256	224	256
FOV phase (%)	93.8	100	93.8
Base resolution	320	320	320
Slabs	1	1	1
Slices per slab	208	256	208
Slice orientation	Sagittal	Sagittal	Sagittal
PAT mode	GRAPPA	GRAPPA	GRAPPA
Acceleration Factor PE	2	2	2
Reference lines PE	32	32	32
Acquisition parameters | T1-weighted structural			
Pulse sequence	3D single-echo T1-weighted MPRAGE	3D single-echo T1-weighted MPRAGE	3D multi-echo T1-weighted MPRAGE
TR (ms)	2400	2400	2500
TE (ms)	2.2	2.1	1.8 / 3.6 / 5.4 / 7.2
TI (ms)	1000	1000	1000
Flip angle (degree)	8	8	8
Coil elements	HEA; HEP	HEA; HEP	HEA; HEP
Bandwidth (Hz/Px)	220	210	744 / 744 / 744 / 744
Fat suppression	Water excitation fast	Water excitation fast	Water excitation fast
Scan time (min:sec)	6:38	7:40	8:22
Acquisition parameters | T2-weighted structural			
Pulse sequence	3D T2-weighted SPACE	3D T2-weighted SPACE	3D T2-weighted SPACE
TR (ms)	3200	3200	3200
TE (ms)	563	565	564
Flip angle mode	variable	variable	variable
Coil elements	HC1-7; NC1,2	HEA; HEP	HEA; HEP
Bandwidth (Hz/Px)	744	744	744
Turbo factor	314	314	314
Fat suppression	None	None	None
Scan time (min:sec)	6:38	7:40	8:22
Other			
Data release version	N/A	"1200 subjects data release"	"HCP-Development Lifespan 2.0 release"
Structural preprocessing pipeline	HCP "minimal pre-processing" pipeline (v4.1.3 with FreeSurfer v6.0) (Glasser et al., 2013, Harms et al., 2018)	HCP "minimal pre-processing" pipeline (v3.21 with FreeSurfer v5.3.0-HCP) (Glasser et al., 2013, Harms et al., 2018)	HCP "minimal pre-processing" pipeline (v4.3.0 with FreeSurfer v6.0) (Glasser et al., 2013, Harms et al., 2018)
Manual editing after automated segmentation	NO	NO	NO

Table S2. Comparison of structural magnetic resonance imaging (MRI) protocols. A detailed report of the imaging protocols and relevant parameters used in the 3q29Del, HCP Young Adult and HCP Development

datasets are provided in this table for increased transparency. HCP Young Adult and Development datasets were pooled to derive the control dataset; their corresponding imaging protocols were previously shown to be largely congruent, with most differences rooted in challenges related to scanning developmental populations (Harms et al., 2018). Note that the original "1200 Subjects Release" by the HCP Young Adult project includes structural MRI scans for N = 1,113 participants. A subset of these data comes from monozygotic twins, who have been previously reported to exhibit high to moderate correlations in brain morphology (e.g., White et al., 2002). To minimize bias in our standard error estimates, one sibling from each known monozygotic twin-pair that was scanned by the HCP Young Adult project was removed from the original dataset in the present study (N = 154 monozygotic twin-pairs based on available genotyping and/or self-report data**;** in cases of discrepancy between genotyping and self-report data, we relied on genetically verified data for final filtering). We additionally removed all subjects with unknown zygosity information *(*N = 3) from the HCP Young Adult dataset for stringency. Hence, the final sample size of the HCP Young Adult data included in the present study was N = 956. Note that there were no monozygotic twin-pairs in the 3q29Del dataset. Zygosity information was not publicly available for the HCP Development dataset. Importable imaging protocols for all HCP datasets are available at https://www.humanconnectome.org/hcp-protocols. *Abbreviations*: 3q29 deletion syndrome, 3q29Del; Human Connectome Project, HCP; magnetization-prepared rapid gradient-echo, MPRAGE; Sampling perfection with application optimized contrast using different angle evolutions, SPACE; repetition time, TR; echo time, TE; inversion time, TI; volumetric navigators, vNavs; Field-of-view, FOV; parallel acquisition technique, PAT; phase-encoding, PE; generalized auto-calibrating partial parallel acquisition, GRAPPA; quality control, QC.

Table S3. Extended linear regression results testing the effect of diagnostic group on volumetric measures of interest and polynomial modeling of age. A-H) The main effect of diagnostic group is reported in bold for clarity. ANOVAs were performed to sequentially compare simpler models to more complex models to identify the best-fitting polynomial function of age for each VOI (highlighted in blue). The relationship between the best-fitting polynomial function of age and VOIs is plotted in the right bottom corner of each panel using data pooled across diagnostic groups. Final inferences are based on heteroskedasticity-robust estimates, which are provided above non-robust OLS estimates (in grey brackets). Contrast coding: reference levels for the diagnostic group and sex variables are healthy control and female, respectively.

A. VOI: Absolute Total Cerebellum Volume (cm^3)

Degree of polynomial	Explanatory variables	*b*	CI (95%)	p-value	perm. p-value
Linear (Model 1)	Intercept	140.44	138.52 – 142.36	**< 2.00E-16*** **	
	Age (years)	-0.10	-0.17 – -0.02	**0.01****	**0.01****
	Sex [Male]	16.50	15.27 – 17.74	**< 2.00E-16*** **	**1.00E-04*** **
	Diagnostic Group [3q29Del]	**-16.25**	**-21.50 – -11.00**	**1.57E-09*** **	**1.00E-04*** **
	R^2 / R^2 adjusted	0.31 / 0.31			
	F-statistic (OLS)	241.7 on 3 and 1627 DF, p-value < 2.20E-16***			
Quadratic (Model 2) *Best-fit*	Intercept	133.50	128.97 – 138.03 [129.05 – 137.96]	**< 2.00E-16*** ** [< 2.00E-16***]	
	Age (years)	0.68	0.22 – 1.14 [0.22 – 1.13]	**3.72E-03**** [3.63E-03**]	**3.30E-03*** **
	Age^2	-0.02	-0.03 – -0.01 [-0.03 – -0.01]	**6.22E-04*** ** [7.31E-04***]	**1.00E-03*** **
	Sex [Male]	16.22	14.97 – 17.48 [14.98 – 17.47]	**< 2.00E-16*** ** [< 2.00E-16***]	**1.00E-04*** **
	Diagnostic Group [3q29Del]	**-15.26**	**-20.01 – -10.51 [-20.53 – -10.00]**	**3.76E-10*** ** [1.53E-08***]	**1.00E-04*** **
	R^2 / R^2 adjusted	0.31 / 0.31			
	Robust Wald test	184.0 on 4 and 1626 DF, p-value < 2.20E-16***			
	[F-statistic (OLS)	185.3 on 4 and 1626 DF, p-value < 2.20E-16***]			
Cubic (Model 3)	Intercept	127.70	117.23 – 138.16	**< 2.00E-16*** **	
	Age (years)	1.69	-0.02 – 3.39	0.06†	0.06†
	Age^2	-0.07	-0.15 – 0.01	0.11	0.11
	Age^3	0.001	-0.001 – 0.002	0.23	0.23
	Sex [Male]	16.25	15.01 – 17.49	**< 2.00E-16*** **	**1.00E-04*** **
	Diagnostic Group [3q29Del]	**-15.10**	**-20.37 – -9.83**	**2.25E-08*** **	**1.00E-04*** **
	R^2 / R^2 adjusted	0.31 / 0.31			
	F-statistic (OLS)	148.6 on 5 and 1625 DF, p-value < 2.20E-16***			

Model 1 vs Model 2 – ANOVA Table:

	Resid. DF	Resid. SS	DF	SS	F-value	Pr(>F)
1	1627	260917				
2	1626	259092	1	1824.90	11.45	7.31E-04***

Model 2 vs Model 3 – ANOVA Table:

	Resid. DF	Resid. SS	DF	SS	F-value	Pr(>F)
2	1626	259092				
3	1625	258862	1	230.30	1.45	0.23

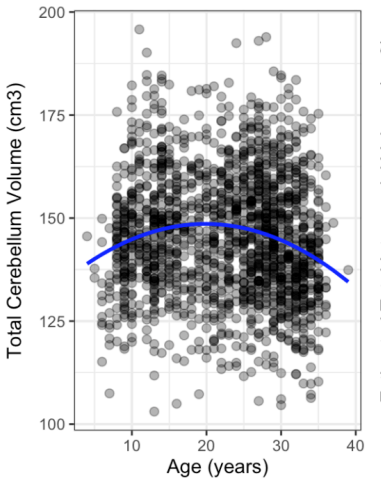

B. VOI: Absolute Cerebellar Cortex Volume (cm^3)

Degree of polynomial	Explanatory variables	*b*	CI (95%)	p-value	perm. p-value
Linear (Model 1)	Intercept	116.86	115.29 – 118.43	**< 2.00E-16*** **	
	Age (years)	-0.25	-0.31 – -0.19	**3.87E-15*** **	**1.00E-04*** **
	Sex [Male]	13.27	12.25 – 14.28	**< 2.00E-16*** **	**1.00E-04*** **
	Diagnostic Group [3q29Del]	**-15.85**	**-20.15 – -11.55**	**7.27E-13*** **	**1.00E-04*** **
	R^2 / R^2 adjusted	0.32 / 0.32			
	F-statistic (OLS)	257.9 on 3 and 1627 DF, p-value < 2.20E-16***			
Quadratic (Model 2) *Best-fit*	Intercept	113.52	109.73 – 117.31 [109.86 – 117.18]	**< 2.00E-16*** ** [**< 2.00E-16*****]	
	Age (years)	0.13	-0.26 – 0.51 [-0.25 – 0.50]	0.52 [0.51]	**0.50**
	Age^2	-0.01	-0.02 – -0.0001 [-0.02 – -0.0001]	**0.04*** [**0.04***]	**0.04***
	Sex [Male]	13.13	12.10 – 14.17 [12.11 – 14.15]	**< 2.00E-16*** ** [**< 2.00E-16*****]	**1.00E-04*** **
	Diagnostic Group [3q29Del]	**-15.38**	**-19.53 – -11.22 [-19.70 – -11.06]**	**5.86E-13*** ** [**4.28E-12*****]	**1.00E-04*** **
	R^2 / R^2 adjusted	0.32 / 0.32			
	Robust Wald test	193.2 on 4 and 1626 DF, p-value < 2.20E-16***			
	[F-statistic (OLS)	194.8 on 4 and 1626 DF, p-value < 2.20E-16***]			
Cubic (Model 3)	Intercept	107.48	98.89 – 116.07	**< 2.00E-16 *** **	
	Age (years)	1.18	-0.23 – 2.58	$0.10^{\dagger}$	$0.10^{\dagger}$
	Age^2	-0.06	-0.13 – 0.01	$0.08^{\dagger}$	$0.08^{\dagger}$
	Age^3	0.001	-0.0002 – 0.002	0.13	0.13
	Sex [Male]	13.16	12.14 – 14.17	**< 2.00E-16 *** **	**1.00E-04 *** **
	Diagnostic Group [3q29Del]	**-15.21**	**-19.53 – -10.88**	**7.57E-12 *** **	**1.00E-04 *** **
	R^2 / R^2 adjusted	0.32 / 0.32			
	F-statistic (OLS)	156.4 on 5 and 1625 DF, p-value < 2.20E-16 ***			

Model 1 vs Model 2 – ANOVA Table:

	Resid. DF	Resid. SS	DF	SS	F-value	Pr(>F)
1	1627	174977				
2	1626	174554	1	422.96	3.94	0.04 *

Model 2 vs Model 3 – ANOVA Table:

	Resid. DF	Resid. SS	DF	SS	F-value	Pr(>F)
2	1626	174554				
3	1625	174305	1	249.44	2.33	0.13

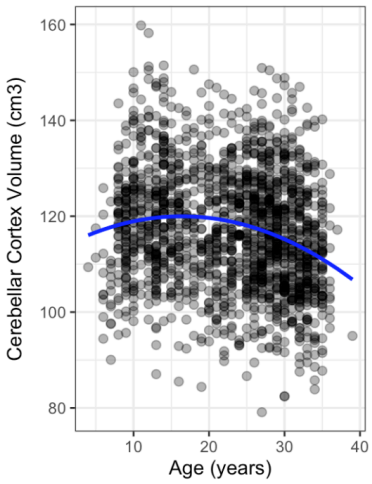

C. VOI: Absolute Cerebellar White Matter Volume (cm^3)

Degree of polynomial	Explanatory variables	*b*	CI (95%)	p-value	perm. p-value
Linear (Model 1)	Intercept	23.58	23.07 – 24.10	**< 2.00E-16*** **	
	Age (years)	0.15	0.13 – 0.17	**< 2.00E-16*** **	**1.00E-04*** **
	Sex [Male]	3.24	2.90 – 3.57	**< 2.00E-16*** **	**1.00E-04*** **
	Diagnostic Group [3q29Del]	**-0.40**	**-1.80 – 1.01**	**0.58**	**0.57**
	R^2 / R^2 adjusted	0.26 / 0.26			
	F-statistic (OLS)	187.3 on 3 and 1627 DF, p-value < 2.20E-16 ***			
Quadratic (Model 2) *Best-fit*	Intercept	19.98	18.82 – 21.15 [18.80 – 21.16]	**< 2.00E-16*** ** [< 2.00E-16***]	
	Age (years)	0.55	0.43 – 0.67 [0.43 – 0.67]	**< 2.00E-16*** ** [< 2.00E-16***]	**1.00E-04*** **
	Age^2	-0.01	-0.01 – -0.01 [-0.01 – -0.01]	**8.88E-11*** ** [4.94E-11***]	**1.00E-04*** **
	Sex [Male]	3.09	2.76 – 3.43 [2.76 – 3.42]	**< 2.00E-16*** ** [< 2.00E-16***]	**1.00E-04*** **
	Diagnostic Group [3q29Del]	**0.11**	**-2.42 – 2.65 [-1.28 – 1.51]**	**0.93 [0.87]**	**0.87**
	R^2 / R^2 adjusted	0.28 / 0.27			
	Robust Wald test	155.1 on 4 and 1626 DF, p-value < 2.20E-16***			
	[F-statistic (OLS)	155.1 on 4 and 1626 DF, p-value < 2.20E-16***]			
Cubic (Model 3)	Intercept	20.22	17.45 – 23.00	**< 2.00E-16*** **	
	Age (years)	0.51	0.06 – 0.96	**0.03***	0.03*
	Age^2	-0.01	-0.03 – 0.02	0.52	0.53
	Age^3	0.00	-0.0004 – 0.0003	0.85	0.85
	Sex [Male]	3.09	2.76 – 3.42	**< 2.00E-16*** **	**1.00E-04*** **
	Diagnostic Group [3q29Del]	**0.11**	**-1.29 – 1.51**	**0.88**	**0.87**
	R^2 / R^2 adjusted	0.28 / 0.27			
	F-statistic (OLS)	124.0 on 5 and 1625 DF, p-value < 2.20E-16 ***			

Model 1 vs Model 2 – ANOVA Table:

	Resid. DF	Resid. SS	DF	SS	F-value	Pr(>F)
1	1627	18695				
2	1626	18205	1	490.30	43.79	4.94E-11***

Model 2 vs Model 3 – ANOVA Table:

	Resid. DF	Resid. SS	DF	SS	F-value	Pr(>F)
2	1626	18205				
3	1625	18204	1	0.39	0.04	0.85

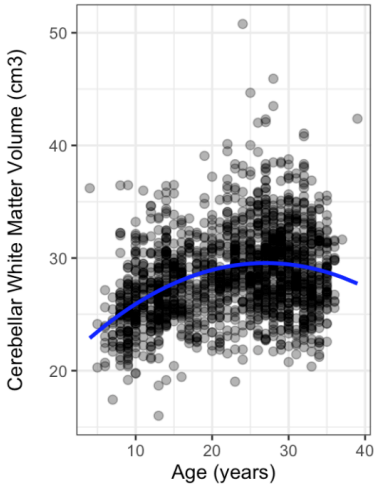

D. VOI: Cerebellar Cortex to Cerebellar White Matter Volume Ratio

Degree of polynomial	Explanatory variables	*b*	CI (95%)	p-value	perm. p-value
Linear (Model 1)	Intercept	4.88	4.82 – 4.94	**< 2.00E-16*** **	
	Age (years)	-0.03	-0.03 – -0.03	**< 2.00E-16*** **	**1.00E-04*** **
	Sex [Male]	0.01	-0.03 – 0.05	0.56	0.56
	Diagnostic Group [3q29Del]	**-0.42**	**-0.58 – -0.25**	**5.35E-07*** **	**1.00E-04*** **
	R^2 / R^2 adjusted	0.31 / 0.31			
	F-statistic (OLS)	240.4 on 3 and 1627 DF, p-value < 2.20E-16***			
Quadratic (Model 2) *Best-fit*	Intercept	5.38	5.22 – 5.53 [5.22 – 5.53]	**< 2.00E-16*** ** [**< 2.00E-16*** **]	
	Age (years)	-0.09	-0.10 – -0.07 [-0.10 – -0.07]	**< 2.00E-16*** ** [**< 2.00E-16*** **]	**1.00E-04*** **
	Age^2	0.001	0.001 – 0.002 [0.001 – 0.002]	**9.59E-13*** ** [**2.46E-15*** **]	**1.00E-04*** **
	Sex [Male]	0.03	-0.01 – 0.07 [-0.01 – 0.07]	0.11 [0.11]	0.11
	Diagnostic Group [3q29Del]	**-0.49**	**-0.86 – -0.12 [-0.65 – -0.33]**	**9.82E-03** * [**2.92E-09*** **]	**1.00E-04*** **
	R^2 / R^2 adjusted	0.33 / 0.33			
	Robust Wald test	179.4 on 4 and 1626 DF, p-value < 2.20E-16***			
	[F-statistic (OLS)	203.2 on 4 and 1626 DF, p-value < 2.20E-16***]			
Cubic (Model 3)	Intercept	5.30	4.98 – 5.62	**< 2.00E-16*** **	
	Age (years)	-0.07	-0.13 – -0.02	**0.01** *	**0.01** *
	Age^2	0.001	-0.002 – 0.003	0.63	0.63
	Age^3	0.00	0.00 – 0.0001	0.60	0.59
	Sex [Male]	0.03	-0.01 – 0.07	0.10^{t}	0.11
	Diagnostic Group [3q29Del]	**-0.49**	**-0.65 – -0.33**	**3.61E-09*** **	**1.00E-04*** **
	R^2 / R^2 adjusted	0.33 / 0.33			
	F-statistic (OLS)	162.6 on 5 and 1625 DF, p-value < 2.2E-16 ***			

Model 1 vs Model 2 – ANOVA Table:

	Resid. DF	Resid. SS	DF	SS	F-value	Pr(>F)
1	1627	250.16				
2	1626	240.70	1	9.46	63.90	2.46E-15***

Model 2 vs Model 3 – ANOVA Table:

	Resid. DF	Resid. SS	DF	SS	F-value	Pr(>F)
2	1626	240.70				
3	1625	240.66	1	0.04	0.27	0.60

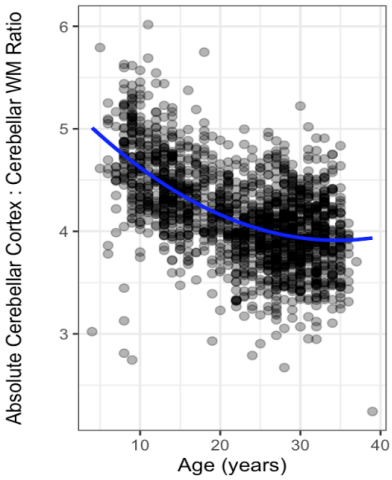

E. VOI: Estimated Total Intracranial Volume (eICV) (cm3)

Degree of polynomial	Explanatory variables	*b*	CI (95%)	p-value	perm. p-value
Linear (Model 1)	Intercept	1511.99	1490.34 – 1533.63	**< 2.00E-16*** **	
	Age (years)	-0.97	-1.81 – -0.12	**0.03***	0.02*
	Sex [Male]	209.85	195.94 – 223.77	**< 2.00E-16*** **	**1.00E-04*** **
	Diagnostic Group [3q29Del]	**-211.79**	**-270.97 – -152.61**	**3.26E-12*** **	**1.00E-04*** **
	R^2 / R^2 adjusted	0.36 / 0.36			
	F-statistic (OLS)	306.8 on 3 and 1627 DF, p-value < 2.20E-16***			
Quadratic (Model 2) *Best-fit*	Intercept	1415.02	1367.87 – 1462.17 [1364.89 – 1465.14]	**< 2.00E-16*** ** [**< 2.00E-16*** **]	
	Age (years)	9.89	4.84 – 14.94 [4.75 – 15.03]	**1.26E-04*** ** [**1.65E-04*** **]	**2.00E-04*** **
	Age^2	-0.25	-0.37 – -0.13 [-0.37 – -0.14]	**3.66E-05*** ** [**2.79E-05*** **]	**1.00E-04*** **
	Sex [Male]	206.00	192.06 – 219.93 [192.03 – 219.96]	**< 2.00E-16*** ** [**< 2.00E-16*** **]	**1.00E-04*** **
	Diagnostic Group [3q29Del]	**-197.99**	**-253.23 – -142.74 [-257.22 – -138.75]**	**3.05E-12*** ** [**7.39E-11*** **]	**1.00E-04*** **
	R^2 / R^2 adjusted	0.37 / 0.37			
	Robust Wald test	232.5 on 4 and 1626 DF, p-value < 2.20E-16***			
	[F-statistic (OLS)	236.9 on 4 and 1626 DF, p-value < 2.20E-16***]			
Cubic (Model 3)	Intercept	1419.77	1301.95 – 1537.60	**< 2.00E-16*** **	
	Age (years)	9.06	-10.14 – 28.27	0.36	0.36
	Age^2	-0.21	-1.16 – 0.74	0.66	0.66
	Age^3	-0.001	-0.02 – 0.01	0.93	0.93
	Sex [Male]	205.98	192.01 – 219.95	**< 2.00E-16*** **	**1.00E-04*** **
	Diagnostic Group [3q29Del]	**-198.12**	**-257.44 – -138.79**	**7.69E-11*** **	**1.00E-04*** **
	R^2 / R^2 adjusted	0.37 / 0.37			
	F-statistic (OLS)	189.4 on 5 and 1625 DF, p-value < 2.20E-16***			

Model 1 vs Model 2 – ANOVA Table:

	Resid. DF	Resid. SS	DF	SS	F-value	Pr(>F)
1	1627	33159001				
2	1626	32802768	1	356233	17.66	2.79E-05***

Model 2 vs Model 3 – ANOVA Table:

	Resid. DF	Resid. SS	DF	SS	F-value	Pr(>F)
2	1626	32802768				
3	1625	32802613	1	154.45	0.01	0.93

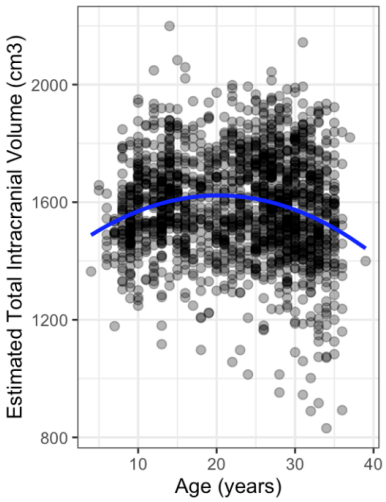

F. VOI: eICV-Adjusted Total Cerebellum Volume (cm^3)

Degree of polynomial	Explanatory variables	*b*	CI (95%)	p-value	perm. p-value
Linear (Model 1) *Best-fit*	Intercept	144.44	142.97 – 145.92 [142.90 – 145.99]	**< 2.00E-16*** ** [**< 2.00E-16*** **]	
	Age (years)	-0.05	-0.11 – 0.01 [-0.11 – 0.01]	0.12 [0.12]	0.12
	Sex [Male]	5.38	4.38 – 6.38 [4.39 – 6.37]	**< 2.00E-16*** ** [**< 2.00E-16*** **]	**1.00E-04*** **
	Diagnostic Group [3q29Del]	**-5.02**	**-9.25 – -0.80** [**-9.24 – -0.81**]	**0.02*** [**0.02***]	**0.02***
	R^2 / R^2 adjusted	0.07 / 0.07			
	Robust Wald test	39.0 on 3 and 1627 DF, p-value < 2.20E-16***			
	[F-statistic (OLS)	40.1 on 3 and 1627 DF, p-value < 2.20E-16***]			
Quadratic (Model 2)	Intercept	142.64	139.06 – 146.23	**< 2.00E-16*** **	
	Age (years)	0.15	-0.21 – 0.52	0.41	**0.41**
	Age^2	-0.005	-0.01 – 0.004	0.28	0.27
	Sex [Male]	5.31	4.31 – 6.31	**< 2.00E-16*** **	**1.00E-04*** **
	Diagnostic Group [3q29Del]	**-4.77**	**-9.01 – -0.53**	**0.03***	**0.03***
	R^2 / R^2 adjusted	0.07 / 0.07			
	F-statistic (OLS)	30.4 on 4 and 1626 DF, p-value < 2.20E-16***			
Cubic (Model 3)	Intercept	136.59	128.16 – 145.02	**< 2.00E-16*** **	
	Age (years)	1.21	-0.17 – 2.58	0.09†	0.08†
	Age^2	-0.06	-0.13 – 0.01	0.09†	0.09†
	Age^3	0.001	-0.0002 – 0.002	0.12	0.12
	Sex [Male]	5.33	4.33 – 6.33	**< 2.00E-16*** **	**1.00E-04*** **
	Diagnostic Group [3q29Del]	**-4.60**	**-8.84 – -0.35**	**0.03***	**0.03***
	R^2 / R^2 adjusted	0.07 / 0.07			
	F-statistic (OLS)	24.8 on 5 and 1625 DF, p-value < 2.20E-16***			

Model 1 vs Model 2 – ANOVA Table:

	Resid. DF	Resid. SS	DF	SS	F-value	Pr(>F)
1	1627	168327				
2	1626	168204	1	122.66	1.19	0.28

Model 2 vs Model 3 – ANOVA Table:

	Resid. DF	Resid. SS	DF	SS	F-value	Pr(>F)
2	1626	168204				
3	1625	167953	1	250.74	2.43	0.12

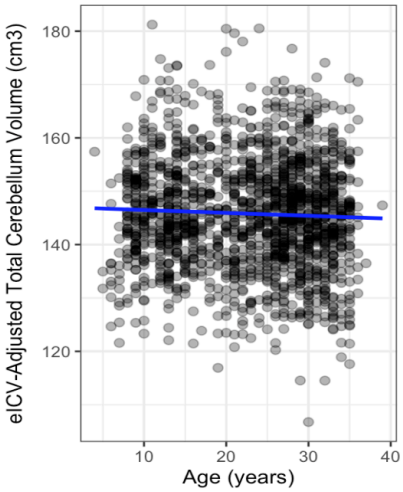

G. VOI: eICV-Adjusted Cerebellar Cortex Volume (cm^3)

Degree of polynomial	Explanatory variables	*b*	CI (95%)	p-value	perm. p-value
Linear (Model 1) *Best-fit*	Intercept	119.88	118.60 – 121.17 [118.58 – 121.19]	**< 2.00E-16***** **[< 2.00E-16***]**	
	Age (years)	-0.21	-0.26 – -0.16 [-0.26 – -0.16]	**1.37E-15***** **[1.42E-15***]**	**1.00E-04*****
	Sex [Male]	4.87	4.03 – 5.72 [4.03 – 5.71]	**< 2.00E-16***** **[< 2.00E-16***]**	**1.00E-04*****
	Diagnostic Group [3q29Del]	**-7.38**	**-10.98 – -3.78** **[-10.95 – -3.81]**	**6.03E-05***** **[5.28E-05***]**	**1.00E-04*****
	R^2 / R^2 adjusted	0.11 / 0.11			
	Robust Wald test	67.5 on 3 and 1627 DF, p-value < 2.20E-16***			
	[F-statistic (OLS)	70.1 on 3 and 1627 DF, p-value < 2.20E-16***]			
Quadratic (Model 2)	Intercept	120.42	117.38 – 123.46	**< 2.00E-16*****	
	Age (years)	-0.27	-0.58 – 0.04	0.09†	0.09†
	Age^2	0.001	-0.01 – 0.01	0.70	0.70
	Sex [Male]	4.89	4.05 – 5.74	**< 2.00E-16*****	**1.00E-04*****
	Diagnostic Group [3q29Del]	**-7.46**	**-11.05 – -3.86**	**4.92E-05*****	**2.00E-04*****
	R^2 / R^2 adjusted	0.11 / 0.11			
	F-statistic (OLS)	52.6 on 4 and 1626 DF, p-value < 2.20E-16 ***			
Cubic (Model 3)	Intercept	114.19	107.05 – 121.33	**< 2.00E-16*****	
	Age (years)	0.81	-0.35 – 1.98	0.17	0.17
	Age^2	-0.05	-0.11 – 0.00	0.07†	0.07†
	Age^3	0.001	0.00 – 0.002	0.06†	0.06†
	Sex [Male]	4.92	4.07 – 5.76	**< 2.00E-16*****	**1.00E-04*****
	Diagnostic Group [3q29Del]	**-7.28**	**-10.88 – -3.69**	**7.40E-05*****	**3.00E-04*****
	R^2 / R^2 adjusted	0.12 / 0.11			
	F-statistic (OLS)	2442.8 on 5 and 1625 DF, p-value < 2.20E-16***			

Model 1 vs Model 2 – ANOVA Table:

	Resid. DF	Resid. SS	DF	SS	F-value	Pr(>F)
1	1627	120694				
2	1626	120683	1	10.95	0.15	0.70

Model 2 vs Model 3 – ANOVA Table:

	Resid. DF	Resid. SS	DF	SS	F-value	Pr(>F)
2	1626	120683				
3	1625	120418	1	265.34	3.58	0.06†

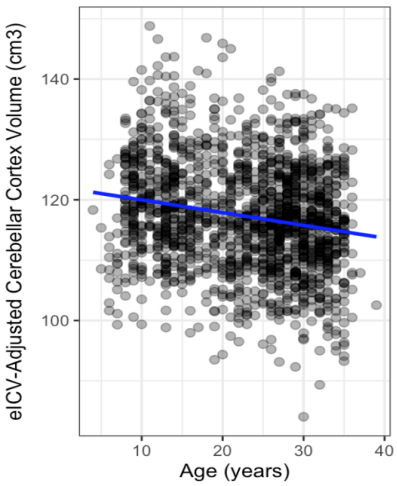

H. VOI: eICV-Adjusted Cerebellar White Matter Volume (cm^3)

Degree of polynomial	Explanatory variables	*b*	CI (95%)	p-value	perm. p-value
Linear (Model 1)	Intercept	24.56	24.12 – 25.00	**< 2.00E-16*** **	
	Age (years)	0.16	0.14 – 0.18	**< 2.00E-16*** **	**1.00E-04*** **
	Sex [Male]	0.51	0.23 – 0.79	**4.33E-04*** **	**8.00E-04*** **
	Diagnostic Group [3q29Del]	**2.36**	**1.16 – 3.55**	**1.22E-04*** **	**3.00E-04*** **
	R^2 / R^2 adjusted	0.18 / 0.18			
	F-statistic (OLS)	118.2 on 3 and 1627 DF, p-value < 2.20E-16***			
Quadratic (Model 2) *Best-fit*	Intercept	22.22	21.22 – 23.23 [21.21 – 23.24]	**< 2.00E-16*** ** [**< 2.00E-16*****]	
	Age (years)	0.42	0.31 – 0.53 [0.32 – 0.53]	**6.39E-14*** ** [**2.53E-15*****]	**1.00E-04*** **
	Age^2	-0.01	-0.01 – -0.004 [-0.01 – -0.004]	**3.94E-06*** ** [6.12E-07***]	**1.00E-04*** **
	Sex [Male]	0.41	0.13 – 0.70 [0.13 – 0.70]	**4.51E-03** ** [**4.07E-03****]	**4.50E-03** **
	Diagnostic Group [3q29Del]	**2.69**	**0.10 – 5.28 [1.49 – 3.89]**	**0.04* [1.15E-05***]**	**1.00E-04*** **
	R^2 / R^2 adjusted	0.19 / 0.19			
	Robust Wald test	106.7 on 4 and 1626 DF, p-value < 2.20E-16***			
	[F-statistic (OLS)	96.2 on 4 and 1626 DF, p-value < 2.20E-16***]			
Cubic (Model 3)	Intercept	22.40	20.02 – 24.78	**< 2.00E-16 *** **	
	Age (years)	0.39	0.004 – 0.78	**0.04***	**0.04***
	Age^2	-0.005	-0.02 – 0.01	0.64	0.63
	Age^3	0.00	-0.003 – 0.003	0.87	0.87
	Sex [Male]	0.41	0.13 – 0.70	**4.16E-03** **	**4.50E-03** **
	Diagnostic Group [3q29Del]	**2.68**	**1.48 – 3.88**	**1.23E-05*** **	**1.00E-04*** **
	R^2 / R^2 adjusted	0.19 / 0.19			
	F-statistic (OLS)	77.0 on 5 and 1625 DF, p-value < 2.20E-16***			

Model 1 vs Model 2 – ANOVA Table:

	Resid. DF	Resid. SS	DF	SS	F-value	Pr(>F)
1	1627	13626				
2	1626	13420	1	206.93	25.07	6.12E-07***

Model 2 vs Model 3 – ANOVA Table:

	Resid. DF	Resid. SS	DF	SS	F-value	Pr(>F)
2	1626	13420				
3	1625	13419	1	0.21	0.03	0.87

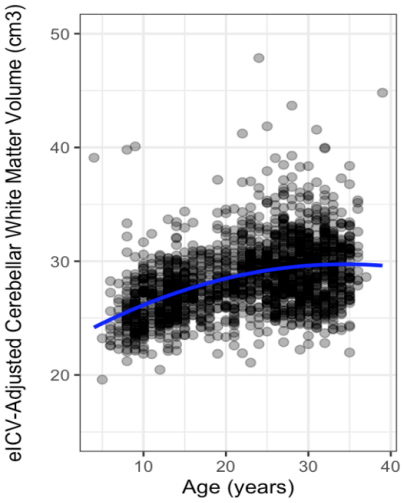

Control N = 1,608, 3q29Del N = 23. p-value ≤ 0.001 '***', p-value ≤ 0.01 '**', p-value ≤ 0.05 '*', p-value ≤ 0.1 '†'. *Abbreviations*: 3q29 deletion syndrome, 3q29Del; VOI, volumetric measure of interest; eICV, estimated total intracranial volume; unstandardized coefficient estimate, *b*; confidence interval, CI; degrees of freedom, DF; sum of squares, SS; analysis of variance, ANOVA; permutation, perm; ordinary least squares, OLS; residual, resid.

VOI	EDF	p-value		
		s(Age) (years)	Sex [Male]	Diagnostic Group [3q29Del]
Total Cerebellum Volume (cm^3)				
Absolute Volume	5.73	1.47E-06***	< 2.00E-16*** (male > female)	**3.47E-07*** (3q29Del < control)**
eICV-Adjusted Volume	4.35	0.09†	< 2.00E-16*** (male > female)	**0.05***
Cerebellar Cortex Volume (cm^3)				
Absolute Volume	5.98	< 2.00E-16***	< 2.00E-16*** (male > female)	**5.32E-10*** (3q29Del < control)**
eICV-Adjusted Volume	5.36	< 2.00E-16***	< 2.00E-16*** (male > female)	**4.67E-04*** (3q29Del < control)**
Cerebellar White Matter Volume (cm^3)				
Absolute Volume	5.26	< 2.00E-16***	< 2.00E-16*** (male > female)	**0.89**
eICV-Adjusted Volume	3.99	< 2.00E-16***	**4.87E-03**** (male > female)	**2.52E-05*** (3q29Del > control)**
eICV (cm^3)				
Absolute Volume	5.00	5.05E-06***	< 2.00E-16*** (male > female)	**5.01E-10*** (3q29Del < control)**

Table S4. Summary of supplemental results from penalized cubic spline models testing the effect of diagnostic group on volumetric measures of interest. To more flexibly account for linear and non-linear trajectories of volumetric change across age without requiring *a priori* selection of candidate models, we fit generalized additive models (GAM) with a cubic spline basis to our data as a supplemental method. Smoothing parameters were selected by the restricted maximum likelihood (REML) approach. EDF represents how complex the developmental pattern of the estimated volumetric trajectory is across age. EDF = 1 is equivalent to a straight line, EDF = 2 is equivalent to a quadratic curve, etc., with higher EDFs describing increased wiggliness. s(Age) represents the spline term of age. The main effect of diagnostic group is reported in bold for clarity. The p-values for sex and diagnostic group are derived from standard t-tests of whether the indicator of sex/diagnostic group are significant in determining each VOI. The p-values for s(Age) are derived from an approximate F-test of whether the smooth term of age is significant in the penalized cubic spline models for each VOI. Contrast coding: reference levels for the diagnostic group and sex variables are healthy control and female, respectively. For categorical variables, the direction of the corresponding effect in significant tests (*p's*

≤ 0.05) is specified by the ">" (greater than) or "<" (less than) symbols. Control *N* = 1,608**,** 3q29Del *N* = 23. p-value ≤ 0.001 '***', p-value ≤ 0.01 '**', p-value ≤ 0.05 '*', p-value ≤ 0.1 '†'. *Abbreviations*: 3q29 deletion syndrome, 3q29Del; estimated total intracranial volume, eICV; volumetric measure of interest, VOI; effective degrees of freedom, EDF.

Table S5. Exploratory modeling of diagnostic group by sex interaction effects on volumetric measures. **A-H)** Interrogated interaction effects are reported in bold. Covariates in each regression model reflect the best-fitting models from Table S3. Final inferences are based on heteroskedasticity-robust estimates, provided above non-robust OLS estimates (in grey brackets). Contrast coding: reference levels for the diagnostic group and sex variables are healthy control and female, respectively.

VOI	Explanatory variables	*b*	CI (95%)	p-value	perm. p-value
A. Absolute Total Cerebellum Volume (cm^3)	Intercept	133.53	128.99 – 138.08 [129.08 – 137.99]	**< 2.00E-16***** **[< 2.00E-16***]**	
	Age (years)	0.67	0.21 – 1.13 [0.22 – 1.13]	**4.18E-03**** **[3.96E-03**]**	**3.10E-03****
	Age^2	-0.02	-0.03 – -0.01 [-0.03 – -0.01]	**7.13E-04*** **[8.03E-04***]**	**1.10E-03****
	Sex [Male]	16.28	15.01 – 17.55 [15.03 – 17.53]	**< 2.00E-16*** **[< 2.00E-16***]**	**1.00E-04****
	Group [3q29Del]	-12.95	-21.59 – -4.32 [-21.27 – -4.63]	**3.30E-03**** **[2.29E-03**]**	**2.20E-03****
	Group x Sex	**-3.82**	**-13.91 – 6.27** **[-14.48 – 6.84]**	**0.46** **[0.48]**	**0.48**
	R^2 / R^2 adjusted	0.31 / 0.31			
	Robust Wald test [F-statistic (OLS)	148.1 on 5 and 1625 DF, p-value < 2.20E-16*** 148.3 on 5 and 1625 DF, p-value < 2.20E-16***]			
B. Absolute Cerebellar Cortex Volume (cm^3)	Intercept	113.56	109.77 – 117.35 [109.90 – 117.22]	**< 2.00E-16*** **[< 2.00E-16***]**	
	Age (years)	0.12	-0.26 – 0.50 [-0.26 – 0.49]	0.54 [0.53]	**0.52**
	Age^2	-0.01	-0.02 – 0.0001 [-0.02 – 0.0001]	0.06† [0.06†]	**0.06†**
	Sex [Male]	13.20	12.16 – 14.24 [12.17 – 14.22]	**< 2.00E-16*** **[< 2.00E-16***]**	**1.00E-04****
	Group [3q29Del]	-12.59	-19.84 – -5.34 [-19.42 – -5.76]	**6.71E-04*** **[3.06E-04***]**	**2.00E-04****
	Group x Sex	**-4.61**	**-13.25 – 4.03** **[-13.36 – 4.14]**	**0.30** **[0.30]**	**0.30**
	R^2 / R^2 adjusted	0.32 / 0.32			
	Robust Wald test [F-statistic (OLS)	155.6 on 5 and 1625 DF, p-value < 2.20E-16 *** 156.0 on 5 and 1625 DF, p-value < 2.20E-16 ***]			
C. Absolute Cerebellar White Matter Volume (cm^3)	Intercept	19.98	18.82 – 21.14 [18.80 – 21.16]	**< 2.00E-16*** **[< 2.00E-16***]**	
	Age (years)	0.55	0.43 –0.67 [0.43 – 0.67]	**< 2.00E-16*** **[< 2.00E-16***]**	**1.00E-04****
	Age^2	-0.01	-0.01 – -0.01 [-0.01 – -0.01]	5.63E-11*** **[4.53E-11***]**	**1.00E-04****
	Sex [Male]	3.08	2.75 – 3.41 [2.75 – 3.41]	**< 2.00E-16*** **[< 2.00E-16***]**	**1.00E-04****
	Group [3q29Del]	-0.36	-3.85 – 3.13 [-2.57 – 1.84]	0.84 [0.75]	**0.75**
	Group x Sex	**0.79**	**-4.17 – 5.74** **[-2.04 – 3.61]**	**0.76** **[0.58]**	**0.58**
	R^2 / R^2 adjusted	0.28 / 0.27			
	Robust Wald test [F-statistic (OLS)	121.5 on 5 and 1625 DF, p-value < 2.20E-16*** 124.1 on 5 and 1625 DF, p-value < 2.20E-16***]			

D. Cerebellar Cortex to Cerebellar White Matter Volume Ratio	Intercept	5.38	5.22 – 5.53 [5.24 – 5.51]	**< 2.00E-16***** **[< 2.00E-16***]**	
	Age (years)	-0.09	-0.10 – -0.07 [-0.10 – -0.07]	**< 2.00E-16***** **[< 2.00E-16***]**	**1.00E-04*****
	Age^2	0.001	0.001 – 0.002 [0.001 – 0.002]	**5.16E-13***** **[1.87E-15***]**	**1.00E-04*****
	Sex [Male]	0.03	-0.004 – 0.07 [-0.003 – 0.07]	0.07† [0.08†]	**0.09**†
	Group [3q29Del]	-0.37	-0.86 – 0.11 [-0.63 – -0.12]	**0.13** **[3.96E-03**]**	**6.40E-03****
	Group x Sex	**-0.19**	**-0.91 – 0.52** **[-0.52 – 0.13]**	**0.60** **[0.25]**	**0.25**
	R^2 / R^2 adjusted	0.33 / 0.33			
	Robust Wald test [F-statistic (OLS)	144.8 on 5 and 1625 DF, p-value < 2.20E-16*** 162.9 on 5 and 1625 DF, p-value < 2.20E-16***]			
E. Estimated Total Intracranial Volume (eICV) (cm^3)	Intercept	1416.29	1369.41 – 1463.16] [1366.23 – 1466.34]	**< 2.00E-16***** **[< 2.00E-16***]**	
	Age (years)	9.66	4.64 – 14.69 [4.53 – 14.79]	**1.69E-04***** **[2.29E-04***]**	**3.00E-04*****
	Age^2	-0.25	-0.37 – -0.13 [-0.37 – -0.13]	4.86E-05*** **[3.92E-05***]**	**1.00E-04*****
	Sex [Male]	208.09	194.04 – 222.14 [194.05 – 222.13]	**< 2.00E-16***** **[< 2.00E-16***]**	**1.00E-04*****
	Group [3q29Del]	-107.56	-191.51 – -23.61 [-201.01 – -14.11]	**0.01**** **[0.02*]**	**0.03***
	Group x Sex	**-149.64**	**-249.96 – -49.33** **[-269.37 – -29.91]**	**3.48E-03**** **[0.01**]**	**0.01****
	R^2 / R^2 adjusted	0.37 / 0.37			
	Robust Wald test [F-statistic (OLS)	192.4 on 5 and 1625 DF, p-value < 2.20E-16*** 191.3 on 5 and 1625 DF, p-value < 2.20E-16***]			
F. eICV-Adjusted Total Cerebellum Volume (cm^3)	Intercept	144.46	142.99 – 145.94 [142.92 – 146.00]	**< 2.00E-16***** **[< 2.00E-16***]**	
	Age (years)	-0.05	-0.11 – 0.01 [-0.11 – 0.01]	0.12 [0.12]	0.12
	Sex [Male]	5.33	4.32 – 6.33 [4.33 – 6.32]	**< 2.00E-16***** **[< 2.00E-16***]**	**1.00E-04*****
	Group [3q29Del]	-7.41	-13.80 – -1.02 [-14.11 – -0.72]	**0.02*** **[0.03*]**	**0.03***
	Group x Sex	**3.94**	**-4.41 – 12.30** **[-4.64 – 12.53]**	**0.35** **[0.37]**	**0.37**
	R^2 / R^2 adjusted	0.07 / 0.07			
	Robust Wald test [F-statistic (OLS)	29.6 on 4 and 1626 DF, p-value < 2.20E-16*** 30.3 on 4 and 1626 DF, p-value < 2.20E-16***]			
G. eICV-Adjusted Cerebellar Cortex Volume (cm^3)	Intercept	119.89	118.60 – 121.17 [118.58 – 121.19]	**< 2.00E-16***** **[< 2.00E-16***]**	
	Age (years)	-0.21	-0.26 – -0.16 [-0.26 – -0.16]	**1.48E-15***** **[1.50E-15***]**	**1.00E-04*****
	Sex [Male]	4.85	4.00 – 5.70 [4.01 – 5.70]	**< 2.00E-16***** **[< 2.00E-16***]**	**1.00E-04*****
	Group [3q29Del]	-8.24	-13.39 – -3.10 [-13.91 – -2.57]	**1.71E-03**** **[4.42E-03**]**	**4.30E-03****
	Group x Sex	**1.43**	**-5.62 – 8.48** **[-5.84 – 8.70]**	**0.69** **[0.70]**	**0.70**
	R^2 / R^2 adjusted	0.11 / 0.11			
	Robust Wald test [F-statistic (OLS)	51.0 on 4 and 1626 DF, p-value < 2.20E-16*** 52.56 on 4 and 1626 DF, p-value < 2.20E-16***]			

H. eICV-Adjusted Cerebellar White Matter Volume (cm^3)	Intercept	22.20	21.21 – 23.19 [21.19 – 23.21]	**< 2.00E-16***** **[< 2.00E-16***]**	
	Age (years)	0.43	0.32 – 0.53 [0.32 – 0.53]	**8.45E-15***** **[1.32E-15***]**	**1.00E-04*****
	Age^2	-0.01	-0.01 – -0.004 [-0.01 – -0.004]	**1.55E-06***** **[4.10E-07***]**	**1.00E-04*****
	Sex [Male]	0.38	0.10 – 0.65 [0.09 – 0.66]	**8.15E-03**** **[9.49E-03**]**	**9.30E-03****
	Group [3q29Del]	1.04	-2.56 – 4.64 [-0.85 – 2.93]	0.57 [0.28]	**0.27**
	Group x Sex	**2.73**	**-2.29 – 7.75** **[0.31 – 5.15]**	**0.29** **[0.03*]**	**0.03***
	R^2 / R^2 adjusted	0.19 / 0.19			
	Robust Wald test [F-statistic (OLS)	87.5 on 5 and 1625 DF, p-value < 2.20E-16*** 78.16 on 5 and 1625 DF, p-value < 2.20E-16***]			

Control N = 1,608 (Female N = 861, Male N = 747), 3q29Del N = 23 (Female N = 9, Male N = 14). p-value ≤ 0.001 '***', p-value ≤ 0.01 '**', p-value ≤ 0.05 '*', p-value ≤ 0.1 '†'. *Abbreviations*: 3q29 deletion syndrome, 3q29Del; VOI, volumetric measure of interest; eICV, estimated total intracranial volume; unstandardized coefficient estimate, *b*; confidence interval, CI; degrees of freedom, DF; permutation, perm; ordinary least squares, OLS.

Outcome variable	Explanatory variables	*b*	CI (95%)	p-value	perm. p-value
eICV-Adjusted Cerebellar White Matter Volume (cm^3) **Sex: Male**	Intercept	21.14	19.36 – 22.93 [19.41 – 22.88]	**< 2.00E-16*** [< 2.00E-16***]	
	Age (years)	0.56	0.36 – 0.75 [0.38 – 0.73]	**1.94E-08*** [8.15E-10***]	**1.00E-04***
	Age^2	-0.01	-0.01 – -0.005 [-0.01 – -0.004]	**1.74E-04*** [2.48E-05***]	**1.00E-04***
	Diagnostic group [3q29Del]	**4.09**	**0.50 – 7.68** **[2.35 – 5.83]**	**0.03*** [4.59E-06***]	**1.00E-04***
	R^2 / R^2 adjusted Robust Wald test [F-statistic (OLS)	0.18 / 0.18 62.1 on 3 and 757 DF, p-value **< 2.00E-16*** 57.0 on 3 and 757 DF, p-value **< 2.00E-16***]			
eICV-Adjusted Cerebellar White Matter Volume (cm^3) **Sex: Female**	Intercept	23.35	22.27 – 24.43 [22.16 – 24.54]	**< 2.00E-16*** [< 2.00E-16***]	
	Age (years)	0.32	0.20 – 0.44 [0.20 – 0.44]	**9.95E-08*** [3.16E-07***]	**1.00E-04***
	Age^2	-0.004	-0.01 – -0.001 [-0.01 – -0.001]	**4.24E-03**** [4.83E-03**]	**4.90E-03****
	Diagnostic group [3q29Del]	**0.88**	**-2.64 – 4.39** **[-0.79 – 2.54]**	**0.62** **[0.30]**	**0.29**
	R^2 / R^2 adjusted Robust Wald test [F-statistic (OLS)	0.21 / 0.20 89.4 on 3 and 866 DF, p-value **< 2.00E-16*** 75.5 on 3 and 866 DF, p-value **< 2.00E-16***]			

Table S6. Post hoc analysis of the suggestive sex by diagnostic group interaction effect on eICV-adjusted cerebellar white matter volumes. For further inspection of the suggestive diagnostic group by sex interaction effect described in Table S5H and Fig. S8, here we report results from a *post hoc* analysis of the effect of diagnostic group on eICV-adjusted cerebellar white matter volumes in males and females, separately. Sex-stratified multiple linear regression models include age and age^2 as covariates based on the best-fitting polynomial model for this VOI from Table S3H. Main effect of diagnostic group is reported in bold for clarity. Results indicate that male 3q29Del subjects have larger eICV-adjusted cerebellar white matter volumes than male controls ($p \leq 0.05$), whereas this effect was not significant in female 3q29Del subjects compared with female controls ($p > 0.05$). Inferences are based on heteroskedasticity-robust estimates in males versus females, which are provided above non-robust OLS estimates (in grey brackets). Robust Wald test statistics are reported to assess the overall significance of each model, along with exact p-values calculated by non-asymptotic permutation marginal tests. Since the heteroskedasticity-robust estimates for the corresponding sex by diagnostic group interaction failed to reach significance in Table S3H ($p > 0.05$), we consider the evidence in

favor of this sex-specific effect to be weak. Male N = 761 (Control N = 747, 3q29Del N = 14), Female N = 870 (Control N = 861, 3q29Del N = 9). Contrast coding: reference level for the diagnostic group variable is healthy control. p-value ≤ 0.001 '***', p-value ≤ 0.01 '**', p-value ≤ 0.05 '*', p-value ≤ 0.1 '†'. *Abbreviations*: 3q29 deletion syndrome, 3q29Del; estimated total intracranial volume, eICV; VOI, volumetric measure of interest; unstandardized coefficient estimate, *b*; confidence interval, CI; degrees of freedom, DF; permutation, perm

VOI	Summary of multiple linear regression findings	Diagnostic group	
		Control Mean ± SD	**3q29Del** Mean ± SD
Total Cerebellum Volume (cm^3)			
All subjects			
Absolute Volume	✓ (3q29Del < control)	145.86 ±15.17	132.74 ±12.81
Diagnostic group X Sex	*ns*	—	—
eICV-Adjusted Volume	✓ (3q29Del < control)	145.86 ± 10.51	141.97 ± 11.31
Diagnostic group X Sex	*ns*	—	—
Male subjects			
Absolute Volume	✓ (3q29Del < control)	154.76 ± 13.47	137.58 ± 9.78
eICV-Adjusted Volume	✓ (3q29Del < control)	148.72 ± 10.80	145.64 ± 10.48
Female subjects			
Absolute Volume	✓ (3q29Del < control)	138.13 ± 12.00	125.22 ± 13.83
eICV-Adjusted Volume	✓ (3q29Del < control)	143.37 ± 9.59	136.26 ± 10.63
Cerebellar Cortex Volume (cm^3)			
All subjects			
Absolute Volume	✓ (3q29Del < control)	117.39 ± 12.52	105.34 ± 11.55
Diagnostic group X Sex	*ns*	—	—
eICV-Adjusted Volume	✓ (3q29Del < control)	117.39 ± 9.12	112.31 ± 9.82
Diagnostic group X Sex	*ns*	—	—
Male subjects			
Absolute Volume	✓ (3q29Del < control)	124.61 ± 10.98	108.88 ± 9.35
eICV-Adjusted Volume	✓ (3q29Del < control)	120.06 ± 9.21	114.96 ± 9.31
Female subjects			
Absolute Volume	✓ (3q29Del < control)	111.12 ± 10.18	99.84 ± 12.99
eICV-Adjusted Volume	✓ (3q29Del < control)	115.07 ± 8.38	108.18 ± 9.63
Cerebellar White Matter Volume (cm^3)			
All subjects			
Absolute Volume	*ns*	28.47 ± 3.89	27.40 ± 5.84
Diagnostic group X Sex	*ns*	—	—
eICV-Adjusted Volume	✓ (3q29Del > control)	28.47 ± 3.13	29.66 ± 6.11
Diagnostic group X Sex	✓ (suggestive interaction effect)	—	—
Male subjects			
Absolute Volume	*ns*	30.15 ± 4.02	28.70 ± 6.35
eICV-Adjusted Volume	✓ (3q29Del > control; inspection of suggestive interaction effect)	28.67 ± 3.46	30.68 ± 6.64
Female subjects			
Absolute Volume	*ns*	27.01 ± 3.12	25.37 ± 4.54
eICV-Adjusted Volume	*ns* (inspection of suggestive interaction effect)	28.30 ± 2.80	28.08 ± 5.12

Cerebellar Cortex to White Matter Volume Ratio			
All subjects			
Absolute Volume Ratio	✓ (3q29Del < control)	4.16 ± 0.46	3.99 ± 0.83
Diagnostic group X Sex	*ns*	—	—
Male subjects			
Absolute Volume Ratio	✓ (3q29Del < control)	4.18 ± 0.48	3.97 ± 0.90
Female subjects			
Absolute Volume Ratio	✓ (3q29Del < control)	4.15 ± 0.45	4.02 ± 0.76
eICV (cm^3)			
All subjects			
Absolute Volume	✓ (3q29Del < control)	1587.49 ± 178.02	1413.33 ± 116.47
Diagnostic group X Sex	✓ (male effect > female effect)	—	—
Male subjects			
Absolute Volume	✓ (3q29Del < control)	1701.33 ± 141.52	1435.33 ± 103.17
Female subjects			
Absolute Volume	✓ (3q29Del < control)	1488.71 ± 144.31	1379.12 ± 133.59

Table S7. Summary of multiple linear regression findings and descriptive statistics for volumetric measures of interest in 3q29Del and control groups. Diagnostic group differences and diagnostic group by sex interaction effects identified in the current study (*p's* ≤ 0.05) are marked by the "✓" symbol; the direction of the corresponding effect is specified by the ">" (greater than) or "<" (less than) symbols. Descriptive statistics (mean and SD) for each volumetric measure of interest are provided on the right for separate groups. Control *N* = 1,608 (Female *N* = 861, Male *N* = 747), 3q29Del *N* = 23 (Female *N* = 9, Male *N* = 14). *Abbreviations*: 3q29 deletion syndrome, 3q29Del; VOI, volumetric measure of interest; estimated total intracranial volume, eICV; standard deviation, SD; not significant, ns.

	PFAC/MCM - (*N* = 11)	**PFAC/MCM +** *(N* = 13)	**Test statistics**
Sex, *n/N (%)*			
Male	7/11 (63.64%)	8/13 (61.54%)	OR = 0.92, 95% CI = 0.13 – 6.39, p-value [a] = 1
Female	4/11 (36.36%)	5/13 (38.46%)	
Age (in years)			
Mean ± SD	17.64 ± 11.76	12.23 ± 5.72	*t = -1.47,* DF = 22, p-value [b] = 0.16[b]
Median [Range]	15 [4 – 39]	10 [6 – 21]	
Ethnicity, *n/N (%)*			
Non-Hispanic / Latino	11/11 (100%)	12/13 (92.31%)	OR = INF, 95% CI = 0.02 – INF, *p-value* [a] = 1
Hispanic / Latino	0/11 (0%)	1/13 (7.69%)	
Race, *n/N (%)*			
White	10/11 (90.91%)	12/13 (92.31%)	OR = 0.84, 95% CI = 0.01 – 71.84 p-value [a] = 1
More than one race	1/11 (9.09%)	1/13 (7.69%)	
History of head injury[#], *n/N (%)*			
Negative	6/8 (75.00%)	11/13 (84.62%)	OR = 0.56, 95% CI = 0.03 – 9.62, p-value [a] = 0.62
Positive	2/8 (25.00%)	2/13 (15.38%)	
History of neonatal complications during delivery[#], *n/N (%)* *"Did the baby have any trouble at birth?" (e.g., birth injuries, jaundice, fetal hypoxia, respiratory distress syndrome, hemorrhage); "Was the baby premature?"*			
Negative	3/8 (37.50%)	7/13 (53.85%)	OR = 0.53, 95% CI = 0.06 – 4.21, p-value [a] = 0.66
Positive	5/8 (62.50%)	6/13 (46.15%)	
History of maternal complications during pregnancy[#], *n/N (%)* *"Did the mother have any illness or injury during pregnancy?" (e.g., preeclampsia, infection, physical trauma)*			
Negative	4/8 (50.00%)	9/13 (69.23%)	OR = 0.46, 95% CI = 0.05 – 3.90, p-value [a] = 0.65
Positive	4/8 (50.00%)	4/13 (30.77%)	
Combined history of head injury, neonatal complications during delivery, and/or maternal complications during pregnancy[#], *n/N (%)*			
Negative	2/8 (25.00%)	4/13 (30.77%)	OR= 0.76, 95% CI= 0.05 – 7,55, p-value [a] = 1
Positive	6/8 (75.00%)	9/13 (69.23%)	

Table S8. Demographic and relevant clinical characteristics of 3q29Del subjects with versus without posterior fossa arachnoid cyst or mega cisterna magna findings. There was no significant difference between PFAC/MCM positive (+) and negative (-) 3q29Del subjects in demographic characteristics or in clinical characteristics that have been proposed to be associated with the etiology of secondary (acquired) cysts

in previous literature (*p's* > 0.05). [a]Fisher's exact test, [b]Student's two sample t-test. [#]3q29Del *N* = 21 due to missing data. *Abbreviations:* 3q29 deletion syndrome, 3q29Del; posterior fossa arachnoid cyst, PFAC; mega cisterna magna, MCM; standard deviation, SD; odds ratio, OR; confidence interval, CI.

Standardized test scores	**3q29Del** (*N* = 23)
Visual-motor Integration (*Beery VMI-6)*	
Mean ± SD	67.83 ± 15.87
Median [Range]	70 [45 – 96]
Supplemental test: Motor Coordination (*Beery VMI-6)*	
Mean ± SD	62.65 ± 15.68
Median [Range]	63 [45 – 90]
Supplemental test: Visual Perception (*Beery VMI-6)*	
Mean ± SD	74.74 ± 18.20
Median [Range]	79 [45 – 101]
Composite IQ *(WASI-II/ DAS-II)*	
Mean ± SD	73.48 ± 13.30
Median [Range]	75 [46 – 96]
Supplemental test: Verbal IQ *(WASI-II/ DAS-II)*	
Mean ± SD	79.87 ± 19.13
Median [Range]	85 [31 – 106]
Supplemental test: Non-verbal IQ *(WASI-II/ DAS-II)*	
Mean ± SD	74.61 ± 13.80
Median [Range]	75 [53 – 98]

Table S9. Descriptive statistics for standardized test scores for sensorimotor and cognitive abilities among 3q29Del subjects. *Abbreviations*: 3q29 deletion syndrome, 3q29Del; intelligence quotient, IQ; Wechsler Abbreviated Scale of Intelligence, WASI; Differential Ability Scales, DAS; visual-motor integration, VMI; standard deviation, SD.

Outcome variables	Explanatory variables	*b*	CI (95%)	p-value
Visual-motor Integration *(standardized score, Beery VMI-6)*	Intercept	100.65	17.78 – 183.51	0.02*
	Age (years)	-0.63	-1.72 – 0.46	0.24
	Sex [Male]	-4.22	-19.46 – 11.02	0.57
	Cerebellar Cortex Volume (cm^3)	**-0.20**	**-0.95 – 0.56**	**0.59**
	R^2 / R^2 adjusted	0.13 / -0.01		
	Robust Wald Test	0.6 on 3 and 19 DF, p-value = 0.63		
	Intercept	44.93	15.79 – 74.07	4.44E-03**
	Age (years)	-0.57	-1.24 – 0.10	0.09†
	Sex [Male]	-10.47	-24.59 – 3.65	0.14
	Cerebellar WM Volume (cm^3)	**1.38**	**0.36 – 2.41**	**0.01****
	R^2 / R^2 adjusted	0.35 / 0.25		
	Robust Wald Test	4.0 on 3 and 19 DF, p-value = 0.02*		
Supplemental test: Motor Coordination *(standardized score, Beery VMI-6)*	Intercept	44.27	-44.76 – 133.29	0.31
	Age (years)	0.28	-0.71 – 1.28	0.56
	Sex [Male]	-5.78	-20.33 – 8.78	0.42
	Cerebellar Cortex Volume (cm^3)	**0.17**	**-0.60 – 0.94**	**0.65**
	R^2 / R^2 adjusted	0.05 / -0.10		
	Robust Wald Test	0.4 on 3 and 19 DF, p-value = 0.77		
	Intercept	46.45	15.79 – 77.11	5.03E-03**
	Age (years)	0.20	-0.53 – 0.92	0.58
	Sex [Male]	-6.58	-21.59 – 8.42	0.37
	Cerebellar WM Volume (cm^3)	**0.63**	**-0.45 – 1.71**	**0.24**
	R^2 / R^2 adjusted	0.09 / -0.05		
	Robust Wald Test	0.8 on 3 and 19 DF, p-value = 0.53		
Supplemental test: Visual Perception *(standardized score, Beery VMI-6)*	Intercept	109.13	24.51 – 193.76	0.01**
	Age (years)	-0.60	-1.68 – 0.48	0.26
	Sex [Male]	-5.46	-22.30 – 11.38	0.51
	Cerebellar Cortex Volume (cm^3)	**-0.21**	**-0.96 – 0.54**	**0.57**
	R^2 / R^2 adjusted	0.10 / -0.04		
	Robust Wald Test	0.6 on 3 and 19 DF, p-value = 0.62		
	Intercept	65.04	30.90 – 99.18	7.88E-04***
	Age (years)	-0.52	-1.34 – 0.29	0.19
	Sex [Male]	-10.06	-30.39 – 10.28	0.31
	Cerebellar WM Volume (cm^3)	**0.87**	**-0.83 – 2.56**	**0.30**
	R^2 / R^2 adjusted	0.16 / 0.03		
	Robust Wald Test	0.8 on 3 and 19 DF, p-value = 0.52		
Composite IQ *(standardized score, WASI-II/ DAS-II)*	Intercept	62.45	-4.14 – 129.04	0.06†
	Age (years)	0.06	-0.86 – 0.97	0.90
	Sex [Male]	-5.15	-18.74 – 8.44	0.44
	Cerebellar Cortex Volume (cm^3)	**0.13**	**-0.47 – 0.72**	**0.66**
	R^2 / R^2 adjusted	0.03 / -0.12		
	Robust Wald Test	0.2 on 3 and 19 DF, p-value = 0.88		
	Intercept	42.69	19.34 – 66.03	1.14E-03**
	Age (years)	-0.03	-0.56 – 0.50	0.90
	Sex [Male]	-8.66	-20.51 – 3.18	0.14
	Cerebellar WM Volume (cm^3)	**1.33**	**0.36 – 2.31**	**9.89E-03****
	R^2 / R^2 adjusted	0.34 / 0.23		
	Robust Wald Test	3.1 on 3 and 19 DF, p-value = 0.05*		

Supplemental test: Verbal IQ *(standardized score, WASI-II/ DAS-II)*	Intercept	46.24	-32.13 – 124.61	0.23
	Age (years)	0.28	-0.72 – 1.29	0.56
	Sex [Male]	-9.09	-25.92 – 7.74	0.27
	Cerebellar Cortex Volume (cm^3)	**0.33**	**-0.36 – 1.02**	**0.33**
	R^2 / R^2 adjusted	0.06 / -0.08		
	Robust Wald Test	0.5 on 3 and 19 DF, p-value = 0.66		
	Intercept	43.93	12.21 – 75.64	9.20E-03**
	Age (years)	0.10	-0.65 – 0.85	0.78
	Sex [Male]	-11.58	-28.35 – 5.18	0.16
	Cerebellar WM Volume (cm^3)	**1.51**	**0.13 – 2.89**	**0.03***
	R^2 / R^2 adjusted	0.23 / 0.11		
	Robust Wald Test	2.9 on 3 and 19 DF, p-value = 0.06†		
Supplemental test: Non-verbal IQ *(standardized score, WASI-II/ DAS-II)*	Intercept	94.11	33.85 – 154.37	4.04E-03**
	Age (years)	-0.52	-1.55 – 0.50	0.30
	Sex [Male]	-5.40	-19.42 – 8.63	0.43
	Cerebellar Cortex Volume (cm^3)	**-0.08**	**-0.64 – 0.48**	**0.77**
	R^2 / R^2 adjusted	0.14 / 0.003		
	Robust Wald Test	0.5 on 3 and 19 DF, p-value = 0.67		
	Intercept	53.59	23.85 – 83.33	1.29E-03**
	Age (years)	-0.52	-1.11 – 0.07	0.08†
	Sex [Male]	-10.37	-22.86 – 2.12	0.10†
	Cerebellar WM Volume (cm^3)	**1.28**	**0.17 – 2.39**	**0.03***
	R^2 / R^2 adjusted	0.41 / 0.31		
	Robust Wald Test	3.0 on 3 and 19 DF, p-value = 0.6†		

Table S10. Extended multiple linear regression results testing the relationships between tissue-specific cerebellar volumes and sensorimotor and cognitive abilities among 3q29Del subjects. Main effects of cerebellar cortex and white matter volumes are reported in bold. Regression parameters reflect heteroskedasticity-robust estimates, computed to address observed violations of statistical assumptions. Regression results indicate significant relationships between cerebellar white matter volume and visual-motor integration skills ($p \leq 0.01$) and composite IQ ($p \leq 0.01$) among 3q29Del subjects. In supplemental analyses, cerebellar white matter volume was found to have a significant relationship with both verbal ($p \leq 0.05$), and non-verbal IQ ($p \leq 0.05$). See Table 5 for results from secondary models including estimated total intracranial volume as an additional covariate. 3q29Del $N = 23$. Contrast coding: reference level for the sex variable is female. p-value ≤ 0.001 '***', p-value ≤ 0.01 '**', p-value ≤ 0.05 '*', p-value ≤ 0.1 '†'. *Abbreviations*: 3q29 deletion syndrome, 3q29Del; volumetric measure of interest, VOI; intelligence quotient, IQ; Wechsler Abbreviated Scale of Intelligence, WASI; Differential Ability Scales, DAS; visual-motor integration, VMI; white matter, WM; unstandardized coefficient estimate, *b*; confidence interval, CI; degrees of freedom, DF.

Standardized test scores	PFAC/MCM - (*N* = 11)	PFAC/MCM + (*N* = 13)	Test statistics
Visual-motor Integration (*Beery VMI-6)* Mean ± SD Median [Range]	66.64 ± 16.45 68 [45 – 86]	68.85 ± 15.30 70 [45 – 96]	*t* = 0.34, DF = 22, p-value = 0.74[a]
Supplemental test: Motor Coordination (*Beery VMI-6)* Mean ± SD Median [Range]	64.00 ± 15.95 63 [45 – 90]	60.38 ± 15.79 58 [45 – 83]	*W* = 60.00, p-value = 0.52[b]
Supplemental test: Visual Perception (*Beery VMI-6)* Mean ± SD Median [Range]	69.09 ± 19.36 63 [45 – 98]	78.38 ± 16.41 79 [45 – 101]	*t* = 1.27, DF = 22, p-value = 0.22[a]
Composite IQ *(WASI-II/ DAS-II)* Mean ± SD Median [Range]	74.91 ± 12.83 75 [54 – 96]	70.77 ± 14.45 72 [46 – 89]	*t* = -0.74, DF = 22, p-value = 0.47[a]
Supplemental test: Verbal IQ *(WASI-II/ DAS-II)* Mean ± SD Median [Range]	84.73 ± 17.19 85 [57 – 106]	74.00 ± 20.24 80 [31 – 93]	*W* = 52.50, p-value = 0.28[b]
Supplemental test: Non-verbal IQ *(WASI-II/ DAS-II)* Mean ± SD Median [Range]	73.09 ± 12.71 72 [54 – 98]	75.54 ± 14.60 79 [53 – 97]	*t* = 0.43, DF = 22, p-value = 0.67[a]

Table S11. Standardized test scores for sensorimotor and cognitive abilities in 3q29Del subjects with versus without posterior fossa arachnoid cyst or mega cisterna magna findings. There was no significant difference between PFAC/MCM positive (+) versus negative (-) 3q29Del subjects in visual-motor integration, motor coordination or visual perception scores measured by the Beery-Buktenica Developmental Test of VMI, or in composite, verbal or non-verbal IQ scores measured by the WASI / DAS (*p's* > 0.05). [a]Student's two sample t-test, [b]Wilcoxon rank sum test with continuity correction. Non-parametric statistics are reported in cases where the data do not meet parametric assumptions. *Abbreviations*: 3q29 deletion syndrome, 3q29Del; posterior fossa arachnoid cyst, PFAC; mega cisterna magna, MCM; intelligence quotient, IQ; WASI, Wechsler Abbreviated Scale of Intelligence; DAS, Differential Ability Scales; VMI, visual-motor integration; standard deviation, SD.

Supplemental Figures

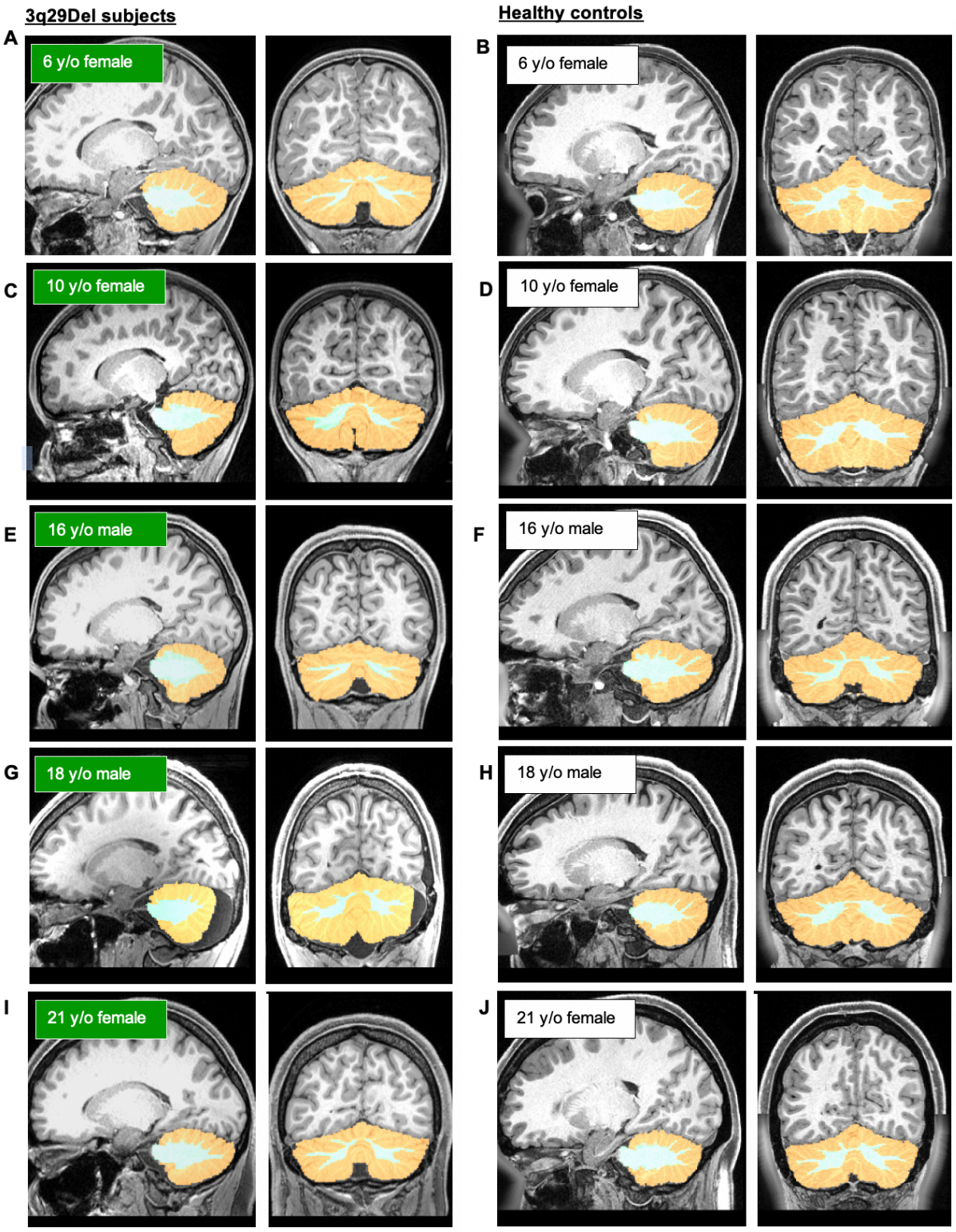

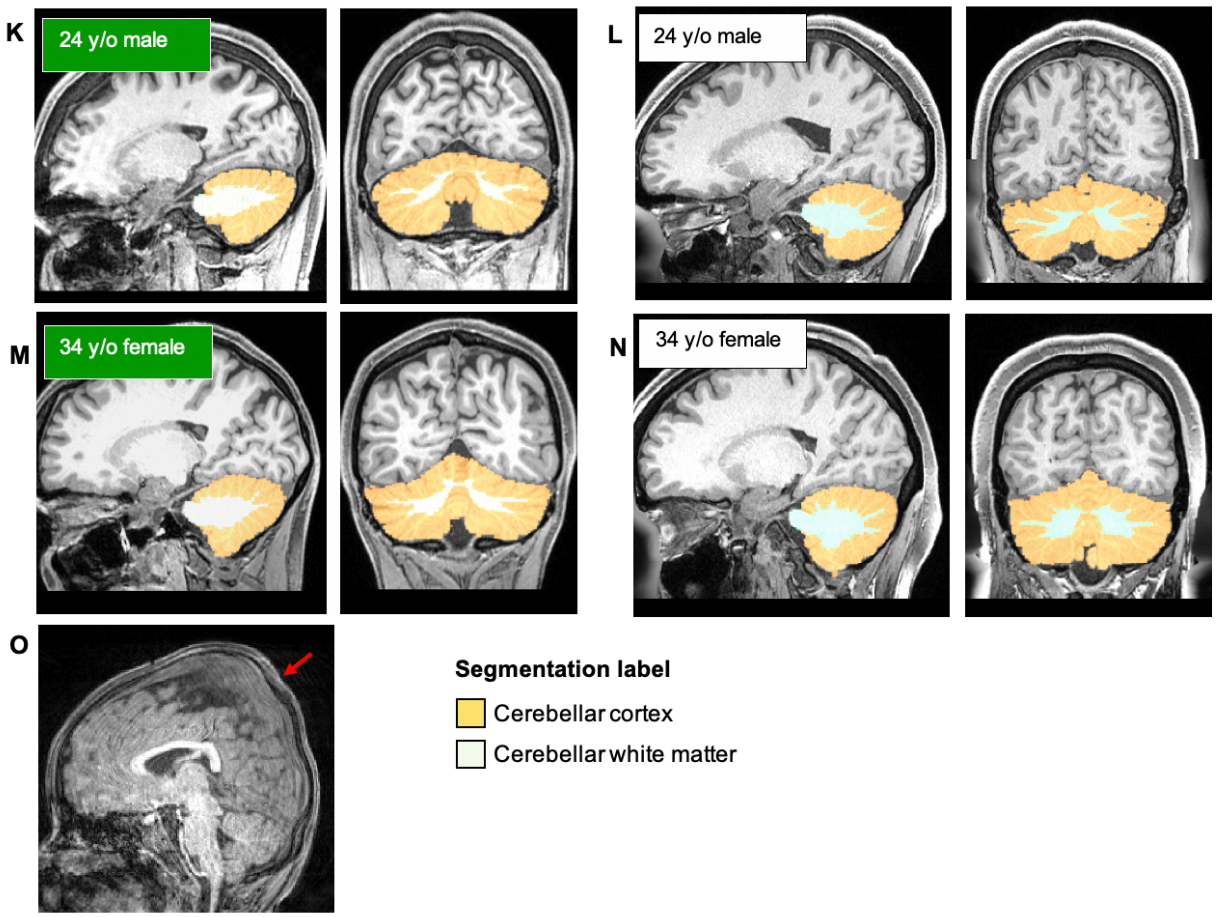

Figure S1. Example cerebellar segmentation masks for representative age- and sex-matched 3q29Del and healthy control pairs. A-N) For quality control, cerebellar cortex and white matter segmentation masks were overlaid on T1-weighted MR images acquired from N = 23 age- and sex-matched case-control pairs randomly selected from the dataset. Representative images for seven randomly selected case-control pairs are provided in this figure for illustration in sagittal and coronal planes. 3D volumes were segmented using FreeSurfer's automated subcortical segmentation algorithm in both diagnostic groups, as implemented in the HCP "minimal pre-processing" pipeline (Glasser et al., 2013; Harms et al., 2018). Image quality, tissue contrast and the boundaries of delineation for cerebellar voxel classifications were examined by two independent raters using the Connectome Workbench tool (https://www.humanconnectome.org/software/get-connectome-workbench). These outputs were found to be highly consistent within and between diagnostic groups, independent of age, sex, and presence or absence of radiologically observable posterior fossa abnormalities. **O)**

A representative T1-weighted sagittal MR image of a 6-year-old male 3q29Del subject who was excluded from volumetric analyses due to motion artifact and a skull deformity interfering with reliable volume estimations. Upon radiological examination, this 3q29Del subject was found to have plagiocephaly (red arrow). An example MR image is provided to illustrate our basis for exclusion. *Abbreviations*: 3q29 deletion syndrome, 3q29Del; years old, y/o.

Harms MP, Somerville LH, Ances BM, Andersson J, Barch DM, Bastiani M, et al. (2018): Extending the Human Connectome Project across ages: Imaging protocols for the Lifespan Development and Aging projects. *Neuroimage*. 183:972-984.

Glasser MF, Sotiropoulos SN, Wilson JA, Coalson TS, Fischl B, Andersson JL, et al. (2013): The minimal preprocessing pipelines for the Human Connectome Project. *Neuroimage*. 80:105-124.

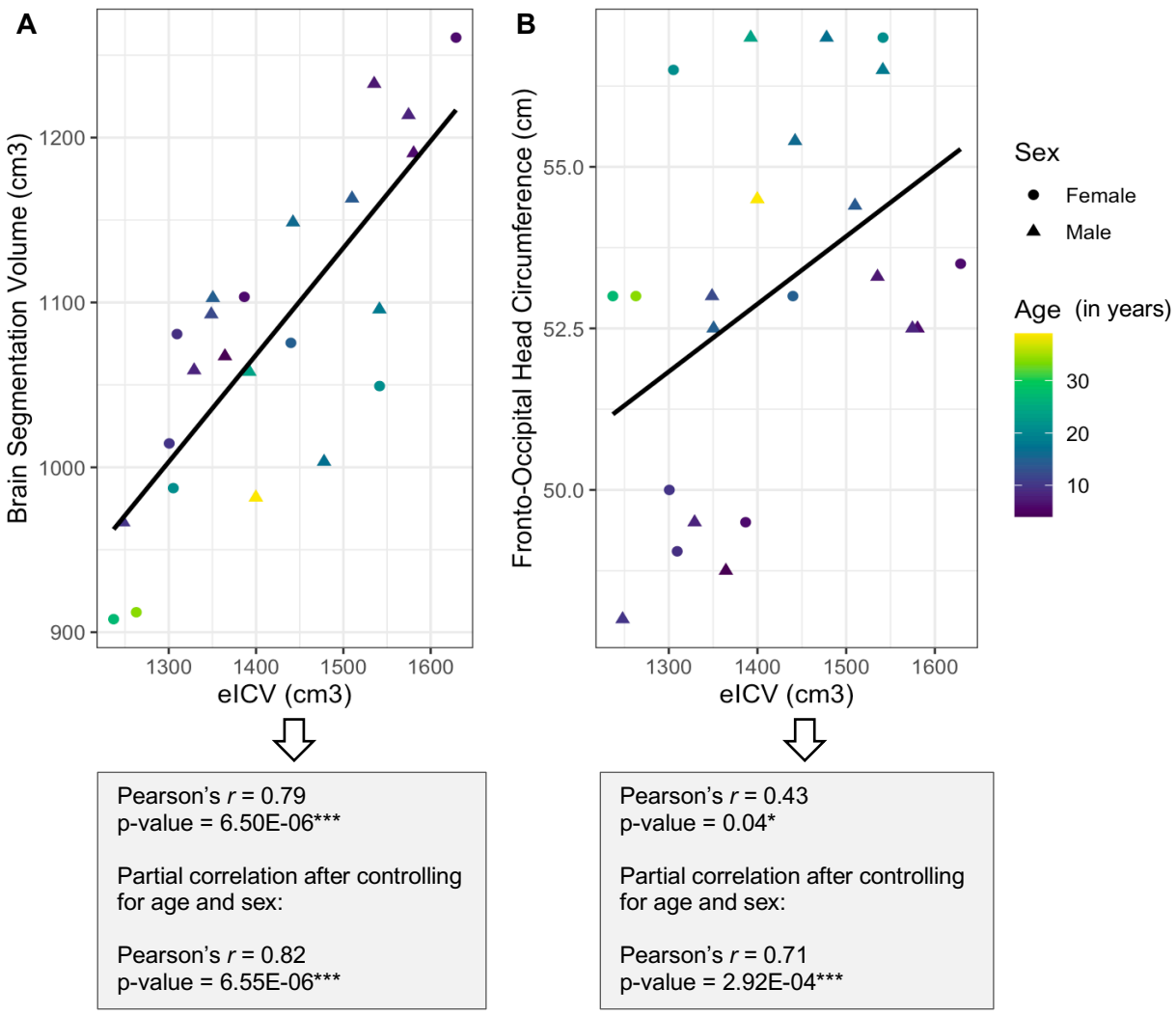

Figure S2. Relationships between estimated total intracranial volume, total brain volume and head circumference among 3q29Del subjects. Morphometric analysis of regional brain structure confronts the challenge of accounting for head size variation. A widely used automated procedure for head size correction, which has been validated against manually delineated measurements of total intracranial volume (ICV), is the atlas-based head size normalization technique developed by FreeSurfer. This method exploits the relationship between ICV and the linear transform to MNI space to calculate an estimated total intracranial volume (eICV) for each subject, as described in Buckner et al. (2004). Since direct quality control of ICV segmentations is not attainable in this framework (due to lack of available segmentation masks), we assessed the quality of our eICV data by testing the Pearson's correlations between **A)** eICV and total brain volume (i.e., the "brain segmentation

volume" label in FreeSurfer: volume of all voxels that are not background / brain stem) and **B)** eICV and fronto-occipital head circumference, which was determined by our team using standardized tape measurement in $N = 23$ 3q29Del subjects. Consistent with previous literature (Hshieh et al., 2016; Wolf et al., 2003 and others), these variables showed a significant positive correlation with eICV in our 3q29Del dataset, with moderate to strong correlation coefficients (p-values ≤ 0.05), providing an indirect metric for quality control. Note that visual inspection of the alignments from which eICV values were calculated did not reveal any errors. *Abbreviations*: 3q29 deletion syndrome, 3q29Del.

Buckner RL, Head D, Parker J, Fotenos AF, Marcus D, Morris JC, et al. (2004): A unified approach for morphometric and functional data analysis in young, old, and demented adults using automated atlas-based head size normalization: reliability and validation against manual measurement of total intracranial volume. *Neuroimage*. 23:724-738.

Hshieh TT, Fox ML, Kosar CM, Cavallari M, Guttmann CR, Alsop D, et al. (2016): Head circumference as a useful surrogate for intracranial volume in older adults. *Int Psychogeriatr*. 28:157-162.

Wolf H, Kruggel F, Hensel A, Wahlund LO, Arendt T, Gertz HJ (2003): The relationship between head size and intracranial volume in elderly subjects. *Brain Res*. 973:74-80.

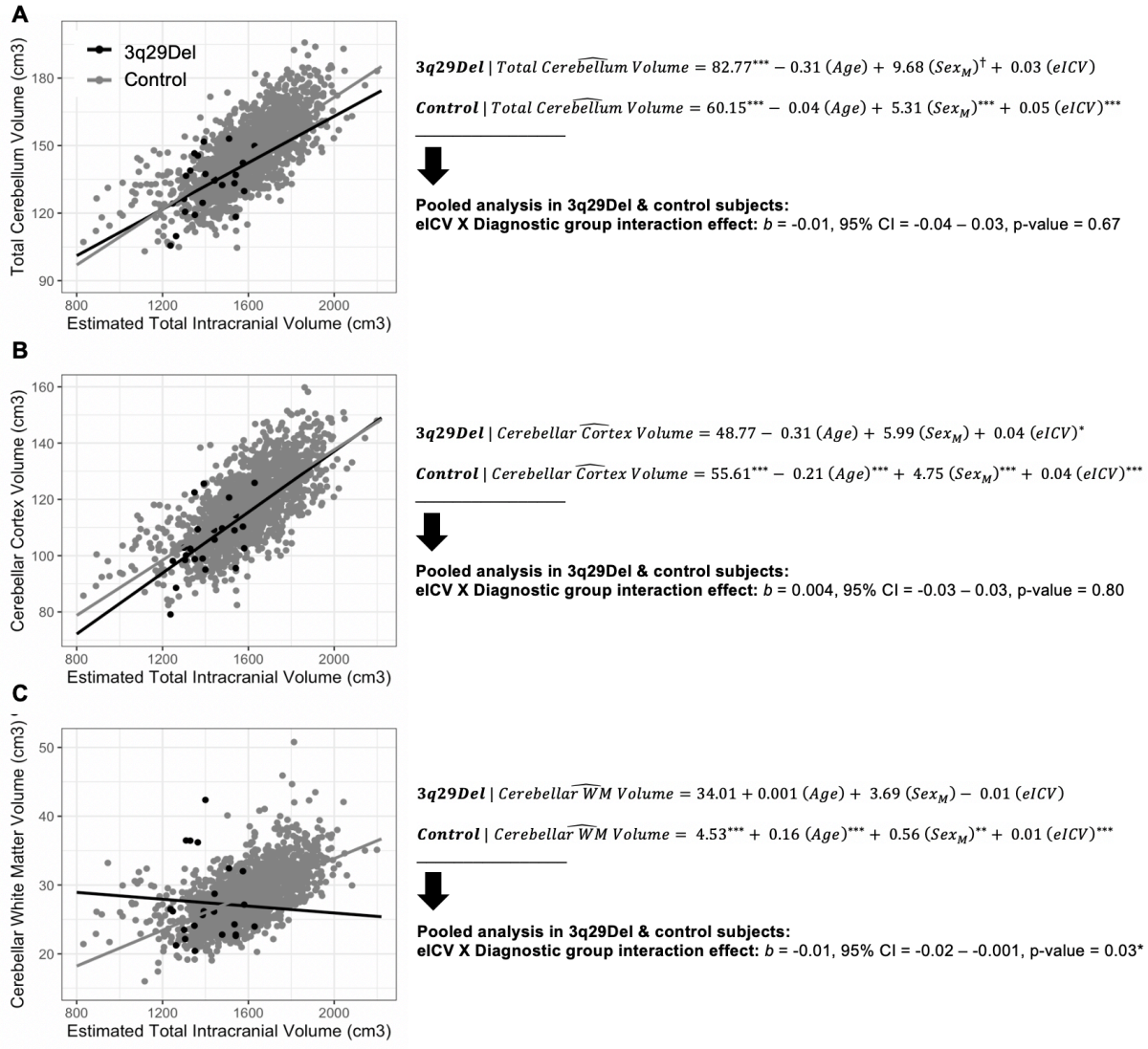

Figure S3. Relationships between eICV and A) total cerebellum, B) cerebellar cortex, and C) cerebellar white matter volumes among 3q29Del subjects versus controls. The grey and black lines represent the estimated linear regression lines for control and 3q29Del groups, respectively. Corresponding multiple linear regression equations for each outcome, with age and sex added as covariates, are provided on the right. Four out of six group-specific intercepts were significantly different from zero (p's ≤ 0.05), indicating that the data do not meet the assumptions for using the "proportion method" for head size adjustment. When 3q29Del and control data were pooled, a significant interaction effect was identified between eICV and diagnostic group on cerebellar white matter volumes, while correcting for age and sex ($p \leq 0.05$), with a significant positive slope

observed among controls ($b = 0.01, p \leq 0.05$) and a negative but not significant slope observed among 3q29Del subjects ($b = -0.01, p > 0.05$). These inhomogeneous regression slopes, along with non-zero intercept tests support the implementation of the "residual method" as a more statistically appropriate approach to the eICV-adjustment of cerebellar volumes in downstream analyses. Refer to Mathalon et al. (1993), O'Brien et al. (2011) and Voevodskaya et al. (2014) for details on statistical considerations for head size adjustment. 3q29Del N = 23, Control N = 1,608. Contrast coding: reference level for the sex variable in regression models is female. p-value ≤ 0.001 '***', p-value ≤ 0.01 '**', p-value ≤ 0.05 '*', p-value ≤ 0.1 '†'. *Abbreviations*: 3q29 deletion syndrome, 3q29Del; unstandardized coefficient estimate*, b*; confidence interval*,* CI; white matter, WM; estimated total intracranial volume, eICV; male, M.

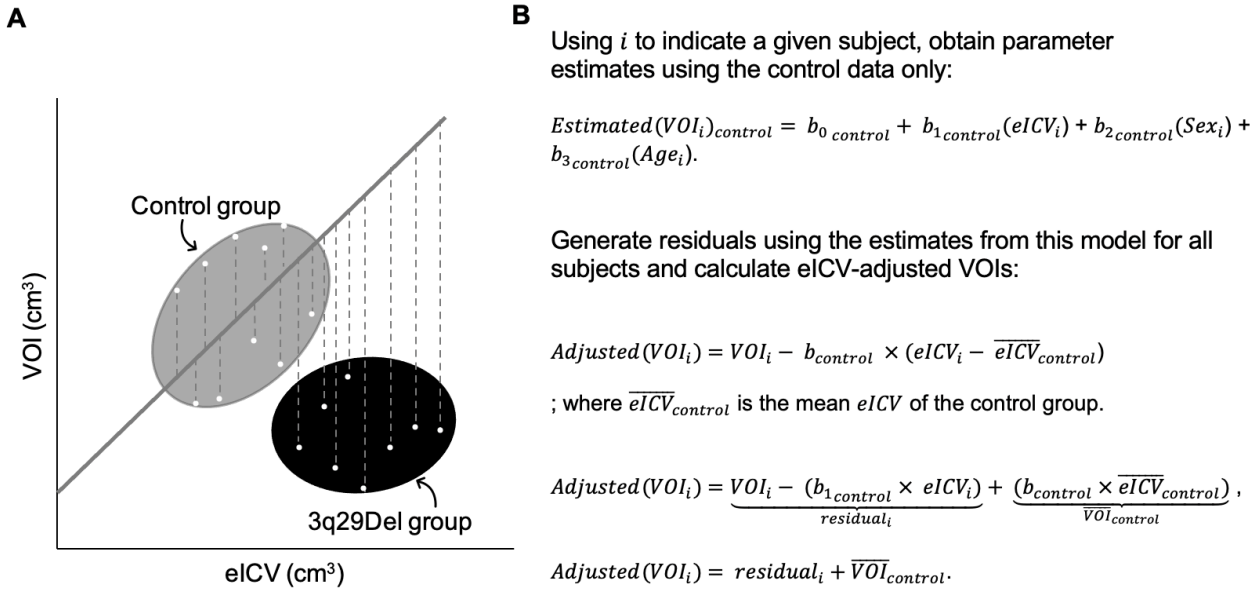

Figure S4. Correction of cerebellar volumes for head size variation in volumetric case-control analyses. Absolute cerebellar volumes were adjusted for eICV using the residual method for head size correction (statistical justification for methodology is outlined in Fig. S3). **A)** A schematic illustration of the residual method for calculating eICV-adjusted VOIs, modified from O'Brien et al. (2011). The gray and black ellipses denote illustrative scatterplots for control and 3q29Del groups, respectively. The solid gray line represents a least-square derived linear regression between eICV and a given VOI, computed based on data from the control group only. Dashed vertical lines illustrate a sample of residuals calculated from this regression line for both control and 3q29Del subjects. **B)** Formulas used for calculating eICV-adjusted VOIs based on the residual approach (disregarding error). We assume that the regression slope, *b1* represents the normative relationship between eICV and cerebellar volumes and that this relationship is not necessarily sustained in the 3q29Del group. Using the residual approach, we regress the VOI of healthy controls on the eICV of healthy controls, including age and sex as covariates, and use the estimates obtained from this linear regression model to calculate residuals for all subjects from both diagnostic groups. Hence, each residual represents the deviation of a given subject's observed VOI from what would be expected of a control subject with the same eICV. Previous work has shown that the residual method is generally robust to systematic and random errors in MRI datasets

(Sanfilipo et al., 2004), which provides advantages for detecting true group differences in combined datasets. Refer to Mathalon et al. (1993), O'Brien et al. (2011) and Voevodskaya et al. (2014) for details on statistical considerations for head size adjustment. *Abbreviations*: 3q29 deletion syndrome, 3q29Del; estimated total intracranial volume, eICV; volumetric measure of interest, VOI.

Mathalon DH, Sullivan EV, Rawles JM, Pfefferbaum A (1993): Correction for head size in brain-imaging measurements. *Psychiatry Res*. 50:121-139.

O'Brien LM, Ziegler DA, Deutsch CK, Frazier JA, Herbert MR, Locascio JJ (2011): Statistical adjustments for brain size in volumetric neuroimaging studies: some practical implications in methods. *Psychiatry Res*. 193:113-122.

Sanfilipo MP, Benedict RH, Zivadinov R, Bakshi R (2004): Correction for intracranial volume in analysis of whole brain atrophy in multiple sclerosis: the proportion vs. residual method. *Neuroimage*. 22:1732-1743.

Voevodskaya O, Simmons A, Nordenskjold R, Kullberg J, Ahlstrom H, Lind L, et al. (2014): The effects of intracranial volume adjustment approaches on multiple regional MRI volumes in healthy aging and Alzheimer's disease. *Front Aging Neurosci*. 6:264.

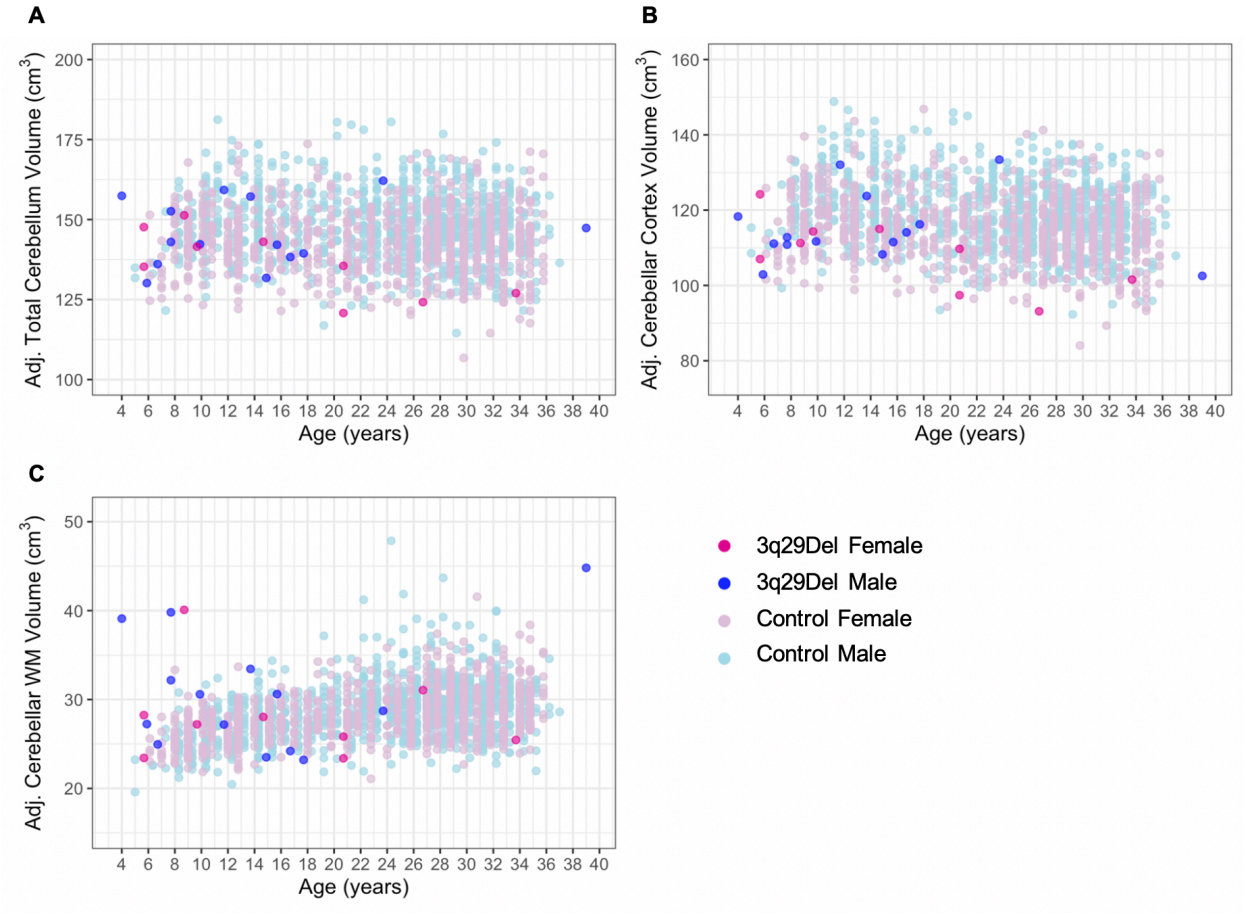

Figure S5. Scatter plots showing the distribution of eICV-adjusted A) total cerebellum volume, B) cerebellar cortex volume, and C) cerebellar white matter volume as a function of age among male and female subjects in each diagnostic group. A slight jitter was added systematically to all panels to minimize overplotting. Control *N* = 1,608 (Female *N* = 861, Male *N* = 747)**,** 3q29Del *N* = 23 (Female *N* = 9, Male *N* = 14). *Abbreviations*: 3q29 deletion syndrome, 3q29Del; adjusted for estimated total intracranial volume, adj.; white matter, WM.

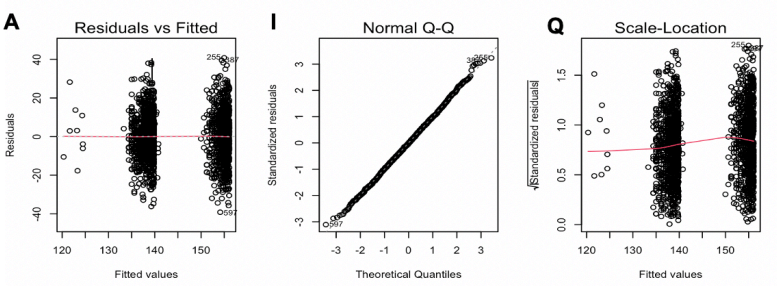

VOI: Absolute Total Cerebellum Volume
Best fit: Model 2 (refer to Table S3A)

Shapiro-Wilk test: W = 1.00, p-value = 0.80
Studentized Breusch-Pagan test: BP = 13.19, p-value = 0.01**.

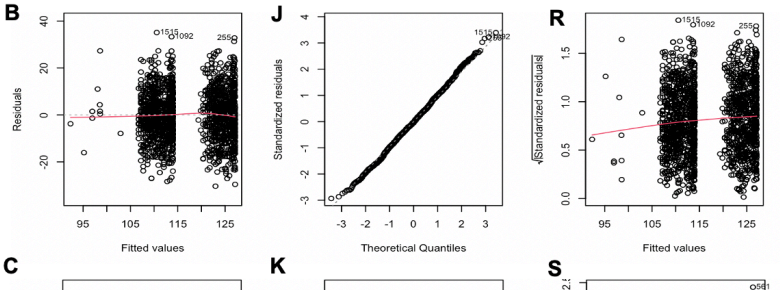

VOI: Absolute Cerebellar Cortex Volume
Best fit: Model 2 (refer to Table S3B)

Shapiro-Wilk test: W = 1.00, p-value = 0.30
Studentized Breusch-Pagan test: BP = 11.05, p-value = 0.03*.

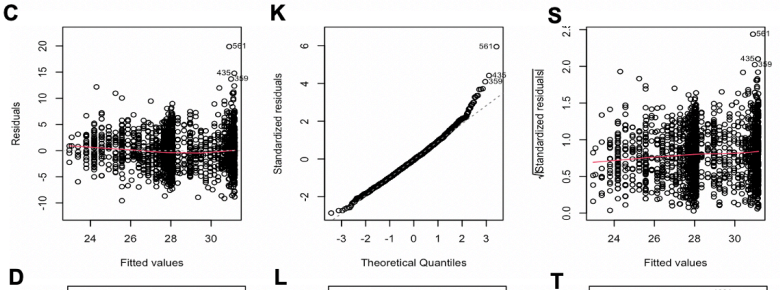

VOI: Absolute Cerebellar White Matter Volume
Best fit: Model 2 (refer to Table S3C)

Shapiro-Wilk test: W = 0.99, p-value = 2.15E-11***
Studentized Breusch-Pagan test: BP = 71.94, p-value = 8.85E-15***.

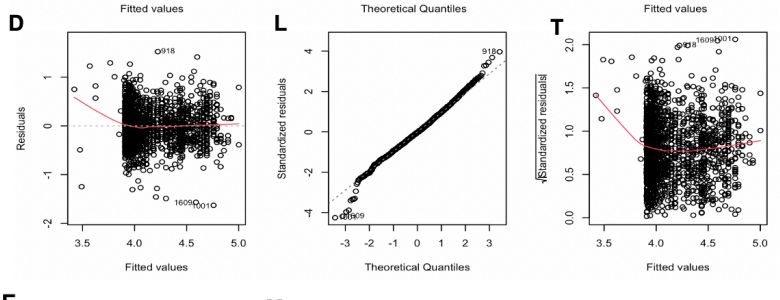

VOI: Cerebellar Cortex to Cerebellar White Matter Volume Ratio
Best fit: Model 2 (refer to Table S3D)

Shapiro-Wilk test: W = 0.99, p-value = 1.09E-06***
Studentized Breusch-Pagan test: BP = 180.9, p-value < 2.2E-16***.

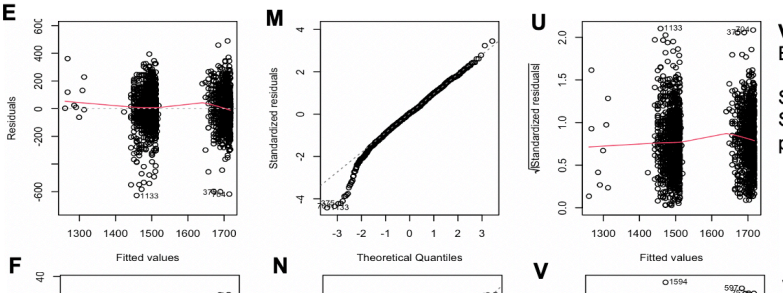

VOI: eICV
Best fit: Model 2 (refer to Table S3E)

Shapiro-Wilk test: W = 0.98, p-value = 1.66E-12***
Studentized Breusch-Pagan test: BP = 16.01, p-value = 3.00E-03**.

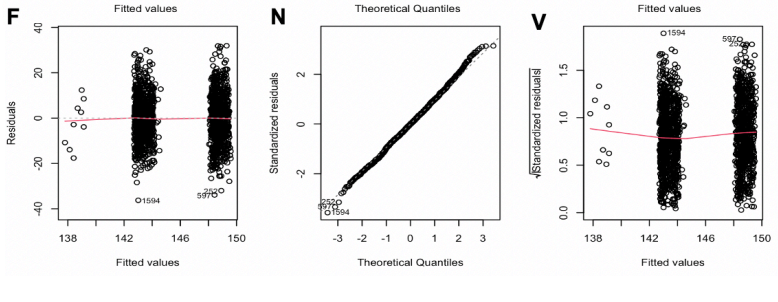

VOI: eICV-Adjusted Total Cerebellum Volume
Best fit: Model 1 (refer to Table S3F)

Shapiro-Wilk test: W = 1.00, p-value = 0.26
Studentized Breusch-Pagan test: BP = 12.86, p-value = 4.95E-03**.

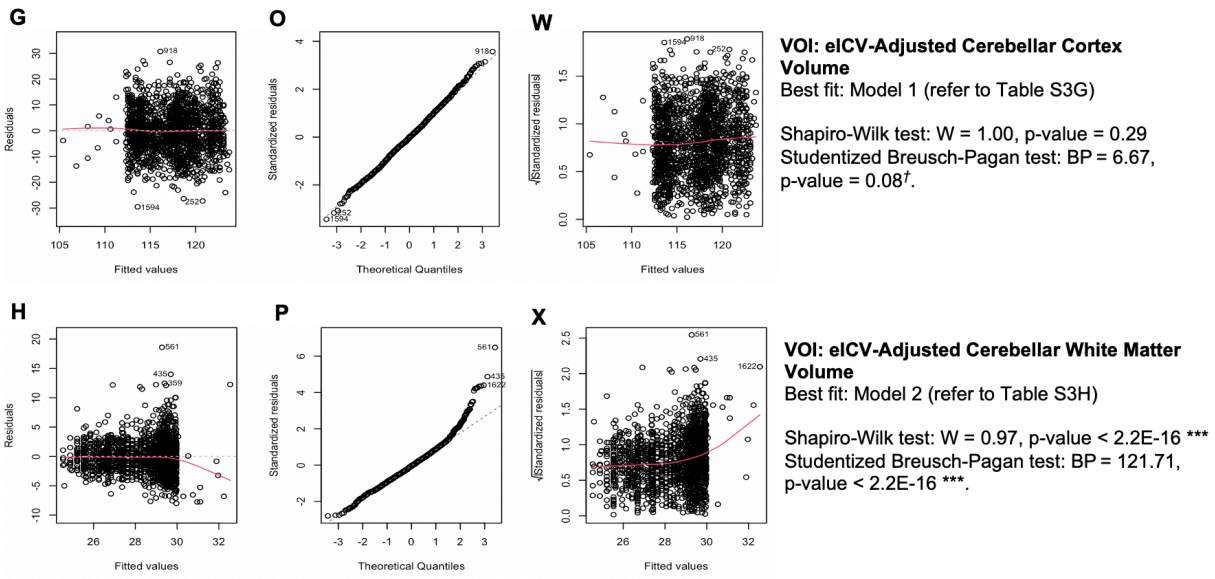

Figure S6. Regression diagnostics: testing the assumptions of ordinary least squares regression for best-fitting models from Table S3. A-H) Plots of residuals versus predicted values for checking the assumptions of linearity and homoscedasticity in multiple linear regression. The residuals should appear approximately linear and be evenly spread around the red *y = 0* line (i.e., slope & y-intercept = 0) to assume a linear relationship between the predictors and the outcome variables and to assume homoscedasticity. **I-P)** QQ-plots of residuals for checking the normality assumption. The normal probability plot of residuals should approximately follow a 45-degree straight line to indicate that all errors are normally distributed around zero. Shapiro-Wilk normality tests were performed to additionally check that the residuals are normally distributed. **Q-X)** Scale-location plots for checking the homoscedasticity assumption. Standardized residuals reflect residuals divided by estimated standard error. Variance of the errors should be approximately the same for any combination of values of the independent variables. Studentized Breusch-Pagan tests were performed to additionally check for homoscedasticity. Given several observed violations of necessary linear regression assumptions, we calculated heteroscedasticity-robust estimates for final inferences. p-value ≤ 0.001 '***', p-value ≤ 0.01 '**', p-value ≤ 0.05 '*', p-value ≤ 0.1 '†'. *Abbreviations*: volumetric measure of interest, VOI; estimated total intracranial volume, eICV.

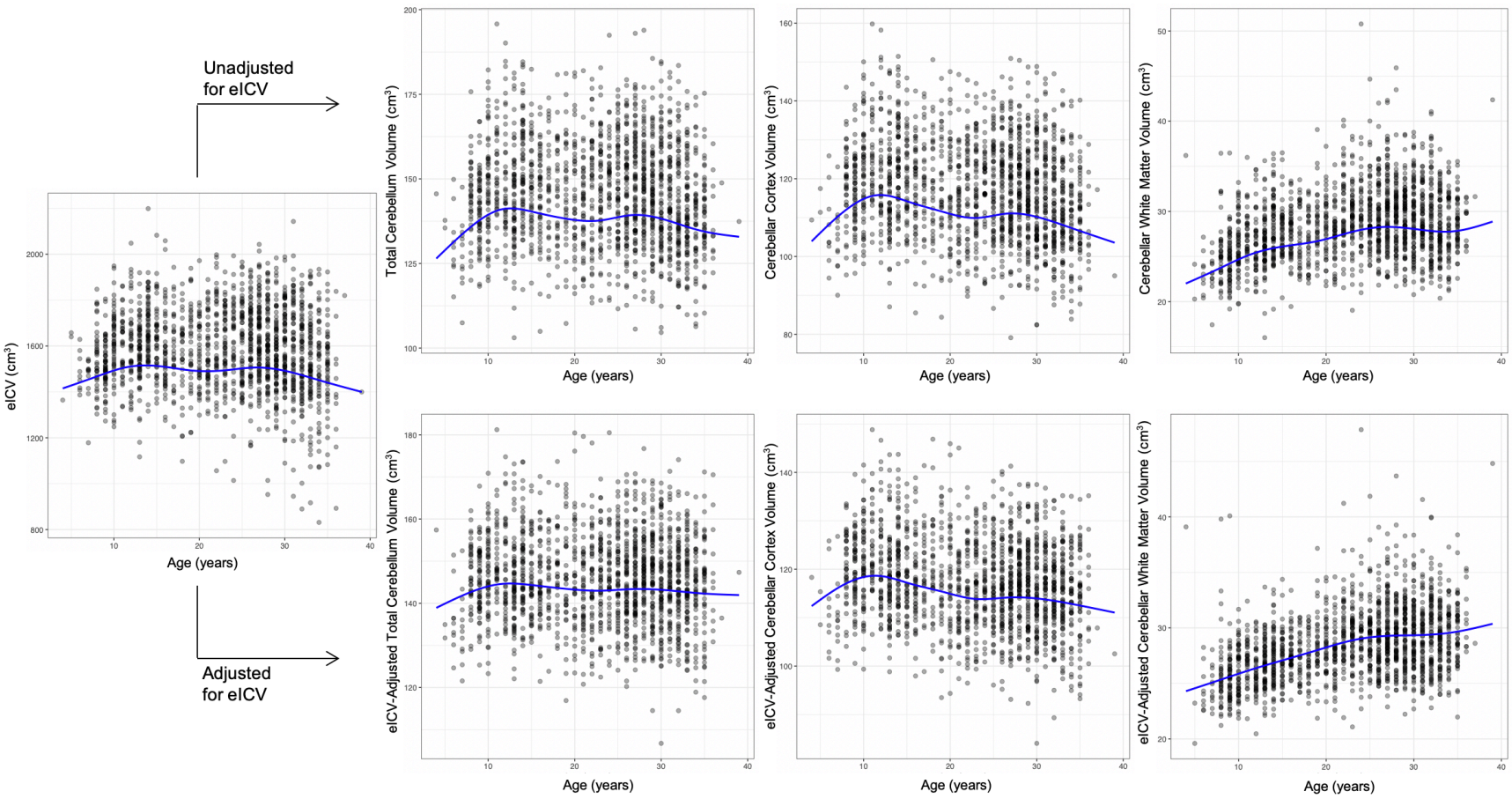

Figure S7. Developmental trajectories for volumetric measures of interest estimated by the penalized cubic spline approach. Each dot represents volumetric data for a single study subject. Blue solid lines represent the estimated mean volumes. An indicator of sex (male / female), an indicator of diagnostic group (3q29Del / healthy control) and a spline term of age were included in each generalized additive model (GAM). Control *N* = 1,608**,** 3q29Del *N* = 23. *Abbreviations*: 3q29 deletion syndrome, 3q29Del; estimated total intracranial volume, eICV.

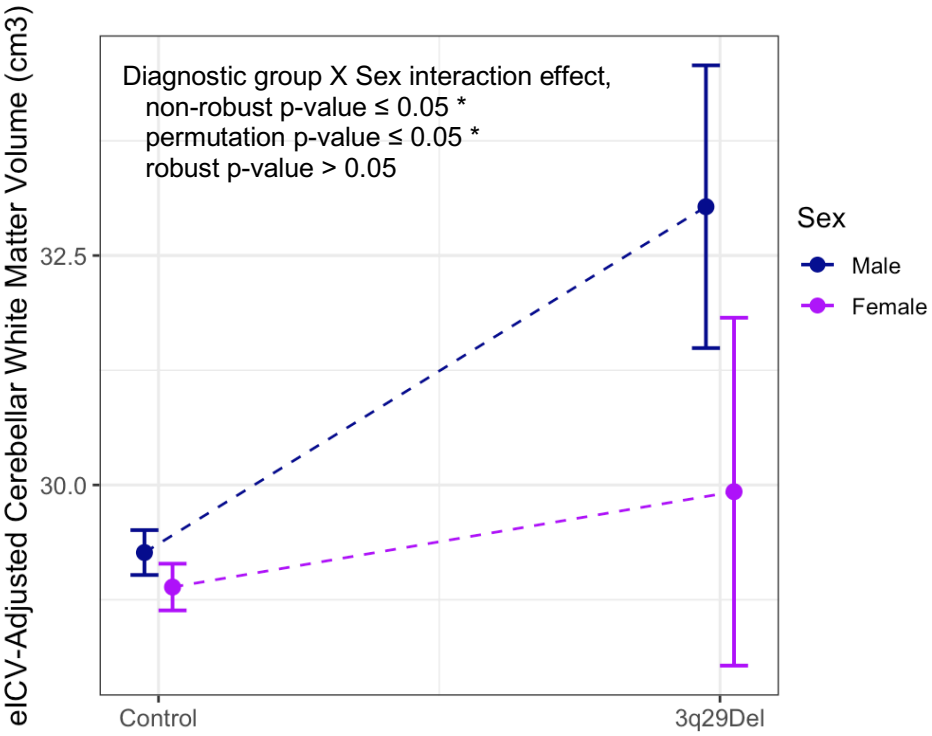

Figure S8. Predictor effect plot showing a suggestive interaction effect between diagnostic group and sex on eICV-adjusted cerebellar white matter volumes. Predicted values of eICV-adjusted cerebellar white matter volume across male versus female 3q29Del and control groups were computed from the exploratory interaction model reported in Table S5H, while covariates (age, age^2) were held fixed. Error bars indicate the 95% confidence interval. Non-robust OLS estimates, and permutation testing from Table S5H suggested a diagnostic group by sex interaction effect on eICV-adjusted cerebellar white matter volumes (non-robust $p \leq 0.05$, permutation $p \leq 0.05$), however this effect was not significant ($p > 0.05$) when robust standard error estimates were calculated to account for the heteroskedasticity in the data. We provide a graphic illustration of this finding for visual inspection of underlying trends, but we consider the evidence in favor of this sex-specific effect to be weak. Control N = 1,608 (Female N = 861, Male N = 747), 3q29Del N = 23 (Female N = 9, Male N = 14). p-value ≤ 0.001 '***', p-value ≤ 0.01 '**', p-value ≤ 0.05 '*', p-value ≤ 0.1 '†' *Abbreviations*: 3q29 deletion syndrome, 3q29Del; estimated total intracranial volume, eICV; ordinary least squares, OLS.

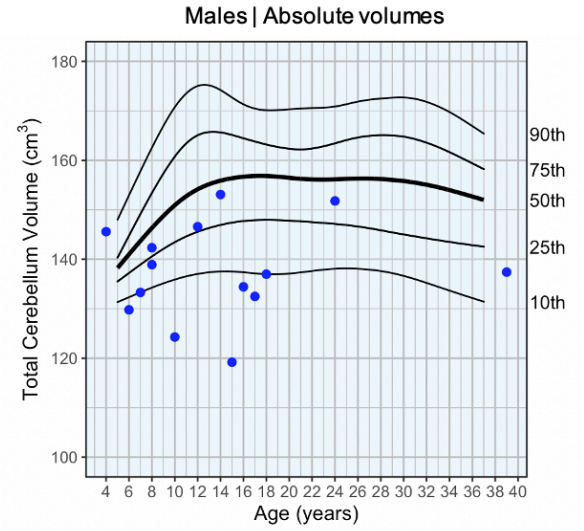
Males | Absolute volumes
Total Cerebellum Volume (cm3)
Age (years)
90th
75th
50th
25th
10th

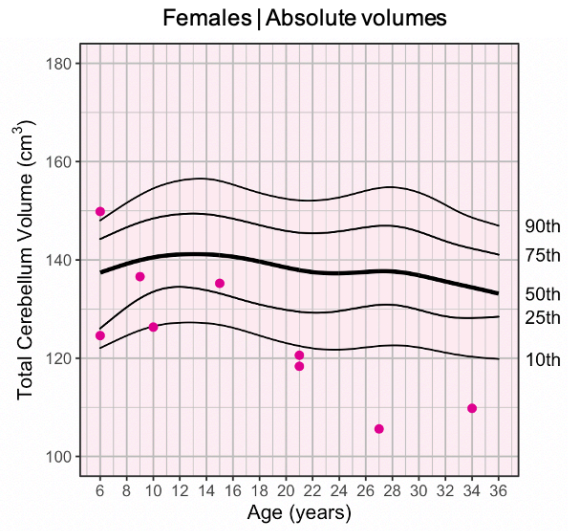
Females | Absolute volumes
Total Cerebellum Volume (cm3)
Age (years)
90th
75th
50th
25th
10th

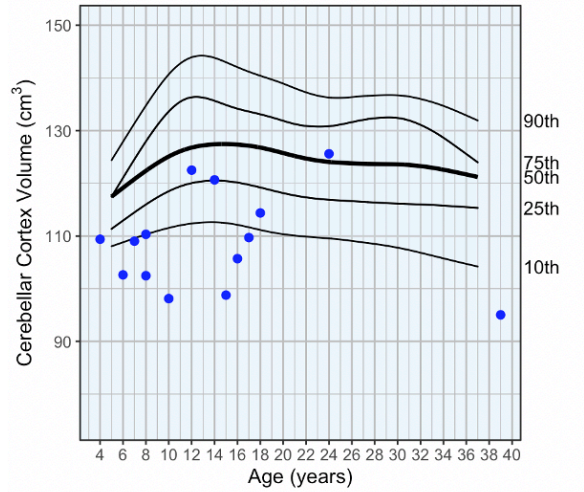
Cerebellar Cortex Volume (cm3)
Age (years)
90th
75th
50th
25th
10th

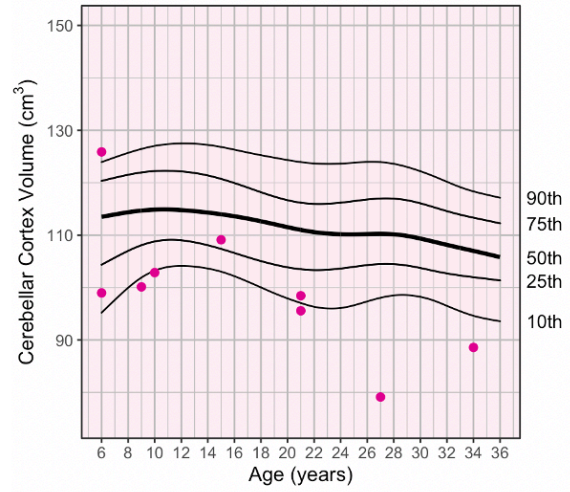
Cerebellar Cortex Volume (cm3)
Age (years)
90th
75th
50th
25th
10th

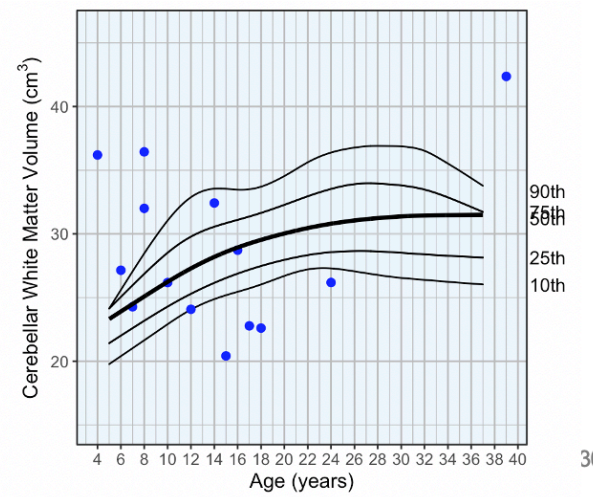
Cerebellar White Matter Volume (cm3)
Age (years)
90th
50th
25th
10th

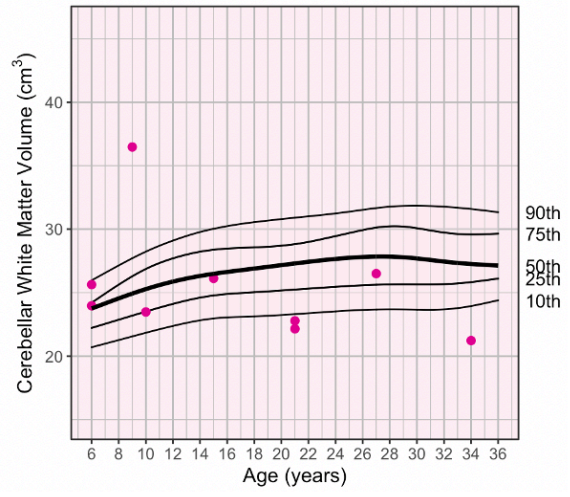
Cerebellar White Matter Volume (cm3)
Age (years)
90th
75th
50th
25th
10th

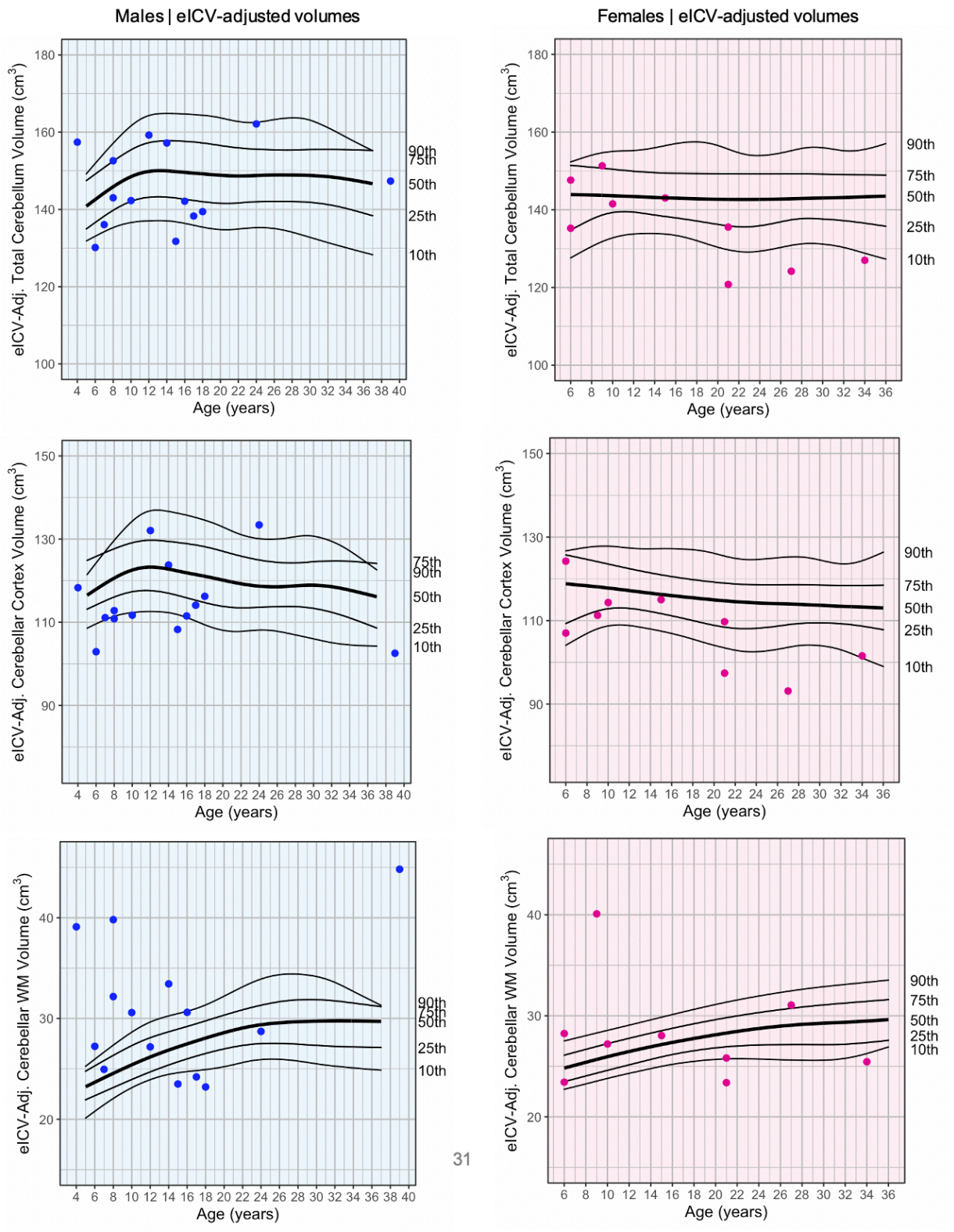
Males | eICV-adjusted volumes
Females | eICV-adjusted volumes
eICV-Adj. Total Cerebellum Volume (cm3)
eICV-Adj. Cerebellar Cortex Volume (cm3)
eICV-Adj. Cerebellar WM Volume (cm3)
Age (years)
90th
75th
50th
25th
10th

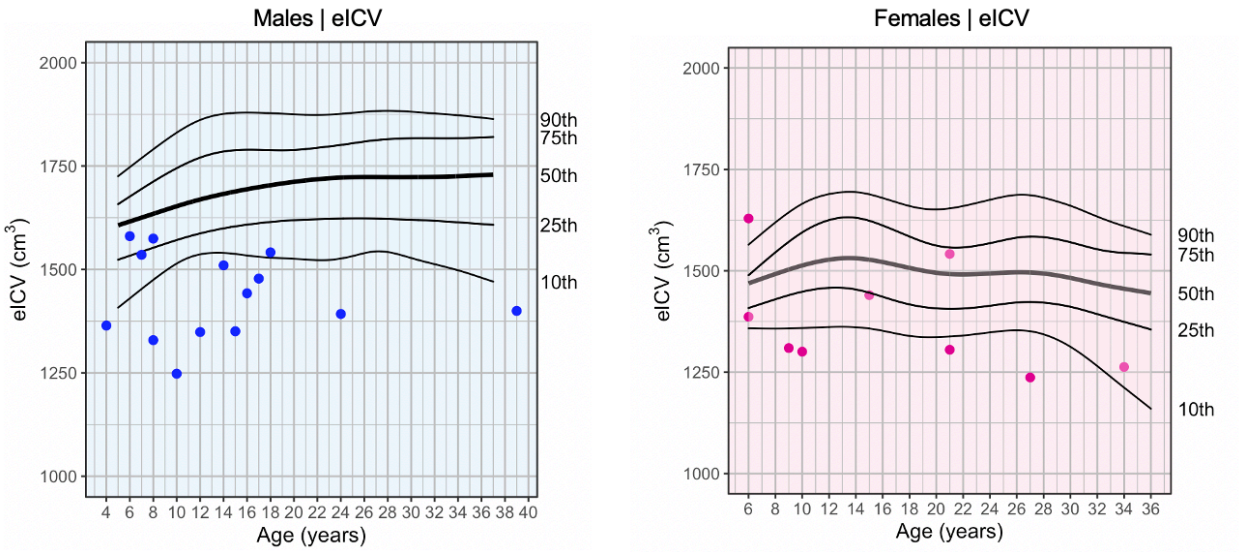

Figure S9. Estimated normative percentile curves for cerebellar volumes and eICV, stratified by sex. Black solid lines represent the 10th, 25th, 50th (median, thicker), 75th, and 90th percentiles estimated by fitting quantile splines to volumetric data from *N* = 861 female healthy controls and *N* = 747 male healthy controls, separately. Pink dots represent data points for *N* = *9* 3q29Del female subjects *and* blue dots represent data points for *N* = *14* 3q29Del male subjects, whose volumetric measures are being compared to sex-stratified reference percentiles in healthy controls. A spline term of age was included as a covariate in each quantile spline model, as described by Oh et al. (2004). Due to the relative sparsity of volumetric data at the youngest and oldest endpoints of the age range covered in the present study, slight overlaps are observed in percentile bands. *Abbreviations*: 3q29 deletion syndrome, 3q29Del; estimated total intracranial volume, eICV; adjusted, adj.

Oh HS, Nychka D, Brown T, Charbonneau P (2004): Period analysis of variable stars by robust smoothing. *Journal of the Royal Statistical Society: Series C (Applied Statistics). 53*(1):15-30.

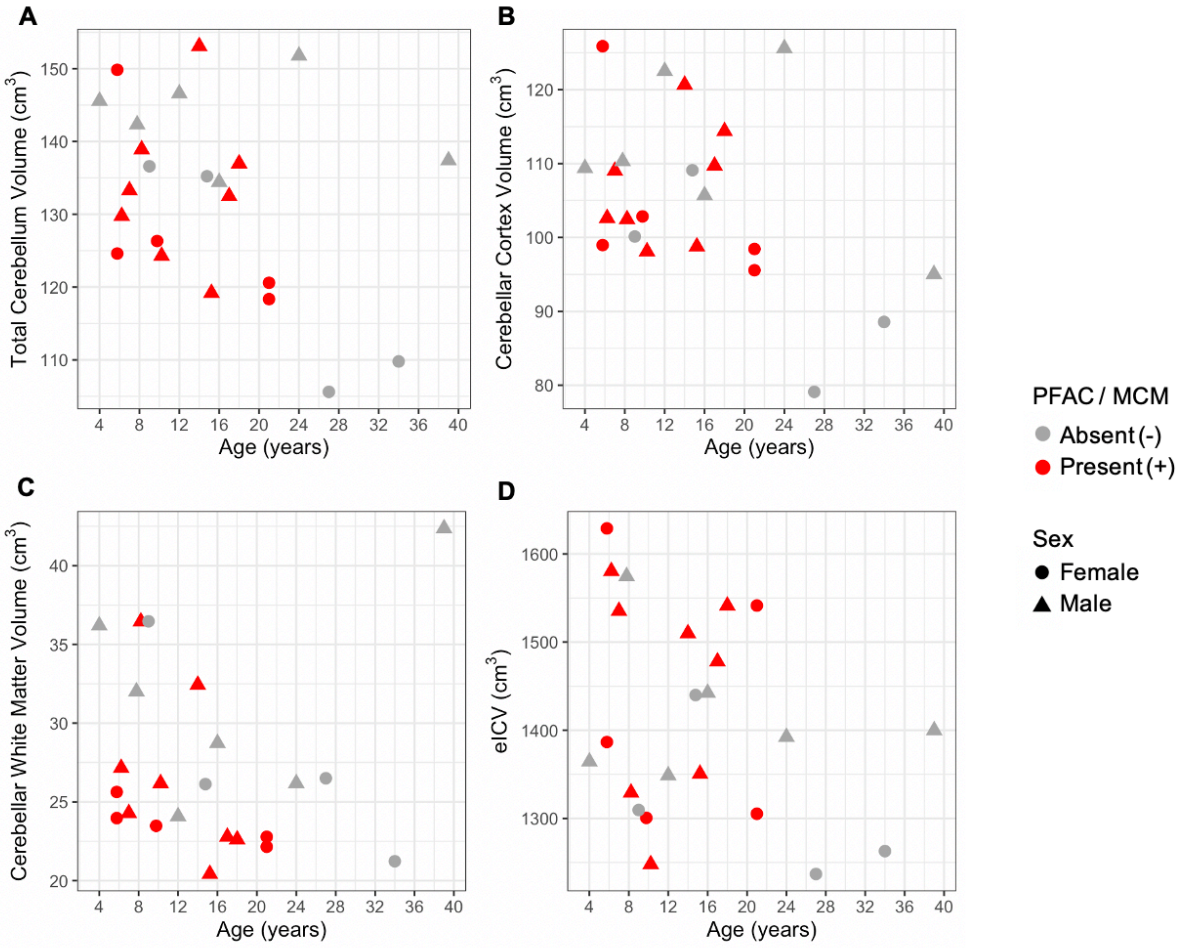

Figure S10. Scatter plots showing the distribution of A) total cerebellum volume, B) cerebellar cortex volume, C) cerebellar white matter volume, and D) eICV as a function of age among 3q29Del subjects with versus without posterior fossa arachnoid cyst or mega cisterna magna findings. A slight jitter was added systematically to all panels to minimize overplotting. 3q29Del N = 23 (Female N = 9, Male N = 14). *Abbreviations*: 3q29 deletion syndrome, 3q29Del; estimated total intracranial volume, eICV; posterior fossa arachnoid cyst, PFAC; mega cisterna magna, MCM.

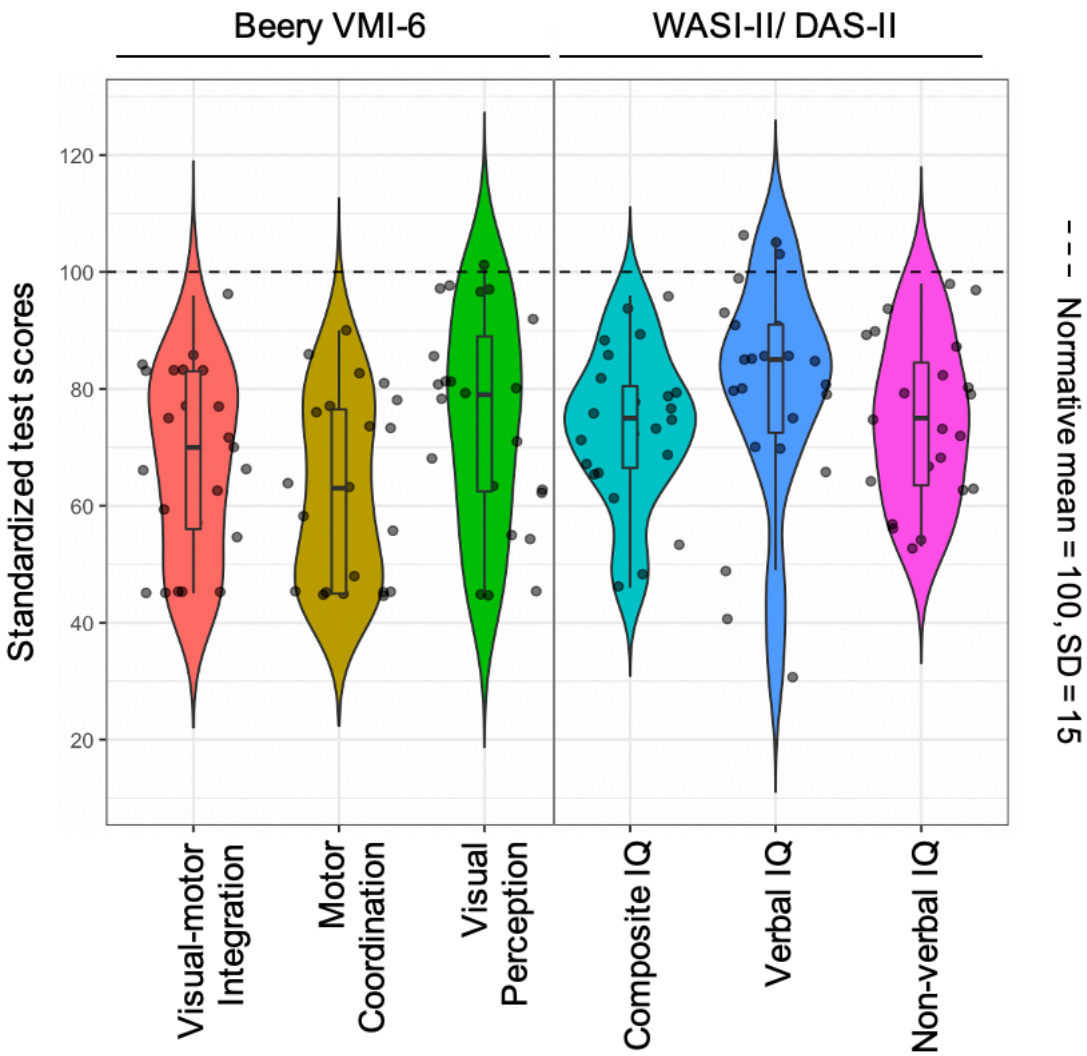

Figure S11. Violin plots with box plots visualizing the distribution of standardized test scores for sensorimotor and cognitive abilities among 3q29Del subjects. Violin plots represent the distribution of standardized test scores (normative mean = 100, SD = 15) for visual-motor integration, motor coordination and visual perception skills measured by the Beery-Buktenica Developmental Test of VMI, and for composite, verbal and non-verbal IQ scores measured by the WASI / DAS. Boxplots visualize the five-number summary statistics for each measure (minimum, lower quartile, median, upper quartile and maximum). Higher scores indicate better performance. 3q29Del *N* = 23. *Abbreviations*: 3q29 deletion syndrome, 3q29Del; intelligence quotient, IQ; Wechsler Abbreviated Scale of Intelligence, WASI; Differential Ability Scales, DAS; visual-motor integration, VMI; standard deviation, SD.

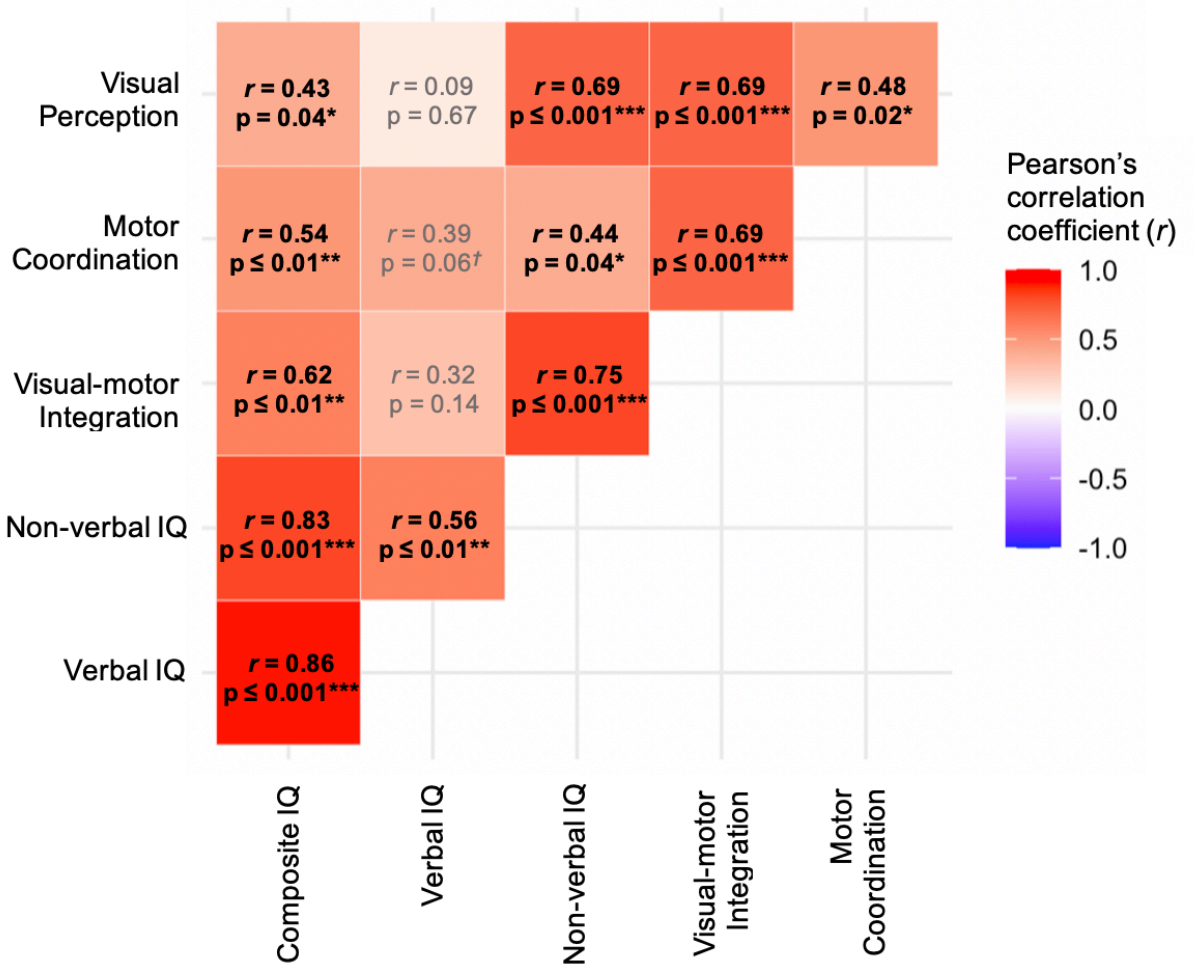

Figure S12. Heatmap visualization of pairwise Pearson's correlations between standardized test scores for sensorimotor and cognitive abilities among 3q29Del subjects. We assessed the pairwise Pearson's correlations among all behavioral measures to determine the extent to which our findings may be interrelated. In the 3q29Del sample, composite IQ, verbal IQ and non-verbal IQ scores were significantly correlated with one another (*p's* ≤ 0.01, moderate-very strong). Similarly, visual-motor integration, motor coordination, and visual perception scores showed significant pairwise correlations with each other (*p's* ≤ 0.05, moderate-strong). Composite IQ scores had significant correlations with visual-motor integration (*p* ≤ 0.01, strong), motor coordination (*p* ≤ 0.01, moderate), and visual perception scores (*p* ≤ 0.05, moderate), which were largely driven by significant correlations observed between non-verbal IQ and motor coordination scores (*p* ≤ 0.05, moderate) and between non-verbal IQ and visual perception scores (*p* ≤ 0.001, strong). Verbal IQ scores did not correlate

significantly with visual-motor integration, motor coordination, or visual perception scores (*p's* > 0.05, very weak-weak). All correlation coefficients (*r*) were positive. Significant test results (*p's* ≤ 0.05) are reported in bold for clarity. The strength of the computed correlation coefficients was evaluated based on the following criteria: $|r|$ = 0 – 0.19, very weak; $|r|$ = 0.20 – 0.39, weak; $|r|$ = 0.40 – 0.59, moderate; $|r|$ = 0.60 – 0.79, strong; $|r|$ = 0.80 – 1, very strong. 3q29Del N = 23. p-value ≤ 0.001 '***', p-value ≤ 0.01 '**', p-value ≤ 0.05 '*', p-value ≤ 0.1 '†'. *Abbreviations*: 3q29 deletion syndrome, 3q29Del; IQ, intelligence quotient.

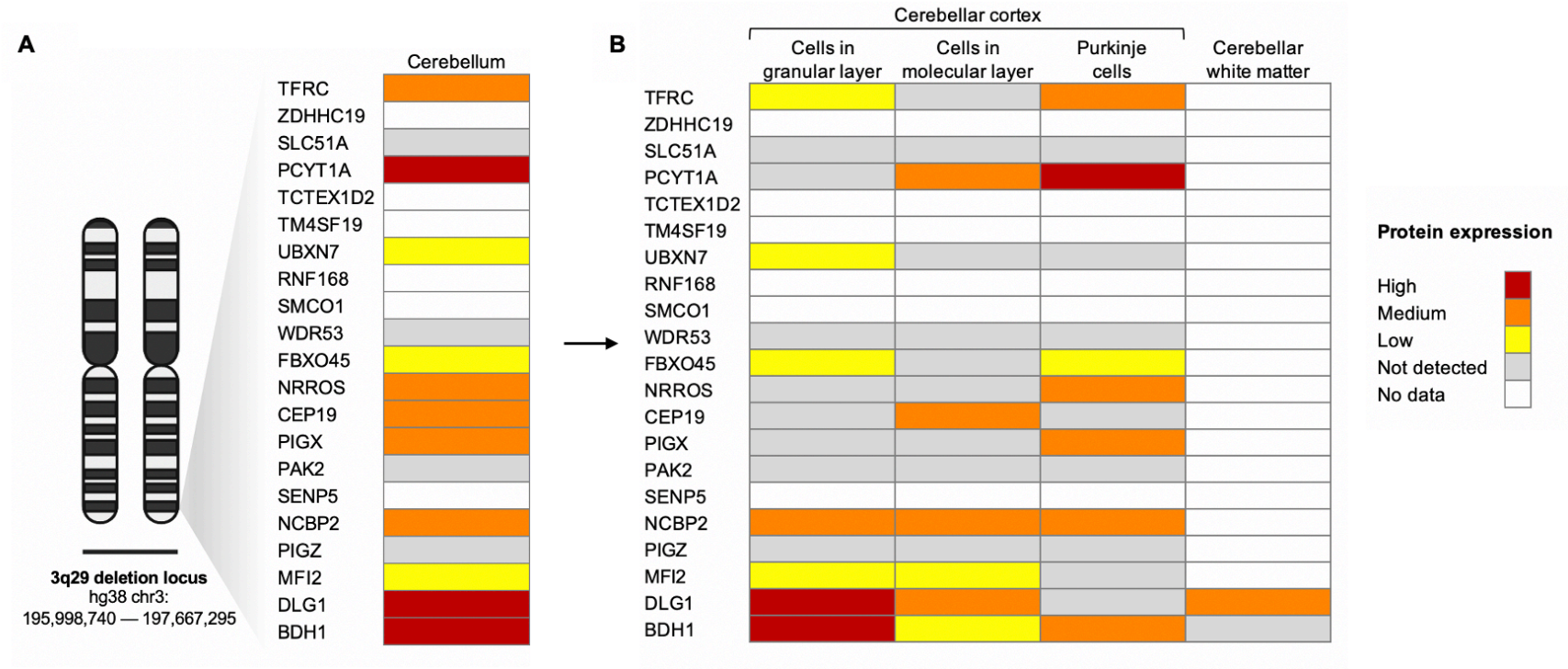

Figure S13. Cerebellar protein expression profiles of 3q29 interval genes annotated by the Human Protein Atlas. In **A)** protein expression profiles of 21 protein coding genes located in the 3q29 interval are provided for the human cerebellum. In **B)** protein expression profiles of 3q29 interval genes are provided for annotated cerebellar subregions, using the same units. All annotations were obtained from the Human Protein Atlas (version 20.1) and were established by evaluation of immunohistochemical staining patterns, RNA-sequencing data, and available protein/gene characterization data, as described by Uhlen et al. (2010 & 2015). Protein expression profiles were characterized in normal human tissues as "High", "Medium", "Low" or "Not detected". The "No data" category indicates that there was no available protein expression information on the Human Protein Atlas for a given query. Note that, for FBXO45, RNA-based expert annotation could not be performed by the Human Protein Atlas due to inconclusive results (query date: 10.02.2021); hence the protein expression profile provided for this gene relies on immunohistochemistry findings only. The data visualized in this figure can be accessed via http://www.proteinatlas.org.

Uhlen M, Oksvold P, Fagerberg L, et al. (2010): Towards a knowledge-based human protein atlas. *Nature Biotechnology*. *28*(12):1248-1250.

Uhlen M, Fagerberg L, Hallström BM, et al. (2015): Tissue-based map of the human proteome. *Science*. 347(6220).

Supplemental References

Ali ZS, Lang SS, Bakar D, Storm PB, Stein SC (2014): Pediatric intracranial arachnoid cysts: comparative effectiveness of surgical treatment options. *Childs Nerv Syst*. 30:461-469.

Bosemani T, Orman G, Boltshauser E, Tekes A, Huisman TA, Poretti A (2015): Congenital abnormalities of the posterior fossa. *Radiographics*. 35:200-220.

Buckner RL, Head D, Parker J, Fotenos AF, Marcus D, Morris JC, et al. (2004): A unified approach for morphometric and functional data analysis in young, old, and demented adults using automated atlas-based head size normalization: reliability and validation against manual measurement of total intracranial volume. *Neuroimage*. 23:724-738.

Cornips EM, Overvliet GM, Weber JW, Postma AA, Hoeberigs CM, Baldewijns MM, et al. (2010): The clinical spectrum of Blake's pouch cyst: report of six illustrative cases. *Childs Nerv Syst*. 26:1057-1064.

Dewey J, Hana G, Russell T, Price J, McCaffrey D, Harezlak J, et al. (2010): Reliability and validity of MRI-based automated volumetry software relative to auto-assisted manual measurement of subcortical structures in HIV-infected patients from a multisite study. *Neuroimage*. 51:1334-1344.

Doherty D, Millen KJ, Barkovich AJ (2013): Midbrain and hindbrain malformations: advances in clinical diagnosis, imaging, and genetics. *Lancet Neurol*. 12:381-393.

Eilers PH, Marx BD (1996): Flexible smoothing with B-splines and penalties. *Statistical science*. 11(2):89-121.

Elam JS, Glasser MF, Harms MP, Sotiropoulos SN, Andersson JLR, Burgess GC, et al. (2021): The Human Connectome Project: A retrospective. *Neuroimage*. 244:118543.

Fischl B, Salat DH, Busa E, Albert M, Dieterich M, Haselgrove C, et al. (2002): Whole brain segmentation: automated labeling of neuroanatomical structures in the human brain. *Neuron*. 33:341-355.

Graven P (1989): Smoothing noisy data with spline function: estimating the correct degree of smoothing by the method of generalized cross-validatIon. *Number. Math*. 31:377-403.

Kollias SS, Ball WS, Jr., Prenger EC (1993): Cystic malformations of the posterior fossa: differential diagnosis clarified through embryologic analysis. *Radiographics*. 13:1211-1231.

Koyabu D, Werneburg I, Morimoto N, Zollikofer CP, Forasiepi AM, Endo H, et al. (2014): Mammalian skull heterochrony reveals modular evolution and a link between cranial development and brain size. *Nature communications*. 5:1-9.

Lee DK, Yoon U, Kwak K, Lee JM (2015): Automated Segmentation of Cerebellum Using Brain Mask and Partial Volume Estimation Map. *Comput Math Methods Med*. 2015:167489.

Limperopoulos C, Robertson RL, Estroff JA, Barnewolt C, Levine D, Bassan H, et al. (2006): Diagnosis of inferior vermian hypoplasia by fetal magnetic resonance imaging: potential pitfalls and neurodevelopmental outcome. *Am J Obstet Gynecol*. 194:1070-1076.

Marcus DS, Harms MP, Snyder AZ, Jenkinson M, Wilson JA, Glasser MF, et al. (2013): Human Connectome Project informatics: quality control, database services, and data visualization. *Neuroimage*. 80:202-219.

Marin-Sanabria EA, Yamamoto H, Nagashima T, Kohmura E (2007): Evaluation of the management of arachnoid cyst of the posterior fossa in pediatric population: experience over 27 years. *Childs Nerv Syst*. 23:535-542.

Mayer KN, Latal B, Knirsch W, Scheer I, von Rhein M, Reich B, et al. (2016): Comparison of automated brain volumetry methods with stereology in children aged 2 to 3 years. *Neuroradiology*. 58:901-910.

McKinney AM (2017): Mega Cisterna Magna and Retrocerebellar Arachnoid Cysts. *Atlas of Normal Imaging Variations of the Brain, Skull, and Craniocervical Vasculature*: Springer, pp 19-41.

Nelson MD, Jr., Maher K, Gilles FH (2004): A different approach to cysts of the posterior fossa. *Pediatr Radiol*. 34:720-732.

Nychka D, Gray G, Haaland P, Martin D, O'connell M (1995): A nonparametric regression approach to syringe grading for quality improvement. *Journal of the American Statistical Association*. 90(432):1171–1178.

Nychka D, Furrer R, Paige J, Sain S (2021): "fields: Tools for spatial data". R package version 12.5, https://github.com/dnychka/fieldsRPackage

Parisi MA, Dobyns WB (2003): Human malformations of the midbrain and hindbrain: review and proposed classification scheme. *Mol Genet Metab*. 80:36-53.

Reinsch CH (1967): Smoothing by spline functions. *Numerische mathematik*. 10(3):177-183.

R Development Core Team (2021): R: A Language and Environment for Statistical Computing. Vienna, Austria: R Foundation for Statistical Computing.

Sanfilipo MP, Benedict RH, Zivadinov R, Bakshi R (2004): Correction for intracranial volume in analysis of whole brain atrophy in multiple sclerosis: the proportion vs. residual method. *Neuroimage*. 22:1732-1743.

Tarui T, Limperopoulos C, Sullivan NR, Robertson RL, du Plessis AJ (2014): Long-term developmental outcome of children with a fetal diagnosis of isolated inferior vermian hypoplasia. *Arch Dis Child Fetal Neonatal Ed*. 99:F54-58.

Tortori-Donati P, Fondelli MP, Rossi A, Carini S (1996): Cystic malformations of the posterior cranial fossa originating from a defect of the posterior membranous area. Mega cisterna magna and persisting Blake's pouch: two separate entities. *Childs Nerv Syst*. 12:303-308.

Wahba G (1980): Spline bases, regularization, and generalized cross validation for solving approximation problems with large quantities of noisy data. University of WISCONSIN.

Wood SN (2011): Fast stable restricted maximum likelihood and marginal likelihood estimation of semiparametric generalized linear models. *Journal of the Royal Statistical Society: Series B (Statistical Methodology)*. 73(1):3-36.

Wood SN (2013): On p-values for smooth components of an extended generalized additive model. *Biometrika*. 100(1), 221-228.

Wood SN (2017): Generalized additive models: an introduction with R. CRC press.

CHAPTER 4. Psychosis spectrum symptoms among individuals with schizophrenia-associated copy number variants and evidence of cerebellar correlates of symptom severity

Esra Sefik, Ryan M. Guest, Katrina Aberizk, Roberto Espana, Katrina Goines, Derek Novacek, Melissa M. Murphy, Adam E. Goldman-Yassen, Joseph F. Cubells, Opal Ousley, Longchuan Li, Sarah Shultz, Elaine F. Walker, Jennifer G. Mulle

Adapted from manuscript currently under review. Preprint citation is provided below:

Sefik E, Guest RM, Aberizk K, Espana R, Goines K, Novacek D, et al. (2022): Psychosis spectrum symptoms among individuals with schizophrenia-associated copy number variants and evidence of cerebellar correlates of symptom severity.
medRxiv.2022.2003.2003.22271848.

Abstract

The 3q29 deletion (3q29Del) is a copy number variant (CNV) with the highest known effect size for psychosis-risk (>40-fold increased risk). Systematic research on this CNV offers promising avenues for identifying mechanisms underlying psychosis and related disorders. Relative to other high-impact CNVs like 22q11.2Del, far less is known about the phenotypic presentation and pathophysiology of 3q29Del. Emerging findings indicate that posterior fossa abnormalities are common among 3q29Del carriers; however, their clinical relevance is unknown. Here, we report the first in-depth evaluation of psychotic symptoms in study participants with 3q29Del (*N* = 23), using the Structured Interview for Psychosis-Risk Syndromes (SIPS), and compare to SIPS data from 22q11.2Del participants (*N* = 31) and healthy controls (*N* = 279). We also investigate the relationship between psychotic symptoms, cerebellar morphology, and cystic/cyst-like malformations of the posterior fossa in 3q29Del by structural brain imaging. Cumulatively, 48% of the 3q29Del sample exhibited a psychotic disorder (N=4) or attenuated positive symptoms (*N* = 7), with three individuals with attenuated symptoms meeting the frequency and timing criteria for clinical high risk for psychosis. Males with 3q29Del scored higher in negative symptoms than females. 3q29Del participants had more severe ratings than controls on all domains and exhibited less severe negative symptoms than 22q11.2Del participants. An inverse relationship was identified between positive symptom severity and cerebellar cortex volume in 3q29Del, while cystic/cyst-like malformations yielded no clinical link with psychosis. Overall, our findings establish the unique and shared profiles of psychotic symptoms across two CNVs and highlight cerebellar involvement in elevated psychosis-risk in 3q29Del.

Introduction

The identification of copy number variants (CNVs) that confer high risk for serious mental illnesses has provided new substrates to investigate the etiology of psychotic disorders. The 3q29 and 22q11.2 deletions (Del) are two CNVs that significantly increase risk for a range of neuropsychiatric disorders, especially schizophrenia and other psychotic disorders (1-12). Thus, systematic research on these CNVs holds promise for shedding light on the neuropathology underlying psychosis.

22q11.2Del is caused by a hemizygous 1.5- to 3.0-Mb deletion involving 45 protein-coding genes. The deletion affects 1 in 2,148-4,000 individuals (13-17) and is estimated to convey a >20-fold increased risk for developing schizophrenia (18, 19). Standardized measures have been used to examine the clinical high risk (CHR) or the "prodromal" symptoms that may precede the onset of psychosis in 22q11.2Del syndrome and the general population. Before the first psychotic episode, typically during late adolescence and early adulthood, individuals often exhibit a period of functional decline coinciding with the emergence of attenuated psychotic symptoms (20-23). Those identified at CHR present with these "warning" signs and are at substantial risk for future psychosis (24). Published reports in 22q11.2Del have shown that about 30-60% of study participants manifest attenuated psychotic symptoms which are known to be linked with elevated risk for subsequent conversion to psychosis (25, 26).

Individuals with 3q29Del are hemizygous for a 1.6-Mb interval containing 21 protein-coding genes. Compared to 22q11.2Del, 3q29Del was only recently identified (27) and is less common, with a prevalence of approximately 1 in 30,000 individuals (10); consequently the associated phenotypes are just now being documented. Like 22q11.2Del, 3q29Del is pleiotropic; it elevates risk for a range of physical and psychiatric disabilities, including low birth weight, failure to thrive, cardiac defects, cognitive deficits, and autism spectrum disorder (9, 28). Current evidence suggests that 3q29Del confers an equal or greater risk for psychosis than 22q11.2Del. Recent reports revealed that the 3q29 deletion confers a >40-fold increased risk for schizophrenia (1, 8, 29). It is not known whether early clinical signs of psychosis risk are elevated among individuals with 3q29Del.

Our team recently documented the neurodevelopmental and psychiatric manifestations associated with

3q29Del (10, 30). 3q29Del individuals participated in in-depth evaluation of psychiatric symptoms and magnetic resonance imaging (MRI). Here, we report detailed results on psychotic symptoms in study participants with 3q29Del, as assessed by the Structured Interview for Psychosis-Risk Syndromes (SIPS) (31, 32). Using this gold-standard instrument, we determined the proportion of 3q29Del participants with attenuated or florid psychotic symptoms and contrasted this with the symptom profile in 22q11.2Del participants and healthy controls (HC).

Next, we asked whether psychosis susceptibility in 3q29Del is associated with morphometric features of the brain measured by structural MRI. Recent radiological findings by our team have revealed that cerebellar hypoplasia and cystic/cyst-like malformations of the posterior fossa, are significantly elevated in 3q29Del (10). Our group has also shown quantitively that study participants with 3q29Del exhibit abnormal cerebellar volumes compared with HCs (33). In the current study, we demonstrate that these neuroanatomical phenotypes may have clinical relevance. This is the first known investigation of the relationship between psychotic symptoms and neuroimaging findings in 3q29Del syndrome and suggests the cerebellum may be a primary site of pathology.

Methods and Materials

Participants

The 3q29Del sample: Twenty-three individuals with 3q29Del, ages 8.08-39.12 (mean ± SD = 16.94 ± 8.24 years) were evaluated using the SIPS (31, 32). Study participants were ascertained from the 3q29 registry (28) and between August 2017-February 2020 traveled to Atlanta, GA for deep phenotyping with gold-standard instruments and MRI. Deletion status was confirmed from the clinical genetics report and/or medical records. The project protocol and a summary of findings have been previously described (10, 30).

Comparison samples: The HC comparison sample included 279 healthy individuals, ages 12.07-34.41 (mean ± SD = 20.08 ± 4.61 years), from the second cohort of the North American Prodromal Longitudinal Study (NAPLS2), who were evaluated with the SIPS between June 2009-October 2012. NAPLS2 is a multi-site

consortium investigating the trajectories of individuals at CHR (34). These HCs chosen for the present analysis neither met criteria for any psychotic disorder nor reported any attenuated psychotic symptoms and had no history of a central nervous system disorder, intellectual disability, substance dependence in the previous six months, or a first-degree relative with a psychotic disorder.

The 22q11.2Del comparison sample included SIPS data from 31 individuals with 22q11.2Del, ages 13.85-29.77 (mean ± SD = 19.75 ± 4.12 years), from the 22q11.2 Clinic in Atlanta, GA (25, 26, 35). Participants were ascertained from a case registry, with the deletion confirmed via fluorescence in situ hybridization (FISH). Participants were often referred for FISH as minors due to cardiovascular defects, language difficulties or immunological problems. Individuals identified as adults were referred as part of clinical care within a genetics or heart clinic, as described in (25). Data were collected between February 2006-June 2007.

Assessment of attenuated and florid psychotic symptoms

All study participants were administered the SIPS semi-structured clinical interview by trained personnel. The 19 items in the SIPS are grouped within four domains: positive, negative, disorganization, and general. Each item is rated on a scale from 0 (*Absent*) to 6 (*Severe and Psychotic* for positive symptoms, *Extreme* for others), with a rating of 3 (*Moderate*) indicating clinical significance. Item ratings were summed to produce a total score for each domain. For adolescents and adults with 3q29Del meeting criteria for a psychotic disorder, the Structured Clinical Interview for DSM-5 (SCID-5) (36) specified the diagnosis. All study participants provided informed consent to participate. These studies were approved by Emory University's Institutional Review Board.

Structural MRI acquisition and processing in 3q29Del

T1- and T2-weighted structural MRI was performed in 17 3q29Del participants with available SIPS data, ages 8.08-39.12 (mean ± SD = 18.13 ± 9.03 years). Of the six 3q29Del participants who had SIPS data but did not complete MRI, five were medically ineligible and one declined to participate. Images were acquired on a Siemens Magnetom Prisma 3T scanner in the sagittal plane using a 32-channel Prisma head coil and an

80mT/m gradient. T1-weighted 3D images were acquired in the sagittal plane using a single-echo MPRAGE sequence (37) with the following parameters: TE=2.24ms, TR=2400ms, TI=1000ms, bandwidth=210Hz/pixel, FOV=256x256mm, resolution=0.8mm isotropic. T2-weighted 3D images were acquired in the sagittal plane using a SPACE sequence (38) with the following parameters: TE=563ms, TR=3200ms, bandwidth=745Hz/pixel, FOV=256x256mm, resolution=0.8mm isotropic. Further details on neuroimaging parameters have been described (10, 33).

All MR images were processed using the "minimal structural pre-processing" pipeline established by the Human Connectome Project (HCP, v.4.1.3) with FreeSurfer (v.6.0) (http://surfer.nmr.mgh.harvard.edu/). We performed automatic segmentation as described in (39), using a previously described probabilistic atlas and Bayesian classification rule that assigns anatomical labels to each voxel based on estimates derived from a manually labeled training set (40). Since it is currently unfeasible to achieve a topologically correct reconstruction and automatic segmentation of the cerebellar cortical surface from *in vivo* MRI data, we treated the cerebellum as a volumetric structure and extracted cerebellar cortex and cerebellar white matter volumes for each 3q29Del participant, using a "coarse parcellation" scheme (41). Tissue-specific volumes were then summed to derive a global metric of total cerebellar volume; these three measures constitute the regions of interest (ROI) in the present study. A similar approach has been successfully used in previous literature (42-50), allowing for methodological consistency.

Finally, we used estimated total intracranial volume (eICV) as a proxy for premorbid brain size (51). eICV was calculated by FreeSurfer as described in (52) and has been reported to show high correlations with manually delineated intracranial volume (53-55). We report results from both eICV-adjusted and unadjusted analyses (56), given previous reports of microcephaly (27, 57, 58), and eICV reduction in 3q29Del (33). See Supplemental Materials for extended methods.

Statistical analyses

All analyses were conducted using *R* v.4.0.3 (59). The frequencies of florid or attenuated psychotic symptoms were compared between the 3q29Del and 22q11.2Del groups using Fisher's exact test. To assess the

variation in symptom profiles between groups, a series of analyses of covariance (ANCOVA) were performed; first, by domain and then item-wise to identify symptoms that may be elevated in 3q29Del. Partial eta-squared (η^2_p) was used to assess effect sizes. Pairwise comparisons for 3q29Del vs. HC and 3q29Del vs. 22q11.2Del were performed using Tukey's test. Since we observed several violations of the statistical assumptions required for ANCOVA (partially due to a likely floor effect in the HC sample), SIPS scores were log-transformed in between-group analyses. Age and sex were considered as potential covariates.

For neuroimaging analyses in 3q29Del, we used multiple linear regression to examine the relationship between ROI volumes and SIPS ratings for positive, negative and disorganization symptom domains separately. In models where a significant relationship was identified, we subsequently added eICV as an additional covariate to test whether results reflect a link with the cerebellum beyond global variability in head size. We also employed an additional categorical approach that relies on diagnostic criteria to determine the presence of either a psychotic disorder or attenuated psychotic symptom syndrome (APSS). Binary logistic regression was used to estimate the probability that either of these diagnoses are present in the 3q29Del sample given cerebellar volumes as the predictor. Multiple comparisons correction was applied at the ROI level using the Bonferroni method, with a rounded *p-value* threshold of 0.02 (0.05/3 ROIs).

In all models, age and sex were considered as covariates. Standard diagnostics were performed for testing regression assumptions. Multicollinearity was assessed in models with eICV by computing variance inflation factor scores. Given observed violations of linear regression assumptions using ordinary least squares, we additionally calculated heteroscedasticity-robust estimates (estimation-type: HC1) (60); final inferences from linear regression are based on robust estimates.

Finally, we tested whether psychotic symptoms differ between 3q29Del participants with versus without cystic/cyst-like malformations of the posterior fossa, which were identified by a board-certified neuroradiologist (33). Fisher's exact test was used for diagnostic comparisons. Student's t-test and Wilcoxon signed-rank test were used for dimensional comparisons. Given limited power due to smaller sample size in the neuroimaging arm, we also report trend-level associations using a less conservative alpha ($p \leq 0.10$) to inform future hypotheses. All analyses were two-tailed. See Supplemental Materials for extended methods.

Results

Presence of attenuated and florid psychotic symptoms in 3q29Del and 22q11.2Del.

Demographics of the 3q29Del sample are presented in Table 1 and Fig. S1; information for 22q11.2Del and HCs are provided in Table S1. Four out of the 23 3q29Del participants (17%) met criteria for a psychotic disorder: schizophrenia (N = 1); schizoaffective disorder, bipolar type (N = 1); and unspecified schizophrenia spectrum and other psychotic disorder (N = 2). Two of these individuals had a prior diagnosis of a psychotic disorder; two did not. These four individuals (3 males, 1 female) tended to be older than those without a psychotic disorder (with psychosis: mean age = 26.66; without psychosis: mean age = 14.89). However, cognitive ability was similar between the groups (with psychosis: mean FSIQ = 73.00; without psychosis: mean FSIQ = 73.89). Those participants meeting criteria for a psychotic disorder reported past or current symptoms that met a rating of *Severe and Psychotic* for unusual thought content, suspiciousness, and/or perceptual abnormalities; these participants reported prodromal symptoms beginning in late childhood or early adolescence (on average between ages 11-12). In contrast, only one out of the 31 22q11.2Del participants (3%) met criteria for a psychotic disorder.

We next excluded individuals with a psychotic disorder and sought to analyze sub-threshold symptoms of psychosis in the remaining individuals with complete data (N = 19 in 3q29Del, N = 29 in 22q11.2Del). Seven 3q29Del participants (37%) exhibited clinically significant attenuated positive symptoms (i.e., at least one positive symptom ≥ 3). Three of these individuals (16%) met the frequency and timing criteria to qualify for APSS (31). Nineteen 22q11.2Del participants (66%) exhibited clinically significant attenuated positive symptoms. The information necessary for assessing APSS was unavailable for this group.

Cumulatively, 48% of the 3q29Del sample showed either florid or attenuated psychotic symptoms, as compared to 67% of the 22q11.2Del sample (Table 2); the comparison of these frequencies revealed no significant difference between the groups (p = 0.26). Too few participants with 3q29Del (N = 3) were taking antipsychotics to determine treatment effects.

Group differences in demographics and symptom profiles.

SIPS symptom ratings are presented in Table 3 for each study group. There was a significant age difference between the 3q29Del sample and HCs ($p \leq 0.01$), and between the 3q29Del and 22q11.2Del samples ($p \leq 0.05$), with 3q29Del participants being younger on average. Given these age differences, as well as evidence from community samples indicating increases in psychotic-like experiences through adolescence followed by a decline in early adulthood (61-63), we first assessed whether the relationship between age and symptom severity differs between study samples. Results are presented in Table S2 and Fig. S2. The correlations between symptom severity and age were positive and often highest in magnitude for 3q29Del, positive and modest in 22q11.2Del, but negative in HCs, which is consistent with the group differences in the mean and range of age.

Next, ANCOVAs were performed to contrast the average symptom ratings by domain of the 3q29Del sample against HCs and 22q11.2Del, adjusting for sex. As the mean age and correlations between symptom severity and age varied between groups, age was initially not adjusted for in the comparison of symptom profiles, as covariate adjustment using the ANCOVA framework assumes homogeneity between groups. There was a significant effect of diagnostic group on all domains: positive [$F(2, 328) = 112.87$, $p \leq 0.001$, $\eta^2_p = 0.41$], negative [$F(2, 329) = 135.00$, $p \leq 0.001$, $\eta^2_p = 0.45$], disorganization [$F(2, 329) = 166.30$, $p \leq 0.001$, $\eta^2_p = 0.50$], general [$F(2, 328) = 74.56$, $p \leq 0.001$, $\eta^2_p = 0.31$]. Pairwise contrasts between 3q29Del and the two other groups were conducted correcting for multiple comparisons, with a rounded *p-value* threshold of 0.01 for each domain (0.05/4 domains). Comparisons revealed that individuals with 3q29Del were rated significantly higher than HCs on all SIPS domains (p's ≤ 0.01): positive [$t(328) = 8.12$, $p \leq 0.001$], negative [$t(329) = 8.21$, $p \leq 0.001$], disorganization [$t(329) = 11.10$, $p \leq 0.001$], and general [$t(328) = 6.59$, $p \leq 0.001$]. In contrast, the average ratings for the 3q29Del group did not significantly differ from ratings in 22q11.2Del for positive [$t(328) = -2.84$, $p = 0.01$], disorganization [$t(329) = -1.81$, $p = 0.16$], or general [$t(328) = -2.24$, $p = 0.06$]. However, the 22q11.2Del group exhibited greater negative symptoms than 3q29Del [$t(329) = -3.75$, $p \leq 0.001$].

To compare group profiles of specific items, a series of ANCOVAs were conducted with the same approach. Bonferroni correction was applied, with a rounded *p-value* threshold of 0.003 (0.05/19 items). For almost all items on the SIPS, there was a significant effect of diagnostic group on severity (p's ≤ 0.003). Fig. 1

presents the symptom profile for each diagnostic group. Comparing the 3q29Del sample with HCs revealed more severe ratings on all items (p's ≤ 0.003), except for sleep disturbance, t(329) = 2.55, p = 0.01, which was nominally significant. Differences between 3q29Del and 22q11.2Del groups were primarily in the negative symptom domain. Participants with 22q11.2Del exhibited more severe social anhedonia [t(329) = -6.09, $p \leq$ 0.001], avolition [t(329) = -4.19, $p \leq 0.001$], experience of emotions and self [t(329) = -4.16, $p \leq 0.001$], and impaired ideational richness [t(329) = -3.10, p = 0.002]. Lastly, individuals with 22q11.2Del were rated as more impaired in personal hygiene [t(329) = -4.27, $p \leq 0.001$], and as experiencing greater dysphoric mood [t(328) = -4.43, $p \leq 0.001$]. The only group difference in positive symptoms was more severe suspiciousness in 22q11.2Del [t(329) = -4.18, $p \leq 0.001$]. When the above analysis was conducted with the inclusion of age as an additional covariate, the same pattern of results was found.

The pairwise comparisons are presented in Table 3, along with the untransformed values for the means and standard errors of each group for interpretability on the original scale. See Table S3 for adjusted means and standard errors after log-transformation. Of note, the 3q29Del group was found to exhibit similar estimates for general cognitive ability compared with the 22q11.2Del group (Table S1), which mitigates the potential confounding effect of IQ on between-group differences.

Sex differences within groups.

We also examined sex differences for the three diagnostic groups (Fig. S3). Statistical analyses included a set of ANCOVAs adjusted for age, given the absence of violations in homogeneity of slopes within group. As these analyses were conducted to explore whether there were sex differences in symptoms similar to those observed in research on CHR and psychotic patients, multiple comparisons correction was not made. The differences in domain scores between males and females with 3q29Del were significant only for negative symptoms [F(1, 20) = 4.85, p = 0.04, η^2_p = 0.20], with males exhibiting more severe symptoms than females. Similarly, negative symptoms differed by sex among the 22q11.2Del group [F(1, 28) = 5.10, p = 0.03, η^2_p = 0.15], and the HC group [F(1, 276) = 6.94, p = 0.01, η^2_p = 0.02], with males exhibiting more severe symptoms than females. Lastly, only among HCs, positive symptoms varied between sexes [F(1, 276) = 3.93, p = 0.05, η^2_p

= 0.01], with males demonstrating greater severity. Notably, relatively small effect sizes were found in the HC group for both symptom domains.

Structural cerebellar correlates of psychosis-risk in 3q29Del.

Prior work by our group using structural MRI scans acquired from a larger 3q29Del sample (including the scans analyzed in the present study) has shown that cerebellar hypoplasia and posterior fossa arachnoid cysts are frequently observed among individuals with 3q29Del (10). Our team has also shown in the same sample that 3q29Del participants exhibit smaller cerebellar cortex and larger cerebellar white matter volumes than healthy controls, and the prevalence of cystic/cyst-like malformations of the posterior fossa is significantly elevated in this syndrome (33).

To determine whether the severity of psychotic symptoms in participants with 3q29Del is associated with structural cerebellar abnormalities previously documented in this population (10, 33) (see Fig. 2A for a representative MR image), we first modeled the dimensional relationship between SIPS ratings for three major symptom domains relevant to psychotic disorders (positive, negative, disorganization) and global and tissue-specific cerebellar volumes in participants with 3q29Del. Table S4 summarizes demographic, clinical, and volumetric data from the 3q29Del subsample with available neuroimaging and SIPS data. Note that there were no significant differences between left and right hemispheric cerebellar volumes (*p's* > 0.05) (Fig. S4); hence, each ROI reflects bilateral volumes.

Our results (Fig. 2B-D, Tables S5A-J) indicate a significant inverse relationship between positive symptom severity and cerebellar cortex volume in 3q29Del, while correcting for age and sex. Smaller cerebellar cortical volumes were associated with greater positive symptoms (b = -0.43, p = 0.02), and this effect remained significant in a secondary model that includes eICV for head size correction (b = -0.29, p = 0.03) (Fig. 2B, Tables S5B-C). Results also indicate a trend-level inverse association between positive symptom severity and total cerebellum volume (b = -0.27, p = 0.10) (Fig. 2D, Table S5A), and a trend-level positive association between disorganization symptom severity and cerebellar white matter volume (b = -0.28, p = 0.09) (Fig. 2C, Table S5J), while correcting for age and sex. There was no relationship between negative symptom severity and

ROI volumes (p's > 0.10).

Given ongoing discussions regarding the merits and limitations of dimensional versus categorical assessment of psychosis (64-66), we next took a categorical approach and asked whether the probability of meeting diagnostic criteria for either a psychotic disorder or APSS would recapitulate the results from our dimensional approach. Our findings from logistic regression indicate no significant relationship between interrogated volumes and the likelihood of these outcomes in 3q29Del, while correcting for age and sex (p's > 0.10) (Tables S6A-C). Detailed regression results can be found in Tables S5-6. See Fig. S5 for sensitivity analysis.

Finally, we found no significant association between diagnostic and dimensional indices of psychotic symptoms and the presence of cystic/cyst-like malformations of the posterior fossa in 3q29Del (p's > 0.05) (Table S7). There was a trend-level relationship between these radiological findings and the odds of APSS (p = 0.08), which may warrant future consideration. See Supplemental Materials for extended results.

Discussion

Rare pathogenic CNVs that arise from recurrent chromosomal rearrangements are now robustly implicated in psychosis-risk (2-4, 67, 68), with eight CNV loci surpassing genome-wide significance (1). Among these loci, the 3q29 deletion has the largest estimated effect size (1, 8), offering a promising opportunity to link a specific genetic mechanism to brain and behavioral phenotypes underlying at least one form of psychosis. Recently, we documented the broader phenotypic spectrum of 3q29Del by direct evaluation of the largest sample of 3q29Del study participants reported to date (10, 30). In the present study, we substantially extended these findings by systematically characterizing the comprehensive profile of psychotic symptoms in 3q29Del and investigating the potential effects of sex and age on severity. Furthermore, we compared the profiles of 3q29Del to HCs and 22q11.2Del. This is particularly important since cross-CNV similarities or differences in symptomology may suggest overlapping or divergent pathogenic mechanisms. Finally, we investigated the neuroanatomical correlates of psychosis-risk in 3q29Del by employing a hypothesis-driven approach, focusing on macrostructural properties of the cerebellum. Overall, our findings target important gaps in our understanding of the link between 3q29Del and exceptionally increased genetic risk for psychotic illnesses.

First, the present study confirmed that a significant proportion of 3q29Del participants meet diagnostic criteria for psychosis (4/23, 17%) or manifest one or more clinically significant attenuated positive symptoms (7/23, 30%), with 43% (3/7) meeting the frequency and timing criteria for APSS. Cumulatively, 48% of the 3q29Del sample showed either florid or attenuated psychotic symptoms, as compared to 67% of the 22q11.2Del sample. The rates of psychosis-related phenotypes observed here are especially striking considering the young ages of the 3q29Del participants. Based on published demographic data on CHR groups, the mean age at ascertainment is between 17 and 18 (69-71). Among those 3q29Del individuals not already meeting criteria for a psychotic disorder, the mean age was 15. Thus, most of the 3q29Del sample is below the typical age of onset for psychosis and the prodrome. Notably, the prevalence of psychosis or clinically significant attenuated positive symptoms is 67% (6/9) among 3q29Del individuals aged 17 and older (Fig. S1). Given this finding and previously published rates of transition to psychosis in CHR groups (72), it is likely that more transitions to florid psychosis are to be expected in the present 3q29Del sample.

In this context, we note that the 22q11.2Del sample was ascertained through cardiology or immunology clinics, whereas 3q29Del participants were ascertained through a registry. Contrary to the expectation that a clinically ascertained sample may be more severely affected, there were no significant differences in the rates of florid or attenuated psychotic symptoms between the 3q29Del and 22q11.2Del samples. However, since we were unable to determine the prevalence of APSS among 22q11.2Del participants, the true frequency of formal psychosis-risk syndromes could not be compared between these samples. 3q29Del participants with a psychotic disorder presented with prodromal symptoms around late childhood to early adolescence, consistent with several reports in 22q11.2Del (11, 73-75), although findings vary (76-79). The profile documented in the current sample indicates that monitoring and identification of early signs among individuals with 3q29Del are warranted. Proper assessment and treatment is necessary to reduce distress and improve functioning; among CHR, interventions may delay or prevent the onset of florid psychosis (80); thus, early intervention among 3q29Del may also attenuate psychosis severity and improve outcomes.

Further, the relation of sex and age with symptoms in the 3q29Del group is similar to that observed in CHR and psychotic samples (61-63). Males tend to score higher in negative symptoms than females, and both

positive and negative symptoms tend to increase with age, although due to the small sample of 3q29Del participants this correlation was not statistically significant. It should be noted that studies of both community and clinical samples reveal increases in psychotic-like experiences during adolescence that extends to about 19 years of age, then begins to decline for those who do not transition to psychosis. The mean age and age-range of the HC group in the present study is in the period when experiences are normatively in decline, hence the inverse relation between age and severity in that group. Given this finding, we performed both age-adjusted and unadjusted analyses to assess the variation in psychotic symptom profiles between groups; both approaches produced the same pattern of results.

Our findings from these group comparisons indicate that individuals with 3q29Del are rated significantly higher than HCs on all SIPS domains, while they show remarkable similarity to individuals with 22q11.2Del in average ratings for the positive, disorganization, and general symptom domains. However, the 22q11.2Del group exhibited a more severe profile than 3q29Del in the negative symptom domain. This finding parallels an earlier study that compared individuals at CHR with 22q11.2Del to individuals at CHR without 22q11.2Del; the 22q11.2Del group had greater negative symptoms, although the two groups showed comparable positive and global symptoms (81). Interestingly, individuals with 22q11.2Del also present with greater negative symptoms when compared to Williams Syndrome or idiopathic developmental disabilities (82). Several lines of evidence also point to higher rates of major depressive disorder in 22q11.2Del (83, 84), which is a potential secondary source of negative symptoms. In contrast, most individuals with 3q29Del had relatively well-preserved hedonic experiences and social motivation (9). It is conceivable that the pronounced profile of negative symptoms observed in 22q11.2Del compared to 3q29Del reflects some level of divergence in etiopathogenetic mechanisms. Disturbances of the brain reward system have been suggested to be central in the pathogenesis of negative symptoms (85); hence, reward processing may be an important future direction for cross-comparison studies in these CNVs. We also note that the less severe negative symptoms seen in 3q29Del may suggest a more favorable profile for functional outcomes and response to intervention in psychotic symptoms, considering the previously reported inverse relationship between negative symptom severity and global functioning (86, 87), as well as prior reports of negative symptoms being more resistant to

treatment (88).

Moreover, our results revealed a significant relationship between cerebellar morphology and severity of psychosis-risk symptoms in 3q29Del, driven by both a tissue-specific and symptom-specific association between cerebellar cortex volume and positive symptoms. Cystic/cyst-like malformations of the posterior fossa yielded no link with psychotic symptoms, suggesting the relationship is specific to cerebellar cortex. Besides its critical role in motor coordination, the cerebellum has been suggested to perform a parallel role in the coordination of thoughts (89-92) through internal models that enable predictive function. An internal model is a system that, when given its current state, can predict the outcome of an action without performing the action (93). The cerebellum is proposed to be a key node in the neural systems that enable the formation and implementation of such models (94). Accordingly, cerebellar dysfunction has been hypothesized to lead to perceptual abnormalities, such as auditory hallucinations (95, 96) and a loss of coherence in speech output (97, 98), which are among the core symptoms of psychosis. Notably, perceptual abnormalities and disorganized communication showed the most severe positive symptom ratings in the present 3q29Del sample.

The potential involvement of cerebellar dysfunction in schizophrenia has been speculated since the 1990s (99-101). Congruently, emerging findings indicate an increased prevalence of psychosis among patients with cerebellar pathology (102, 103). The cerebellar cognitive-affective syndrome, which follows from cerebellar lesions, has substantial overlap with the phenomenology of psychosis (104-107). In addition, there are reports of cerebellar abnormalities in idiopathic psychosis (108-119) and pathology in Purkinje cells, the output neurons of the cerebellar cortex, has been documented in schizophrenia (120-122). Further, altered functional or structural connectivity and morphology of the cerebellum has been identified in CHR groups (50, 123-131). Notably, a recent study of the Philadelphia Neurodevelopmental Cohort found cerebellar gray matter volume to be a robust predictor of psychotic-like experiences in a large community sample of youths (132), which is consistent with our findings.

Thus, various lines of evidence point to cerebellar involvement in psychotic symptoms. However, how exactly cerebellar abnormalities relate to psychosis remains unknown and the considerable heterogeneity reported in extant literature constitutes a major challenge in addressing this gap. The association that we

identified between cerebellar cortex volume and positive symptom severity in 3q29Del may help elucidate one part of this question, as this finding suggests that one or more genes affected by the hemizygous deletion of the 3q29 interval modulate the link between cerebellar development and psychosis-risk. In fact, many genes located in this interval, including *DLG1* and *BDH1*, which have been proposed as drivers of neuropsychiatric phenotypes (133, 134), show medium-high expression in the cerebellum (https://www.proteinatlas.org/). Its protracted development may increase the cerebellum's susceptibility to perturbations of these genes (135, 136).

Our results indicate that diagnostic dichotomization does not recapitulate the dimensional brain-behavior relationship identified in 3q29Del. There may be several reasons for this finding. One explanation is the statistical drawback (reduced power) associated with dichotomizing continuous variables (137). Another explanation may be misclassification bias (138); young participants have not yet moved through the highest risk period for psychosis and may transition to APSS or psychosis at a later timepoint; this may have biased the categorical results toward the null. Additionally, a binary split presupposes a true cutpoint between opposite sides of diagnostic criteria. For example, an APSS diagnosis requires attenuated psychotic symptoms to have begun within the past year or to have been rated one or more points higher compared to 12 months ago (31), which could lead to the diagnostic exclusion of individuals who have a longer and more gradual prodrome (139). Hence, such criteria, although useful in other applications, may lead to arbitrary divisions of a complex continuum. To conclude, our findings support cerebellar cortex morphology as a likely trait marker of psychosis-risk in 3q29Del, which we operationalize as a multidimensional continuum with varying degrees of severity, distress, and functional impairment.

Our study has several limitations. First, our sample size was limited due to the rare prevalence of 3q29Del, which prevented analyses of interactions. Demands of study participation (e.g., travel to GA) may have barred individuals with more severe presentations from participating; thus, symptom severity could be underestimated. Additionally, the complex architecture of the cerebellum presents challenges for MRI; future work with improved segmentation techniques will explore finer associations with cerebellar subregions. Furthermore, cerebellar connections with cerebral association cortices (140), as well as the basal ganglia (141), warrant future investigation to address questions related to circuitry. Finally, given the cross-sectional design, our findings do

not necessarily reflect causation. Longitudinal follow-up as well as targeted investigations of the cerebellum in the mouse model of 3q29Del (142) will be conducted for causal inference and mechanistic insights.

Altogether, our findings indicate that clinical signs of psychosis risk are elevated in 3q29Del participants. Furthermore, our results establish the unique and shared profiles of psychotic symptoms across 3q29Del and 22q11.2 Del and highlight cerebellar involvement in elevated psychosis-risk in 3q29Del.

Acknowledgements

We acknowledge the 3q29Del study population, their families and the 3q29 Project members. We thank the Marcus Autism Center for providing clinical assessment resources. Funding for this work was provided by National Institutes of Health (NIH) grants R01 MH110701, R01 MH118534, and National Institutes of Mental Health (NIMH) grant U01MH081988. REDCap is supported by grant UL1 TR000424. Funding for work in 22q11.2Del was provided by grants awarded to Joseph Cubells and Opal Ousley from the Robert W. Woodruff Fund and the Predictive Health Initiative of Emory University. We would like to thank the following NAPLS2 PIs for their contributions to the healthy control dataset: Jean Addington, Carrie E. Bearden, Kristin Cadenhead, Tyrone D. Cannon, Barbara A. Cornblatt, Daniel H. Mathalon, Thomas H. McGlashan, Diana O. Perkins, Larry J. Seidman, Ming T. Tsuang, and Scott W. Woods.

Data availability

The 3q29Del data collected in this study are deposited in the NIMH Data Archive (nda.nih.gov) (behavioral data: collection 2614, embargoed until September 2022; neuroimaging data: collection 3126, embargoed until November 2023). Prior to these dates, the 3q29Del data are available from Jennifer Mulle upon reasonable request. The NAPLS2 data used in this article are available from Elaine F. Walker on behalf of the NAPLS Consortium upon reasonable request. The 22q11.2Del data used in this article are available from Opal Ousley and Joseph F. Cubells upon reasonable request.

Tables

		3q29Del (*N* = 23)	
	3q29Del (*N* = 23)	**With a psychotic disorder (*N* = 4)**	**Without a psychotic disorder (*N* = 19)**
Age (in years) *M* ± *SD* Median [Range]	16.94 ± 8.24 15.89 [8.08 – 39.12]	26.66 ± 9.55 25.70 [16.13 – 39.12]	14.89 ± 6.51 14.01 [8.08 – 34.64]
Sex, *N (%)*			
Male	14 (61%)	3 (75%)	11 (58%)
Female	9 (39%)	1 (25%)	8 (42%)
Race, *N (%)*			
White	20 (87%)	4 (100%)	16 (84%)
More than one race	3 (13%)	0 (0%)	3 (16%)
Ethnicity, *N (%)*			
Hispanic/Latino	1 (4%)	0 (0%)	1 (5%)
Non-Hispanic/Latino	22 (96%)	4 (100%)	18 (95%)
General cognitive abilities *M* ± *SD* Median [Range]	73.74 ± 11.98 75 [46 – 99]	73.00 ± 14.72 76 [61 – 94]	73.89 ± 11.80 76 [46 – 99]
Antipsychotic usage, *N (%)*	3 (13%)	1 (25%)	2 (11%)

Table 1. Demographic and relevant clinical information for individuals with 3q29Del. Descriptive statistics are reported separately for the total 3q29Del sample, and the sample stratified by the presence/absence of a psychotic disorder. Abbreviations: deletion, Del; mean, *M*; standard deviation, *SD*.

	3q29Del (*N* = 23)	22q11.2Del (*N* = 31)
	Clinically significant, *N* (%)	Clinically significant, *N* (%)
Positive Symptom Domain	11 (48%)	20 (67%)
P1. Unusual Thought Content	5 (22%)	4 (13%)
P2. Suspiciousness	3 (13%)	9 (29%)
P3. Grandiosity	2 (9%)	4 (13%)
P4. Perceptual Abnormalities	7 (30%)	6 (19%)
P5. Disorganized Communication	7 (30%)	7 (23%)

Table 2. Rates of clinically significant psychotic symptoms (i.e., at least one SIPS item rated ≥ 3) among subjects with 3q29Del and 22q11.2Del. For P5 and the positive symptom domain total, 22q11.2Del *N* = 30 due to missing data from one 22q11.2Del subject. Note that 13 3q29Del subjects and 10 22q11.2Del subjects had more than one P item with a ≥ 3 rating. *Abbreviations:* Structured Interview for Psychosis-Risk Syndromes, SIPS; deletion, Del.

	HC (*N* = 279)		22q11.2Del (*N* = 31)		3q29Del (*N* = 23)		Pairwise comparisons	
SIPS symptom domains and items	Mean	Std. Error	Mean	Std. Error	Mean	Std. Error	3q29Del vs. HC	3q29Del vs. 22q11.2Del
Positive Symptom Domain[a]	1.07	0.10	8.17	0.75	7.00	1.48	< 0.001	0.01
P1. Unusual Thought Content[a]	0.25	0.03	1.68	0.23	1.52	0.47	< 0.001	0.01
P2. Suspiciousness[a,b]	0.26	0.03	1.74	0.23	1.00	0.34	< 0.001	< 0.001
P3. Grandiosity[a]	0.21	0.03	0.94	0.26	0.74	0.23	0.002	0.35
P4. Perceptual Abnormalities[a]	0.22	0.03	1.81	0.25	1.91	0.43	< 0.001	0.37
P5. Disorganized Communication[a]	0.13	0.02	1.83	0.21	1.83	0.34	< 0.001	0.38
Negative Symptom Domain[a,b]	1.46	0.13	13.13	1.00	8.35	1.32	< 0.001	< 0.001
N1. Social Anhedonia[a,b]	0.27	0.04	3.00	0.28	1.35	0.31	< 0.001	< 0.001
N2. Avolition[a,b]	0.29	0.05	2.23	0.28	1.17	0.31	< 0.001	< 0.001
N3. Expression of Emotion[a]	0.11	0.02	1.65	0.26	1.35	0.36	< 0.001	0.04
N4. Experience of Emotion and Self[a,b]	0.09	0.02	1.26	0.26	0.57	0.23	< 0.001	< 0.001
N5. Ideational Richness[a,b]	0.26	0.03	2.90	0.28	2.13	0.40	< 0.001	0.002
N6. Occupational Functioning[a]	0.44	0.07	2.10	0.28	1.78	0.37	< 0.001	0.17
Disorganization Symptom Domain[a]	0.66	0.07	6.55	0.65	5.48	0.74	< 0.001	0.16
D1. Odd Behavior or Appearance[a]	0.08	0.02	1.58	0.26	1.26	0.28	< 0.001	0.10
D2. Bizarre Thinking[a]	0.04	0.01	0.81	0.19	0.87	0.28	< 0.001	0.78
D3. Trouble with Focus and Attention[a]	0.46	0.05	2.68	0.15	2.74	0.38	< 0.001	0.36
D4. Personal Hygiene[a,b]	0.09	0.02	1.48	0.28	0.61	0.21	< 0.001	< 0.001
General Symptom Domain[a]	1.34	0.13	7.71	0.72	6.09	1.04	< 0.001	0.63
G1. Sleep Disturbance	0.48	0.05	1.71	0.25	1.13	0.32	0.01	0.02
G2. Dysphoric Mood[a,b]	0.41	0.05	2.52	0.29	1.17	0.33	0.002	< 0.001
G3. Motor Disturbances[a]	0.20	0.03	1.81	0.28	1.78	0.31	< 0.001	0.86
G4. Impaired Tolerance to Normal Stress[a]	0.25	0.04	1.68	0.24	2.00	0.36	< 0.001	0.55

Table 3. The overall results of the ANCOVA between the SIPS ratings of each diagnostic group and pairwise comparisons. The unadjusted means and standard errors for both deletion groups and HCs are shown. Pairwise comparisons reflect p-values calculated on log-transformed sex-adjusted data. Refer to Table S3 for log-transformed sex-adjusted means and standard errors for each group. '[a]' indicates significant difference ($p \leq 0.01$ for domain, $p \leq 0.003$ for item) between 3q29Del and HC; '[b]' indicates significant difference ($p \leq 0.01$ for domain, $p \leq 0.003$ for item) between 3q29Del and 22q11.2Del. For P5 and the positive symptom domain

total, 22q11.2Del *N* = 30 due to missing data from one 22q11.2Del subject. For G2 and the general symptom domain total, HC *N* = 278 due to missing data from one HC subject. *Abbreviations:* Structured Interview for Psychosis-Risk Syndromes, SIPS; healthy controls, HC; deletion, Del; analysis of covariance, ANCOVA; standard, std.

Figures

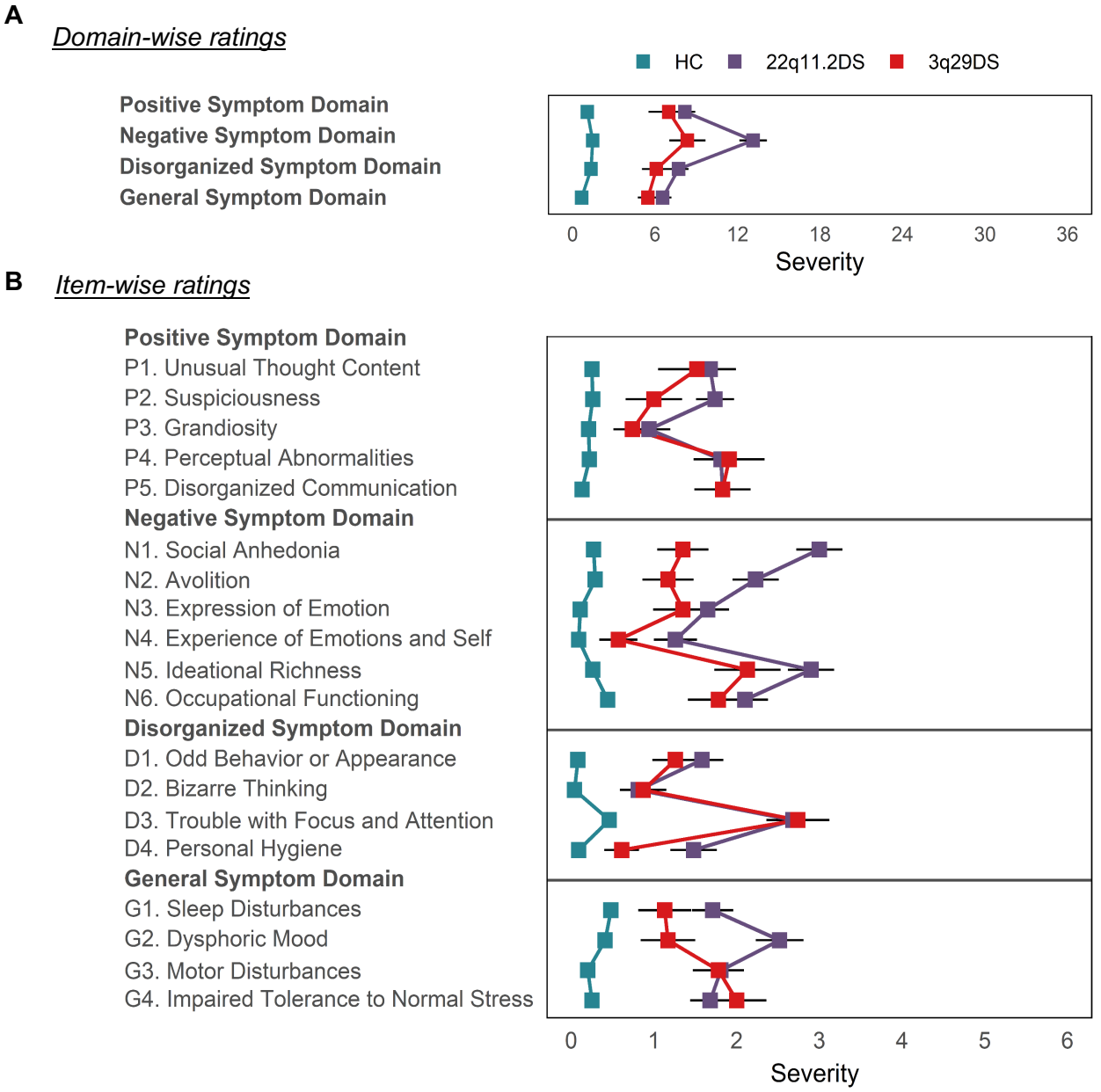

Figure 1. The unadjusted means of individual SIPS ratings for each diagnostic group. Standard error bars are shown. In panel **A)** SIPS domain totals are presented for each group. In panel **B)** item-specific SIPS ratings are presented for each group. For P5 and the positive symptom domain total, 22q11.2Del $N = 30$ due to missing data from one 22q11.2Del subject. For G2 and the general symptom domain total, HC $N = 278$ due to missing data from one HC subject. *Abbreviations:* Structured Interview for Psychosis-Risk Syndromes, SIPS; healthy controls, HC; deletion, Del; deletion syndrome, DS.

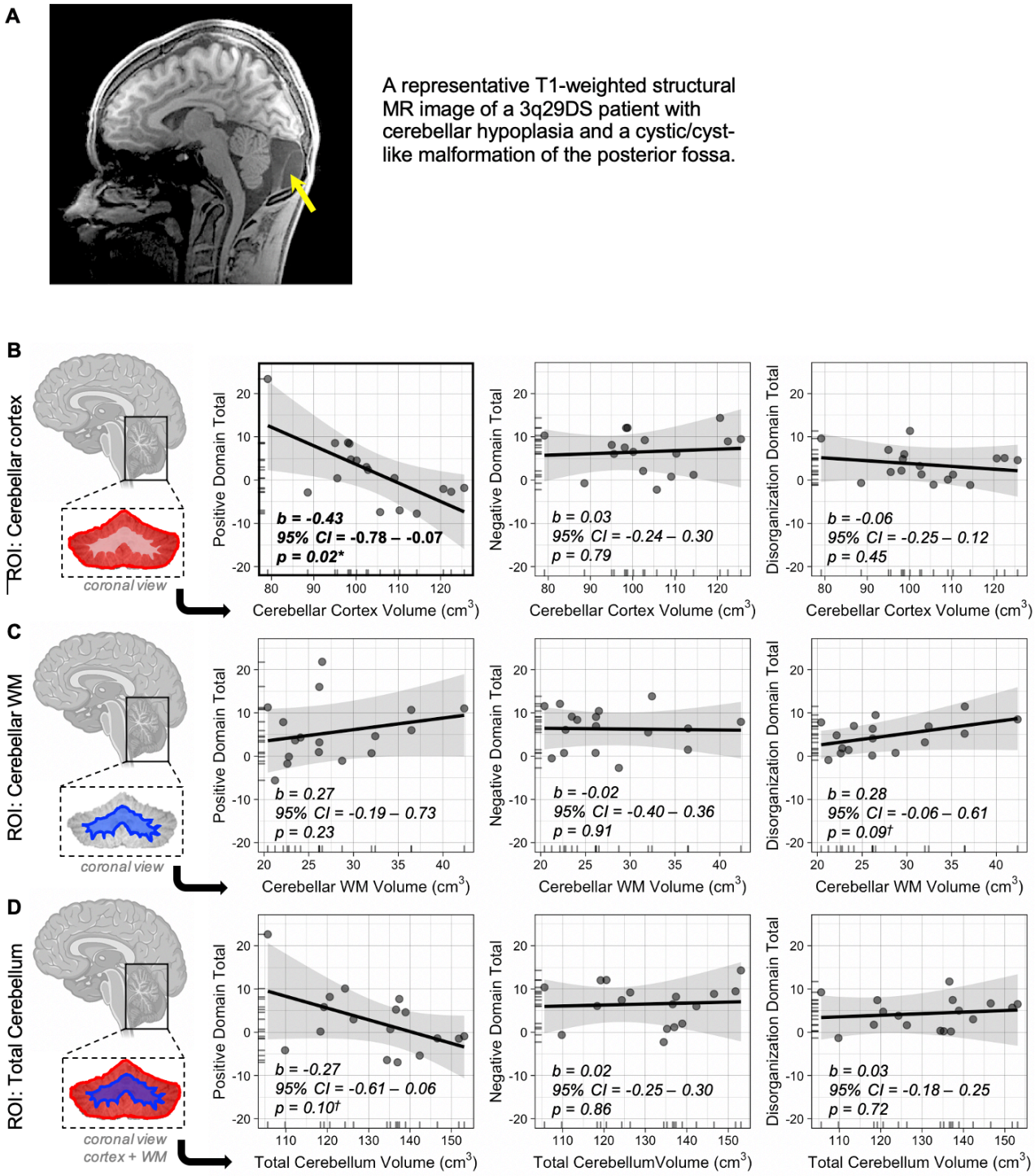

Figure 2. The relationships between cerebellar structure and psychosis-risk symptoms in 3q29Del. A) The sagittal view of a representative T1-weighted structural MRI scan from a 3q29Del subject with cerebellar hypoplasia and a cystic/cyst-like malformation of the posterior fossa (yellow arrow). **B-D)** Predictor effect plots show the relationships between SIPS ratings for three major symptom domains relevant to psychotic

disorders and global and tissue-specific cerebellar volumes among subjects with 3q29Del (N = 17). Predicted values of positive, negative and disorganization symptom ratings indexed by the SIPS (y-axis) were computed from the best-fit multiple linear regression models from Table S5, while covariates (age and sex) were held fixed. The shaded area is a pointwise confidence band for the fitted values. Rug plots on both sides of each graph show the distribution of the predictor and outcome variables and data points represent partial residuals. Schematic illustrations of the three ROIs are provided next to their corresponding predictor effect plots for clarity. Parameter estimates on each plot reflect the main effect of **B)** cerebellar cortex volume, **C)** cerebellar WM volume and **D)** total cerebellum volume on domain-specific symptom severity ratings and reflect heteroskedasticity-robust estimates. Regression results indicate a significant inverse relationship between cerebellar cortex volume and positive symptom severity, with smaller volumes predicting more severe symptoms among 3q29Del subjects (bold panel). '*' indicates significant association after Bonferroni correction ($p \leq 0.02$). '†' indicates trend-level association ($p \leq 0.10$). *Abbreviations:* Magnetic resonance imaging, MRI; region of interest, ROI; Structured Interview for Psychosis-Risk Syndromes, SIPS; white matter, WM; deletion, Del; deletion, Del.

References

1. Marshall CR, Howrigan DP, Merico D, Thiruvahindrapuram B, Wu W, Greer DS, et al. (2017): Contribution of copy number variants to schizophrenia from a genome-wide study of 41,321 subjects. *Nat Genet*. 49:27-35.

2. Malhotra D, Sebat J (2012): CNVs: harbingers of a rare variant revolution in psychiatric genetics. *Cell*. 148:1223-1241.

3. Rees E, Walters JT, Georgieva L, Isles AR, Chambert KD, Richards AL, et al. (2014): Analysis of copy number variations at 15 schizophrenia-associated loci. *Br J Psychiatry*. 204:108-114.

4. Stefansson H, Rujescu D, Cichon S, Pietilainen OP, Ingason A, Steinberg S, et al. (2008): Large recurrent microdeletions associated with schizophrenia. *Nature*. 455:232-236.

5. Clements CC, Wenger TL, Zoltowski AR, Bertollo JR, Miller JS, de Marchena AB, et al. (2017): Critical region within 22q11.2 linked to higher rate of autism spectrum disorder. *Mol Autism*. 8:58.

6. Ousley O, Evans AN, Fernandez-Carriba S, Smearman EL, Rockers K, Morrier MJ, et al. (2017): Examining the Overlap between Autism Spectrum Disorder and 22q11.2 Deletion Syndrome. *Int J Mol Sci*. 18.

7. Serur Y, Sofrin Frumer D, Daon K, Sobol-Havia D, Weinberger R, Shulman C, et al. (2019): Psychiatric disorders and autism in young children with 22q11.2 deletion syndrome compared to children with idiopathic autism. *Eur Psychiatry*. 55:116-121.

8. Mulle JG (2015): The 3q29 deletion confers >40-fold increase in risk for schizophrenia. *Mol Psychiatry*. 20:1028-1029.

9. Pollak RM, Murphy MM, Epstein MP, Zwick ME, Klaiman C, Saulnier CA, et al. (2019): Neuropsychiatric phenotypes and a distinct constellation of ASD features in 3q29 deletion syndrome: results from the 3q29 registry. *Mol Autism*. 10:30.

10. Sanchez Russo R, Gambello MJ, Murphy MM, Aberizk K, Black E, Burrell TL, et al. (2021): Deep phenotyping in 3q29 deletion syndrome: recommendations for clinical care. *Genet Med*. 23:872-880.

11. Vorstman JAS, Morcus MEJ, Duijff SN, Klaassen PWJ, Heineman-de Boer JA, Beemer FA, et al. (2006): The 22q11.2 deletion in children: high rate of autistic disorders and early onset of psychotic symptoms. *J Am Acad Child Adolesc Psychiatry*. 45:1104-1113.

12. Schneider M, Debbane M, Bassett AS, Chow EW, Fung WL, van den Bree M, et al. (2014): Psychiatric disorders from childhood to adulthood in 22q11.2 deletion syndrome: results from the International Consortium on Brain and Behavior in 22q11.2 Deletion Syndrome. *Am J Psychiatry*. 171:627-639.

13. Devriendt K, Fryns JP, Mortier G, van Thienen MN, Keymolen K (1998): The annual incidence of DiGeorge/velocardiofacial syndrome. *J Med Genet*. 35:789-790.

14. Botto LD, May K, Fernhoff PM, Correa A, Coleman K, Rasmussen SA, et al. (2003): A population-based study of the 22q11.2 deletion: phenotype, incidence, and contribution to major birth defects in the population. *Pediatrics*. 112:101-107.

15. McDonald-McGinn DM, Kirschner R, Goldmuntz E, Sullivan K, Eicher P, Gerdes M, et al. (1999): The Philadelphia story: the 22q11.2 deletion: report on 250 patients. *Genet Couns*. 10:11-24.

16. Mcdonald-Mcginn DM, Tonnesen MK, Laufer-Cahana A, Finucane B, Driscoll DA, Emanuel BS, et al. (2001): Phenotype of the 22q11. 2 deletion in individuals identified through an affected relative: Cast a wide FISH ing net! *Genetics in Medicine*. 3:23-29.

17. Blagojevic C, Heung T, Theriault M, Tomita-Mitchell A, Chakraborty P, Kernohan K, et al. (2021): Estimate of the contemporary live-birth prevalence of recurrent 22q11.2 deletions: a cross-sectional analysis from population-based newborn screening. *CMAJ Open*. 9:E802-E809.

18. McDonald-McGinn DM, Sullivan KE, Marino B, Philip N, Swillen A, Vorstman JA, et al. (2015): 22q11.2 deletion syndrome. *Nat Rev Dis Primers*. 1:15071.

19. Fung WL, McEvilly R, Fong J, Silversides C, Chow E, Bassett A (2010): Elevated prevalence of generalized anxiety disorder in adults with 22q11.2 deletion syndrome. *Am J Psychiatry*. 167:998.

20. Vorstman JA, Breetvelt EJ, Duijff SN, Eliez S, Schneider M, Jalbrzikowski M, et al. (2015): Cognitive decline preceding the onset of psychosis in patients with 22q11.2 deletion syndrome. *JAMA Psychiatry*. 72:377-385.

21. Goulding SM, Holtzman CW, Trotman HD, Ryan AT, Macdonald AN, Shapiro DI, et al. (2013): The prodrome and clinical risk for psychotic disorders. *Child Adolesc Psychiatr Clin N Am*. 22:557-567.

22. Yung AR, McGorry PD (1996): The initial prodrome in psychosis: descriptive and qualitative aspects. *Aust N Z J Psychiatry*. 30:587-599.

23. Yung AR, McGorry PD (1996): The prodromal phase of first-episode psychosis: past and current conceptualizations. *Schizophr Bull*. 22:353-370.

24. Salazar de Pablo G, Radua J, Pereira J, Bonoldi I, Arienti V, Besana F, et al. (2021): Probability of Transition to Psychosis in Individuals at Clinical High Risk: An Updated Meta-analysis. *JAMA Psychiatry*. 78:970-978.

25. Shapiro DI, Cubells JF, Ousley OY, Rockers K, Walker EF (2011): Prodromal symptoms in adolescents with 22q11.2 deletion syndrome and schizotypal personality disorder. *Schizophr Res*. 129:20-28.

26. Weisman O, Guri Y, Gur RE, McDonald-McGinn DM, Calkins ME, Tang SX, et al. (2017): Subthreshold Psychosis in 22q11.2 Deletion Syndrome: Multisite Naturalistic Study. *Schizophr Bull*. 43:1079-1089.

27. Cox DM, Butler MG (2015): A clinical case report and literature review of the 3q29 microdeletion syndrome. *Clin Dysmorphol*. 24:89-94.

28. Glassford MR, Rosenfeld JA, Freedman AA, Zwick ME, Mulle JG, Unique Rare Chromosome Disorder Support G (2016): Novel features of 3q29 deletion syndrome: Results from the 3q29 registry. *Am J Med Genet A*. 170A:999-1006.

29. Singh T, Neale BM, Daly MJ, Consortium obotSEM-A (2020): Exome sequencing identifies rare coding variants in 10 genes which confer substantial risk for schizophrenia. *medRxiv*.2020.2009.2018.20192815.

30. Murphy MM, Lindsey Burrell T, Cubells JF, Espana RA, Gambello MJ, Goines KCB, et al. (2018): Study protocol for The Emory 3q29 Project: evaluation of neurodevelopmental, psychiatric, and medical symptoms in 3q29 deletion syndrome. *BMC Psychiatry*. 18:183.

31. Miller TJ, McGlashan TH, Rosen JL, Cadenhead K, Cannon T, Ventura J, et al. (2003): Prodromal assessment with the structured interview for prodromal syndromes and the scale of prodromal symptoms: predictive validity, interrater reliability, and training to reliability. *Schizophr Bull.* 29:703-715.

32. Miller TJ, McGlashan TH, Rosen JL, Somjee L, Markovich PJ, Stein K, et al. (2002): Prospective diagnosis of the initial prodrome for schizophrenia based on the Structured Interview for Prodromal Syndromes: preliminary evidence of interrater reliability and predictive validity. *Am J Psychiatry.* 159:863-865.

33. Sefik E, Li Y, Sholar B, Evans L, Pincus J, Ammar Z, et al. (2022): Structural deviations of the posterior fossa and the cerebellum and their cognitive links in a neurodevelopmental deletion syndrome. *med*R*xiv*.2022.2003.2001.22271659.

34. Addington J, Liu L, Buchy L, Cadenhead KS, Cannon TD, Cornblatt BA, et al. (2015): North American Prodrome Longitudinal Study (NAPLS 2): The Prodromal Symptoms. *J Nerv Ment Dis.* 203:328-335.

35. Rockers K, Ousley O, Sutton T, Schoenberg E, Coleman K, Walker E, et al. (2009): Performance on the Modified Card Sorting Test and its relation to psychopathology in adolescents and young adults with 22q11.2 deletion syndrome. *J Intellect Disabil Res.* 53:665-676.

36. First MB, Williams JB, Karg RS, Spitzer RL (2015): Structured clinical interview for DSM-5—Research version (SCID-5 for DSM-5, research version; SCID-5-RV). *Arlington, VA: American Psychiatric Association.*1-94.

37. Mugler JP, 3rd, Brookeman JR (1990): Three-dimensional magnetization-prepared rapid gradient-echo imaging (3D MP RAGE). *Magn Reson Med.* 15:152-157.

38. Mugler JP, 3rd, Bao S, Mulkern RV, Guttmann CR, Robertson RL, Jolesz FA, et al. (2000): Optimized single-slab three-dimensional spin-echo MR imaging of the brain. *Radiology.* 216:891-899.

39. Glasser MF, Sotiropoulos SN, Wilson JA, Coalson TS, Fischl B, Andersson JL, et al. (2013): The minimal preprocessing pipelines for the Human Connectome Project. *Neuroimage.* 80:105-124.

40. Fischl B, Salat DH, Busa E, Albert M, Dieterich M, Haselgrove C, et al. (2002): Whole brain segmentation: automated labeling of neuroanatomical structures in the human brain. *Neuron.* 33:341-355.

41. Schmahmann JD, Doyon J, McDonald D, Holmes C, Lavoie K, Hurwitz AS, et al. (1999): Three-dimensional MRI atlas of the human cerebellum in proportional stereotaxic space. *Neuroimage.* 10:233-260.

42. Hoogendam YY, van der Geest JN, van der Lijn F, van der Lugt A, Niessen WJ, Krestin GP, et al. (2012): Determinants of cerebellar and cerebral volume in the general elderly population. *Neurobiol Aging*. 33:2774-2781.

43. Laidi C, d'Albis MA, Wessa M, Linke J, Phillips ML, Delavest M, et al. (2015): Cerebellar volume in schizophrenia and bipolar I disorder with and without psychotic features. *Acta Psychiatr Scand*. 131:223-233.

44. McDonald CR, Hagler DJ, Jr., Ahmadi ME, Tecoma E, Iragui V, Dale AM, et al. (2008): Subcortical and cerebellar atrophy in mesial temporal lobe epilepsy revealed by automatic segmentation. *Epilepsy Res*. 79:130-138.

45. Cerasa A, Messina D, Nicoletti G, Novellino F, Lanza P, Condino F, et al. (2009): Cerebellar atrophy in essential tremor using an automated segmentation method. *AJNR Am J Neuroradiol*. 30:1240-1243.

46. Lisdahl KM, Thayer R, Squeglia LM, McQueeny TM, Tapert SF (2013): Recent binge drinking predicts smaller cerebellar volumes in adolescents. *Psychiatry Res*. 211:17-23.

47. Walhovd KB, Fjell AM, Reinvang I, Lundervold A, Dale AM, Eilertsen DE, et al. (2005): Effects of age on volumes of cortex, white matter and subcortical structures. *Neurobiol Aging*. 26:1261-1270; discussion 1275-1268.

48. Zhao G, Walsh K, Long J, Gui W, Denisova K (2018): Reduced structural complexity of the right cerebellar cortex in male children with autism spectrum disorder. *PLoS One*. 13:e0196964.

49. Laidi C, Boisgontier J, Chakravarty MM, Hotier S, d'Albis MA, Mangin JF, et al. (2017): Cerebellar anatomical alterations and attention to eyes in autism. *Sci Rep*. 7:12008.

50. Cao H, Chen OY, Chung Y, Forsyth JK, McEwen SC, Gee DG, et al. (2018): Cerebello-thalamo-cortical hyperconnectivity as a state-independent functional neural signature for psychosis prediction and characterization. *Nat Commun*. 9:3836.

51. Davis P, Wright E (1977): A new method for measuring cranial cavity volume and its application to the assessment of cerebral atrophy at autopsy. *Neuropathology and applied neurobiology*. 3:341-358.

52. Buckner RL, Head D, Parker J, Fotenos AF, Marcus D, Morris JC, et al. (2004): A unified approach for morphometric and functional data analysis in young, old, and demented adults using automated atlas-based

head size normalization: reliability and validation against manual measurement of total intracranial volume. *Neuroimage*. 23:724-738.

53. Shen L, Saykin AJ, Kim S, Firpi HA, West JD, Risacher SL, et al. (2010): Comparison of manual and automated determination of hippocampal volumes in MCI and early AD. *Brain Imaging Behav*. 4:86-95.

54. Nordenskjold R, Malmberg F, Larsson EM, Simmons A, Brooks SJ, Lind L, et al. (2013): Intracranial volume estimated with commonly used methods could introduce bias in studies including brain volume measurements. *Neuroimage*. 83:355-360.

55. Malone IB, Leung KK, Clegg S, Barnes J, Whitwell JL, Ashburner J, et al. (2015): Accurate automatic estimation of total intracranial volume: a nuisance variable with less nuisance. *Neuroimage*. 104:366-372.

56. O'Brien LM, Ziegler DA, Deutsch CK, Frazier JA, Herbert MR, Locascio JJ (2011): Statistical adjustments for brain size in volumetric neuroimaging studies: some practical implications in methods. *Psychiatry Res*. 193:113-122.

57. Willatt L, Cox J, Barber J, Cabanas ED, Collins A, Donnai D, et al. (2005): 3q29 microdeletion syndrome: clinical and molecular characterization of a new syndrome. *Am J Hum Genet*. 77:154-160.

58. Ballif BC, Theisen A, Coppinger J, Gowans GC, Hersh JH, Madan-Khetarpal S, et al. (2008): Expanding the clinical phenotype of the 3q29 microdeletion syndrome and characterization of the reciprocal microduplication. *Mol Cytogenet*. 1:8.

59. R Development Core Team (2021): R: A Language and Environment for Statistical Computing. Vienna, Austria: R Foundation for Statistical Computing.

60. MacKinnon JG, White H (1985): Some heteroskedasticity-consistent covariance matrix estimators with improved finite sample properties. *Journal of econometrics*. 29:305-325.

61. Sullivan SA, Kounali D, Cannon M, David AS, Fletcher PC, Holmans P, et al. (2020): A Population-Based Cohort Study Examining the Incidence and Impact of Psychotic Experiences From Childhood to Adulthood, and Prediction of Psychotic Disorder. *Am J Psychiatry*. 177:308-317.

62. Hafner H (2019): From Onset and Prodromal Stage to a Life-Long Course of Schizophrenia and Its Symptom Dimensions: How Sex, Age, and Other Risk Factors Influence Incidence and Course of Illness. *Psychiatry J*. 2019:9804836.

63. Waford RN, MacDonald A, Goines K, Novacek DM, Trotman HD, Elaine FW, et al. (2015): Demographic correlates of attenuated positive psychotic symptoms. *Schizophr Res*. 166:31-36.

64. Helzer JE, Kraemer HC, Krueger RF (2006): The feasibility and need for dimensional psychiatric diagnoses. *Psychol Med*. 36:1671-1680.

65. Allardyce J, Suppes T, Van Os J (2007): Dimensions and the psychosis phenotype. *Int J Methods Psychiatr Res*. 16 Suppl 1:S34-40.

66. Potuzak M, Ravichandran C, Lewandowski KE, Ongur D, Cohen BM (2012): Categorical vs dimensional classifications of psychotic disorders. *Compr Psychiatry*. 53:1118-1129.

67. Girirajan S, Campbell CD, Eichler EE (2011): Human copy number variation and complex genetic disease. *Annu Rev Genet*. 45:203-226.

68. Sullivan PF (2017): Schizophrenia and the dynamic genome. *Genome Med*. 9:22.

69. Addington J, Cadenhead KS, Cornblatt BA, Mathalon DH, McGlashan TH, Perkins DO, et al. (2012): North American Prodrome Longitudinal Study (NAPLS 2): overview and recruitment. *Schizophr Res*. 142:77-82.

70. Cui H, Giuliano AJ, Zhang T, Xu L, Wei Y, Tang Y, et al. (2020): Cognitive dysfunction in a psychotropic medication-naive, clinical high-risk sample from the ShangHai-At-Risk-for-Psychosis (SHARP) study: Associations with clinical outcomes. *Schizophr Res*. 226:138-146.

71. Bourgin J, Duchesnay E, Magaud E, Gaillard R, Kazes M, Krebs MO (2020): Predicting the individual risk of psychosis conversion in at-risk mental state (ARMS): a multivariate model reveals the influence of nonpsychotic prodromal symptoms. *Eur Child Adolesc Psychiatry*. 29:1525-1535.

72. Fusar-Poli P, Bonoldi I, Yung AR, Borgwardt S, Kempton MJ, Valmaggia L, et al. (2012): Predicting psychosis: meta-analysis of transition outcomes in individuals at high clinical risk. *Arch Gen Psychiatry*. 69:220-229.

73. Debbane M, Glaser B, David MK, Feinstein C, Eliez S (2006): Psychotic symptoms in children and adolescents with 22q11.2 deletion syndrome: Neuropsychological and behavioral implications. *Schizophr Res.* 84:187-193.

74. Usiskin SI, Nicolson R, Krasnewich DM, Yan W, Lenane M, Wudarsky M, et al. (1999): Velocardiofacial syndrome in childhood-onset schizophrenia. *J Am Acad Child Adolesc Psychiatry.* 38:1536-1543.

75. Chawner S, Niarchou M, Doherty JL, Moss H, Owen MJ, van den Bree MBM (2019): The emergence of psychotic experiences in the early adolescence of 22q11.2 Deletion Syndrome. *J Psychiatr Res.* 109:10-17.

76. Murphy KC, Jones LA, Owen MJ (1999): High rates of schizophrenia in adults with velo-cardio-facial syndrome. *Arch Gen Psychiatry.* 56:940-945.

77. Ivanov D, Kirov G, Norton N, Williams HJ, Williams NM, Nikolov I, et al. (2003): Chromosome 22q11 deletions, velo-cardio-facial syndrome and early-onset psychosis. Molecular genetic study. *Br J Psychiatry.* 183:409-413.

78. Bassett AS, Chow EW, AbdelMalik P, Gheorghiu M, Husted J, Weksberg R (2003): The schizophrenia phenotype in 22q11 deletion syndrome. *Am J Psychiatry.* 160:1580-1586.

79. Bassett AS, Hodgkinson K, Chow EW, Correia S, Scutt LE, Weksberg R (1998): 22q11 deletion syndrome in adults with schizophrenia. *Am J Med Genet.* 81:328-337.

80. Preti A, Cella M (2010): Randomized-controlled trials in people at ultra high risk of psychosis: a review of treatment effectiveness. *Schizophr Res.* 123:30-36.

81. Armando M, Girardi P, Vicari S, Menghini D, Digilio MC, Pontillo M, et al. (2012): Adolescents at ultra-high risk for psychosis with and without 22q11 deletion syndrome: a comparison of prodromal psychotic symptoms and general functioning. *Schizophrenia research.* 139:151-156.

82. Mekori-Domachevsky E, Guri Y, Yi J, Weisman O, Calkins ME, Tang SX, et al. (2017): Negative subthreshold psychotic symptoms distinguish 22q11.2 deletion syndrome from other neurodevelopmental disorders: A two-site study. *Schizophr Res.* 188:42-49.

83. Antshel KM, Fremont W, Roizen NJ, Shprintzen R, Higgins AM, Dhamoon A, et al. (2006): ADHD, major depressive disorder, and simple phobias are prevalent psychiatric conditions in youth with velocardiofacial syndrome. *J Am Acad Child Adolesc Psychiatry*. 45:596-603.

84. Antshel KM, Shprintzen R, Fremont W, Higgins AM, Faraone SV, Kates WR (2010): Cognitive and psychiatric predictors to psychosis in velocardiofacial syndrome: a 3-year follow-up study. *J Am Acad Child Adolesc Psychiatry*. 49:333-344.

85. Barch DM, Dowd EC (2010): Goal representations and motivational drive in schizophrenia: the role of prefrontal-striatal interactions. *Schizophr Bull*. 36:919-934.

86. Ventura J, Hellemann GS, Thames AD, Koellner V, Nuechterlein KH (2009): Symptoms as mediators of the relationship between neurocognition and functional outcome in schizophrenia: a meta-analysis. *Schizophr Res*. 113:189-199.

87. Schneider M, Armando M, Schultze-Lutter F, Pontillo M, Vicari S, Debbane M, et al. (2019): Prevalence, course and psychosis-predictive value of negative symptoms in 22q11.2 deletion syndrome. *Schizophr Res*. 206:386-393.

88. Fusar-Poli P, Papanastasiou E, Stahl D, Rocchetti M, Carpenter W, Shergill S, et al. (2015): Treatments of Negative Symptoms in Schizophrenia: Meta-Analysis of 168 Randomized Placebo-Controlled Trials. *Schizophr Bull*. 41:892-899.

89. Schmahmann JD (1998): Dysmetria of thought: clinical consequences of cerebellar dysfunction on cognition and affect. *Trends Cogn Sci*. 2:362-371.

90. Ito M (1993): Movement and thought: identical control mechanisms by the cerebellum. *Trends Neurosci*. 16:448-450; discussion 453-444.

91. Ito M (2008): Control of mental activities by internal models in the cerebellum. *Nat Rev Neurosci*. 9:304-313.

92. Moberget T, Gullesen EH, Andersson S, Ivry RB, Endestad T (2014): Generalized role for the cerebellum in encoding internal models: evidence from semantic processing. *J Neurosci*. 34:2871-2878.

93. Wolpert DM, Ghahramani Z, Jordan MI (1995): An internal model for sensorimotor integration. *Science*. 269:1880-1882.

94. Ito M (2006): Cerebellar circuitry as a neuronal machine. *Progress in neurobiology*. 78:272-303.

95. Ford JM, Mathalon DH (2005): Corollary discharge dysfunction in schizophrenia: can it explain auditory hallucinations? *International Journal of Psychophysiology*. 58:179-189.

96. Frith C (2005): The neural basis of hallucinations and delusions. *Comptes rendus biologies*. 328:169-175.

97. Picard H, Amado I, Mouchet-Mages S, Olie JP, Krebs MO (2008): The role of the cerebellum in schizophrenia: an update of clinical, cognitive, and functional evidences. *Schizophr Bull*. 34:155-172.

98. Moberget T, Ivry RB (2019): Prediction, psychosis, and the cerebellum. *Biological Psychiatry: Cognitive Neuroscience and Neuroimaging*. 4:820-831.

99. Andreasen NC, Paradiso S, O'leary DS (1998): "Cognitive dysmetria" as an integrative theory of schizophrenia: a dysfunction in cortical-subcortical-cerebellar circuitry? *Schizophrenia bulletin*. 24:203-218.

100. Andreasen NC, O'Leary DS, Cizadlo T, Arndt S, Rezai K, Ponto L, et al. (1996): Schizophrenia and cognitive dysmetria: a positron-emission tomography study of dysfunctional prefrontal-thalamic-cerebellar circuitry. *Proceedings of the National Academy of Sciences*. 93:9985-9990.

101. Andreasen NC, Nopoulos P, O'Leary DS, Miller DD, Wassink T, Flaum M (1999): Defining the phenotype of schizophrenia: cognitive dysmetria and its neural mechanisms. *Biological psychiatry*. 46:908-920.

102. Leroi I, O'Hearn E, Marsh L, Lyketsos CG, Rosenblatt A, Ross CA, et al. (2002): Psychopathology in patients with degenerative cerebellar diseases: a comparison to Huntington's disease. *Am J Psychiatry*. 159:1306-1314.

103. Liszewski CM, O'Hearn E, Leroi I, Gourley L, Ross CA, Margolis RL (2004): Cognitive impairment and psychiatric symptoms in 133 patients with diseases associated with cerebellar degeneration. *J Neuropsychiatry Clin Neurosci*. 16:109-112.

104. Schmahmann JD, Sherman JC (1998): The cerebellar cognitive affective syndrome. *Brain: a journal of neurology*. 121:561-579.

105. Schmahmann JD (2004): Disorders of the cerebellum: ataxia, dysmetria of thought, and the cerebellar cognitive affective syndrome. *The Journal of neuropsychiatry and clinical neurosciences*. 16:367-378.

106. Schmahmann JD, Weilburg JB, Sherman JC (2007): The neuropsychiatry of the cerebellum - insights from the clinic. *Cerebellum*. 6:254-267.

107. Argyropoulos GPD, van Dun K, Adamaszek M, Leggio M, Manto M, Masciullo M, et al. (2020): The Cerebellar Cognitive Affective/Schmahmann Syndrome: a Task Force Paper. *Cerebellum*. 19:102-125.

108. Shenton ME, Dickey CC, Frumin M, McCarley RW (2001): A review of MRI findings in schizophrenia. *Schizophr Res*. 49:1-52.

109. Shepherd AM, Laurens KR, Matheson SL, Carr VJ, Green MJ (2012): Systematic meta-review and quality assessment of the structural brain alterations in schizophrenia. *Neurosci Biobehav Rev*. 36:1342-1356.

110. Moberget T, Doan N, Alnæs D, Kaufmann T, Córdova-Palomera A, Lagerberg T, et al. (2018): Cerebellar volume and cerebellocerebral structural covariance in schizophrenia: a multisite mega-analysis of 983 patients and 1349 healthy controls. *Molecular psychiatry*. 23:1512-1520.

111. Wassink TH, Andreasen NC, Nopoulos P, Flaum M (1999): Cerebellar morphology as a predictor of symptom and psychosocial outcome in schizophrenia. *Biol Psychiatry*. 45:41-48.

112. Bottmer C, Bachmann S, Pantel J, Essig M, Amann M, Schad LR, et al. (2005): Reduced cerebellar volume and neurological soft signs in first-episode schizophrenia. *Psychiatry Res*. 140:239-250.

113. Kim T, Lee KH, Oh H, Lee TY, Cho KIK, Lee J, et al. (2018): Cerebellar Structural Abnormalities Associated With Cognitive Function in Patients With First-Episode Psychosis. *Front Psychiatry*. 9:286.

114. Gupta CN, Calhoun VD, Rachakonda S, Chen J, Patel V, Liu J, et al. (2015): Patterns of Gray Matter Abnormalities in Schizophrenia Based on an International Mega-analysis. *Schizophr Bull*. 41:1133-1142.

115. Chen YL, Tu PC, Lee YC, Chen YS, Li CT, Su TP (2013): Resting-state fMRI mapping of cerebellar functional dysconnections involving multiple large-scale networks in patients with schizophrenia. *Schizophr Res*. 149:26-34.

116. Levitt JJ, McCarley RW, Nestor PG, Petrescu C, Donnino R, Hirayasu Y, et al. (1999): Quantitative volumetric MRI study of the cerebellum and vermis in schizophrenia: clinical and cognitive correlates. *Am J Psychiatry*. 156:1105-1107.

117. Nopoulos PC, Ceilley JW, Gailis EA, Andreasen NC (1999): An MRI study of cerebellar vermis morphology in patients with schizophrenia: evidence in support of the cognitive dysmetria concept. *Biol Psychiatry*. 46:703-711.

118. Keller A, Castellanos FX, Vaituzis AC, Jeffries NO, Giedd JN, Rapoport JL (2003): Progressive loss of cerebellar volume in childhood-onset schizophrenia. *Am J Psychiatry*. 160:128-133.

119. He H, Luo C, Luo Y, Duan M, Yi Q, Biswal BB, et al. (2019): Reduction in gray matter of cerebellum in schizophrenia and its influence on static and dynamic connectivity. *Hum Brain Mapp*. 40:517-528.

120. Maloku E, Covelo IR, Hanbauer I, Guidotti A, Kadriu B, Hu Q, et al. (2010): Lower number of cerebellar Purkinje neurons in psychosis is associated with reduced reelin expression. *Proceedings of the National Academy of Sciences*. 107:4407-4411.

121. Mavroudis IA, Petrides F, Manani M, Chatzinikolaou F, Ciobica AS, Padurariu M, et al. (2017): Purkinje cells pathology in schizophrenia. A morphometric approach. *Rom J Morphol Embryol*. 58:419-424.

122. Greenstein D, Lenroot R, Clausen L, Chavez A, Vaituzis AC, Tran L, et al. (2011): Cerebellar development in childhood onset schizophrenia and non-psychotic siblings. *Psychiatry Res*. 193:131-137.

123. Dean DJ, Bernard JA, Orr JM, Pelletier-Baldelli A, Gupta T, Carol EE, et al. (2014): Cerebellar Morphology and Procedural Learning Impairment in Neuroleptic-Naive Youth at Ultrahigh Risk of Psychosis. *Clin Psychol Sci*. 2:152-164.

124. Smieskova R, Fusar-Poli P, Allen P, Bendfeldt K, Stieglitz RD, Drewe J, et al. (2010): Neuroimaging predictors of transition to psychosis--a systematic review and meta-analysis. *Neurosci Biobehav Rev*. 34:1207-1222.

125. Pantelis C, Velakoulis D, McGorry PD, Wood SJ, Suckling J, Phillips LJ, et al. (2003): Neuroanatomical abnormalities before and after onset of psychosis: a cross-sectional and longitudinal MRI comparison. *Lancet*. 361:281-288.

126. Borgwardt SJ, McGuire PK, Aston J, Berger G, Dazzan P, Gschwandtner U, et al. (2007): Structural brain abnormalities in individuals with an at-risk mental state who later develop psychosis. *Br J Psychiatry Suppl.* 51:s69-75.

127. Merritt K, Luque Laguna P, Irfan A, David AS (2021): Longitudinal Structural MRI Findings in Individuals at Genetic and Clinical High Risk for Psychosis: A Systematic Review. *Front Psychiatry.* 12:620401.

128. Bernard JA, Orr JM, Mittal VA (2017): Cerebello-thalamo-cortical networks predict positive symptom progression in individuals at ultra-high risk for psychosis. *Neuroimage Clin.* 14:622-628.

129. Borgwardt SJ, Riecher-Rossler A, Dazzan P, Chitnis X, Aston J, Drewe M, et al. (2007): Regional gray matter volume abnormalities in the at risk mental state. *Biol Psychiatry.* 61:1148-1156.

130. Koutsouleris N, Schmitt GJ, Gaser C, Bottlender R, Scheuerecker J, McGuire P, et al. (2009): Neuroanatomical correlates of different vulnerability states for psychosis and their clinical outcomes. *Br J Psychiatry.* 195:218-226.

131. Koutsouleris N, Gaser C, Bottlender R, Davatzikos C, Decker P, Jager M, et al. (2010): Use of neuroanatomical pattern regression to predict the structural brain dynamics of vulnerability and transition to psychosis. *Schizophr Res.* 123:175-187.

132. Moberget T, Alnæs D, Kaufmann T, Doan NT, Córdova-Palomera A, Norbom LB, et al. (2019): Cerebellar gray matter volume is associated with cognitive function and psychopathology in adolescence. *Biological psychiatry.* 86:65-75.

133. Sefik E, Purcell RH, Emory 3q P, Walker EF, Bassell GJ, Mulle JG (2021): Convergent and distributed effects of the 3q29 deletion on the human neural transcriptome. *Transl Psychiatry.* 11:357.

134. Carroll LS, Williams HJ, Walters J, Kirov G, O'Donovan MC, Owen MJ (2011): Mutation screening of the 3q29 microdeletion syndrome candidate genes DLG1 and PAK2 in schizophrenia. *Am J Med Genet B Neuropsychiatr Genet.* 156B:844-849.

135. Wang VY, Zoghbi HY (2001): Genetic regulation of cerebellar development. *Nat Rev Neurosci.* 2:484-491.

136. ten Donkelaar HJ, Lammens M, Wesseling P, Thijssen HO, Renier WO (2003): Development and developmental disorders of the human cerebellum. *J Neurol*. 250:1025-1036.

137. Altman DG, Royston P (2006): The cost of dichotomising continuous variables. *BMJ*. 332:1080.

138. Kirkwood BRSJACBS (2019): *Essential medical statistics*. Malden, MA: Blackwell Science.

139. Powers AR, Addington J, Perkins DO, Bearden CE, Cadenhead KS, Cannon TD, et al. (2020): Duration of the psychosis prodrome. *Schizophrenia research*. 216:443-449.

140. Palesi F, Tournier JD, Calamante F, Muhlert N, Castellazzi G, Chard D, et al. (2015): Contralateral cerebello-thalamo-cortical pathways with prominent involvement of associative areas in humans in vivo. *Brain Struct Funct*. 220:3369-3384.

141. Bostan AC, Dum RP, Strick PL (2010): The basal ganglia communicate with the cerebellum. *Proc Natl Acad Sci U S A*. 107:8452-8456.

142. Rutkowski TP, Purcell RH, Pollak RM, Grewenow SM, Gafford GM, Malone T, et al. (2021): Behavioral changes and growth deficits in a CRISPR engineered mouse model of the schizophrenia-associated 3q29 deletion. *Mol Psychiatry*. 26:772-783.

Supplemental Materials

Extended Methods

Assessment of attenuated and florid psychotic symptoms

In both deletion samples and HCs, the SIPS semi-structured clinical interview was administered by trained personnel, with two main aims: 1) to determine the presence of psychosis, present or past, and 2) to assess the severity of attenuated symptoms (Miller et al., 2003). The 19 items in the SIPS are grouped within four domains: positive, negative, disorganization, and general. Each item is rated on a scale from 0 (*Absent*) to 6 (*Severe and Psychotic* for positive symptoms, *Extreme* for others), with a rating of 3 (*Moderate*) indicating clinical significance. The intensity of experience, any associated distress and impairment, and insight (for positive symptoms) were considered for each rating. Item ratings were summed to produce a total score for each domain. The onset and worsening of symptoms were collected for 3q29Del to determine the presence of a psychosis-risk syndrome. The basis of ratings for 3q29Del and 22q11.2Del also relied on the reports of guardians when present. Overall, the instrument maintains excellent inter-rater reliability (Miller et al., 2003) and is comparable to the performance of another valid instrument in the CHR field (Fusar-Poli et al., 2015). For adolescents and adults with 3q29Del meeting criteria for a psychotic disorder, the Structured Clinical Interview for DSM-5 (SCID-5) (First et al., 2015) specified the diagnosis.

All participants provided written consent to participate in each respective project; in cases when the participant was a minor, a parent or legal guardian provided consent and the minor provided assent. The informed consent process and study procedures were in accordance with Emory University Institutional Review Board for the 3q29Del and 22q11.2Del samples. For NAPLS2, the study procedures were approved by the review boards of each individual site, including Emory University.

Cognitive assessment protocols

The 3q29Del sample: Participants who were 18-years-old or older completed the Vocabulary, Similarities, Block Design and Matrix Reasoning subtests of the second edition of the Wechsler Abbreviated Scale of Intelligence (WASI-II) (Wechsler, 2011). The scores from all four subsets were then combined to form

a Full Score Intelligence Quotient (FSIQ) score to estimate general cognitive ability. Participants who were between seven and 17-years-old completed the Verbal Similarities, Word Definitions, Sequential and Quantitative Reasoning and Matrices subtests of the second edition (school-age form) of the Differential Ability Scales (DAS-II) (Elliot, 2007). Younger participants completed the Verbal Comprehension, Naming Vocabulary, Picture Similarities and Matrices subtests of the second edition (early years form) of the Differential Ability Scales (DAS-II) (Elliot, 2007). The scores from all four subsets were then combined to form a General Conceptual Ability (GCA) composite score to estimate general cognitive ability. See Murphy et al. (2018) for detailed study protocol.

The 22q11.2Del sample**:** Participants who were 17-years-old or older completed the Vocabulary, Arithmetic, Similarities, and Block Design subtests of the third edition of the Wechsler Adult Intelligence Scale (WAIS-III) (Wechsler, 1997). Younger participants completed the equivalent subtests in the third edition of the Wechsler Intelligence Scale for Children (WISC-III) (Wechsler, 1991). As participants completed only a portion of each intelligence scale, an estimation of intellectual functioning hinged upon performance on these subtests. Sattler (2002) identified short-form combinations of individual subtests that could reliably estimate intellectual functioning. The most valid short form for each intelligence scale was selected for this sample from these combinations; see Appendices A and C in Sattler (2002) for reliability and validity coefficients and conversion tables. For the WISC-III, the best performing short form included the sum of Arithmetic, Vocabulary and Block Design (r = 0.88), whereas for the WAIS-III the short form included all four administered subtests (r = 0.92). The sum of the scaled scores within each combination were used to derive the estimated full scale deviation quotients (Sattler, 2002).

Healthy controls: All participants were administered two subtests from the first edition of the Wechsler Abbreviated Scale of Intelligence (WASI-I): Vocabulary and Block Design (Wechsler, 1999). The four-subtest WASI was developed from the Wechsler intelligence scales in order to briefly approximate FSIQ, as it relies on its own two- and four-subtest short forms. Two-subtest estimates of FSIQ from the WASI strongly correlate with estimates from the WAIS-III among neurotypical samples (r = 0.87) (Weschler, 1999). Performance on these two subtests (Vocabulary and Block Design) were utilized to estimate FSIQ.

Extended methods for structural magnetic resonance imaging

T1- and T2-weighted structural magnetic resonance imaging (MRI) was performed in 17 3q29Del participants with available SIPS data, ages 8.08-39.12 (mean ± SD = 18.13 ± 9.03 years), at the Emory University Center for Systems Imaging Core. Images were acquired on a Siemens Magnetom Prisma 3T scanner in the sagittal plane using a 32-channel Prisma head coil with 3D MPRAGE and SPACE sequences, after completion of a training protocol using a mock scanner. To avoid bias and variability associated with hand-drawn measurements, we performed automatic segmentation of acquired images by using FreeSurfer. As recommended, two trained evaluators (ES, LL) inspected the MRI scans to determine whether technical problems (e.g., motion artifacts) or notable pathology (e.g., arachnoid cysts) interfere with segmentation quality; all scans included in this study passed quality control. Note that when compared with manual delineation, segmentations obtained by the FreeSurfer software were found by others to yield well-defined boundaries for the cerebellum comparable in accuracy to manual labeling; a previous quantitative evaluation of robustness and accuracy indicated an excellent dice similarity index, as well as high recall and precision values for cerebellar segmentation results acquired by FreeSurfer (Fischl et al., 2002; Lee et al., 2015). In this framework, cerebellar cortex refers to the tightly folded outer mantle that mostly contains gray matter, while cerebellar white matter refers to the inner core that mostly contains myelinated nerve fibers.

Extended statistical analyses

In between-group analyses, since we observed several violations of the statistical assumptions required for ANCOVA (partially due to a likely floor effect in the HC sample), all SIPS scores were log-transformed to improve normality and homogeneity of variances. Age and sex were considered as potential covariates prior to assessing the variation in psychotic symptom profiles between groups. We ran an exploratory Pearson correlation analysis between age and SIPS domain scores separately by diagnostic group and performed Fisher's *r*-to-*Z* transformation to assess the significance of the difference between resulting coefficients. Additionally, we examined sex differences among 3q29Del participants as well as within the comparison groups, using

ANCOVAs by symptom domain and then item-wise, while adjusting for age. In sex-specific analyses, assumption violations were observed only in the HC group, hence log-transformation was applied only to HC scores in these analyses. Note that since general symptoms are considered non-specific to psychosis (e.g., impaired tolerance to stress), they were excluded from downstream neuroimaging analyses in the 3q29Del sample.

List of R packages used for statistical analyses

Pearson's chi-squared tests, Fisher's exact tests, t-tests (paired and unpaired) and Wilcoxon signed-rank tests were performed using the standard R *chisq.test(), fisher.test(), t.test()* and *wilcox.test()* functions. Analyses of variance (ANOVA) and analyses of covariance (ANCOVA) were performed by the standard R *anova()* function. Partial eta-squared was used to assess effect sizes via the *eta_squared()* function from the *effectsize* package (https://CRAN.R-project.org/package=effectsize). Pairwise comparisons for 3q29Del vs. HCs and 3q29Del vs. 22q11.2Del were performed to assess the relative severity of attenuated symptoms using the *glht()* function from the *multcomp* package (https://CRAN.R-project.org/package=multcomp). The standard R *cor.test()* function was used to perform Pearson's correlations. Fisher's *r*-to-*Z* transformation for exploratory correlation analyses between age and symptom domain scores was performed by using the *cocor.indep.groups()* function from the *cocor* package (https://CRAN.R-project.org/package=cocor). The multiple linear regression and binary logistic regression models reported in the neuroimaging arm of the study were performed via the standard R *lm()* and g*lm()* functions (family=binomial, link=logit), respectively. Wald statistics were calculated by the *waldtest()* function from the *lmtest* package (https://CRAN.R-project.org/package=lmtest). Heteroscedasticity-robust estimates were calculated using the *vcovHC()* function from the *sandwich* package (https://CRAN.R-project.org/package=sandwich). Diagnostics plots for linear regression were inspected using the R base function *plot()*. Shapiro-Wilk tests were performed using the standard R *shapiro.test()* function to check for assumptions of normality. Breusch-Pagan and Levene's test were performed using the *bptest()* function from the *lmtest* package (https://CRAN.R-project.org/package=lmtest) and the *levene_test()* function from the *rstatix* package (https://CRAN.R-project.org/package=rstatix) to check for homogeneity of variances, respectively.

Graphics were generated by the *ggplot2* (https://CRAN.R-project.org/package=ggplot2), *ggpubr (https://cran.r-project.org/package=ggpubr)* and *jtools* (https://cran.r-project.org/package=jtools) packages

Extended Results

Sex differences in SIPS ratings within groups

We examined within-group sex differences for the three diagnostic groups. Statistical analyses included a set of ANCOVAs adjusted for age; values for HCs were log-transformed given assumption violations within this group. As these analyses were conducted to explore whether there were sex differences in symptoms similar to those observed in research on CHR and psychotic patients, correction for multiple comparisons was not made. The unadjusted means and standard errors for each group are presented in Fig. S3.

The differences in domain scores between males and females with 3q29Del were nonsignificant for positive [$F(1,20) = 1.60$, $p = 0.22$], disorganization [$F(1,20) = 1.90$, $p = 0.18$], and general [$F(1,20) = 1.13$, $p = 0.30$] symptoms. Sex did explain variation in negative symptoms [$F(1, 20) = 4.85$, $p = 0.04$, $\eta^2_p = 0.20$], as males exhibited more severe symptoms (age-adjusted mean ± *SD* = 10.42 ± 5.58) than females (age-adjusted mean ± *SD* = 5.12 ± 5.61). Similarly, among the 22q11.2Del group, there was no sex difference in positive [$F(1, 27) = 2.40$, $p = 0.13$], disorganization [$F(1, 28) = 4.19$, $p = 0.05$], or general [$F(1, 28) = 3.07$, $p = 0.09$] symptoms. Only negative symptoms differed by sex [$F(1, 28) = 5.10$, $p = 0.03$, $\eta^2_p = 0.15$], with males with 22q11.2Del exhibiting more severe symptoms (age-adjusted mean ± *SD* = 15.50 ± 5.31) than females (age-adjusted mean ± *SD* = 11.20 ± 5.32). Sex differences among HCs evidenced a similar pattern, with no sex differences for disorganization [$F(1, 276) = 1.21$, $p = 0.27$], or general [$F(1, 276) = 2.96$, $p = 0.09$] symptoms, and negative symptoms were rated higher in males (log-transformed age-adjusted mean ± *SD* = 0.311 ± 3.08) than females (log-transformed age-adjusted mean ± *SD* = 0.21 ± 3.10) [$F(1, 276) = 6.94$, $p = 0.01$, $\eta^2_p = 0.02$]. However, sex differences among HCs were observed in positive symptoms [$F(1, 276) = 3.93$, $p = 0.05$, $\eta^2_p = 0.01$], with greater severity among males (log-transformed age-adjusted mean ± *SD* = 0.25 ± 2.79) versus females (log-transformed age-adjusted mean ± *SD* = 0.18 ± 2.78).

Sex differences were also tested in item-wise ratings within each group, while adjusting for age. For

3q29Del, only one item, impaired ideational richness, marginally varied by sex, with males rated higher [$F(1,20) = 4.71$, $p = 0.04$, $\eta^2_p = 0.19$]. In contrast, males were rated significantly higher than females with 22q11.2Del on ratings for suspiciousness [$F(1,20) = 4.32$, $p = 0.05$, $\eta^2_p = 0.13$], social anhedonia [$F(1,28) = 6.06$, $p = 0.02$, $\eta^2_p = 0.18$], experience of emotion and self [$F(1,20) = 5.43$, $p = 0.03$, $\eta^2_p = 0.16$], and bizarre thinking [$F(1,20) = 6.22$, $p = 0.02$, $\eta^2_p = 0.18$]. Lastly, for HCs, males were rated higher than females on grandiosity [$F(1,276) = 10.27$, $p = 0.001$, $\eta^2_p = 0.04$], disorganized communication [$F(1,276) = 6.02$, $p = 0.01$, $\eta^2_p = 0.02$], and occupational functioning [$F(1,276) = 7.77$, $p = 0.014$, $\eta^2_p = 0.03$].

Supplemental Tables

	3q29Del (*N* = 23)	HC (*N* = 279)	22q11.2Del (*N* = 31)	Pairwise comparisons with 3q29Del: 3q29Del vs. HC	Pairwise comparisons with 3q29Del: 3q29Del vs. 22q11.2Del
Age (in years)					
M ± *SD* Median [Range]	16.94 ± 8.24 15.89 [8.08 – 39.12]	20.08 ± 4.761 20.04 [12.07 – 34.41]	19.75 ± 4.12 19.10 [13.85 – 29.77]	*p-value*[a] = 0.003**	*p-value*[a] = 0.02*
Sex, *N (%)*					
Male Female	14 (61%) 9 (39%)	141 (51%) 138 (49%)	14 (45%) 17 (55%)	*p-value*[b] = 0.46	*p-value*[b] = 0.39
Race, *N (%)*					
White Black or African American Asian More than one race Other (e.g., Native Hawaiian or Pacific Islander)	20 (87%) 0 (0%) 0 (0%) 3 (13%) 0 (0%)	152 (55%) 48 (17%) 30 (11%) 29 (10%) 20 (7%)	13 (76%) 3 (18%) 1 (6%) 0 (0%) 0 (0%)	*p-value*[c] = 0.006**	*p-value*[c] = 0.02*
Ethnicity, *N (%)*					
Hispanic/Latino Non-Hispanic/Latino	1 (4%) 22 (96%)	50 (18%) 229 (82%)	2 (11%) 17 (89%)	*p-value*[c] = 0.14	*p-value*[c] = 0.58
General cognitive abilities					
M ± *SD* Median [Range]	73.74 ± 11.98 75 [46 – 99]	111.00 ± 14.16 112 [72 – 139]	73.71 ± 15.91 71 [46 – 109]	*p-value*[a] = < 0.001***	*p-value*[a] = 0.88

Table S1. Demographic and relevant clinical information for the HC and 22q11.2Del samples and comparison with 3q29Del. [a] Wilcoxon rank sum test with continuity correction, [b] Pearson's chi-squared test with Yates' continuity correction. [c] Fisher's exact test (due to smaller subsamples). There were no significant differences in the sex or ethnicity compositions of the 3q29Del vs HC groups, or the 3q29Del vs 22q11.2Del groups (p's > 0.05). There was a significant age difference between the 3q29Del vs HC groups ($p \leq 0.01$), and the 3q29Del vs 22q11.2Del groups ($p \leq 0.05$), with the 3q29Del group being younger on average. There were significant differences in the race composition of the 3q29Del vs HC groups ($p \leq 0.01$), and the 3q29Del vs

22q11.2Del groups ($p \leq 0.05$), with the 3q29Del group having a larger fraction of subjects identifying as "White". There was no significant difference between the 3q29Del vs 22q11.2Del groups in general cognitive ability ($p > 0.05$). As expected, there was a significant difference between the 3q29Del vs HC groups in general cognitive ability ($p \leq 0.001$), with 3q29Del subjects exhibiting lower scores than HCs on average. For general cognitive abilities, HC $N = 262$ due to missing data. For race and ethnicity, 22q11.2Del $N = 17$ and $N = 19$, respectively due to missing data. Percentages reflect fraction of subjects with complete data. Two-tailed significance levels: *p-value* ≤ 0.001 '***', *p-value* ≤ 0.01 '**', *p-value* ≤ 0.05 '*', *p-value* ≤ 0.1 '†'. *Abbreviations:* healthy control, HC; deletion, Del; mean, *M*; standard deviation, *SD*.

	Pearson's correlation coefficients between age and symptom ratings			Pairwise comparisons of group-specific correlation coefficients	
SIPS Domains	**HC** (*N* = 279)	**22q11.2Del** (*N* = 31)	**3q29Del** (*N* = 23)	**3q29Del vs. HC**	**3q29Del vs. 22q11.2Del**
Positive Symptom Domain	-0.11[a]	0.19	0.40[a]	z = 2.31 *p*-value = 0.02	z = 0.78 *p*-value = 0.43
Negative Symptom Domain	-0.15*[a]	0.02	0.37[a]	z = 2.33 *p*-value = 0.02	z = 1.26 *p*-value = 0.21
Disorganization Symptom Domain	-0.08	0.15	0.15	z = 1.00 *p*-value = 0.32	z = 0.00 *p*-value = 1.00
General Symptom Domain	-0.03	0.25	0.26	z = 1.28 *p*-value = 0.20	z = 0.04 *p*-value = 0.97

Table S2. Correlations between SIPS symptom ratings and age at visit, stratified by symptom domain and diagnostic group. To assess the relationship between age and SIPS symptom ratings, Pearson correlations were calculated between age and SIPS domain scores in each study group, separately. Correlation coefficients were positive and highest in magnitude for 3q29Del, positive and modest in 22q11.2Del, but negative in HCs. This is consistent with the group differences in the mean and range of age. The 3q29Del group is younger and encompasses an age-range that is typically associated with an increase in symptom severity. The 22q11.2Del and HC groups are older, and the age range in HCs extends into young adulthood when psychotic-like experiences typically decline. Given the group variation in sample size, power for detecting significant correlations between age and symptom severity was lowest in 3q29Del, highest for the HCs, and moderate in 22q11.2Del. Fisher's *r*-to-*Z* transformation was subsequently performed to test the significance of between-group differences in these correlation coefficients. The last two columns of the above table present results from these pairwise comparisons in 3q29Del vs HC, and in 3q29Del vs 22q11.2Del. Correlations between age and positive and negative symptom domain ratings showed a significant difference between 3q29Del and HC groups (p's ≤ 0.05). *Significant group-specific Pearson correlation ($p \leq 0.05$). [a] Significant difference between groups in correlation coefficients, based on Fisher's *r*-to-*Z* transformation ($p \leq 0.05$). For the positive symptom domain total, 22q11.2Del $N = 30$ due to missing data. For the general symptom domain total, HC $N = 278$ due to missing data. *Abbreviations:* Structured Interview for Psychosis-Risk Syndromes, SIPS; healthy controls, HC; deletion, Del.

	HC (*N* = 279)		22q11.2Del (*N* = 31)		3q29Del (*N* = 23)	
SIPS symptom domains and items	Adjusted mean	Std. Error	Adjusted mean	Std. Error	Adjusted mean	Std. Error
Positive Symptom Domain	0.21	0.02	0.93	0.05	0.71	0.06
P1. Unusual Thought Content	0.07	0.01	0.39	0.03	0.26	0.04
P2. Suspiciousness	0.07	0.01	0.39	0.03	0.20	0.03
P3. Grandiosity	0.05	0.01	0.21	0.03	0.16	0.03
P4. Perceptual Abnormalities	0.06	0.01	0.40	0.03	0.36	0.03
P5. Disorganized Communication	0.04	0.01	0.41	0.03	0.37	0.03
Negative Symptom Domain	0.26	0.02	1.12	0.05	0.81	0.06
N1. Social Anhedonia	0.07	0.01	0.56	0.03	0.29	0.03
N2. Avolition	0.07	0.01	0.45	0.03	0.23	0.04
N3. Expression of Emotion	0.03	0.01	0.35	0.03	0.27	0.03
N4. Experience of Emotion and Self	0.02	0.01	0.27	0.02	0.13	0.03
N5. Ideational Richness	0.07	0.01	0.54	0.03	0.40	0.04
N6. Occupational Functioning	0.09	0.01	0.43	0.04	0.35	0.04
Disorganization Symptom Domain	0.15	0.01	0.83	0.04	0.71	0.05
D1. Odd Behavior or Appearance	0.02	0.01	0.34	0.02	0.27	0.03
D2. Bizarre Thinking	0.01	0.01	0.19	0.02	0.18	0.02
D3. Trouble with Focus and Attention	0.11	0.01	0.55	0.03	0.51	0.04
D4. Personal Hygiene	0.02	0.01	0.30	0.02	0.14	0.03
General Symptom Domain	0.57	0.04	2.03	0.13	1.60	0.15
G1. Sleep Disturbance	0.11	0.01	0.37	0.04	0.23	0.04
G2. Dysphoric Mood	0.10	0.01	0.49	0.04	0.24	0.04
G3. Motor Disturbances	0.05	0.01	0.38	0.03	0.37	0.03
G4. Impaired Tolerance to Normal Stress	0.06	0.01	0.37	0.03	0.40	0.04

Table S3. Sex-adjusted means and standard errors of SIPS ratings after log-transformation. The log-transformed sex-adjusted means and standard errors for both deletion groups and HCs are reported above. For P5 and the positive symptom domain total, 22q11.2Del $N = 30$ due to missing data from one 22q11.2Del subject. For G2 and the general symptom domain total, HC $N = 278$ due to missing data from one HC subject. *Abbreviations:* Structured Interview for Psychosis-Risk Syndromes, SIPS; healthy controls, HC; deletion, Del; standard, std.

	3q29Del sub-sample with available neuroimaging and SIPS data (*N* = 17)
Demographic characteristics	
Age (in years)	
M ± *SD*	18.13 ± 9.03
Median [Range]	15.89 [8.08 – 39.12]
Sex, *N* (%)	
Male	10 (59%)
Female	7 (41%)
Race, *N (%)*	
White	15 (88%)
More than one race	2 (12%)
Ethnicity, *N* (%)	
Hispanic/Latino	1 (6%)
Non-Hispanic/Latino	16 (94%)
Clinical characteristics	
Psychotic disorder dx., *N (%)*	3 (18%)
Attenuated psychotic symptom syndrome dx., *N (%)*	3 (18%)
Positive symptom domain total, SIPS	
M ± *SD*	7.65 ± 7.86
Median [Range]	6.00 [0 – 25]
Negative symptom domain total, SIPS	
M ± *SD*	8.18 ± 5.53
Median [Range]	7.00 [0 – 17]
Disorganization symptom domain total, SIPS	
M ± *SD*	5.41 ± 3.81
Median [Range]	5.00 [0 – 11]
General cognitive abilities	
M ± *SD*	71.94 ± 12.02
Median [Range]	73 [46 – 94]
Antipsychotic usage, *N (%)*	2 (12%)
Neuroimaging measures	
Total cerebellum volume (cm^3)	
M ± *SD*	131.62 ± 13.82
Median [Range]	135.23 [105.61 – 153.09]
Cerebellar cortex volume (cm^3)	
M ± *SD*	103.96 ± 12.21
Median [Range]	102.46 [79.11 – 125.60]
Cerebellar white matter volume (cm^3)	
M ± *SD*	27.66 ± 6.25
Median [Range]	26.18 [20.42 – 42.37]
Estimated total intracranial volume (cm^3)	
M ± *SD*	1384.30 ± 108.26
Median [Range]	1350.52 [1236.90 – 1574.65]

Table S4. Demographic, clinical, and MRI-derived volumetric information for the 3q29Del subsample with available neuroimaging and SIPS data. *Abbreviations:* Deletion, Del; magnetic resonance imaging, MRI; Structured Interview for Psychosis-Risk Syndromes, SIPS; mean, *M*; standard deviation, *SD;* diagnosis, dx.

Table S5. Extended linear regression results: The effect of cerebellar volumetric measures on domain-specific symptom ratings in 3q29Del and polynomial modeling of age. Heteroskedasticity-robust Wald tests were performed to compare simpler models to more complex models to identify the best fitting polynomial function of age for each ROI. The addition of a quadratic age term does not yield a significantly better fit to the data (*p's* > 0.05); hence we favor parsimony and base our statistical inferences on model 1 (highlighted in blue). In **A-J)** the main effect of cerebellar volume is highlighted in grey for clarity. 3q29Del *N* = 17. *Abbreviations:* 3q29 deletion syndrome, 3q29Del; region of interest, ROI; unstandardized coefficient estimate, *b*; confidence interval, *CI*; degrees of freedom, DF; standard error, *SE;* estimated total intracranial volume, eICV; variance inflation factor, VIF. Contrast coding: reference level for the sex variable is female. Two-tailed significance levels: *p-value* ≤ 0.001 '***', *p-value* ≤ 0.01 '**', *p-value* ≤ 0.05 '*', *p-value* ≤ 0.1 '†'.

A. Outcome: Positive Symptom Domain Total

Degree of polynomial	*Explanatory variables*	*b*	*CI (95%)*	*SE b*	*p-value*
Linear (Model 1) Best-fit	Intercept	33.62	-11.49 – 78.73	20.88	0.13
	Age (years)	0.26	-0.24 – 0.75	0.23	0.28
	Sex [Male]	8.88	2.48 – 15.27	2.96	0.01**
	Total Cerebellum Volume (cm^3)	**-0.27**	**-0.61 – 0.06**	**0.16**	**0.10†**
	R^2 / R^2 adjusted	0.34 / 0.19			
	Robust Wald test	F-statistic = 4.02 on 3 and 13 DF, *p-value* = 0.03*			
Quadratic (Model 2)	Intercept	40.16	-8.33 – 88.66	22.26	0.10†
	Age	-0.34	-2.14 – 1.47	0.83	0.69
	Age^2	0.01	-0.03 – 0.06	0.02	0.51
	Sex [Male]	8.54	2.47 – 14.62	2.79	0.01**
	Total Cerebellum Volume (cm^3)	**-0.28**	**-0.64 – 0.08**	**0.16**	**0.11**
	R^2 / R^2 adjusted	0.36 / 0.15			
	Robust Wald test	F-statistic = 4.07 on 4 and 12 DF, *p-value* = 0.03*			

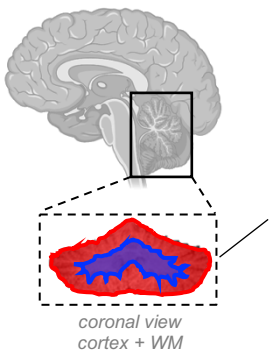

ROI: Total cerebellum volume

Model 1 vs Model 2 – Robust Wald Test:

	Residual DF	DF	F-value	Pr(>F)
1	13			
2	12	1	0	0.99

Final model: Model 1

B. Outcome: Positive Symptom Domain Total

Degree of polynomial	*Explanatory variables*	*b*	*CI (95%)*	*SE b*	*p-value*
Linear (Model 1) Best-fit	Intercept	43.39	4.75 – 82.04	17.89	**0.03***
	Age (years)	0.18	-0.22 – 0.58	0.18	0.36
	Sex [Male]	9.70	4.21 – 15.19	2.54	**0.002****
	Cerebellar Cortex Volume (cm^3)	**-0.43**	**-0.78 – -0.07**	**0.16**	**0.02***
	R^2 / R^2 adjusted	0.49 / 0.37			
	Robust Wald test	F-statistic = 11.07 on 3 and 13 DF, *p-value* < 0.001***			
Quadratic (Model 2)	Intercept	42.69	5.29 – 80.09	17.17	**0.03***
	Age	0.49	-1.47 – 2.45	0.90	0.60
	Age^2	-0.01	-0.05 – 0.04	0.02	0.74
	Sex [Male]	10.22	3.08 – 17.35	3.27	0.01**
	Cerebellar Cortex Volume (cm^3)	**-0.45**	**-0.87 – -0.03**	**0.19**	**0.04***
	R^2 / R^2 adjusted	0.49 / 0.32			
	Robust Wald test	F-statistic = 5.95 on 4 and 12 DF, *p-value* = 0.01**			

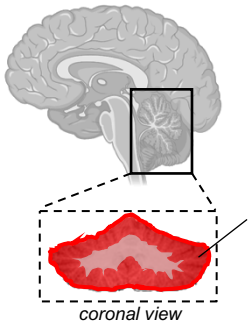

Model 1 vs Model 2 – Robust Wald Test:

	Residual DF	DF	F-value	Pr(>F)
1	13			
2	12	1	0	0.99

Final model: Model 1

C. Outcome: Positive Symptom Domain Total

	Explanatory variables	*b*	*CI (95%)*	*SE b*	*p-value*	*VIF*
Secondary model with eICV correction	Intercept	70.23	31.12 – 109.34	**17.95**	**0.002****	
	Age (years)	0.21	-0.23 – 0.64	0.20	0.32	1.20
	Sex [Male]	10.18	5.48 – 14.89	**2.16**	< 0.001***	**1.43**
	eICV (cm^3)	-0.03	-0.05 – -0.01	0.01	0.01**	1.37
	Cerebellar Cortex Volume (cm^3)	**-0.29**	**-0.56 – -0.02**	**0.12**	**0.03***	**1.99**
	R^2 / R^2 adjusted	0.61 / 0.48				
	Robust Wald test	F-statistic = 28.78 on 4 and 12 DF, *p-value* < 0.001***				

VIF > 5 was treated as indicative of a problematic amount of collinearity.

D. Outcome: Positive Symptom Domain Total

Degree of polynomial	*Explanatory variables*	*b*	*CI (95%)*	*SE b*	*p-value*
Linear (Model 1) Best-fit	Intercept	-8.00	-20.09 – 4.10	5.60	0.18
	Age (years)	0.34	-0.07 – 0.76	0.19	0.10†
	Sex [Male]	3.65	-4.27 – 11.57	3.66	0.34
	Cerebellar White Matter Volume (cm^3)	**0.27**	**-0.19 – 0.73**	**0.21**	**0.23**
	R^2 / R^2 adjusted	0.26 / 0.09			
	Robust Wald test	F-statistic = 11.58 on 3 and 13 DF, *p-value* < 0.001***			
Quadratic (Model 2)	Intercept	-11.11	-66.04 – 43.82	25.21	0.67
	Age	0.55	-2.90 – 4.01	1.58	0.73
	Age^2	-0.00	-0.08 – 0.07	0.04	0.89
	Sex [Male]	3.64	-4.75 – 12.03	3.85	0.36
	Cerebellar White Matter Volume (cm^3)	**0.31**	**-0.70 – 1.33**	**0.47**	**0.51**
	R^2 / R^2 adjusted	0.26 / 0.01			
	Robust Wald test	F-statistic = 7.10 on 4 and 12 DF, *p-value* = 0.004**			

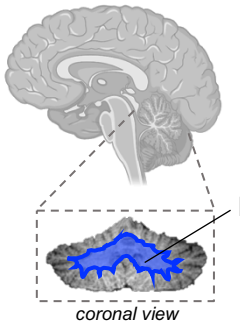

Model 1 vs Model 2 – Robust Wald Test:

	Residual DF	DF	F-value	Pr(>F)
1	13			
2	12	1	0	0.99

Final model: Model 1

E. Outcome: Negative Symptom Domain Total

Degree of polynomial	*Explanatory variables*	*b*	*CI (95%)*	*SE b*	*p-value*
Linear (Model 1) Best-fit	Intercept	-1.46	-36.03 – 33.11	16.00	0.93
	Age (years)	0.28	0.05 – 0.52	0.11	0.02*
	Sex [Male]	2.76	-4.21 – 9.74	3.23	0.41
	Total Cerebellum Volume (cm^3)	**0.02**	**-0.25 – 0.30**	**0.13**	**0.86**
	R^2 / R^2 adjusted	0.24 / 0.07			
	Robust Wald test	F-statistic = 3.90 on 3 and 13 DF, *p-value* = 0.03*			
Quadratic (Model 2)	Intercept	-4.68	-42.10 – 32.74	17.17	0.79
	Age	0.57	-0.78 – 1.93	0.62	0.37
	Age^2	-0.01	-0.04 – 0.02	0.01	**0.66**
	Sex [Male]	2.93	-4.70 – 10.55	3.50	0.42
	Total Cerebellum Volume (cm^3)	**0.03**	**-0.25 – 0.30**	**0.13**	**0.84**
	R^2 / R^2 adjusted	0.25 / 0.002			
	Robust Wald test	F-statistic = 2.39 on 4 and 12 DF, *p-value* = 0.12			

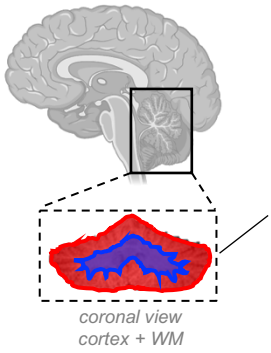

Model 1 vs Model 2 – Robust Wald Test:

	Residual DF	DF	F-value	Pr(>F)
1	13			
2	12	1	0	0.99

Final model: Model 1

F. Outcome: Negative Symptom Domain Total

Degree of polynomial	*Explanatory variables*	*b*	*CI (95%)*	*SE b*	*p-value*
Linear (Model 1) Best-fit	Intercept	-2.15	-29.68 – 25.37	12.74	0.87
	Age (years)	0.29	0.04 – 0.54	0.12	0.03*
	Sex [Male]	2.71	-3.78 – 9.19	3.00	0.38
	Cerebellar Cortex Volume (cm^3)	**0.03**	**-0.24 – 0.30**	**0.13**	**0.79**
	R^2 / R^2 adjusted	0.24 / 0.07			
	Robust Wald test	F-statistic = 3.54 on 3 and 13 DF, *p-value* = 0.05*			
Quadratic (Model 2)	Intercept	-2.69	-29.62 – 24.24	12.36	0.83
	Age	0.53	-0.97 – 2.03	0.69	0.46
	Age^2	-0.01	-0.04 – 0.03	0.02	0.74
	Sex [Male]	3.10	-4.99 – 11.19	3.71	0.42
	Cerebellar Cortex Volume (cm^3)	**0.02**	**-0.29 – 0.33**	**0.14**	**0.90**
	R^2 / R^2 adjusted	0.25 / -0.001			
	Robust Wald test	F-statistic = 2.12 on 4 and 12 DF, *p-value* = 0.14			

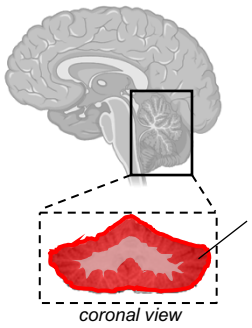

Model 1 vs Model 2 – Robust Wald Test:

	Residual DF	DF	F-value	Pr(>F)
1	13			
2	12	1	0	0.99

Final model: Model 1

G. Outcome: Negative Symptom Domain Total

Degree of polynomial	*Explanatory variables*	*b*	*CI (95%)*	*SE b*	*p-value*
Linear (Model 1) Best-fit	Intercept	1.95	-8.00 – 11.91	4.61	0.68
	Age (years)	0.28	0.02 – 0.54	0.12	0.04*
	Sex [Male]	3.19	-2.15 – 8.53	2.47	0.22
	Cerebellar White Matter Volume (cm^3)	**-0.02**	**-0.40 – 0.36**	**0.18**	**0.91**
	R^2 / R^2 adjusted	0.24 / 0.06			
	Robust Wald test	F-statistic = 3.37 on 3 and 13 DF, *p-value* = 0.05*			
Quadratic (Model 2)	Intercept	-4.62	-42.17 – 32.94	17.24	0.79
	Age	0.72	-1.57 – 3.00	1.05	0.51
	Age^2	-0.01	-0.06 – 0.04	0.02	0.69
	Sex [Male]	3.17	-2.52 – 8.87	2.62	0.25
	Cerebellar White Matter Volume (cm^3)	**0.08**	**-0.64 – 0.79**	**0.33**	**0.82**
	R^2 / R^2 adjusted	0.25 / 0.003			
	Robust Wald test	F-statistic = 2.14 on 4 and 12 DF, *p-value* = 0.14			

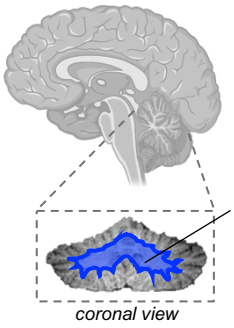

Model 1 vs Model 2 – Robust Wald Test:

	Residual DF	DF	F-value	Pr(>F)
1	13			
2	12	1	0	0.99

Final model: Model 1

H. Outcome: Disorganization Symptom Domain Total

Degree of polynomial	*Explanatory variables*	*b*	*CI (95%)*	*SE b*	*p-value*
Linear (Model 1) Best-fit	Intercept	-1.89	-26.83 – 23.05	11.54	0.87
	Age (years)	0.08	-0.15 – 0.31	0.11	0.45
	Sex [Male]	1.81	-4.64 – 8.26	2.98	0.55
	Total Cerebellum Volume (cm^3)	**0.04**	**-0.18 – 0.25**	**0.10**	**0.72**
	R^2 / R^2 adjusted	0.12 / -0.09			
	Robust Wald test	F-statistic = 0.70 on 3 and 13 DF, *p-value* = 0.57			
Quadratic (Model 2)	Intercept	1.80	-23.62 – 27.23	11.67	0.88
	Age	-0.25	-1.35 – 0.85	0.50	0.63
	Age^2	0.01	-0.02 – 0.03	0.01	0.50
	Sex [Male]	1.62	-5.17 – 8.41	3.12	0.61
	Total Cerebellum Volume (cm^3)	**0.03**	**-0.19 – 0.25**	**0.10**	**0.76**
	R^2 / R^2 adjusted	0.14 / -0.14			
	Robust Wald test	F-statistic = 0.91 on 4 and 12 DF, *p-value* = 0.49			

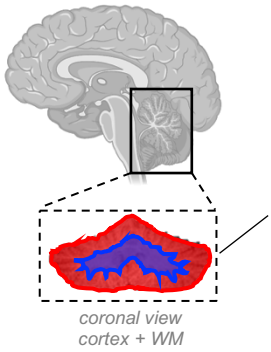

Model 1 vs Model 2 – Robust Wald Test:

	Residual DF	DF	F-value	Pr(>F)
1	13			
2	12	1	0	0.99

Final model: Model 1

I. Outcome: Disorganization Symptom Domain Total

Degree of polynomial	*Explanatory variables*	*b*	*CI (95%)*	*SE b*	*p-value*
Linear (Model 1) Best-fit	Intercept	9.57	-10.29 – 29.42	9.19	0.32
	Age (years)	0.04	-0.22 – 0.30	0.12	0.74
	Sex [Male]	3.14	-1.61 – 7.88	2.20	0.18
	Cerebellar Cortex Volume (cm^3)	**-0.06**	**-0.25 – 0.12**	**0.08**	**0.45**
	R^2 / R^2 adjusted	0.13 / -0.06			
	Robust Wald test	F-statistic = 0.74 on 3 and 13 DF, *p-value* = 0.55			
Quadratic (Model 2)	Intercept	10.14	-12.14 – 32.41	10.22	0.34
	Age	-0.21	-1.58 – 1.16	0.63	0.74
	Age^2	0.01	-0.02 – 0.04	0.01	0.67
	Sex [Male]	2.72	-3.54 – 8.97	2.87	0.36
	Cerebellar Cortex Volume (cm^3)	**-0.05**	**-0.29 – 0.19**	**0.11**	**0.68**
	R^2 / R^2 adjusted	0.15 / -0.13			
	Robust Wald test	F-statistic = 1.14 on 4 and 12 DF, *p-value* = 0.39			

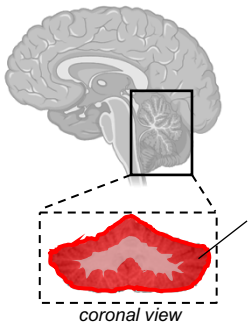

Model 1 vs Model 2 – Robust Wald Test:

	Residual DF	DF	F-value	Pr(>F)
1	13			
2	12	1	0	0.99

Final model: Model 1

J. Outcome: Disorganization Symptom Domain Total

Degree of polynomial	*Explanatory variables*	*b*	*CI (95%)*	*SE b*	*p-value*
Linear (Model 1) Best-fit	Intercept	-3.96	-10.97 – 3.05	3.24	0.24
	Age (years)	0.05	-0.13 – 0.24	0.09	0.54
	Sex [Male]	1.34	-3.31 – 5.98	2.15	0.54
	Cerebellar White Matter Volume (cm^3)	**0.28**	**-0.06 – 0.61**	**0.15**	**0.09†**
	R^2 / R^2 adjusted	0.29 / 0.13			
	Robust Wald test	F-statistic = 6.19 on 3 and 13 DF, *p-value* = 0.01**			
Quadratic (Model 2)	Intercept	-11.07	-31.63 – 9.49	9.44	0.26
	Age	0.53	-0.68 – 1.75	0.56	0.36
	Age^2	-0.01	-0.04 – 0.02	0.01	0.40
	Sex [Male]	1.32	-3.53 – 6.17	2.22	0.56
	Cerebellar White Matter Volume (cm^3)	**0.38**	**-0.11 – 0.87**	**0.22**	**0.11**
	R^2 / R^2 adjusted	0.32 / 0.10			
	Robust Wald test	F-statistic = 4.51 on 4 and 12 DF, *p-value* = 0.02*			

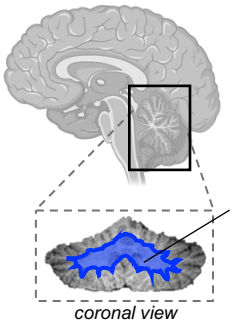

Model 1 vs Model 2 – Robust Wald Test:

	Residual DF	DF	F-value	Pr(>F)
1	13			
2	12	1	0	0.99

Final model: Model 1

Table S6. Extended logistic regression results: The effect of cerebellar volumetric measures on the probability of a psychotic disorder or APSS diagnosis in 3q29Del and polynomial modeling of age. A-C) Logistic regression models include sex, age, and/or age^2 (when appropriate) as covariates. Analysis of variance (ANOVA) with likelihood ratio test was performed to sequentially compare simpler models (model 1) to more complex models (model 2) to identify the best fitting polynomial function of age for each ROI. Results indicate that the addition of a quadratic age term in model 2 does not yield a significantly better fit to the data than model 1 in any of our analyses (*p's* > 0.05); hence we favor parsimony and base our statistical inferences on model 1 (highlighted in blue). In all models, the main effect of cerebellar volume is highlighted in gray for clarity. 3q29Del *N* = 17. *Abbreviations:* 3q29 deletion syndrome, 3q29Del; attenuated psychotic symptom syndrome, APSS; region of interest, ROI; odds ratio, *OR*; confidence interval, *CI*; degrees of freedom, DF; standard error, *SE*. Contrast coding: reference level for the sex variable is female. Two-tailed significance levels: p-value ≤ 0.001 '***', p-value ≤ 0.01 '**', p-value ≤ 0.05 '*', p-value ≤ 0.1 '†'.

A. Binary outcome: Presence / absence of a psychotic disorder or APSS diagnosis

Degree of polynomial	*Explanatory variables*	*OR*	*CI (95%)*	*SE*	*p-value*
Linear (Model 1) Best-fit	Intercept	2.77	0.00 – 4028197.83	18.89	0.88
	Age (years)	1.09	0.96 – 1.29	0.08	0.25
	Sex [Male]	4.34	0.24 – 173.78	6.86	0.35
	Total Cerebellum Volume (cm^3)	**0.97**	**0.87 – 1.08**	**0.05**	**0.56**
	Tjur's R^2	0.14			
Quadratic (Model 2)	Intercept	7.64	0.00 – 67707088.23	57.13	0.79
	Age	0.97	0.50 – 1.90	0.32	0.93
	Age^2	1.00	0.99 – 1.02	0.01	0.73
	Sex [Male]	3.98	0.22 – 162.76	6.29	0.38
	Total Cerebellum Volume (cm^3)	**0.97**	**0.87 – 1.08**	**0.05**	**0.57**
	Tjur's R^2	0.15			

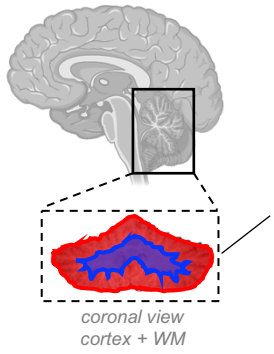

Model 1 vs Model 2 – ANOVA with likelihood ratio test:

	Residual DF	Residual Deviance	DF	Deviance	Pr(> Chi)
1	13	19.40			
2	12	19.28	1	0.12	0.83

Final model: Model 1

B. Binary outcome: Presence / absence of a psychotic disorder or APSS diagnosis

Degree of polynomial	*Explanatory variables*	*OR*	*CI (95%)*	*SE*	*p-value*
Linear (Model 1) Best-fit	Intercept	72.82	0.00 – 125831051.98	458.80	0.50
	Age (years)	1.07	0.93 – 1.29	0.08	0.36
	Sex [Male]	6.87	0.43 – 389.88	10.95	0.23
	Cerebellar Cortex Volume (cm^3)	**0.93**	**0.81 – 1.04**	**0.06**	**0.24**
	Tjur's R^2	0.20			
Quadratic (Model 2)	Intercept	67.04	0.00 – 130020106.90	427.82	0.51
	Age	1.10	0.54 – 2.35	0.39	0.78
	Age^2	1.00	0.98 – 1.02	0.01	0.93
	Sex [Male]	7.19	0.38 – 436.11	12.10	0.24
	Cerebellar Cortex Volume (cm^3)	**0.93**	**0.80 – 1.05**	**0.06**	**0.26**
	Tjur's R^2	0.20			

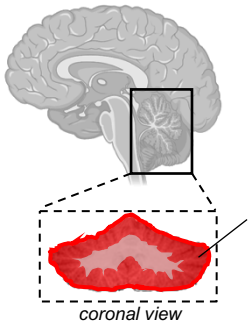

Model 1 vs Model 2 – ANOVA with likelihood ratio test:

	Residual DF	Residual Deviance	DF	Deviance	Pr(> Chi)
1	13	18.24			
2	12	18.24	1	0.01	0.94

Final model: Model 1

C. Binary outcome: Presence / absence of a psychotic disorder or APSS diagnosis

Degree of polynomial	*Explanatory variables*	*OR*	*CI (95%)*	*SE*	*p-value*
Linear (Model 1) Best-fit	Intercept	0.00	0.00 – 1.12	0.01	0.17
	Age (years)	1.13	0.97 – 1.42	0.11	0.21
	Sex [Male]	2.00	0.17 – 37.92	2.58	0.59
	Cerebellar White Matter Volume (cm^3)	**1.15**	**0.92 – 1.57**	**0.15**	**0.31**
	Tjur's R^2	0.20			
Quadratic (Model 2)	Intercept	0.00	0.00 – 103.47	0.00	0.24
	Age	1.30	0.57 – 3.34	0.56	0.54
	Age^2	1.00	0.98 – 1.02	0.01	0.73
	Sex [Male]	1.90	0.16 – 35.91	2.45	0.62
	Cerebellar White Matter Volume (cm^3)	**1.17**	**0.89 – 1.66**	**0.18**	**0.28**
	Tjur's R^2	0.20			

Model 1 vs Model 2 – ANOVA with likelihood ratio test:

	Residual DF	Residual Deviance	DF	Deviance	Pr(> Chi)
1	13	18.44			
2	12	18.32	1	0.12	0.73

Final model: Model 1

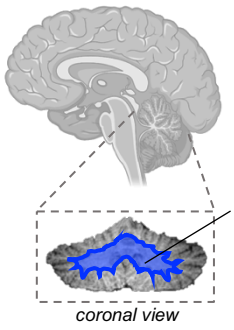

	3q29Del sub-sample with available neuroimaging and SIPS data (*N* = 17)		
	Subjects without PFAC / MCM findings (*N* = 9)	**Subjects with PFAC / MCM findings** (*N* = 8)	**Test statistics**
Diagnostic evaluation of psychotic symptoms			
Psychosis or APSS dx., *n (%)*			OR = 1.19,
Absent	6 (66.67%)	5 (62.50%)	95% CI = 0.11 – 13.47,
Present	3 (33.33%)	3 (37.50%)	*p-value*[a] = 1
Psychosis dx., *n (%)*			OR = 0,
Absent	6 (66.67%)	8 (100%)	95% CI = 0.00 – 2.54,
Present	3 (33.33%)	0 (0%)	*p-value*[a] = 0.21
APSS dx., *n (%)*			OR = INF,
Absent	9 (100%)	5 (62.50%)	95% CI = 0.52 – INF,
Present	0 (0%)	3 (37.50%)	*p-value*[a] = 0.08[†]
Dimensional evaluation of psychotic symptoms			
SIPS Positive Symptom Domain			
Mean ± SD	7.56 ± 9.53	7.75 ± 6.11	*W* = 42.00,
Median [Range]	3 [0 – 25]	8 [1 – 17]	*p-value*[b] = 0.60
SIPS Negative Symptom Domain			
Mean ± SD	7.56 ± 6.21	8.88 ± 4.97	*t* = 0.48, DF = 15,
Median [Range]	6 [0 – 17]	7.5 [2 – 16]	*p-value*[c] = 0.64
SIPS Disorganization Symptom Domain			
Mean ± SD	6.00 ± 4.56	4.75 ± 2.92	*t* = -0.66, DF = 15,
Median [Range]	8 [0 – 11]	5 [1 – 9]	*p-value*[c] = 0.52

Table S7. Nested comparison of diagnostic and dimensional phenotypes in 3q29Del subjects with versus without posterior fossa arachnoid cyst and mega cisterna magna findings. [a] Fisher's exact test, [b] Wilcoxon rank sum test with continuity correction, [c] Student's two sample t-test. Results from diagnostic evaluation of psychotic symptoms indicate that there is no statistically significant difference between 3q29Del subjects with versus without PFAC/MCM findings in the prevalence of psychotic disorder and/or APSS diagnoses (p's > 0.05). There was a trend-level association ($p \leq 0.1$) between the odds of meeting diagnostic criteria for APSS and having a PFAC/MCM finding, which may warrant consideration in future studies with larger sample sizes. Results from dimensional evaluation of psychotic symptoms indicate that there was no statistically significant difference between 3q29Del subjects with versus without PFAC/MCM findings in SIPS domain totals for positive, negative or disorganization symptoms (p's > 0.05). Non-parametric test statistics are reported in cases where the data do not meet parametric assumptions. Note that given well-established

challenges in differentiating PFACs from MCM using conventional MRI (i.e., shared characteristics in appearance), we considered the prevalence rate of these two neuroanatomical findings jointly. *Abbreviations:* 3q29 deletion, 3q29Del; diagnosis, dx; posterior fossa arachnoid cyst, PFAC; mega cisterna magna, MCM; attenuated psychotic symptom syndrome, APSS; Structured Interview for Psychosis-Risk Syndromes, SIPS; standard deviation, SD; degrees of freedom, DF; odds ratio, OR; infinity, INF. Two-tailed significance levels: *p-value* ≤ 0.001 '***', *p-value* ≤ 0.01 '**', *p-value* ≤ 0.05 '*', *p-value* ≤ 0.1 '†'.

Supplemental Figures

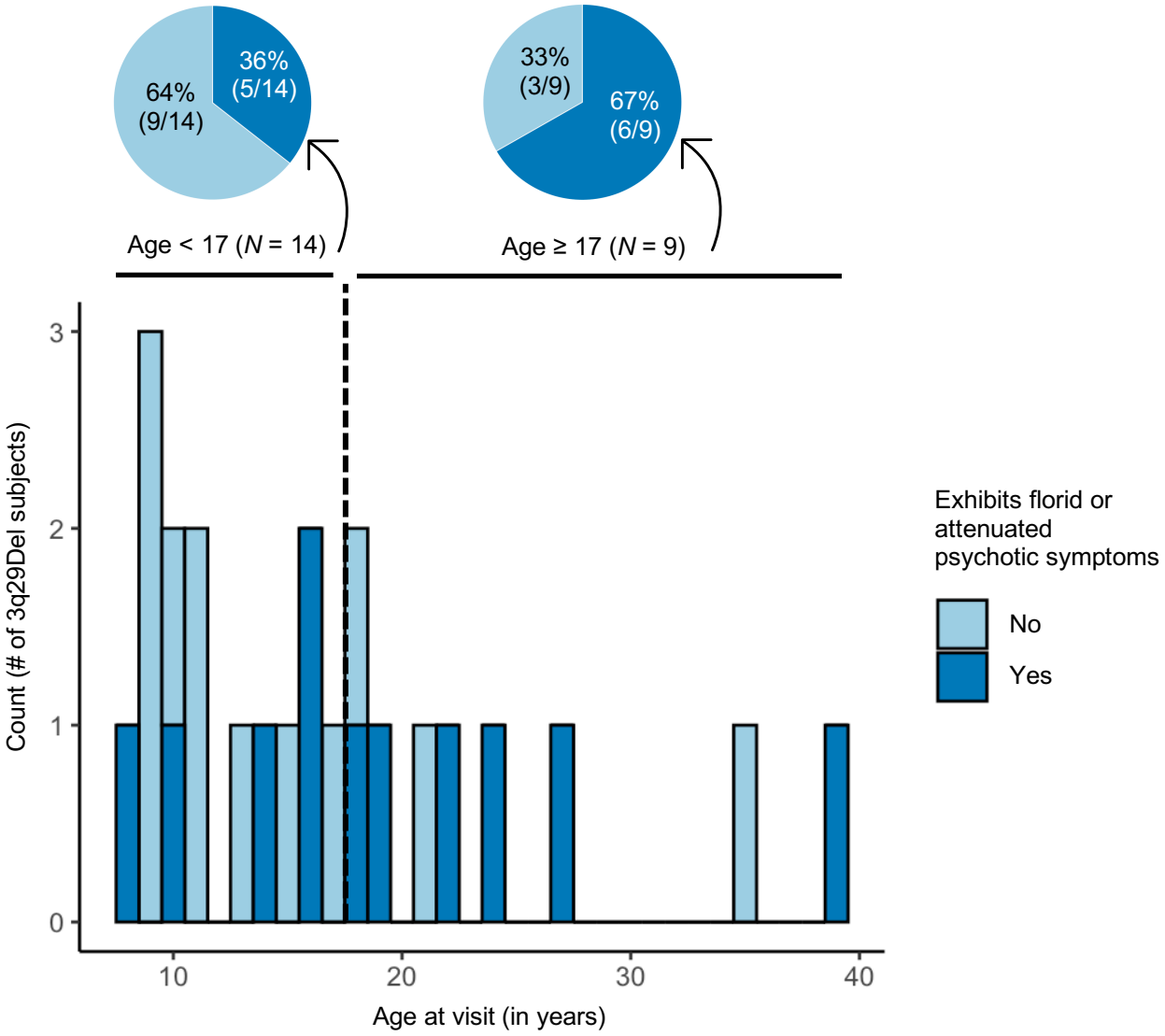

Figure S1. Age-stratified prevalence rates of florid or attenuated psychotic symptoms in 3q29Del. 48% of the 3q29Del sample (11/23) meets diagnostic criteria for psychosis or exhibits one or more clinically significant attenuated positive symptoms (i.e., at least one positive symptom rated three or higher on the SIPS). Based on published demographic data on CHR groups in the general population, the mean age at ascertainment is between 17 and 18 years. Thus, the majority of the 3q29Del subjects in the present sample (61%, 14/23) fall below the estimated age for typical onset of both psychosis and the psychosis prodrome (dashed line on histogram marks age 17 years). When stratified by age-group (age < 17 years vs age ≥ 17 years), our results

indicate that the prevalence rate of psychosis or clinically significant attenuated positive symptoms among 3q29Del subjects younger than age 17 is 36% (5/14), whereas this rate is 67% (6/9) among those aged 17 and older. *Abbreviations:* Deletion, Del; Structured Interview for Psychosis-Risk Syndromes, SIPS; clinical high risk, CHR.

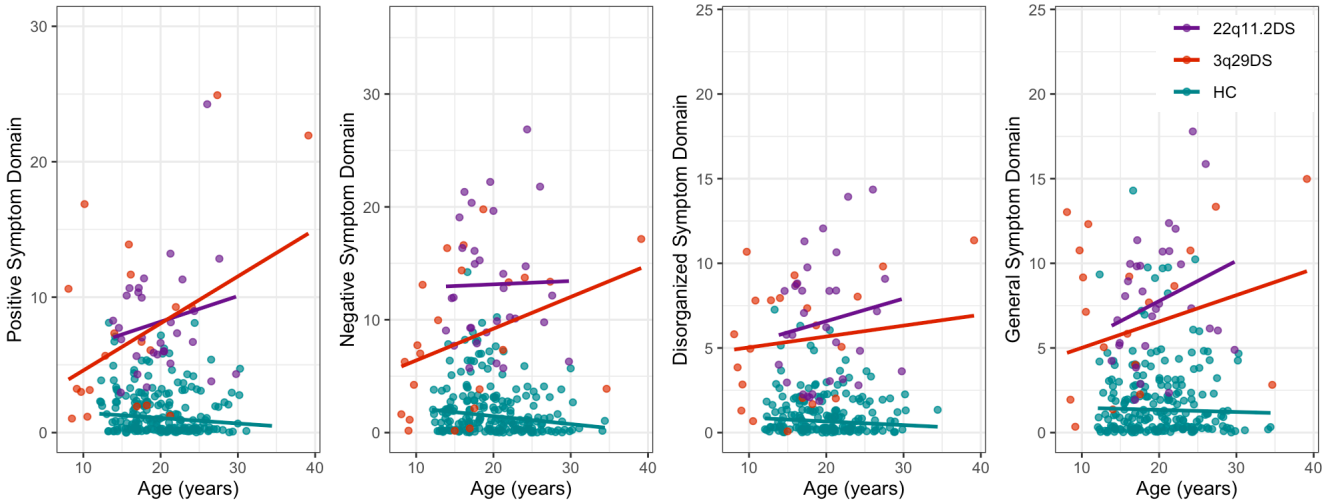

Figure S2. Scatter plots of the relationship between SIPS symptom ratings and age at visit, stratified by symptom domain and diagnostic group. The scatterplots above are provided for visual evaluation of the correlation results reported in Table S2. Solid lines represent the line of linear fit for each group. A slight jitter was systematically added to each plot to minimize overplotting. *Abbreviations:* Structured Interview for Psychosis-Risk Syndromes, SIPS; healthy controls, HC; deletion syndrome, DS.

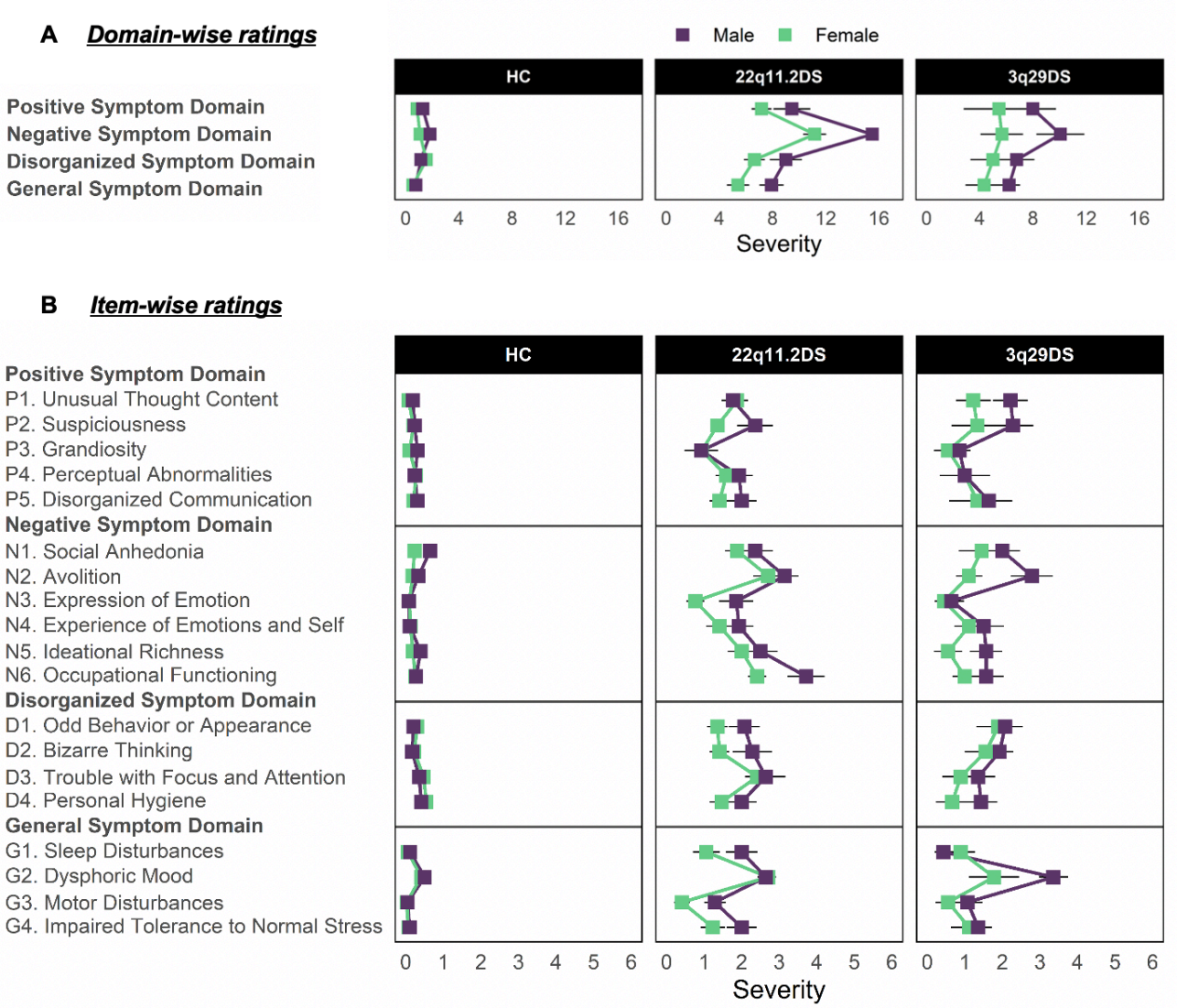

Figure S3. Sex-specific SIPS ratings among deletion groups and HCs. Sex differences were investigated in SIPS domain totals (panel **A**) and item-specific SIPS ratings (panel **B**) within each group. Plots reflect the unadjusted means of individual SIPS ratings for each group. Standard error bars are shown. For P5 and the positive symptom domain total, 22q11.2Del $N = 30$ due to missing data from one 22q11.2Del subject. For G2 and the general symptom domain total, HC $N = 278$ due to missing data from one HC subject. *Abbreviations:* Structured Interview for Psychosis-Risk Syndromes, SIPS; healthy controls, HC; deletion, Del; deletion syndrome, DS.

A

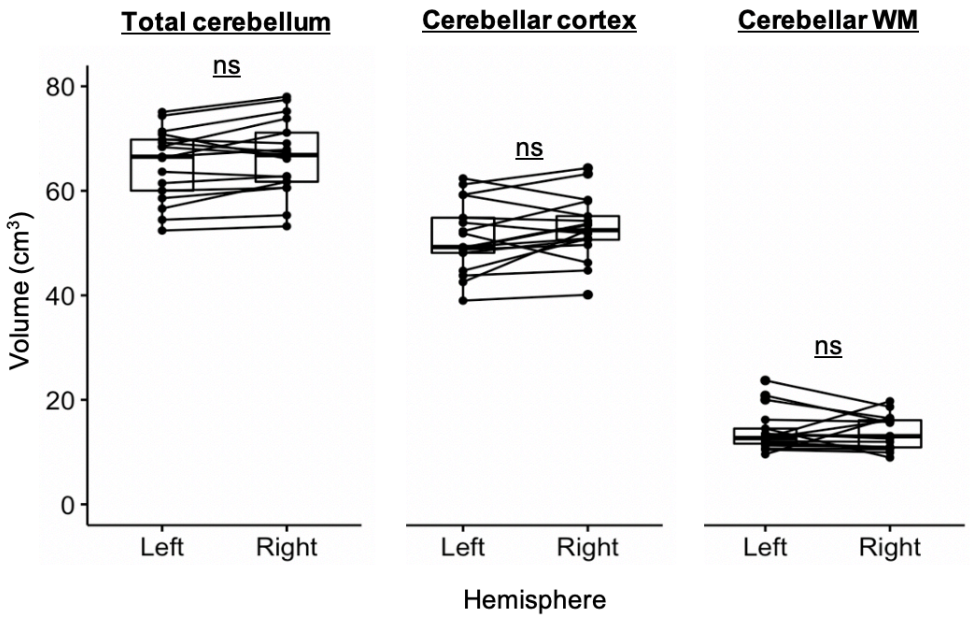

B

ROI (cm^3)	Left Hemisphere	Right Hemisphere	Difference (Left - Right)	*p-value*
Total cerebellum volume				
Mean ± SD	65.15 ± 6.86	66.46 ± 7.22	-1.31 ± 2.75	0.07
Median (range)	66.54 (52.39 – 75.08)	66.85 (53.22 – 78.01)	-1.35 (-5.35 – 4.70)	
Cerebellar cortex volume				
Mean ± SD	51.14 ± 6.74	52.82 ± 6.13	-1.69 ± 4.11	0.11
Median (range)	49.24 (38.99 – 62.39)	52.47 (40.12 – 64.37)	-1.65 (-9.92 – 5.61)	
Cerebellar WM volume				
Mean ± SD	14.02 ± 3.97	13.64 ± 3.21	0.37 ± 3.60	0.13
Median (range)	12.69 (9.60 – 23.72)	13.05 (8.96 – 19.74)	0.40 (-7.05 – 5.56)	

Figure S4. Comparison of hemisphere-specific ROI volumes in the 3q29Del subsample with available neuroimaging and SIPS data. A) Box plots showing the paired distribution of left and right hemispheric ROI volumes in 3q29Del (N = 17). **B)** Descriptive statistics and results of paired-samples tests for inter-hemispheric differences in ROI volumes. There were no significant volumetric differences between the two hemispheres of any of the ROIs investigated in this study ($p > 0.05$). Hence, left and right hemispheric volumes were added to derive a single bilateral volume for each ROI in downstream analyses. *Abbreviations:* Deletion, Del; Structured Interview for Psychosis-Risk Syndromes, SIPS; magnetic resonance imaging, MRI; region of interest, ROI; white matter, WM; standard deviation, SD; not significant, ns.

A

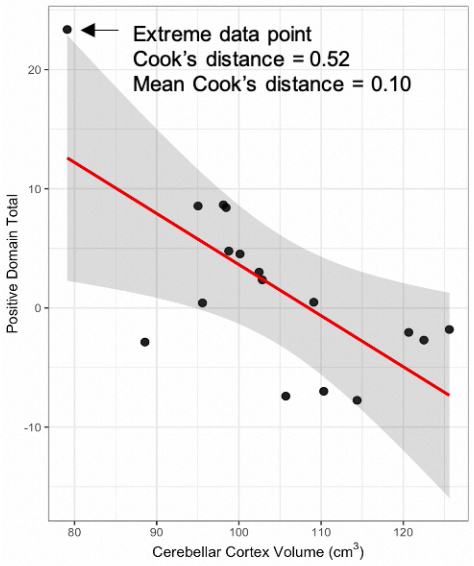

B

Regression analysis after removal of one extreme data point:

Outcome: Positive Symptom Domain Total (*N* = 16)				
Explanatory variables	***b***	***CI (95%)***	***SE b***	***p-value***
Intercept	26.91	-1.44 – 55.26	13.01	0.06†
Age (years)	0.15	-0.24 – 0.54	0.18	0.42
Sex [Male]	9.87	3.60 – 16.14	2.88	0.005**
Cerebellar Cortex Volume (cm^3)	**-0.28**	**-0.54 – -0.01**	**0.12**	**0.04***
R^2 / R^2 adjusted	0.50 / 0.37			
Robust Wald test	F-statistic = 4.86 on 3 and 12 DF, *p-value* = 0.02*			

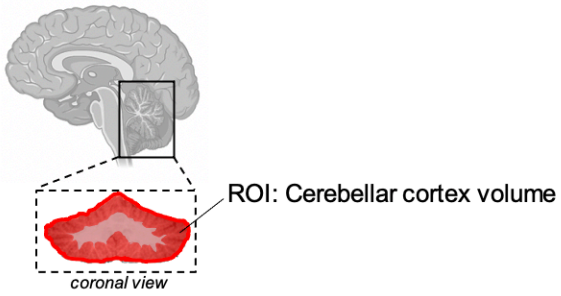

Figure S5. Sensitivity analysis: The relationship between cerebellar cortex volume and positive symptom severity in 3q29Del after removal of an extreme data point. A) Predictor effect plot showing the relationship between cerebellar cortex volume and positive symptom ratings in *N* = 17 3q29Del subjects. Visual inspection suggests that one datapoint (black arrow) may have high leverage on findings; the mean Cook's distance in the sample = 0.10, while the Cook's distance for this subject = 0.52. As values greater than 4 times the mean Cook's distance of the sample may be classified as influential, we performed a sensitivity analysis by removing this datapoint. **B)** Multiple linear regression results in *N* = 16 3q29Del subjects. The main effect of cerebellar cortex volume on positive symptom severity is highlighted in grey for clarity. Results indicate that the coefficient of determination (R^2) remains relatively stable after removal of the extreme datapoint. Although statistical power is reduced due to slightly smaller sample size, there is still a significant inverse relationship between cerebellar cortex volume and positive symptom severity, while correcting for age and sex ($p \leq 0.05$). *Abbreviations:* 3q29 deletion, 3q29Del; unstandardized coefficient estimate, *b*; confidence interval, *CI*; degrees of freedom, DF; standard error, *SE*. Contrast coding: reference level for the categorical sex variable is female. Two-tailed significance levels: *p-value* ≤ 0.001 '***', *p-value* ≤ 0.01 '**', *p-value* ≤ 0.05 '*', *p-value* ≤ 0.1 '†'.

Supplemental References

Elliott CD (2007): *Manual for the Differential Abilities Scales, 2nd ed.* San Antonio, TX: Harcourt Assessment.

First MB, Williams JB, Karg RS, Spitzer RL (2015): Structured clinical interview for DSM-5—Research version (SCID-5 for DSM-5, research version; SCID-5-RV). *Arlington, VA: American Psychiatric Association.*1-94.

Fischl B, Salat DH, Busa E, Albert M, Dieterich M, Haselgrove C *et al.* (2002): Whole brain segmentation: automated labeling of neuroanatomical structures in the human brain. *Neuron* 33(3): 341-355.

Fusar-Poli P, Cappucciati M, Rutigliano G, Schultze-Lutter F, Bonoldi I, Borgwardt S, et al. (2015): At risk or not at risk? A meta-analysis of the prognostic accuracy of psychometric interviews for psychosis prediction. *World Psychiatry*. 14:322-332.

Lee DK, Yoon U, Kwak K, Lee JM (2015): Automated Segmentation of Cerebellum Using Brain Mask and Partial Volume Estimation Map. *Comput Math Methods Med* 2015: 167489.

Miller TJ, McGlashan TH, Rosen JL, Cadenhead K, Cannon T, Ventura J, et al. (2003): Prodromal assessment with the structured interview for prodromal syndromes and the scale of prodromal symptoms: predictive validity, interrater reliability, and training to reliability. *Schizophr Bull.* 29:703-715.

Murphy MM, Lindsey Burrell T, Cubells JF, Espana RA, Gambello MJ, Goines KCB, et al. (2018): Study protocol for The Emory 3q29 Project: evaluation of neurodevelopmental, psychiatric, and medical symptoms in 3q29 deletion syndrome. *BMC Psychiatry* 18:183.

Sattler JM (2002): *Assessment of children: Cognitive applications*. San Diego, CA: Jerome M. Sattler, Publisher, Inc.

Wechsler D (1991): *Manual for the Wechsler Intelligence Scale for Children-III*. San Antonio, TX: The Psychological Corporation.

Wechsler D (1997): *Manual for the Wechsler Adult Intelligence Scale-III*. San Antonio, TX: The Psychological Corporation.

Wechsler D (1999): *Manual for the Wechsler Abbreviated Scale of Intelligence*. San Antonio, TX: The Psychological Corporation.

Wechsler D (2011): *Manual for the Wechsler Abbreviated Scale of Intelligence*, *2nd ed.* Bloomington, MN: Pearson.

CHAPTER 5. Conclusions

This chapter closes this dissertation with a summary of the foregoing chapters, the broader implications of our findings for the fields of neuroscience and psychiatric genetics and a detailed roadmap for future directions.

Summary of research findings

As described in detail in this dissertation, copy number variation (CNV) of DNA sequences represents a significant source of genetic diversity (1-5) and constitutes a far more important substrate for human evolution and adaptation than previously recognized (6-9). Accumulating findings indicate the existence of multiple rare and recurrent CNVs that increase susceptibility to neurodevelopmental and psychiatric disorders with exceptionally large effect sizes (10-22). Given their defined genomic boundaries and high penetrance, systematic research on these CNVs offers a promising opportunity to link specific genetic mechanisms to brain and behavioral phenotypes underlying complex mental illnesses. The ultimate objective of this dissertation was to improve our neurobiological understanding of the largest known genetic risk factor for schizophrenia, the 3q29 deletion (3q29Del) (10, 23-25), in pursuit of this goal.

In chapter 1, a general introduction of the background and overarching aims of this dissertation were presented.

In chapter 2, we focused on addressing the current gap in our understanding of the impact that 3q29Del exerts on the human neural transcriptome. To systematically formulate unbiased hypotheses about molecular mechanisms linking 3q29Del to neuropsychiatric illness, we conducted a systems-level network analysis of the non-pathological adult human cortical transcriptome and generated evidence-based predictions that relate individual 3q29 interval genes to novel biological functions and specific disease associations. We found that the 21 protein-coding genes located in the interval segregate into seven clusters of highly co-expressed genes, demonstrating both convergent and distributed effects across the interrogated transcriptomic landscape. Pathway analysis of these clusters indicated involvement of this locus in not only nervous-system specific

functions, including axon guidance, and synaptic signaling and organization, but also in core cellular functions, including transcriptional regulation, post-translational modifications, chromatin remodeling and mitochondrial metabolism. Top network-neighbors of 3q29 genes showed significant overlap with known schizophrenia, autism spectrum disorder (ASD) and intellectual disability-risk genes, suggesting that 3q29Del biology is relevant to idiopathic disease. Leveraging "guilt by association", we proposed nine specific 3q29 interval genes *(BDH1, CEP19, DLG1, FBXO45, PIGZ, RNF168, SENP5, UBXN7, WDR53)*, including one highly connected hub gene *(UBXN7)*, as prioritized drivers of neuropsychiatric risk in this syndrome. Additionally, we empirically demonstrated the validity of our graph-based predictions in an experimental system by conducting RNA-sequencing in mice harboring a homologous deletion to the human 3q29Del locus. These results provide testable hypotheses for experimental analysis on causal drivers and mechanisms of the largest known genetic risk factor for schizophrenia. These data also highlight the study of normal function in non-pathological post-mortem tissue to further our understanding of psychiatric genetics, especially for rare syndromes like 3q29Del, where access to neural tissue from carriers is unavailable or limited. The mechanistic hypotheses that were formulated in this chapter have directly informed the design of several ongoing experiments in our laboratory, including our work on single-cell RNA-sequencing (scRNA-Seq) of the isocortex in a CRISPR-Cas9 engineered mouse model of 3q29Del, as well as in human induced pluripotent stem cell (hiPSC) derived cerebral organoids. Future work will interrogate the extent to which scRNA-Seq findings from these experiments converge with graph-based predictions presented in this chapter.

In chapter 3, we performed direct and systematic evaluations of human subjects with 3q29Del, with the goal of linking syndromic phenotypes to specific abnormalities in brain structure. To achieve this goal, we conducted the first ever *in vivo* quantitative neuroimaging study in 3q29Del subjects using structural magnetic resonance imaging (MRI), with a focus on the cerebellum and its primary tissue-types. Additionally, we performed a whole-brain radiological evaluation, and examined the association between neuroanatomical findings and standardized behavioral measures to probe gene-brain-behavior relationships. We found a >100-fold increase in posterior fossa abnormalities, particularly in cystic and cyst-like malformations, among 3q29Del carriers. Additionally, we found a significant reduction in the cerebellar volumes of 3q29Del subjects,

independent of other radiological anomalies discovered in this region. Upon further inspection, we found a reduction in cerebellar cortex volume but a concomitant expansion in cerebellar white matter volume, indicating non-uniform changes in these two structures. Interestingly, sex played a moderating role in a subset of neuroanatomical findings. We additionally found that cerebellar white matter changes are associated with cognitive disability and diminished visual motor integration skills in 3q29Del subjects, while cystic/cyst-like malformations yielded no behavioral link, suggesting that the cerebellum is a possible mechanistic intermediary between this genetic lesion and syndromic phenotypes. Overall, our findings from this chapter indicate that abnormal development of posterior fossa structures may be a neuroimaging-based biomarker in one of the largest known genetic risk factors for schizophrenia. These data also add to the emerging body of neuroscientific literature implicating the cerebellum as crucial to not only motor but also non-motor functions of the human brain and present a novel point of genetic convergence with cerebellar pathology reported in idiopathic forms of neurodevelopmental disease.

In chapter 4, we reported the first in-depth evaluation of psychotic symptoms in study subjects with 3q29Del, using the gold-standard Structured Interview for Psychosis-Risk Syndromes (SIPS). We compared this profile to a large sample of healthy controls and participants with another well-known schizophrenia associated CNV, the 22q11.2 deletion (22q11.2Del). Additionally, we examined the effect of age and sex on symptom severity and investigated the relationship between psychotic symptoms and findings from structural brain imaging in 3q29Del to probe the neural substrates of elevated psychosis risk in this syndrome. We found that 48% of 3q29Del subjects exhibit either florid or attenuated psychotic symptoms, which was especially striking considering their young ages. We also found that 3q29Del subjects have more severe ratings than controls on all SIPS domains, while they show remarkable similarity to 22q11.2Del in positive, disorganization, and general symptoms, but diverge from 22q11.2Del in negative symptoms. Additionally, we identified an inverse relationship between positive symptom severity and cerebellar cortex volume among 3q29Del subjects, suggesting that the cerebellar abnormalities identified in chapter 3 may also moderate the relationship between this genetic lesion and vulnerability for certain aspects of psychosis. Overall, our findings in this chapter establish the unique and shared profiles of psychotic symptoms across two high-impact CNVs and highlight

cerebellar involvement in elevated psychosis-risk in one of the largest known genetic risk factors for schizophrenia.

Altogether, the findings reported in the present dissertation substantially advance our understanding of the role that 3q29Del plays in heightened vulnerability for severe neurodevelopmental and psychiatric disorders. These data will provide a strong foundation for subsequent studies investigating the precise neurobiological mechanisms underlying the remarkable risk of neuropsychiatric disease conferred by this CNV. Continued research in this area has the potential to inform clinical practice and diagnostic subtyping, and in the long-term aid in the development of novel, targeted interventions for highly heterogeneous and debilitating disorders like schizophrenia.

Future directions

The findings and predictions presented in this dissertation raise a number of opportunities for formulating future studies, both in terms of theory development and empirical research. In individual data chapters, we have already proposed several new adaptations, tests, and experiments to refine and expand upon our results. Here, we specifically focus on and develop a more detailed roadmap for three interrelated future directions that can serve as immediate extensions of the work described in previous sections.

Future directions for neuroimaging and deep phenotyping of individuals with 3q29Del to refine cerebellar contributions to disease

First, a more comprehensive investigation of the link between cognitive function and cerebellar morphology is needed to parse out the specific cognitive subprocesses that cerebellar dysfunction may be related to beyond IQ among carriers of 3q2Del. By direct and systematic evaluation of 3q29Del study subjects, our group has recently shown that executive functioning skills (25), which are required to control and coordinate goal-directed behaviors (26), show clinically significant deficits in this syndrome. Subdomains of executive function such as working memory and cognitive flexibility have traditionally been considered frontal lobe functions, but more recent evidence suggests that this view may be an oversimplification. Converging evidence indicates that executive functioning skills are dependent on a larger neural circuit that encompasses multiple

brain regions, including the cerebellum (27, 28), although the cerebellum itself has received little experimental attention in this regard. Future research should interrogate whether tissue-specific changes in cerebellar volume correlate with specific executive functioning skills among individuals with 3q29Del, which can be measured by both standardized questionnaires such as the Behavior Rating Inventory of Executive Function (29) and performance-based tools like the Wisconsin Card Sorting task or Digit Span and Letter-Number Sequencing tests (30).

Furthermore, given the link that we discovered between positive symptom severity and cerebellar cortex volumes among 3q29Del participants, and the existing literature on executive functions being a potential neurocognitive endophenotype in schizophrenia (31-33), this work can be further expanded to interrogate the relationships between cerebellar structure, specific subdomains of executive function, and dimensions of psychosis-risk in 3q29Del through mediation analyses, which may yield a more integrated understanding of seemingly distinct syndromic phenotypes. In this context, the inclusion of an age- and sex-matched healthy control group in behavioral analyses will be an important addition that can help elucidate whether identified brain-behavior relationships are specific to 3q29Del or represent a more generalizable association.

Another important direction is to follow study participants over time to determine the temporal order of variables and investigate whether longitudinal patterns of structural change in cerebellar cortex and white matter covary with changes in behavioral and clinical phenotypes. This will be particularly important since many 3q29Del subjects included in the present sample were below the typical age of onset for psychosis at time of scanning and our findings predict that more subjects will transition to frank psychosis over time.

Finally, it should be highlighted that while the cytoarchitecture of the cerebellum is highly homogenous, its inputs from and outputs to distinct cerebral regions are not (34-37). The cerebellum is topographically organized, with the anterior cerebellum (lobules I-IV) and lobule VIII receiving majority of inputs from sensory-motor areas of the neocortex, while lobules VI and VII (including Crus I-II and lobule VIIB) are connected more to the associative and prefrontal areas of the neocortex. The posterior vermis is thought to be the anatomical substrate of the limbic cerebellum, lobule IX is essential for the visual guidance of movement and Lobule X is considered the substrate of the vestibulocerebellum (involved with balance and vestibular

reflexes). Given this heterogeneity in the functional organization of the cerebellum, it will be imperative to implement a higher resolution segmentation technique such as the Spatially Unbiased Atlas Template of the Human Cerebellum (SUIT) (38) to determine whether specific subregions of the cerebellum show differential structural vulnerabilities and phenotypic correlations among individuals with 3q29Del.

Future directions for high resolution neuroimaging of the cerebellum in the 3q29Del mouse model

Leveraging the 3q29Del mouse model in future experiments can help us map out the developmental trajectory of the cerebellar pathology identified in humans, and yield insights into evolutionarily conserved aspects of this pathology at the cellular and molecular levels. As described in earlier chapters, the 3q29 interval is completely syntenic in mice. Our group has shown that mice with the orthologous deletion exhibit phenotypes consistent with the human syndrome, including diminished weight throughout development, deficits in social interaction, impaired spatial memory, exaggerated acoustic startle responses, and attenuated locomotor activity in response to amphetamine (39). In addition, pilot structural MRI data collected in a small sample of adult 3q29Del mice and wild type littermates showed a significant reduction of total cerebellar volume in 3q29Del mice, replicating the human cerebellar phenotype. Hence, these transgenic mice present a valuable experimental system that can be used to interrogate the biology of the 3q29Del syndrome.

To elucidate the temporal evolution of the cerebellar abnormalities observed in these pilot data, future work should image a larger sample of wild type and mutant mice at multiple developmental time points either cross-sectionally or longitudinally by using *ex vivo* or *in vivo* structural MRI techniques. Notably*, ex vivo* protocols enable the acquisition of high-resolution images since the brain can be dissected to fit into a sensitive coil and imaged overnight on high field MR systems. This level of resolution can reveal subtle anatomical aberrations that cannot be identified by conventional neuroimaging techniques in humans. However, tissues prepared for *ex vivo* imaging can suffer from morphological disruption due to fixation and perfusion. Hence, the trade-offs between longitudinal *in vivo* and cross-sectional *ex vivo* imaging should be considered during experimental design.

Given the sigmoidal growth curve that normative cerebellar development follows in mice (40), timepoints for neuroimaging should be chosen to effectively sample across phases of slow and rapid cerebellar

growth. In the mouse brain, total cerebellar volume undergoes slow growth in the late embryonic period (E16-E18), followed by a rapid increase during the early postnatal period (P0-P20) and the peak reached within the juvenile period (P20-25) (40). Hence, P2, P10, P20 and P120 may be ideal timepoints to compare the rates of change in cerebellar volumetric growth across developmental time between wild type and 3q29Del mice.

The addition of cerebellum-dependent motor learning tasks to these experiments, such as Pavlovian eye-blink conditioning (41, 42), as well as perceptual decision-making tasks that have been shown to index cerebellar involvement in working memory (43, 44) could also strengthen future investigations by complementing mouse neuroimaging findings with cerebellum-related behavioral readouts.

Future directions for transcriptomic investigation of the cerebellum in the 3q29Del mouse model

Leveraging the 3q29Del mouse model can also help address what cellular or molecular changes are induced by 3q29Del in the cerebellum at distinct developmental timepoints that can be selected based on findings from neuroimaging. Using single-cell transcriptional profiling (scRNA-Seq), future work should investigate which genes are differentially expressed in the cerebella of mutant mice compared with wild type littermates and what biological pathways and processes are enriched among these dysregulated genes.

Unlike bulk-RNA sequencing (bulk-RNA-Seq), which averages gene expression across all cells in a given tissue, scRNA-Seq can profile the transcriptome of the cerebellum at single-cell resolution, which provides a unique opportunity to conduct an unbiased analysis of the entire cellular composition of the cerebellum. As reported in earlier chapters, most 3q29 interval genes are expressed in the cerebellum but there is limited knowledge about which genes are expressed in which distinct cell types. The cerebellum contains at least six different types of neurons, including glutamatergic granule cells and GABAergic Purkinje cells, as well as a remarkable heterogeneity of glial and endothelial cells, all expressing a distinct repertoire of genes (45, 46). A true understanding of the molecular and cellular determinants of the pathological cerebellum in 3q29Del requires a transcriptomic investigation of all cerebellar cell types to identify the specific cell type or cell types and driver genes that contribute to disease.

Findings that emerge from scRNA-Seq experiments can then be compared to the WGCNA-based

predictions reported in earlier chapters of this dissertation to determine whether empirical findings from the cerebellum of 3q29Del mice converge with network-level operations of 3q29 interval genes in the non-pathological adult human cortical transcriptome.

Altogether, the research directions outlined in this section build upon this dissertation as a foundation and have the potential to bring us closer to elucidating the exact neural impact that one of the strongest known genetic risk factors for schizophrenia exerts on one of the least understood regions of the human brain.

References

1. Iafrate AJ, Feuk L, Rivera MN, Listewnik ML, Donahoe PK, Qi Y, et al. (2004): Detection of large-scale variation in the human genome. *Nat Genet*. 36:949-951.

2. Sebat J, Lakshmi B, Troge J, Alexander J, Young J, Lundin P, et al. (2004): Large-scale copy number polymorphism in the human genome. *Science*. 305:525-528.

3. Redon R, Ishikawa S, Fitch KR, Feuk L, Perry GH, Andrews TD, et al. (2006): Global variation in copy number in the human genome. *Nature*. 444:444-454.

4. Korbel JO, Urban AE, Affourtit JP, Godwin B, Grubert F, Simons JF, et al. (2007): Paired-end mapping reveals extensive structural variation in the human genome. *Science*. 318:420-426.

5. Carvalho CM, Zhang F, Lupski JR (2011): Structural variation of the human genome: mechanisms, assays, and role in male infertility. *Syst Biol Reprod Med*. 57:3-16.

6. Cheng Z, Ventura M, She X, Khaitovich P, Graves T, Osoegawa K, et al. (2005): A genome-wide comparison of recent chimpanzee and human segmental duplications. *Nature*. 437:88-93.

7. Dumas L, Kim YH, Karimpour-Fard A, Cox M, Hopkins J, Pollack JR, et al. (2007): Gene copy number variation spanning 60 million years of human and primate evolution. *Genome Res*. 17:1266-1277.

8. Lupski JR (2007): An evolution revolution provides further revelation. *Bioessays*. 29:1182-1184.

9. Zhang F, Gu W, Hurles ME, Lupski JR (2009): Copy number variation in human health, disease, and evolution. *Annu Rev Genomics Hum Genet*. 10:451-481.

10. Marshall CR, Howrigan DP, Merico D, Thiruvahindrapuram B, Wu W, Greer DS, et al. (2017): Contribution of copy number variants to schizophrenia from a genome-wide study of 41,321 subjects. *Nat Genet*. 49:27-35.

11. Sanders SJ, He X, Willsey AJ, Ercan-Sencicek AG, Samocha KE, Cicek AE, et al. (2015): Insights into Autism Spectrum Disorder Genomic Architecture and Biology from 71 Risk Loci. *Neuron*. 87:1215-1233.

12. Leppa VM, Kravitz SN, Martin CL, Andrieux J, Le Caignec C, Martin-Coignard D, et al. (2016): Rare Inherited and De Novo CNVs Reveal Complex Contributions to ASD Risk in Multiplex Families. *Am J Hum Genet*. 99:540-554.

13. Takumi T, Tamada K (2018): CNV biology in neurodevelopmental disorders. *Curr Opin Neurobiol.* 48:183-192.

14. Malhotra D, Sebat J (2012): CNVs: harbingers of a rare variant revolution in psychiatric genetics. *Cell.* 148:1223-1241.

15. Kaminsky EB, Kaul V, Paschall J, Church DM, Bunke B, Kunig D, et al. (2011): An evidence-based approach to establish the functional and clinical significance of copy number variants in intellectual and developmental disabilities. *Genet Med.* 13:777-784.

16. Girirajan S, Campbell CD, Eichler EE (2011): Human copy number variation and complex genetic disease. *Annu Rev Genet.* 45:203-226.

17. Sebat J, Lakshmi B, Malhotra D, Troge J, Lese-Martin C, Walsh T, et al. (2007): Strong association of de novo copy number mutations with autism. *Science.* 316:445-449.

18. Girirajan S, Brkanac Z, Coe BP, Baker C, Vives L, Vu TH, et al. (2011): Relative burden of large CNVs on a range of neurodevelopmental phenotypes. *PLoS Genet.* 7:e1002334.

19. Cooper GM, Coe BP, Girirajan S, Rosenfeld JA, Vu TH, Baker C, et al. (2011): A copy number variation morbidity map of developmental delay. *Nat Genet.* 43:838-846.

20. Chawner SJ, Watson CJ, Owen MJ (2021): Clinical evaluation of patients with a neuropsychiatric risk copy number variant. *Curr Opin Genet Dev.* 68:26-34.

21. Moreno-De-Luca A, Myers SM, Challman TD, Moreno-De-Luca D, Evans DW, Ledbetter DH (2013): Developmental brain dysfunction: revival and expansion of old concepts based on new genetic evidence. *Lancet Neurol.* 12:406-414.

22. Moreno-De-Luca D, Cubells JF (2011): Copy number variants: a new molecular frontier in clinical psychiatry. *Curr Psychiatry Rep.* 13:129-137.

23. Mulle JG (2015): The 3q29 deletion confers >40-fold increase in risk for schizophrenia. *Mol Psychiatry.* 20:1028-1029.

24. Mulle JG, Dodd AF, McGrath JA, Wolyniec PS, Mitchell AA, Shetty AC, et al. (2010): Microdeletions of 3q29 confer high risk for schizophrenia. *Am J Hum Genet.* 87:229-236.

25. Sanchez Russo R, Gambello MJ, Murphy MM, Aberizk K, Black E, Burrell TL, et al. (2021): Deep phenotyping in 3q29 deletion syndrome: recommendations for clinical care. *Genet Med.* 23:872-880.

26. Cristofori I, Cohen-Zimerman S, Grafman J (2019): Executive functions. *Handb Clin Neurol.* 163:197-219.

27. Bellebaum C, Daum I (2007): Cerebellar involvement in executive control. *Cerebellum.* 6:184-192.

28. Beuriat PA, Cohen-Zimerman S, Smith GNL, Krueger F, Gordon B, Grafman J (2020): A New Insight on the Role of the Cerebellum for Executive Functions and Emotion Processing in Adults. *Front Neurol.* 11:593490.

29. Gioia GA, Isquith PK, Guy SC, Kenworthy L (2000): Test review behavior rating inventory of executive function. *Child Neuropsychology.* 6:235-238.

30. Wechsler D, Kodama H (1949): *Wechsler intelligence scale for children*. Psychological corporation New York.

31. Aydin E, Cansu Ulgen M, Tabo A, Devrim Balaban O, Yesilyurt S, Yumrukcal H (2017): Executive function and genetic loading in nonpsychotic relatives of schizophrenia patients. *Psychiatry Res.* 248:105-110.

32. Wobrock T, Ecker UK, Scherk H, Schneider-Axmann T, Falkai P, Gruber O (2009): Cognitive impairment of executive function as a core symptom of schizophrenia. *World J Biol Psychiatry.* 10:442-451.

33. Donati FL, D'Agostino A, Ferrarelli F (2020): Neurocognitive and neurophysiological endophenotypes in schizophrenia: An overview. *Biomarkers in Neuropsychiatry.* 3:100017.

34. Stoodley CJ, Schmahmann JD (2010): Evidence for topographic organization in the cerebellum of motor control versus cognitive and affective processing. *Cortex.* 46:831-844.

35. Stoodley CJ, Schmahmann JD (2009): Functional topography in the human cerebellum: a meta-analysis of neuroimaging studies. *Neuroimage.* 44:489-501.

36. Kelly RM, Strick PL (2003): Cerebellar loops with motor cortex and prefrontal cortex of a nonhuman primate. *J Neurosci.* 23:8432-8444.

37. Strick PL, Dum RP, Fiez JA (2009): Cerebellum and nonmotor function. *Annu Rev Neurosci.* 32:413-434.

38. Diedrichsen J (2006): A spatially unbiased atlas template of the human cerebellum. *Neuroimage*. 33:127-138.

39. Rutkowski TP, Purcell RH, Pollak RM, Grewenow SM, Gafford GM, Malone T, et al. (2021): Behavioral changes and growth deficits in a CRISPR engineered mouse model of the schizophrenia-associated 3q29 deletion. *Mol Psychiatry*. 26:772-783.

40. Chuang N, Mori S, Yamamoto A, Jiang H, Ye X, Xu X, et al. (2011): An MRI-based atlas and database of the developing mouse brain. *Neuroimage*. 54:80-89.

41. Gormezano I, Schneiderman N, Deaux E, Fuentes I (1962): Nictitating membrane: classical conditioning and extinction in the albino rabbit. *Science*. 138:33-34.

42. McCormick DA, Thompson RF (1984): Cerebellum: essential involvement in the classically conditioned eyelid response. *Science*. 223:296-299.

43. Deverett B, Koay SA, Oostland M, Wang SS (2018): Cerebellar involvement in an evidence-accumulation decision-making task. *Elife*. 7.

44. Deverett B, Kislin M, Tank DW, Wang SS (2019): Cerebellar disruption impairs working memory during evidence accumulation. *Nat Commun*. 10:3128.

45. Wizeman JW, Guo Q, Wilion EM, Li JY (2019): Specification of diverse cell types during early neurogenesis of the mouse cerebellum. *Elife*. 8.

46. Aldinger KA, Thomson Z, Phelps IG, Haldipur P, Deng M, Timms AE, et al. (2021): Spatial and cell type transcriptional landscape of human cerebellar development. *Nat Neurosci*. 24:1163-1175.